horticulturae

Special Issue Reprint

Biotic and Abiotic Stress Responses of Horticultural Plants

Edited by
Changxia Li and Yue Wu

mdpi.com/journal/horticulturae

MDPI

Biotic and Abiotic Stress Responses of Horticultural Plants

Biotic and Abiotic Stress Responses of Horticultural Plants

Guest Editors

Changxia Li
Yue Wu

MDPI

Basel • Beijing • Wuhan • Barcelona • Belgrade • Novi Sad • Cluj • Manchester

Guest Editors

Changxia Li
College of Agriculture
Guangxi University
Nanning
China

Yue Wu
College of Horticulture
Gansu Agricultural
University
Lanzhou
China

Editorial Office
MDPI AG
Grosspeteranlage 5
4052 Basel, Switzerland

This is a reprint of the Special Issue, published open access by the journal *Horticulturae* (ISSN 2311-7524), freely accessible at: https://www.mdpi.com/journal/horticulturae/special_issues/B0K917NYDS.

For citation purposes, cite each article independently as indicated on the article page online and as indicated below:

Lastname, A.A.; Lastname, B.B. Article Title. *Journal Name* **Year**, *Volume Number*, Page Range.

ISBN 978-3-7258-6326-6 (Hbk)
ISBN 978-3-7258-6327-3 (PDF)
https://doi.org/10.3390/books978-3-7258-6327-3

Contents

horticulturae

MDPI

Editorial

Advances and Future Directions in Biotic and Abiotic Stress Responses of Horticultural Plants

Changxia Li [1,*] and Yue Wu [2]

[1] College of Agriculture, Guangxi University, Nanning 530004, China
[2] College of Horticulture, Gansu Agricultural University, Lanzhou 730070, China; wuy@gsau.edu.cn
* Correspondence: licx@gxu.edu.cn

1. Introduction

Horticultural plants are fundamental to global nutrition, economic stability, and ecosystem services. However, their productivity and quality are perpetually threatened by a complex array of biotic and abiotic stresses. Biotic stresses, including pests and pathogens, cause substantial pre- and post-harvest losses [1,2], while abiotic stresses such as drought, salinity, and extreme temperatures, intensified by climate change, pose ever-growing challenges to sustainable cultivation [3,4]. Understanding the intricate physiological, molecular, and biochemical mechanisms that underpin plant stress responses is paramount for developing resilient crop varieties and innovative management strategies. This Special Issue, "Biotic and Abiotic Stress Responses of Horticultural Plants", brings together cutting-edge research and comprehensive reviews that illuminate these mechanisms and present pathways toward enhanced horticultural sustainability.

2. Biotic Stress Responses: From Pest Management to Molecular Defense

The battle against biotic stressors requires a multi-pronged approach, integrating traditional management with modern biotechnology. Invasive species like the oriental fruit fly (*Bactrocera dorsalis*) continue to devastate fruit production, necessitating advanced control strategies ranging from biological controls to RNA interference (RNAi) and CRISPR-Cas9 gene editing, as detailed by Jaffar et al. [5]. Similarly, pervasive pests such as aphids, whiteflies, and spider mites demand constant vigilance and integrated pest management (IPM) protocols [6]. Beyond pests, pathogens including bacteria, fungi, and viruses trigger sophisticated plant immune responses. Shamshiri et al. (contribution 1) demonstrated that infection with Cucumber Mosaic Virus (CMV) and Turnip Mosaic Virus (TuMV) significantly reduced the yield and quality of saffron by negatively impacting its morphological and physiological traits and altering the biosynthesis of its key apocarotenoid metabolites and associated gene expression. Zhang et al. (contribution 2) revealed that the *MIR396d-p3* negatively regulated apple resistance to the fungal pathogen *Colletotrichum gloeosporioides* by targeting and suppressing the expression of the disease resistance-related genes *MdUGT89A2* and *MdRGA3*. Ma et al. (contribution 3) reported that resistance to clubroot disease in radish involved rapid and coordinated activation of defense pathways, including R gene-mediated recognition, MAPK-Ca^{2+}-ROS signaling, and jasmonic acid regulation, while susceptibility was characterized by delayed responses and pathogen-induced metabolic hijacking. Ginger rhizomes activated the plant–pathogen interaction pathway, including PTI and ETI immune responses, along with ROS and NO signaling, to defend against *Fusarium solani* infection during postharvest storage (contribution 4). Jones et al. [7] synthesized 50 years of research to show that plant immunity, mediated by cell surface

and intracellular receptors, provides the foundational knowledge for designing durable resistance, such as stacking immune receptor genes to control crop diseases. Furthermore, the menace of root-knot nematodes (*Meloidogyne* spp.) underscores the need for innovative control measures. Vashisth et al. [8] reviewed the potential of genetic engineering and RNAi technology to develop nematode-resistant crops, highlighting a promising frontier in durable resistance breeding.

3. Abiotic Stress Responses: Unraveling Mechanisms for Climate Resilience

Abiotic stresses trigger a cascade of molecular events, from stress perception to the activation of protective genes and metabolites. Waadt et al. [9] comprehensively synthesized recent advances in understanding how plant hormones, particularly abscisic acid, mediate sophisticated sensing, signaling, and response mechanisms to confer tolerance against major abiotic stresses such as drought, salinity, and flooding. It further highlighted the critical role of hormonal crosstalk, innovative biosensors for monitoring hormone dynamics, and the potential for translating these molecular insights into developing climate-resilient crops. Kumar et al. [10] reviewed how histone acetylation dynamics, regulated by HATs and HDACs, control plant development and stress responses by modulating chromatin structure and gene expression. Laloum et al. [11] indicated the critical role of alternative splicing in fine-tuning plant abiotic stress tolerance, particularly through its regulation of ABA signaling components and splicing factors. Wang et al. (contribution 5) reported that specific members of the ABF gene family in kiwifruit (*Actinidia chinensis*), particularly AcABF2, AcABF3, AcABF8, AcABF9, and AcABF10, are upregulated under drought stress and are positively correlated with increased abscisic acid (ABA) levels, suggesting their crucial role in enhancing drought tolerance through the ABA signaling pathway. Wang et al. (contribution 6) demonstrated that cucumber seedlings' tolerance to high-temperature and high-humidity stress increases with their leaf stage, with four-leaf seedlings being the most resilient due to less severe photosynthetic inhibition and oxidative damage compared to the more sensitive one- and two-leaf stages. Red light enhances the salt tolerance of hydroponically grown pea seedlings by improving chlorophyll content, antioxidant enzyme activity, ion homeostasis, and reducing oxidative damage under saline conditions (contribution 7). The application of biochar and hydroretentive polymers mitigated water-deficit stress in *Satureja rechingeri* by improving water status and reducing oxidative stress, as evidenced by decreased antioxidant enzyme activity and malondialdehyde content (contribution 8).

4. Sustainable Practices and Integrated Future Strategies

The transition to sustainable horticulture is imperative. Practices like intercropping not only improve resource efficiency but also suppress diseases. Lv et al. [12] found that intercropping faba bean with wheat suppressed Fusarium wilt by altering the rhizosphere microbiome and root exudate profile. The integration of multi-omics data—genomics, transcriptomics, proteomics, and metabolomics—is revolutionizing our understanding. Gao et al. [13] comprehensively summarized the role of various plant microRNAs in regulating salt stress tolerance through genetic engineering, highlighting their molecular mechanisms, target genes, and potential applications in developing salt-resistant crops. Moreover, optimizing irrigation and fertilization management, as evaluated by Hui et al. [14], remains crucial for improving seed yield by enhancing topsoil nutrient availability, leaf photosynthetic efficiency, and seed morphological traits.

5. Conclusions

This Special Issue encapsulates the significant strides made in deciphering how horticultural plants perceive and respond to environmental challenges. The collective works underscore that solutions lie at the intersection of fundamental discovery and applied innovation. By leveraging advanced biotechnological tools, adopting sustainable agronomic practices, and fostering interdisciplinary collaboration, we can fortify our horticultural systems against an uncertain climate future. The journey toward stress-resilient horticulture is ongoing, and the insights gathered here provide a robust foundation for the research and actions that will follow.

Author Contributions: Writing—original draft preparation, C.L.; logical conception, C.L. and Y.W.; writing—review and editing, C.L. All authors have read and agreed to the published version of the manuscript.

Conflicts of Interest: The authors declare no conflicts of interest.

List of Contributions:

1. Shamshiri, M.; Sánchez, C.; Rico, S.; Mokhtassi-Bidgoli, A.; Ayyari, M.; Rezadoost, H.; Shams-Bakhsh, M. Molecular, Metabolic, and Physiological Responses to Progressive Biotic Stress Caused by Cucumber Mosaic Virus and Turnip Mosaic Virus in Saffron. *Horticulturae* **2025**, *11*, 96.
2. Zhang, B.; Tang, J.; Ji, Z.; Du, Y.; Cong, J.; Zhou, Z. MIR396d-p3 Negatively Regulates Apple Resistance to *Colletotrichum gloeosporioides* via MdUGT89A2 and MdRGA3. *Horticulturae* **2025**, *11*, 351.
3. Ma, Y.; Li, X.; Cui, F.; Yu, Q.; Liu, B.; Guo, X.; Liu, L. Transcriptome Analysis Reveals Key Pathways and Candidate Genes for Resistance to Plasmodiophora brassicae in Radish. *Horticulturae* **2025**, *11*, 777.
4. Zhang, L.; Jia, Q.; Liu, L.; Liu, Y. Integrated Transcriptomic and Functional Analyses Reveal the Role of the Plant–Pathogen Interaction Pathway in *Fusarium solani* Infection of Zingiber officinale. *Horticulturae* **2025**, *11*, 791.
5. Wang, H.; Zi, Y.; Rong, X.; Zhang, Q.; Nie, L.; Wang, J.; Ren, H.; Zhang, H.; Liu, X. Expression Analysis of the ABF Gene Family in Actinidia chinensis Under Drought Stress and the Response Mechanism to Abscisic Acid. *Horticulturae* **2025**, *11*, 715.
6. Wang, X.; Pan, Y.; Liu, H.; Meng, H.; Cheng, Z. Physiological Responses of Cucumber Seedlings to Combined High-Temperature and High-Humidity Stress at Different Leaf Stages. *Horticulturae* **2024**, *10*, 1369.
7. Xu, K.; Sun, X.; Sun, C.; Wang, Y.; Zhu, H.; Xu, W.; Feng, D. Enhanced Salt Tolerance of Pea (*Pisum sativum* L.) Seedlings Illuminated by LED Red Light. *Horticulturae* **2025**, *11*, 150.
8. Beiranvandi, M.; Akbari, N.; Ahmadi, A.; Mumivand, H.; Nazarian Firouzabadi, F.; Argento, S. Impact of Biochar and Hydroretentive Polymers on the Biochemical and Physiological Traits of *Satureja rechingeri* Jamzad Under Water Deficit Stress. *Horticulturae* **2025**, *11*, 169.

References

1. Wan, F.H.; Yang, N.W. Invasion and Management of Agricultural Alien Insects in China. *Annu. Rev. Entomol.* **2016**, *61*, 77–98. [CrossRef] [PubMed]
2. Savary, S.; Willocquet, L.; Pethybridge, S.J.; Esker, P.; McRoberts, N.; Nelson, A. The global burden of pathogens and pests on major food crops. *Nat. Ecol. Evol.* **2019**, *3*, 430–439. [CrossRef] [PubMed]
3. Zhang, H.M.; Zhu, J.H.; Gong, Z.Z.; Zhu, J.K. Abiotic stress responses in plants. *Nat. Rev. Genet.* **2022**, *23*, 104–119. [CrossRef] [PubMed]
4. Ballagón, D.; Terán, F.; de Oliveira, T.; Santa-Catarina, C.; Gómez-Cadena, A. Citrus rootstocks modify scion antioxidant system under drought and heat stress combination. *Plant Cell Rep.* **2022**, *41*, 593–602. [CrossRef] [PubMed]
5. Jaffar, S.; Rizvi, S.A.H.; Lu, Y. Understanding the invasion, ecological adaptations, and management strategies of *Bactrocera dorsalis* in China: A Review. *Horticulturae* **2023**, *9*, 1004. [CrossRef]

6. Varadharajan, V.; Rajendran, R.; Muthuramalingam, P.; Runthala, A.; Madhesh, V.; Swaminathan, G.; Murugan, P.; Srinivasan, H.; Park, Y.; Shin, H.; et al. Multi-omics approaches against abiotic and biotic stress-a review. *Plants* **2025**, *14*, 865. [CrossRef] [PubMed]
7. Jones, J.D.G.; Staskawicz, B.J.; Dangl, J.L. The plant immune system: From discovery to deployment. *Cell* **2024**, *187*, 2095–2116. [CrossRef] [PubMed]
8. Vashisth, S.; Kumar, P.; Chandel, V.G.S.; Kumar, R.; Verma, S.C.; Chandel, R.S. Unraveling the enigma of root-knot nematodes: From origins to advanced management strategies in agriculture. *Planta* **2024**, *260*, 36. [CrossRef] [PubMed]
9. Waadt, R.; Seller, C.A.; Hsu, P.K.; Takahashi, Y.; Munemasa, S.; Schroeder, J.I. Plant hormone regulation of abiotic stress responses. *Nat. Rev. Mol. Cell Biol.* **2022**, *23*, 680–694. [CrossRef] [PubMed]
10. Kumar, V.; Thakur, J.K.; Prasad, M. Histone acetylation dynamics regulating plant development and stress responses. *Cell Mol. Life Sci.* **2021**, *78*, 4467–4486. [CrossRef] [PubMed]
11. Laloum, T.; Martín, G.; Duque, P. Alternative splicing control of abiotic stress responses. *Trends Plant Sci.* **2018**, *23*, 140–150. [CrossRef] [PubMed]
12. Lv, J.X.; Dong, Y.; Dong, K.; Zhao, Q.; Yang, Z.X.; Chen, L. Intercropping with wheat suppressed Fusarium wilt in faba bean and modulated the composition of root exudates. *Plant Soil* **2020**, *448*, 153–164. [CrossRef]
13. Gao, Z.; Ma, C.; Zheng, C.; Yao, Y.; Du, Y. Advances in the regulation of plant salt-stress tolerance by miRNA. *Mol. Biol. Rep.* **2022**, *49*, 5041–5055. [CrossRef] [PubMed]
14. Hui, J.; Sun, Y.; Wei, K.; Cartmill, A.D.; Lo'pez, I.F.; Ma, C.; Zhang, Q. Optimizing irrigation and fertilization management enhances alfalfa seed yield components through improved soil nutrient availability and leaf photosynthetic efficiency. *Front. Plant Sci.* **2025**, *16*, 1655710. [CrossRef] [PubMed]

horticulturae

MDPI

Article

Physiological Responses of Cucumber Seedlings to Combined High-Temperature and High-Humidity Stress at Different Leaf Stages

Xi'ao Wang [1,2], Yupeng Pan [1], Hanqiang Liu [1], Huanwen Meng [1] and Zhihui Cheng [1,*]

[1] College of Horticulture, Northwest A&F University, Yangling, Xianyang 712100, China; chuntian882@163.com (X.W.); yupeng.pan@nwafu.edu.cn (Y.P.); hanqiang0216@nwafu.edu.cn (H.L.); menghw2005@163.com (H.M.)

[2] Spice and Beverage Research Institute, Chinese Academy of Tropical Agricultural Sciences (CATAS), Xinglong, Wanning 571533, China

* Correspondence: chengzh@nwafu.edu.cn

Abstract: The growth and development of plants are closely tied to growth stages, such as germination, flower bud differentiation, photosynthesis, water and fertilizer use efficiency, stress resistance, etc. Previous studies on the stress resistance of plants with different leaf stages have primarily focused on single-factor environmental conditions. However, there has been a lack of systematic research on the physiology of plant seedlings under combined high-temperature and high-humidity (HH) stress, and the relationship between cucumber growth stages and HH tolerance remains unclear. In this study, we analyzed the phenotype, photosynthetic characteristics, reactive oxygen species content, and antioxidant enzyme activity of cucumber seedlings at 1-, 2-, 3-, and 4-leaf stages under control (25 °C + 80%RH, CK) and HH (42 °C + 95%RH) stress, aiming to clarify the relationship between growth stage and cucumber HH tolerance. The results indicated that the HH tolerance of cucumber seedlings increases with leaf stage. Seedlings at 1-leaf and 2-leaf stages were most sensitive to HH, whereas 4-leaf seedlings showed the greatest tolerance. Under HH stress, the biomass, chlorophyll content, net photosynthetic rate, and photosynthetic electron transfer rate were significantly reduced compared to CK. Simultaneously, there was an increase in reactive oxygen species content and antioxidant enzyme activity. The relative values for dry weight, total chlorophyll content, net photosynthetic rate, Fv/Fm, qP, ETR, and Y (II) in 1-leaf and 2-leaf seedlings were significantly lower, while ROS accumulation and changes in antioxidant enzyme activity were significantly higher compared to 4-leaf seedlings. This lays a foundation for future studies on the growth and physiological response of cucumber plants at different growth stages under varying temperature and humidity combined stresses.

Keywords: cucumber; growth stage; high-temperature and high-humidity stress; dual stress; physiology

1. Introduction

Vegetables are one of the essential foods in people's daily diets, with high nutritional and economic value. To meet the market demand for year-round production and balanced supply, most vegetables are grown in facilities. However, during the growth and development of vegetables, they are often subjected to various abiotic stresses within the facility, such as salt stress [1], nitrate stress [2], drought stress [3], heat stress [4], and heavy metal stress [5], which greatly affect the yield and quality of vegetables. Meanwhile, HH stress is also one of the main stresses faced by facility crops, which not only limits their vegetative growth but also significantly reduces their photosynthesis and production. When seedlings were subjected to HH stress, the growth of their leaves and roots were inhibited. Similar results were reported by Weng et al. [6], as well as a significant decrease in plant dry weight and leaf dry weight [7,8]. Pollen abortion occurred, fruit setting rate decreased, and ovary

development was restricted [9]. In addition, it was reported that HH stress would make it easy to cause diseases which seriously threaten the yield and quality of vegetables [10,11].

At present, only a few studies on the HH tolerance of vegetables have been reported. It was determined that Fv/Fm, Pn, chlorophyll content, leaf length, leaf width, plant height, MDA, and stem diameter could be used as identification indexes of early tolerance to HH stress [6]. With the occurrence times and accumulative days of HH stress events, the growth of tomato was inhibited, the corresponding losses of physiological indexes of tomato increased, and flower bud differentiation was also affected [12,13]. Moreover, Zheng et al. [14] found that the activities of sucrose-metabolizing enzymes in young tomato fruits were changed under HH stress, which reduced fruit soluble sugar content. In cucumber, researchers found that HH stress has a serious impact on photosynthesis and yield formation in cucumber [15,16]. In our previous research, HH stress had a significant inhibitory effect on the vegetative growth, reproductive growth, and physiological status of cucumber [7]. The strength of cucumber's HH tolerance may be related to the leaf stage of seedlings, which should be further studied.

It was concerning that there were significant differences in the HH resistance of different varieties [17]. The leaf stage of seedlings may also be one of the main factors affecting the stress tolerance of plants [18], which has been reported in wheatgrass [19], plantain trees [20], *Elymus sibiricus* [21], maize [22], etc. Shao et al. discovered that the most significant effects of waterlogging and high-temperature combined stresses on maize yield occurred at the third-leaf stage, followed by the sixth-leaf stage and tasselling stage [22]. The aging process of *E. sibiricus* was associated with an increase in oxidative stress, indicating that there was an increase in ABA, particularly in the roots [21]. In our previous study, it was shown that cucumber plants at the 6-leaf stage were more tolerant than those at the 2- and 4-leaf stages under low-temperature and high-humidity stress [23]. Similarly, we wondered if there would be similar patterns of cucumber seedlings under HH stress.

In this study, we analyzed the phenotype, photosynthetic characteristics, reactive oxygen species content, and antioxidant enzyme activities of cucumber seedlings at different leaf stages under HH stress, aiming to clarify the relationship between growth stage and HH tolerance. This research will lay a foundation for the physiological and molecular response of plants under HH stress and provide a reference for further studies of other combined stresses.

2. Materials and Methods

2.1. Plant Materials and Experimental Treatment

The cultivar 'Jinchun No. 4' used in this experiment was considered a variety sensitive to HH, which was purchased from Tianjin Kerun Cucumber Research Institute. The cucumber seeds were firstly soaked in hot water at 55 °C for 15 min, then soaked in 25 °C water for 4 h, and germinated in a constant-temperature incubator at 28 °C for 24 h. When the cucumber seeds germinated and the buds were 1–2 mm exposed, we selected the germinated seeds that grew consistently and sowed them in 50-well trays. They were cultivated in growth chambers (Jiangnan, Ningbo) at 25/18 °C (14 h/10 h), a relative humidity of 80% (80%RH), and daytime photosynthetically active radiation of 200 $\mu mols^{-1}m^{-2}$. When the seedlings grew to the 1-, 2-, 3-, and 4-leaf stages, the seedlings were subjected to high-temperature and high-humidity stress (42 °C + 95%RH, HH) and the control treatment (25 °C + 80%RH, CK). The treatments lasted for 8 h and temperature and humidity recorders (Jinan, China, Jianda Renke) were used to monitor the internal environment of the growth chambers in real time during the whole treatment. Three replicates were set for each leaf stage, with 10 seedlings per replicate. Before this experiment, cucumber seedlings at the same leaf stage with consistent growth conditions were selected. The physiology indexes of the seedlings were sampled at 6 h after treatment, and the phenotypes and growth indexes of the seedlings at different leaf stages were analyzed when the treatments finished.

2.2. Biomass

After 8 h of treatment, seedlings at different leaf stages were quickly washed with clean water, wiped to remove the free water on the leaf surface, and then used for biomass measurement, including leaf fresh weight, top part fresh weight, and root fresh weight. Then, all these samples were transferred into envelopes, heated at 105 °C for 30 min, and then dried at 65 °C until reaching a constant weight, which lasted about 3 days. After that, the dry weights of leaves, top parts, and roots were measured and analyzed. Each index of cucumber seedlings at different leaf stages was measured with three biological replicates.

2.3. Photosynthesis and Chlorophyll Fluorescence

After 6 h of treatment, the first fully spread leaf of each treatment was selected for photosynthesis and chlorophyll fluorescence determination. The photosynthetic parameters were measured using a LI-COR6800 plant photosynthesis analyzer (LI-COR, Lincoln, NE, USA), which included the net photosynthetic rate (A), intercellular CO_2 concentration (Ci), transpiration rate (E), and stomatal conductance (gsw). Before powering on, the CO_2 steel cylinder should be firstly installed, and the desiccant H_2O scrub, H_2O humidifier, and soda lime CO_2 scrub should also be tested and correctly equipped. When the blade chamber is closed, the machine performs warmup tests by checking itself for 10 to 15 min. After that, the parameters of the environment were set as follows: 500 μmol s^{-1} flow rate, 0.1 kPa press valve, 10,000 rpm fan speed, and 'sun + sky' ambient. We created a new record file, clamped on the blade, and matched the IRGAs, then logged our remarks in the files.

Leaves were fully adapted to dark conditions which were placed with leaf clamps in a dark environment for no less than 30 min before this experiment. Chlorophyll fluorescence parameters were measured using a Dual PAM-100 dual-channel chlorophyll fluorescence analyzer (Walz, Effeltrich, Germany) under the 'Fluo+P700' measure mode, and then began to test the device by setting the measure light, saturated pulsed light, and actinic light. When the height of ΔF(Fm'-F) showed between 1/3 and 2/3 of Fv(Fm-Fo) in slow kinetics, we began to measure all these chlorophyll fluorescence parameters including PSII maximum photochemical efficiency (Fv/Fm), photochemical quenching coefficient (qP), electron transfer rate (ETR), non-photochemical quenching coefficient (NPQ), actual photochemical efficiency of PSII (Y(II)), quantum yield of unregulated energy dissipation (Y(NO)), and quantum yield of non-photochemical quenching (Y(NPQ)). All the data above can be downloaded from the report.

2.4. Chlorophyll Content

Samples were taken from the first fully spread leaf at each leaf stage 6 h after treatment. Three replicates were taken for each treatment and then were stored in a −80 °C freezer for future use. The chlorophyll content indexes, including chlorophyll a, chlorophyll b, carotenoids, total chlorophyll content, and total pigment content A, were determined by dissolving a 0.1 g leaf sample in 9 mL of 95% ethanol, and extracting for 24 h in a dark environment, inverting and mixing every 6 h. Then, we measured the absorbance at 665 nm, 649 nm, and 470 nm using a UV-4802 spectrophotometer (Unico, Shanghai, China) with 95% ethanol as the control. Total chlorophyll content was calculated by the mathematical expression given below.

$$\text{Chlorphyll a} = 13.95A_{665} - 6.88A_{649} \quad (1)$$

$$\text{Chlorphyll b} = 24.96A_{649} - 7.32A_{665} \quad (2)$$

$$\text{Carotenoids} = \frac{1000A_{470} - 2.05\text{Chlorphyll a} - 114\text{Chlorphyll b}}{245} \quad (3)$$

$$\text{Total chlorphyll} = \text{Chlorphyll a} + \text{Chlorphyll b} \quad (4)$$

$$\text{Total pigment} = \text{Chlorphyll a} + \text{Chlorphyll b} + \text{Carotenoids} \quad (5)$$

2.5. Reactive Oxygen Species and Antioxidant Enzyme Activity

Samples were taken as per the method in Section 2.4, and used for reactive oxygen species determination, including hydrogen peroxide (H_2O_2) and superoxide anions ($O_2^{\bullet -}$). The activities of antioxidant enzymes, such as superoxide dismutase (SOD), peroxidase (POD), and catalase (CAT), were also measured. The method for determining the indexes above was also performed with reference to Amin et al. [23] with a little revision.

For H_2O_2 determination, we added 0.2 g leaf samples to 0.1% trichloroacetic acid, and then fully ground them. After that, they were subjected to a 4 °C centrifuge at 12,000 r/min for 15 min. Next, 0.5 mL of supernatant was mixed with 0.5 mL 10 mM PBS7.0 and 1 mL 1 M KI, and the data were analyzed at 390 nm after 1 h of dark treatment.

$O_2^{\bullet -}$ was extracted with 65 mM PBS7.8, and we added 1 mL of supernatant to 0.75 mL PBS7.8 and 0.25 mL 10 mM hydroxylamine hydrochloride after being centrifuged at 10,000 r/min for 10 min. Then, we let the reaction solution stand at room temperature for half an hour, and extracted 2 mL of the reaction solution into 2 mL 7 mM α-naphthylamine and 2 mL p-aminobenzene sulfonic acid. After that, the data were measured and recorded at 530 nm after a 30 min water bath at 30 °C.

Leaf samples of about 0.5 g were taken and added to 6 mL 0.05 M PBS 7.8 for the reaction solution preparation. After that, the reaction solution was centrifuged at 4 °C at 11,000 r/min for 20 min, and the supernatant could be extracted for the determination of SOD, POD, and CAT.

A few kinds of solution were prepared for the SOD preparation, including 0.13 M methionine (Met), 0.75 mM nitro-blue tetrazolium (NBT), 0.02 mM riboflavin (Rib), and 0.1 mM EDTA-Na_2. We took 0.05 mL of the reaction solution and added it to a mixed solution including 1.5 mL PBS 7.8, 0.3 mL Met, 0.3 mL NBT, 0.3 mL EDTA-Na_2, 0.25 mL dH_2O, and 0.3 mL Rib. We placed the reaction solution in a fully illuminated environment for about 10 min to 20 min until the reaction solution became dark blue, and covered the reaction solution with a black cloth to terminate it immediately. The data were measured at 560 nm and two tubes without enzyme solution were used as the control, one of which was in the dark during the whole experiment, and the other was in light.

The reaction solution for POD measurement was prepared with 0.7 mL 0.05 M PBS 7.0, 1 mL 0.2% 2-methoxyphenol, and 1 mL 0.3% H_2O_2. The enzyme solution was added into the reaction solution and the absorbance was measured at 470 nm at 30 s intervals for 3 min.

Catalase activity was assayed by measuring a 30% H_2O_2 reduction; 1.9 mL 0.05 M PBS 7.0 and 1 mL 0.3% H_2O_2 were mixed and prepared for the reaction, and 0.1 mL was added to the reaction solution and the 30% concentration of H_2O_2 at 240 nm was measured at 30 s intervals for 3 min.

2.6. Data Processing

The relative values of each leaf stage were calculated and the calculation formula was as follows:

$$R = \frac{X_T}{X_{CK}} \quad (6)$$

X_T is the treatment value and X_{CK} is the control value in Formula (1), and multiple comparisons were conducted between different leaf stages using Tukey's test, $p < 0.05$. All the indexes for cucumber seedlings were measured at the same leaf age stages with 3 replicates under treatment and control separately. The relative values were compared in pairs. In addition, all the data were statistically analyzed using IBM SPSS Statistics 26.0 and presented using GraphPad Prism 6 software.

3. Results

3.1. Growth of Cucumber Seedlings with Different Leaf Stages Under HH Stress

The sensitivity of cucumber seedlings to HH treatment varied among different leaf stages. In brief, the tolerance to HH gradually increased with the increase in leaf stages. At 8 h after HH treatment, all leaves and growth tips of the 1-leaf seedlings were wilted and the whole plant was dead. For seedlings of the 2-leaf stage, the leaves showed severe chlorosis, with a curled growth tip, but the seedlings were still upright and not dead. In comparison, although the growth tips of the 3-leaf seedlings were curled, and parts of the leaves were damaged, the injured area was significantly smaller than that of the 2-leaf seedlings. However, there was only a little injury on the leaf edges of the 4-leaf seedlings, while other parts of those leaves remained dark green, with normal growth pip and normal plant growth (Figure 1).

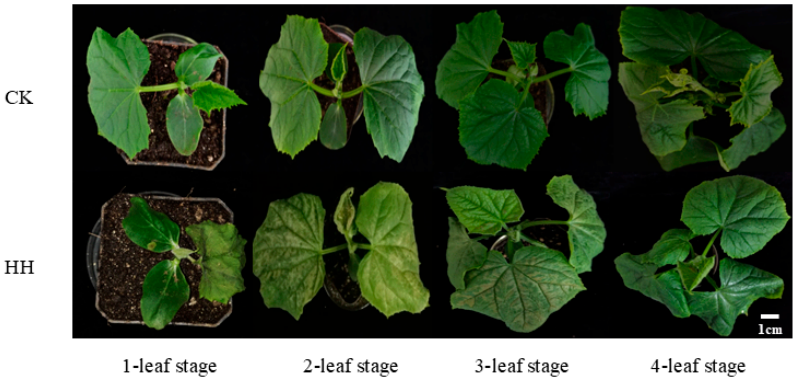

Figure 1. Phenotypes of different leaf-stage cucumber seedlings at 8 h after HH stress.

For biomass, there were significant differences among the seedlings of different leaf stages under HH stress. Overall, the relative biomass of seedlings increased with the increase in the leaf stages. However, there was no significant difference in the relative values of each part of the seedlings between the 3-leaf and the 4-leaf seedlings (Figure 2), indicating that the 3-leaf and the 4-leaf seedlings had similar HH tolerance. The relative values of the leaf fresh weight, top part fresh weight, root fresh weight, and whole-plant fresh weight of the 1-leaf and the 2-leaf seedlings were significantly lower than those of the 4-leaf seedlings (Table S1), and there was no significant difference between the 1-leaf and the 2-leaf seedlings (Figure 2A–D). The relative values of leaf dry weight, top part dry weight, root dry weight, and whole-plant dry weight of the 1-leaf and the 2-leaf seedlings were significantly lower than those of the 4-leaf seedlings (Table S1, Figure 2E–H). The relative values of leaf dry weight, top part dry weight, and whole-plant dry weight of the 1-leaf seedlings were also significantly lower than those of the 2-leaf seedlings (Table S1, Figure 2E,F,H). All of the above indicate that HH stress significantly affected the dry matter accumulation of cucumber seedlings, and the effect decreased with the increase in the leaf stages. The relative values of root fresh weight and root dry weight of the 1-leaf seedlings decreased by 0.15 and 0.13, respectively, compared to the 4-leaf seedlings (Table S1). There was no significant difference in the relative values of root fresh weight and root dry weight between adjacent leaf stages (Figure 2C,G).

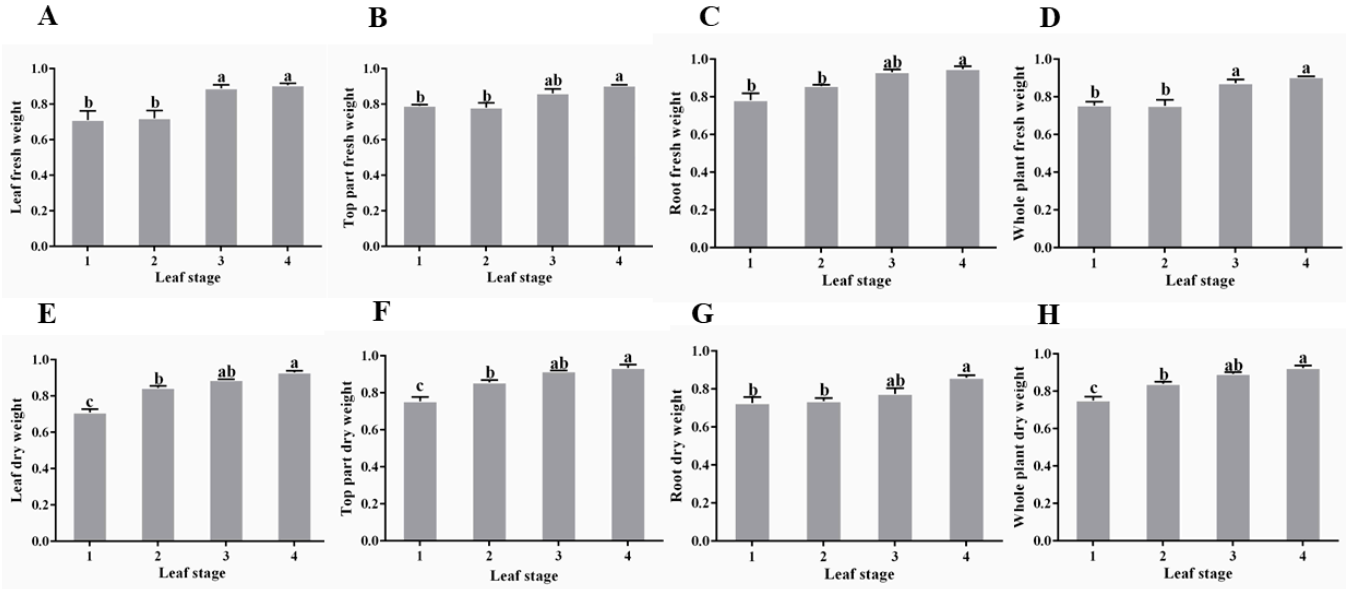

Figure 2. Relative biomass of different leaf-stage cucumber seedlings 8 h after treatments. (**A**) Leaf fresh weight; (**B**) top part fresh weight; (**C**) root fresh weight; (**D**) whole-plant fresh weight; (**E**) leaf dry weight; (**F**) top part dry weight; (**G**) root dry weight; (**H**) whole-plant dry weight. Values are means ± SD from three biological replicates, ANOVA and Tukey HSD test, $p < 0.05$. Different letters on the bars represent significant differences while same letters represent non-significant difference among treatment.

3.2. Photosynthesis of Cucumber Seedlings with Different Leaf Stages Under HH Stress

Chlorophyll and carotenoids are the main photosynthetic pigments of plants, and the relative value of chlorophyll content can partly reflect the HH tolerance of cucumbers at different leaf stages. Overall, the relative values of chlorophyll a, chlorophyll b, carotenoids, total chlorophyll content, and total pigment content increased continuously with the increase in cucumber leaf stages. The relative values of different pigments of the 4-leaf seedlings were significantly higher than those of the 1-leaf seedlings, while there was no significant difference between the 1-leaf and the 2-leaf seedlings (Table S2, Figure 3). There was a significant difference in chlorophyll b and total pigment content between the 2-leaf seedlings and the 3-leaf seedlings, with decreases of 0.08 and 0.09, respectively (Table S2, Figure 3B,E). Only total pigment content showed a significant difference between the 3-leaf and the 4-leaf seedlings, while there was no significant difference among other types of pigments (Table S2, Figure 3E).

There were significant differences in the relative values of photosynthetic parameters among cucumbers at different leaf stages (Table S3). After HH stress, the relative values of the net photosynthetic rate of seedlings at all leaf stages were less than 1, indicating the inhibitive effects, but the decrease in the 4-leaf seedlings was the smallest, only 0.38, and the net photosynthetic rate of the 4-leaf seedlings was significantly higher than those of the 1-leaf, the 2-leaf, and the 3-leaf seedlings (Table S3, Figure 4A), indicating that the 4-leaf seedlings had the strongest resistance to HH stress among all leaf stages. For the 1-leaf and the 2-leaf seedlings, the relative values of stomatal conductance were significantly higher than those of the 3-leaf and the 4-leaf seedlings (Table S3). It was indicated that the increase in stomatal conductance of the 1-leaf and the 2-leaf seedlings under HH stress was significantly higher than that of the 3-leaf and the 4-leaf seedlings compared to the control condition (Table S3, Figure 4B). The relative values of the intercellular carbon dioxide concentration for seedlings at all leaf stages were greater than 1 (Table S3). The relative value of the 4-leaf seedlings was the lowest (1.05) and significantly lower than that of the 1-leaf and the 2-leaf seedlings (Table S3, Figure 4C), indicating that HH stress could lead to an increase in the intercellular carbon dioxide concentration in cucumber

seedlings compared with the control condition, and the increase in the 4-leaf seedlings was the smallest. In addition, the transpiration rate of seedlings at different leaf stages significantly increased to varying extents under HH stress, indicating that the transpiration rate of the 1-leaf seedlings increased the most (0.78), and was significantly higher than that of the 3-leaf and the 4-leaf seedlings (Table S3, Figure 4D).

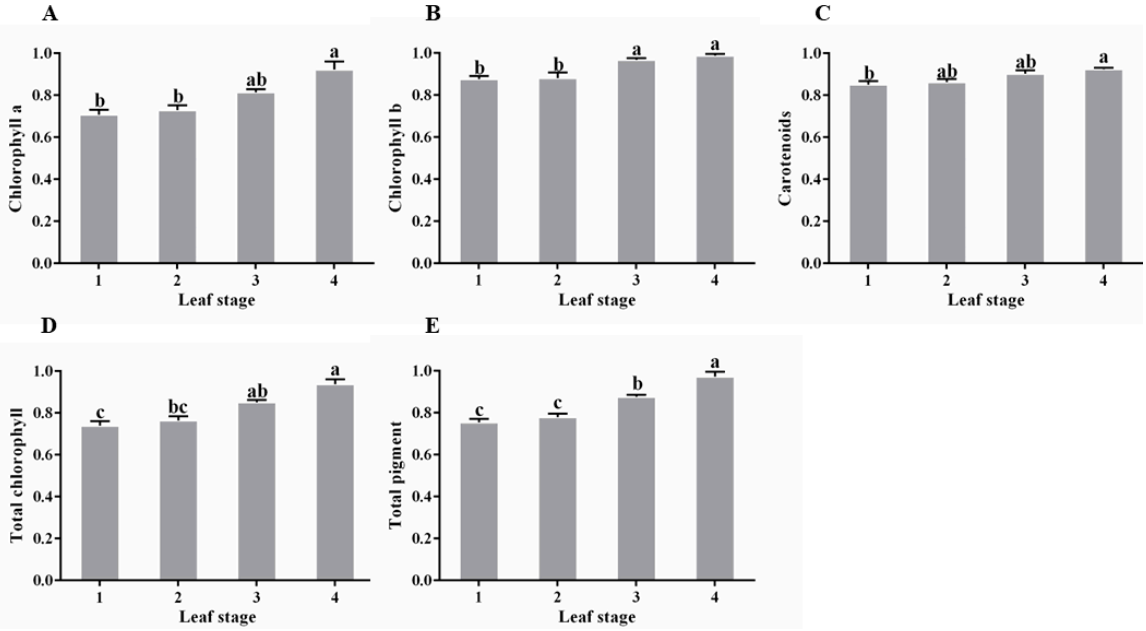

Figure 3. Relative values of photosynthetic pigment content of different leaf-stage cucumber seedlings 6 h after HH stress: (**A**) chlorophyll a; (**B**) chlorophyll b; (**C**) carotenoids; (**D**) total chlorophyll; (**E**) total pigment. Values are means ± SD from three biological replicates, ANOVA and Tukey HSD test, $p < 0.05$. Different letters on the bars represent significant differences while same letters represent non-significant difference among treatment.

HH stress had a serious and different-degree impact on the photosynthetic electron transfer process in the PSII of seedlings at different leaf stages (Figure 5). Although the relative values of Fv/Fm for different leaf-stage seedlings were all less than 1, the 4-leaf seedlings had the smallest decreased value (0.07), while the 1-leaf seedlings had the largest decrease (0.47) (Table S4, Figure 5A). qP represented the opening degree of PSII reaction centers. Although the relative value of qP of the 4-leaf seedlings was less than 1 (0.93) under HH stress, it was significantly higher than those of the 1-leaf (0.72) and the 2-leaf (0.82) seedlings (Table S4, Figure 5B). In contrast, the relative value of NPQ of the 1-leaf seedlings was significantly higher than those of the 2-leaf, the 3-leaf, and the 4-leaf seedlings (Table S4, Figure 5C), showing that the 1-leaf seedlings consumed the most energy for heat dissipation under HH stress. The relative values of ETR and Y(II) for seedlings at different leaf stages showed the same trends of change. Although the ETR and Y(II) of 3-leaf and 4-leaf seedlings decreased after HH stress, the degree of reduction was significantly lower than those of the 1-leaf and the 2-leaf seedlings (Table S4, Figure 5D,E). In addition, the relative values of Y(NPQ) and Y(NO) for the 3-leaf and the 4-leaf seedlings were significantly lower than those of the 1-leaf and the 2-leaf seedlings, which were close to 1, indicating that the HH tolerance of the 3-leaf and the 4-leaf seedlings was significantly higher than that of the 1-leaf and the 2-leaf seedlings (Table S4, Figure 5F,G).

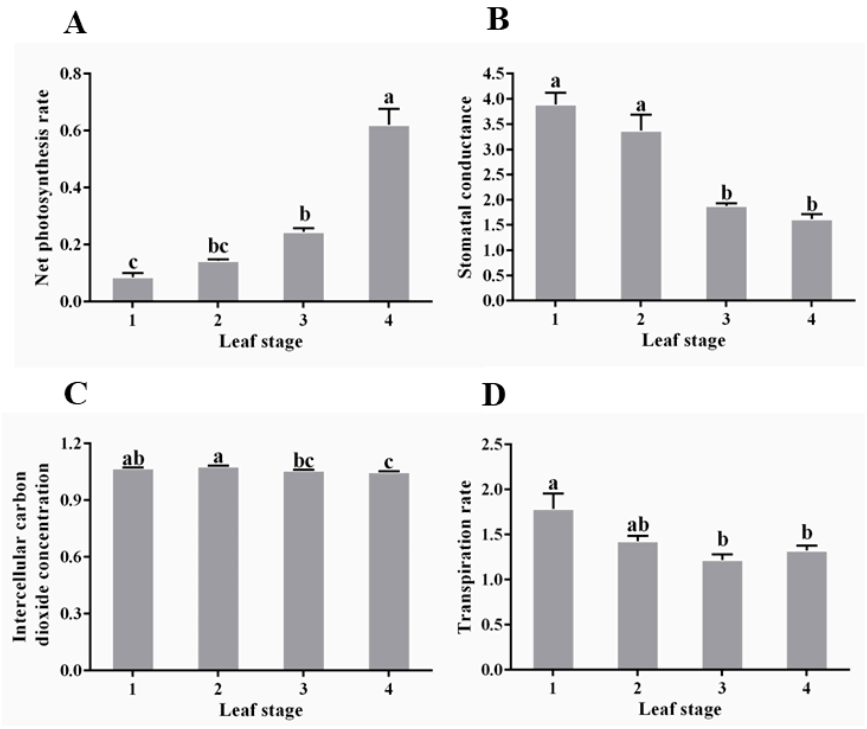

Figure 4. Relative values of photosynthesis parameters of different leaf-stage cucumber seedlings 6 h after HH stress. (**A**) Net photosynthesis rate; (**B**) stomatal conductance; (**C**) intercellular carbon dioxide concentration; (**D**) transpiration rate. Values are means ± SD from three biological replicates, ANOVA and Tukey HSD test, $p < 0.05$. Different letters on the bars represent significant differences while same letters represent non-significant difference among treatment.

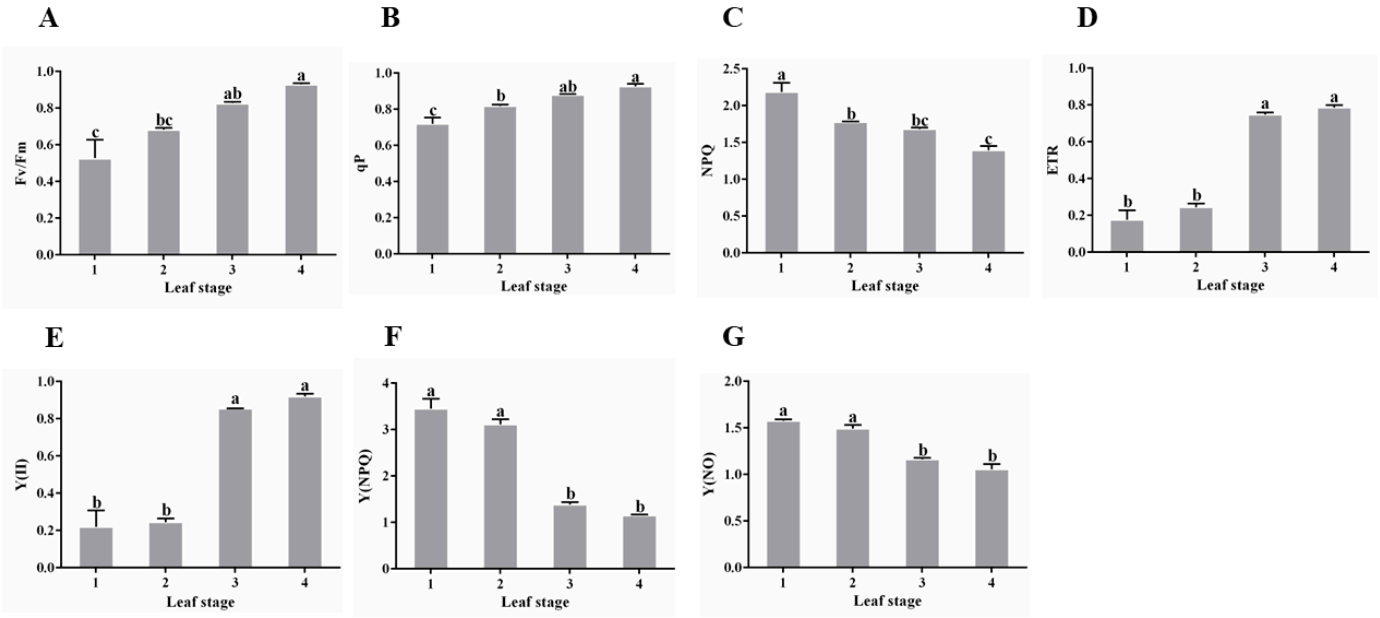

Figure 5. Relative values of chlorophyll fluorescence parameters in different leaf-stage cucumber seedlings 6 h after HH stress. (**A**) Fv/Fm; (**B**) qP; (**C**) NPQ; (**D**) ETR; (**E**) Y(II); (**F**) Y(NPQ); (**G**) Y(NO). Values are means ± SD from three biological replicates, ANOVA and Tukey HSD test, $p < 0.05$. Different letters on the bars represent significant differences while same letters represent non-significant difference among treatment.

3.3. Antioxidant Properties of Cucumber Seedlings with Different Leaf Stages Under HH Stress

There were significant differences in the accumulation of reactive oxygen species (ROS) in seedlings of different leaf stages under HH stress. As shown in Table S5 and Figure 6, the relative values of $O_2^{\bullet -}$ and H_2O_2 in different leaf-stage seedlings were both greater than 1 and gradually decreased with an increase in leaf stages. This indicated that HH stress significantly increased the accumulation of $O_2^{\bullet -}$ and H_2O_2 in young seedlings.

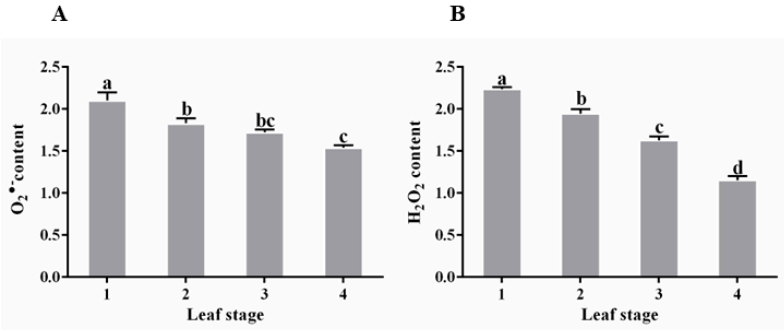

Figure 6. Relative value of reactive oxygen species content in different leaf-stage cucumber seedlings 6 h after HH stress. (**A**) $O_2^{\bullet -}$ content; (**B**) H_2O_2 content. Values are means ± SD from three biological replicates, ANOVA and Tukey HSD test, $p < 0.05$. Different letters on the bars represent significant differences while same letters represent non-significant difference among treatment.

There were significant differences in antioxidant enzyme activities among cucumber seedlings at different leaf stages. After 6 h of HH stress, the relative values of SOD activity in seedlings were all greater than 1, while the relative values of POD activity and CAT activity were both less than 1 (Table S5, Figure 7), indicating that HH stress increased the activity of SOD, while it lowered the activity of POD and CAT in plants. The relative values of SOD activity in the 1-leaf and the 2-leaf seedlings were significantly higher than those in the 3-leaf and the 4-leaf seedlings, while the relative values of POD activity were significantly lower than those in the 3-leaf and the 4-leaf seedlings (Table S5, Figure 7A,B). For CAT activity, the relative values in the 4-leaf seedlings were significantly higher than those in the 1-leaf, the 2-leaf, and the 3-leaf seedlings (Table S5, Figure 7C). All the above results indicated that the antioxidant enzyme activity changes in the 1-leaf and the 2-leaf seedlings were significantly higher than those in the 4-leaf seedlings under HH stress.

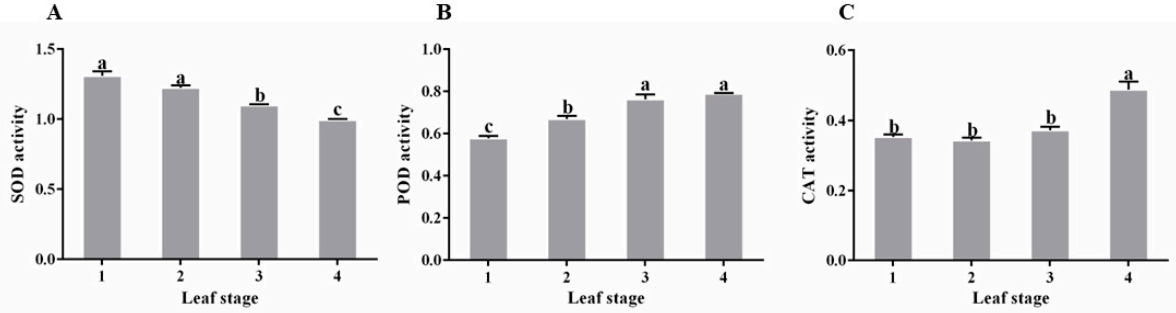

Figure 7. Relative values of antioxidant enzyme activities in different leaf-stage cucumber seedlings 6 h after HH stress. (**A**) SOD activity. (**B**) POD activity. (**C**) CAT activity. Values are means ± SD from three biological replicates, ANOVA and Tukey HSD test, $p < 0.05$. Different letters on the bars represent significant differences while same letters represent non-significant difference among treatment.

4. Discussion

The tolerance of plants to abiotic stress depends not only on the type and duration of stress, but also on the plant growth stage [24]. The growth stage is a major driving force for changes in the traits and performance of plants. Wu et al. found that younger garlic plants

were more sensitive to low temperatures and showed significant inhibition of vegetative growth [25]. Elder plants always exhibited stronger self-regulation abilities, and were less sensitive to environmental changes in many traits [26]. Our previous research on cucumber seedling tolerance to low-temperature and high-humidity conditions found that the fresh and dry weights of plants at different leaf stages were significantly reduced compared to the control, while the decrease in the 2-leaf seedlings was significantly higher than that of the 4-leaf and the 6-leaf plants [23]. Until now, there have only been a few reports on the growth response of plants to HH stress at a single growth stage [7,27], and studies on trait responses at different growth stages are scarce. This study found significant differences in the phenotypes of seedlings at different leaf stages after 8 h HH stress (Figure 1). One-leaf seedlings wilted and died, while the two-leaf, the three-leaf, and the four-leaf seedlings still grew upright. After HH stress, the damaged area of leaves decreased with the increase in leaf stages. In terms of biomass, the relative values of fresh and dry weight, whether on the top part or root part, were all less than 1, indicating that HH stress inhibited the accumulation of biomass (Table S1, Figure 2). The relative values of fresh weight and dry weight increased with the increase in leaf stages, indicating that the higher the leaf stage of cucumber seedlings, the stronger their water retention capacity and dry matter accumulation ability, and the stronger their resistance to HH stress.

The chloroplast is one of the main target organs of plants under oxidative stress, and chlorophyll content is related to the resistance of plants to stress [28]. Pshibytko et al. found that the total chlorophyll content in leaves of 4-day-old barley plants significantly decreased after being subjected to high-temperature stress [29]. Amin et al. found that the chlorophyll content of cucumber seedlings at different leaf stages significantly decreased after low-temperature and high-humidity stress, and the degree of decrease continued to weaken with increasing leaf stage [23]. It has been reported that HH stress could significantly reduce the chlorophyll content of tomato seedlings [27], but the chlorophyll content of different leaf-stage plants under HH stress was currently unclear. In this study, the degree of leaf chlorosis varied among seedlings of different leaf stages under HH stress (Figure 1), which might be related to the decrease in chlorophyll content (Table S2, Figure 3E). This research also showed that relative values of various chlorophyll indicators in the 4-leaf seedlings were significantly higher than those in the 1-leaf and the 2-leaf seedlings. Except for the relative value of pigment content in the 4-leaf seedlings, which was significantly higher than that in the 3-leaf seedlings, there was no significant difference with other indicators compared to the 3-leaf seedlings (Table S2, Figure 3). This indicated that the chlorophyll content of the 1-leaf and the 2-leaf seedlings was more sensitive to HH stress compared to the 4-leaf seedlings.

The leaves are the main organ of photosynthesis. Their photosynthetic capacity is greatly influenced by the external environment, and vary with different leaf stages. There were significant differences in the relative values of net photosynthetic rate, stomatal conductance, intercellular carbon dioxide concentration, and transpiration rate among seedlings of different leaf stages (Table S3, Figure 4). Although the net photosynthetic rate of different leaf-stage seedlings decreased after HH stress, the relative value of the 4-leaf seedlings was significantly higher than that of other leaf-stage seedlings (Table S3, Figure 4A). Due to the influence of chlorophyll content on light absorption and conversion, it was believed that this was also the main factor leading to different degrees of net photosynthetic rate decline among different leaf-stage seedlings (Figures 3 and 4A). Tong et al. found that the transpiration rate of cucumber seedlings significantly increased after HH stress [7]. In this study, we further found that the increase in transpiration rate was related to leaf stages, and the increased degree of transpiration rate of the 3-leaf and the 4-leaf seedlings was significantly lower than that of the 1-leaf seedlings (Table S3, Figure 4D). The stomatal conductance and transpiration rate showed the same trend of change, and the increase in stomatal conductance of the 3-leaf and the 4-leaf seedlings was significantly smaller than that of the 1-leaf and the 2-leaf seedlings (Table S3, Figure 4B,D). In addition, although the relative intercellular CO_2 concentration of the 4-leaf seedlings

was significantly lower than that of the 1-leaf and the 2-leaf seedlings, the relative net photosynthetic rate of the 4-leaf seedlings was significantly higher than that of the 1-leaf and the 2-leaf seedlings (Table S3, Figure 4A,C). Shang et al. believed that this was because elder plants stored more energy and carbon sources during growth than younger plants [30], and therefore they had stronger regulatory ability and were less affected by changes in environmental factors.

The PSII reaction center is sensitive to HH stress in terms of photosynthetic electron transfer. Yang et al. found that the Fv/Fm, qP, and ETR of tomato seedlings under HH stress were significantly reduced compared to the control [31]. Tong et al. showed that there was no significant difference in Fv/Fm and NPQ between cucumber seedlings under HH stress and control, while qP and ETR decreased significantly [7], which was not completely consistent with the results obtained in this study. In our study, we found that the Fv/Fm, qP, ETR, and Y (II) of seedlings at different leaf stages showed varying degrees of decrease after HH stress, while NPQ, Y (NO), and Y (NPQ) showed an upward trend (Figure 5). Furthermore, our analysis also revealed that the decrease in Fv/Fm, qP, ETR, and Y (II) of the 4-leaf seedlings was significantly lower than that of the 1-leaf and the 2-leaf seedlings after HH stress, and the increase in NPQ, Y (NO), and Y (NPQ) was also significantly lower than that of the 1-leaf and the 2-leaf seedlings (Table S4, Figure 5). Therefore, it was believed that the 4-leaf seedlings had significantly stronger HH tolerance than the 1-leaf and the 2-leaf seedlings due to their higher PSII reaction center opening ratio, lower energy dissipation, higher light energy utilization efficiency, and stronger self-regulation ability.

The self-repair ability of different leaf-stage seedlings under abiotic stress gradually increases with the increase in leaf stages. The activities of SOD, POD, and CAT in cucumber seedlings were significantly upregulated under low-temperature and high-humidity stress compared to the control, and the increase was greater with leaf stage [23]. As far as we know, there is no report on the antioxidant enzyme activities of cucumber seedlings at different leaf stages under HH stress. Only a few studies found that HH stress could significantly affect antioxidant enzyme activities. However, the reports on changes in SOD, POD, and CAT activities were not consistent [7,32]. This study found that the activities of SOD, POD, and CAT showed different trends under HH stress, with SOD activity significantly increasing and POD and CAT activities significantly decreasing (Table S5, Figure 7). This might be closely related to the time point of sampling. During the ROS clearing process, different antioxidant enzymes had a sequential effect, and these antioxidant enzymes generally showed a dynamic trend of first increasing and then decreasing after stress. Therefore, to understand the changes in antioxidant enzyme activities in cucumber seedlings under HH stress, it is necessary to take samples and measurements at various time points during the whole process to clarify the biochemical mechanism of cucumber seedlings responding to HH stress. In addition, there were significant differences in the changes in antioxidant enzyme activities among seedlings at different leaf stages. The changes in SOD, POD, and CAT activities in the 4-leaf seedlings were significantly lower than those of the 1-leaf, the 2-leaf, and the 3-leaf seedlings (Table S5, Figure 7), indicating that the 4-leaf seedlings with strong HH tolerance had stronger self-regulation abilities, which was consistent with patterns observed in biomass and photosynthetic indicators.

Overall, this study showed that cucumber seedlings with elder leaf stages had stronger HH tolerance, while seedlings at younger leaf stages suffered more severe damage (Figure 1), presented much more decline in biomass (Table S1, Figure 2) and photosynthesis effect (Tables S2–S4, Figures 4 and 5), showed a larger accumulation of reactive oxygen species (Table S5, Figure 6), and a greater change in antioxidant enzyme activities (Table S5, Figure 7).

In addition, Kuk and Shin reported that the youngest leaf on the same cucumber plant at the four-leaf stage was more tolerant than elder leaves to 5 °C low-temperature stress [33], because of less of an increase in lipid peroxidation and H_2O_2 content, lower photosynthetic activity and chlorophyll a fluorescence (Fv/Fm), higher induction of antioxidant activity, and the expression of APX isozymes in response to low temperature. However, Munné-

Bosch and Lalueza measured oxidative stress markers in leaves and organelles, together with ABA levels in leaves of 2- and 7-year-old *Cistus clusii* dunal plants and concluded that meristematic tissues maintained the capacity to make new leaves with no symptoms of oxidative stress for several years, the leaves of elder plants show higher oxidative stress than those of young plants when exposed to adverse climatic conditions, age-induced oxidative stress occur both in chloroplasts and mitochondria, and newly emerged leaves accumulate higher amounts of ABA even without environmental stress as plants age [34]. Therefore, further research could be conducted to clarify the effects and mechanism of HH stress on different-age leaves of the same plant and on different-age plants at the adult stages of cucumber.

5. Conclusions

High-temperature and high-humidity stress did serious harm to cucumber seedlings. This study explored the physical effect on seedlings with various leaf stages under HH stress. It was shown that seedlings at the 1-leaf and the 2-leaf stages were the most sensitive to HH, and the 4-leaf seedlings were the most tolerant to HH. Compared with the control, biomass, chlorophyll content, net photosynthetic rate, and photosynthetic electron transfer rate of cucumber seedlings under HH stress were significantly decreased. At the same time, reactive oxygen species content and antioxidant enzyme activity were increased. The relative values of various indicators such as dry weight, total chlorophyll content, net photosynthetic rate, Fv/Fm, qP, ETR, and Y (II) of the 1-leaf and the 2-leaf seedlings were significantly lower than those of the 4-leaf seedlings, while the relative values of ROS accumulation and changes in antioxidant enzyme activity were significantly higher than those of the 4-leaf seedlings. Our findings contribute to a deeper understanding of seedling damage under HH stress and provide a piece of important information for further basic mechanism research towards the HH tolerance of cucumber plants.

Supplementary Materials: The following supporting information can be downloaded at: https://www.mdpi.com/article/10.3390/horticulturae10121369/s1, Table S1: Biomass of different leaf-stage cucumber seedlings at 8 h after treatments; Table S2: Photosynthetic pigment content of different leaf-stage cucumber seedlings at 6 h after treatments; Table S3: Photosynthesis of different leaf-stage cucumber seedlings at 6 h after treatments; Table S4: Chlorophyll fluorescence parameters of different leaf-stage cucumber seedlings at 6 h after treatments; Table S5: Reactive oxygen species content and antioxidant enzyme activities of different leaf-stage cucumber seedlings at 6 h after treatments.

Author Contributions: Conceptualization, X.W. and Z.C.; Methodology, H.M.; Software, Y.P.; Validation, X.W., Y.P., and H.L.; Formal analysis, X.W.; Investigation, Z.C.; Resources, H.M.; Data curation, X.W.; Writing, original draft preparation, X.W.; Review and editing, Z.C.; Visualization, X.W.; Supervision, Z.C.; Project administration, Z.C. and H.M.; Funding acquisition, Z.C. All authors have read and agreed to the published version of the manuscript.

Funding: This research was funded by the National Key Research and Development Program of China (2016YFD0101705), the National Natural Science Foundation of China (32202493), and the Key Research and Development Program of Shaanxi Province of China (Program No. 2024NC-YBXM-042).

Data Availability Statement: The original contributions presented in this study are included in this article; further inquiries can be directed to the corresponding author.

Conflicts of Interest: The authors declare no conflicts of interest.

References

1. Yu, Y.; Zhang, H.N.; Xing, H.Y.; Cui, N.; Liu, X.Y.; Meng, X.N.; Wang, X.Y.; Fan, L.; Fan, H.Y. Regulation of growth and salt resistance in cucumber seedlings by hydrogen-rich water. *J. Plant Growth Regul.* **2023**, *42*, 134–153. [CrossRef]
2. Gou, T.Y.; Yang, L.; Hu, W.X.; Chen, X.H.; Zhu, Y.X.; Guo, J.; Gong, H.J. Silicon improves the growth of cucumber under excess nitrate stress by enhancing nitrogen assimilation and chlorophyll synthesis. *Plant Physiol. Biochem.* **2020**, *152*, 53–61. [CrossRef]
3. Das, A.; Kumari, K.; Munshi, A.D.; Raju, D.; Talukdar, A.; Singh, D.; Hongal, D.; Iquebal, M.A.; Bhatia, R.; Bhattacharya, R.C.; et al. Physio-chemical and molecular modulation reveals underlying drought resilience mechanisms in cucumber (*Cucumis sativus* L.). *Sci. Hortic.* **2024**, *328*, 112855. [CrossRef]

4. Hongal, D.A.; Raju, D.; Kumar, S.; Talukdar, A.; Das, A.; Kumari, K.; Dash, P.K.; Chinnusamy, V.; Das Munshi, A.; Behera, T.K.; et al. Elucidating the role of key physio-biochemical traits and molecular network conferring heat stress tolerance in cucumber. *Front. Plant Sci.* **2023**, *14*, 1128928. [CrossRef] [PubMed]
5. Martinez-Alonso, A.; Nicolás-Espinosa, J.; Carvajal, M.; Bárzana, G. The differential expressions of aquaporins underline the diverse strategies of cucumber and tomato against salinity and zinc stress. *Physiol. Plant.* **2024**, *176*, e14222. [CrossRef] [PubMed]
6. Weng, J.Y.; Li, P.L.; Rehman, A.S.; Wang, L.K.; Gao, X.; Niu, Q.L. Physiological response and evaluation of melon (*Cucumis melo* L.) germplasm resources under high temperature and humidity stress at seedling stage. *Sci. Hortic.* **2021**, *288*, 110317. [CrossRef]
7. Tong, P.J.; Cheng, Z.H.; Meng, H.W. Physiological response of cucumber seedlings to high temperature and humidity stress. *J. Northwest A&F Univ.* **2021**, *49*, 85–93+103.
8. Xu, C.; Yang, Z.Q.; Wang, M.T.; Han, W.; Wei, T.T. Regulating effect of air humidity on tomato growth and root exudates during flowering period under high temperature condition. *Chin. J. Agrometeorol.* **2020**, *41*, 552–563.
9. Matsui, T.; Kobayasi, K.; Kagata, H.; Horie, T. Correlation between viability of pollination and length of basal dehiscence of the theca in rice under a hot-and-humid condition. *Plant Prod. Sci.* **2005**, *8*, 109–114. [CrossRef]
10. Yang, S.; Shi, Y.; Zou, L.; Huang, J.; Shen, L.; Wang, Y.; Guan, D.; He, S. Pepper *CaMLO6* negatively regulates *Ralstonia solanacearum* resistance and positively regulates high temperature and high humidity responses. *Plant Cell Physiol.* **2020**, *61*, 1223–1238. [CrossRef]
11. Yang, S.; Cai, W.W.; Wu, R.J.; Huang, Y.; Lu, Q.L.; Huang, X.Y.; Zhang, Y.P.; Wu, Q.; Cheng, X.G.; Wan, M.Y.; et al. Differential CaKAN3-CaHSF8 associations underlie distinct immune and heat responses under high temperature and high humidity conditions. *Nat. Commun.* **2023**, *14*, 4477. [CrossRef] [PubMed]
12. Zhang, Q.; Zhang, X.Y.; Yang, Z.Q.; Huang, Q.Q.; Qiu, R.J. Characteristics of plastic greenhouse high-temperature and high-humidity events and their impacts on facility tomatoes growth. *Front. Earth Sci.* **2022**, *10*, 848924. [CrossRef]
13. Ucak, A.B.; Kociecka, J.; Liberacki, D.; Saltuk, B.; Atilgan, A.; Stachowski, P.; Rolbiecki, R. The effects of high temperature and low humidity on crop water stress index of seed of seed pumpkin plants (*Cucurbita pepo* L.) in semi-arid climate conditions. *Acta Sci. Pol. Hortorum Cultus* **2024**, *23*, 63–73. [CrossRef]
14. Zheng, Y.J.; Yang, Z.Q.; Wei, T.T.; Zhao, H.L. Response of tomato sugar and acid metabolism and fruit quality under different high temperature and relative humidity conditions. *Phyton-Int. J. Exp. Bot.* **2022**, *91*, 2033–2054. [CrossRef]
15. Li, Y.; Yang, Z.Q.; Li, S.Y.; Zhang, Y.D.; Han, Z. Effect mechanism of high temperature and high humidity stress on yield formation of cucumber. *Chin. J. Agrometeorol.* **2022**, *43*, 392–407.
16. Li, Y.C.; Yang, Z.Q.; Yang, L.; Luo, J.; Zhang, F.Y. Effects of high temperature and high humidity conditions at seedling stage on the chlorophyll fluorescence characteristics in the center of photosystem II of cucumber leaves. *Chin. J. Agrometeorol.* **2022**, *43*, 912–922.
17. Weng, J.Y.; Rehman, A.; Li, P.L.; Chang, L.Y.; Zhang, Y.D.; Niu, Q.L. Physiological and transcriptomic analysis reveals the responses and difference to high temperature and humidity stress in two melon genotypes. *Int. J. Mol. Sci.* **2022**, *23*, 734. [CrossRef]
18. Rankenberg, T.; Geldhof, B.; van Veen, H.; Holsteens, K.; Van de Poel, B.; Sasidharan, R. Age-dependent abiotic stress resilience in plants. *Trends Plant Sci.* **2021**, *26*, 692–705. [CrossRef]
19. Jiang, B.; Gao, G.; Ruan, M.; Bian, Y.; Geng, F.; Yan, W.; Xu, X.; Shen, M.; Wang, J.; Chang, R.; et al. Quantitative assessment of abiotic stress on the main functional phytochemicals and antioxidant capacity of wheatgrass at different seedling age. *Front. Nutr.* **2021**, *8*, 731555. [CrossRef] [PubMed]
20. Akhbarfar, G.; Nikbakht, A.; Etemadi, N.; Gailing, O. Physiological and biochemical responses of plantain trees (*Platanus orientalis* L.) derived from different ages to drought stress and *Ascophyllum nodosum* L. extract. *J. Soil Sci. Plant Nutr.* **2023**, *23*, 5945–5961. [CrossRef]
21. Qi, J.; Wu, Z.; Liu, Y.; Meng, X. Effects of plant age on antioxidant activity and endogenous hormones in *Alpine elymus* sibiricus of the Tibetan Plateau. *PeerJ* **2023**, *11*, e15150. [CrossRef] [PubMed]
22. Shao, J.Y.; Wang, Q.H.; Liu, P.; Zhao, B.; Han, W.; Zhang, J.W.; Ren, B.Z. The complex stress of waterlogging and high temperature accelerated maize leaf senescence and decreased photosynthetic performance at different growth stages. *J. Agron. Crop Sci.* **2024**, *210*, e12689. [CrossRef]
23. Amin, B.; Atif, M.J.; Wang, X.; Meng, H.; Ghani, M.I.; Ali, M.; Ding, Y.; Li, X.; Cheng, Z. Effect of low temperature and high humidity stress on physiology of cucumber at different leaf stages. *Plant Biol.* **2021**, *23*, 785–796. [CrossRef]
24. Rahman, K.; Ahmed, N.; Raihan, M.R.H.; Nowroz, F.; Jannat, F.; Rahman, M.; Hasanuzzaman, M. Jute responses and tolerance to abiotic stress: Mechanisms and approaches. *Plants* **2021**, *10*, 1595. [CrossRef] [PubMed]
25. Wu, C.; Wang, M.; Dong, Y.; Cheng, Z.; Meng, H. Effect of plant age and vernalization on bolting, plant growth and enzyme activity of garlic (*Allium sativum* L.). *Sci. Hortic.* **2016**, *201*, 295–305. [CrossRef]
26. Funk, J.L.; Larson, J.E.; Vose, G. Leaf traits and performance vary with plant age and water availability in *Artemisia californica*. *Ann. Bot.* **2021**, *127*, 495–503. [CrossRef]
27. Yuan, C.H.; Yang, Z.Q.; Zhao, H.L. Compensatory growth of tomato after high temperature and high humidity stress. *Chin. J. Ecol.* **2020**, *39*, 487–496.
28. Munné-Bosch, S.; Alegre, L. Plant aging increases oxidative stress in chloroplasts. *Planta* **2002**, *214*, 608–615. [PubMed]

29. Pshibytko, N.L.; Kalitukho, L.N.; Zhavoronkova, N.B.; Kabashnikova, L.F. The pool of chlorophyllous pigments in barley seedlings of different ages under heat shock and water deficit. *Russ. J. Plant Physiol.* **2004**, *51*, 15–20. [CrossRef]
30. Shang, T.Q.; Sun, Z.H. Photosynthetic characteristics and monoterpenes emission are related to foliage ontogeny in *Cinnamomum camphora*. *Chin. J. Appl. Environ. Biol.* **2019**, *1*, 89–99.
31. Yang, Z.Q.; Zhang, M.Y.; Yang, S.Q.; Wang, L.; Li, K.W.; Li, J. Effect of high humidity and high temperature interaction on photosynthetic characteristics of greenhouse tomato crops. *Chin. J. Ecol.* **2018**, *37*, 57–63.
32. Wang, L.; Yang, Z.Q.; Yang, S.Q.; Li, J.; Li, K.W.; Hou, M.Y. Effects of high temperature and different air humidity on growth and senescence characteristics for tomato seedlings. *Chin. J. Agrometeorol.* **2017**, *38*, 761–770.
33. Kuk, Y.I.; Shin, J.S. Mechanisms of low-temperature tolerance in cucumber leaves of various ages. *J. Am. Soc. Hortic. Sci.* **2007**, *132*, 294–301. [CrossRef]
34. Munné-Bosch, S.; Lalueza, P. Age-related changes in oxidative stress markers and abscisic acid levels in a drought-tolerant shrub, *Cistus clusii* grown under Mediterranean field conditions. *J. Planta* **2007**, *225*, 1039–1049. [CrossRef]

horticulturae

MDPI

Article

Molecular, Metabolic, and Physiological Responses to Progressive Biotic Stress Caused by Cucumber Mosaic Virus and Turnip Mosaic Virus in Saffron

Marzieh Shamshiri [1], Conchi Sánchez [2,*], Saleta Rico [2], Ali Mokhtassi-Bidgoli [3], Mahdi Ayyari [4], Hassan Rezadoost [5] and Masoud Shams-Bakhsh [1,*]

[1] Department of Plant Pathology, Faculty of Agriculture, Tarbiat Modares University, Tehran 1411713116, Iran; m.shamshiri.1992@gmail.com
[2] Misión Biológica de Galicia, Consejo Superior de Investigaciones Científicas, 15780 Santiago de Compostela, Spain; saleta@mbg.csic.es
[3] Department of Agronomy, Faculty of Agriculture, Tarbiat Modares University, Tehran 1411713116, Iran; mokhtassi@modares.ac.ir
[4] Department of Horticultural Science, Faculty of Agriculture, Tarbiat Modares University, Tehran 1411713116, Iran; m.ayyari@modares.ac.ir
[5] Department of Phytochemistry, Medicinal Plants and Drugs Research Institute, Shahid Beheshti University, G. C., Evin, Tehran 1983969411, Iran; h_rezadoost@sbu.ac.ir
* Correspondence: conchi@mbg.csic.es (C.S.); shamsbakhsh@modares.ac.ir (M.S.-B.)

Abstract: The economic value of the saffron stigma is primarily due to three crucial apocarotenoids: crocin, picrocrocin, and safranal, which contribute to its color, flavor, and aroma. These compounds make saffron highly valuable in various industries. Plant viruses like the cucumber mosaic virus (CMV) and turnip mosaic virus (TuMV) are significant threats to agricultural crops worldwide, causing economic losses. To elucidate the influence of viral stress on the quality of saffron, morphological, physiological, biochemical, and molecular indexes were assessed. Under the stress of both viruses, typical viral symptoms appeared. The lowest contents of leaf pigments, flowering performance, petal anthocyanin, greenness, and photosynthesis properties were observed in plants infected with CMV and TuMV. According to high-performance liquid chromatography (HPLC) analysis, CMV inoculation led to the highest reduction in crocin and safranal content, while inducing the highest increase in picrocrocin compared to the mock treatment. Gene expression analysis involved in the biosynthesis of crucial secondary metabolites showed a high correlation with the content of each metabolite. CMV inoculation resulted in the lowest expression of *CsALDH31l* and the highest expression of *CsUGT709G1* compared with the mock treatment. Our findings demonstrate the association between virus stress and changes in the metabolism of the saffron medicinal plant.

Keywords: Apocarotenoides; CMV: cucumber mosaic virus; Crocus sativus; expression analysis; HPLC (High performance liquid chromatography); Iridaceae; TuMV (turnip mosaic virus)

1. Introduction

Saffron (*Crocus sativus* L.) is a monocotyledonous herbaceous plant belonging to the Iridiaceae family I [1,2]. Stigmas are the most valuable part of the plant; when dried, they become saffron, which is the most expensive spice in the world [1,3,4]. Iran is the leading producer of saffron globally, accounting for almost 90% of the total world production. Other significant saffron-producing countries include India, Greece, Morocco, and Spain, with

contributions also from Afghanistan, Italy, Azerbaijan, and Kashmir. The saffron market is expected to grow with Iran maintaining its dominant position in saffron production [2].

The distinctive qualities of saffron are attributed to its secondary metabolites, particularly the apocarotenoids crocin, picrocrocin, and safranal, which are responsible for its red color, bitter taste, and specific aroma, respectively [5,6]. Crocin is the most important pigment, giving saffron a reddish-yellow-golden color. Picrocrocin is a colorless monoterpene glycoside and a precursor of safranal, the second most abundant component of saffron. Safranal, a monoterpene aldehyde, is a significant component of aromatic and volatile compounds in Iranian saffron [2,6]. The quality of the saffron spice is determined by the concentration of these compounds according to the International Standardization Organization (ISO 3632-1:2011) [7], and the National Nutrient Value of the United States Department of Agriculture (USDA) [6].

Anthocyanins, a type of flavonoid, are natural water-soluble pigments with different colors in plants [8], have pleiotropic effects, and might help protect plants against pathogenic agents by playing a role in pests and disease resistance [9]. They also have antioxidant functions and play an important role in eliminating reactive oxygen species [8]. Environmental factors and biotic and abiotic stresses can also affect anthocyanin synthesis in plants [8]. Research has identified key genes involved in the synthesis of the basic secondary metabolites of saffron. *CsALDH31l* plays a crucial role in crocin synthesis [10,11], while *CsUGT709G1* is responsible for the synthesis of picrocrocin and safranal [11–13].

Despite saffron's high economic value and extensive cultivation, the plant is vulnerable to several viruses that significantly impact its production and quality. Several plant viruses cause disease in Crocus spp. cultivars such as *C. chrysanthus*, *C. vernus* and *C. sativus* [14], including saffron latent virus (SaLV) [15], turnip mosaic virus TuMV [16–18], cucumber mosaic virus CMV [19], iris sever mosaic virus (ISMV) [20–22], ornithogalum mosaic virus [23], tomato spotted wilt virus (TSWV) [24], iris mild mosaic virus [25,26] and bean yellow mosaic virus [27,28] were identified. The impact of viral infection on plant compounds has been explored in various studies, highlighting the complex interactions between pathogens and host metabolism. For instance, researchers examined the impact of SaLV on saffron and TuMV on stem mustard (*Brassica juncea* var. *tsatsai*), parsley yellow leaf curl virus (PYLCV), and sesame curly top virus (SeCTV) on parsley; CMV-Fny on green basil; co-infection of CMV and beet curly top virus (BCTV) on sugar beet, pepper, and bean plants; CMV on *Passiflora edulis*; and CMV on *Agastache anethiodora* [15,29–34]. Saffron quality can be influenced by the climatic conditions of different geographical areas and the presence of viruses, which affect the composition of secondary metabolites [15]. Therefore, evaluating the responses of virus-inoculated and non-inoculated plants growing in the same geographical area and under the same environmental conditions will provide relevant information about the influence of the virus on plant performance and saffron quality.

The present study aims to investigate the effect of two important plant viruses, CMV and TuMV, on the morphological, physiological, and phytochemical traits, as well as on the main bioactive secondary metabolites of saffron at the biochemical and molecular levels. In addition, the interaction of the inoculation period (year) and post-inoculation time on different parameters related to the performance of saffron were evaluated. Understanding these interactions is crucial for developing strategies to mitigate the impact of viral infections on saffron.

2. Materials and Methods

2.1. Experimental Design, Plant Material and Growth Conditions

Saffron corms obtained from the saffron production region (Torbat-e-Heydarieh, Khorasan, Razavi Province, Iran) in 2021 were planted in pots filled with a sterilized mixture

of peat, perlite, and soil (1:1:1 ratio, $v/v/v$). Plants were grown in a greenhouse under controlled conditions at a temperature of 10 ± 5 °C and a light/dark cycle of 16/8 h. The experiment was conducted in Research Greenhouses located at the Faculty of Agriculture, Tarbiat Modares University, Tehran, Iran. The study was arranged in a completely randomized design with 335 pots per treatment, each containing 9 plants. We tested three different treatments: two sets of viral-inoculated plants and a mock treatment. The experimental procedure was repeated thoroughly over the two growing seasons. Saffron is grown as a perennial crop under field conditions, and assessing the plant's responses to viral stress is inadequate if limited to just the first year. Consequently, the different timing treatments applied in this study illustrate the effects of the virus throughout the growing season, as well as the consequences of viral accumulation over a two-year span. This suggests that the virus had sufficient time to influence plant characteristics. To test the effect of the post-inoculation period, plants derived from healthy corms potted in 2021 and either inoculated with the virus or left uninoculated were assessed at the end of each growing season in 2021 (group A) and 2022 (group B). In addition, to study the effect of the inoculation year in 2022, the experiment was repeated using plants grown from healthy corms from those sowed in 2021, and these plants were evaluated in 2022 (group C).

2.2. Viral Inoculation and Virus Detection

Two plant viruses with RNA genomes, TuMV-UK1 [35] and CMV-Fny [36], were separately sap-inoculated into the leaves when the plants reached the leaf stage. Viruses were transferred from infected pumpkin and turnip plants to saffron plants. The inoculum was prepared in 0.1 M phosphate buffer (pH 7.4), and for the mock treatment, plant leaves were treated with phosphate buffer without the virus. Plants were kept in a greenhouse under previously described conditions. The presence of viruses in leaf samples showing symptoms was determined using a back-inoculation test on pumpkin, turnip, and canola as their indicator plants and RT-PCR. The extract from the saffron plants treated with either TuMV or CMV, as well as from TuMV-mock or CMV-mock, was subsequently inoculated into its respective indicator plants at the first true leaf stage. The integrity of the total RNA extracted from fresh saffron leaf tissue using the RNX-Plus kit (SinaClon, Tehran, Iran) was checked using 1.2% agarose gel electrophoresis. cDNA was synthesized using the Easy™ cDNA Synthesis Kit (Parstous, Mashhad, Iran) according to the manufacturer's protocol and used in PCR reactions with specific primer pairs for TuMV [35] or CMV [37]. For TuMV and CMV samples, PCR reactions generated a 986 bp fragment, including 54 bp of the 3′-end of the NIb gene, the entire CP gene, and 65 bp of the 3′-UTR, as well as a 625 bp fragment of the CP gene. An internal 18S rDNA gene-specific primer pair [38] was used as an internal control, amplifying a 459 bp DNA fragment. The primer sequences are listed in Table S1. Previously, possible background viral infection was randomly tested in non-inoculated leaf tissue samples. The infection status of saffron samples was evaluated by RT-PCR using general and specific primer pairs for several important virus families reported in saffron, including TuMV, CMV, and tospovirus genera [39] (Table S1).

2.3. Determination of Morphological and Physiological Indexes

The response of saffron to virus inoculation was assessed through various morphological and physiological traits. Morphological traits included leaf area (cm^2) and fresh weight of flowers (g $plant^{-1}$). Flowering performance was monitored by recording the daily number of flowers for each treatment, and the fresh weight of the stigma was measured upon harvest. Physiological indexes evaluated 30 days after the flowering stage included greenness (Spad), photosynthesis rate (Photo, μmol CO_2 m^{-2} s^{-1}), transpiration rate (Trmmol, mol/m^2/s), and instantaneous water use efficiency (WUE, μmol CO_2 $mmol^{-1}$ H_2O).

The leaf greenness index was recorded using a chlorophyll meter (Minolta Chlorophyll Meter SPAD-502 is manufactured by Konica Minolta, Inc., headquartered in Tokyo, Japan). The photosynthesis rate, transpiration rate, and instantaneous water use efficiency were determined using a photosynthesis meter (Li-Cor, Li-6400 XT Portable Photosynthesis System is manufactured by LI-COR Biosciences, headquartered in Lincoln, Nebraska, USA). Conditions within the measuring chamber were maintained with photosynthetically active radiation (PAR) at 1500 μmol m^{-2} s^{-1}, leaf temperature between 25 °C and 35 °C, reference CO_2 content at 480 μmol mol^{-1}, and reference H_2O content at 1 mmol mol^{-1}. Reference CO_2 and H_2O levels were manually adjusted before measurements.

2.4. Determination of Biochemical Indexes

Assessed biochemical indexes included photosynthetic pigments (chlorophyll a, chlorophyll b, total chlorophyll, and carotenoid content) and anthocyanin content. Photosynthetic pigments were evaluated using the method described by Lichtenthaler [40]. Absorbance was measured at 665 nm for chlorophyll a, 652 nm for chlorophyll b, and 470 nm for carotenoids. The results were reported as μg mL^{-1} based on the formulas provided by Warren [41]. The petal anthocyanin content (mg L^{-1}) was measured using the differential pH method described by Lee et al. [42]. Absorbance readings were taken at 520 nm and 700 nm, and the petal anthocyanin content was expressed as mg L^{-1} equivalent of cyanidin-3-glycoside in the extract. Saffron petal extracts were prepared according to the method described by Fuleki and Francis [43]. Potassium chloride buffer solution (0.025 M, pH 1) and sodium acetate buffer solution (0.4 M, pH 4.5) were prepared following the method of Mónica Giusti and Wrolstad [44].

2.5. HPLC Analysis of Secondary Metabolites

The contents of the secondary metabolites crocin, picrocrocin, and safranal in extracts from the stigmas of CMV-inoculated, TuMV-inoculated, and mock plants were analyzed by HPLC.

Ethanol extraction was performed using 10 mg of powdered stigma for picrocrocin and crocin quantification, and 60 mg was used to determine the safranal content. The samples were diluted with 10 mL of 80% ethanol and then subjected to 15 min of sonification in dark conditions. After centrifugation, the supernatant was used for chromatography [45]. HPLC analysis was performed in a KNAUER system equipped with a K1001 binary pumpchromium well, a multiple wavelength UV-vis diode-array detector (DAD), model 2800, and a KNAUER Eurospher RP C18 column (4.6 × 250 mm, ×55 μm) following the method described by Kabiri et al., [45]. The mobile phase consisted of acetonitrile (A) and water (B), using a linear gradient: 90% A for 5 min, decreased to 20% A over 20 min, and held for an additional 5 min. The flow rate was 1 mL/min. The detection wavelengths were set at 250 nm for safranal, 308 nm for picrocrocin, and 440 nm for crocin. Each sample was analyzed in triplicate, and all steps of the experiment were performed at room temperature. Method validation was based on the International Committee of Harmonization (ICH) regulations [45]. Parameters such as linearity, band purity, precision, replication, limit of detection (LOD), and limit of quantification (LOQ) were evaluated. Each component was identified by comparing the retention times with the reference compound and confirming with MS spectra. Peak purity was verified using UV spectra between 200 and 700 nm. Method reproducibility and precision were assessed by calculating the relative standard division (RSD) of the three replicates for each component.

2.6. qRT-PCR Assay

Total RNA from leaves of CMV-inoculated, TuMV-inoculated, and mock plants was extracted using the "FavorPrepTM Plant total RNA Purification Mini Kit" (Favorgen Biotech corp., Ping Tung, Taiwan). RNA was treated with DNase I (Promega, Madison, WI, USA) for DNA digestion. Quality and quantity were determined using a NanoDrop spectrophotometer 2000c (Thermo Fisher Scientific™,Waltham, Massachusetts, USA), and RNA integrity was checked by electrophoresis on a 1.2% agarose gel. cDNA was synthesized from 1 µg of total RNA using the High Capacity cDNA Reverse Transcription Kit (Applied Biosystems, Foster City, CA, USA) according to the manufacturer's instructions. qRT-PCR was performed in an optical 48-well plate using a Step One Real-Time PCR System (Applied Biosystems, Foster City, CA, USA) and NZYSupreme qPCR Green Master Mix (NZYtech, Lisboa, Portugal) to monitor dsDNA synthesis. PCR reactions contained 400 µM of each primer, 1.5 µL of cDNA template (12.5 ng of input RNA), and 2x of NZYSupreme qPCR Green Master Mix in a final volume of 20 µL. The PCR thermal profile was 95 °C for 2 min, 40 cycles of 95 °C for 5 s, and 60 °C for 30 s. Melt curves were generated at the end of each run to ensure the uniformity of the product. Selected target genes in the saffron secondary metabolite pathway included *CsALDH31l* (MF596165.1), a marker for the biosynthesis of crocin, and *CsUGT709G1* (KX385186.1), which is involved in the biosynthesis of picrocrocin and safranal. Amplification of Ubiquitin (BM005694.1) was used as an internal control to normalize the expression data. Primer sequences for target and endogenous genes are listed in Table S2. Three biological replicates and three technical replicates were assessed for each sample. Relative gene expression levels were calculated using the Comparative Ct Method [46] and expressed as relative values to mock samples. Results are presented as mean ± standard error from three biological replicates. All calculations and normalizations were performed using the DataAssist v3.0 software (Applied Biosystems, Thermo Fisher Scientific, Foster City, CA, USA).

2.7. Statistical Analysis

Statistical analyses were performed using SAS 9.4 software (SAS Institute, Cary, NC, USA). Residual normality was checked using the univariate procedure before the analysis of variance. A combined ANOVA was conducted using a general linear model (GLM). Means were compared using the least significant difference test (LSD) at $p \leq 0.05$. Principal component analysis (PCA) was applied to illustrate the relationships between the dependent and independent variables using XLSTAT 2019.2.2 software.

3. Results

3.1. Assessment of the Virus Infection

Saffron samples inoculated with CMV and TuMV showed mosaic patterns and leaf curling 8–10 days post-inoculation (dpi). Additionally, the flowers exhibited deformities, asymmetrical shapes, and occasional stigma curling (Figure 1). The back-inoculation test confirmed the presence of CMV and TuMV in pumpkin, turnip, and canola as their indicator plants (Figure 2). Screening by RT-PCR with specific primers successfully amplified 625 bp and 986 bp fragments for CMV-inoculated and TuMV-inoculated plants, respectively (Figure 3). No background amplification of CMV, TuMV viruses, or tospovirus genera was observed in reactions performed with RNA samples isolated from non-inoculated plants, except for a 459 bp fragment corresponding to the 18S internal gene (Figure 4).

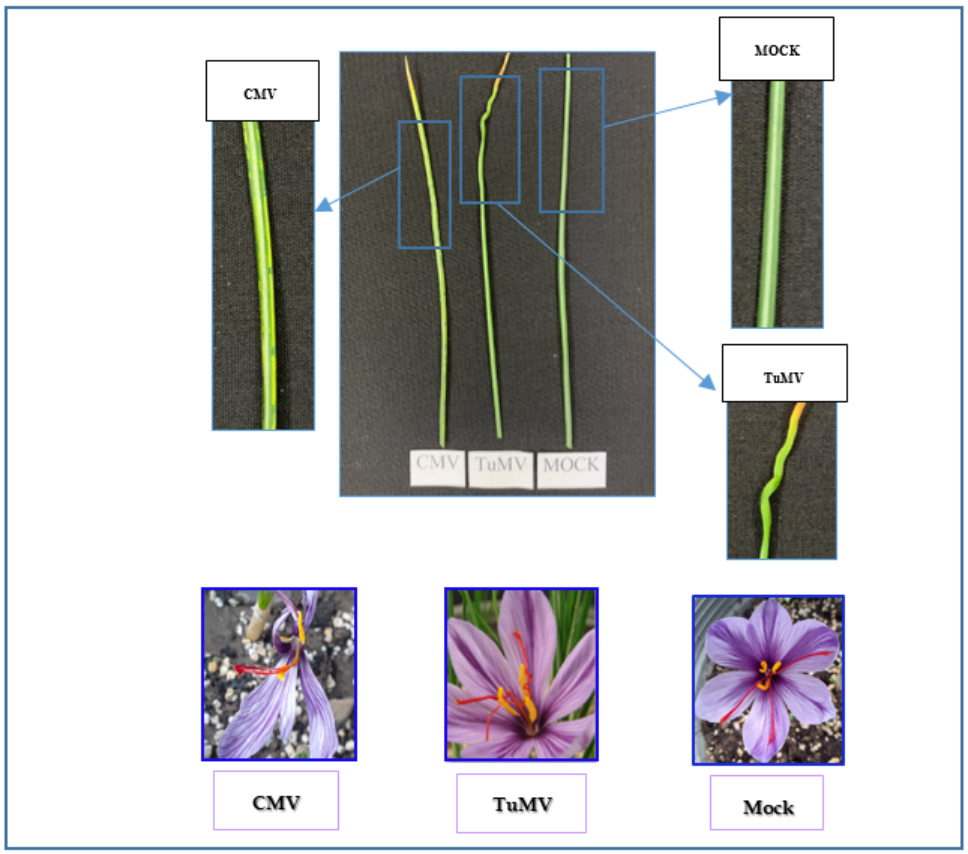

Figure 1. Symptoms of sap-inoculation plants with CMV, TuMV, and Mock.

Figure 2. Detection of CMV and TuMV by back-inoculation in indicator plants (**left**: pumpkin, **center**: turnip, **right**: canola).

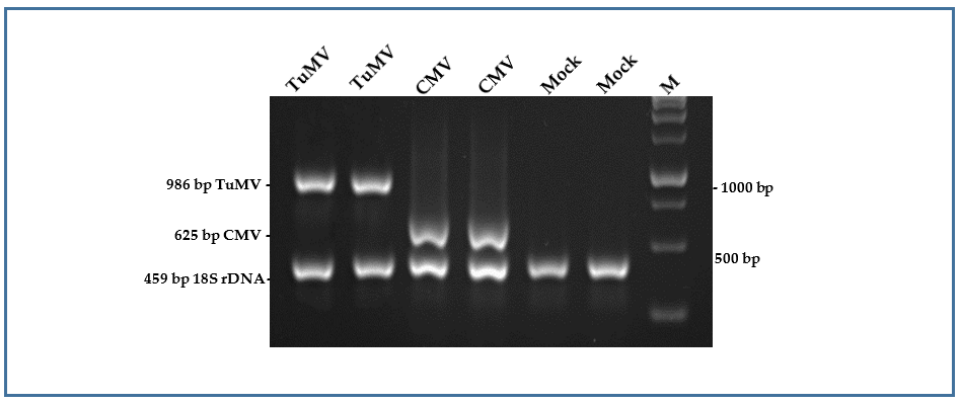

Figure 3. Agarose gel showing the bands corresponding to 18S rDNA (459 bp), CMV (625 bp), and TuMV (986 bp) obtained by RT-PCR in sap-inoculated plants. Lane M: GeneRuler 1 Kb DNA ladder.

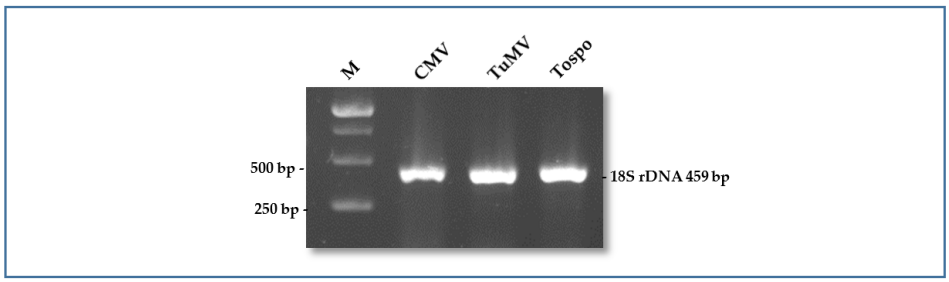

Figure 4. Agarose gel showing the RT-PCR reactions of samples from control plants not inoculated with virus showing only the 18S rDNA.

3.2. Effect of Virus Infection on Morpho-Physiological Traits of Saffron Plants

To test the effect of virus infection on morphological characteristics, leaf area and flowering were measured in plant organs from mock and virus-inoculated plants (Table 1). The mean leaf area dropped significantly in CMV- and TuMV-inoculated plants, with reductions of 33% and 38%, respectively, compared to mock plants (Table 1). The lowest leaf area (6.79 cm^2) was recorded in TuMV-treated plants, followed by CMV-inoculated plants (7.52 cm^2), with values significantly lower than those of mock plants (11.25 cm^2). Regarding fresh flower weight, a significant decrease (−29%) was observed in CMV- and TuMV-treated plants compared to the mock treatment (Table 1).

Table 1. The effect of viral treatments on different traits of saffron. CMV: CMV-inoculated plants TuMV: TuMV-inoculated plants. Mock: mock plants. WUE: water use efficiency. Values are presented as the mean ± standard error. For each parameter, values with different letters are significantly different ($p < 0.05$) according to the LSD test.

Virus Treatment	Petal Anthocyanin (mg L^{-1})	Leaf Area (cm^2 $plant^{-1}$)	Fresh Weight of Flower (g $plant^{-1}$)	Photo (µmol CO_2 m^{-2} s^{-1})	Trmmol (mol/m^2/s)	WUE (µmol CO_2 $mmol^{-1}$ H_2O)	Greeness Index (Spad)
Mock	3.22 ± 0.06 [a]	11.25 ± 0.30 [a]	0.52 ± 0.01 [a]	4.26 ± 0.50 [a]	0.53 ± 0.08 [a]	9.20 ± 1.04 [b]	64.73 ± 0.24 [a]
CMV	2.20 ± 0.03 [b]	7.52 ± 0.15 [b]	0.37 ± 0.01 [b]	2.26 ± 0.25 [b]	0.25 ± 0.03 [b]	11.24 ± 2.03 [b]	44.04 ± 0.27 [c]
TuMV	2.30 ± 0.03 [b]	6.97 ± 0.17 [b]	0.37 ± 0.01 [b]	3.91 ± 0.52 [a]	0.28 ± 0.04 [b]	14.84 ± 1.42 [a]	48.51 ± 0.19 [b]

Virus-inoculated plants exhibited a significant decrease in greenness compared to the mock treatment, with a greater reduction (−32%) in CMV- than in TuMV-treated plants (−32% versus −25%) (Table 1). All analyzed physiological indexes, including photosynthesis rate, transpiration rate, and instantaneous water use efficiency, showed a significant downward trend in virus-inoculated plants compared to the mock treatment. Specifically, CMV infection significantly reduced the photosynthesis rate (−47%) and transpiration rate (−52%) of host plants. A significant reduction in the transpiration rate (−46%) and WUE (−61%) was also detected in TuMV-infected plants.

The effect of the virus inoculation year (2021 and 2022) on the physiological indexes of the saffron plants was assessed at the end of both growth seasons (2021, group A and 2022, group C) to evaluate the consequences of viral accumulation over the two growing seasons. In addition, the effect of elapsed time after starting the experiment and data collection on these indices was estimated by comparing the data collected after the first (group A) and second year (group B) of treatments. As shown in Table 2, the anthocyanin content and photosynthesis rate significantly decreased in groups B and C, regardless of the beginning of the experiment. In group B plants, the transpiration rate significantly decreased, whereas WUE significantly increased (+70%), with no significant differences in these parameters between groups B and C.

Table 2. Effect of virus inoculation year and post-inoculation period on different traits of saffron plants. Plants inoculated in 2021 and evaluated at the end of the growing season in 2021 (group A) and 2022 (group B). Plants inoculated in 2022 were evaluated at the end of the growing season (group C). CMV: CMV-inoculated plants. TuMV: TuMV-inoculated plants. Mock: mock plants. WUE: water use efficiency. Values are presented as the mean ± standard error.

Time Effect	Petal Anthocyanin (mg L^{-1})	Photo (μmol CO_2 m^{-2} s^{-1})	Trmmol (mol/m^2/s)	WUE (μmol CO_2 $mmol^{-1}$ H_2O)
Group A	2.69 ± 0.16 [a]	4.57 ± 0.37 [a]	0.45 ± 0.05 [a]	10.84 ± 0.90 [b]
Group B	2.54 ± 0.12 [b]	2.40 ± 0.45 [b]	0.14 ± 0.02 [b]	18.41 ± 2.21 [a]
Group C	2.49 ± 0.14 [b]	2.50 ± 0.39 [b]	0.35 ± 0.07 [a]	8.06 ± 1.14 [b]

Values with different letters are significantly different ($p < 0.05$) according to the LSD test.

Virus infection adversely affected the flowering of saffron plants, and a significant decrease in this parameter was observed in virus-inoculated plants compared to the mock (Figure 5A). Virus-induced flowering inhibition ranged from 52 to 60% in CMV-infected plants and from 55 to 62% in TuMV-inoculated plants. The greatest reduction (−60% and −62%) was detected in CMV- and TuMV-inoculated plants in 2021 (group A) and was evaluated after the second growth season (group B). Mock plants of groups B and C showed a significant reduction in flowering regardless of the year at the beginning of the experiment. Similarly, virus-inoculated plants in groups B and C exhibited a significant decrease in flowering in comparison to group A, with the greatest inhibition in the second growth season (Figure 5A).

3.3. Biochemical Indexes

The impact of the year of treatment, elapsed time after treatment, and virus infection on plant photosynthetic pigments were analyzed. The interaction effect of these factors was significant, showing notable differences in the chlorophyll content between virus-treated and mock plants at the three analyzed time points, as well as for each treatment between the evaluated periods (Figure 5B–D). Mock plants in groups B and C showed a significant decrease in chlorophyll a content compared to that in group A, without differences between groups B and C (Figure 5B). Chlorophyll a content significantly decreased (−52%) after virus inoculation in plants of group A. Similarly, TuMV-treated plants of groups B and C showed a reduction in chlorophyll a, ranging from 63 to 61%, respectively, with the lowest value (−74%) detected in CMV-treated plants of group B. Overall, for each treatment, the chlorophyll a content followed a similar trend in groups B and C (Figure 5B). Regarding chlorophyll b content, mock plants of groups B and C showed the highest and most significant decrease (Figure 5C), indicating a similar performance of plants growing in 2022 (groups B and C). In CMV- and TuMV-inoculated plants, chlorophyll b content significantly decreased compared to mock plants, with the highest reduction (−67%) in group A compared to the mock treatment. The negative effect of virus inoculation on this parameter was less evident in groups B (−28% in CMV-treated plants) and C (−35% in TuMV-treated plants). However, CMV-treated plants of group B, as well as CMV- and TuMV-treated plants of group C, showed a significant decrease in chlorophyll b compared to their respective mock plants (Figure 5C). The total chlorophyll content followed a similar trend to that of chlorophyll a (Figure 5D). In mock plants, carotenoid content significantly decreased in groups B and C compared to that in group A (Figure 5E). A significant reduction in carotenoids was detected in CMV- and TuMV-inoculated plants compared to mock plants, regardless of the evaluation period. The highest reduction for CMV- and TuMV-treated plants (−54% and −43%, respectively) was detected in plants of group C.

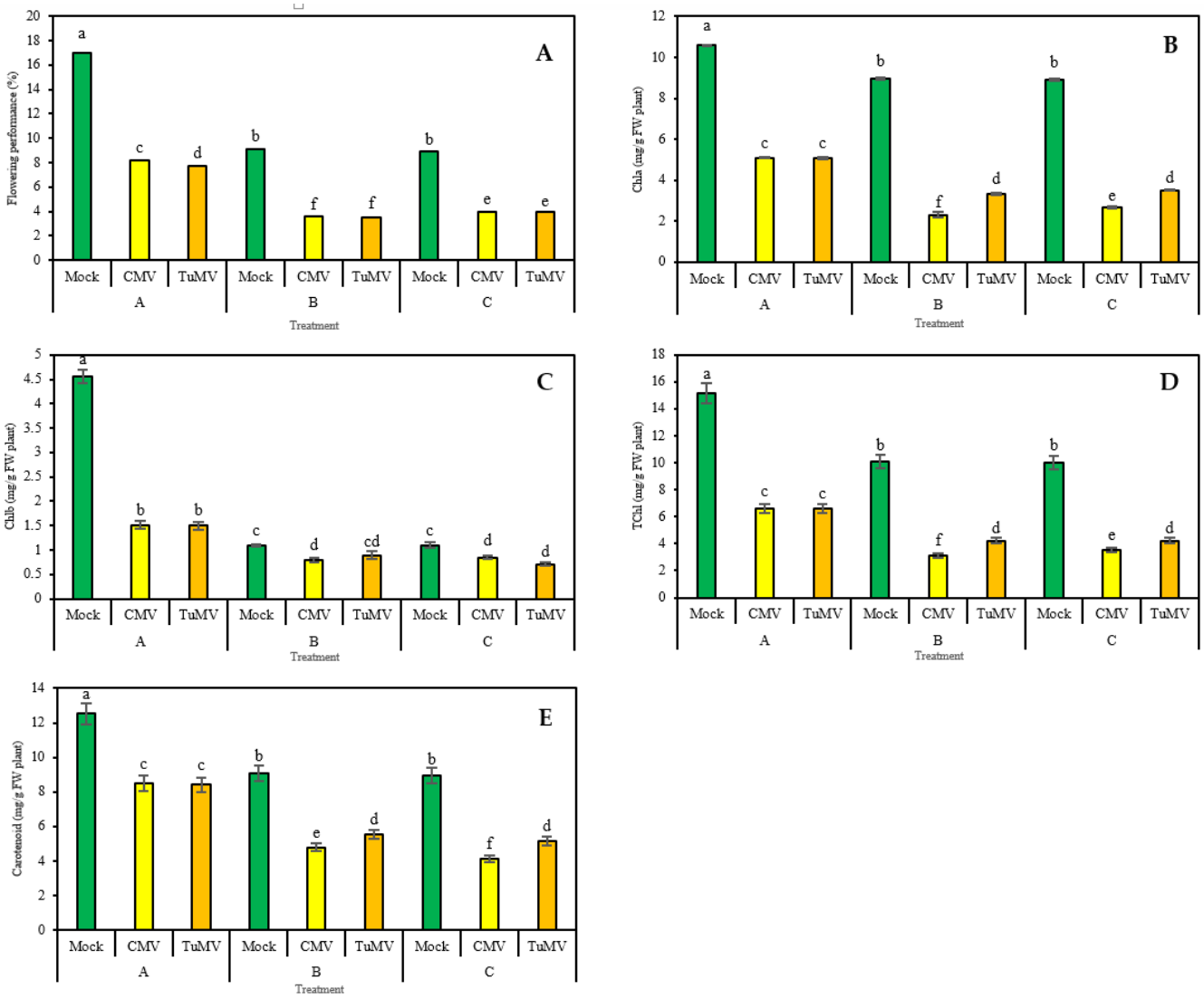

Figure 5. Effect of the virus inoculation year and post-inoculation period on performance of saffron plants. Plants inoculated and not inoculated (mock) with CMV or TuMV in 2021 were evaluated in 2021 (group A) and 2022 (group B). Plants inoculated or not (mock) in 2022 were evaluated at the end of the growing season (group C). (**A**)—Flowering performance (**B**)—Chlorophyll a (**C**)—Chlorophyll b (**D**)—Total chlorophyll content and (**E**)—Carotenoid. According to the least significant difference (LSD) test, for each parameter, bars with different letters are significantly different ($p < 0.05$). Values are means ± standard error of three independent replicates.

Table 1 shows a significant decrease in anthocyanin content in saffron flower petals after inoculation of plants with CMV (−32%) or TuMV (−28%). The overall anthocyanin content of plants over time decreased significantly in groups B and C compared to that in group A (Table 2).

3.4. Effect of Viral Infection on Main Secondary Metabolites of Saffron

The effect of virus infection on the content of the main secondary metabolites (crocin, picrocrocin, and safranal) was evaluated over one and two growing seasons in mock plants and CMV- and TuMV-inoculated plants of groups A and B. As shown in Figure 6A, there was a significant decrease in crocin content in virus-inoculated plants of group A (−6%), with the greatest reduction detected in infected plants of group B (−91% for CMV and −56% for TuMV). Moreover, crocin content showed a significant decrease in mock plants in group B (Figure 6A). In contrast, picrocrocin content significantly increased in

CMV- and TuMV-inoculated plants in group A, with the highest content in CMV-treated plants (Figure 6B). During the second growth season), picrocrocin increased significantly in mock plants of group B, whereas it decreased in CMV-treated plants or remained stable in TuMV-treated plants compared to those of group A. Virus inoculation negatively affected the safranal content, with the lowest level achieved in CMV-treated plants of group A (Figure 6C). In the TuMV-treated plants of groups A and B, safranal levels remained steady during the two growing seasons. In contrast, in mock plants, the growing season strongly affected safranal content, with values four times higher in the second year of growth. These data suggested a distinct effect of the growing season in mock plants and virus-inoculated plants. Figure 6D illustrates the HPLC chromatograms of crocin, picrocrocin, and safranal of saffron.

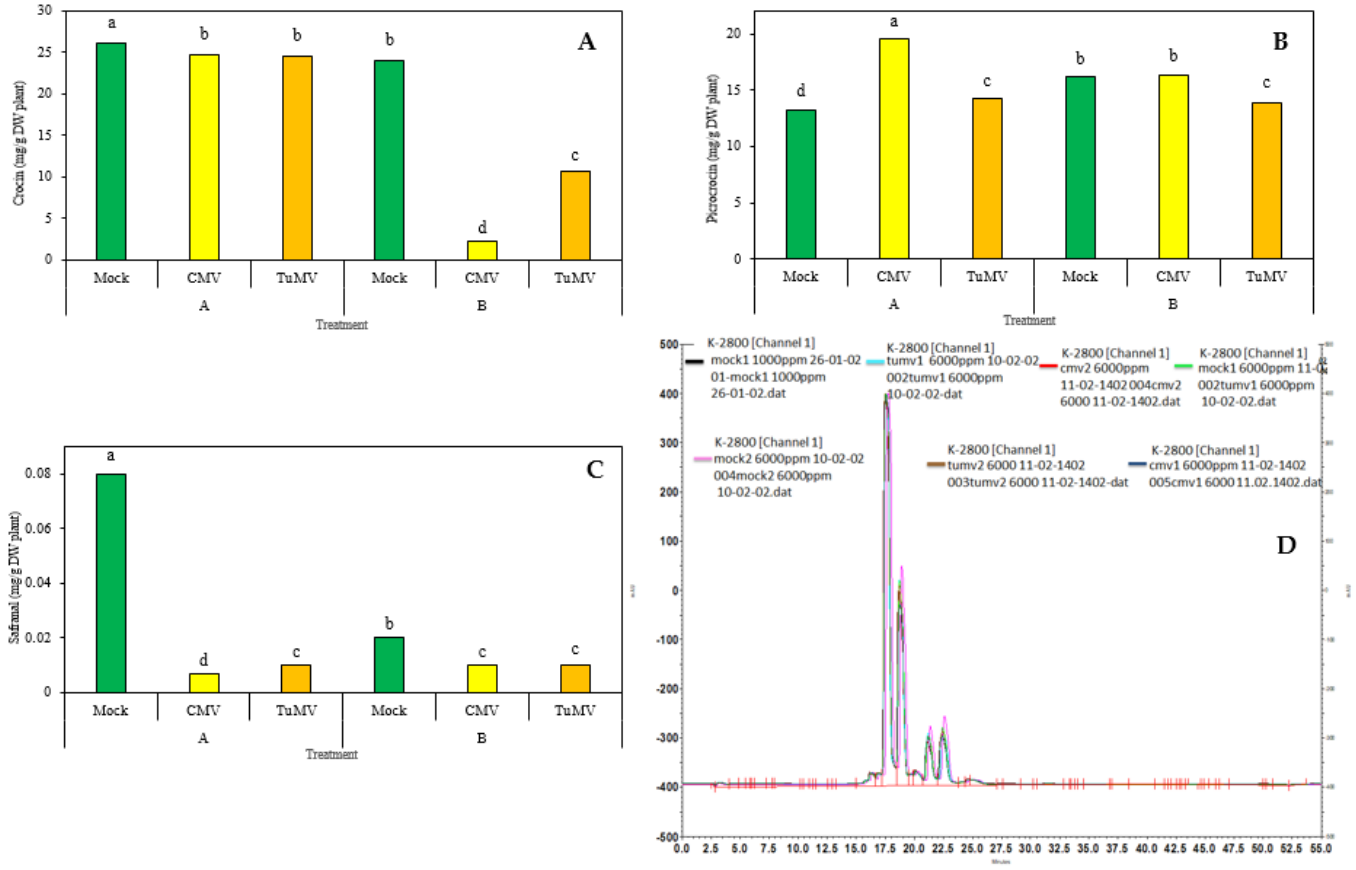

Figure 6. Impact of Virus Inoculation (CMV or TuMV) Year on Saffron Secondary Metabolites. This figure illustrates the influence of the year of inoculation with either CMV or TuMV on the secondary metabolites of saffron. Saffron plants were inoculated with CMV, TuMV, or left uninoculated (mock) in 2021 and subsequently assessed in both 2021 (A) and 2022 (B). The components analyzed include: (**A**) Crocin; (**B**) Picrocrocin; (**C**) Safranal content; (**D**) The comparative HPLC chromatograms depict various saffron samples analyzed for crocin, picrocrocin, and safranal at wavelengths of 440 nm, 250 nm, and 308 nm, respectively. The color coding in the chromatograms is as follows: Black: MOCK-A; Light Green: MOCK-A; Light Blue: TuMV-A; Dark Blue: CMV-A; Pink: MOCK-B; Brown: TuMV-B; Red: CMV-B. According to the least significant difference (LSD) test, for each parameter bars with different letters are significantly different ($p < 0.05$). Values are mean ± standard error of three independent replicates.

3.5. Relative Expression Analysis of CsALDH31l and CsUGT709G1genes

The expression patterns of two key genes involved in the biosynthesis of crocin and picrocrocin in saffron stigmas, *CsALDH31l* and *CsUGT709G1*, were analyzed in response to CMV and TuMV inoculation. *CsALDH31l* was significantly downregulated under

CMV and TuMV treatments, with the lowest relative expression level observed in CMV-inoculated plants, with two times lower values (Figure 7A). Although there were no significant differences in *CsUGT709G1* relative expression between inoculated plants and the mock treatment, a slight upregulation of the gene was observed in CMV-infected plants, while relative expression levels in TuMV-inoculated and mock-treated plants were similar (Figure 7B).

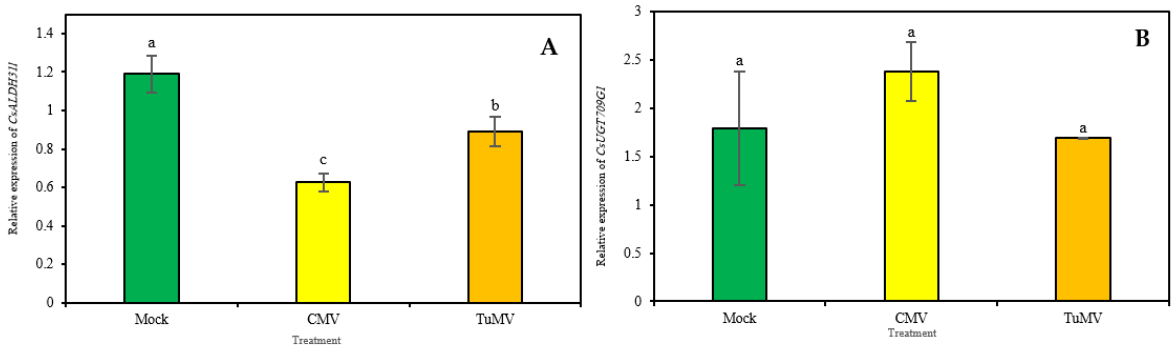

Figure 7. Effect of CMV and TuMV treatments on (**A**)—Relative gene expression of *CsALDH31l* (**B**)—Relative gene expression of *CsUGT709G1*. Data were analyzed by one-way ANOVA, and values are the mean ± standard error of three independent replicates. Bars with different letters are significantly different ($p < 0.05$).

3.6. Morphological, Physiological, Phytochemical, and Molecular Indexes Assessment by PC

To analyze the relationships between the parameters evaluated after one or two growing seasons and the effects of virus inoculation (CMV and TuMV) on saffron plants, PCA was conducted using 12 morphological, physiological, and phytochemical parameters (Figure 8). PCA revealed that the data could be divided into two principal components (PCs), capturing approximately 88% of the total variation. The first PC accounted for 76.22% of the variation, while the second PC accounted for 11.41% of the variation. The mock plants (11, 21, 31) were clearly separated from the viruses (CMV and TuMV)-inoculated plants, regardless of the evaluation date. The mock plants evaluated in the first growing season (11) showed the most positive values in terms of the first component. In contrast, CMV-treated plants evaluated after two growing seasons (22) exhibited the most negative effects among all traits. Mock plants presented the highest flowering performance and carotenoid and chlorophyll content. Meanwhile, the photosynthesis rate and transpiration showed a very high positive correlation with chlorophyll b. Conversely, spad and leaf areas were highly correlated with each other, but not with photosynthesis and chlorophyll b (Figure 8).

Based on PCA related to gene expression and content of secondary metabolites, the first component explains approximately 80% and the second component approximately 20% of the changes in Figure 9. In other words, these changes are justified and reliable by almost 100%. As shown in Figure 9, it is clearly seen that the three treatments are completely separated from each other and placed in three different regions of the figure. In fact, the three treatments worked completely differently with respect to the level of gene expression and the content of metabolites. In the case of TuMV, the level of gene expression and metabolite content decreased, while CMV and mock showed a higher level of gene expression and the corresponding metabolite content. As shown in Figure 9, high expression levels of *CsUGT709G1* and high picrocrocin content are associated with CMV infection. Moreover, high expression of *CsALDH31l* and, consequently, high production of crocin content were observed in the mock treatment. On the other hand, the expression of *CsUGT709G1* could affect the amount of safranal production, but it cannot be stated because

the ratio of the effect of *CsUGT709G1* expression on the production rate of picrocrocin was much higher than the ratio of its effect on safranal. In other words, the genes that had a more direct effect on the production of a particular metabolite are clustered together. PCA showed a correlation between the mock plants and secondary metabolite content (Figure 9).

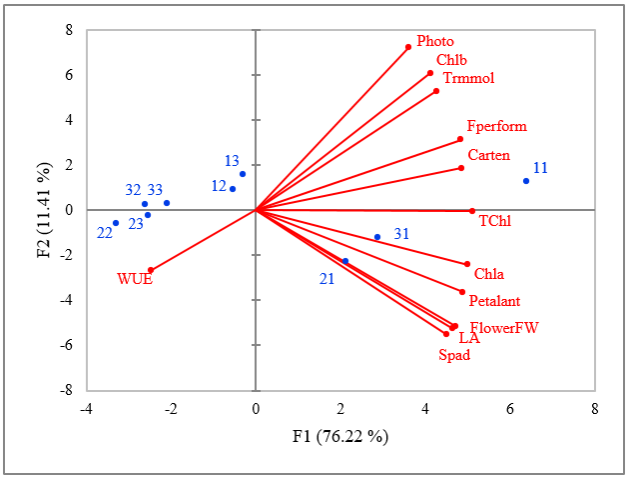

Figure 8. Principal component analysis (PCA) biplot visualizing the relationship between different morphological, physiological and phytochemical traits, including: LA: Leaf area (cm^2 $plant^{-1}$); Flower FW: Fresh weight of flower (g $plant^{-1}$), Fperform: flowering performance (%), Photo: Photosynthetic rate (µmol CO_2 m^{-2} s^{-1}), Trmmol: Transpiration rate (mmol H_2O m^{-2} s^{-1}), WUE: Instantaneous water use efficiency (µmol CO_2 $mmol^{-1}$ H_2O), Spad: Greenness index (Spad), Chla: Chlorophyll a (mg g^{-1} FW plant), Chlb: Chlorophyll b (mg g^{-1} FW plant), TChl: Total chlorophyll (mg g^{-1} FW plant), Carten: Carotenoid (mg g^{-1} FW plant), Petalant: Petal anthocyanin content (mg g^{-1} FW plant), 11: Mock-group A, 12: CMV-group A, 13: TuMV-group A, 21: Mock-group B, 22: CMV-group B, 23: TuMV-group B, 31: Mock-group C, 32: CMV-C, 33:TuMV-C.

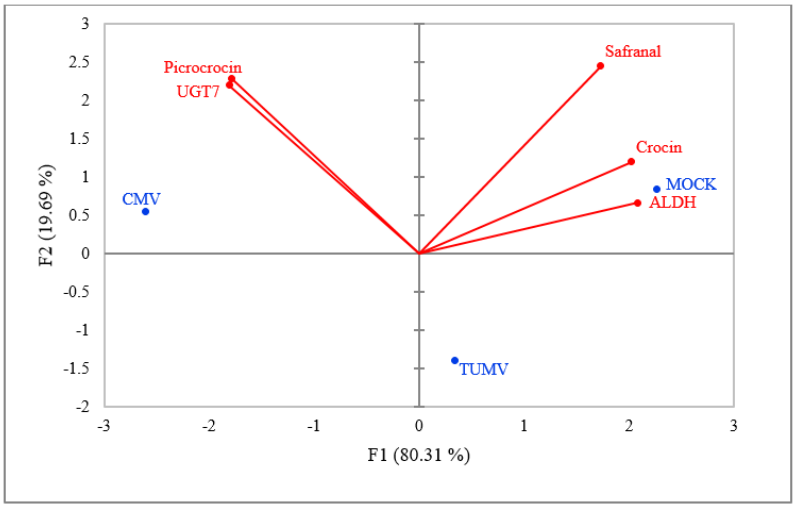

Figure 9. Principal component analysis biplot of the critical gene expression levels in the biosynthesis pathway of crocin and picrocrocin in treated saffron plants with different viruses, including CMV and TuMV, compared to the mock treatment. ALDH: *CsALDH31l* gene, UGT7: *CsUGT709G1* gene.

4. Discussion

Plants are continuously interacting with various biological organisms, including viruses, which can impact plant metabolism both positively and negatively. Plant viruses, as obligate biotrophic pathogens, alter the physiological and metabolic processes of their hosts to support their own replication and spread. This often results in severe damage to

important plant products. These interactions induce physiological, phytochemical, and molecular changes in plants, enriching their defense signaling pathways [47,48]. Secondary metabolites are small organic compounds that play vital biological roles during biotic and abiotic stress in plants. To thoroughly assess the impact of the virus on this plant over an adequate period of time, various indices were evaluated at multiple time points. Therefore, we studied the effect of two important plant viruses, CMV and TuMV, on the morphological, physiological, phytochemical, and molecular properties of saffron over two years, evaluating the effect of the post-inoculation period (one or two years), as well as the effect of the inoculation year.

Our findings demonstrated that viral infections, particularly by CMV and TuMV, have a detrimental impact on the morphological characteristics of saffron plants. The infection of parsley plants with CMV significantly impacted their morphological characteristics, resulting in a reduction in plant biomass [30]. CMV caused severe mosaic and yellowing of leaves, while TuMV induced leaf curling, mosaic patterns, zigzag leaf shapes, and gradual changes in the leaf tip color, alongside stigma-curling symptoms. These symptoms were correlated with a notable reduction in leaf area and fresh flower weight, consistent with previous studies on biotic and abiotic stress responses in saffron and other crops [49,50]. The decrease in leaf area likely represents a defensive plant response to reduce water loss and enhance survival under stress conditions [51]. Similar effects have been observed in other studies, where viral infections led to reduced plant growth and altered morphological traits, such as those recorded in CMV-infected Bambara groundnut and TuMV-infected stem mustard [29,52].

Our results indicated a direct relationship between leaf area and fresh weight of flowers, with the highest values for both parameters in mock plants, whereas the fresh weight of flowers decreased when virus-induced leaf area reduction occurred. Subsequently, the photosynthesis rate, leaf pigment content, and flowering performance are negatively affected by virus infection.

Photosynthesis and pigment content were adversely affected by viral infections. CMV-inoculated plants exhibited the lowest levels of chlorophyll a, b, and total chlorophyll, consistent with findings in different crops under abiotic stresses [50] and viral infections, leading to decreased chlorophyll levels and disrupted photosynthesis. The appearance of symptoms associated with CMV in various plants has led to reduced greenness, disrupted photosynthesis, and, consequently, a decline in photosynthetic pigments. [29–32,53]. This disruption is likely due to virus-induced alterations in chloroplast structure and function, affecting energy production and photosynthetic efficiency [54–57]. We found that the flowering performance of saffron plants was negatively affected by biotic stress induced by CMV and TuMV, but this parameter has also been reduced under abiotic stress, like storage period at low temperatures and drought [49]. The saffron plant behavior in terms of flowering performance and chlorophyll and carotenoid content changed throughout the evaluation period, not only by the virus inoculation treatments but also by the post-inoculation period and inoculation year. In mock plants, these parameters decreased significantly in group B compared to group A, without relevant changes between groups B and C derived from corms established in 2021 and 2022, respectively. These data suggest possible changes in the quality or decay of corms from 2021 to 2022, leading to alterations in the development and properties of plants generated from daughter corms that have undergone a dormant phase. Therefore, the lower performance of plants in group B than in group A might be due to physiological status decay of corms in the second growing season. The effects of uncontrolled abiotic stresses, which altered plant yields in 2022, cannot be ruled out.

Our study highlights that viral stress significantly alters the secondary metabolism of saffron, affecting crocin, picrocrocin, and safranal levels. Viral treatment (CMV infection in particular) led to the highest reduction in crocin and safranal content, while increasing picrocrocin levels. These results align with previous research indicating that viral infections can reprogram plants' secondary metabolism to enhance defense mechanisms [47]. These changes are associated with the altered expression of genes involved in the biosynthesis of these metabolites [13]. Specifically, CMV infection resulted in the lowest expression of *CsALDH31l*, which is crucial for crocin synthesis, and the highest expression of *CsUGT709G1*, which is involved in picrocrocin synthesis. This regulatory shift further supports the core link between viral stress, gene expression, and metabolic responses, highlighting the complex nature of plant-virus interactions [58].

Furthermore, viral treatments reduce anthocyanin content in saffron petals, suggesting that viral stress affects flavonoid biosynthesis, which is crucial for plant defense [9]. Anthocyanins are known to decrease under stress conditions, and their reduced levels in viral treatments suggest a potential defense response against viral pathogens [59]. Previous studies have shown the vital role of anthocyanins in plant defense against biological stress factors [8,9,60].

PCA analysis revealed strong correlations among various indexes, indicating that morphological and physiological indexes are interconnected. With the increase in leaf area, the amount of greenness also increased, and the decrease in greenness under viral treatment was not only because of the leaf area, but also because of the virus-induced effects on chlorophyll. Despite sufficient chlorophyll levels, plants under viral stress redirected resources towards strengthening their defense pathways rather than maximizing photosynthetic potential, converting chlorophyll a to chlorophyll b.

Overall, our research provides compelling evidence that viral stress significantly influences the metabolism and physiological processes of saffron plants, leading to reduced growth, altered photosynthesis, and changes in secondary metabolite production. The correlation between gene expression, secondary metabolite levels, and other physiological and morphological indexes highlights the complex interplay between viral infection and plant metabolic responses. Understanding these interactions can help to develop strategies to mitigate the adverse effects of viral infections on economically important crops, thereby ensuring better yield and quality.

5. Conclusions

The study highlights the detrimental effects of CMV and TuMV on saffron, demonstrating significant reductions in leaf area, flower fresh weight, and overall flowering performance. Inoculated plants exhibited typical viral symptoms, including leaf mosaic and stigma curling. Notably, CMV treatment resulted in the lowest chlorophyll and carotenoid levels, alongside a marked decrease in crocin and safranal content, while picrocrocin levels peaked in 2021. A strong correlation was found between secondary metabolite content and the expression of key biosynthetic genes (*CsALDH31l* and *CsUGT709G1*), although no correlation existed for safranal synthesis. Additionally, viral treatments adversely affected anthocyanin levels, greenness, photosynthesis rates, stomatal transpiration, and water use efficiency. Taken together, according to our results, it can be stated that viral infection diminishes the quality of saffron stigma and petals and the quantity of saffron from the viewpoint of flowering performance. Future studies should investigate the molecular mechanisms of saffron's secondary metabolite production in response to viral infections and develop strategies to improve its resilience against CMV and TuMV.

Supplementary Materials: The following supporting information can be downloaded at https://www.mdpi.com/article/10.3390/horticulturae11010096/s1, Table S1: Primer sequences used to detect the virus in plants and internal control; Table S2: Primer sequences used to assess genes involved in secondary metabolites pathways and the reference gene.

Author Contributions: Conceptualization, M.S.-B., M.S.; data curation: M.S., S.R., A.M.-B.; formal analysis, A.M.-B.; investigation, M.S.; resources, M.S.-B., H.R., C.S., A.M.-B.; supervision, M.S.-B., M.A., C.S.; software, A.M.-B., validation, A.M.-B.; writing—original draft, M.S.; writing—review and editing, C.S., S.R., M.S.-B. All authors have read and agreed to the published version of the manuscript.

Funding: This research was partially funded by the Xunta de Galicia through project number IN607A 2021/06.

Data Availability Statement: The original contributions presented in this study are included in the article/Supplementary Materials. Further inquiries can be directed to the corresponding authors.

Acknowledgments: This work has been supported by Tarbiat Modares University, Tehran, Iran. We also extend our heartfelt thanks to the Misión Biológica de Galicia, Consejo Superior de Investigaciones Científicas, 15780 Santiago de Compostela, Spain, and Shahid Beheshti University, Tehran, Iran, for the fund and support.

Conflicts of Interest: The authors declare no conflicts of interest.

References

1. Aissa, R.; Ibourki, M.; Bouzid, H.A.; Bijla, L.; Oubannin, S.; Sakar, E.H.; Jadouali, S.; Hermansyah, A.; Goh, K.W.; Ming, L.C.; et al. Phytochemistry, quality control and medicinal uses of Saffron (*Crocus sativus* L.): An updated review. *J. Med. Life* **2023**, *16*, 822–836. [CrossRef] [PubMed]
2. Kothari, D.; Thakur, R.; Kumar, R. Saffron (*Crocus sativus* L.): Gold of the spices—A comprehensive review. *Hortic. Environ. Biotechnol.* **2021**, *62*, 661–677. [CrossRef]
3. Moratalla-López, N.; Bagur, M.J.; Lorenzo, C.; Martínez-Navarro, M.E.; Salinas, M.R.; Alonso, G.L. Bioactivity and bioavailability of the major metabolites of *Crocus sativus* L. Flower. *Molecules* **2019**, *24*, 2527. [CrossRef] [PubMed]
4. Shahandeh, H. Soil conditions for sustainable saffron production. In *Saffron: Science, Technology and Health*; Woodhead Publishing Series in Food Science, Technology and Nutrition; Woodhead Publishing: Sawston, UK, 2020; pp. 59–66. [CrossRef]
5. Caballero-Ortega, H.; Pereda-Miranda, R.; Abdullaev, F.I. HPLC quantification of major active components from 11 different saffron (*Crocus sativus* L.) sources. *Food Chem.* **2007**, *100*, 1126–1131. [CrossRef]
6. Pandita, D. Saffron (*Crocus sativus* L.): Phytochemistry, therapeutic significance and omics-based biology. In *Medicinal and Aromatic Plants: Expanding Their Horizons Through Omics*; Elsevier Inc.: Amsterdam, The Netherlands, 2021; pp. 325–396. [CrossRef]
7. *ISO 3632-1:2011*; Spices—Saffron (*Crocus sativus* L.). Food Products SC 7, Spices, Culinary Herbs and Condiments. International Organization for Standardization: Geneva, Switzerland, 2011.
8. Li, Z.; Ahammed, G.J. Plant stress response and adaptation via anthocyanins: A review. *Plant Stress* **2023**, *10*, 100230. [CrossRef]
9. Sivankalyani, V.; Feygenberg, O.; Diskin, S.; Wright, B.; Alkan, N. Increased anthocyanin and flavonoids in mango fruit peel are associated with cold and pathogen resistance. *Postharvest Biol. Technol.* **2016**, *111*, 132–139. [CrossRef]
10. Ahrazem, O.; Argandoña, J.; Fiore, A.; Rujas, A.; Rubio-Moraga, Á.; Castillo, R.; Gómez-Gómez, L. Multi-species transcriptome analyses for the regulation of crocins biosynthesis in Crocus. *BMC Genom.* **2019**, *4*, 81–90. [CrossRef]
11. Diretto, G.; Ahrazem, O.; Rubio-Moraga, Á.; Fiore, A.; Sevi, F.; Argandoña, J.; Gómez-Gómez, L. *UGT709G1*: A novel uridine diphosphate glycosyltransferase involved in the biosynthesis of picrocrocin, the precursor of safranal in saffron (*Crocus sativus*). *New Phytol.* **2019**, *224*, 725–740. [CrossRef]
12. López, A.J.; Frusciante, S.; Niza, E.; Ahrazem, O.; Rubio-Moraga, Á.; Diretto, G.; Gómez-Gómez, L. A new glycosyltransferase enzyme from family 91, ugt91p3, is responsible for the final glucosylation step of crocins in saffron (*Crocus sativus* L.). *Int. J. Mol. Sci.* **2021**, *22*, 8815. [CrossRef]
13. Moradi, S.; Kafi, M.; Aliniaeifard, S.; Moosavi-Nezhad, M.; Pedersen, C.; Gruda, N.S.; Salami, S.A. Monochromatic blue light enhances crocin and picrocrocin content by upregulating the expression of underlying biosynthetic pathway genes in saffron (*Crocus sativus* L.). *Front. Hortic.* **2022**, *1*, 960423. [CrossRef]
14. Samuitienė, M.; Navalinskienė, M.; Jackevičienė, E. Arabis mosaic virus on ornamental plants. *Biologija* **2008**, *54*, 264–268. [CrossRef]

15. Parizad, S.; Dizadji, A.; Habibi, M.K.; Winter, S.; Kalantari, S.; Movi, S.; Lorenzo Tendero, C.; Alonso, G.L.; Moratalla-Lopez, N. The effects of geographical origin and virus infection on the saffron (*Crocus sativus* L.) quality. *Food Chem.* **2019**, *295*, 387–394. [CrossRef]
16. Chen, J.; Chen, J.S. Occurrence and control of mosaic disease (turnip mosaic virus) in saffron (*Crocus sativus*). *Zhejiang Nongye Kexue* **2000**, *3*, 132–135.
17. Hedari, M.; Hosseini, S.A.; Douri, R. Detection and Phylogenetic Analysis of Turnip mosaic virus on Saffron (*Crocus sativus*) in Iran. *J. Appl. Res. Plant Prot.* **2017**, *7*, 17–28.
18. Tavoosi, M.; Moradi, Z.; Mehrvar, M. First report of Turnip mosaic virus infecting saffron in Iran. *VirusDisease* **2022**, *33*, 489–491. [CrossRef]
19. Chen, Y.K.; Derks, A.F.; Langeveld, S.; Goldbach, R.; Prins, M. High sequence conservation among cucumber mosaic virus isolates from lily. *Arch. Virol.* **2001**, *146*, 1631–1636. [CrossRef]
20. Langeveld, S.A.; Dore, J.M.; Memelink, J.; Derks, A.F.L.M.; van der Vlugt, C.I.M.; Asjes, C.J.; Bol, J.F. Identification of potyviruses using the polymerase chain reaction with degenerate primers. *J. Gen. Virol.* **1991**, *72*, 1531–1541. [CrossRef]
21. Tavoosi, M.; Hosseini, S.A. Molecular Detection and Investigation of Irish severe mosaic virus in Saffron, Fields of Razavi and South Khorasan. *J. Saffron Res.* **2021**, *9*, 323–334. [CrossRef]
22. Van der Vlugt, C.I.M.; Langeveld, S.A.; Goldbach, R.W. Molecular cloning and sequence analysis of the 3′-terminal region of iris severe mosaic virus RNA. *Arch. Virol.* **1994**, *136*, 397–406. [CrossRef]
23. Liao, F.R.; Lin, W.Z.; Chen, X.H.; Chen, Q.; Chen, H.Y.; Huang, P.Y.; Fang, Z.P.; Wu, Y.; Shen, J.G.; Lin, S.M. Molecular identification and sequence analysis of ornithogalum mosaic virus in Saffron (*Crocus sativus*) corms. *Sci. Agric. Sin.* **2017**, *50*, 4046–4054. [CrossRef]
24. Farkhoond, S.; Hosseini, S.A.; Salari, K.; Hossein, M.; Fard, A. Detection and phylogenetic analysis of saffron and tomato isolates of Tomato spotted wilt virus from South Khorasan. *Iran. J. Plant Prot. Sci.* **2018**, *48*, 217–227. [CrossRef]
25. Navalinskiene, M.; Samuitiene, M. Viruses affecting some bulb and corm flower crops. *Biologija* **2001**, *4*, 40–42.
26. Miglino, R.; Jodlowska, A.; van Schadewijk, A.R. First report of Narcissus mosaic virus infecting *Crocus* spp. cultivars in the Netherlands. *Plant Dis.* **2005**, *89*, 342. [CrossRef]
27. Russo, M.; Martelli, G.P.; Cresti, M.; Ciampolini, F. Bean yellow mosaic virus in saffron. *Phytopathol. Mediterr.* **1979**, *18*, 189–191.
28. Grilli Caiola, M. Virus-like particles in cells of saffron flowers. *Phytopathol. Zeitschrift.* **1982**, *105*, 92–95.
29. Guo, D.P.; Guo, Y.P.; Zhao, J.P.; Liu, H.; Peng, Y.; Wang, Q.M.; Chen, J.S.; Rao, G.Z. Photosynthetic rate and chlorophyll fluorescence in leaves of stem mustard (*Brassica juncea* var. tsatsai) after turnip mosaic virus infection. *Plant Sci.* **2005**, *168*, 57–63. [CrossRef]
30. Shamshiri, M.; Ayyari, M.; Mokhtassi-Bidgoli, A.; Shams-Bakhsh, M. Effect of viral-inoculation on the morphology, physiology, and phytochemistry of parsley (*Petroselinum crispum*). *Physiol. Mol. Plant Pathol.* **2024**, *134*, 102477. [CrossRef]
31. Saadati, M.; Ayyari, M.; Shams-bakhsh, M. Effect of the cucumber mosaic virus-Fny infection on the physiological and phytochemical properties of three green basil (*Ocimum basilicum* L.) landraces. *Iran. J. Plant Pathol.* **2022**, *57*, 303–319. [CrossRef]
32. Astaraki, S.; Safaie, N.; Shams -Bakhsh, M. Reaction of sugar beet, pepper and bean plants to co -infection with Cucumber mosaic virus and Beet curly top viruses. *Iran. J. Plant Pathol.* **2020**, *56*, 221–236.
33. Lan, H.; Lai, B.; Zhao, P.; Dong, X.; Wei, W.; Ye, Y.; Wu, Z. Cucumber mosaic virus infection modulated the phytochemical contents of Passiflora edulis. *Microb. Pathog.* **2020**, *138*, 103828. [CrossRef]
34. Bruni, R.; Bianchi, A.; Bellardi, M.G. Essential oil composition of Agastache anethiodora Britton (Lamiaceae) infected by cucumber mosaic virus (CMV). *Flavour Fragr. J.* **2007**, *22*, 66–70. [CrossRef]
35. Sánchez, F.; Martı'nez-Herrera, D.; Aguilar, I.; Ponz, F. Infectivity of turnip mosaic potyvirus cDNA clones and transcripts on the systemic host Arabidopsis thaliana and local lesion hosts. *Virus Res.* **1998**, *55*, 207–219. [CrossRef]
36. Rizzo, T.M.; Palukaitis, P. Construction of full-length cDNA clones of cucumber mosaic virus RNAs 1, 2 and 3: Generation of infectious RNA transcripts. *Mol. Genet. Genom.* **1990**, *222*, 249–256. [CrossRef]
37. Asghari, N.; Koolivand, D.; Eini, O. Differential expression of HSP90 and AGO genes in tomato infected by Cucumber mosaic virus. *Crop Biotech.* **2020**, *10*, 31–42. [CrossRef]
38. Faria, J.C.; Albino, M.M.C.; Dias, B.B.A.; Cançado, L.J.; da Cunha, N.B.; de M. Silva, L.; Vianna, G.R.; Aragão, F.J.L. Partial resistance to Bean golden mosaic virus in a transgenic common bean (*Phaseolus vulgaris* L.) line expressing a mutated rep gene. *Plant Sci.* **2006**, *171*, 565–571. [CrossRef]
39. Huang, K.S.; Li, S.L.; Sun, J.H.; Wang, Y.C.; Jan, F.J.; Chen, T.C. Development of a generic method for inspection of tospoviruses. *Eur. J. Plant Pathol.* **2018**, *150*, 457–469. [CrossRef]
40. Lichtenthaler, H.K. Chlorophylls and Carotenoids: Pigments of Photosynthetic Biomembranes. *Methods Enzymol.* **1987**, *148*, 350–382.
41. Warren, C.R. Rapid measurement of chlorophylls with a microplate reader. *J. Plant Nutr.* **2008**, *31*, 1321–1332. [CrossRef]
42. Lee, D.J.; Schoenberger, R.; Archibald, J.; McCollum, S. Development of a machine vision system for automatic date grading using digital reflective near-infrared imaging. *J. Food Eng.* **2008**, *86*, 388–398. [CrossRef]

43. Fuleki, T.; Francis, F.J. Quantitative methods for anthocyanins. 2. determination of total anthocyanin and degradation index for cranberry juice. *J. Food Sci.* **1968**, *33*, 78–83. [CrossRef]
44. Mónica Giusti, M.; Wrolstad, R.E. Characterization and measurement of anthocyanins by uv-visible spectroscopy. In *Handbook of Food Analytical Chemistry*; Wiley: Hoboken, NJ, USA, 2001; pp. 1–13. [CrossRef]
45. Kabiri, M.; Rezadoost, H.; Ghassempour, A. A comparative quality study of saffron constituents through HPLC and HPTLC methods followed by isolation of crocins and picrocrocin. *LWT* **2017**, *84*, 1–9. [CrossRef]
46. Schmittgen, T.D.; Livak, K.J. Analyzing real-time PCR data by the comparative CT method. *Nat. Protoc.* **2008**, *3*, 1101–1108. [CrossRef]
47. Mishra, J.; Srivastava, R.; Trivedi, P.K.; Verma, P.C. Effect of virus infection on the secondary metabolite production and phytohormone biosynthesis in plants. *3 Biotech* **2020**, *10*, 1–16. [CrossRef]
48. Srivastava, R.; Rai, K.M.; Srivastava, R. Plant biosynthetic engineering through transcription regulation: An insight into molecular mechanisms during environmental stress. In *Biosynthetic Technology and Environmental Challenges. Energy, Environment, and Sustainability*; Springer: Singapore, 2018; pp. 51–72. [CrossRef]
49. Mzabri, I.; Legsayer, M.; Chetouani, M.; Aamar, A.; Kouddane, N.; Boukroute, A.; Bekkouch, I.; Berrichi, A. Saffron (*Crocus sativus* L.) yield parameter assessment of abiotic stressed corms stored in low temperature. *J. Mater. Environ. Sci.* **2017**, *8*, 3588–3597.
50. Mzabri, I.; Legsayer, M.; Aliyat, F.; Maldani, M.; Kouddane, N.E.; Boukroute, A.; Bekkouch, I.; Berrichi, A. Effect of Drought Stress on the Growth and Development of Saffron (*Crocus sativus* L.) in Eastern Morocco. *Atlas J. Biol.* **2017**, 364–370. [CrossRef]
51. Lebon, G.; Duchêne, E.; Brun, O.; Magné, C.; Clément, C. Flower abscission and inflorescence carbohydrates in sensitive and non-sensitive cultivars of grapevine. *Sex. Plant Reprod.* **2004**, *17*, 71–79. [CrossRef]
52. Buhari, S.M.; Salaudeen, M.T.; Wada, A.C. Effects of cucumber mosaic virus on yield components and yield of bambara groundnut. *Bull. Sci. Res.* **2022**, *4*, 35–45. [CrossRef]
53. Pichersky, E.; Raguso, R.A. Why do plants produce so many terpenoid compounds? *New Phytol.* **2018**, *220*, 692–702. [CrossRef]
54. Jang, C.; Seo, E.Y.; Nam, J.; Bae, H.; Gim, Y.G.; Kim, H.G.; Cho, I.S.; Lee, Z.W.; Bauchan, G.R.; Hammond, J.; et al. Insights into *Alternanthera mosaic* virus TGB3 functions: Interactions with Nicotiana benthamiana PsbO correlate with chloroplast vesiculation and veinal necrosis caused by TGB3 over-expression. *Front. Plant Sci.* **2013**, *4*, 5. [CrossRef]
55. Tu, Y.; Jin, Y.; Ma, D.; Li, H.; Zhang, Z.; Dong, J.; Wang, T. Interaction between PVY HC-Pro and the NtCF1 β-subunit reduces the amount of chloroplast ATP synthase in virus-infected tobacco. *Sci. Rep.* **2015**, *5*, 15605. [CrossRef] [PubMed]
56. Bhattacharyya, D.; Chakraborty, S. Chloroplast: The Trojan horse in plant–virus interaction. *Mol. Plant Pathol.* **2018**, *19*, 504–518. [CrossRef] [PubMed]
57. Zhao, J.; Zhang, X.; Hong, Y.; Liu, Y. Chloroplast in plant-virus interaction. *Front. Microbiol.* **2016**, *7*, 1565. [CrossRef] [PubMed]
58. Ahrazem, O.; Rubio-Moraga, A.; Argandoña-Picazo, J.; Castillo, R.; Gómez-Gómez, L. Intron retention and rhythmic diel pattern regulation of carotenoid cleavage dioxygenase 2 during crocetin biosynthesis in saffron. Plant Mol. *Biol.* **2016**, *91*, 355–374. [CrossRef]
59. Heydari, S.; Rezaei, R.; Haghayegh, G.H. Effect of drying processes on stability of anthocyanin extracts from saffron petal. *Evol. Trends Eng. Technol.* **2014**, *2*, 13–18. [CrossRef]
60. Zhang, Y.; Butelli, E.; De Stefano, R.; Schoonbeek, H.J.; Magusin, A.; Pagliarani, C.; Wellner, N.; Hill, L.; Orzaez, D.; Granell, A.; et al. Anthocyanins double the shelf life of tomatoes by delaying overripening and reducing susceptibility to gray mold. *Curr. Biol.* **2013**, *23*, 1094–1100. [CrossRef]

horticulturae

MDPI

Article

Enhanced Salt Tolerance of Pea (*Pisum sativum* L.) Seedlings Illuminated by LED Red Light

Kexin Xu [1,2,†], Xiaoan Sun [3,†], Chitao Sun [4], Yuqing Wang [5], Haiyan Zhu [3], Wanli Xu [1,*] and Di Feng [1,*]

[1] Key Laboratory of Saline-Alkali Soil Improvement and Utilization (Saline-Alkali Land in Arid and Semiarid Regions), Ministry of Agriculture and Rural Affairs, China, Institute of Agricultural Resources and Environment, Xinjiang Academy of Agricultural Sciences, Urumchi 830091, China; coco271568@163.com
[2] College of Tropical Agriculture and Forestry, Hainan University, Haikou 570208, China
[3] Weifang University of Science and Technology, Shouguang 262700, China; seannyx@outlook.com (X.S.); shgzhhyan@outlook.com (H.Z.)
[4] College of Water Conservancy and Civil Engineering, Shandong Agricultural University, Taian 271018, China; sunchitao@163.com
[5] Agricultural College, South China Agricultural University, Guangzhou 510642, China; wyq17860231824@outlook.com
* Correspondence: wlxu2005@163.com (W.X.); fengdi2008sunny@163.com (D.F.)
† These authors contributed equally to this work.

Abstract: Light quality is an important variable affecting plant growth, so we aimed to explore the impact of light quality on plants under salt stress. The salt tolerance of pea (*Pisum sativum* L.) seedlings illuminated by LED red light and 4:1 of red/blue light in a hydroponic system was evaluated at three salinity levels (0, 50, and 100 mmol/L of NaCl) for their morphological and physiological parameters and their root growth characteristics in response to salt stress. Results demonstrated that, as salt stress intensified, the plant height, aboveground fresh/dry mass, root growth indices, and chlorophyll content of pea seedlings exhibited a decreasing trend, while the malondialdehyde (MDA) content and the activity of superoxide dismutase (SOD), peroxidase (POD), and catalase (CAT) in leaves increased. Also, more sodium (Na^+) but less potassium (K^+) ions were detected due to the change in electrolyte balance. Compared with pea seedlings under no salt stress, the growth rate, plant height, and K^+ ion content significantly increased with the red light treatments, but both lights did not affect the aboveground fresh/dry mass, chlorophyll content, or root growth index. Under medium salt stress (50 mmol/L), red light helped generate more chlorophylls by 17.06%, accelerate leaf electrolyte exudation by 23.84%, accumulate more K^+ ions by 46.32%, and increase the K^+/Na^+ ratio by 45.45%. When pea seedlings were stressed by 100 mmol/L salinity stress, red light was able to maintain the leaf chlorophyll level by 114.66%, POD enzyme activity by 157.78%, MDA amount by 14.16%, leaf and stem electrolyte leakage rate by 38.76% and 21.80%, respectively, K^+ ion content by 45.47%, and K^+/Na^+ ratio by 69.70%. In conclusion, the use of red light has proven to enhance the salt tolerance of pea seedlings in a hydroponic system, which can and should be a promising approach to prime pea seedlings for more salt tolerance.

Keywords: pea; LED red light; salt stress; physiological responses; growth indicators

1. Introduction

Salt stress is one of the most important factors inhibiting plant growth [1]. Seed germination and the seedling stage are the periods most sensitive to soil salinity. If plant salt stress occurs at these early and vulnerable stages, the entire growth and later development

can be severely hindered [2]. Understanding mechanisms involved in crop salt tolerance is of great importance and can lead to finding ways to enhance crop tolerance against salt stress in modern agricultural production. Many attempted, endeavoring, and encouraging approaches in this area include breeding for salt-tolerant varieties [3], adversity exercises (including cross-adaptation) [4,5], use of exogenous substances [6], and lighting modulation and priming [7]. Among these, the approach of adjusting light quality is a novel technology to change physiological responses or adjust key metabolisms for enhanced salt tolerance in crops, having the advantage of being fast, safe, and without limitation by various development stages, and therefore has become one of the most researched fields.

Light quality refers to the composition of light wavelengths and their proportions. It can be divided into ultraviolet light, visible light, and infrared light. Among them, the two kinds of light that have the most important influence on plant photosynthesis are blue light (with a wavelength of 450–495 nm) and red light (with a wavelength of 620–760 nm) in visible light. Plants perceive changes in light quality through photoreceptors and adapt to a series of environmental conditions. For example, blue light is mainly absorbed by phototropin and cryptochrome, affecting plant photosynthesis, phototropism, and photoperiodism. Red light is mainly absorbed by phytochrome, influencing seed germination and flowering, along with seedling morphogenesis and photosynthesis [8]. Goins et al. [9] found that red LED light caused less main stem development but longer main stem length during wheat vegetative growth than white light, while red LED light supplemented with some blue light helped produce larger plants and more grains at harvest. Liu et al. [10] treated 'Miaoxiang 7' strawberry with red light and found enhanced photosynthesis in the leaves and high soluble solids and vitamin C in the fruits. Li et al. [11] found that red/blue (3:1) light proved to significantly increase the net photosynthetic rate, gas exchange, photosynthetic electron transfer capacity, photochemical efficiency, and aboveground and root biomass accumulation in pepper seedlings compared with white light. Chrysanthemums exposed to blue and far red light demonstrated a longer internode length than those exposed to red light [12], probably due to the fact that red light significantly affects photosynthesis through generating more chlorophylls but simultaneously inhibiting carbohydrates from moving out of source organs, specifically leaves [13,14]. In the context of physiological development, the application of red light promoted cell division and elongation, along with stem elongation [14,15]. Cultivated lily plants under exposure to a high percentage of red (80%) and blue light (20%) as background have been used as an effective way to promote extensive stem elongation [16]. While red light positively enhanced the K^+ uptake in cucumber and spinach [17,18], blue light hindered it. However, blue light enhanced the K^+ uptake in leek and garlic [19].

Under salt stress, different red/blue light ratios have been reported to affect gene expressions such as VvLhcs and light harvesting chlorophyll genes found in *Vitis vinifera* [19] and increase the aboveground biomass of lettuce. When red light is combined with blue, the bluer wavelength usually reduces lettuce plant growth, but, compared with dichromatic light, both blue and red light increases leaf size and epidermal cell area but reduces root dry mass, SPAD index, stomatal density, and leaf thickness [20]. In addition, changes in the ratio of red/far-red light can affect plant salt resistance by modulating the production of different physiological metabolites in plants [19,20]. Moreover, a pretreatment of red light has proven to promote the activity of antioxidant enzymes, accumulation of the biomass in healing tissues, and UV-A tolerance in lettuce photosynthetic cells [21–25]. In summary, red light plays an important role in plant growth and development, photosynthesis, maturation and senescence, fruit quality, and plant resistance to various stresses.

Legumes are economically important crops and pea sprouts are favored by consumers as fresh for their nutritional value and health benefits [26]. No study has been reported

on the salt tolerance of pea sprouts or seedlings through modulating lighting quality. Therefore, the aim of this experiment was to investigate the effect of LED red light on pea salt tolerance at its germination and seedling stages in a hydroponic system through investigating its growth and physiological parameters. The effect of red light on the salt tolerance of pea seedlings may shade some light on the potential impact of red light on the salt tolerance of mature pea plants or other field crops.

2. Results and Analyses

2.1. Effect of Salt Stress on Seed Germination

The germination rate of pea seeds with all treatments increased during the 3-day assessment. However, a higher salinity level seemed to hinder seed germination in the first two days, while there was no difference in the seed germination rate on the third day (Figure 1). Compared with CK, the germination rate of pea seeds with the 50 mmol/L and 100 mmol/L salt treatments was 31.1% and 48.7% on day 1, and 8.8% and 33.9% on day 2 post sowing, respectively. There was no significant difference in the germination rate between treatments (99.7%, 97.6%, and 96.0% respectively) on day 3 post sowing, suggesting that high salinity up to a 100 mmol/L level delayed seed germination but did not reduce the final germination rate in 3 days.

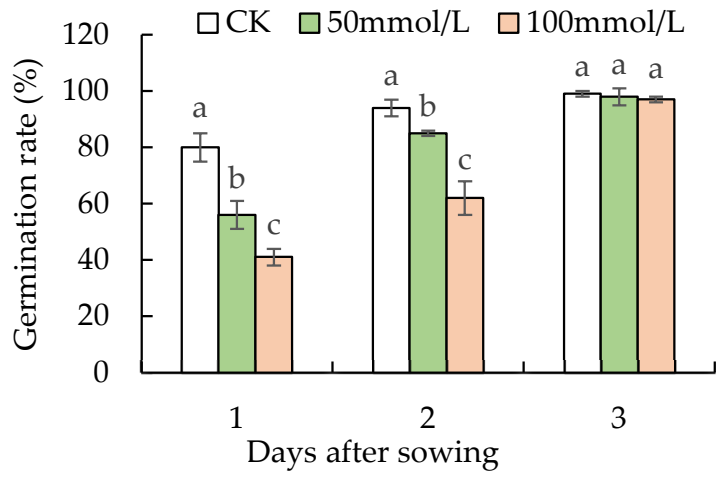

Figure 1. Seedling emergence under different concentrations of salt solutions. Different lowercase letters represent differences between treatments on the same day at the 0.05 level of significance.

2.2. Effect of Red Light on Aboveground Mass of Pea under Salt Stress

In the first 6 days after seed germination, under the same light conditions, the plant height of seedlings with the F1, F2, R1, and R2 treatments decreased by 42.82%, 58.42%, 36.57%, and 40.08%, respectively, compared with their corresponding F0 or R0 treatments (Figures 2 and 3a). Twelve days after seed germination, the plant height of these seedlings with the F1, F2, R1, and R2 treatments decreased by 67.09%, 78.14%, 50.86%, and 57.88%, respectively, compared with their CKs (F0 and R0). For the same salinity levels, the plant height of seedlings with the R0 treatment increased by 26.47% and 15.15% in 6 and 12 days after seed germination, respectively, compared with that of seedlings with the F0 treatment. There was no significant difference in the plant height of seedlings between the R1 and F1 treatments 6 days after germination. However, 12 days after seed germination, the plant height of seedlings with the R1 treatment increased by 47.73% compared with those with the F1 treatment. Also, at 6 and 12 days after seed germination, the plant height of seedlings with the R2 treatment increased by 34.62% and 93.75%, respectively, compared with that of the seedlings with the F2 treatment. Evidently, red light enhances the growth of pea seedlings whether there is salt stress or not compared with the control.

As shown in Figure 3b, the aboveground fresh mass of seedlings with the F1, F2, R1, and R2 treatments was 54.21%, 77.22%, 51.11%, and 60.79% lower than that of seedlings with the F0 or R0 treatment, respectively, under the same light conditions 6 days after seed germination. Twelve days after seed germination, the aboveground fresh mass of seedlings with the F1, F2, R1, and R2 treatments was 61.83%, 75.47%, 51.33%, and 52.12% lower than that of seedlings with the F0 or R0 treatment, respectively. For the same salinity levels, there was no significant difference in the aboveground fresh mass of seedlings between the R0 and F0 treatment at both 6 and 12 days after seed germination. However, the aboveground fresh mass of seedlings with the R1 treatment increased by 33.70% and 24.37%, respectively, compared with that of seedlings with the F1 treatment. And the aboveground fresh mass of seedlings with the R2 treatment increased by 15.91% and 56.70%, respectively, compared with that of seedlings with the F2 treatment. It was evident that, in the absence of salt stress, red light did not change the aboveground fresh mass. But, when pea seedlings were under salt stress, the redlight treatment was more effective than red/blue light in increasing the aboveground fresh mass of pea seedlings.

Under the same light conditions, the aboveground dry mass of pea seedlings with the F1, F2, R1, and R2 treatments decreased by 49.32%, 72.97%, 50.00%, and 64.56%, respectively, 6 days after seed germination compared with that of seedlings with their respective F0 or R0 treatments. Twelve days after germination, the aboveground dry mass of F1 and F2 treatments decreased by 60.26% and 75.17%, respectively, and that of R1 and R2 treatments decreased by 43.70% and 49.61%, respectively, compared with that of F0 (Figure 3c). Also, at 12 days after germination, the aboveground dry mass of F1 and F2 treatments decreased by 60.26% and 75.17%, and that of R1 and R2 treatments decreased by 43.70% and 49.61%, respectively, compared with that of R0 treatment. For the same salinity levels, there was no significant difference in aboveground dry mass between R0 and F0 and R1 and F1 treatments at 6 days and 12 days after germination. However, at 12 days after germination, the aboveground dry mass of R2 treatment was 70.67% higher than that of F2, which was a significant increase. It can be seen that, under no/low salt stress, red light did not affect aboveground dry mass in the same way as the control, but, under high salt stress, red light treatment promoted an increase in aboveground dry mass in comparison with the control.

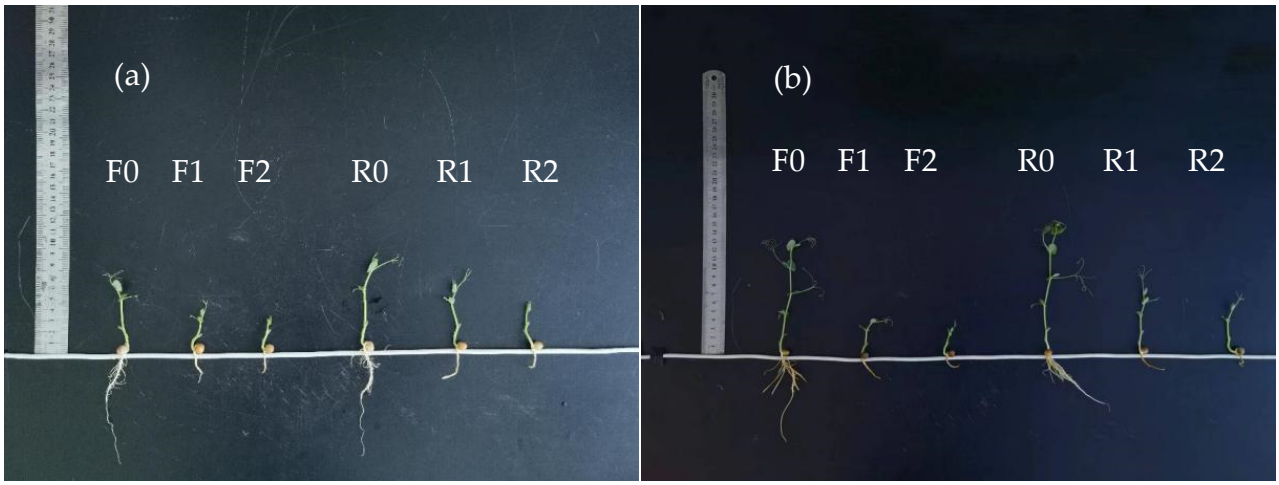

Figure 2. Growth of pea seedlings under different light quality and salt stress at 6 days after germination (**a**) and 12 days after germination (**b**).

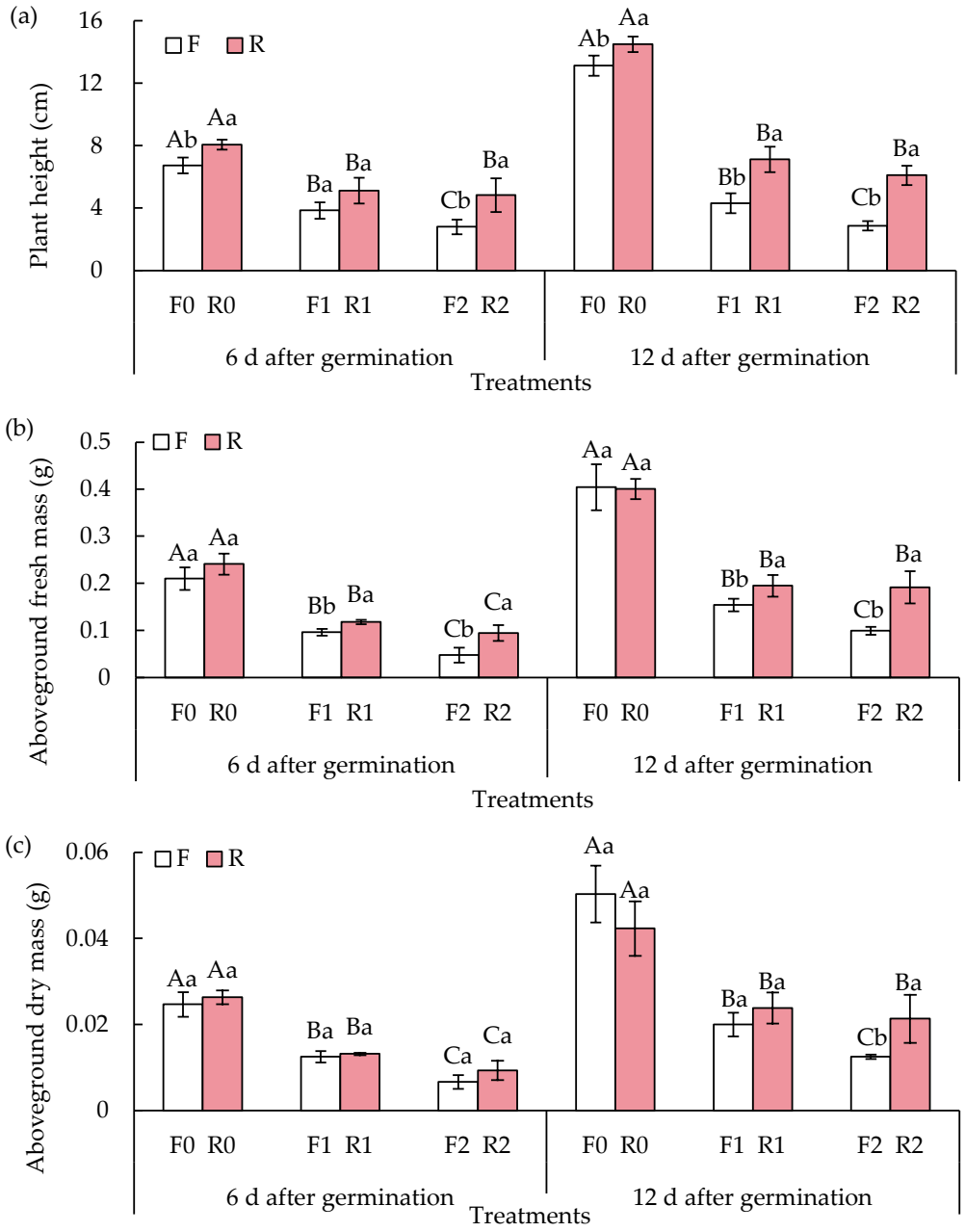

Figure 3. Evaluation of aboveground growth of pea seedlings: (**a**) plant height, (**b**) aboveground fresh mass, (**c**) aboveground dry mass with different treatments. Different uppercase letters indicate significant differences in different salt concentrations of the same light quality ($p < 0.05$), and different lowercase letters indicate significant differences in different light qualities of the same salt concentration ($p < 0.05$).

2.3. Effect of Red Light on Root Growth of Pea Seedlings Under Salt Stress

Table 1 presents the total root length (cm), total root surface area (cm^2), total root volume (cm^3), average root diameter (mm), and root fresh/dry weight (g) of pea. For the total root length, under the same light quality, at 6 d after germination, it was reduced by 84.35% and 85.00% in F1 and F2 treatments compared with F0 treatment, respectively, and was reduced by 73.09% and 82.01% in R1 and R2 treatments compared with R0 treatment, respectively. At 12 d after germination, the total root length in F1 and F2 treatments was 88.08% and 89.11% lower compared with F0 treatment, respectively, while that of R1 and R2 treatments was reduced by 81.48% and 87.85% compared with R0 treatment, respectively. Under the same salt treatments, there was no significant difference in total root length

between R0 and F0 treatments at 6 d and 12 d after germination. However, the total root length of R1 treatment increased significantly by 57.66% and 65.53% over F1 treatment at 6 d and 12 d after germination, respectively, and R2 treatment had no significant difference in total root length compared with F2 treatment. This indicates that the redlight treatment favored the increase in total root length to some extent under light salt stress compared with the control.

Table 1. Comparison of growth parameters of pea roots on different days between various light and salinity treatments.

Days After Sowing (d)	Treatments	Total Root Length (cm)	Total Root Surface Area (cm^2)	Total Root Volume (cm^3)	Average Root Diameter (mm)	Root Dry Mass (g)
6	F0	58.00 ± 12.84 Aa	9.83 ± 1.21 Aa	0.134 ± 0.016 Aa	0.547 ± 0.022 Aa	0.017 ± 0.002 Ba
	F1	9.08 ± 0.72 Bb	1.22 ± 0.15 Bb	0.013 ± 0.002 Bb	0.428 ± 0.009 Bb	0.006 ± 0.001 Ba
	F2	8.70 ± 0.24 Ba	1.16 ± 0.12 Bb	0.012 ± 0.002 Bb	0.425 ± 0.011 Ba	0.004 ± 0.001 Cb
	R0	53.19 ± 14.55 Aa	8.38 ± 2.45 Aa	0.105 ± 0.033 Aa	0.500 ± 0.004 Aa	0.018 ± 0.002 Aa
	R1	14.31 ± 2.01 Ba	2.04 ± 0.34 Ba	0.023 ± 0.005 Ba	0.463 ± 0.013 Ba	0.005 ± 0.001 Ba
	R2	9.57 ± 0.53 Ba	1.40 ± 0.05 Ca	0.017 ± 0.001 Ba	0.44 ± 0.009 Ba	0.005 ± 0.001 Ca
12	F0	85.72 ± 7.99 Aa	15.05 ± 1.38 Aa	0.210 ± 0.020 Aa	0.559 ± 0.005 Aa	0.027 ± 0.003 Aa
	F1	10.22 ± 0.34 Bb	1.30 ± 0.19 Bb	0.013 ± 0.004 Ba	0.405 ± 0.023 Ba	0.009 ± 0.001 Ba
	F2	9.33 ± 0.59 Ba	1.05 ± 0.14 Ba	0.010 ± 0.003 Ba	0.360 ± 0.017 Ca	0.003 ± 0.001 Ca
	R0	91.3 ± 19.19 Aa	15.62 ± 2.9 Aa	0.213 ± 0.037 Aa	0.548 ± 0.010 Aa	0.029 ± 0.001 Aa
	R1	16.91 ± 2.09 Ba	1.73 ± 0.13 Ba	0.014 ± 0.002 Ba	0.328 ± 0.012 Ba	0.007 ± 0.001 Ba
	R2	11.09 ± 0.73 Ca	1.10 ± 0.15 Ca	0.009 ± 0.002 Ca	0.316 ± 0.011 Ba	0.006 ± 0.001 Ba

Note: Different uppercase letters indicate significant differences in different salt concentrations of the same light quality ($p < 0.05$), and different lowercase letters indicate significant differences in different light qualities of the same salt concentration ($p < 0.05$).

Regarding the total root surface area, under the same light quality, at 6 d after germination, that of F1 and F2 treatments was 87.55% and 88.16% lower than that of the F0 treatment, respectively; that of R1 and R2 treatments was 75.59% and 83.24% lower than that of the R0 treatment, respectively. Under the same salt treatments, there was no significant difference in total root surface area between R0 and F0 treatments at 6 d and 12 d after germination. The total root surface area of R1 treatment increased significantly by 67.11% and 33.29% over F1 treatment at 6 d and 12 d after germination, respectively. At 6 d after germination, the total root surface area of R2 treatment increased by 20.63% compared with F2 treatment, which was a significant increase, but, at 12 d after germination, the difference between R2 and F2 treatments was not significant. It suggests that the red light treatment favored the increase in total root surface area under salt stress compared with the control.

In terms of the total root volume, under the same light quality, at 6 d after germination, the total root volume of F1 and F2 treatments was reduced by 90.13% and 90.71%, respectively, and that of R1 and R2 treatments was reduced by 77.78% and 84.13%, respectively, compared with the R0 treatment. At 12 d after germination, it was reduced by 93.60% and 95.45% in F1 and F2 treatments, respectively, and by 93.38% and 95.88% in R1 and R2 treatments, respectively, compared with F0 treatment. Under the same salt treatment, there was no significant difference in total root volume between the R0 and F0 treatments at 6 d and 12 d after germination. At 6 d after germination, the total root volume of the R1 treatment increased by 76.47% over the F1 treatment, which was a significant increase, while, at 12 d after germination, the differences between R1 and F1 treatments were not significant. At 6 d after germination, the total root volume of R2 treatment increased significantly by 33.93% compared with F2 treatment, and, at 12 d after germination, the difference between R2 and F2 treatments was not significant. It indicates that the red light treatment favored the increase in total root volume under salt stress compared with the control.

Concerning the average root diameter, under the same light quality, at 6 d after germination, the average root diameter of F1 and F2 treatments decreased by 21.80% and

22.29%, respectively, and that of R1 and R2 treatments decreased by 7.27% and 12.01%, respectively, compared with the R0 treatment. At 12 d after germination, the mean root diameters of the F1 and F2 treatments were reduced by 27.51% and 35.56%, respectively, and the mean root diameters of the R1 and R2 treatments were reduced by 40.17% and 42.24%, respectively, compared with the R0 treatment. Under the same salt stress, at 6 d after germination, the average root diameter of R1 increased significantly by 8.26% over that of F1 treatment, while, at 6 d and 12 d after germination, the differences between R0 and F0 and R2 and F2 treatments were not significant. It suggests that the red light treatment under light salt stress favored the increase in mean root diameter to some extent compared with the control.

For the root dry mass, under the same light quality, at 6 d after germination, the root dry mass of the F1 and F2 treatments was reduced by 64.36% and 76.24%, respectively, and that of the R1 and R2 treatments was reduced by 73.58% compared with that of the R0 treatment. At 12 d after germination, the root dry mass of the F1 and F2 treatments was reduced by 67.68 g and 87.80 g, respectively, compared with the F0 treatment, and the root dry mass of the R1 and R2 treatments was reduced by 75.86 g and 79.31 g, respectively, compared with the R0 treatment. At 12 d after germination under the same salt stress, there was no significant difference in root dry mass between R0 and F0 treatments and between R1 and F1 treatments, whereas R2 showed a significant increase of 100.00% in root dry mass over F2. This indicates that prolonged exposure to red light reduces the reduction in the dry mass of pea roots by salt stress compared with the control light under high salt stress.

2.4. Effect of Red Light on Chlorophyll Content of Pea Under Salt Stress

The chlorophyll content of hemp pea under salt stress in the control red and blue light treatments versus the red light treatments is evidently shown in Figure 4. With the same light quality, compared with the F0 treatment, the chlorophyll content of the F1 and F2 treatments was reduced by 34.32% and 69.77%, respectively. Compared with the R0 treatment, the chlorophyll content of the R1 and R2 treatments was reduced by 28.40% and 39.56%, respectively. Under the same salt stress, there was no significant difference in chlorophyll content between the R0 and F0 treatments. The chlorophyll content of the R1 treatment increased by 17.06% over the F1 treatment, and the chlorophyll content of the R2 treatment increased by 114.66% compared with the F2 treatment, with a significant increase. It indicates that the red light treatment promotes the increase in chlorophyll content in hemp pea under salt stress more than the control.

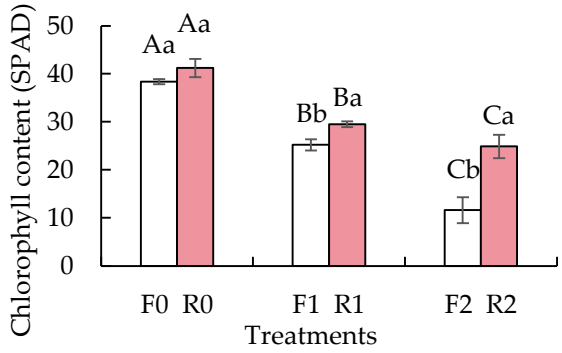

Figure 4. The chlorophyll content of pea seedlings between different light and salinity treatments on the 12th day after sowing. Different uppercase letters indicate significant differences in different salt concentrations of the same light quality ($p < 0.05$), and different lowercase letters indicate significant differences in different light qualities of the same salt concentration ($p < 0.05$).

2.5. Effect of Red Light on Antioxidant Enzyme Activities of Pea Seedlings Under Salt Stress

The MDA content and activities of SOD, POD, and CAT enzymes in the leaves of pea seedlings significantly increased with the salinity level in the hydroponic solution (Figure 5). Under the same salinity level, the MDA content in leaves with the R2 treatment was 14.16% less than that in the F2 treatment, but no such significant differences were observed between the R0 and F0 treatments, or between the R1 and F1 treatments. A significantly reduced SOD enzyme activity (by 34.76% and 26.83%) was detected in leaves with the R0 and R2 treatments, but not with R1. The POD enzyme activity significantly increased in leaves with both R1 and R2 treatments (by 73.53% and 157.78%, respectively, $p < 0.05$). There was no significant difference in the CAT enzyme activity in leaves with the two light quality treatments. Since SOD and POD enzymes are relatively sensitive to light quality, the salt-stressed pea seedlings illuminated by red light tended to reduce the MDA content and SOD enzyme activity but increased the POD enzyme activity significantly in comparison with those activities in the F treatments.

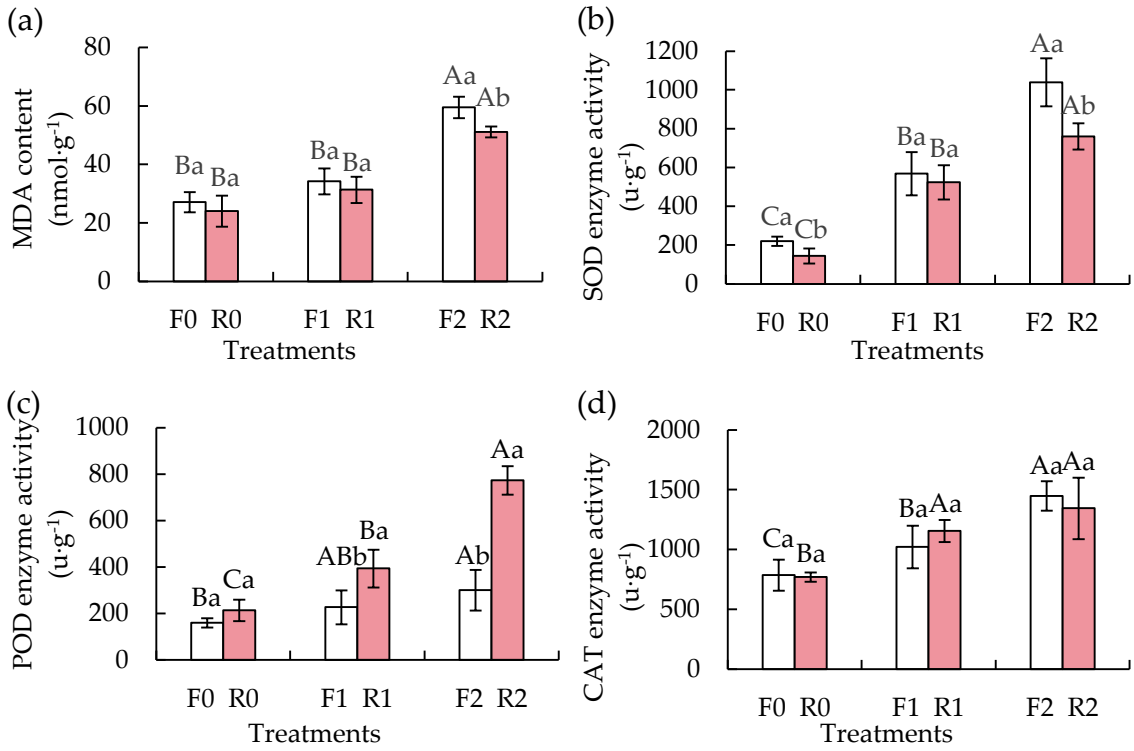

Figure 5. Evaluation of antioxidant enzyme activities: (**a**) malondialdehyde (MDA) content, (**b**) superoxide dismutase (SOD) activity, (**c**) peroxidase (POD) activity, and (**d**) catalase (CAT) activity in leaves of pea seedlings between different light and salinity treatments on the 12th day after sowing. Different uppercase letters indicate significant differences in different salt concentrations of the same light quality ($p < 0.05$), and different lowercase letters indicate significant differences in different light qualities of the same salt concentration ($p < 0.05$).

2.6. Effect of Red Light on the Electrolyte Leakage Rate in Pea Seedlings Under Salt Stress

Under the illumination of the same light quality, the leaf electrolyte leakage rate in seedlings with the F1 and F2 (compared with F0) and R1 and R2 (compared with R0) treatments increased by 44.30%, 116.17%, 10.46%, and 33.06%, respectively (Figure 6a). Under the same salinity level, no significant difference in the leaf electrolyte leakage rate was observed between R0 and F0, while a significantly reduced rate of 23.84% in R1 compared with F1 and of 38.76% in R2 compared with F2 was observed. Under the illumination of the same light quality, the stem electrolyte leakage rate in seedlings with

the F1 and F2 (compared with F0) and R1 and R2 (compared with R0) treatments increased by 53.06%, 108.58%, 37.89%, and 36.78%, respectively (Figure 6b). Under the same salinity level, no significant difference in the stem electrolyte leakage rate was observed between the R0 and F0 treatments or between the R1 and F1 treatments, while a significantly lower rate of 21.80% in R2 compared with F2 was observed. Under the illumination of the same light quality, the root electrolyte leakage rate in seedlings with the F1 and R1 treatments did not change significantly compared with their respective F0 and R0 treatments, but increased by 14.24% and 40.57% in roots with the F2 and R2 treatments compared with their respective F0 and R0 treatments (Figure 6c). There was no such significant difference in roots between R0 and F0, R1 and F1, and R2 and F2 treatments under the same salinity levels. Therefore, illumination with red light caused the electrolyte to leak less through the membranes in the leaves and stems of pea seedlings under salt stress.

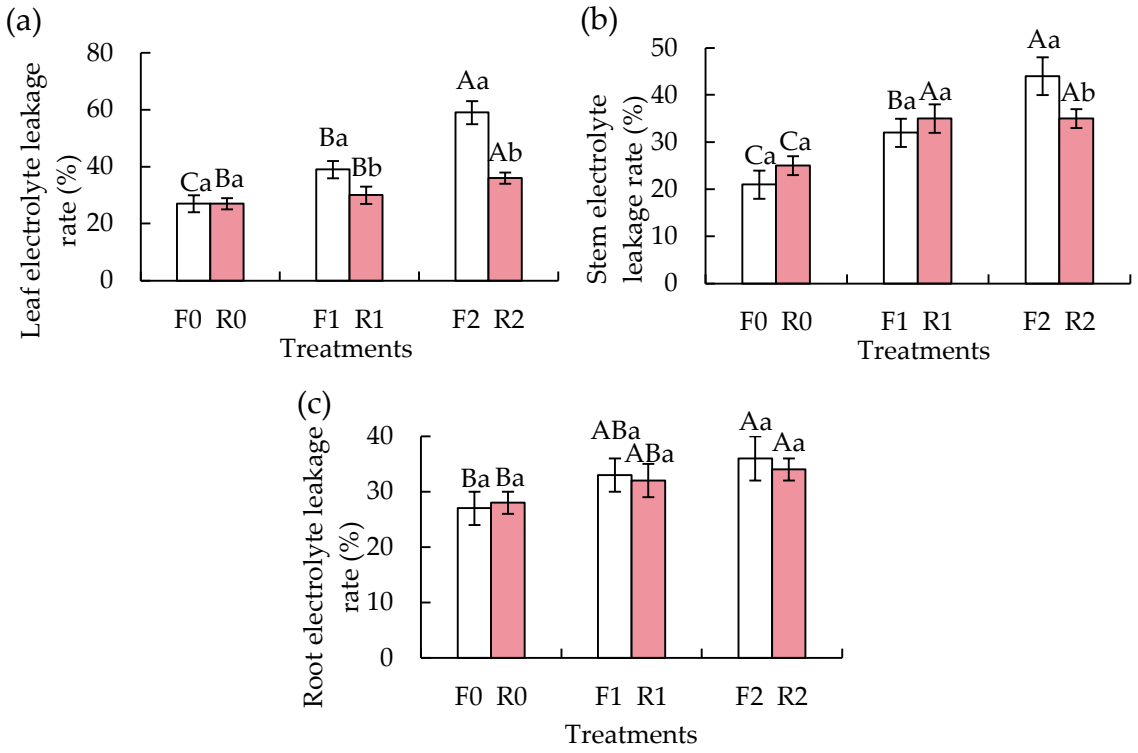

Figure 6. The electrolyte leakage rate of different parts of pea seedlings: (**a**) in leaves, (**b**) in stems, and (**c**) in roots between different light and salinity treatments on the 12th day after sowing. Different uppercase letters indicate significant differences in different salt concentrations of the same light quality ($p < 0.05$), and different lowercase letters indicate significant differences in different light qualities of the same salt concentration ($p < 0.05$).

2.7. Effect of Red Light on the K^+ and Na^+ Content and K^+/Na^+ Ratio in Pea Seedlings Under Salt Stress

Under the illumination of the same light quality, the K^+ content decreased by 29.99%, 35.48%, 11.09%, and 18.54% in seedlings with the F1 and F2 (compared with F0) and R1 and R2 (compared with R0) treatments, respectively (Figure 7a). Meanwhile, under the same salt stress, the K^+ content in seedlings with the R0, R1, and R2 increased significantly by 15.22%, 46.32%, and 45.47%, compared with their respective F0, F1, and F2 treatments, respectively. Under the illumination of the same light quality, the Na^+ content in seedlings with the F1, F2, R1, and R2 treatments increased by 1668.39%, 2897.81%, 1889.01%, and 2773.05%, respectively, compared with their respective F0 or R0 treatments (Figure 7b). There was no significant difference in the Na^+ content in seedlings when comparing the R0 to F0 and R1 to F1 treatments. However, seedlings with the R2 treatment showed a

significant reduction of 14.28% in the Na^+ content compared with the F2 treatment. In terms of the K^+/Na^+ ratio, there were significant reductions of 96.04% and 97.85% in seedlings with F1 and F2 (compared with F0), and of 95.53% and 97.16% in seedlings with R1 and R2 (compared with R0) under the illumination of the same light quality (Figure 7c). Meanwhile, there were such significant differences of 28.82%, 45.45%, and 69.70% increases in seedlings when comparing the R0 to F0, R1 to F1, and R2 to F2 treatments, respectively. It was evident that red light increased the K^+ content and the K^+/Na^+ ratio in pea seedlings with or without salt stress but reduced the Na^+ content in seedlings under severe salt stress.

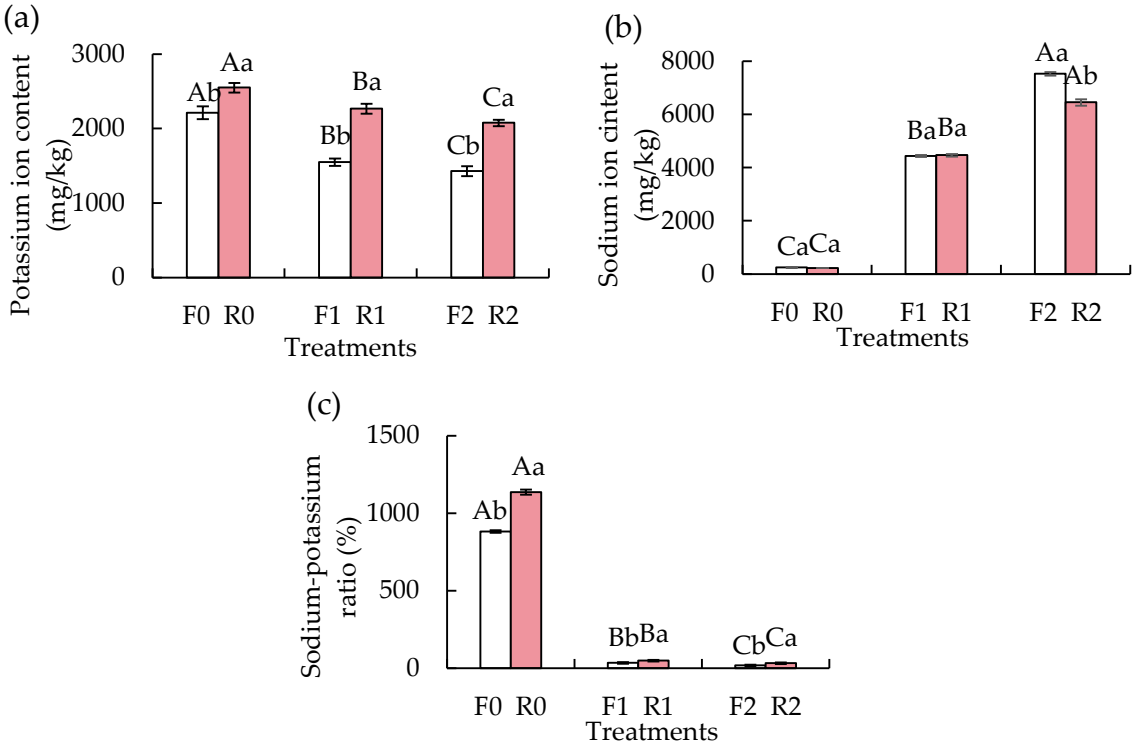

Figure 7. Effect of different lights and salinity levels on the K^+ (**a**) and Na^+ (**b**) content and K^+/Na^+ ratio (**c**) of pea seedlings on the 12th day after sowing. Different uppercase letters indicate significant differences in different salt concentrations of the same light quality ($p < 0.05$), and different lowercase letters indicate significant differences in different light qualities of the same salt concentration ($p < 0.05$).

3. Discussion

3.1. The Impact of Salt Stress on Crops

Salt stress is an inevitable constraint that the environment imposes on crop production, agricultural development, and ecological conservation, which negatively affects plant growth, development, and reproduction [27]. Our data analysis demonstrated that the process of the pea seed germination was delayed at first under salt stress, but, 3 days after sowing, the final germination rate did not change significantly, suggesting that salt-stressed pea seeds absorbed less water first due to osmotic stress but quickly adjusted to tolerate an unlethal salinity (<100 mmol/L) in their final germination, which was basically consistent with the results reported by Ya et al. [28].

3.2. The Role of Light Quality in Plant Growth and Development

The light environment is crucial for plant growth and development as it influences morphological adjustment, photosynthesis, morphogenesis, root development, metabolisms, photoperiod modulation, and gene expression in plants [29]. Light quality, being one of the

core constituents of the light environment and the most significant technical parameter in supplementary light for facility crops, has always drawn attention. Different wavelengths of light possess different levels of energy, which can impact plant growth and development by modulating photoreceptors, transcription factors, and plant hormones [16,17]. Light quality is capable of affecting the antioxidant capacity of crops, regulating carbon and nitrogen metabolism, and enabling crops to adapt to various abiotic stress environments [18,19]. Among them, red and blue light are most essential in promoting photosynthetic efficiency [30–32]. The illustration of mechanisms involved in sensing quality and intensity of red, blue, or both bended lights by pea seedlings to affect the growth, development, and metabolism is demonstrated in Figure 8.

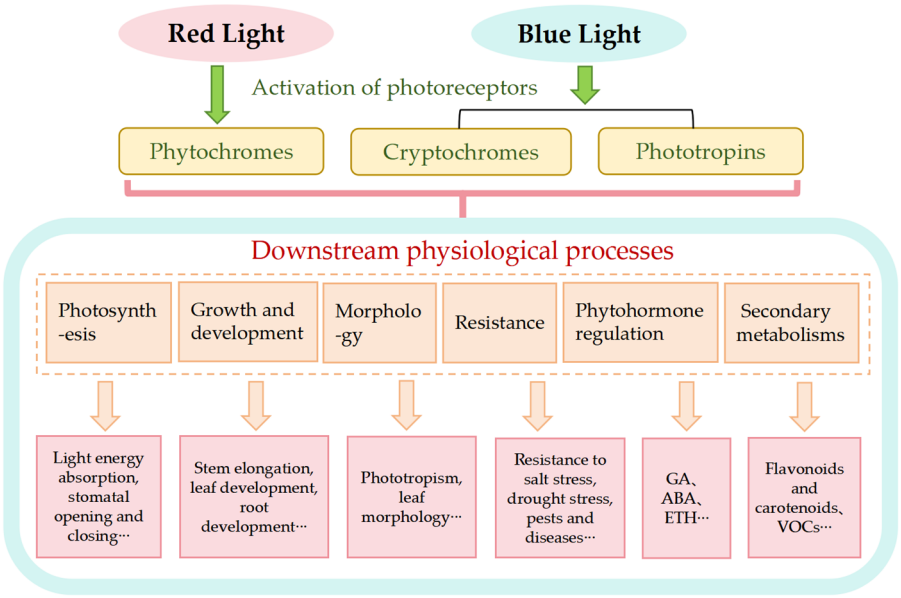

Figure 8. The effect of the quality of red and blue lights on the growth, development, and metabolisms of hydroponically cultivated pea seedlings.

In this experiment, red light has proven to be more effective than red/blue (4:1) light in enhancing the growth and height of normal pea seedlings. However, neither of the two lights significantly affected the aboveground fresh/dry mass, chlorophyll content, or root growth indexes, which is basically in agreement with the findings on the effect of red light on tomato growth reported by Mansoori et al. [33]. Under the same salt stress, both growth rate and fresh mass of pea seedlings with the red light treatment were greater than those of seedlings with the red/blue (4:1) light treatment, while the dry matter mass of pea seedlings under the illumination of red light was significantly greater than that of seedlings under the illumination of red/blue (4:1) light treatments only on day 12 with the highest salinity level (100 mmol/L). Red light shows a less inhibitory effect on root growth and development whether under salt stress or not and significantly increases the chlorophyll content of seedlings at different salt stress levels. The difference of growth parameters measured between two different treatments of light quality may be due to the variations of physiological and biochemical levels in response to different light quality acquired by photoreceptors in plants [34,35]. It is generally considered that red light either enhances the tolerance of pea seedlings against salt stress or makes them more sensitive to light quality by promoting the chlorophyll synthesis catalyzed by increased enzyme activities, reducing osmotic damages to cell membranes, improving photosynthetic efficiency, and initiating more dry matter accumulation [7].

3.3. The Situation Related to Antioxidant Enzymes

Abiotic stresses disrupt the balance between ROS production and its elimination, likely resulting in an excessive accumulation of ROS and ultimately leading to oxidative stress [36]. MDA is an oxidative end product of the free radical-induced lipid peroxidation and can indirectly reflect the intensity of oxidative stress [37]. SOD, POD, and CAT are essential antioxidant enzymes that remove excess ROS [38].

Many studies have demonstrated that the activities and efficiencies of antioxidant enzymes in response to abiotic stresses in plants vary depending on the ratio of red to blue light, plant species, genotype, and stages of plant growth and development [39–41]. In this study, all leaves of pea seedlings showed an increasing trend in the SOD, POD, and CAT activities and the MDA content as salt stress intensified. However, the antioxidant enzyme activity demonstrated some variation in seedlings under different lights, in which SOD and POD enzymes showed higher activities and were more responsive to light quality. Under the same salt stress, the SOD activity and MDA content of the red light treatment were lower than those of the seedlings illuminated by red/blue (4:1) light, suggesting that the lack of blue light was unfavorable to increasing the SOD activity, which could be a consequence of lower superoxide production [42,43]. Additionally, the POD activity of pea seedlings illuminated by red light was greater than that of seedlings illuminated by red/blue (4:1) light, which is consistent with the previous findings on the effect of light on antioxidant enzyme activities [44,45]. It is evident that there are certain synergies and antagonisms between various physiological metabolisms in pea seedlings under salt stress. Under illumination by red light, the changes in SOD and POD activities showed an opposite trend, likely due to a delayed signaling transduction in plants or other interfering factors involved in the complexity of the enzymatic activities or diversified responses of plants to oxidative stress and complex regulatory networks [46]. POD and SOD enzyme sensitivity to a certain type of illumination may be due to the fact that light signal pathways can modulate gene expression and secondary signal pathways, adjust synthesis and breakdown of enzymes participating in light-effecting metabolisms, and affect their efficacies [47–51].

3.4. The Situation Related to Ionic Balance

Under NaCl-generated salt stress, the increase in Na^+ accumulation and decrease in K^+ uptake by plants break the balance of interior ions, causing ionic toxicity and nutrient deficits in plants, and ultimately affecting plant growth and development [52,53]. The results derived from this experiment demonstrated that red light illumination was favorable to the increase in K^+ content and decrease in Na^+ content, which indicated that a high proportion of red light was required to promote the uptake of K^+ by plant cells, reduce the uptake of Na^+, and increase the K^+-Na^+ ratio in order to alleviate the inhibitory effect of ionic imbalance caused by salt stress on the growth of pea seedlings. In addition, salt stress increases the electrolyte leakage rate [54], which can be mitigated by red light illumination on pea seedlings under salt stress, suggesting that red light could alleviate the oxidative damage to cell membranes through reducing the electrolyte leakage rate in pea seedlings.

Light intensity can affect the salt tolerance of crops. When the light intensity is less than 500 $\mu mol/m^2/s$, it is considered to be relatively low for some plants such as peas [55]. Above that light intensity level, a relatively higher light intensity is conducive to increasing the photosynthetic rate of plants and then alleviating the damage caused by salt stress to plants through various physiological pathways such as increasing the synthesis of osmotic regulatory substances, etc. [56]. Therefore, we believe that the slight difference between the light intensity of the two lamps (390.2 $\mu mol/m^2/s$ and 324.8 $\mu mol/m^2/s$, respectively) we used did not affect the results at all at such a low intensity. In the future, research on the

optimal combination of light quality and light intensity for improving the salt tolerance of plants should be further explored.

4. Materials and Methods

4.1. Materials

Pea seeds were soaked and germinated and their sprouts were planted in 30 cm × 22 cm × 3.5 cm trays and placed on a 4-shelf rack (40 cm high, 100 cm long, and 50 cm wide). Spectra outputs from the various basal lamp/filter combinations were recorded with a calibrated spectroradiometer (LI-COR 1800, Lincoln, NE, USA) placed horizontally in the cabinets used for the experiments, with the sensor covered by the glass lid of the vessel. Different light treatments and salt treatments were carried out at the same time. Four LED light tubes were fixed on the top of each shelf (four lamps per layer) and the whole rack was fully covered with black cloth. The test lighting spectrum was set up with two LED light sources at a 4:1 ratio of red/blue and red light with a photosynthetic active radiation of 390.2 μmol/m^2/s and 324.8 μmol/m^2/s (T8 36W Grow Light, Beijing Yasheng Zengguang Physical Agricultural Technology Development Co., Ltd., Beijing, China), and the light intensity of 2740 Lx and 2270 Lx, respectively (Figure 9).

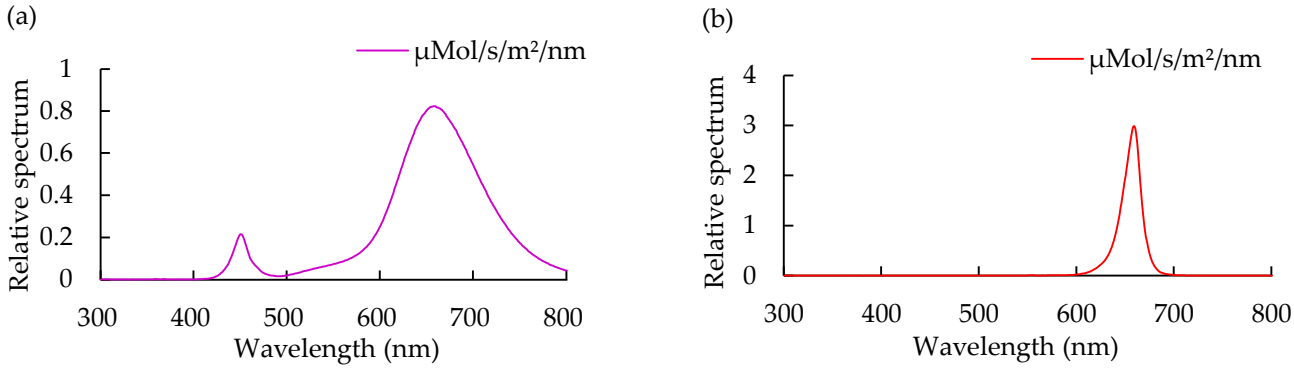

Figure 9. Spectral distribution of red/blue lighting (**a**) and red lighting (**b**).

4.2. Methods

The pea variety 'Green Valley Pea No.2' was purchased from Beijing Green Valley Sprouts Co., Ltd., Beijing, China). Pea seeds were soaked in distilled water for 10 h, then placed in Petri dishes with filter paper moistened with 0, 50, and 100 mmol/L NaCl hydroponic solution, with 25 seeds in each Petri dish, and 10 Petri dishes under each concentration gradient, for a total of 750 seeds. The seeds were placed in a shaded environment for germination. The germination percentage of each treatment was counted at 1, 2, and 3 d after sowing.

$$\text{Germination rate (\%)} = \text{number of seeds germinated/total seeds used} \times 100\% \quad (1)$$

To test the salt stress-mitigating effect of red light on pea seedlings, germinated seeds were transplanted in hydroponic cases composed of a plastic box with an internal plastic grid that was illuminated with red/blue lights or red light. Three NaCl solutions at a concentration of 0 (CK), 50, or 100 mmol/L were used for hydroponic cultivation under two light treatments. Each treatment of lighting and salinity combination was replicated three times, with 125 seeds in each of them. Seedlings cultivated in hydroponic cases in the fresh nutrient solution were watered with 0, 50, or 100 mmol/L NaCl solution, respectively, illuminated for 12 h, and kept in the dark for 12 h at 25 ± 1 °C throughout the whole experiment. The hydroponic cases with various light treatments were placed randomly on

the shelves in a density to avoid any possible shading. Lighting tubes were anchored 36 cm above the hydroponic cases. Since the red/blue light at a 4:1 ratio has been regularly used as a supplemental light for leafy vegetables, it was chosen for the three salinity levels as the control groups designated as F0, F1, and F2, while red light in combination with three salinity levels were grouped as R0, R1, and R2.

Morphological parameters such as plant height, plant fresh mass and dry mass, and root characters were measured at 6 and 12 days after seed germination. Five seedlings per treatment were measured with a ruler for their height each time, then separated into their aboveground part and roots, and weighed respectively for their fresh mass using an electronic balance (with an accuracy of ~0.01 g). To obtain their dry mass, both the aboveground part and roots were dried in an oven at 105 °C for 30 min and then kept at 75 °C until they were completely dry. Finally, they were weighed using an electronic balance with an accuracy of 0.0001 g. Fresh root samples were scanned by a root scanner (EPSON EXPRESSION 10000 XL, Epson (Beijing, China) Co., Ltd., Beijing, China), and then analyzed using a root analysis system (WinRHIZO STD4800 LA2400, Regent Co., Ltd., Toronto, ON, Canada), for total root length (cm), total root surface area (cm^2), total root volume (cm^3), and average diameter of the roots (mm).

Physiological parameters of pea seedlings under each treatment were investigated on the 12th day after sowing. The SPAD value of the 3rd and 4th unfolded leaves at the top of each seedling was measured with a chlorophyll meter to determine the chlorophyll content (TYS-4N Handheld Chlorophyll Analyzer, Beijing Zhongke Weihe Technology Development Co., Ltd., Beijing, China). The content of K^+ and Na^+ ions was measured with the flame photometric method. The rate of electrolyte leakage used to indicate the permeability and the degree of damage to cell membranes was determined by the protocol described by Dionisio-Sese et al. [57]. Leaves of pea seedlings were sampled, rinsed with tap water, and dried by filter paper. Then, 0.3 g of a sample leaf was cut into small pieces, emerged in deionized water in a 25 mL testing tube, and soaked for 3 h to measure the first EC (EC_1) using a conductivity meter (Thunder Magnetic DDS-307A, Shanghai Yidian Scientific Instrument Co., Ltd., Shanghai, China). The second EC (EC_2) was determined after the leaf sample in the testing tube was boiled for 30 min and cooled to room temperature. The permeability rate was calculated by EC (%) = $EC_1/EC_2 \times 100\%$. The third unfolded true leaves below the growing tip of all remaining seedlings under each treatment were cut and mixed to determine antioxidant enzymatic activities of superoxide dismutase (SOD), peroxidase (POD), catalase (CAT), and malondialdehyde (MDA). SOD, POD, CAT, and MDA were determined using the SOD (SOD-2-Y), POD (POD-2-Y), CAT (CAT-2-Y), or MDA (MDA-2-Y) detection kit, respectively (Comin Biotechnology Co., Ltd. Suzhou, China) [58]. Briefly, leaf samples maintained under −80 °C were ground with liquid nitrogen. In the Na_2HPO_4/NaH_2PO_4 buffer, SOD, POD, CAT, and MDA were extracted by homogenizing on ice (0.1 g leaf tissues for each SOD, POD, CAT, and MDA assay with 1 mL buffer). After the extraction of SOD, POD, CAT, and MDA, the homogenates were centrifuged at 8000× *g* at 4 °C for 10 min. For the pro assay, the homogenates were shaken in a boiling water bath (90 °C) for 10 min, cooled, and then centrifuged at 1000× *g* at 25 °C for 10 min.

SOD activity was determined by measuring its ability to inhibit the photochemical reduction of nitroblue tetrazolium (NBT) at 560 nm. One unit of SOD activity (U) was defined as the amount of enzyme that caused a 50% decrease in the SOD-inhibited NBT reduction. The reaction mixture consisted of 240 µL potassium phosphate buffer (K_2HPO_4/KH_2PO_4) plus ethylenediaminetetraacetic acid, 510 µL xanthine, 6 µL xanthine oxidase, and 180 µL NBT. Control and blank tubes were performed in the same manner but contained 90 µL supernatant and distilled water, respectively. In the control and blank tubes, the solu-

tions were mixed thoroughly and absorbance levels at 560 nm were determined using a spectrophotometer (752Pro UV-Vis Spectrophotometer, Lengguang Technology Co., Ltd., Shanghai, China). The results were expressed as units (U) of fresh weight (FW, U/g).

POD activity was determined by measuring the oxidation of guaiacol in the presence of hydrogen peroxide (H_2O_2) at 470 nm. One unit of POD activity (U) was defined as the amount of enzyme required to increase the absorbance at 470 nm by 0.01 per min per mL. The reaction mixture consisted of 15 μL supernatant, 270 μL distilled water, 520 μL sodium acetate and acetic acid, 130 μL H_2O_2, and 135 μL guaiacol. The reaction mixture was mixed immediately, and the increase in absorbance at 470 nm from 30 s (A_1) up to 1.5 min (A_2) was determined using a spectrophotometer. POD activity was calculated using the formula POD = 7133 × (A_2-A_1)/FW (U/g).

CAT activity was determined by the amount of H_2O_2 consumption at 240 nm. One unit of CAT activity (U) was defined as the amount of enzyme catalyzing the decomposition of 1 nmol of H_2O_2 per min. The reaction mixture consisted of 100 μL H_2O_2 and 20 mL sodium phosphate (Na_2HPO_4/NaH_2PO_4) buffer. A 35 μL aliquot of the supernatant was mixed thoroughly with 1 mL reaction mixture, and then the decrease in absorbance at 240 nm (A_1) up to 1 min (A_2) was determined using a spectrophotometer. CAT activity was calculated using the formula CAT = 678 × (A_1-A_2)/FW (U/g).

To measure MDA activity, the reaction mixture consisted of 0.6 mL trichloroacetic acid and thiobarbituric acid. A 0.2 mL aliquot of the supernatant was added and the sample was placed in a boiling water bath (90 °C) for 30 min. After cooling, the mixture was centrifuged at 10,000× *g* at 25 °C for 10 min. The absorbance levels of the supernatant at 532 nm (A532) and 600 nm (A600) were recorded and expressed as U/g FW. The MDA content was calculated using the formula MDA = 25.8 × (A532−A600)/FW (U/g).

4.3. Data Analysis

The experimental data were processed, analyzed, and plotted using EXCEL software. ANOVA and significance tests were performed using SPSS 17.0 data processing software with the LSD method.

5. Conclusions

Under salt stress, red light, compared with red/blue (4:1) light, significantly increased the height, aboveground fresh mass, aboveground dry mass, root growth indexes, chlorophyll content, POD enzyme activity, and K^+/Na^+ ratio in leaves, but decreased the MDA content, SOD enzyme activity, Na^+ content, and stem and leaf electrolyte leakage rate in pea seedlings. In summary, red light can be used to improve the salt tolerance of pea seedlings. The results may provide a theoretical basis for the use of light quality to regulate plant salt tolerance or enhance the tolerance of crop seedlings against abiotic stresses.

Author Contributions: The research presented here was carried out in collaboration between all authors. D.F. conceived the idea and designed this study; K.X. carried out the experiment and data analysis; K.X., Y.W., X.S. and H.Z. prepared the first draft of the manuscript; D.F., X.S., C.S. and W.X. revised the manuscript. All authors have read and agreed to the published version of the manuscript.

Funding: This study was supported by the "Tianshan Elite Scholars" program for innovative leading talents in science and technology (No. 2022TSYCLJ0039).

Data Availability Statement: Data are contained within the article.

Conflicts of Interest: The authors declare that they have no known competing financial interests or personal relationships that could have appeared to influence the work reported in this paper. The authors declare no conflict of interest.

References

1. Hu, T.; Zhang, G.; Zheng, F.; Cao, Y. Research progress in plant salt stress response. *Mol. Plant Breed.* **2018**, *16*, 006–3015.
2. Sun, H.; Wu, H.; Li, M.; Zhang, Q.; Han, Y.; Du, J. Effects of melatonin seed soaking on growth and physiological characteristics of kidney bean seedlings under salt stress. *J. Henan Agric. Sci.* **2021**, *50*, 111–120.
3. Afzal, M.; Hindawi, S.E.S.; Alghamdi, S.S.; Migdadi, H.H.; Khan, M.A.; Hasnain, M.U.; Arslan, M.; Habib ur Rahman, M.; Sohaib, M. Potential breeding strategies for improving salt tolerance in crop plants. *J. Plant Growth Regul.* **2023**, *42*, 3365–3387. [CrossRef]
4. Su, M.; Wei, X.; Han, T.; Ma, W.; Luo, Q. Effects of salt-tolerance exercise on survival rate and physiological characteristics of cherry tomato seedlings under salt stress. *North. Hortic.* **2019**, *2*, 8–14.
5. Gong, M.; Chen, B.; Li, Z.; Guo, L. Heat-shock-induced cross adaptation to heat, chilling, drought and salt stress in maize seedlings and involvement of H_2O_2. *J. Plant Physiol.* **2001**, *158*, 1125–1130. [CrossRef]
6. Feng, D.; Gao, Q.; Liu, J.; Tang, J.; Hua, Z.; Sun, X. Categories of exogenous substances and their effect on alleviation of plant salt stress. *Eur. J. Agron.* **2023**, *142*, 126656. [CrossRef]
7. Wang, Y.; Bian, Z.; Pan, T.; Cao, K.; Zou, Z. Improvement of tomato salt tolerance by the regulation of photosynthetic performance and antioxidant enzyme capacity under a low red to far-red light ratio. *Plant Physiol. Biochem.* **2021**, *167*, 806–815. [CrossRef] [PubMed]
8. Leivar, P.; Quail, P.H. PIFs: Pivotal components in a cellular signaling hub. *Trends Plant Sci.* **2011**, *16*, 19–28. [CrossRef]
9. Goins, G.D.; Yorio, N.C.; Sanwo, M.M.; Brown, C.S. Photomorphogenesis, photosynthesis, and seed yield of wheat plants grown under red light-emitting diodes (LEDs) with and without supplemental blue lighting. *J. Exp. Bot.* **1997**, *48*, 1407–1413. [CrossRef]
10. Liu, Q.; Lian, H.; Liu, S.; Sun, Y.; Yu, X.; Guo, H. Effects of different LED light qualities on photosynthetic characteristics, fruit production and quality of strawberry. *Chin. J. Appl. Ecol.* **2015**, *26*, 1743–1750.
11. Li, Y.; Xin, G.; Shi, Q.; Yang, F.; Wei, M. Response of photomorphogenesis and photosynthetic properties of sweet pepper seedlings exposed to mixed red and blue light. *Front. Plant Sci.* **2023**, *13*, 984051. [CrossRef] [PubMed]
12. Dierck, R.; Dhooghe, E.; Van Huylenbroeck, J.; Van Der Straeten, D.; De Keyser, E. Light quality regulates plant architecture in different genotypes of Chrysanthemum morifolium Ramat. *Sci. Hortic.* **2017**, *218*, 177–186. [CrossRef]
13. Bondada, B.R.; Syvertsen, J.P. Leaf chlorophyll, net gas exchange and chloroplast ultrastructure in citrus leaves of different nitrogen status. *Tree Physiol.* **2003**, *23*, 553–559. [CrossRef]
14. Dou, H.; Niu, G.; Gu, M.; Masabni, J.G. Effects of light quality on growth and phytonutrient accumulation of Herbs under controlled environments. *Horticulturae* **2017**, *3*, 36. [CrossRef]
15. Bugbee, B. Toward an optimal spectral quality for plant growth and development: The importance of radiation capture. In Proceedings of the VIII International Symposium on Light in Horticulture, East Lansing, MI, USA, 22–26 May 2016; Volume 1134, pp. 1–12.
16. Flores-Pérez, S.; Castillo-González, A.M.; Valdez-Aguilar, L.A.; Avítia-García, E. Use of different proportions of red and blue LEDs to improve the growth of *Lilium* spp. *Rev. Mex. Cienc. Agrícolas* **2021**, *12*, 835–847.
17. Xu, J.; Guo, Z.; Jiang, X.; Ahammed, G.J.; Zhou, Y. Light regulation of horticultural crop nutrient uptake and utilization. *Hortic. Plant J.* **2021**, *7*, 367–379. [CrossRef]
18. Miao, Y.; Chen, Q.; Qu, M.; Gao, L.; Hou, L. Blue light alleviates 'red light syndrome' by regulating chloroplast ultrastructure, photosynthetic traits and nutrient accumulation in cucumber plants. *Sci. Hortic.* **2019**, *257*, 108680. [CrossRef]
19. Wei, Y.; Lu, X.; Bao, J.; Zhang, C.; Yan, H.; Li, K.; Gong, M.; Li, S.; Ma, S. Identification and expression analysis of chlorophyll a/b binding protein gene family in grape (*Vitis vinifera*). *Physiol. Mol. Biol. Plants* **2022**, *28*, 1147–1158. [CrossRef]
20. Izzo, L.G.; Mickens, M.A.; Aronne, G.; Gómez, C.J.P.P. Spectral effects of blue and red light on growth, anatomy, and physiology of lettuce. *Physiol. Plant.* **2021**, *172*, 2191–2202. [CrossRef]
21. Kreslavski, V.D.; Lyubimov, V.Y.; Shirshikova, G.N.; Shmarev, A.N.; Kosobryukhov, A.A.; Schmitt, F.-J.; Friedrich, T.; Allakhverdiev, S.I. Preillumination of lettuce seedlings with red light enhances the resistance of photosynthetic apparatus to UV-A. *J. Photochem. Photobiol. B Biol.* **2013**, *122*, 1–6. [CrossRef]
22. Adil, M.; Abbasi, B.H.; ul Haq, I. Red light controlled callus morphogenetic patterns and secondary metabolites production in *Withania somnifera* L. *Biotechnol. Rep.* **2019**, *24*, e00380. [CrossRef] [PubMed]
23. Yu, Y.; Qin, W.; Li, Y.; Zhang, C.; Wang, Y.; Yang, Z.; Ge, X.; Li, F. Red light promotes cotton embryogenic callus formation by influencing endogenous hormones, polyamines and antioxidative enzyme activities. *Plant Growth Regul.* **2019**, *87*, 187–199. [CrossRef]
24. Manivannan, A.; Soundararajan, P.; Park, Y.G.; Wei, H.; Kim, S.H.; Jeong, B.R. Blue and red light-emitting diodes improve the growth and physiology of in vitro-grown carnations 'Green Beauty' and 'Purple Beauty'. *Hortic. Environ. Biotechnol.* **2017**, *58*, 12–20. [CrossRef]

25. Manivannan, A.; Soundararajan, P.; Halimah, N.; Ko, C.H.; Jeong, B.R. Blue LED light enhances growth, phytochemical contents, and antioxidant enzyme activities of *Rehmannia glutinosa* cultured in vitro. *Hortic. Environ. Biotechnol.* **2015**, *56*, 105–113. [CrossRef]
26. Yang, G.; Xu, J.; Xu, Y.; Guan, X.; Ramaswamy, H.S.; Lyng, J.G.; Li, R.; Wang, S. Recent developments in applications of physical fields for microbial decontamination and enhancing nutritional properties of germinated edible seeds and sprouts: A review. *Crit. Rev. Food Sci. Nutr.* **2024**, *64*, 12638–12669. [CrossRef] [PubMed]
27. Shilev, S. Plant-growth-promoting bacteria mitigating soil salinity stress in plants. *Appl. Sci.* **2020**, *10*, 7326. [CrossRef]
28. Ya, X.; Yang, D.; Zhou, G.; Chen, J.; Liu, Z. Identification and evaluation of salt tolerance of pea resources. *J. Sichuan Agric. Univ.* **2022**, *40*, 505–511.
29. Liu, Z.; Feng, D.; Xu, K.; Zhu, H.; Sun, X.; Zhang, J.; Yu, L.; Sang, X. Effect of blue light on the growth of tomato seedlings under salt stress. *China Cucurbits Veg.* **2023**, *36*, 126–131.
30. Zheng, L.; He, H.; Song, W. Application of light-emitting diodes and the effect of light quality on horticultural crops: A review. *HortScience* **2019**, *54*, 1656–1661. [CrossRef]
31. Li, Y.; Xin, G.; Liu, C.; Shi, Q.; Yang, F.; Wei, M. Effects of redand blue light on leaf anatomy, CO_2 assimilation and the photosynthetic electrontransport capacity of sweet pepper (*Capsicum annuum* L.) seedlings. *BMC Plant Biol.* **2020**, *20*, 1–16.
32. Jung, W.-S.; Chung, I.-M.; Hwang, M.H.; Kim, S.-H.; Yu, C.Y.; Ghimire, B.K. Application of light-emitting diodes for improving the nutritional quality and bioactive compound levels of some crops and medicinal plants. *Molecules* **2021**, *26*, 1477. [CrossRef] [PubMed]
33. Mansoori, M.; Wu, B.-S.; Addo, P.W.; MacPherson, S.; Lefsrud, M. Growth responses of tomato plants to different wavelength ratios of amber, red, and blue light. *Sci. Hortic.* **2023**, *322*, 112459. [CrossRef]
34. Zhang, L.; Chang, Q.; Guo, Q.; Hou, X.; Liu, L.; Zhu, Z.; Chen, S. Different light-quality colored films affect growth, photosynthesis, chloroplast ultrastructure, and triterpene acid accumulation in *Glechoma longituba* plants. *Photosynthetica* **2022**, *61*, 264–274. [CrossRef] [PubMed]
35. Kang, B.; Grancher, N.; Koyffmann, V.; Lardemer, D.; Burney, S.; Ahmad, M. Multiple interactions between cryptochrome and phototropin blue-light signalling pathways in *Arabidopsis thaliana*. *Planta* **2008**, *227*, 1091–1099. [CrossRef] [PubMed]
36. Gill, S.S.; Tuteja, N. Reactive oxygen species and antioxidant machinery in abiotic stress tolerance in crop plants. *Plant Physiol. Biochem.* **2010**, *8*, 16. [CrossRef] [PubMed]
37. Saleem, M.H.; Rehman, M.; Zahid, M.; Imran, M.; Xiang, W.; Liu, L. Morphological changes and antioxidative capacity of jute (*Corchorus capsularis*, Malvaceae) under different color light-emitting diodes. *Braz. J. Bot.* **2019**, *42*, 581–590. [CrossRef]
38. You, J.; Chan, Z. ROS regulation during abiotic stress responses in crop plants. *Front. Plant Sci.* **2015**, *6*, 165102. [CrossRef]
39. Choi, C.Y.; Kim, N.N.; Shin, H.S.; Park, H.G.; Cheon, S.G.; Kil, G.S. The effect of various wavelengths of light from light-emitting diodes on the antioxidant system of marine cyanobacteria, *Synechococcus* sp. *Mol. Cell. Toxicol.* **2013**, *9*, 295–302. [CrossRef]
40. Ye, S.; Shao, Q.; Xu, M.; Li, S.; Wu, M.; Tan, X.; Su, L. Effects of light quality on morphology, enzyme activities, and bioactive compound contentsin *Anoectochilus roxburghii*. *Front. Plant Sci.* **2017**, *8*, 857. [CrossRef] [PubMed]
41. Liu, Y.; Wang, T.; Fang, S.; Zhou, M.; Qin, J. Responses of morphology, gas exchange, photochemical activity of photosystem II, andantioxidant balance in *Cyclocarya paliurus* to light spectra. *Front. Plant Sci.* **2018**, *9*, 419445. [CrossRef]
42. Rehman, M.; Fahad, S.; Saleem, M.H.; Hafeez, M.; Rahman, M.U.; Liu, F.; Deng, G. Red light optimized physiological traits and enhanced the growth of ramie (*Boehmeria nivea* L.). *Photosynthetica* **2020**, *58*, 922–931. [CrossRef]
43. Cao, K.; Yu, J.; Xu, D.; Ai, K.; Bao, E.; Zou, Z. Exposure to lower red to far-red light ratios improve tomato tolerance to salt stress. *BMC Plant Biol.* **2018**, *18*, 1–12. [CrossRef]
44. Liang, Z.; Li, Q.; Xu, W. Effects of different light quality on growth, active ingredients and enzymes activities of *Salvia miltiorrhiza*. *China J. Chin. Mater. Medica* **2012**, *37*, 2055–2060.
45. Xu, H.; Fu, Y.; Li, T.; Wang, R. Effects of different LED light wavelengths on the resistance of tomato against *Botrytis cinerea* and the corresponding physiological mechanisms. *J. Integr. Agric.* **2017**, *16*, 106–114. [CrossRef]
46. Medina-Puche, L.; Lozano-Durán, R. Plasma membrane-to-organelle communication in plant stress signaling. *Curr. Opin. Plant Biol.* **2022**, *69*, 102269. [CrossRef]
47. Sun, Y.; Xu, W.; Jia, Y.; Wang, M.; Xia, G. The wheat TaGBF1 gene is involved in the blue-light response and salt tolerance. *Plant J.* **2015**, *84*, 1219–1230. [CrossRef] [PubMed]
48. Li, X.; Han, H.; Wei, Y.; Hu, T.; Qiang, W.; Wang, X.; Zhang, M. Phytochrome interacting factor 3 mediates low light signaling to regulate isorhynchophylline biosynthesis in *Uncaria rhynchophylla*. *Sci. Rep.* **2024**, *14*, 25032. [CrossRef] [PubMed]
49. Tian, T.; Hu, H.Y.; Ma, Y.S.; Qin, J.W.; Li, C.T.; Li, Y. Effects of light quality on agronomic traits, antioxidant capacity and nutritional composition of *Sarcomyxa edulis*. *Sci. Rep.* **2024**, *14*, 24762. [CrossRef]
50. Schmoll, M. Regulation of plant cell wall degradation by light in Trichoderma. *Fungal Biol. Biotechnol.* **2018**, *24*, 10. [CrossRef] [PubMed]

51. Gechev, T.; Willekens, H.; Van Montagu, M.; Inzé, D.; Van Camp, W.; Toneva, V.; Minkov, I. Different responses of tobacco antioxidant enzymes to light and chilling stress. *J. Plant Physiol.* **2003**, *160*, 509–515. [CrossRef]
52. Hassan, I.A. Interactive effects of salinity and ozone pollution on photosynthesis, stomatal conductance, growth, and assimilate partitioning of wheat (*Triticum aestivum* L.). *Photosynthetica* **2004**, *42*, 111–116. [CrossRef]
53. Qiu, L.; Wu, D.; Ali, S.; Cai, S.; Zhang, G. Evaluation of salinity tolerance and analysis of allelic function of HvHKT1 and HvHKT2 in Tibetan wild barley. *Theor. Appl. Genet.* **2011**, *122*, 695–703. [CrossRef]
54. Madani, S.M.; Piri, S.; Sedaghathoor, S. The response of three mandarin cultivars grafted on sour orange rootstock to salinity stress. *Int. J. Fruit Sci.* **2022**, *22*, 264–274. [CrossRef]
55. Zhang, Y.; Zheng, J.; Zhan, Y.; Yu, Z.; Liu, S.; Lu, S.; Li, Y.; Li, Z.; Liang, X.; Li, H.; et al. *GmPLP1* negatively regulates soybean resistance to high light stress by modulating photosynthetic capacity and reactive oxygen species accumulation in a blue lightdependent manner. *Plant Biotechnol. J.* **2023**, *21*, 2625–2640. [CrossRef] [PubMed]
56. Yang, J.; Qu, X.; Li, T.; Gao, Y.; Du, H.; Zheng, L.; Ji, M.; Zhang, P.; Zhang, Y.; Hu, J.; et al. HY5-HDA9 orches-trates the transcription of *HsfA2* to modulate salt stress responsein *Arabidopsis*. *J. Integr. Plant Biol.* **2023**, *65*, 45–63. [CrossRef]
57. Dionisio-Sese, M.L.; Tobita, S. Antioxidant responses of rice seedlings to salinity stress. *Plant Sci.* **1998**, *135*, 1–9. [CrossRef]
58. Pan, L.; Zhang, X.; Wang, J.; Ma, X.; Zhou, M.; Huang, L.; Nie, G.; Wang, P.; Yang, Z.; Li, J. Transcriptional profiles of drought-related genes in modulating metabolic processes and antioxidant defenses in *Lolium multiflorum*. *Front. Plant Sci.* **2016**, *7*, 1–15. [CrossRef] [PubMed]

horticulturae

MDPI

Article

Impact of Biochar and Hydroretentive Polymers on the Biochemical and Physiological Traits of *Satureja rechingeri* Jamzad Under Water Deficit Stress

Mojgan Beiranvandi [1], Nasser Akbari [1], Abdolreza Ahmadi [1,*], Hasan Mumivand [2], Farhad Nazarian Firouzabadi [1] and Sergio Argento [3]

[1] Department of Agroecology, Faculty of Agriculture, Lorestan University, Khorramabad P.O. Box 456, Iran; mojganbeiranvandi98@gmail.com (M.B.); akbari.n@lu.ac.ir (N.A.); nazarian.f@lu.ac.ir (F.N.F.)
[2] Department of Horticultural Science, Faculty of Agriculture, Lorestan University, Khorramabad P.O. Box 456, Iran; mumivand.h@lu.ac.ir
[3] National Research Council of Italy, Institute of Biomolecular Chemistry (CNR-ICB), Via P. Gaifami, 18, 95126 Catania, Italy; sergio.argento@cnr.it
* Correspondence: ahmadi.a@lu.ac.ir

Abstract: *Satureja rechingeri* is a valuable medicinal plant, but its growth can be significantly impacted by water deficit stress. To investigate the effects of biochar (BC) and hydroretentive polymers (HPs) on various eco-physiological traits of savory under a water deficit, an experiment was conducted over two consecutive cropping seasons (2017–2019). A randomized complete block design with a split-plot factorial arrangement and three replications was used. The treatments consisted of three levels of irrigation (95 ± 5, 75 ± 5, and 55 ± 5% FC), which were applied to the main plots, and combinations of two levels of biochar and two levels of HPs, which were applied to subplots. The results show that a water deficit reduced the relative water content (RWC), chlorophyll content, and dry matter yield of the shoots. Furthermore, the activity of catalase (CAT), peroxidase (POD), ascorbate peroxidase (APX), and malondialdehyde (MDA) increased in two-year-old plants. The MDA content significantly decreased by 15.6% in the second year compared to in the first year under a water deficit. The application of HPs caused a decrease of 26.4%, 32.5%, and 27.5% in POD, CAT, and APX enzyme activities, respectively, compared to their control levels. In the biochar treatment, there was a significant reduction in the activity of POD, APX, and CAT in the leaves.

Keywords: drought stress; enzymatic antioxidant activities; plant pigments; soil amendments

1. Introduction

Satureja rechingeri Jamzad is a perennial medicinal herb belonging to the Lamiaceae family. It holds significant value in Iranian flora due to its aromatic properties and therapeutic potential [1]. This herb typically grows up to 20 cm in height, featuring small, strongly scented leaves. It thrives in rocky, arid environments and exhibits remarkable tolerance to dry conditions [2]. Research has shown that *S. rechingeri* biosynthesizes several bioactive compounds, including essential oils, flavonoids, and phenolic acids, which contribute to its potential medicinal properties [3–5]. For instance, studies have demonstrated that the essential oil extracted from *S. rechingeri* exhibits antimicrobial and antioxidant activities, making it a promising candidate for treating bacterial infections and preventing oxidative damage to cells [6]. In addition to its medicinal benefits, *S. rechingeri* has been suggested to possess

natural insecticidal properties due to its strong scent and chemical composition. This characteristic makes it a safer and more environmentally friendly alternative to synthetic insecticides [7]. The essential oil of *S. rechingeri* contains biologically active compounds such as carvacrol and thymol, which are primarily responsible for its therapeutic effects. Savory species also produce antimicrobial secondary metabolites, including essential oils, as part of their natural growth and defense mechanisms against pathogens and drought stress [4].

Plants, including *S. rechingeri*, undergo various morphological, physiological, and biochemical changes when exposed to drought stress. These alterations can affect plant establishment, height, leaf and root characteristics, shoot and root dry weight, and overall yield [5]. Additionally, drought stress impacts photosynthetic efficiency, stomatal conductance, relative leaf water content, respiration, osmotic regulation, carbohydrate accumulation, proline levels, sugar content, protein synthesis, cell membrane integrity, and hormonal balance. Plants employ a range of strategies to cope with drought stress, including enzymatic and non-enzymatic defense mechanisms [8,9]. Under stressful conditions, an excessive buildup of reactive oxygen species (ROS) can occur, leading to cellular oxidative damage [10]. To counteract this, plants activate defense mechanisms such as catalase (CAT), superoxide dismutase (SOD), peroxidase (POD), ascorbate peroxidase (APX), and polyphenol oxidase (PPO) [11,12]. Additionally, to mitigate the adverse effects of drought stress, plants employ various physiological, biochemical, and cellular strategies. These adaptations are crucial for maintaining sustainable growth and productivity, especially in arid and semi-arid regions [13].

Drought stress remains a significant constraint on plant growth and productivity, particularly in water-scarce regions [14]. Soil management practices, such as the application of biochar and hydroretentive polymers (HPs), have been shown to improve soil fertility, water availability, and root zone conditions, making them effective tools for drought mitigation [15–17]. Biochar, a carbon-rich material produced through the pyrolysis of organic materials like biomass and manure, has been widely studied for its ability to enhance soil fertility and water retention [18–20]. Similarly, HPs are hydrophilic materials capable of absorbing and retaining large amounts of water, making them valuable for improving plant water availability in agriculture [21,22]. These polymers are commonly used in agriculture to enhance plant water availability [23,24].

Numerous studies have evaluated the effects of biochar and hydroretentive polymers on the eco-physiological characteristics of plants under drought stress [25]. For example, research has demonstrated that plants treated with biochar exhibit significant improvements in leaf water potential, the photosynthetic rate, and stomatal conductance compared to untreated plants [26]. Similarly, the application of superabsorbent polymers has been shown to increase shoot dry weight, root length density, and leaf relative water content in savory plants under drought stress [4]. Furthermore, the combined use of biochar and superabsorbent polymers has synergistic effects on plant growth and physiology, enhancing drought resilience and ultimately improving productivity [27]. In another study, the combined application of biochar and superabsorbent polymers significantly increased plant height, shoot and root dry weight, and chlorophyll content compared to individual treatments [17]. This finding suggests that the combined use of these amendments offers a more effective strategy for alleviating the adverse effects of drought stress on savory. Such approaches can enhance the plant water status, improve photosynthetic efficiency, promote growth, and ultimately lead to higher productivity. The primary aim of this research was to investigate how the physio-morphological properties of *S. rechingeri* are influenced by cow manure biochar, both independently and in combination with HPs, under drought stress conditions.

2. Materials and Methods

2.1. Materials

To perform this experiment, savory (*S. rechingeri*) seeds were collected from their natural habitats in Ilam province, Iran, from 375 to 915 m above sea level, at the flowering stage, and they were planted in pots in February 2017. After 70 days, seedlings in the 8- to 10-leaf stage were transferred to the medicinal plant research farm of the Faculty of Agriculture, Lorestan University, Khorramabad, Iran (46.21° E, 32.3° N, altitude), 1100 m above sea level, with an annual average precipitation and temperature of 461 mm and 18.2 °C, respectively. The experiments were conducted during two consecutive cropping seasons in 2017 and 2019. The monthly temperatures and precipitation at the experimental farm during the two growing seasons are presented in Table 1.

Table 1. Monthly air temperature and total precipitation at the experimental sites in Khorramabad, Iran, during the two growing seasons in 2018 and 2019.

Months	Temperature (°C)				Total Precipitation (mm)	
	Max		Min			
	2018	2019	2018	2019	2018	2019
March	16	18	10	9.6	211	195
April	18.2	18.9	13.2	11.1	153	134
May	21.2	24	17.2	16.9	51.4	70.3
June	37.26	39.4	20.6	18.6	0	0
July	40.1	44	24.9	24.0	0	0
August	46.3	48.1	30.2	27.3	0	0
September	33.3	35	19.1	18.4	0	0
October	21.86	30.8	13.2	12.1	12.6	27.2

2.2. Soil Characterization

Before the experiment, random soil samples were taken from the field site at a depth of 0–30 cm. Following sampling, the soil was ground, air-dried, and filtered through a 2 mm sieve before routine physicochemical properties were determined. The soil particle size distribution was measured using sieving and pipette methods [28]. At the test sites, the soil was a clay loam (43% silt, 39% clay, and 18% sand) with 1.15% organic matter. The recovery of soil organic carbon was measured by the Walkley–Black method [29]. A Theta Probe device was used to determine the water-holding capacity (WHC%) (Spectrum Technology Inc, Hamburg, Germany), and the total nitrogen, phosphorus, and potassium concentrations were determined by the Kjeldahl method [30]. The chemical properties of the soil under investigation are summarized in Table 2.

Table 2. Some chemical properties of the investigated soil before the amendment application.

Soil Particle Size Distribution	TN	TC	$CaCO_3$	P	Available N	K^+	Ca^{2+}	Mg^{2+}	ECe	pH
	%	%	%	mg kg^{-1}	%	mg kg^{-1}	mg kg^{-1}	mg kg^{-1}	dS m^{-1}	-
43% silt, 39% clay, 18% sand	0.09	1.15	19.8	10.8	0.059	355	0.43	98.4	0.57	8

TN, total nitrogen; TC, total carbon; P, phosphorus; [K^+, Ca^{2+}, Mg^{2+}], soluble cation concentrations; ECe, electrical conductivity of soil saturated paste extract.

2.3. Experimental Design and Treatments

Treatments were arranged as a split-plot factorial with a randomized complete block design arrangement, with three replications during two consecutive cropping seasons. Three levels of irrigation [95 ± 5 (D_0), 75 ± 5 (D_1), and 55 ± 5 (D_2) percent of field capacity], two levels of biochar (0- and 5-ton ha^{-1}) [BC], and two rates of hydroretentive polymers (0 and 240 kg ha^{-1}) [HPs] (as subplots) were used. Each experimental plot comprised four rows spaced 50 cm apart, with each row measuring 3 m in length, resulting in a planting density of 4 plants per square meter. The main plots within each block were separated by one meter, while the blocks themselves were spaced two meters apart. Seeds were collected during the flowering stage from natural habitats and sown in pots in February 2017. By early May 2018, when the plants had reached a height of approximately 6–8 cm, they were transplanted to the farm. Throughout the growing season, no pesticides were applied, and weed control was carried out manually. As *S. rechingeri* is a biennial plant, replanting was not required. The selection of biochar and HPs should be tailored to the soil type to optimize their effectiveness. Soil type—whether clay, sandy, or loam—plays a critical role in influencing water and nutrient absorption and retention, which directly impacts plant performance [31].

The biochar used in this study had been produced at 450–650 °C for 4 h from cow manure with the following characteristics: a particle size (PS) < 2 mm; a bulk density (BD) of 0.65 Mg m^{-3}; a total porosity (TP) of 83.4%; a pH of 8.5–8.8; a cation exchange capacity (CEC) of 12.9–14 cmol kg^{-1}; and an electrical conductivity (EC) of 12.88 ds/m. The biochar was mixed with soil to a depth of 0–20 cm before planting [21]. A hydroretentive polymer was used as the superabsorbent in this experiment with the following characteristics: a PS of 0.2; a BD of 0.7 Mg m^{-3}; a TP of 52.2%; a pH of 7.70; a CEC of 400 mol kg^{-1}; and an EC of 13.21 ds/m. The HP amounts appropriate for each treatment were placed at a depth of 20 cm beneath the seedlings [27].

2.4. Measurements of Chlorophyll Content and Photosynthesis Parameters

At the end of each stress period (the fifth day after applying the water deficit stress), the chlorophyll content index of the SPAD (soil and plant analyzer development) value was determined with a portable chlorophyll meter (SPAD-502 Plus, Konica Minolta, Lincoln, Japan). Forty to fifty days after the initiation of the watering treatments, the photosynthesis parameters, which included the net photosynthesis rate (PN), stomatal conductance (gs), and transpiration (E) of two upper and fully expanded leaves, were measured using a Li-COR 6400 portable photosynthesis system (Li-COR, Lincoln, NE, USA) on a sunny day between 10:00 and 11:00 am. During the measurement, the photosynthetic photon flux density was maintained at 750 μmol m^{-2} s^{-1} using an internal red/blue LED light source, and CO_2 concern was set to 400 μmol^{-1} by mixing external air with CO_2 from an attached source. The leaf temperature was recorded as 27–28 °C, with a sample relative humidity higher than 70%.

2.4.1. Measurement of RWC (%)

The relative water content (RWC) was determined by selecting the youngest developed leaf from each treatment in each replication. The leaves were weighed immediately after harvesting to obtain their fresh weight. The leaves were then placed in test tubes with distilled water and left for 4 h under low-light conditions at room temperature (25 °C) to estimate their turgid masses. After drying the leaf samples in an oven at 72 °C for 48 h, the dry mass of the leaves was measured. The RWC was calculated using Equation (1) [32]:

$$\mathrm{RWC}(\%) = \left(\frac{\text{Fresh Weight} - \text{Dry Weight}}{\text{Turgid Weight} - \text{Dry Weight}} \times 100 \right) \quad (1)$$

2.4.2. Measurement of MDA

Malondialdehyde was identified by Buege and Steven [33] as the product of lipid peroxidation that reacts with thiobarbituric acid to produce a red species absorbing at 535 nm. For this purpose, TCA-TBA-HCI stock was prepared by mixing 15% *w/v* trichloroacetic acid; 0.375% *w/v* thiobarbituric acid; and 0.25 N hydrochloric acid. This solution was mildly heated to assist in the dissolution of the thiobarbituric acid. In this study, the malondialdehyde concentration was calculated using the described methods with minor modifications. In a Chinese mortar, 0.5 g of fresh leaves was ground with 5 mL of a 20% trichloroacetic acid solution containing 0.5% thiobarbituric acid. The extract was centrifuged, then heated at 80 °C for 25 min, cooled, and centrifuged again. To correct for any additional compounds, the absorbance value of the samples was obtained at a wavelength of 532 nm (A532) and then subtracted from their absorbance value at a wavelength of 600 nm (A600). The malondialdehyde concentration of the sample was calculated using an extinction coefficient of $1.56 \times 10 \sim M^{-I}\ cm^{-1}$ (Equation (2)).

$$\text{MDA } (\mu\text{mol g FW}^{-1}) = \lfloor (\text{A532} - \text{A600}) \rfloor \times 1000 \quad (2)$$

2.4.3. Enzymatic Antioxidant Activities

To determine the antioxidant activity, a fresh leaf sample weighing 0.3 g was ground in 1.5 mL of cold 50 mM phosphate buffer (pH 7.8), and the resulting suspension was transferred to 2 mL microtubes. The microtubes were then placed in a refrigerated centrifuge for 20 min at a temperature of four degrees Celsius with a revolution speed of 14,000 per minute. The method described in [34] was used to measure the activity of ascorbate peroxidase (APX) [35]. Peroxidase (POD) activity was determined using the standard method, and absorbance readings were recorded at 470 nm [36]. Catalase (CAT) activity was measured according to the method described in [37].

2.5. Statistical Analyses

A combined analysis of variances (in randomized complete block split-plot factorial field experiments with three replications) was performed on the data obtained from the 2-year study using PROC GLM of SAS version 9.1 (SAS Institute, Cary, NC, USA 1990). Means were statistically compared using LSD ($p < 0.05$).

3. Results

3.1. Analysis of Variance of Studied Traits

The results of the analysis of variance showed that year had a significant effect on the malondialdehyde (MDA) concentration ($p < 0.05$) and biomass production ($p < 0.01$) (Table S1). Water stress and the hydroretentive polymer (HP) had a considerable impact on all traits ($p < 0.01$). The effects of biochar on SPAD, MDA, ascorbate peroxidase (APX), the net photosynthesis rate (PN), the transpiration rate (E), stomata conductance (GS), biomass production (BIO), and the leaf relative water content (RWC) were significant ($p < 0.01$). The interaction effect of water deficit × biochar on peroxidase (POD), the transpiration rate, SPAD, the RWC, MDA, and stomata conductance was significant. Similarly, the interaction effect of water deficit × HP on SPAD, POX, APX, MDA, and the RWC was significant ($p < 0.01$) (Table S1).

3.2. Effects of Biochar, Water Deficit, and Superabsorbent on SPAD

The results indicate that there was a significant difference in the chlorophyll meter number (SPAD) between the different levels of water deficit (Table S1). The SPAD values of the leaves in the treatments of 75 ± 5% (D_1) and 55 ± 5% (D_2) showed an increase

of 33.2 and 11.8%, respectively, compared to those in D_0 (95 ± 5% FC) (Table 3). The application of biochar (BC) and the hydroretentive polymer (HP) increased the SPAD value by 1.7% and 46.1%, respectively, compared to the control treatment (without BC and the HP) (Table 4). A comparison of the mean BC × D interaction effects on SPAD showed that its value increased with the water deficit levels with the use of biochar. The highest SPAD value, with an average of 30.5, was obtained from the D_0BC_1 treatment (95 ± 5% water requirement +10 t ha^{-1} BC), and no statistically significant difference was observed compared to the control. The lowest value of 22.6 was obtained in the D_2BC_1 treatment (55 ± 5% FC + BC), which caused a 25.5% increase in the SPAD value compared to the control (without BC) (Table 4). These outcomes indicate the positive and more effective role of biochar over soil quality and nutrient availability in improving the physiological attributes of *Satureja rechingeri*. Similarly, the effect of D×HP on the SPAD value decreased in parallel with the intensification of the water shortage in both conditions, with and without the HP, but the effect of the application of the HP on its activity level differed depending on the level of irrigation; no statistically significant difference was observed between the use and non-use of the HP in D_1, but its use at D_1 and D_2 levels increased the SPAD value by 83.5% and 47.1%, respectively, compared to the control (without the HP) (Table 5). Nevertheless, at both levels of application and the non-application of SA, the SPAD value decreased in parallel with the intensification of the lack of moisture (Table 5).

Table 3. Mean comparisons of the main effects of year, water deficit, biochar, and hydroretentive polymer on gas exchange parameters and physiological properties in savory.

Traits / Treatment	SPAD	MDA (µmol g Fw^{-1})	POX (Unit mg^{-1} Protein)	CAT	APX ($\mu molCO_2$ $m^{-2}s^{-1}$)	PN	E (Mmol H_2O $m^{-2}s^{-1}$)	GS (mol H_2O $m^{-2}s^{-1}$)	BIO (g $plant^{-1}$)	RWC %
Years										
Y_1	25.7 a	23.7 a	5.00 a	3.51 a	5.10 a	20.5 a	4.99 a	0.468 a	11.9 b	70.0 a
Y_2	26.0 a	20.5 b	5.20 a	3.72 a	4.86 a	20.2 a	4.93 a	0.459 a	24.0 a	71.5 a
Deficit stress										
D_0	20.3 c	12.9 a	4.52 b	2.11 c	2.75 c	27.2 a	6.71 a	0.559 a	24.8 a	84.2 a
D_1	26.8 b	22.1 b	4.61 b	3.82 b	5.61 b	19.6 b	4.91 b	0.449 b	18.1 b	69.6 b
D_2	30.4 a	31.4 c	6.18 a	4.91 a	6.58 a	14.4 c	3.10 c	0.382 c	11.0 c	58.5 c
Biochar										
BC_0	24.9 b	22.8 a	5.17 a	3.41 a	5.31 a	19.0 b	4.12 b	0.432 b	15.7 b	68.6 b
BC_1	26.8 a	21.4 b	5.04 a	3.83 a	4.65 b	21.6 a	5.03 a	0.495 a	18.3 a	72.9 a
Hydroretentive polymer										
HP_0	20.6 b	24.8 a	5.88 a	4.12 a	5.79 a	19.3 b	4.49 b	0.448 b	16.8 b	66.5 b
HP_1	30.1 a	19.4 b	4.33 b	3.11 b	4.20 b	21.5 a	5.33 a	0.479 a	19.1 a	74.9 a

Abbreviations: Y, years; D_0, D_1, and D_2: water deficit at 95 ± 5, 75 ± 5, and 55 ± 5% FC, respectively; BC_0, BC_1: 0 and 10 t ha^{-1} biochar, respectively; HP_0 and HP_1: 0 and 240 kg ha^{-1} hydroretentive polymer, respectively; SPAD, photosynthesis index; MDA, malondialdehyde; POX, peroxidase; CAT, catalase; APX, ascorbate peroxidase; PN, net photosynthesis rate; E, transpiration rate; GS, stomata conductance; BIO, biomass production; RWC, relative water content. Different letters in each column indicate significant differences among the treatments ($p < 0.05$, LSD test).

Table 4. The interaction effect of water deficit × biochar on SPDA, MDA, POX, transpiration, stomatal conductance (gs), and RWC of savory.

Traits / Treatment	SPAD -	MDA µmol g Fw^{-1}	POX Unit mg^{-1} protein	E mmol H_2O $m^{-2}s^{-1}$	GS mol H_2O $m^{-2}s^{-1}$	RWC %
D_0BC_0	30.4 a	13.0 d	4.65 cd	5.97 b	0.544 a	84.1 a
D_0BC_1	30.5 a	12.8 d	4.39 d	7.44 a	0.575 a	84.2 a

Table 4. *Cont.*

Traits / Treatment	SPAD	MDA	POX	E	GS	RWC
	-	μmol g Fw^{-1}	Unit mg^{-1} protein	mmol H_2O $m^{-2}s^{-1}$	mol H_2O $m^{-2}s^{-1}$	%
D_1BC_0	26.3 b	23.6 b	4.28 d	4.64 d	0.418 c	68.2 c
D_1BC_1	27.3 b	20.6 c	4.95 c	5.20 c	0.480 b	71.1 b
D_2BC_0	18.0 d	31.9 a	6.57 a	2.86 f	0.333 d	53.5 e
D_2BC_1	22.6 c	30.9 a	5.79 b	3.35 e	0.431 c	63.4 d
LSD5%	2.16	1.61	0.476	0.446	3.21	2.88

Abbreviations: D_0, D_1, and D_2: water deficit at 95 ± 5, 75 ± 5, and 55 ± 5% FC, respectively; BC_0, BC_1: 0 and 10 t ha^{-1} biochar; SPAD, photosynthesis index; MDA, malondialdehyde; POX, peroxidase; E, transpiration rate; GS, stomata conductance; RWC, relative water content. Different letters in each column indicate significant differences among the treatments ($p < 0.05$, LSD test).

Table 5. Interaction effect of water deficit × superabsorbent on SPAD, MDA POX, APX, and RWC of savory.

Traits / Treatment	SPAD	MDA	POX	APX	RWC
	-	μmol g Fw^{-1}	Unit mg^{-1} protein	Unit mg^{-1} protein	%
D_0HP_0	30.1 b	14.1 e	4.59 c	2.88 c	83.7 a
D_0HP_1	30.8 b	11.7 f	3.93 d	2.62 d	84.6 a
D_1HP_0	18.9 d	24.5 c	5.29 b	6.12 b	63.5 c
D_1HP_1	34.7 a	19.6 d	4.45 c	5.12 c	75.8 b
D_2HP_0	15.9 e	35.8 a	7.74 a	8.39 a	52.4 d
D_2HP_1	24.8 c	27.0 b	4.62 c	4.78 c	64.5 c
LSD5%	2.16	1.61	0.476	0.552	2.88

Abbreviations: D_0, D_1, and D_2: deficit stress at 95 ± 5, 75 ± 5, and 55 ± 5% FC; HP_0 and HP_1: 0 and 6 g $plant^{-1}$ superabsorbent; SPAD, photosynthesis index; MDA, malondialdehyde; POD, peroxidase; APX, ascorbate peroxidase; RWC, relative water content. Different letters in each column indicate significant differences among the treatments ($p < 0.05$, LSD test).

3.3. Effects of Biochar, Water Deficit, and Superabsorbent on MDA

Except for malondialdehyde (MDA), no changes were noticed in the other traits under water deficit stress (Table 3). The content of MDA decreased by 15.6% under the water deficit in the second year compared to in the first year. This can be attributed to the sustained stress experienced over the two years. The highest concentration of MDA (31.4 μmol g Fw^{-1}) was obtained from treatment D_2 (55 ± 5% FC) (Table 3). These results indicate that the water deficit led to a decrease in the RWC and dry matter yield, while the amount of MDA and soluble sugars increased following drought stress. In the treatments involving the application of biochar and the hydroretentive polymer, the process of increasing MDA was slow, resulting in a decrease of 6.2% and 21.8% in the MDA concentration compared to the control level (without BC and the HP) (Table 3). This result indicates that the application of biochar creates favorable conditions for plants to maintain low levels of MDA, thereby preventing the lipid peroxidation of cell membranes caused by oxidative stress and protecting them from damage due to water deficit. As the level of membrane fat peroxidation increases, so does MDA production. Also, the results of this research show that the mutual effects of BC and the water deficit led to a significant decrease in MDA. This may imply that the release of active oxygen and the destruction of membrane fat are prevented. The highest concentration of MDA (31.9 mg/g FW^{-1}) was associated with the D_2BC_0 treatment, whereas the lowest concentration (12.8 mg/g FW^{-1}) of MDA was observed in the D_0BC_1 treatment. There was no statistically significant difference between the application and control treatment of BC at the water deficit levels of

95 ± 5 (D_0) and 75 ± 5 (D_2). However, biochar use at the water deficit level of 75 ± 5 (D_1) resulted in a 12.7% decrease in the MDA concentration compared to the control (without BC) (Table 4). In fact, by providing water to the plant, BC prevents the degradation of cell membrane fat and thus inhibits the activity of oxygen radicals. Examining the process of MDA production during the experiment showed that the MDA amount significantly increased in proportion to the increase in the field water deficit stress in the HP_0 and HP_1 treatments (Table 5). The amount of MDA in the three stress treatments (95 ± 5, 75 ± 5, and 55 ± 5% FC) showed a different trend to that in the two HP and HP_0 treatments. The MDA concentration increased regardless of HP application; however, the effect of HP application differed depending on the water deficit level. So, the use of the HP at the irrigation levels of 95 ± 5 (D_0), 75 ± 5 (D_1), and 55 ± 5 (D_2) caused a decrease of 0.17, 0.20, and 24.5% in MDA, respectively, compared to the control level without the hydroretentive polymer (Table 5), and these values increased under the water stress conditions. By increasing the ability to hold water, the HP moderated the water deficit conditions in the soil and reduced the amount of MDA under the stress conditions.

3.4. Effects of Biochar, Water Deficit, and Superabsorbent on Enzyme Antioxidants

A comparison of the average of the simple effects showed that, as the intensity of the water deficit (D) of the savory plant increased, the activity of antioxidant enzymes (POX, CAT, and APX) also increased (Table 3). The highest activity levels were observed in the D_2 (55 ± 5% FC of water requirement) treatment. Compared to the D_0 (95 ± 5% FC) treatment, the enzyme activity of POX, CAT, and APX increased by 36.7%, 133%, and 139%, respectively (Table 3). Although biochar application did not have a statistically significant effect on the activity of POX and CAT enzymes, its use led to a 14.2% reduction in APX enzyme activity compared to the control treatment (Table 3). Moreover, the application of the HP resulted in reductions of 26.4%, 32.5%, and 27.5% in the activity of POX, CAT, and APX enzymes, respectively, compared to their control levels (Table 3). Interestingly, the interaction effect between irrigation and the HP on the activities of POX and APX enzymes differed significantly under the water deficit and non-water deficit conditions. For instance, in the D_2HP_1 treatment, the activity of POX increased by 17.6% and that of APX increased by 82.4% compared to in the D_0HP_1 treatment. Conversely, applying the superabsorbent at D_0, D_1, and D_2 levels resulted in a decrease of 0.9%, 16.3%, and 75.5% in APX enzyme activity, respectively, compared to the control level (HP_0) (Table 5).

Although the activity of the POX enzyme increased with the intensification of the water deficit in both the application and non-application conditions of biochar, the effect of BC application on POX activity differed depending on the irrigation level. In the D_0 treatment, there was no statistically significant difference between the application and non-application of BC. However, at the D_1 and D_2 levels of irrigation, the application of BC resulted in a 15.6% increase and an 11.9% decrease in POX activity, respectively, compared to the control level (without biochar) (Table 4).

3.5. Effects of Biochar, Water Deficit, and Hydroretentive Polymer on Photosynthetic Parameters

A means comparison revealed a significant decrease in the photosynthetic parameters (photosynthesis, transpiration, and stomatal conductance) and the RWC of the savory plant leaves in parallel with the intensity of drought stress. Among the different treatments, the highest values were observed in the D_0 treatment (95 ± 5% FC), whereas the lowest values were obtained under D_2 (55 ± 5% FC) conditions. Specifically, the net photosynthesis rate, transpiration rate, stomatal conductance rate, and RWC decreased by 0.47%, 53.8%, 31.6%, and 30.5%, respectively, in the 55 ± 5 (D_2) treatment compared to at the 90 ± 5 (D_0) level (Table 3). The reduction in the RWC and the stomata closure represent the

initial impacts of drought stress, resulting from disturbances in the photosynthetic material production system. Furthermore, the response to water stress likely involves the regulation of carbon dioxide availability in the chloroplast, predominantly controlled by stomatal conductance. The application of biochar and the hydroretentive polymer resulted in a significant improvement in various parameters compared to the control group. Specifically, there was a 13.7% and 11.4% increase in net photosynthesis, a 22.1% and 18.7% rise in transpiration, a 14.6% and 6.9% elevation in stomatal conductance, and a 6% and 12.6% improvement in the RWC (Table 3). No statistically significant difference was observed when comparing the application of BC with that of the control at the D_0 (95 $\pm$ 5% FC) level. However, at the 75 $\pm$ 5 (D_1) and 55 $\pm$ 5 (D_2) levels, the application of BC resulted in a significant increase in stomatal conductivity. Specifically, there was a 4.2% and 18.5% elevation in stomatal conductivity compared to the control (without BC) level, as shown in Table 4. Additionally, using BC led to an overall increase in the transpiration rate across all drought stress levels. In D_0, D_1, and D_2, the application of BC caused a 24.6%, 12.1%, and 14.6% rise in transpiration, respectively, compared to the control level (without BC) (Table 4). Furthermore, the RWC decreased as the water deficit intensified in both conditions, regardless of biochar application. However, the effect of BC on the RWC varied depending on the severity of the water deficit levels. In summary, this study revealed no significant difference in stomatal conductivity between the usage of biochar (BC) and non-usage of BC at the 95 $\pm$ 5% (D_0) level. Nevertheless, at the D_1 and D_2 levels, BC usage led to a notable increase of 4.2% and 18.5% in stomatal conductivity compared to the control treatment (without BC) (Table 4). Furthermore, the effect of the HP on the RWC varied depending on the drought stress level. At the D_0 (95 $\pm$ 5% FC) level, there was no statistically significant difference between the application and non-application of SA. However, at the D_1 and D_2 levels, the application of the HP resulted in an increase of 19.4% and 23.1% in the RWC compared to the control level (HP_0) (Table 5).

3.6. Correlation Matrix

A clear correlation was identified among all biochemical, enzymatic, and photosynthetic parameters associated with the savory plant. Notably, there was a positive and significant correlation between biochemical parameters such as peroxidase (POX), catalase (CAT), and ascorbate peroxidase (APX) and photosynthetic characteristics like the transpiration rate. However, these biochemical parameters exhibited a negative correlation with net photosynthesis, the photosynthesis index, stomatal conductance, and the relative water content. Additionally, a significant negative correlation was found among the stomatal conductance, net photosynthesis rate, photosynthesis index, and relative water content (Figure 1). The negative correlation between these factors highlights the delicate balance between water conservation and photosynthesis in plants.

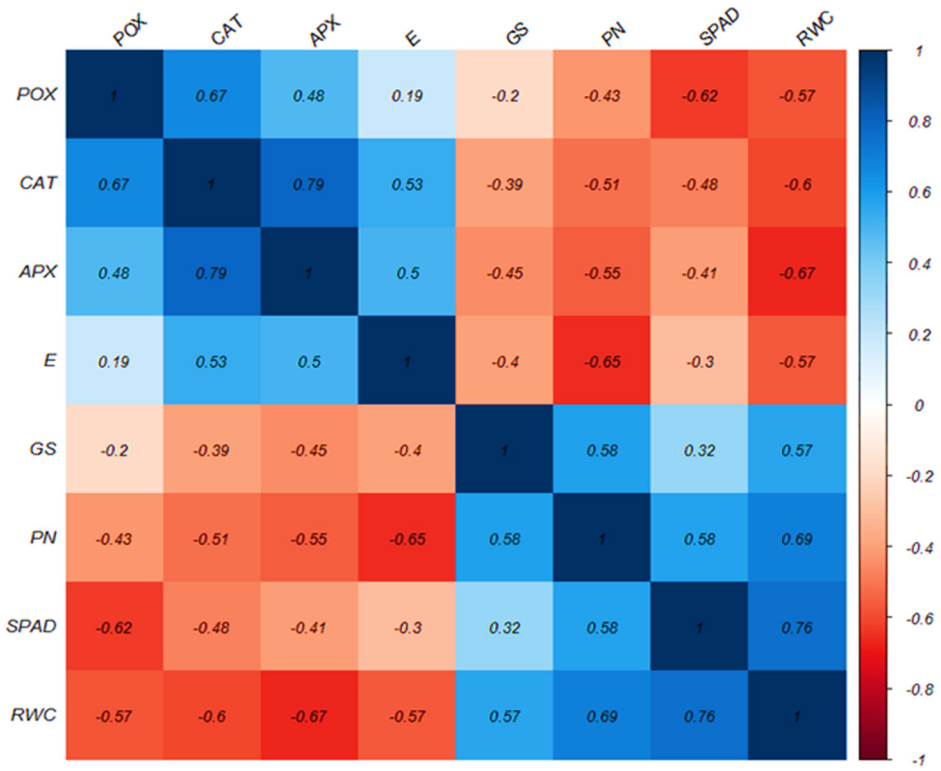

Figure 1. The effect of water deficit on the correlation between biochemical mechanisms of two-year-old *Satureja rechingeri*. POX, peroxidase; CAT, catalase; APX, ascorbate peroxidase; E, transpiration rate; GS, stomata conductance; PN, net photosynthesis rate; SPAD, photosynthesis index; RWC, relative water content.

4. Discussion

Under the conditions of water stress, plants face a decline in photosynthesis, respiration, and nutrient absorption. This can result in stunted growth, reduced chlorophyll levels, and lower crop yields. Furthermore, drought stress can elevate the production of reactive oxygen species (ROS), which can damage cellular membranes and adversely affect overall plant health. Interestingly, the SPAD values of the leaves increased under moisture stress (Table 1). As illustrated in Table 4, drought stress led to a rise in chlorophyll meter readings for the savory plants. This suggests that a higher chlorophyll meter reading under drought conditions may indicate an intensified stress effect on the plant and a subsequent reduction in the leaf area. By decreasing the leaf area during stressful periods, plants minimize their transpiration surface to conserve water; consequently, while the total chlorophyll content may decline, the concentration of chlorophyll per unit leaf area increases (38). Research [38] indicated that the SPAD values of *Malva sylvestris* L. rose with increasing levels of stress. Drought is a significant factor hindering plant growth by reducing photosynthesis [38] and limiting CO_2 uptake into leaves, which further decreases photosynthetic rates and damages chlorophyll. Studies on cotton [39] confirmed the detrimental effects of drought on chlorophyll levels. Afzal et al. [40] noted that variations in chlorophyll meter readings could be influenced by leaf thickness, which may vary based on crop type, growth stage, cultivar, and environmental factors. In this study's findings, the greenness index improved with the application of 10 t ha^{-1} of cow manure biochar and 240 kg ha^{-1} of a hydroretentive polymer. The highest SPAD values were recorded with the interaction between the D_0BC_1 and D_0HP_1 treatments. Yang et al. [41] identified rapid physiological adaptations, such as leaf tubularization, a reduced leaf area, and increased stomatal resistance, as strategies for coping with drought stress. Jia et al. [42] explored how water deficits affect physiology, antioxidant enzymes, and secondary metabolites across various plant species. One

accelerated reaction due to ROS presence is lipid peroxidation in cell membranes leading to the production of aldehydes like malondialdehyde [42]. MDA serves as an indicator of oxidative damage under drought conditions; its elevated levels signify membrane injury. Jia et al. [42] associated increased MDA concentrations with heightened lipid peroxidation and the oxidation of membrane fatty acids. The results indicated that a water deficit at 60% field capacity decreased photosynthetic pigments and dry matter production while increasing MDA levels in aerial parts [43]. The application of biochar can help mitigate these negative effects, as it can improve the soil structure, enhance the water retention capacity, and reduce oxidative stress. These factors contribute to the better performance of plants under drought conditions. The MDA level was consistently higher in the water deficit stress treatment compared to in the water deficit + biochar treatment [44]. The highest MDA concentration was observed under the interaction between the D_2BC_0 and D_2HP_0 treatments. When subjected to stress conditions, plants generate substantial amounts of reactive oxygen species (ROS). Excessive ROS production during drought leads to oxidative stress within plants [45,46]. In severe cases of drought stress, even though plants activate their antioxidant systems, excessive ROS formation can trigger lipid peroxidation, along with damage to pigments, proteins, and other cellular components, ultimately resulting in harm to the plant [47]. To counteract the detrimental effects of reactive oxygen species (ROS), plants develop a sophisticated antioxidant defense system that includes superoxide dismutase (SOD), ascorbate peroxidase (APX), catalase (CAT), and peroxidase (POX). The observed increase in catalase activity in *Satureja rechingeri* suggests that this plant has a notable capacity to withstand drought stress. Recent findings indicate that drought conditions may significantly enhance the activity of antioxidant enzymes. This study revealed that the application of biochar notably reduced the levels of POX and APX in savory leaves. In essence, the use of biochar improved the function of protective enzymes like CAT and POX, which helped to inhibit active oxygen species and subsequently reduced membrane lipid peroxidation. In summary, under drought stress, the addition of water through biochar and hydroretentive polymer treatments increased soil moisture compared to the control conditions. This improvement in moisture levels helped mitigate soil dryness and led to a decrease in the activities of enzymes such as POX and APX relative to those in the control soils. The protective role of antioxidant enzymes against oxidative damage has also been explored in bermudagrass (*Cynodon dactylon* L.) [47]. Consistent with our findings, Wang et al. [48] reported that a water deficit resulted in a reduced relative water content alongside increased malondialdehyde (MDA) levels and heightened activity of superoxide dismutase and peroxidase enzymes in rubber plants (*Ficus elastica*) [49]. Overall, our results indicate a significant increase in the activity of antioxidant enzymes (CAT, POX, and APX) with escalating drought stress. Thus, enhancing antioxidant enzyme activity may play a crucial role in bolstering plant resistance to moisture stress. Although this study did not find a positive correlation between SOD or CAT activity and a higher RWC under moisture stress conditions, there is substantial evidence suggesting that, during the early stages of drought, stomatal closure is a primary limitation on photosynthesis. This closure occurs due to decreased photosynthetic rates under dry conditions, signaling necessary metabolic adjustments within the leaf [50]. Various studies have documented reductions in photosynthetic rates due to drought stress across different plant species [51,52], attributing these declines mainly to stomatal and non-stomatal limitations [53]. To prevent excessive moisture loss through transpiration during drought stress, plants reduce their stomatal conductance; this response consequently limits photosynthesis while potentially improving intrinsic water use efficiency (WUEi) [54]. This aligns with the findings of our study, where we observed a decline in net photosynthesis, transpiration, and stomatal conductance under drought conditions. The D_2 (60% FC) treatment showed the highest values, while the D_0 (100% FC)

treatment showed the lowest. Lyu et al. [43] noted that biochar application can improve soil moisture levels, promote water infiltration, and enhance the water retention capacity, ultimately benefiting agricultural yields. In a comparative study on irrigation and biochar effects, it was found that, as water scarcity increased, stomatal conductance, transpiration rates, and the leaf relative water content (RWC) decreased regardless of biochar application. However, the influence of biochar on these parameters varied with the severity of the water deficit. Our results indicate that a water deficit negatively impacts plant photosynthesis rates; however, biochar application can alleviate some adverse effects associated with reduced water availability. By enhancing electron transfer and protective enzyme activity in plant leaves, biochar can bolster their defense mechanisms against drought stress [43]. A higher RWC suggests that amendments like biochar and hydroretentive polymers (HPs) may help reduce water loss by closing stomatal openings or improving root expansion for better water absorption. Nanda et al. [55] reported that hydroretentive polymers can enhance soil moisture retention and decrease irrigation frequency by up to 50%. Additionally, research indicates that biochar is particularly beneficial in less fertile soils compared to more fertile ones, which is consistent with our findings [56]. The total porosity, water-holding capacity, pH, and electrical conductivity (EC) of the substrate significantly increased with increasing biochar rates, especially in the substrate without SAP. The values of pH and EC were significantly lower in the substrate with SAP than in that without SAP at high biochar application rates (27). Given the comparable performance of biochar and superabsorbent materials, we can conclude that this aligns with the results of our experiment. Thus, incorporating cow manure biochar is a strategic approach for soil management in arid regions. Hydroretentive polymers are macromolecules with hydrophilic components capable of absorbing and retaining significant amounts of water [57]. They have been shown to significantly improve moisture storage and capacity in the root zone under stress conditions [58]. By mitigating the effects of water deficit on plants, they ultimately promote enhanced growth and photosynthetic activity [50].

5. Conclusions

This research shows that drought stress negatively affects savory plants by reducing photosynthesis due to stomatal closure. However, applying biochar (BC) and hydroretentive polymers (HPs) helps mitigate these effects by improving soil properties, water availability, and nutrient absorption. BC and HPs also enhance plant defense mechanisms against stress by reducing lipid peroxidation and maintaining low levels of malondialdehyde (MDA). The combined use of BC and HPs is more effective in enhancing plant characteristics under drought stress compared to individual use. The future application of biochar (BC) and hydroretentive polymers (HPs) in agriculture shows promise in mitigating the detrimental effects of drought stress on plants by enhancing soil properties, water availability, nutrient absorption, and photosynthetic pigments. This combined approach can protect plants from oxidative damage, maintain low levels of malondialdehyde (MDA), and improve physiological processes under stress conditions.

Supplementary Materials: The following supporting information can be downloaded at: https://www.mdpi.com/article/10.3390/horticulturae11020169/s1, Table S1: Analysis of variance (ANOVA) of the effects of water deficit, biochar, and hydroretentive polymer on gas exchange parameters and physiological properties of savory.

Author Contributions: Conceptualization and investigation, M.B., A.A., N.A. and H.M.; data collection, M.B., A.A. and H.M.; writing—original draft, M.B., A.A. and N.A.; software, script evaluation, and editing, M.B., H.M. and F.N.F.; writing—review and editing, M.B., A.A. and S.A.; data curation and formal analysis, M.B., A.A., H.M. and S.A.; visualization and validation, H.M. and

A.A.; methodology and references, M.B., N.A., A.A. and H.M.; supervision, M.B. All authors have read and agreed to the published version of the manuscript.

Funding: This research received no external funding.

Data Availability Statement: The data presented in this study are available on request from the corresponding author.

Acknowledgments: The authors wish to thank Lorestan University, Iran, for the facilities provided for this research.

Conflicts of Interest: The authors declare no conflict of interest.

References

1. Shams, S.; Ismaili, A.; Firouzabadi, F.N.; Mumivand, H.; Sorkheh, K. Comparative transcriptome analysis to identify putative genes involved in carvacrol biosynthesis pathway in two species of *Satureja*, endemic medicinal herbs of Iran. *PLoS ONE* **2023**, *18*, e0281351. [CrossRef] [PubMed]
2. Hadian, J.; Akramian, M.; Heydari, H.; Mumivand, H.; Asghari, B. Composition and in vitro antibacterial activity of essential oils from four *Satureja* species growing in Iran. *Nat. Prod. Res.* **2012**, *26*, 98–108. [CrossRef]
3. Sefidkon, F.; Abbasi, K.; Jamzad, Z.; Ahmadi, S. The effect of distillation methods and stage of plant growth on the essential oil content and composition of *Satureja rechingeri* Jamzad. *Food Chem.* **2007**, *100*, 1054–1058. [CrossRef]
4. Beiranvandi, M.; Akbari, N.; Ahmadi, A.; Mumivand, H.; Nazarian, F. Biochar and super absorbent polymer improved growth, yield, and phytochemical characteristics of *Satureja rechingeri* Jamzad in water-deficiency conditions. *Ind. Crops Prod.* **2022**, *183*, 114959. [CrossRef]
5. Nooshkam, A.; Mumivand, H.; Hadian, J.; Alemardan, A.; Morshedloo, M.R. Drug yield and essential oil and carvacrol contents of two species of Satureja (*S. khuzistanica* Jamzad and *S. rechingeri* Jamzad) cultivated in two different locations. *J. Appl. Res. Med. Aromat. Plant.* **2017**, *6*, 126–130. [CrossRef]
6. Aghbash, B.N.; Pouresmaeil, M.; Dehghan, G.; Nojadeh, M.S.; Mobaiyen, H.; Maggi, F. Chemical composition, antibacterial and radical scavenging activity of essential oils from *Satureja macrantha* C.A.Mey. at different growth stages. *Foods* **2020**, *9*, 494. [CrossRef]
7. Pavela, R.; Morshedloo, M.R.; Mumivand, H.; Khorsand, G.J.; Karami, A.; Maggi, F.; Desneux, N.; Benelli, G. Phenolic monoterpene-rich essential oils from *Apiaceae* and *Lamiaceae* species: Insecticidal activity and safety evaluation on non-target earthworms. *Entomol. Gen.* **2020**, *40*, 421–435. [CrossRef]
8. Ahmadi, S.Z.; Zahedi, B.; Ghorbanpour, M.; Mumivand, H. Comparative morpho-physiological and biochemical responses of *Capsicum annuum* L. plants to multi-walled carbon nanotubes, fullerene C60 and graphene nanoplatelets exposure under water deficit stress. *BMC Plant Biol.* **2024**, *24*, 116. [CrossRef] [PubMed]
9. Mumivand, H.; Ebrahimi, A.; Shayganfar, A.; Khoshro, H.H. Screening of tarragon accessions based on physiological and phytochemical responses under water deficit. *Sci. Rep.* **2021**, *11*, 17839. [CrossRef]
10. Sharma, P.; Jha, A.B.; Dubey, R.S.; Pessarakli, M. Reactive oxygen species, oxidative damage, and antioxidative defense mechanism in plants under stressful conditions. *J. Bot.* **2012**, *2012*, 217037. [CrossRef]
11. Apel, K.; Hirt, H. Reactive oxygen species: Metabolism, oxidative stress, and signal transduction. *Annu. Rev. Plant Biol.* **2004**, *55*, 373–399. [CrossRef] [PubMed]
12. Mumivand, H.; Ebrahimi, A.; Morshedloo, M.R.; Shayganfar, A. Water deficit stress changes in drug yield, antioxidant enzymes activity and essential oil quality and quantity of Tarragon (*Artemisia dracunculus* L.). *Ind. Crops Prod.* **2021**, *164*, 113381. [CrossRef]
13. Forni, C.; Duca, D.; Glick, B.R. Mechanisms of plant response to salt and drought stress and their alteration by rhizobacteria. *Plant Soil* **2017**, *410*, 335–356. [CrossRef]
14. Jiao, Y.; Zhu, G.; Meng, G.; Lu, S.; Qiu, D.; Lin, X.; Li, R.; Wang, Q.; Chen, L.; Zhao, L.; et al. Estimating non-productive water loss in irrigated farmland in arid oasis regions: Based on stable isotope data. *Agric. Water Manag.* **2023**, *289*, 108515. [CrossRef]
15. Phillips, C.E.; Nair, U.S.; Mahmood, R.; Rappin, E.; Pielke, R.A., Sr. Influence of irrigation on diurnal mesoscale circulations: Results from GRAINEX. *Geophys. Res. Lett.* **2022**, *49*, e2021GL096822. [CrossRef]
16. Mumivand, H.; Izadi, Z.; Amirizadeh, F.; Maggi, F.; Morshedloo, M.R. Biochar amendment improves growth and the essential oil quality and quantity of peppermint (*Mentha× piperita* L.) grown under waste water and reduces environmental contamination from waste water disposal. *J. Hazard. Mater.* **2023**, *446*, 130674. [CrossRef]
17. Fouladidorhani, M.; Shayannejad, M.; Shariatmadari, H.; Mosaddeghi, M.R.; Arthur, E. Biochar, manure, and super absorbent increased wheat yields and salt redistribution in a saline-sodic soil. *Agron. J.* **2020**, *112*, 5193–5205. [CrossRef]
18. Sohi, S.P. Carbon storage with benefits. *Science* **2012**, *338*, 1034–1035. [CrossRef]

19. Lehmann, J.; Joseph, S. (Eds.) *Biochar for Environmental Management: Science, Technology and Implementation*; Taylor & Francis: Abingdon, UK, 2024.
20. Yuan, S.; Tan, Z. Effect and mechanism of changes in physical structure and chemical composition of new biochar on Cu (II) adsorption in an aqueous solution. *Soil Ecol. Lett.* **2022**, *4*, 237–253. [CrossRef]
21. Arthur, E.; Danso, E.O.; Beiranvand, M.; Pouladi, N.; Yakubu, A.; Abenney-Mickson, S.; Sabi, E.B. Rice straw biochar effects on Atterberg limits and aggregate characteristics of an Acrisol in Ghana. *Arch. Agron. Soil Sci.* **2020**, *66*, 1861–1872. [CrossRef]
22. Chang, L.; Xu, L.; Liu, Y.; Qiu, D. Superabsorbent polymers used for agricultural water retention. *Polym. Test.* **2021**, *94*, 107021. [CrossRef]
23. Thombare, N.; Mishra, S.; Siddiqui, M.Z.; Jha, U.; Singh, D.; Mahajan, G.R. Design and development of guar gum-based novel, superabsorbent and moisture retaining hydrogels for agricultural applications. *Carbohydr. Polym.* **2018**, *185*, 169–178. [CrossRef]
24. Souza, A.J.J.; Guimarães, R.J.; Dominghetti, A.W.; Scalco, M.S.; Rezende, T.T. Water-retaining polymer and seedling type when planting irrigated coffee. *Rev. Ciênc. Agrôn.* **2016**, *47*, 334–343. [CrossRef]
25. Alotaibi, K.D.; Schoenau, J.J. Addition of biochar to a sandy desert soil: Effect on crop growth, water retention and selected properties. *Agronomy* **2019**, *9*, 327. [CrossRef]
26. Zhang, W.; Wei, J.; Guo, L.; Fang, H.; Liu, X.; Liang, K.; Niu, W.; Liu, F.; Siddique, K.H.M. Effects of two biochar types on mitigating drought and salt stress in tomato seedlings. *Agronomy* **2023**, *13*, 1039. [CrossRef]
27. Fan, R.; Luo, J.; Yan, S.; Zhou, Y.; Zhang, Z. Effects of biochar and super absorbent polymer on substrate properties and water spinach growth. *Pedosphere* **2015**, *25*, 737–748. [CrossRef]
28. Gee, G.W.; Or, D. 2.4 Particle-size analysis. In *Methods of Soil Analysis: Part 4 Physical Methods*; Soil Science Society of America, Inc.: Madison, WI, USA, 2002; pp. 255–293. [CrossRef]
29. Nelson, D.W.; Sommers, L.E. Total carbon, organic carbon, and organic matter. In *Methods of Soil Analysis: Part 2 Chemical and Microbiological Properties*; Soil Science Society of America, Inc.: Madison, WI, USA, 1982; pp. 539–579. [CrossRef]
30. Sáez-Plaza, P.; Michałowski, T.; Navas, M.J.; Asuero, A.G.; Wybraniec, S. An overview of the Kjeldahl method of nitrogen determination. Part I. Early history, chemistry of the procedure, and titrimetric finish. *Crit. Rev. Anal. Chem.* **2013**, *43*, 178–223. [CrossRef]
31. Ekebafe, M.O.; Ekebafe, L.O.; Maliki, M. Utilisation of biochar and superabsorbent polymers for soil amendment. *Sci. Prog.* **2013**, *96*, 85–94. [CrossRef]
32. Sairam, R.K.; Saxena, D.C. Oxidative stress and antioxidants in wheat genotypes: Possible mechanism of water stress tolerance. *J. Agron. Crop Sci.* **2000**, *184*, 55–61. [CrossRef]
33. Buege, J.A.; Aust, S.D. [30] Microsomal lipid peroxidation. In *Methods in Enzymology*; Academic Press: Cambridge, MA, USA, 1978; Volume 52, pp. 302–310. [CrossRef]
34. Bertrand, R.L.; Eze, M.O. Modifying polyacrylamide background color for the nitroblue tetrazolium-based superoxide dismutase staining assay. *Adv. Enzym. Res.* **2014**, *2014*, 22008. [CrossRef]
35. Nakano, Y.; Asada, K. Hydrogen peroxide is scavenged by ascorbate-specific peroxidase in spinach chloroplasts. *Plant Cell Physiol.* **1981**, *22*, 867–880.
36. MacAdam, J.W.; Nelson, C.J.; Sharp, R.E. Peroxidase activity in the leaf elongation zone of tall fescue: I. Spatial distribution of ionically bound peroxidase activity in genotypes differing in length of the elongation zone. *Plant Physiol.* **1992**, *99*, 872–878. [CrossRef]
37. Chanes, B.; Mahely, A.C. Assay of catalase and peroxidase. In *Methods in Enzymology*; Academic Press: New York, NY, USA, 1996; pp. 764–791.
38. Ahmadi, A.; Farzad, T.H.; Feizi, V. Water stress and mineral zeolite application on growth and some physiological characteristics of Mallow (*Malva sylvestris*). *J. Plant Res. (Iran. J. Biol.)* **2015**, *28*, 459–474.
39. Massacci, A.; Nabiev, S.M.; Pietrosanti, L.; Nematov, S.K.; Chernikova, T.N.; Thor, K.; Leipner, J. Response of the photosynthetic apparatus of cotton (*Gossypium hirsutum*) to the onset of drought stress under field conditions studied by gas-exchange analysis and chlorophyll fluorescence imaging. *Plant Physiol. Biochem.* **2008**, *46*, 189–195. [CrossRef]
40. Afzal, A.; Duiker, S.W.; Watson, J.E. Leaf thickness to predict plant water status. *Biosyst. Eng.* **2017**, *156*, 148–156. [CrossRef]
41. Yang, X.; Lu, M.; Wang, Y.; Wang, Y.; Liu, Z.; Chen, S. Response mechanism of plants to drought stress. *Horticulturae* **2021**, *7*, 50. [CrossRef]
42. Jia, Y.; Gray, V.M. Interrelationships between nitrogen supply and photosynthetic parameters in *Vicia faba* L. *Photosynthetica* **2003**, *41*, 605–610. [CrossRef]
43. Bettaieb, I.; Zakhama, N.; Wannes, W.A.; Kchouk, M.E.; Marzouk, B. Water deficit effects on Salvia officinalis fatty acids and essential oils composition. *Sci. Hortic.* **2009**, *120*, 271–275. [CrossRef]
44. Lyu, S.; Du, G.; Liu, Z.; Zhao, L.; Lyu, D. Effects of biochar on photosystem function and activities of protective enzymes in *Pyrus ussuriensis* Maxim. under drought stress. *Acta Physiol. Plant.* **2016**, *38*, 220. [CrossRef]

45. Akbarzadeh, S.; Morshedloo, M.R.; Behtash, F.; Mumivand, H.; Maggi, F. Exogenous β-aminobutyric acid (BABA) improves the growth, essential oil content, and composition of grapefruit mint (*Mentha suaveolens* × *piperita*) under water deficit stress conditions. *Horticulturae* **2023**, *9*, 354. [CrossRef]
46. Del Buono, D.; Ioli, G.; Nasini, L.; Proietti, P. A comparative study on the interference of two herbicides in wheat and Italian ryegrass and on their antioxidant activities and detoxification rates. *J. Agric. Food Chem.* **2011**, *59*, 12109–12115. [CrossRef] [PubMed]
47. Wang, Y.; Yu, J.; Zhou, B.; Sapkota, S.; Wei, F.; Wang, Z. Atrazine and mesotrione-induced oxidative stress and impact on antioxidant enzymes and chlorophyll contents in bermudagrass. *Planta Daninha* **2018**, *36*, e018172227. [CrossRef]
48. Wang, X.; Vignjevic, M.; Jiang, D.; Jacobsen, S.; Wollenweber, B. Improved tolerance to drought stress after anthesis due to priming before anthesis in wheat (*Triticum aestivum* L.) var. Vinjett. *J. Exp. Bot.* **2014**, *65*, 6441–6456. [CrossRef]
49. Jaafar, H.Z.E.; Ibrahim, M.H.; Karimi, E. Phenolics and flavonoids compounds, phenylanine ammonia lyase and antioxidant activity responses to elevated CO_2 in *Labisia pumila* (Myrisinaceae). *Molecules* **2012**, *17*, 6331–6347. [CrossRef]
50. Aghamirzaei, H.; Mumivand, H.; Nia, A.E.; Raji, M.R.; Maroyi, A.; Maggi, F. Effects of Micronutrients on the Growth and Phytochemical Composition of Basil (*Ocimum basilicum* L.) in the Field and Greenhouse (Hydroponics and Soil Culture). *Plants* **2024**, *13*, 2498. [CrossRef]
51. Colom, M.R.; Vazzana, C. Photosynthesis and PSII functionality of drought-resistant and drought-sensitive weeping lovegrass plants. *Environ. Exp. Bot.* **2003**, *49*, 135–144. [CrossRef]
52. Bolla, A.; Voyiatzis, D.; Koukourikou-Petridou, M.; Chimonidou, D. Photosynthetic parameters and cut-flower yield of rose 'Eurored' (HT) are adversely affected by mild water stress irrespective of substrate composition. *Sci. Hortic.* **2010**, *126*, 390–394. [CrossRef]
53. Álvarez, S.; Sánchez-Blanco, J. Mª. Changes in growth rate, root morphology and water use efficiency of potted Callistemon citrinus plants in response to different levels of water deficit. *Sci. Hortic.* **2013**, *156*, 54–62. [CrossRef]
54. Nar, H.; Saglam, A.; Terzi, R.; Várkonyi, Z.; Kadioglu, A. Leaf rolling and photosystem II efficiency in *Ctenanthe setosa* exposed to drought stress. *Photosynthetica* **2009**, *47*, 429–436. [CrossRef]
55. Nanda, S.; Azargohar, R.; Kozinski, J.A.; Dalai, A.K. Characteristic studies on the pyrolysis products from hydrolyzed Canadian lignocellulosic feedstocks. *BioEnergy Res.* **2014**, *7*, 174–191. [CrossRef]
56. El-Naggar, A.; Lee, S.S.; Rinklebe, J.; Farooq, M.; Song, H.; Sarmah, A.K.; Zimmerman, A.R.; Ahmad, M.; Shaheen, S.M.; Ok, Y.S. Biochar application to low fertility soils: A review of current status, and future prospects. *Geoderma* **2019**, *337*, 536–554. [CrossRef]
57. Mohamadnia, Z.; Zohuriaan-Mehr, M.J.; Kabiri, K.; Jamshidi, A.; Mobedi, H. Ionically cross-linked carrageenan-alginate hydrogel beads. *J. Biomater. Sci. Polym. Ed.* **2008**, *19*, 47–59. [CrossRef] [PubMed]
58. Arbona, V.; Iglesias, D.J.; Jacas, J.; Primo-Millo, E.; Talon, M.; Gómez-Cadenas, A. Hydrogel substrate amendment alleviates drought effects on young citrus plants. *Plant Soil* **2005**, *270*, 73–82. [CrossRef]

horticulturae

MDPI

Article

MIR396d-p3 Negatively Regulates Apple Resistance to *Colletotrichum gloeosporioides* via *MdUGT89A2* and *MdRGA3*

Baodong Zhang [1], Jinqi Tang [2], Zhirui Ji [1], Yinan Du [1], Jialin Cong [1] and Zongshan Zhou [1,*]

[1] Research Institute of Pomology, Chinese Academy of Agriculture Sciences, Xingcheng 125100, China; mayday0318143@163.com (B.Z.)
[2] College of Horticulture, China Agricultural University, Beijing 100193, China
* Correspondence: zszhouqrj@163.com

Abstract: Apple (*Malus domestica*) is an economically important fruit crop, but its production is affected by Glomerella leaf spot, a devastating disease caused by the fungal pathogen *Colletotrichum gloeosporioides*. MicroRNA (miRNA) is a kind of non-coding RNA that plays an important role in the process of plant–pathogen interactions. However, little is known about the miRNAs that influence apple resistance against *C. gloeosporioides*. A novel miRNA, *MIR396d-p3*, was identified through small RNA sequencing (sRNA-seq). Functional analyses revealed that *MIR396d-p3* negatively regulates apple resistance to *C. gloeosporioides*. In addition, *MdUGT89A2* and *MdRGA3* were confirmed as targets of *MIR396d-p3* using 5′ RACE and heterologous expression assays. We further found that overexpressing *MdUGT89A2* and *MdRGA3* induce apple disease resistance to *C. gloeosporioides*, while silencing of *MdUGT89A2* and *MdRGA3* reduces resistance to *C. gloeosporioides*. These results indicate that *MIR396d-p3* plays a role in the response to the infection of *C. gloeosporioides* through regulating the expressions of *MdUGT89A2* and *MdRGA3*. This research provides a new perspective on the interaction between apples and *C. gloeosporioides* and offers possible targets for resistance breeding.

Keywords: *MIR396d-p3*; apple glomerella leaf spot; *UGT89A2*; plant immune

1. Introduction

Apple (*Malus domestica*) is a major fruit crop worldwide but suffers significant yield losses due to persistent fungal pathogens [1]. Apple glomerella leaf spot (GLS), caused by *Colletotrichum gloeosporioides* (*C. gloeosporioides*), leads to defoliation and a marked decline in apple yield [2]. The main varieties of apple in the world, such as "Golden Delicious" and "Gala", are universally susceptible to GLS, thereby exacerbating the impact of this disease [3]. High levels of humidity and temperature lead to recurrent outbreaks of GLS that affect both leaves and fruits [4]. Chemical control continues to be the predominant approach for managing apple GLS disease at this time, but treatments have negative repercussions, impacting environmental health and jeopardizing food safety. Deciphering the resistance mechanisms of apples against *C. gloeosporioides*, along with cultivating new resistant germplasm, would be a more effective approach.

MicroRNAs (miRNAs) are small non-coding RNAs that regulate gene expression post-transcriptionally by binding to target mRNAs and inhibiting their translation or promoting degradation [5]. Mounting evidence has revealed that miRNAs perform critical regulatory roles in plant–pathogen interactions [6]. In particular, miRNAs play vital regulatory roles in the response of apple to various fungal pathogens, such as *Botryosphaeria dothidea* [7–10], *Alternaria alternata* [11–13], and *C. gloeosporioides* [14]. However, the precise mechanisms by

which miRNAs mediate apple resistance to *C. gloeosporioides* are still not well understood. Specifically, the role of *miR396* in regulating apple resistance to *C. gloeosporioides* has not yet been reported, while the regulation of immune responses to pathogenic infections by *miR396* in Arabidopsis [15], rice [16], tomato [17], and soybean [18] has been documented.

UDP-glycosyltransferases (*UGTs*) are pivotal biotransformation enzymes that have developed across a wide range of living organisms, including bacteria, fungi, plants, and animals [19]. *UGTs* are essential for the glycosylation of small molecules [20]. This process can modify the homeostasis of these compounds by influencing their chemical activity, degradation, and distribution. *UGTs* are involved in various processes related to plant growth and defense response [21–23]. For example, *UGT73C7* is a pathogen-induced glycosyltransferase in Arabidopsis that enhances disease resistance by redirecting phenylpropanoid metabolism and upregulating the expression of the *SNC1* gene, a key component in plant immunity [21]. In addition, UDP-glucosyltransferase *HvUGT13248* is conferred type II resistance to Fusarium head blight (*FHB*) in barley by glucosylating the mycotoxin deoxynivalenol (*DON*) to its nontoxic form, DON-3-O-glucoside (*D3G*), and demonstrates that mutations in *HvUGT13248* increase susceptibility to *F. graminearum* infection [22]. Given these findings [21,22], we hypothesize that *UGTs* may play a pivotal role in apple resistance to *C. gloeosporioides*. However, there have been no reports on the study of *UGTs* in the disease resistance of apples.

Plant disease resistance genes (*R* genes) are the most recognized group of resistance gene analogs (*RGAs*), playing a vital role in sensing and defending against various plant pathogens [24]. This typical *R* gene structure usually comprises three domains: a leucine-rich repeat (LRR), a nucleotide-binding domain (NBD), and a signaling domain, which includes the Toll/IL-1 receptor (TIR), RESISTANCE TO POWDERY MILDEW 8 (RPW8), and the coiled-coil (CC) domain [25]. In addition, *R* genes and *RGAs* serve as essential genetic resources for managing plant diseases and offering immune protection against significant pathogen-related damage. Therefore, it is essential to dissect the role of *RGAs* in the resistance of apples to *C. gloeosporioides*.

This study used sRNA-seq technology to analyze how apple miRNA responds to the infection of *C. gloeosporioides*. At the same time, a novel miRNA, *MIR396d-p3*, is identified as the research object of this study. Then we predicted and verified through 5′ RACE and heterologous expression assays that *MdUGT89A2* and *MdRGA3* are direct targets of *MIR396d-p3.* To further confirm this regulatory relationship, expression profiling of *MIR396d-p3* and its target genes was detected in susceptible and resistant cultivars. In addition, we found that *MIR396d-p3* regulates resistance to *C. gloeosporioides* by modulating the expression of *MdUGT89A2* and *MdRGA3* through functional analyses. Taken together, this research provides a new perspective on the interaction mechanism between apples and *C. gloeosporioides*.

2. Material and Methods

2.1. Plant Material and Pathogen Cultures

The apple cultivars “Royal Gala” (abbreviated as “GL-3”) and “Fuji” (“FJ”) were maintained in vitro using Murashige and Skoog basal medium containing specific plant growth regulators: 0.6 mg·L^{-1} benzylaminopurine (BAP), 0.4 mg·L^{-1} α-naphthaleneacetic acid (NAA), and 0.2 mg·L^{-1} gibberellin A3 (GA3). The plant materials were grown at 25 ± 1 °C under controlled conditions and a 16/8 h light/dark cycle with a light intensity of 120 μmol m^{-2} s^{-1} in humidity-controlled chambers maintaining saturated moisture. For experimental standardization, in vitro-developed apple plantlets at 28 days of maturity were systematically selected as biological material for subsequent experiments.

Nicotiana benthamiana were sown in a mix (vermiculite, perlite, and soil in a 1:1:1 ratio). *N. benthamiana* plantlets were cultivated under controlled environmental conditions, including a temperature regime of 22 ± 1 °C, a 16/8 h light/dark cycle with a light intensity of 120 μmol m^{-2} s^{-1}, and 80% relative humidity.

The *C. gloeosporioides* strain W16, preserved in our laboratory, was grown on potato dextrose agar (PDA) medium at 28 °C for 3 days [26]. A sterilized toothpick was then employed to abrade the mycelial surface to promote sporulation. After an additional 4 days of incubation, we rinsed the mycelium and spores on the plate with sterile water. We filtered the resulting suspension through four layers of sterile gauze to remove mycelial fragments. We collected the filtrate containing spores and adjusted the spore concentration to 1×10^6 conidia·mL^{-1} for the subsequent experiments.

2.2. sRNA-Seqencing and Identification of Differentially Expressed microRNAs (DE-miRNAs)

To investigate whether miRNAs are involved in the response of apple plants to *C. gloeosporioides* infection, we performed sRNA-seq analysis using the susceptible cultivar "GL-3". Newly emerged apical leaves (3–4 leaves per plant) were inoculated with a conidial suspension of *C. gloeosporioides*. Samples were collected 24 h post-inoculation, with three bottles of leaves pooled as one biological replicate, and three independent biological replicates were subjected to sequencing analysis. Total RNA from "GL-3" plants, both inoculated with *C. gloeosporioides* and uninoculated controls, was extracted using a column method according to the method reported by Zhang et al. [27]. The quantification and purity evaluation of total RNA were performed with Nanodrop (Life Technologies, Carlsbad, CA, USA) and a Bioanalyzer 2100 (Agilent Technologies, Santa Clara, CA, USA). Subsequently, the small RNA libraries were assembled using the 5′-phosphate-dependent method and were sequenced on an Illumina HiSeq 2000/2500 platform [28].

The obtained raw data were selected by aligning them against various RNA databases, including the RFam database and the Repbase database, resulting in valid small RNA data for subsequent analysis [29]. In order to screen for differentially expressed miRNAs, we utilized *p*-values and fold change for selection. The specific criteria were $\log_2|(\text{fold change})| \geq 1$ and $p\text{-value} < 0.05$.

2.3. Bioinformatics Analysis

The target genes of candidate miRNA and the RNA secondary structure of candidate precursor miRNA were predicted using the psRNATarget web server [30] (https://www.zhaolab.org/psRNATarget/, accessed on 21 March 2025) and the UNAFold Web Server (http://www.unafold.org, accessed on 21 March 2025), respectively. To understand how many plant species contain candidate miRNA families and the evolutionary relationship between candidate miRNA and the reported candidate miRNA family in apple, we downloaded all relevant information from the miRBase database. Meanwhile, we used MEGA_12.0.10 software to construct a phylogenetic tree about candidate precursor miRNA.

Similarly, the promoter sequence of candidate miRNA was obtained from the GDR database by aligning it with the apple genome sequence [28], and cis-acting elements in the promoter were analyzed using the PlantCARE web server (https://bioinformatics.psb.ugent.be/webtools/plantcare/html/, accessed on 20 January 2025). Finally, visualization of the results was performed using TBtools v2.061 [31].

2.4. Rapid Amplification of cDNA Ends Assay

Total RNA was obtained as described above. First strand cDNA was synthesized at 42 °C for 90 min and at 70 °C for 15 min using 5′ TS Oligo. Then, rapid amplification of cDNA ends (RACE) was conducted using the 5′ GSP provided in the HiScript-TS 5′/3′ RACE Kit. Nested PCR was then performed for multiple rounds of amplification to obtain

positive bands. Subsequently, 24 randomly selected clones were sent for sequencing to a company.

2.5. Plasmid Construction

35S: *MIR396d-p3* construct. The sequence of the *MIR396d-p3* precursor was introduced into the pFGC5941 vector at the NcoI/BamHI site.

35S: STTM-*MIR396d-p3* construct. A fragment containing two partially complementary sequences of *MIR396d-p3*, separated by a 48-base pair short spacer, was artificially synthesized and introduced into the pFGC5941 binary vector.

35S: *MdUGT89A2*-GUS construct. The full coding sequence of *MdUGT89A2*, excluding the stop codon, was introduced into the pFGC5941 vector at the NcoI/BamHI site.

35S: *MdRGA3*-GUS construct. The complete coding sequence of *MdRGA3*, without the stop codon, was inserted into the pFGC5941 binary vector at the NcoI/BamHI site.

35S: *MdUGT89A2* construct. The coding sequence of *MdUGT89A2* was introduced into the pFGC5941 binary vector.

35S: *MdRGA3* construct. The gene sequence of *MdRGA3* was cloned into the pFGC5941 binary vector.

RNAi construct. Two fragments with the sense and antisense sequences of *MdUGT89A2* and *MdRGA3* were inserted into the flanking regions of the pFGC5941 intron, respectively.

2.6. Agrobacterium-Mediated Transient Transformation

Transformation of all recombinant constructs was performed in *Agrobacterium tumefaciens* GV3101 cells. A single colony of *Agrobacterium* was grown in LB liquid medium containing rifampin (50 $\mu g \cdot mL^{-1}$) and kanamycin (50 $\mu g \cdot mL^{-1}$). Subsequently, the bacteria were suspended in a buffer solution composed of 10 mM $MgCl_2$, 10 mM MES, and 100 μM acetosyringone, with a pH adjusted to 5.6. The suspension was incubated at 25 °C in the dark for 2 h prior to its use in transient transformation experiments.

2.7. Histochemical Staining and GUS Activity Quantification

GUS staining assay was conducted on *N. benthamiana* infiltrated leaves according to previously reported methods [32]. The *N. benthamiana* leaves utilized for histochemical GUS staining were subjected to an incubation at 37 °C overnight. Subsequently, they were placed in a series of ethanol solutions with increasing concentrations (30%, 50%, and 70%) to facilitate visualization.

To further quantify GUS activity, the fluorometric 4-methylumbelliferyl-β-D-glucuronide (*MUG*) method was employed. The specific method should be carried out in accordance with the GUS gene quantitative detection Kit (Coolaber Science & Technology, Beijing, China). A unit of GUS activity is characterized by the production of 1 nM of 4-methylumbelliferone per minute for each milligram of soluble protein. In each treatment, 10 leaves corresponding to each construct were collected for detection.

2.8. RT-qPCR Assay

To validate the expression patterns of miRNAs and their target genes, total RNA was extracted using a column-based method at 4 d post-transfection. For temporal profiling of miRNA expression, additional samples were harvested at 24 and 72 h post-transfection, followed by RNA extraction using the same protocol. First-strand cDNA was generated through the HiScript II 1st Strand cDNA Synthesis Kit (Vazyme Biotech Co., Ltd., Nanjing, China). The expression level of mature *MIR396d-p3* was analyzed using stem-loop real-time quantitative PCR, with 5S rRNA and *MdActin* serving as internal controls. RT-qPCR was conducted in accordance with the instructions provided for ChamQ SYBR qPCR Master

Mix using CFX Connect TM Real-Time System (BIO-RAD, Hercules, CA, USA). The $2^{-\Delta\Delta CT}$ method was used to calculate relative expression levels of the corresponding genes [33].

To quantify fungal biomass, fungal and plant DNA extraction kits (Sangon Biotech, Shanghai, China) were employed to isolate *C. gloeosporioides* DNA and apple genomic DNA from leaf samples collected at 48 h post-inoculation, respectively. Subsequently, the fungal *Cgβ-Tubulin* gene and the apple *MdActin* gene were selected as internal reference genes for biomass quantification. Utilizing the same RT-qPCR reaction conditions and calculation procedures as described for the RT-qPCR assay, biomass data were obtained.

2.9. Statistical Analysis

The statistical analyses were implemented using GraphPad Prism 10 software. The data are expressed as the mean ± standard error (SE). One-way ANOVA followed by Tukey's test ($p < 0.05$) was used to analyze significant differences.

3. Results

3.1. Analysis of Apple Small RNA Sequencing Response to C. gloeosporioides

To investigate whether miRNAs of apple are involved in the response to *C. gloeosporioides* infection, sRNA-seq was conducted, and the clean data were obtained. First, we removed miRNAs mapped to two positions of the same precursor on the genome; the unique count of candidate RNAs was obtained. The length distribution analysis of the above miRNAs is shown in Figure S1B. According to Figure S1B, we found that the most abundant small RNAs produced in the leaves of "GL-3" apple were 24 nt in length, followed by 23 nt, 22 nt, and 21 nt. Additionally, 284 conserved miRNAs belonged to 47 miRNA families (Figure S1A). Among these families, *miR156* is the largest, with a total of 37 members, followed by the *miR166*, *miR167*, and *miR159* families, which contain 17, 15, and 14 members, respectively. Furthermore, there are some miRNA families with only one member, such as *miR1510*, *miR4243*, *miR7533*, *miR7125*, and *miR8775*.

To better understand the DE-miRNAs and their target genes, we performed GO (Gene Ontology) enrichment analysis and KEGG (Kyoto Encyclopedia of Genes and Genomes) analysis on the predicted target genes. The results are shown in Figure S1C,D. According to Figure S1C,D, the target genes of the DE-miRNAs are mainly enriched in biological processes such as defense response, regulation of transcription by RNA polymerase II, cell differentiation, cellular response to iron ions, and signal transduction. The KEGG analysis results indicate that the target genes of the DE-miRNAs play significant roles in pathways related to spliceosomes, plant–pathogen interactions, starch and sucrose metabolism, and *MAPK* signaling. Based on the GO and KEGG analyses, it can be concluded that these target genes of DE-miRNAs play important roles in the response of "GL-3" apple leaves to *C. gloeosporioides* infection.

3.2. Validation of sRNA-Seq Data Using RT-qPCR

To investigate the credibility of sRNA-seq, the expression profiles of nine differentially expressed miRNAs (DE-miRNAs), including *miR395a*, *MIR10994-p5_1ss6TC*, *MIR10986-p3_1ss21GT*, *MIR2916-p5_1ss5AG*, *MIR390a-p3*, *miR156e_R+1*, *MIR395c-p5*, *miR167a*, and *PC-3p-4885_278*, were detected through RT-qPCR at 0 h, 24 h, and 72 h post-infection. As shown in Figure 1, RT-qPCR demonstrated that *miR395a* exhibited a significant increase as the infection time increases; this trend is consistent with the sRNA-seq data. Similarly, the expression levels of *MIR10994-p5_1ss6TC* and *MIR10986-p3_1ss21GT* also show an increase with the increase in the infection time, and the expression levels are also increasing. Interestingly, most of these miRNAs were upregulated at 24 h or 72 h, except *miR167a* and *PC-3p-4885_278*. In general, the results from RT-qPCR aligned well with the sRNA-seq data.

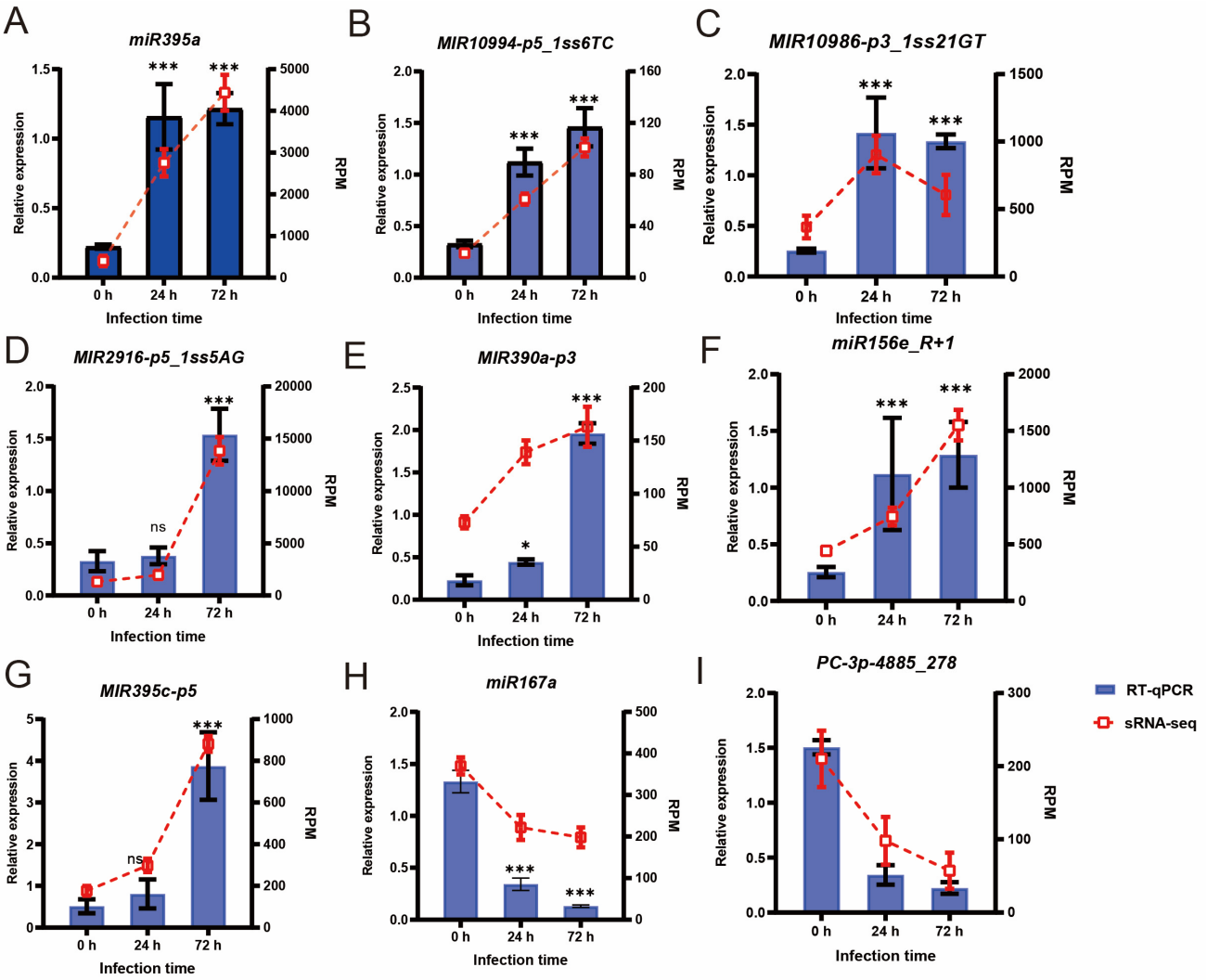

Figure 1. RT-qPCR validation of differentially expressed miRNA (DE-miRNA) expression in apple leaves following *Colletotrichum gloeosporioides* infection. Comparison with sRNA-seq (miRNA) and RNA-seq (transcriptome) data is shown. Blue bars represent qRT-PCR expression levels; red lines indicate RNA-seq and sRNA-seq derived expression. Results are expressed as mean ± SD (n = 3). Statistical significance was determined by one-way ANOVA followed by Tukey's post-hoc test. * ($p < 0.05$), and ***($p < 0.001$) indicate significant differences. ns: not significant.

3.3. Identification and In Silico Analysis of miRNA Response to C. gloeosporioides

To investigate the possible miRNAs response to *C. gloeosporioides*, we selected a miRNA of particular interest, *MIR396d-p3*, based on *p*-values and fold change (FC). This is because *miR396* is a highly conserved small RNA molecule that has been identified in a wide range of plant species. According to the miRBase database (version 22.1), information about the *miR396* family has been found in 52 plant species (Figure S2). *miR396* may hold significant research value. Meanwhile, *MIR396d-p3* expression significantly increased after 24 h of infection, indicating its response to *C. gloeosporioides* infection (Figure 2A). First, we predicted the RNA secondary structure of the *MIR396d-p3* precursor through the UNAFold Web Server. The results were shown as Figure 2B: the *MIR396d-p3* precursor can form a secondary structure, indicating that the miRNA precursor may be stable and capable of being successfully processed into mature miRNA. Meanwhile, by aligning with the apple genome, it was found that the *MIR396d-p3* precursor is located between positions 2032169 and 2032271 on chromosome 2 (Figure 2C).

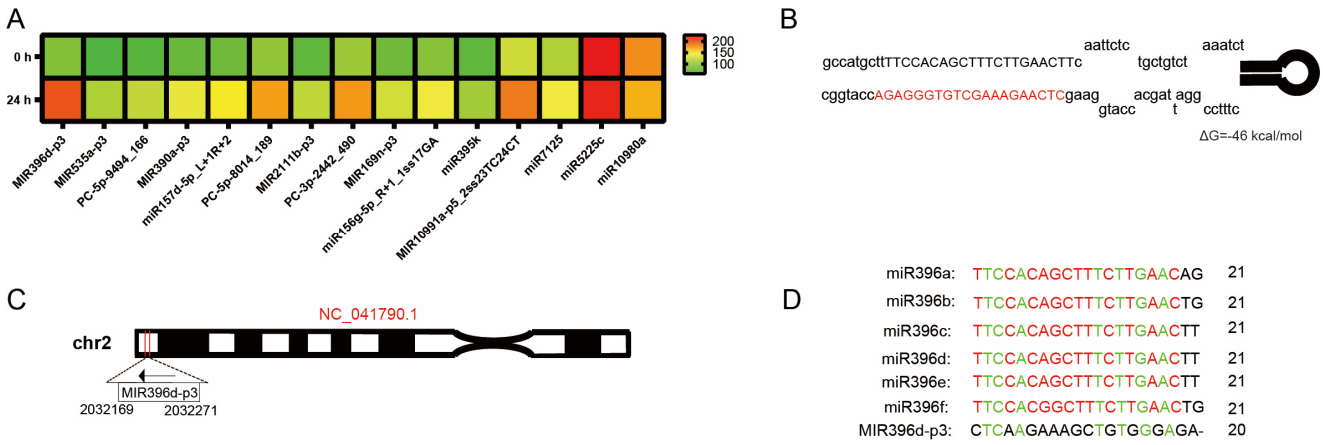

Figure 2. Identification and in silico analysis of *MIR396d-p3*. (**A**) The heatmap showing the *MIR396d-p3* was identified post-infection. (**B**) The secondary structure of a *MIR396d-p3* precursor sequence predicted through RNA-fold web service, with the free-energy value indicated. (**C**) The location of *MIR396d-p3* precursor sequence on chromosome 2 in the genome, with the corresponding NCBI accession number (NC_041790.1) marked. (**D**) Sequence alignment of *mdm-miR396* sequences. Red representative almost identical except for one base, green represents the same base.

To understand which environmental factors might influence *MIR396d-p3*, we predicted the cis-acting elements in the promoter region of the *MIR396d-p3* precursor. The results, shown in Figure S3, indicate that factors such as pathogen infection, light, jasmonic acid, and abscisic acid can influence its expression. In addition, by comparing with the existing apple *miR396* in the miRBase database, we found that apple *miR396* is highly conserved, despite some genetic evolution observed in *MIR396d-p3* (Figures 2D and S4).

3.4. MIR396d-p3 Cleaves MdUGT89A2 and MdRGA3 Transcripts

To screen the target genes of *MIR396d-p3*, we conducted a series of computational predictions through psRNATarget. As shown in Table S1, eight target genes were selected based on their predicted interactions with *MIR396d-p3*, including 1-aminocyclopropane-1-carboxylate synthase 7-like, transcription factor *bHLH111*-like, receptor protein kinase *ZmPK1*, *WAT1*-related protein, disease resistance protein *RGA3*, UDP-glycosyltransferase 89A2 (*UGT89A2*), peroxidase 29, and serine acetyltransferase. Next, we conducted 5′ RACE experiments on these eight target genes and found that only *UGT89A2* and *RGA3* interacted with *MIR396d-p3* (Figure 3A). To further clarify that *MIR396d-p3* can cleave *MdUGT89A2* and *MdRGA3* transcripts, we performed heterologous expression in *N. benthamiana*. First, we constructed 35S:*MIR396d-p3* and the corresponding 35S-*UGT89A2*:GUS, 35S-*RGA*:GUS using the Cloning Kit V2 (Figure 3B). Then, we co-injected them into *N. benthamiana* to assess their expression and detected GUS activity to determine if they interacted. Meanwhile, 35S:GUS served as a positive control, and 35S:*MIR396d-p3* served as a negative control. As shown in Figure 3D, 35S-*UGT89A2*:GUS and 35S-RGA:GUS did not show significant differences compared to 35S:GUS; however, when they were co-expressed with *MIR396d-p3*, their expression levels were significantly reduced, indicating that *MIR396d-p3* can cleave *MdUGT89A2* and *MdRGA3* transcripts. GUS staining also exhibited a similar phenotype (Figure 3C).

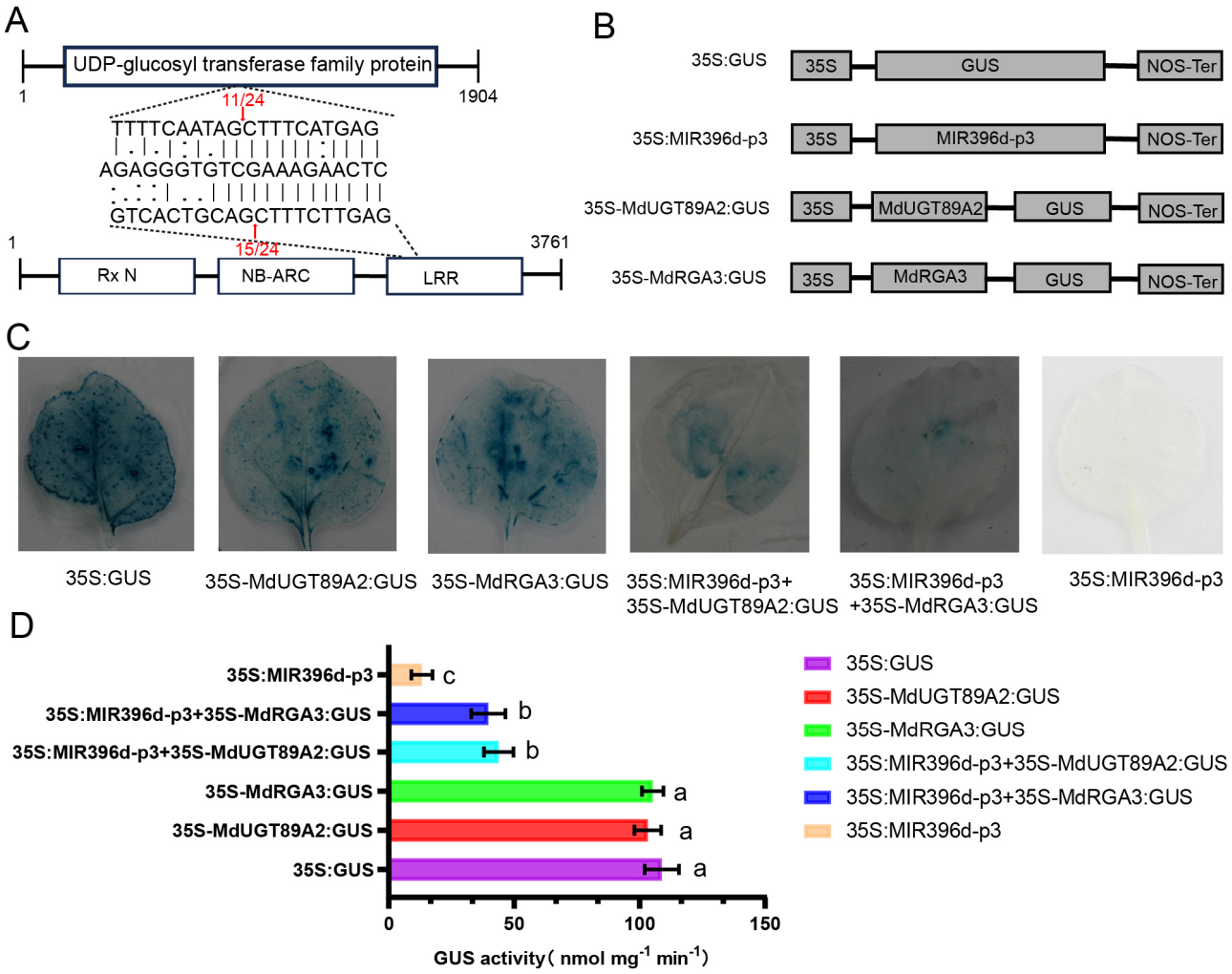

Figure 3. *MIR396d-p3* cleaves *MdUGT89A2* and *MdRGA3* transcripts. (**A**) 5′ RACE identified the cleavage site of the predicted *MIR396d-p3* target. The arrow denotes the cleavage site, and the numbers above indicate the frequency of cleavage at that site in independent clones. (**B**) Schematic diagrams of constructs used for co-transformation of *Nicotiana benthamiana*. (**C**) Histochemical GUS staining of *N. benthamiana* leaves 3 d post-infiltration with the indicated constructs. (**C**) Representative image from three independent experiments. (**D**) Quantification of GUS activity in *N. benthamiana* leaves transiently expressing the indicated constructs. Data represent means ± SD of three technical replicates. Different letters indicate significant difference $p < 0.05$ (one-way ANOVA followed by post hoc Tukey test). All data are shown as means ± SD (n = 9).

To assess the expression pattern of *MIR396d-p3* and its target genes *MdUGT89A2* and *MdRGA3* in the susceptible variety "GL-3" and the resistant variety "FJ", RT-qPCR assay was conducted at 0, 24, and 72 h post-*C. gloeosporioides* infection. As shown in Figure 4, the expression level of *MIR396d-p3* was significantly upregulated in"GL-3", while *MdUGT89A2* and *MdRGA3* were strikingly downregulated. Meanwhile, the expression level of *MIR396d-p3* in "FJ" continuously decreases as the infection time increases, while *MdUGT89A2* and *MdRGA3* were upregulated. Collectively, *MIR396d-p3* can negatively regulate the expression of *MdUGT89A2* and *MdRGA3*.

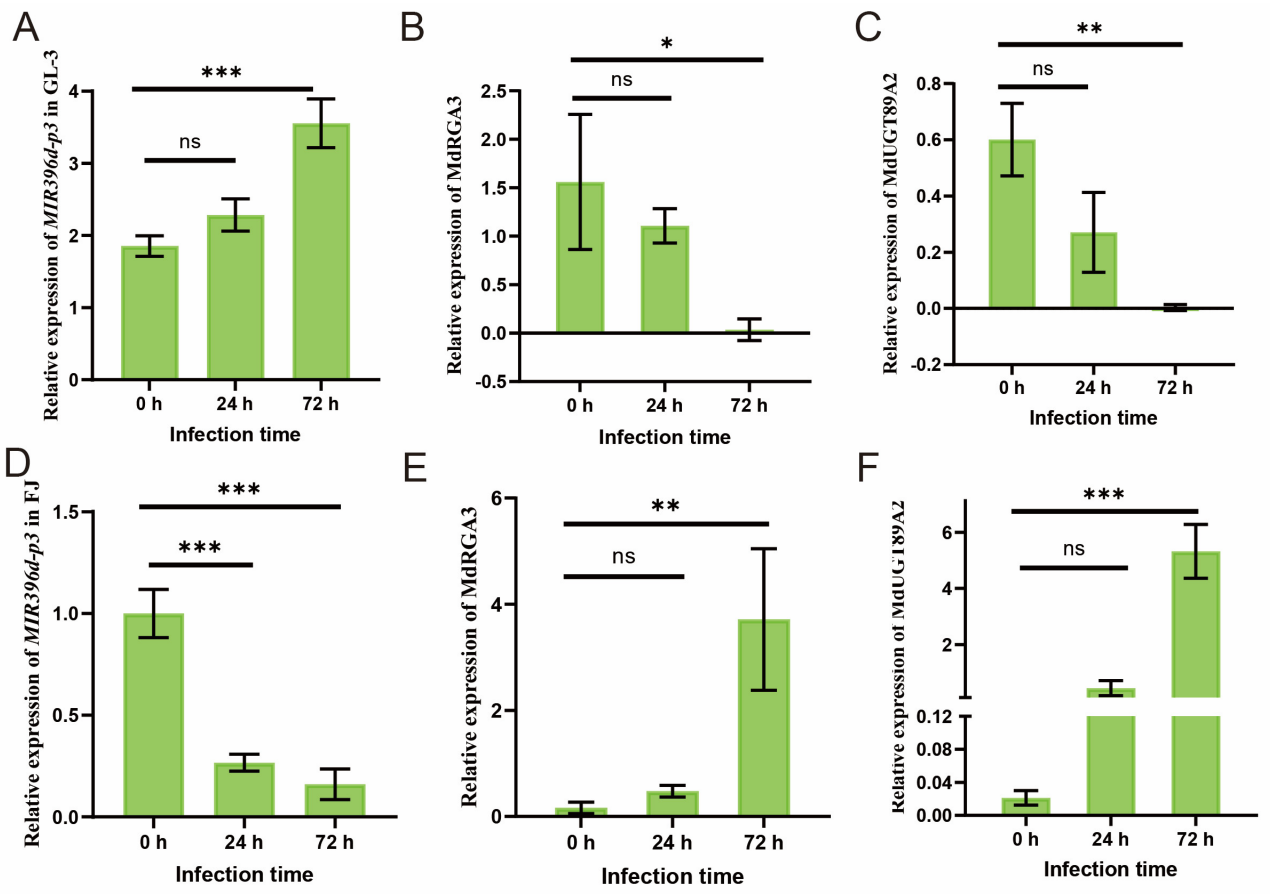

Figure 4. Analyses of expression patterns of *MIR396d-p3* and its target genes *MdUGT89A2* and *MdRGA3* in the apple response to *Colletotrichum gloeosporioides* infection. Expression analysis of mature *MIR396d-p3* in "GL-3" (**A**) and "FJ" (**D**) apple leaves at the indicated time points after inoculation with *C. gloeosporioides* using stem-loop RT-qPCR. Relative expression of *MdRGA3* (**B**) and *MdUGT89A2* (**C**) in "GL-3" apple leaves at 0, 24, and 72 h post-*C. gloeosporioides* infection (qRT-PCR). Relative expression of *MdRGA3* (**E**) and *MdUGT89A2* (**F**) in "FJ" apple leaves at 0, 24, and 72 h post-*C. gloeosporioides* infection (qRT-PCR). A one-way ANOVA was performed, followed by a Tukey's test (a post-hoc test used for multiple comparisons after a significant ANOVA result). Significant differences are marked with asterisks: * $p < 0.05$, ** $p < 0.01$, *** $p < 0.001$. ns: not significant.

3.5. Responsiveness of MIR396d-p3 to C. gloeosporioides Infection

To investigate the involvement of *MIR396d-p3* in the apple's response to *C. gloeosporioides*, we cloned the *MIR396d-p3* precursor into the pFGC5941 vector to construct the *MIR396d-p3* overexpression vector (Figure 5A). Then the overexpressed constructed vector was transformed into the resistant apple cultivar "FJ" via *Agrobacterium*-mediated transformation. The expression level of *MIR396d-p3* was assessed through RT-qPCR at 4 d post-inoculation. As shown in Figure 5B, the expression level of *MIR396d-p3* was significantly higher in the *MIR396d-p3* overexpression plants compared to wild-type "FJ" and the pFGC5941 EV control (EV).

Disease lesion areas were measured at 2 d post-*C.gloeosporioides* inoculation. The OE-*MIR396d-p3* plants exhibited significantly larger lesions compared to "FJ" and EV (Figure 5C,D). In addition, *C. gloeosporioides* biomass in the OE-*MIR396d-p3* plants was significantly higher than in the "FJ" and EV plants (Figure 5E). Based on these results, we therefore predicted that the *MIR396d-p3* is involved in the apple resistance response to *C. gloeosporioides*.

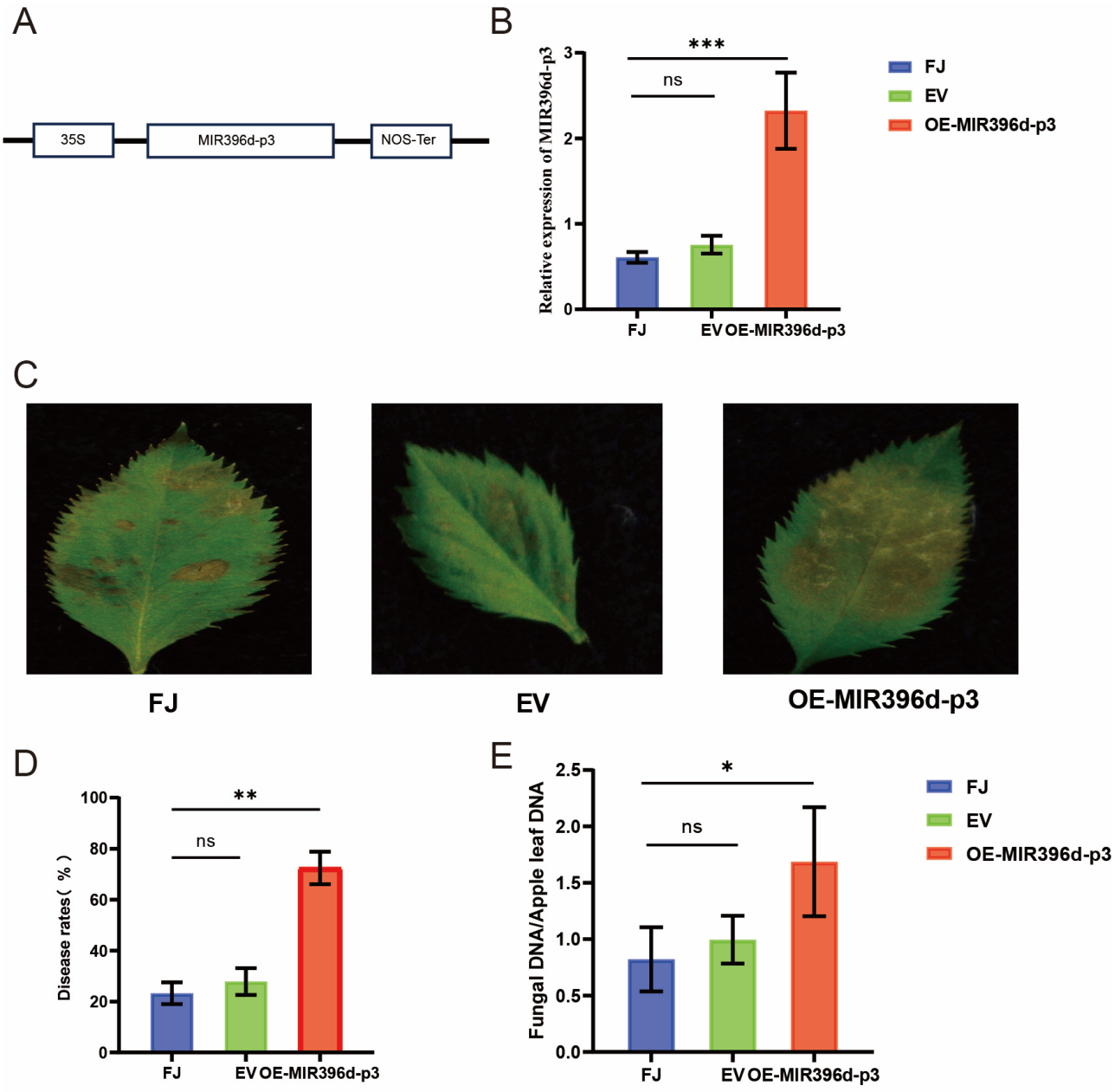

Figure 5. Overexpression of *MIR396d-p3* negatively regulates the resistance of apple to *C. gloeosporioides*. (**A**) Schematic diagrams of constructs used for *MIR396d-p3* overexpression. (**B**) The constitutive expression of mature *MIR396d-p3* (**B**) in non-infiltrated leaves and leaves infiltrated with different constructs by RT-qPCR analysis. (**C**) Representative symptoms in "FJ" leaves infected with *C. gloeosporioides*. The image is a photograph taken after inoculation at 48 h. (**D**) Percentage of infected "FJ" leaves at 48 hpi in different disease level classifications. (**E**) Relative biomass of *C. gloeosporioides* determined by quantitative PCR in infected leaves sampled at 48 hpi. Statistical significance was assessed via one-way ANOVA followed by Tukey's post-hoc test for multiple comparisons. Asterisks denote significant differences (* represent $p < 0.05$, ** represent $p < 0.01$, *** represent $p < 0.001$). ns: not significant.

To further explore the function of *MIR396d-p3* during the *C. gloeosporioides* infection, we constructed an *MIR396d-p3* silencing (STTM-*MIR396d-p3*) vector using STTM technology (Figure 6A). To evaluate the efficiency of silence, the STTM-*MIR396d-p3* vector was introduced into the susceptible apple cultivar "GL-3" via *Agrobacterium*-mediated transformation. We found that the expression level of *MIR396d-p3* was significantly reduced in STTM-*MIR396d-p3* plants, indicating that the *MIR396d-p3* is successfully silencing

(Figure 6B). Subsequently, these leaves were inoculated with *C. gloeosporioides*. After 2 days of inoculation, disease lesion areas were counted. Compared to the "GL-3" and EV plants, the STTM-*MIR396d-p3* plants displayed significantly reduced lesion areas (Figure 6C,D). The reduced *C. gloeosporioides* biomass in STTM-*MIR396d-p3* plants, quantified by RT-qPCR, further supports the observed effect that *MIR396d-p3* silencing enhances apple resistance to *C. gloeosporioides*. These findings strongly indicate *MIR396d-p3* negatively affects resistance to *C. gloeosporioides*.

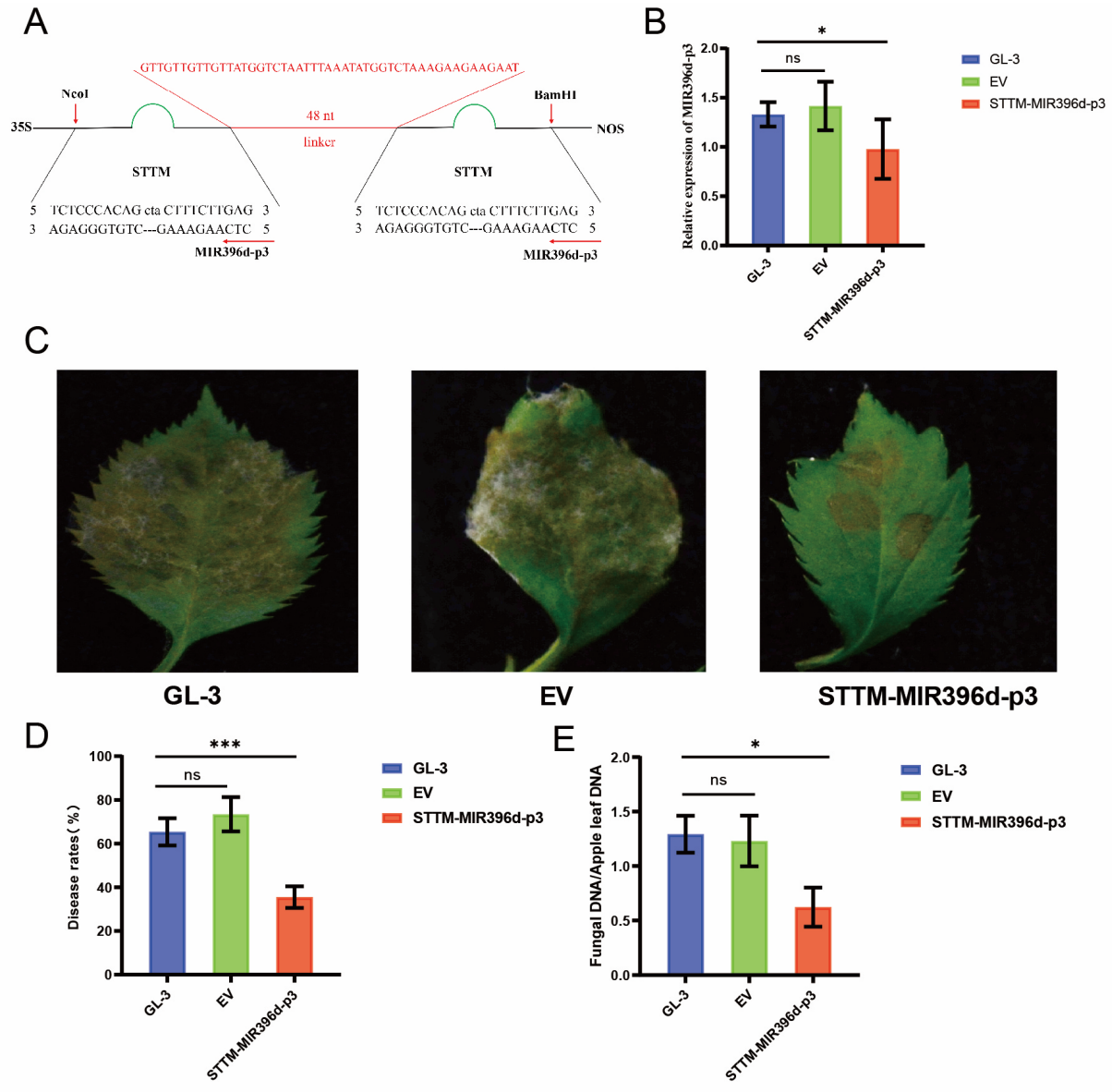

Figure 6. The *C. gloeosporioides* resistance of STTM-*MIR396d-p3* apple "GL-3" leaves. (**A**) Schematic structure of the construct for silencing *MIR396d-p3*. Relative expression levels of (**B**) *MIR396d-p3* in transiently transformed leaves of STTM-*MIR396d-p3*, "GL-3", and empty vector (EV) controls. Photographs of representative leaves with median lesion diameter in STTM-*MIR396d-p3*, "GL-3", and EV controls at 48 h after inoculation with *C. gloeosporioides* (**C**) are shown. (**D**) Determination of lesion diameter for different transformants inoculated with *C. gloeosporioides* were determined and analysed in STTM-*MIR396d-p3*, "GL-3", and EV plants. (**E**) Relative biomass of *C. gloeosporioides* was determined by qPCR. Statistical significance was assessed by one-way ANOVA with Tukey's post-hoc test. Significant differences are indicated by asterisks: * ($p < 0.05$), *** ($p < 0.001$). ns: not significant.

3.6. MdUGT89A2 and MdRGA3 Are Involved in the Resistance to C. gloeosporioides in Apple

We next examined the impact of *MdUGT89A2* and *MdRGA3* on apple's resistance to *C. gloeosporioides*. Full-length *MdUGT89A2* and *MdRGA3* sequences were amplified and cloned into the pFGC5941 vector to generate overexpression constructs (Figure S5). The construct was subsequently introduced into "GL-3" by *Agrobacterium*-mediated infiltration. RT-qPCR analysis confirmed successful overexpression of *MdUGT89A2* and *MdRGA3* in the OE-*MdUGT89A2* and OE-*MdRGA3* plants at 4 d post-transformation, respectively (Figure 7A). Lesion areas were measured 2 days following *C. gloeosporioides* inoculation. The OE-*MdUGT89A2* and OE-*MdRGA3* plants displayed a significantly reduced lesion area compared with the "GL-3" and EV plants. This similar result was further confirmed by the relative biomass (Figure 7D). These results indicated *MdUGT89A2* and *MdRGA3* positively regulate apple resistance to *C. gloeosporioides*.

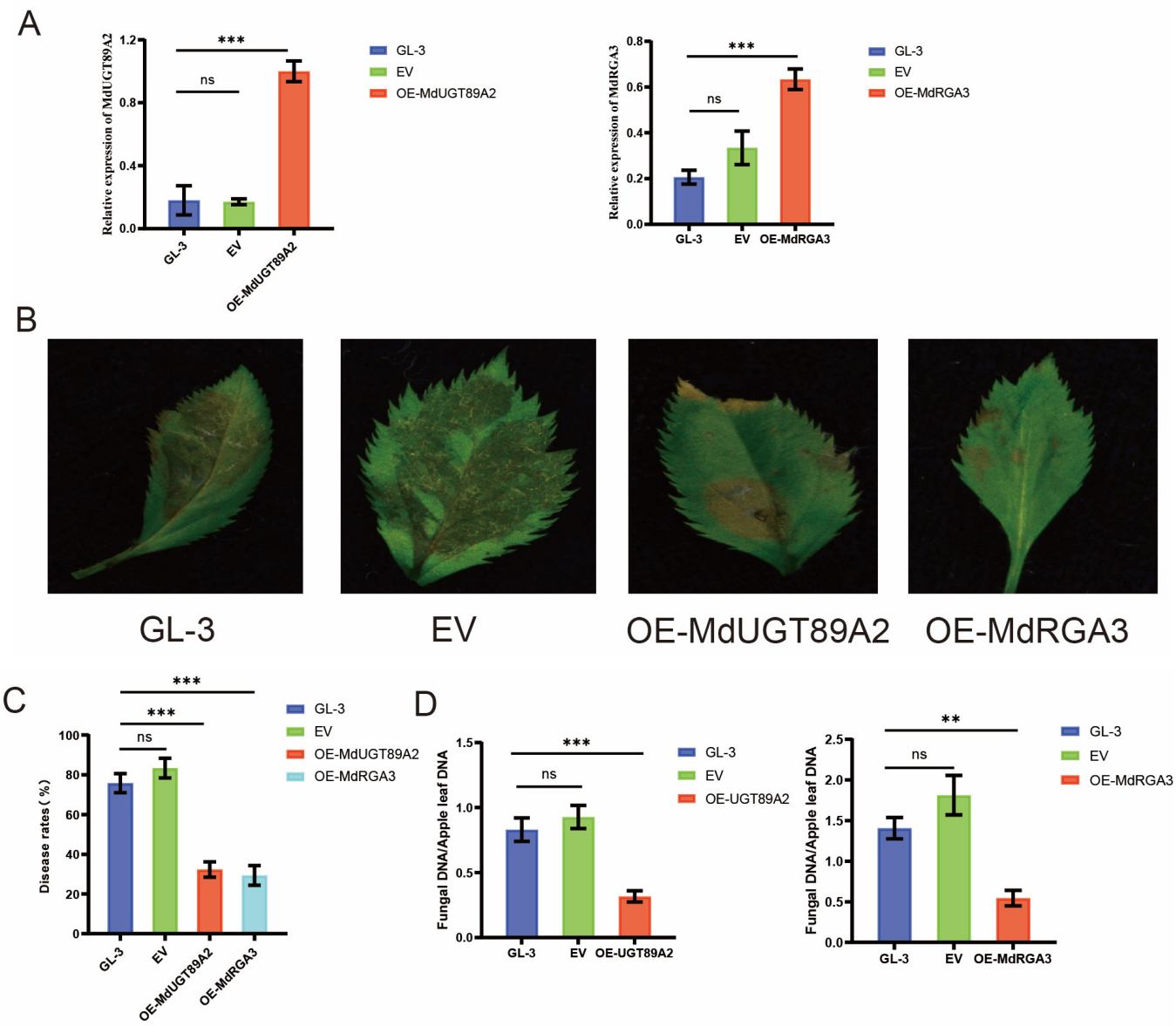

Figure 7. Transient overexpression (OE) of *MdUGT89A2* and *MdRGA3* enhances resistance to *C. gloeosporioides*. (**A**) Relative expression levels of the target genes in different plant lines ("GL-3", EV, OE-*MdUGT89A2*, OE -*MdRGA3*). Error bars represent standard deviations, and significance levels are indicated by asterisks (** indicated $p < 0.01$, *** represented $p < 0.001$, ns: not significant). (**B**) Phenotypes

of leaves from different plant lines, showing the differences in disease-related symptoms. (**C**) Disease severities of different plant lines, expressed as a percentage. Error bars represent standard deviations, and significance levels are indicated by asterisks. (**D**) Quantification of fungal DNA in different plant lines, indicating the accumulation of fungi. Statistical significance (one-way ANOVA, Tukey's post-hoc): ** $p < 0.01$, *** $p < 0.001$.

We used RT-qPCR to detect the expression level of *MdUGT89A2* and *MdRGA3* in the corresponding RNAi-silenced plants and found that *MdUGT89A2* expression was reduced by approximately ~76.74%, while *MdRGA3* expression was reduced by ~69.2%, relative to control plants (Figure 8A). Following inoculation with *C. gloeosporioides*, the lesion size was assessed on RNAi-*MdUGT89A2*, RNAi-*MdRGA3*, "FJ", and EV plants at 2 d post-inoculation. Silencing of *MdUGT89A2* and *MdRGA3* resulted in significantly larger lesions compared to "FJ" and EV plants. Consistent with the larger lesion sizes, *C. gloeosporioides* biomass was significantly elevated in plants with RNAi-mediated silencing of *MdUGT89A2* and *MdRGA3* (Figure 8D). Collectively, *MdUGT89A2* and *MdRGA3* function as positive regulators of apple resistance to *C. gloeosporioides*.

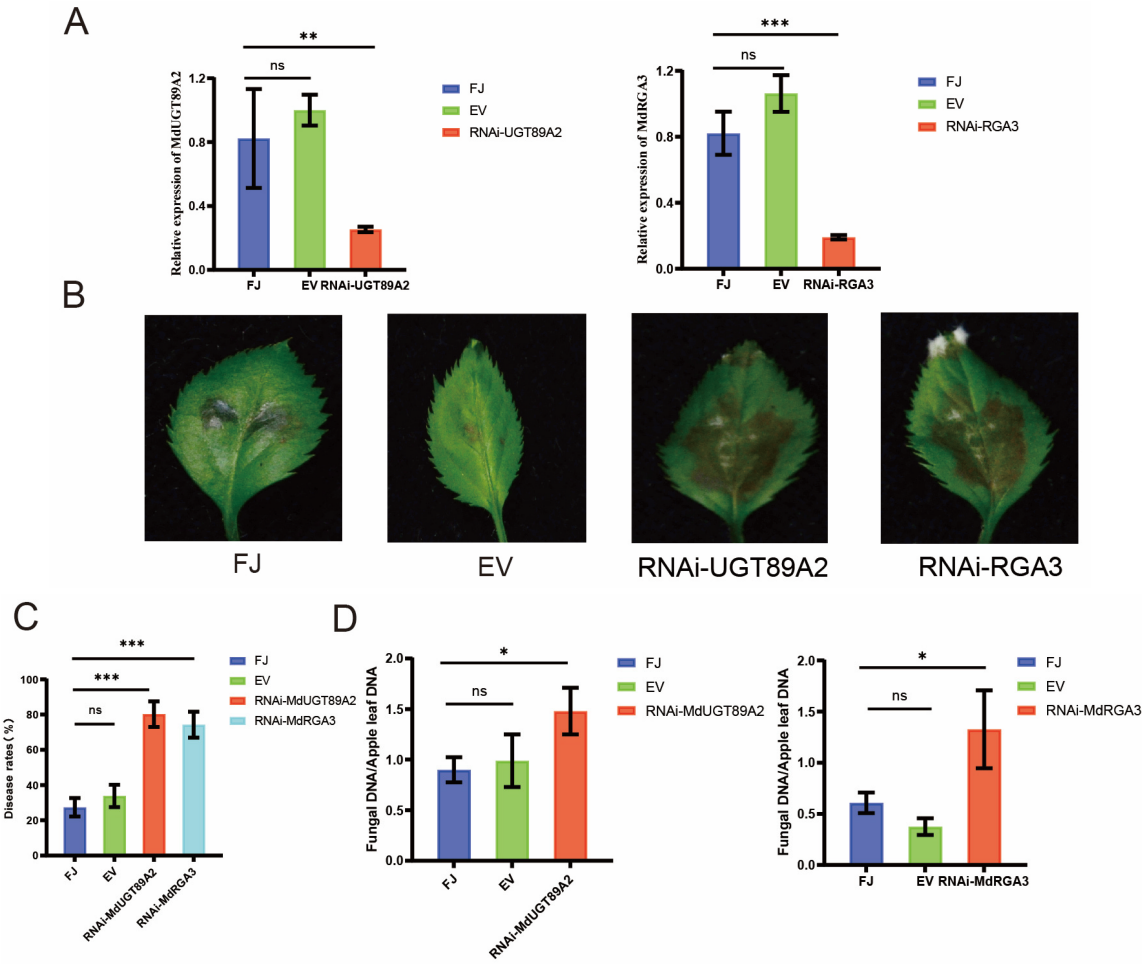

Figure 8. Silencing *MdUGT89A2* and *MdRGA3* comprises disease resistance against *C. gloeosporioides*. (**A**) The expression of the three treatments "FJ", EV, RNAi-*MdUGT89A2*, and RNAi-*MdRGA3* was detected using RT-qPCR. (**B**) Four days after *Agrobacterium* injection, "FJ", EV, RNAi-*MdUGT89A2*, and RNAi-*MdRGA3* were inoculated with *C. gloeosporioides*. These phenotypes as well as lesion area two days after inoculation with *C. gloeosporioides*. (**C**) Lesion area was analyzed statistically as shown. (**D**) Relative *C. gloeosporioides* biomass was determined by RT-qPCR. Comparisons between groups were analyzed using one-way ANOVA and Tukey's post-hoc test. Asterisks mark significant differences: * ($p < 0.05$), ** ($p < 0.01$), *** ($p < 0.001$). ns: not significant.

4. Discussion

In this study, we investigated the role of microRNA (miRNA) in apple's response to *C. gloeosporioides*, the causal agent of GLS. Through sRNA sequencing, a novel miRNA, *MIR396d-p3*, was identified. Bioinformatic analysis of *MIR396d-p3* target genes and its promoter region indicated that *MIR396d-p3* may regulate key aspects of biological processes, including plant defense, signal transduction, plant–pathogen interactions, and light-mediated responses. Previous studies have reported the involvement of Arabidopsis *miR396* in mediating immune responses against fungal pathogens [15]. Therefore, we hypothesize that *MIR396d-p3* may also play a role in apple's defense against *C. gloeosporioides* infection.

MiR396-mediated cleavage of growth-regulating factors (*GRFs*) has been observed in diverse plant species, including switchgrass (*Panicum virgatum*) [34], rice (*Oryza sativa*) [16], Arabidopsis (*Arabidopsis thaliana*) [15], and poplar (*Populus* spp.) [35], tomato (*Solanum lycopersicum*) [36], and soybean (*Glycine max*) [18]. The *miR396-GRF* regulatory module represents a novel and efficient mechanism for modulating plant growth, development, and responses to environmental stresses. Interestingly, our integrated analysis of bioinformatics prediction and experimental validation identified two novel *MIR396d-p3* target genes, *MdUGT89A2* and *MdRGA3*. These previously unreported targets significantly advance our understanding of the *miR396*-mediated regulatory mechanisms underlying plant stress responses.

Plants have independently evolved UDP-glycosyltransferases (*UGTs*) with specific substrate specificities, enabling fine-tuned regulation of defensive secondary metabolites and thereby resisting pathogen infection. They work by attaching glucose to various substances, such as toxins, hormones, and other metabolites [20]. This process usually helps detoxify harmful substances, protecting the plant from damage. In relation to fungal pathogens, *UGTs* can alter mycotoxins produced by the fungus, making them less harmful and impeding the pathogen's ability to cause infection [23]. We found that overexpressing *MdUGT89A2* enhances resistance to *C. gloeosporioides*. This discovery opens new avenues for developing disease-resistant apple varieties by manipulating this crucial regulatory pathway. However, we have not yet studied the potential substrates of *UGT*s and what immune responses are activated in response to pathogen infection. On the other hand, *MdRGA3* belongs to the family of *R* genes, which are essential for recognizing and defending against pathogen attacks [37,38]. Overexpression of *MdRGA3* significantly increases the resistance to *C. gloeosporioides* infection. This further supports the notion that *MdRGA3* is crucial for apple resistance to *C. gloeosporioides*.

miRNAs, as key regulatory molecules, orchestrate a complex network of gene expression in response to pathogen infection, including in apples [39]. For example, *Md-miR156ab* and *Md-miR395* target *WRKY* transcription factors, thereby affecting resistance to *Alternaria alternata* by modulating the expression of pathogenesis-related (*PR*) genes [13]. Similarly, *Md-miR482* has been confirmed to regulate the expression of *NBS-LRR* genes, with overexpression of *miR482* attenuating disease resistance by inhibiting *MdTNL1* expression [12]. To our knowledge, there is no report about the involvement of *miR396* in the interaction between apple and pathogenic fungi. This study is the first to reveal the regulatory role of *MIR396d-p3* in apple–fungal interactions. In addition, *RGA3* (a member of the *R* gene family) and *UGT89A2* (a key regulator of secondary metabolism) were reported as *MIR396d-p3* target genes for the first time. This highlights the complexity of plant immune responses, which are mediated by both *R* genes and the regulation of secondary metabolite biosynthesis. This study not only fills the research gap regarding miRNA in apple—*C. gloeosporioides* interactions but also enriches the molecular basis of apple disease resistance mechanisms through integrating various regulatory networks.

In addition, several strategies can be employed to enhance disease resistance in plant breeding, including traditional breeding methods, marker-assisted selection, and various genetic engineering techniques. One particularly promising approach focuses on manipulating small RNA pathways. This involves either suppressing small RNAs that inhibit defense responses or boosting the expression of genes that confer resistance, thereby enhancing the plant's immune response and the ability to resist pathogenic bacteria.

5. Conclusions

In summary, this study reveals that *MIR396d-p3* negatively regulates apple resistance to *C. gloeosporioides* by suppressing the expression of *MdUGT89A2* and *MdRGA3*. Functional analyses demonstrated that overexpressing *MdUGT89A2* or *MdRGA3* enhances tolerance to *C. gloeosporioides*, while silencing *MdUGT89A2* or *MdRGA3* increases susceptibility to *C. gloeosporioides*. This study identifies a novel *MIR396d-p3-MdUGT89A2/MdRGA3* regulatory axis, deepening the understanding of the mechanism of miRNA in the interaction between apples and pathogenic fungi, and also provided references for potential resistance breeding sites.

Supplementary Materials: The following supporting information can be downloaded at: https://www.mdpi.com/article/10.3390/horticulturae11040351/s1, Supplemental material Figure S1: Statistics plants *miR396* sequences. Numeric distribution of *miR396s* across 52 plant species, with column height representing the quantity. Figure S2: Phylogenetic tree of plants *miR396* precursor sequences. Figure S3. Analysis of cis-acting elements in *MIR396d-p3* promoter. Figure S4: Phylogenetic tree of plants miR396 precursor sequences. Figure S5: Schematic diagrams of the expression constructs for *MdUGT89A2* and *MdRGA3* under the control of the 35S promoter and NOS—Ter terminator. Figure S6: Schematic illustrations of the RNAi constructs for *MdUGT89A2* and *MdRGA3*. Table S1: Description of the target transcripts of the *MIR396d-p3*. Table S2: Primers in this study.

Author Contributions: Writing—original draft preparation, B.Z.; methodology, B.Z. and J.T.; data curation and software, B.Z., J.T., Z.J. and Y.D.; writing—review and editing, B.Z., J.T. and J.C.; software—B.Z., Y.D., J.C.; supervision: Z.Z.; conceptualization, B.Z. and Z.Z.; resources and investigation, Z.Z. All authors have read and agreed to the published version of the manuscript.

Funding: This work was supported by Agricultural Science and Technology Innovation Program (CAAS-ASTIP-2016-RIP) and the Asian regional cooperation special projects.

Data Availability Statement: Data is contained within the article and Supplementary Materials.

Conflicts of Interest: The authors declare no conflicts of interest.

References

1. Hamada, N.A.; Moreira, R.R.; Nesi, C.N.; May De Mio, L.L. Pathogen Dispersal and Glomerella Leaf Spot Progress Within Apple Canopy in Brazil. *Plant Dis.* **2019**, *103*, 3209–3217. [CrossRef] [PubMed]
2. Shi, J.; Zhang, F.; Su, Y.; Jiang, Q.; Yuan, Y.; Nie, X.; Zhou, Y.; Zhang, X.; Wang, Z.; Wang, F.; et al. MdIPT8, an Isopentenyl Transferase Enzyme, Enhances the Resistance of Apple to Colletotrichum Gloeosporioides Infection. *Sci. Hortic.* **2022**, *303*, 111245. [CrossRef]
3. Shang, S.; Liu, G.; Zhang, S.; Liang, X.; Zhang, R.; Sun, G. A Fungal CFEM-containing Effector Targets NPR1 Regulator NIMIN2 to Suppress Plant Immunity. *Plant Biotechnol. J.* **2023**, *22*, 82–97. [CrossRef]
4. Wang, B.; Li, B.-H.; Dong, X.-L.; Wang, C.-X.; Zhang, Z.-F. Effects of Temperature, Wetness Duration, and Moisture on the Conidial Germination, Infection, and Disease Incubation Period of Glomerella Cingulata. *Plant Dis.* **2015**, *99*, 249–256. [CrossRef] [PubMed]
5. Song, X.; Li, Y.; Cao, X.; Qi, Y. MicroRNAs and Their Regulatory Roles in Plant–Environment Interactions. *Annu. Rev. Plant Biol.* **2019**, *70*, 489–525. [CrossRef]
6. Qiao, Y.; Xia, R.; Zhai, J.; Hou, Y.; Feng, L.; Zhai, Y.; Ma, W. Small RNAs in Plant Immunity and Virulence of Filamentous Pathogens. *Annu. Rev. Phytopathol.* **2021**, *59*, 265–288. [CrossRef]

7. Yu, X.; Hou, Y.; Chen, W.; Wang, S.; Wang, P.; Qu, S. Malus Hupehensis miR168 Targets to ARGONAUTE1 and Contributes to the Resistance against Botryosphaeria Dothidea Infection by Altering Defense Responses. *Plant Cell Physiol.* **2017**, *58*, 1541–1557. [CrossRef]
8. Yu, X.; Gong, H.; Cao, L.; Hou, Y.; Qu, S. MicroRNA397b Negatively Regulates Resistance of Malus Hupehensis to Botryosphaeria Dothidea by Modulating MhLAC7 Involved in Lignin Biosynthesis. *Plant Sci.* **2020**, *292*, 110390. [CrossRef]
9. Zhou, T.; Cao, L.; Hu, K.; Yu, X.; Qu, S. miR164–NAC21/22 Module Regulates the Resistance of Malus Hupehensis against Alternaria Alternata by Controlling Jasmonic Acid Signaling. *Plant Sci.* **2023**, *330*, 111635. [CrossRef]
10. Yu, X.; Hou, Y.; Cao, L.; Zhou, T.; Wang, S.; Hu, K.; Chen, J.; Qu, S. MicroRNA Candidate miRcand137 in Apple Is Induced by *Botryosphaeria dothidea* for Impairing Host Defense. *Plant Physiol.* **2022**, *189*, 1814–1832. [CrossRef]
11. Zhang, Q.; Ma, C.; Zhang, Y.; Gu, Z.; Li, W.; Duan, X.; Wang, S.; Hao, L.; Wang, Y.; Wang, S.; et al. A Single-Nucleotide Polymorphism in the Promoter of a Hairpin RNA Contributes to *Alternaria alternata* Leaf Spot Resistance in Apple (*Malus* × *Domestica*). *Plant Cell* **2018**, *30*, 1924–1942. [CrossRef] [PubMed]
12. Liu, F.; Tang, J.; Li, T.; Zhang, Q. The microRNA miR482 Regulates NBS-LRR Genes in Response to ALT1 Infection in Apple. *Plant Sci.* **2024**, *343*, 112078. [CrossRef] [PubMed]
13. Zhang, Q.; Li, Y.; Zhang, Y.; Wu, C.; Wang, S.; Hao, L.; Wang, S.; Li, T. Md-miR156ab and Md-miR395 Target WRKY Transcription Factors to Influence Apple Resistance to Leaf Spot Disease. *Front. Plant Sci.* **2017**, *8*, 526. [CrossRef] [PubMed]
14. Zhang, Y.; Zhang, Q.; Hao, L.; Wang, S.; Wang, S.; Zhang, W.; Xu, C.; Yu, Y.; Li, T. A Novel miRNA Negatively Regulates Resistance to Glomerella Leaf Spot by Suppressing Expression of an NBS Gene in Apple. *Hortic. Res.* **2019**, *6*, 93. [CrossRef]
15. Soto-Suárez, M.; Baldrich, P.; Weigel, D.; Rubio-Somoza, I.; San Segundo, B. The Arabidopsis miR396 Mediates Pathogen-Associated Molecular Pattern-Triggered Immune Responses against Fungal Pathogens. *Sci. Rep.* **2017**, *7*, 44898. [CrossRef]
16. Dai, Z.; Tan, J.; Zhou, C.; Yang, X.; Yang, F.; Zhang, S.; Sun, S.; Miao, X.; Shi, Z. The OsmiR396–OsGRF8–OsF3H-flavonoid Pathway Mediates Resistance to the Brown Planthopper in Rice (*Oryza sativa*). *Plant Biotechnol. J.* **2019**, *17*, 1657–1669. [CrossRef]
17. Zhang, Y.; Xiao, T.; Yi, F.; Yu, J. SimiR396d Targets SiGRF1 to Regulate Drought Tolerance and Root Growth in Foxtail Millet. *Plant Sci.* **2023**, *326*, 111492. [CrossRef]
18. Noon, J.B.; Hewezi, T.; Baum, T.J. Homeostasis in the Soybean miRNA396–*GRF*Network Is Essential for Productive Soybean Cyst Nematode Infections. *J. Exp. Bot.* **2019**, *70*, 1653–1668. [CrossRef]
19. Dimunová, D.; Matoušková, P.; Podlipná, R.; Boušová, I.; Skálová, L. The Role of UDP-Glycosyltransferases in Xenobioticresistance. *Drug Metab. Rev.* **2022**, *54*, 282–298. [CrossRef]
20. Bowles, D.; Isayenkova, J.; Lim, E.-K.; Poppenberger, B. Glycosyltransferases: Managers of Small Molecules. *Curr. Opin. Plant Biol.* **2005**, *8*, 254–263. [CrossRef]
21. Huang, X.; Wang, Y.; Lin, J.; Chen, L.; Li, Y.; Liu, Q.; Wang, G.; Xu, F.; Liu, L.; Hou, B. The Novel Pathogen-responsive Glycosyltransferase UGT73C7 Mediates the Redirection of Phenylpropanoid Metabolism and Promotes *SNC1*-dependent Arabidopsis Immunity. *Plant J.* **2021**, *107*, 149–165. [CrossRef] [PubMed]
22. Bethke, G.; Huang, Y.; Hensel, G.; Heinen, S.; Liu, C.; Wyant, S.R.; Li, X.; Quin, M.B.; McCormick, S.; Morrell, P.L.; et al. UDP-Glucosyltransferase HvUGT13248 Confers Type II Resistance to *Fusarium Graminearum* in Barley. *Plant Physiol.* **2023**, *193*, 2691–2710. [CrossRef] [PubMed]
23. Jiang, H.; Qu, S.; Liu, F.; Sun, H.; Li, H.; Teng, W.; Zhan, Y.; Li, Y.; Han, Y.; Zhao, X. Multi-omics Analysis Identified the *GmUGT88A1* Gene, Which Coordinately Regulates Soybean Resistance to Cyst Nematode and Isoflavone Content. *Plant Biotechnol. J.* **2025**. *early view*. [CrossRef]
24. McHale, L.; Tan, X.; Koehl, P.; Michelmore, R.W. Plant NBS-LRR Proteins: Adaptable Guards. *Genome Biol.* **2006**, *7*, 212. [CrossRef]
25. Huang, S.; Jia, A.; Ma, S.; Sun, Y.; Chang, X.; Han, Z.; Chai, J. NLR Signaling in Plants: From Resistosomes to Second Messengers. *Trends Biochem. Sci.* **2023**, *48*, 776–787. [CrossRef]
26. Wu, J.; Ji, Z.; Wang, N.; Chi, F.; Xu, C.; Zhou, Z.; Zhang, J. Identification of Conidiogenesis-Associated Genes in Colletotrichum Gloeosporioides by Agrobacterium Tumefaciens-Mediated Transformation. *Curr. Microbiol.* **2016**, *73*, 802–810. [CrossRef]
27. Zhang, B.; Zhang, M.; Jia, X.; Hu, G.; Ren, F.; Fan, X.; Dong, Y. Integrated Transcriptome and Metabolome Dissecting Interaction between Vitis Vinifera L. and Grapevine Fabavirus. *Int. J. Mol. Sci.* **2023**, *24*, 3247. [CrossRef]
28. Daccord, N.; Celton, J.-M.; Linsmith, G.; Becker, C.; Choisne, N.; Schijlen, E.; van de Geest, H.; Bianco, L.; Micheletti, D.; Velasco, R.; et al. High-Quality de Novo Assembly of the Apple Genome and Methylome Dynamics of Early Fruit Development. *Nat. Genet.* **2017**, *49*, 1099–1106. [CrossRef]
29. Li, W.; Jia, Y.; Liu, F.; Wang, F.; Fan, F.; Wang, J.; Zhu, J.; Xu, Y.; Zhong, W.; Yang, J. Integration Analysis of Small RNA and Degradome Sequencing Reveals MicroRNAs Responsive to Dickeya Zeae in Resistant Rice. *Int. J. Mol. Sci.* **2019**, *20*, 222. [CrossRef]
30. Dai, X.; Zhao, P.X. psRNATarget: A Plant Small RNA Target Analysis Server. *Nucleic Acids Res.* **2011**, *39*, W155–W159. [CrossRef]
31. Chen, C.; Wu, Y.; Li, J.; Wang, X.; Zeng, Z.; Xu, J.; Liu, Y.; Feng, J.; Chen, H.; He, Y.; et al. TBtools-II: A "One for All, All for One" Bioinformatics Platform for Biological Big-Data Mining. *Mol. Plant* **2023**, *16*, 1733–1742. [CrossRef] [PubMed]

32. Jefferson, R.A.; Kavanagh, T.A.; Bevan, M.W. GUS Fusions: Beta-Glucuronidase as a Sensitive and Versatile Gene Fusion Marker in Higher Plants. *EMBO J.* **1987**, *6*, 3901–3907. [CrossRef] [PubMed]
33. Reid, K.E.; Olsson, N.; Schlosser, J.; Peng, F.; Lund, S.T. An Optimized Grapevine RNA Isolation Procedure and Statistical Determination of Reference Genes for Real-Time RT-PCR during Berry Development. *BMC Plant Biol.* **2006**, *6*, 27. [CrossRef]
34. Liu, Y.; Yan, J.; Wang, K.; Li, D.; Yang, R.; Luo, H.; Zhang, W. MiR396-*GRF* Module Associates with Switchgrass Biomass Yield and Feedstock Quality. *Plant Biotechnol. J.* **2021**, *19*, 1523–1536. [CrossRef]
35. Wang, L.; Hou, J.; Xu, H.; Zhang, Y.; Huang, R.; Wang, D.; He, X.-Q. The PtoTCP20-miR396d-PtoGRF15 Module Regulates Secondary Vascular Development in Populus. *Plant Commun.* **2023**, *4*, 100494. [CrossRef]
36. Sun, L.; Zhu, M.; Zhou, X.; Gu, R.; Hou, Y.; Li, T.; Huang, H.; Yang, R.; Wang, S.; Zhao, W. The miR396a–SlGRF8 Module Regulates Sugar Accumulation in the Roots via SlSTP10 during the Interaction between Root-knot Nematodes and Tomato Plants. *J. Integr. Plant Biol.* **2024**, *66*, 2701–2715. [CrossRef]
37. Wang, J.; Song, W.; Chai, J. Structure, Biochemical Function, and Signaling Mechanism of Plant NLRs. *Mol. Plant* **2023**, *16*, 75–95. [CrossRef]
38. Zhang, J.; Coaker, G.; Zhou, J.-M.; Dong, X. Plant Immune Mechanisms: From Reductionistic to Holistic Points of View. *Mol. Plant* **2020**, *13*, 1358–1378. [CrossRef]
39. Padmanabhan, C.; Zhang, X.; Jin, H. Host Small RNAs Are Big Contributors to Plant Innate Immunity. *Curr. Opin. Plant Biol.* **2009**, *12*, 465–472. [CrossRef]

horticulturae

MDPI

Article

The Effects of Increasing Boron on Growth, Yield, and Nutritional Value of Scallion (*Allium cepa* L.) Grown as a Bunch Harvest

Halil Samet [1,*] and Yakup Çikili [2]

[1] Department of Crop and Animal Production, Izmit Vocational School, Kocaeli University, Kocaeli 41285, Türkiye
[2] Department of Soil Science and Plant Nutrition, Faculty of Agriculture, Çanakkale Onsekiz Mart University, Çanakkale 17100, Türkiye; yakupcikili@gmail.com
* Correspondence: halil.samet@kocaeli.edu.tr

Abstract: Scallions are a highly valued leafy vegetable and are enjoyed worldwide due to their appealing taste and nutritional benefits. A combination of short cultivation cycles and high market demand not only enhances food security but also offers a profitable opportunity for growers. In our study, we aim to evaluate the effect of increasing boron (B) applications, specifically 0, 0.2, 0.4, 0.8, 1.2, and 1.6 mM B supplied as boric acid (H_3BO_3) in the nutrient solution, on several key physiological and agronomic parameters in scallions. Results showed that the effects of increasing B levels on biomass production were insignificant, but the root fresh weight (FW) significantly decreased with all B levels. Higher B levels (1.2 and 1.6 mM) caused decreases of 22.9% and 29.6%, respectively. The effects of all B levels on photosynthetic pigment contents [chlorophyll (Chl) *a*, *b*, *a* + *b*, and carotenoid (Car)], root and shoot membrane permeability (MP), and root, shoot, and leaf nutritional status [phosphorus (P), potassium (K), calcium (Ca), and sodium (Na) concentrations] were found insignificantly. However, all B levels caused a significant increase in the B concentrations of the root, shoot, and leaf of scallions and plants translocated the majority of applied B into their leaves. The translocation factor (TF) of B from the root to the leaf was found to be 138.2%, 133.3%, and 107.3% with 0.8, 1.2, and 1.6 mM B levels, respectively. Moreover, plants exposed to high levels of B showed no significant response or toxicity symptoms. We concluded that B is a phloem mobile element in onion, a non-graminaceous monocotyledonous plant, and therefore accumulates in the upper organs but illustrates partial toxicity symptoms in leaves. Studies with higher B concentrations could be recommended to determine critical B levels for green onion production in B-contaminated areas.

Keywords: boron toxicity; chlorophyll; green onion; membrane permeability; nutritional imbalance

1. Introduction

Although it has been known for nearly a century that boron (B) is an essential micronutrient for plants, its role in plant metabolism can still not be clearly defined. Recent studies show that B plays important roles mainly in synthesizing the cell wall and maintaining its structure and integrity. The amount of B in the cell wall may vary depending on the species of plant, its organs, and the amount of B in the growing medium [1]. Although there are differences between species, plants grown in soils containing extractable B in hot water,

generally above 5 mg kg^{-1}, could exhibit toxicity symptoms [2]. The toxicity mechanism of B is not clear yet; however, it has been suggested that toxicity may be related to the B forms in plants and that soluble B is more effective than total B [3].

The absorbed B by roots, as boric acid (H_3BO_3) or a small amount of borate ($H_3BO_4^-$), can reach all cells by easily moving through lipid bilayers due to its characteristic feature (a small, water-soluble, un-dissociated, and uncharged molecule). Both B compounds tend to complex easily with different sugars and other compounds with cis-hydroxyl groups [4] that are primarily involved in the formation of cell walls. It forms di-ester bridges between two RG-II molecules and cross-links cell wall pectin. The RG-II-pectins are major B-binding fractions and they influence cell wall porosity and plant morphogenesis [5]. Information on how plants localize B to RG-II is still limited [6], but it is believed that as a result of an abnormal decrease in the amount of this cross-linking, there may be a decrease in intercellular binding, causing stunting in plants [7,8]. The main dimerization reaction involved in the B-bridging of RG-II is illustrated in Figure 1. Briefly, two monomeric neutral apiose residues (RG-II molecules), which resist the electrostatic repulsion important for B-bridging, approach each other, and a dimeric RG-II is formed. This dimerization reaction introduces an additional negative charge onto the previously neutral B atom, and three molecules of water and a positive charge are also released.

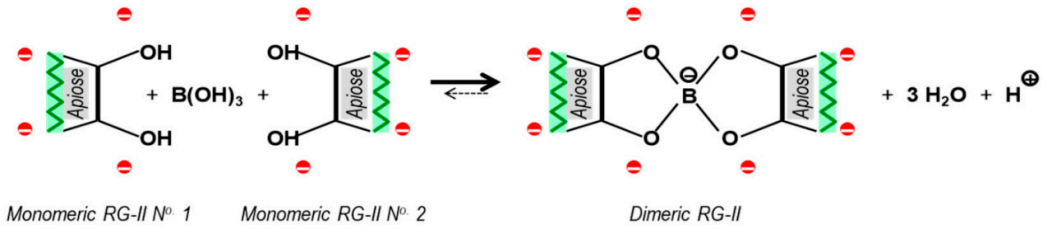

Figure 1. The main dimerization reaction in the B-bridging of monomeric RG-II (red circles indicate the charges of the neighboring anionic sugar residue) [6,9].

The dimeric RG-II is often associated with upright growth, and it has been observed that a higher concentration of borate-cross-linked RG-II in cell walls has contributed to the evolution of lignified secondary walls in higher plants [8]. One of the important functions of B in plants is to form a covalent bridge [RG-II–(B−)–RG-II] between pectin molecules [7]. These bridges can reduce cell wall porosity [10]. It is accepted that species with high cell wall pectin content, such as onion, require more B for cell wall construction than other species and that pectin in the cell wall forms an insoluble complex with B, thus reducing the toxic effect of B [11].

Generally, B is known to be immobile in the phloem in most plant species. However, researchers have reported that B is mobile in some species that use polyols (simple sugars) as primary photosynthetic metabolites and can then transport B to active accumulation sites in the phloem, e.g., vegetative or reproductive organs [12].

Some plant species' ability to move B around depends on how it binds to polyols (sugar alcohols), which are the main byproduct of photosynthesis. Brown and Hu [13] found that a polyol–B–polyol complex is made in the leaves of these species and moved to the active sites by the phloem. It is significantly mobile in species where polyols (e.g., sorbitol, mannitol, etc.) are the primary products of photosynthesis. These species include onions, celery, carrots, olives, beans, peas, and cauliflower [14].

Onion is among the non-graminaceous monocots, like asparagus, and unlike other monocots, it has pectin-rich cell walls [15,16]. Therefore, the tissue B requirements of species such as onion are equal to those of dicotyledonous species. However, some species, such as asparagus, have higher tissue B requirements than dicotyledonous species [17]. B plays a crucial functional role in the formation of pectic networks within the plant

cell wall, primarily through its interaction with rhamnogalacturonan II (RG-II), a pectic polysaccharide. This cross-linking contributes to the structural integrity and porosity of the cell wall, thereby enhancing its extensibility [6]. Such extensibility is crucial for cell wall loosening, a process that enables cell expansion and promotes overall plant growth. Consequently, B is not only vital for maintaining cell wall architecture but also acts as a key regulator of plant developmental processes by influencing cell elongation and tissue differentiation [18].

Scallions are one of the most important leafy vegetables and are widely cultivated in various climatic conditions, both in fields and greenhouses, for bunch consumption [19]. They also provide significant profits to producers due to their ease of vegetative propagation, short growth cycle, tolerance to abiotic stress conditions, and longer shelf life [20]. However, research on this widely produced and consumed crop remains limited, which is why this study was planned.

We aim to identify the critical B concentrations that may induce stress in scallions in this study. In addition, our aim is to enhance the understanding of plant nutrition by investigating the mechanisms of B transport and accumulation, ultimately supporting the development of more effective agricultural practices and environmental management strategies.

2. Materials and Methods

2.1. Experimental Design

We performed this study in a semi-controlled climate room with a temperature of 24 ± 3 °C and a humidity of 50 ± 15 percent in the summer. We used small bulbs (*Allium cepa* L. var. Kartopu) purchased from the local seed market, with a 1.5–2.0 cm diameter. We compacted the perlite-filled plastic pots well with a volume of 1.5 L, and equalized their weights. We saturated the pots with distilled water and allowed them to flow freely under the influence of gravity for 24 h. After draining the excess water, we weighed them to determine the approximate amount of solution. We planted the tiny bulbs in an inert medium (sterile perlite) with three plants per pot. To ensure a gradual acclimation of the test plants to the nutrient environment, we initially applied a quarter-strength and a half-strength modified Hoagland solution during the first week and the second week, respectively. By the third week, once the first true leaves of the plants had reached a length of 3–4 cm, we began applying the full-strength modified nutrient solution until the end of the study. Throughout the experiment, we monitored surface evaporation daily and added the lost water with the nutrient solution accordingly to maintain consistent moisture levels.

We applied to the related pots the B levels [0 (B-free), 0.2, 0.4, 0.8, 1.2, and 1.6 mM B (from H_3BO_3)] by mixing them with nutrient solution and approximately 50–100 mL of B-supplemented full-strength nutrient solution to the related pots daily, depending on their water consumption.

The modified Hoagland solution contains 5 mM calcium nitrate tetrahydrate [$Ca(NO_3)_2 \times 4H_2O$], 5 mM potassium nitrate (KNO_3), 2 mM magnesium sulfate heptahydrate ($MgSO_4 \times 7H_2O$), 1 mM potassium di-hydrogen phosphate (KH_2PO_4), 44.7 μM iron sulfate heptahydrate ($FeSO_4 \times 7H_2O$), 30 μM sodium chloride (NaCl), 9.1 μM manganese sulfate monohydrate ($MnSO_4 \times H_2O$), 0.77 μM zinc sulfate heptahydrate ($ZnSO_4 \times 7H_2O$), 0.32 μM copper sulfate pentahydrate ($CuSO_4 \times 5H_2O$), 0.10 μM ammonium molybdate tetrahydrate [$(NH_4)_2Mo_7O_{24} \times 4H_2O$], and 54.8 μM disodium EDTA dihydrate ($Na_2EDTA \times 2H_2O$) [21]. We adjusted the pH of the medium to 6.0–6.5 during the experimental period.

2.2. Sampling and Harvest of Plants

After 54 days, we harvested the green onions and separated them into roots, shoots, and leaves. We weighed all parts for fresh biomass. Then, to remove any particles that might have adhered to the plant surfaces, we washed these parts under running tap water and rinsed them three times with deionized water. We dried all samples in an air-pressurized oven at 70 °C until a constant mass was obtained. We weighed the dried samples to determine their DW and ground them into powder for ion analysis.

2.3. Determination of Photosynthetic Pigments

Before harvest, for photosynthetic pigment analysis in healthy, fresh leaves, we extracted 250 mg of fresh leaf samples in 10 mL of acetone (90% v/v) with a homogenizer and filtered the extract. Then, we measured the absorbance of the extract at 663, 645, and 470 nm using a spectrophotometer (UV-1201, Shimadzu, Kyoto, Japan) as described by Lichtenthaler [22].

2.4. Determination of Membrane Damage

We measured the MP in fresh leaves using the electrical conductivity (EC, %) method as described by Yan et al. [23]. For this purpose, just before the harvest, we washed leaves and then took out a standard sample using a disc, cut it into 1 cm pieces, and placed it in a beaker containing 10 mL of deionized water. We immersed the leaf samples at 30 °C for 3 h, and then we measured the EC of the solution. After boiling the samples for 2 min, we measured their conductivity again when the solution was cooled to room temperature. We calculated the percentage of MP as follows:

$$\text{MP (EC, \%)} = \text{C1/C2} \times 100$$

where C1 and C2 are the electrolyte conductivities measured before and after boiling, respectively.

2.5. Determination of Nutrient Ion Concentrations

We determined nutrient ion concentrations using the dry-ashed method. For this purpose, 500 mg of each of the shoot and root samples was dry-ashed in a muffle furnace at 500 °C for 6 h, and then the cooled ash was dissolved in a 10 N nitric acid (HNO_3) solution [24]. The B and phosphorus (P) concentrations were measured using a spectrophotometer (Shimadzu UV-1201, Kyoto, Japan). The potassium (K), calcium (Ca), and sodium (Na) concentrations were analyzed using a flame photometer.

2.6. Determination of Bio-Concentration, Translocation, and Accumulation

The bio-concentration factor (BCF) is the ratio of ions in plant organs (root, shoot, or leaf) to the ion concentration in the nutrient solution and was calculated according to the formulation of Equation (1). The translocation factor (TF) is the ratio of ion concentrations in the shoots or leaves to those at the roots, and the net accumulation (NA) of ions is the rate of total ion amounts in the whole plant to dry biomass in the roots and they were calculated using the formulation of Equations (2) and (3), respectively [25]

$$\text{BCF of ion} = [\text{ion}]_{\text{root, shoot, or leaf}}/[\text{ion}]_{\text{nutrient solution}} \quad (1)$$

$$\text{TF of ion} = [\text{ion}]_{\text{shoot or leaf}}/[\text{ion}]_{\text{nutrient solution}} \quad (2)$$

$$\text{NA of ion via roots (mg kg}^{-1}\text{ dry biomass)} = [\text{ion}]_{\text{shoot or leaf}}/\text{dry biomass}_{\text{ root}} \quad (3)$$

where $[ion]_{shoot/root/leaf}$ is the ion concentration in shoots, roots, or leaves; $[ion]_{nutrient\ solution}$ is the ion concentration in the nutrient solution; $dry\ biomass_{root}$ is the dry biomass of roots.

2.7. Statistical Analysis

We carried out this study in three replications according to the randomized plot design. We evaluated the normality of the data distribution using the Shapiro–Wilk test, and according to the test results, we performed the statistical analysis of the experimental data using ANOVA with the MINITAB (version 16) package program. We also used the Pearson correlation coefficient (r) test to show the correlations among all parameters in the root, shoot, and leaves of scallions. We analyzed the multiple comparisons of means among B levels using Tukey's honestly significant difference (HSD) at the significance level (α: 0.05). We showed the significance levels as (*) $p < 0.050$, (**) $p < 0.010$, (***) $p < 0.001$, and (ns) not significant.

3. Results

3.1. Vegetative Growth

All B applications had a significant influence on the FW and DW of roots and shoots, but they had a non-significant influence on the FWs and DWs of shoots (Figure 2). Compared to the control, the FW of roots decreased with all B levels (0.2, 0.4, 0.8, 1.2, and 1.6 mM) by 12.0%, 14.4%, 16.4%, 22.9%, and 29.6%, respectively. The FW of shoots showed a declining tendency with all B applications. In addition, the FW of leaves decreased by 5.7%, 6.0%, and 5.0%, respectively, with high B levels (0.8, 1.2, and 1.6 mM) in contrast to low B levels (Figure 2a). On the other hand, the DW of roots decreased at 0.2, 0.4, 0.8, 1.2, and 1.6 mM B levels by 10.1%, 8.1%, 7.9%, 16.7%, and 22.4%, respectively. Decreases in the DW of shoots were non-significant. We observed that the DW of leaves significantly increased with low B applications (0.2 and 0.4 mM) by 10.1% and 7.4%, respectively; however, there were non-significant changes with high B applications (Figure 2b).

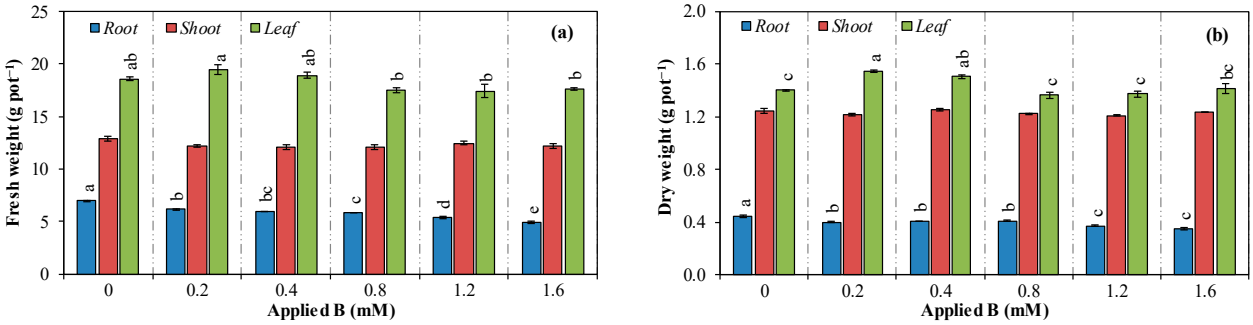

Figure 2. The effects of increasing B levels on (**a**) Fresh weight; (**b**) Dry weight of scallions (Bars indicate means of three replicates ± SE. Different letters on the bars for each parameter differ significantly according to Tukey HSD).

3.2. Photosynthetic Pigment Contents and Membrane Permeability

In scallion, while the B applications did not significantly affect the content of Chl *a* and Chl *a* + *b*, the 0.4, 0.8, 1.2, and 1.6 mM B applications caused notable decreases in Chl *b* contents by 8.3%, 6.2%, 5.9%, and 8.1%, respectively. In addition, low B applications (0.2 and 0.4 mM) significantly increased the Car contents by 5.1% and 4.6%, respectively (Figure 3a).

On the other hand, the root MP value significantly decreased with the 1.2 and 1.6 mM B levels by 20.6% and 15.8%, respectively. Similarly, the shoot MP value considerably decreased with 0.8, 1.2, and 1.6 mM B levels by 11.5%, 19.8%, and 21.5%, respectively (Figure 3b).

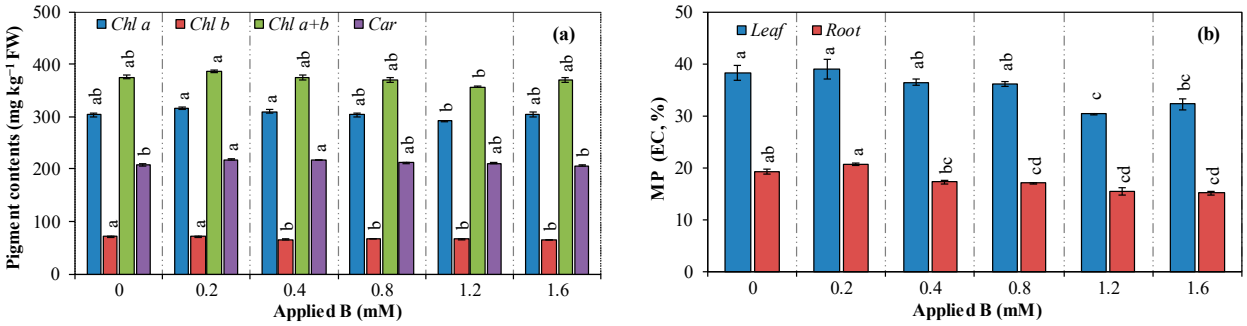

Figure 3. The effects of increasing B levels on (**a**) photosynthetic pigment contents, (**b**) membrane permeability (MP) of scallions (Bars indicate means of three replicates ± SE. Different letters on the bars for each parameter differ significantly according to Tukey HSD).

3.3. Concentration, Translocation, and Accumulation of Nutrients

Applied B levels significantly affected the B concentrations in roots, shoots, and leaves, as well as the TF value of B (Table 1). In comparison with control, all B levels (0.2, 0.4, 0.8, 1.2, and 1.6 mM) caused a notable increase in the root B concentrations by 2.0-, 3.1-, 5.2-, 6.7-, and 7.6-fold, respectively. Furthermore, all B applications significantly increased the shoot B concentrations by 1.8-, 2.6-, 4.1-, 5.1-, and 5.2-fold, respectively. Similarly, these B applications significantly increased the leaf B concentrations by 3.3-, 5.4-, 12.4-, 15.7-, and 15.9-fold, respectively (Table 1). The B concentrations in plant parts, in descending order, were as follows: leaves < shoots < roots. In addition, all B applications (0.2, 0.4, 0.8, 1.2, and 1.6 mM) caused a significant decrease in the TF of B (root to shoot) by 9.2%, 17.9%, 21.3%, 24.5%, and 32.3%, respectively. However, these B levels caused a considerable increase in the TF of B (root to leaf) by 62.7%, 71.2%, 138.2%, 133.8%, and 107.3%, respectively (Table 1).

Table 1. The effects of increasing B levels on concentrations and translocation of B in scallions.

Applied B (mM)	Boron Concentrations (mg kg^{-1})			Translocation Factor of B	
	Root	Shoot	Leaf	Root to Shoot	Root to Leaf
0	59.8 ± 1.01 f	30.0 ± 0.26 e	58.7 ± 5.07 e	0.502 a	0.984 d
0.2	119.6 ± 1.52 e	54.5 ± 0.34 d	191.3 ± 13.2 d	0.456 b	1.601 c
0.4	186.8 ± 4.14 d	76.9 ± 0.40 c	314.5 ± 4.00 c	0.412 c	1.685 c
0.8	309.4 ± 4.38 c	122.1 ± 2.31 b	725.0 ± 1.80 b	0.395 cd	2.344 a
1.2	400.8 ± 3.47 b	151.8 ± 1.13 a	922.1 ± 5.81 a	0.379 d	2.301 a
1.6	456.6 ± 4.39 a	155.0 ± 2.60 a	931.3 ± 1.57 a	0.340 e	2.040 b
F-test	***	***	***	***	***

Values are the mean of three replicates (means ± SE, $n = 3$). Different letters in the same column are significantly different according to Tukey HSD. The *F*-test shows a significant difference at *** $p < 0.001$.

Applied B levels significantly affected the leaves' P, K, Ca, and Na concentrations (Figure 4). The P concentration in roots significantly decreased with 0.4 mM B application by 11.1% but increased with 1.6 mM B application by 16.7% compared to the control. Similarly, the P concentration in shoots markedly decreased with 0.4 mM B application by 12.6%, while other B applications had insignificant effects. Furthermore, 0.2, 0.4, 0.8, 1.2, and 1.6 mM B applications caused a notable increase in the P concentrations in leaves by 6.7%, 6.7%, 20.8%, 11.7%, and 24.2%, respectively (Figure 4a).

The K concentration in roots significantly increased with 0.4 and 0.8 mM B levels by 12.6% and 9.7%, respectively; however, it significantly decreased with a 1.6 mM B application by 7.7% compared to the control. While the K concentration in shoots was not affected by B applications, the K concentration in leaves markedly increased with 0.8 and 1.2 mM B applications by 12.3% and 6.6%, respectively, compared to the control (Figure 4b).

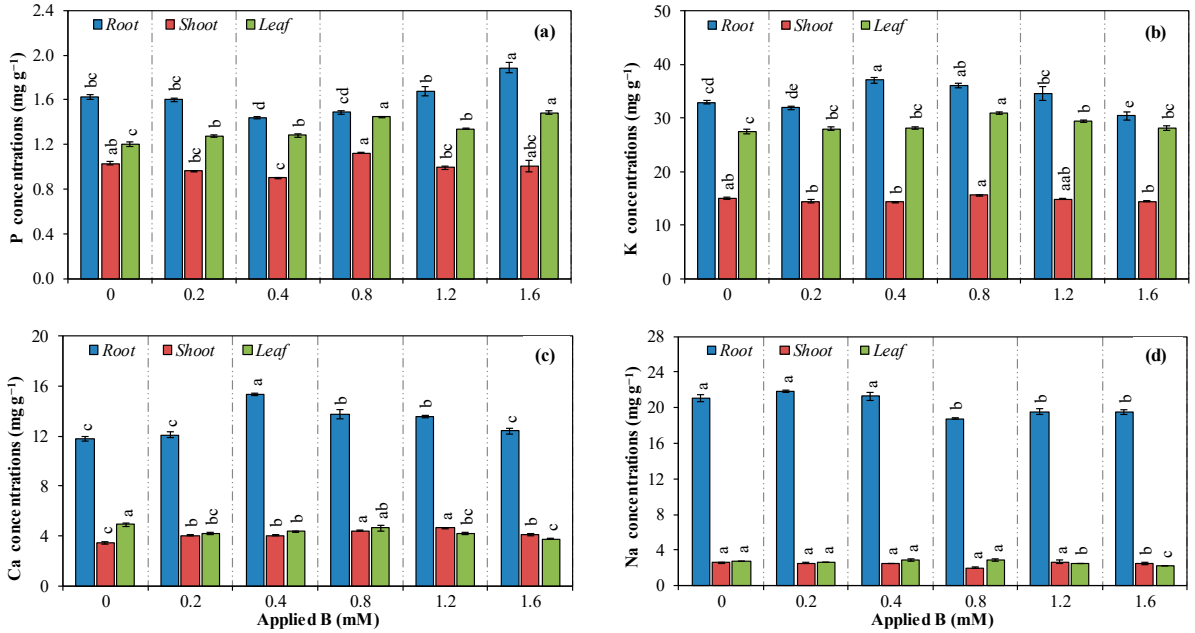

Figure 4. The effects of increasing B levels on (**a**) P concentrations; (**b**) K concentrations; (**c**) Ca concentrations; (**d**) Na concentrations in scallions (Bars indicate means of three replicates ± SE. Different letters on the bars for each parameter differ significantly according to Tukey HSD).

On the other hand, the Ca concentration in roots considerably increased at 0.4, 0.8, and 1.2 mM B levels by 30.3%, 17.1%, and 15.4%, respectively. The Ca concentration in shoots also significantly increased with 0.2, 0.4, 0.8, 1.2, and 1.6 mM B applications by 16.4%, 16.1%, 27.4%, 33.4%, and 17.6%, respectively. However, the Ca concentration in leaves remarkably decreased with 0.2, 0.4, 1.2, and 1.6 mM B applications by 14.3%, 11.2%, 14.5%, and 23.5%, respectively (Figure 4c).

The Na concentration in roots decreased with higher B levels (0.8, 1.2, and 1.6 mM) by 10.8%, 7.1%, and 7.4%, respectively, compared to the control. The Na concentration in shoots significantly decreased at only 1.6 mM B applications by 20.3%, and the Na concentration in leaves significantly decreased with the 1.2 and 1.6 mM B applications by 7.7%, and 15.1%, respectively (Figure 4d).

We found a significant interaction between B applications and the TF of ions (P, K, Ca, and Na) (Table 2). While the 0.8 mM B application caused a notable increase in TF of P from root to shoot by 19.2%, the 1.6 mM B application caused a notable decrease in this parameter by 15.6%, compared to the control. In addition, the 0.4 and 0.8 mM B applications significantly increased the TF of P from root to leaf by 20.4% and 31.8%, respectively.

Table 2. The effects of increasing B levels on the translocation of phosphorus, potassium, and calcium of scallions.

Applied B (mM)	Translocation Factor of P		Translocation Factor of K		Translocation Factor of Ca	
	Root to Shoot	Root to Leaf	Root to Shoot	Root to Leaf	Root to Shoot	Root to Leaf
0	0.634 b	0.740 c	0.455 a	0.836 bc	0.295 b	0.417 a
0.2	0.600 bc	0.800 c	0.453 a	0.878 ab	0.334 a	0.348 b
0.4	0.626 b	0.891 b	0.388 b	0.760 c	0.263 c	0.284 c
0.8	0.756 a	0.975 a	0.433 ab	0.856 ab	0.321 ab	0.337 b
1.2	0.597 bc	0.801 c	0.433 ab	0.851 abc	0.341 a	0.309 bc
1.6	0.535 c	0.788 c	0.477 a	0.928 a	0.329 a	0.302 bc
F-test	***	***	**	***	***	***

Values are the mean of three replicates (means ± SE, $n = 3$). Different letters in the same column are significantly different according to Tukey HSD. *F*-test shows a significant difference at ** $p < 0.010$ and *** $p < 0.001$.

While the 0.4 mM B application caused a notable decrease in the TF of K from root to shoot by 14.7%, the 1.6 mM B application caused a notable increase in the TF of K from root to leaf by 11.0%, compared to the control.

The 0.2, 1.2, and 1.6 mM B applications significantly increased the TF of Ca from root to shoot by 13.2%, 15.6%, and 11.5%, respectively, compared to the control. However, the 0.4 mM B level caused a significant reduction in the TF of Ca from root to shoot of 10.8%. Furthermore, the 0.2, 0.4, 0.8, 1.2, and 1.6 mM B levels caused a notable decrease in the TF of Ca from root to leaf by 16.5%, 31.9%, 19.2%, 25.9%, and 27.6%, respectively (Table 2).

The 0.2, 0.4, 0.8, 1.2, and 1.6 mM B applications significantly affected the BCF of B, P, K, and Ca in roots, shoots, and leaves compared to the control (Figure 5). All B applications (0.2, 0.4, 0.8, 1.2, and 1.6 mM) caused notable decreases in BCF of B in roots, shoots, and leaves. These decreases in roots were 62.9%, 68.1%, 72.1%, 75.5%, and 78.9%, respectively. In addition, the reductions in shoots were 66.3%, 73.9%, 78.2%, and 81.4%, respectively. Similarly, in leaves, they were 85.7%, 39.5%, 45.3%, 35.5%, 42.6%, and 56.1%, respectively (Figure 5a).

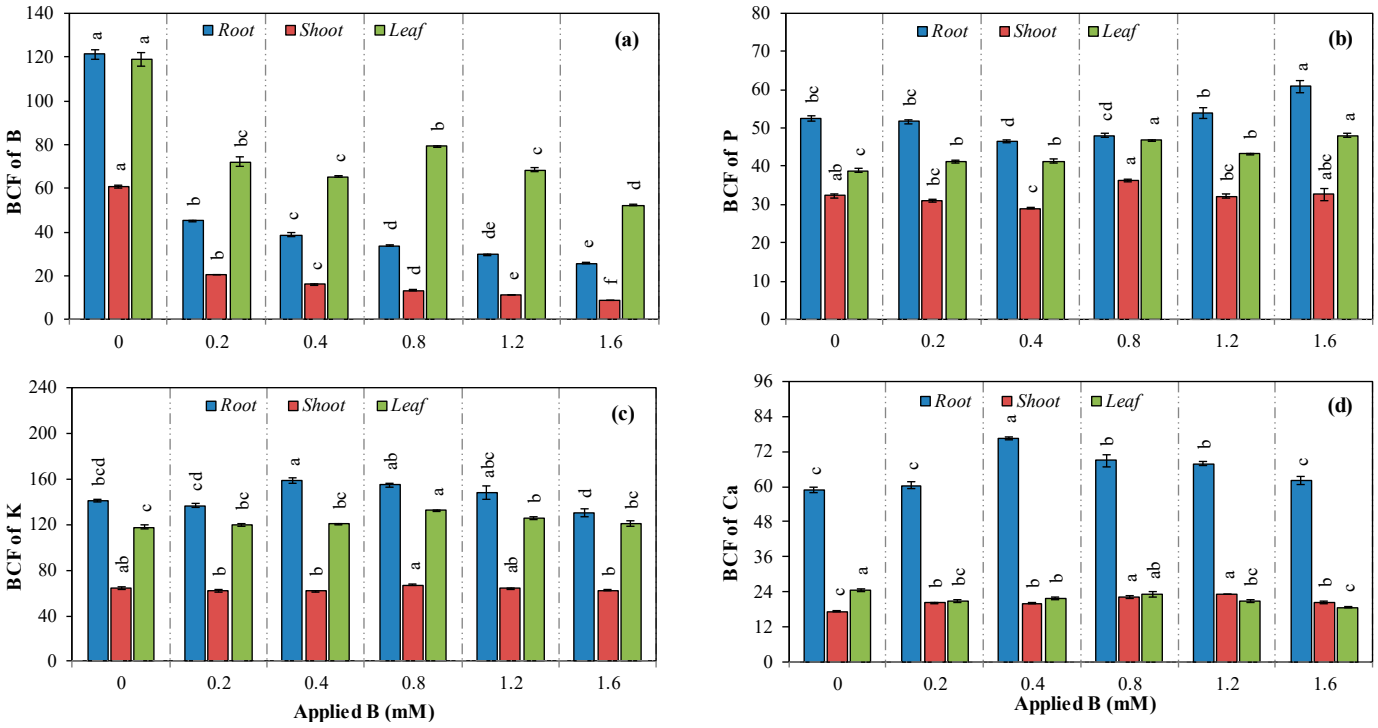

Figure 5. The effects of increasing B levels on (**a**) BCF of B; (**b**) BCF of P; (**c**) BCF of K; (**d**) BCF of Ca in scallions (Bars indicate means of three replicates ± SE. Different letters on the bars for each parameter differ significantly according to Tukey HSD).

The 0.4 mM B application significantly decreased the BCF of P in roots and roots by 11.5% and 9.9%, respectively. However, the 1.6 mM B level increased this parameter by 16.2% in roots. Similarly, 0.8 mM B caused an increase in BCF of P in shoots by 12.7%, compared to the control. On the other hand, all B applications (0.2, 0.4, 0.8, 1.2, and 1.6 mM) significantly increased the BCF of P in leaves by 6.2%, 6.4%, 20.4%, 11.3%, and 23.5%, respectively (Figure 5b).

The 0.4 mM of B application caused a notable increase in the BCF of K in roots by 12.8%. In addition, 0.8 and 1.2 mM B applications caused a notable increase in the BCF of K in leaves by 6.8% and 6.8%, respectively. However, the effects of B applications on the BCF of K in shoots were non-significant (Figure 5c).

On the other hand, the 0.4, 0.8, and 1.2 mM B applications caused a considerable increase in the BCF of Ca in roots by 30.3%, 17.2%, and 15.3%, respectively. However, the 0.2, 0.4, 1.2, and 1.6 mM B applications caused a considerable decrease in the BCF of Ca in leaves by 14.3%, 11.0%, 14.3%, and 23.7%, respectively (Figure 5d).

All B applications (0.2, 0.4, 0.8, 1.2, and 1.6 mM B) caused a considerable increase in the net accumulations of B, K, and Ca via roots compared to the control (Table 3). These increases in the net accumulation of B were 3.1-, 4.8-, 9.3-, 13.1-, and 14.5-fold, respectively. The increases in the net accumulations of K were 14.2%, 14.6%, 14.8%, 18.9%, and 21.0%, respectively. In addition, the increases in the net accumulation of Ca were 10.2%, 18.6%, 14.8%, 19.9%, and 13.8%, respectively.

Table 3. The effects of increasing B levels on net ion accumulations of scallions.

Applied B (mM)	Net Ion Accumulations via Roots (mg g^{-1} DW)				
	B	**P**	**K**	**Ca**	**Na**
0	0.329 ± 0.004 f	8.30 ± 0.21 c	161.8 ± 2.59 b	36.92 ± 0.72 b	36.92 ± 0.63 ab
0.2	1.028 ± 0.031 e	9.48 ± 0.06 bc	184.7 ± 1.63 a	40.69 ± 0.53 a	38.44 ± 0.62 ab
0.4	1.584 ± 0.025 d	8.94 ± 0.15 bc	185.4 ± 2.51 a	43.78 ± 0.55 a	39.44 ± 0.74 a
0.8	3.069 ± 0.024 c	9.67 ± 0.09 b	185.8 ± 1.64 a	42.39 ± 1.00 a	36.20 ± 0.55 b
1.2	4.315 ± 0.062 b	9.89 ± 0.18 b	192.4 ± 4.22 a	44.26 ± 0.83 a	36.98 ± 0.23 ab
1.6	4.774 ± 0.179 a	11.48 ± 0.55 a	195.8 ± 6.55 a	42.01 ± 0.87 a	36.22 ± 0.67 b
F-test	***	***	***	***	**

Values are the mean of three replicates (means ± SE, $n = 3$). Different letters in the same column are significantly different, according to Tukey's HSD. *F*-test shows a significant difference at ** $p < 0.010$ and *** $p < 0.001$.

On the other hand, only high B applications (0.8, 1.2, and 1.6 mM) caused a notable increase in the net accumulations of P by 16.5%, 19.2%, and 38.3%, respectively. The B applications did not significantly affect the net accumulation of Na (Table 3).

3.4. Correlation Analysis

Evaluations based on plant biomass production, photosynthetic pigment contents, and B behaviors (translocation, concentration, and accumulation) determined variables showing statistically significant relationships. The data reveal that the root FW of scallion leaves exhibited a highly significant and negative correlation with the B concentrations in the root, shoot, and leaf tissues, as well as with net ion accumulations of B, P, Ca, and K. The correlation coefficients for these relationships ranged from 0.691 to 0.926, indicating a strong inverse relationship between root FW and the concentrations of these ions. In contrast, the root FW showed a notable positive correlation with the BCF of B in the root, shoot, and leaf, as well as with the MP values in both the root and leaf tissues. The correlation coefficients for these positive relationships ranged from 0.696 to 0.885 (Figure 6).

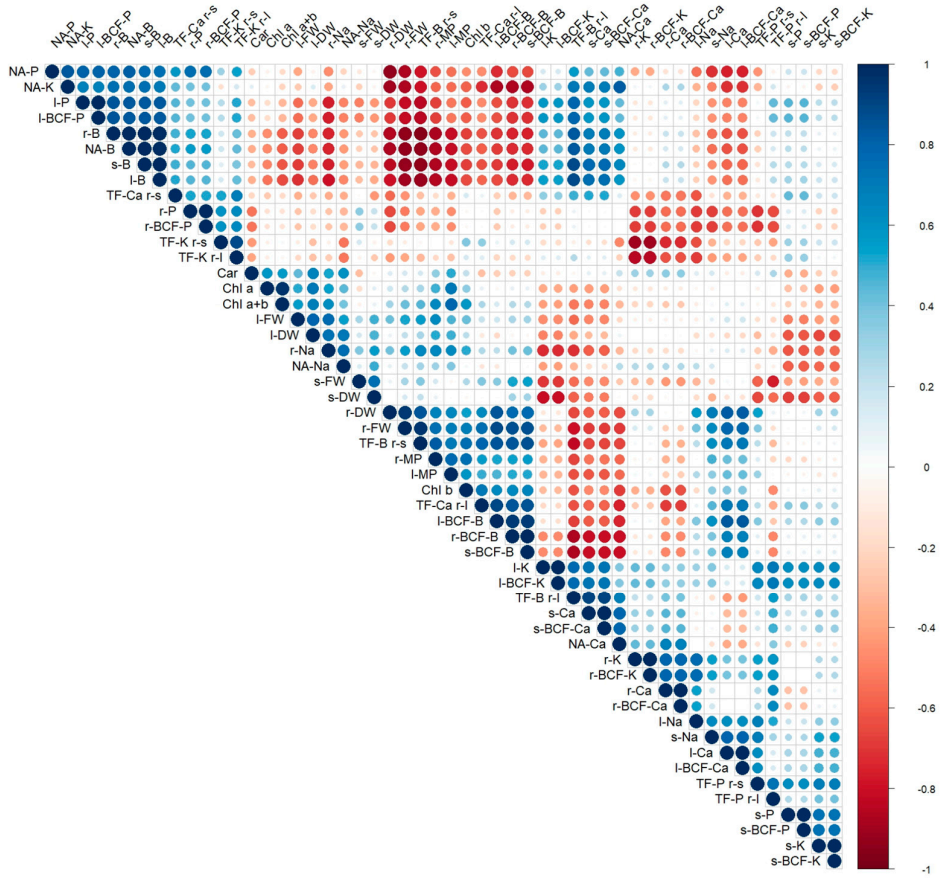

Figure 6. The correlation matrix illustrates the relationships among parameters measured in scallions' root, shoot, and leaf tissues. In the matrix, both the color and size of the circles reflect the strength and direction of the correlations: blue circles indicate positive correlations, while red circles denote negative correlations. Larger circles correspond to stronger correlation coefficients. Abbreviations: r, root; s, shoot; l, leaf; r–s, root to shoot; r–l, root to leaf.

4. Discussion

Excessive B in the rooting medium negatively affects the physiological, biochemical, and metabolic functions of plants and may reduce yield and quality [26]. In our study, increasing B applications resulted in a significant reduction in both the FWs and DWs of the roots, whereas the shoot and leaf biomass remained unaffected (Figure 1). When examining B concentrations, it was seen that B concentrations in upper organs (shoot + leaves) were approximately 2–2.5-fold higher than those in the roots (Table 2). The B distribution in plant parts may be closely related to the genetic structure of the onion. This may be partially explained by the fact that sorbitols, the primary photosynthetic products in onion plants, are highly mobile and tend to accumulate in leaves [13]. The absence of dramatic toxicity symptoms in leaves (Figure 7) may also support this result. Additionally, previous research has demonstrated that excessive B in the rooting medium can inhibit root growth [27]. In agreement with these findings, Francois [28] observed that even when applying a range of B concentrations (0.5, 1, 5, 10, 15, and 20 mg kg^{-1}) to the nutrient solution, there was no significant effect on the biomass production of green onion leaves [29].

Changes in plant'photosynthetic pigment contents (especially Chl and carotenoids) are considered an important indicator of negativity due to abiotic stress factors. The B levels applied in our study caused certain changes in the content of these pigments in scallions (Figure 3). For instance, there was a non-significant decrease in Chl *a* content, whereas there was a significant decrease in Chl *b* content. This result is from a previous work, which reported that during the process of Chl degradation due to B toxicity, Chl *b* is

converted to Chl *a*, and thus the Chl *a*/*b* ratio might increase [29]. Ito et al. [30] revealed that the reduction of Chl *b* in leaves exposed to high B application depends on the different mechanisms such as greater degradation of Chl *b*, an increment of Chl *b* in conversion to Chl *a*, a reduction in conversion of Chl *a* to Chl *b*, or the combination of these mechanisms. The Car contents of scallions significantly increased with only low B applications (Figure 3a).

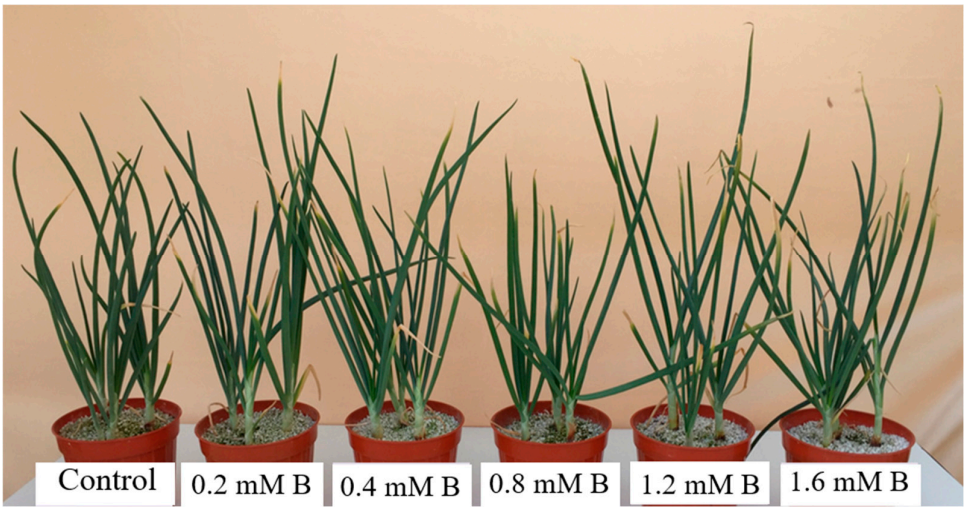

Figure 7. The effects of increasing B levels on the growth of scallions.

At the same time, MP value in roots and shoots significantly decreased with the high B applications, contrary to expectations (Figure 3b). Notably, positive correlations were observed between the root FW and MP values of the root and leaf, suggesting that as the root FW increased, MP values in the plant tissues also tended to increase (Figure 6). The tendency of B, which is abundant in the growth medium, to form complexes easily with different sugars and other compounds containing cis-hydroxyl groups may partially support this conclusion. Kobayashi et al. [31] reported that the B–RG-II complex cross-links pectin polysaccharide chains and thus functions to form a pectin network in cell walls. The Car pigments, components of thylakoid membranes, protect Chl from photo-oxidation by absorbing and transferring light to Chl [32]. Nevertheless, Bolaños et al. [33] noted that B has a vital role in the stabilization of molecules by cis-diol groups, independent of its other functions. The insignificant effects of B applications on biomass production in leaves (Figure 2), some photosynthetic pigment contents (Chl *a*, Chl *a* + *b*) (Figure 3a), and MP (Figure 3b) could be explained by the specific B mobility in onion.

Onions are known to produce complex sugar alcohol (polyol) and therefore have high phloem B mobility [14]. The transport of B in the phloem was discussed in previous sections, but its mobility is highly variable among plant species. In species-producing sugar alcohols like onions, the borate anion binds to these sugar alcohols to form complexes that are crucial for transporting B from mature leaves to young leaves via the phloem [13,34]. In contrast, in sucrose-producing species like wheat, complexes such as bis–sucrose–borate have been identified, resulting in a lower concentration of B within the phloem [35]. Brown and Hu [13], who applied ^{10}B-enriched boric acid to leaves, reported that onions and carrots are important mannitol-producing plants. As seen in Figure 7, the absence of serious B toxicity symptoms in scallions exposed to high B indicates that this plant is tolerant of high B doses. Onion leaf injury remained restricted to the tip of the leaves, without marginal chlorosis. Onions showed a notable tolerance to high B treatments, especially 10, 15, or 20 mg L^{-1} B doses [28]. This tolerance could be related to the role of B in di-ester bridges between two RG-II molecules (Figure 1). These major B-binding fractions may affect cell wall porosity and plant morphogenesis [5], due to an increase in intercellular bindings [7,8].

Many researchers reported that there appears to be a linear relationship between the B levels applied to the rooting medium and the B concentration in the plant tissue [36–38]. However, this relationship could be disrupted by some conditions, such as the location of the study (greenhouse or field conditions) [39], working in a nutrient solution or a soilless environment, etc. [40]. In our study, the B applications caused a significant increase in the B concentrations of plant organs (the roots, shoots, and leaves), and the leaves have an approximately 2-fold higher B concentration than the roots in plants exposed to high B (Table 1). The distribution of B concentrations in plant organs is ordered as shoot < root < leaf. Differences between B concentrations in plant organs and the lack of toxicity symptoms can be explained by B mobility in plant species as above. These findings are in agreement with the results of Subedi [41], who studied the accumulation and distribution of B in wheat varieties. This researcher reported the total B concentrations in the leaves by 68%, in the roots by 16%, and in the bulbs by 10%. In addition, Samet and Çıkılı [38] stated that purslane leaves exposed to 0.37, 0.74, 1.48, and 2.96 mM B contained 2.64-, 3.42-, 3.14-, and 4.28-fold more B than in their roots, respectively.

Leaf P concentrations increased significantly with all B levels (Figure 4a), while leaf K concentrations increased only with 0.8 and 1.2 mM B levels (Figure 4b). On the other hand, leaf Ca and Na concentrations decreased significantly only with 1.2 and 1.6 mM B levels (Figure 4c,d). Francois [42] studied the effect of B on radish growth in sand culture, and he reported that Ca and P concentrations showed a notable reduction with excess B, while K, Mg, and Na concentrations remained unchanged. The same researcher found that P, K, Ca, Na, and Mg in the leaves and bulbs of onions were not affected significantly by increasing B levels [28].

While a larger TF value of nutrient elements indicates a higher plant's transfer capacity of elements from the root to the shoot or leaves, the higher elements' BCF value indicates that the plant has a higher accumulation potential of these nutrients. In the present study, translocation for P, K, and Ca elements in both shoots and roots was found to be lower than 1 (Table 2). This indicated that only limited quantities of these elements could be transported to the aboveground parts of scallions, which might be due to lower mobility [43,44]. However, the TF value of B in leaves was larger than 1 (Table 1), implying that B was more readily accumulated in the leaves, which had also been observed by other researchers [45]. In addition, over the range of 0.2–1.6 mM of B supply, the TF value of B, P, and K in leaves was found to be greater than in shoots (Tables 1 and 2). This may be due to the higher accumulation of B, P, and K in leaves compared to shoots (Figure 4). On the other hand, higher B application caused a greater increase in the TF value for B in leaves, contrary to shoots (Table 1). This may also be related to the fact that translocation from roots to shoots is low with low B applications because the B in the roots is bound to the root's cell wall [1]. These findings showed that scallions have a high transfer capacity of B, P, and K to leaves, contrary to Ca. The fact that the Ca concentration in the roots is approximately 8-fold higher than in the leaves (Figure 4c) and that the BCF of Ca is higher than in the roots (Figure 5d) indicates that calcium is accumulated in the roots. The uptake and transport of Ca are primarily involved by physiological (cation exchange capacity of the rhizosphere, root, and shoot) and molecular mechanisms (Ca transporter proteins and channels), which affect the accumulation and partitioning of Ca in plant parts [46]. Furthermore, applying 0.4 mM B increased the Ca concentration in the roots, while applying higher B decreased it (Figure 4c). This could be explained by the fact that insufficient B in the rooting medium will change the intracellular Ca ion concentration. A significant positive correlation was observed between the Ca concentration and root FW, as well as the Ca accumulation in the plant leaves (Figure 6). This suggests that the increase in root FW may contribute to higher calcium concentration and accumulation in the leaves. González-Fontes et al. [47] reported

that Ca and B have a vital role in jointly stabilizing and maintaining the structure and function of the cell wall, and there is a close connection between the Ca and B interaction and the physiological processes taking place in the cell wall.

Net ion accumulation indicates the amount of ions accumulated in the upper organs by the resulting dry root biomass [48]. The results presented in Table 3 showed that increasing B levels caused a significant increase in the net accumulation of B, P, K, and Ca, except for Na. Gradual and significant increases in net B accumulation in plants may result from plant exposure to increased B levels (Table 1). B is mobile in plants that use complex sugar alcohols (polyols) as the primary photosynthetic metabolite, like onions, and is carried from the roots to the upper parts of the plant by the transpiration stream (via xylem), where it joins with polyols to form a complex. Complexes of polyol–B–polyol can pass through the phloem and reach the actively developing meristematic tissues [49]. At higher B applications (0.8, 1.2, and 1.6 mM), in contrast to net B accumulation, the closeness of net P, K, Ca, and Na accumulation data could be explained by the strong tolerance of onions to B toxicity. On the other hand, a significant negative correlation was observed between root FW and net ion accumulation via the root, indicating a strong inverse relationship between root FW and the ion accumulations (Figure 6). Root DW (Figure 2b) and MP values (Figure 3b) measured at the same B levels show that onion roots were not seriously damaged at these B levels. The fact that no effective deficiency symptoms were seen in the onion leaves in Figure 5 may support this hypothesis.

5. Conclusions

Boron exhibits unique characteristics compared to other plant nutrients, particularly in terms of its narrow threshold between deficiency and toxicity, species-specific uptake and transport mechanisms, and its diverse physiological roles. In this study, green onions did not show a significant response to high B levels. However, important information was obtained regarding the effects of B on the ion concentrations, net ion accumulations, and bio-concentrations. For example, the applied B levels caused significant increases in P, K, and Ca net ion accumulation. The BCF of P also increased with higher B levels (0.8, 1.2, and 1.6 mM). Collectively, these findings partially confirmed the potential relationship between increasing B levels and ion behavior (transport and accumulation) and also revealed the complex interactions of B uptake, transport, and accumulation in metabolism. The fact that the expected results cannot be obtained with increasing B levels may be related to the genetic structure of the onion. Evidence suggests that onion (*Allium* sp.), as a non-gramineous monocot, displays distinct phloem mobility of B, unlike many other plant species where B transport is primarily limited to the xylem. Phloem mobility may enable a more efficient internal redistribution of B, potentially contributing to a higher tolerance. In addition, B is known to play a critical role in the structural integrity of cell walls by forming diester bonds between two rhamnogalacturonan II (RG-II) molecules, which is particularly associated with maintaining upright growth and cell wall stability. Furthermore, the partial limitations in observing toxicity symptoms may be attributed to the relatively low B concentrations applied to the rooting medium. Therefore, future studies employing higher B levels may offer a clearer finding of the physiological roles of B and its behavior in green onions. Given these findings, we suggest B concentrations in experiments above 1.6 mM to reach more definitive conclusions about response thresholds in onion varieties.

In the broader context, the increasing contamination of agricultural lands and water resources worldwide compels farmers to produce crops on polluted soils or to use contaminated water for irrigation. In such environments, knowing the ability of plants to tolerate abiotic stress can help minimize yield losses and ensure access to safe and sustainable food sources. Nevertheless, findings derived from greenhouse experiments conducted under

controlled hydroponic conditions should be validated through field trials carried out in soil-based systems to enhance their applicability to agricultural settings.

Author Contributions: The authors (H.S. and Y.Ç.) collaborated on the following issues: methodology, validation, analysis, investigation, data collection, writing, review, and editing of the original draft. Furthermore, All authors have read and agreed to the published version of the manuscript.

Funding: This research received no external funding.

Data Availability Statement: The raw data supporting the conclusions of this article will be made available by the authors on request.

Conflicts of Interest: There are no conflicts of interest among the authors in this study.

References

1. Goldbach, H.E.; Wimmer, M.A.; Findeklee, P. Discussion paper: Boron—How can the critical level be defined? *J. Plant Nutr. Soil Sci.* **2000**, *163*, 115–121. [CrossRef]
2. Yau, S.K.; Hamblin, J.; Ryan, J. Phenotypic variation in boron toxicity tolerance in barley, durum, and bread wheat. *Rachis* **1994**, *13*, 20–25.
3. Wimmer, M.A.; Goldberg, S.; Gupta, U.C. Boron. In *Handbook of Plant Nutrition*; Barker, A., Pilbeam, D., Eds.; CRC Press: Boca Raton, FL, USA, 2015; pp. 305–346.
4. Loomis, W.D.; Durst, R.W. Chemistry and biology of boron. *BioFactors* **1992**, *3*, 229–239.
5. Xiao, C.; Anderson, C.T. Roles of pectin in biomass yield and processing for biofuels. *Front. Plant Sci.* **2013**, *4*, 67. [CrossRef]
6. Begum, R.A.; Fry, S.C. Arabinogalactan-proteins as boron-acting enzymes, cross-linking the rhamnogalacturonan-II domains of pectin. *Plants* **2023**, *12*, 3921. [CrossRef]
7. O'Neill, M.A.; Eberhard, S.; Albersheim, P.; Darvill, A.G. Requirement of borate cross-linking of cell wall rhamnogalacturonan II for Arabidopsis growth. *Science* **2001**, *294*, 846–849. [CrossRef]
8. Matsunaga, T.; Ishii, T.; Matsumoto, S.; Masanobu, H.; Darvill, A.; Albersheim, P.; O'Neill, M.A. Occurrence of the Primary Cell Wall Polysaccharide Rhamnogalacturonan II in Pteridophytes, Lycophytes, and Bryophytes. Implications for the Evolution of Vascular Plants. *Plant Physiol.* **2004**, *134*, 339–351. [CrossRef]
9. Avci, U.; Peña, M.J.; O'Neill, M.A. Changes in the abundance of cell wall apiogalacturonan and xylogalacturonan and conservation of rhamnogalacturonan II structure during the diversification of the Lemnoideae. *Planta* **2018**, *247*, 953–971. [CrossRef]
10. Begum, R.A.; Messenger, D.J.; Fry, S.C. Making and breaking of boron bridges in the pectic domain rhamnogalacturonan-II at apoplastic pH in vivo and in vitro. *Plant J.* **2023**, *113*, 1310–1329. [CrossRef]
11. Hu, H.; Brown, P.H.; Labavitch, J.M. Species variability in boron requirement is correlated with cell wall pectin. *J. Exp. Bot.* **1996**, *47*, 227–232. [CrossRef]
12. Brown, P.H.; Bellaloui, N.; Wimmer, M.A.; Bassil, E.S.; Ruiz, J.; Hu, H.; Pfeffer, H.; Dannel, F.; Römheld, V. Boron in plant biology. *Plant Biol.* **2002**, *4*, 205–223. [CrossRef]
13. Brown, P.H.; Hu, H. Boron mobility and consequent management in different crops. *Better Crops* **1998**, *82*, 28–31.
14. Brdar-Jokanović, M. Boron toxicity and deficiency in agricultural plants. *Int. J. Mol. Sci.* **2020**, *21*, 1424–1444. [CrossRef] [PubMed]
15. Redgwell, R.J.; Selvendran, R.R. Structural features of cell wall polysaccharides of onion (*Allium cepa*). *Carbohydr. Res.* **1986**, *157*, 183–199. [CrossRef]
16. Waldron, K.W.; Selvendran, R.R. Composition of the cell walls of different asparagus (*Asparagus officinalis*) tissues. *Physiol. Plant.* **1990**, *80*, 568–575. [CrossRef]
17. Jones, J.B., Jr.; Wolf, B.; Mills, H.A. *Plant Analysis Handbook. A Practical Sampling, Preparation, Analysis, and Interpretation Guide*; Micro-Macro Publishing Inc.: Athens, GA, USA, 1991; pp. 127–189.
18. González-Fontes, A.; Rexach, J.; Navarro-Gochicoa, M.T.; Herrera-Rodríguez, M.B.; Beato, V.M.; Maldonado, J.M.; Camacho-Cristóbal, J.J. Is boron involved solely in structural roles in vascular plants? *Plant Signal. Behav.* **2008**, *3*, 24–26. [CrossRef]
19. Manna, D.; Maity, T.K. Growth, yield, and bulb quality of onion (*Allium cepa* L.) in response to foliar application of boron and zinc. *J. Plant Nutr.* **2016**, *39*, 438–441. [CrossRef]
20. Francke, A.; Majkowska-Gadomska, J.; Kaliniewicz, Z.; Jadwisieńczak, K. No Effect of Biostimulants on the Growth, Yield, and Nutritional Value of Shallots Grown for Bunch Harvest. *Agronomy* **2022**, *12*, 1156. [CrossRef]
21. Hoagland, D.R.; Arnon, D.I. The water-culture method for growing plants without soil. *Calif. Agric. Exp. Stn. Circ.* **1950**, *347*, 1–32.
22. Lichtenthaler, H.K. Chlorophylls and carotenoids: Pigments of photosynthetic biomembranes. *Methods Enzymol.* **1987**, *148*, 350–382. [CrossRef]

23. Yan, B.; Dai, Q.; Liu, X.; Huang, S.; Wang, Z. Flooding-induced membrane damage, lipid oxidation, and activated oxygen generation in corn leaves. *Plant Soil* **1996**, *179*, 261–268. [CrossRef]
24. Miller, R.O. High-temperature oxidation: Dry ashing. In *Handbook of Reference Methods for Plant Analysis*; Kalra, P.Y., Ed.; Taylor and Francis/CRC Press: Boca Raton, FL, USA, 1998; pp. 66–69.
25. Soda, S.; Hamada, T.; Yamaoka, Y.; Ike, M.; Nakazato, H.; Saeki, Y.; Kasamatsu, T.; Sakurai, Y. Constructed wetlands for advanced treatment of wastewater with a complex matrix from a metal-processing plant: Bioconcentration and translocation factors of various metals in *Acorus gramineus* and *Cyperus alternifolius*. *Ecol. Eng.* **2012**, *39*, 63–70. [CrossRef]
26. Herrera-Rodríguez, M.B.; González-Fontes, A.; Rexach, J.; Camacho-Cristobal, J.J.; Maldonado, J.M.; Navarro-Gochicoa, M.T. Role of boron in vascular plants and response mechanisms to boron stresses. *Plant Stress* **2010**, *4*, 115–122.
27. Reid, R.; Fitzpatrick, K. Influence of leaf tolerance mechanisms and rain on boron toxicity in barley and wheat. *Plant Physiol.* **2009**, *151*, 413–420. [CrossRef]
28. Francois, L.E. Yield and quality responses of garlic and onion to excess boron. *HortScience* **1991**, *26*, 547–549. [CrossRef]
29. Trifunović-Momčilov, M.; Milošević, S.; Marković, M.; Đurić, M.; Jevremović, S.; Dragićević, I.Č.; Subotić, A.R. Changes in photosynthetic pigments content in non-transformed and AtCKX transgenic centaury (*Centaurium erythraea* Rafn) shoots grown under salt stress in vitro. *Agronomy* **2021**, *11*, 2056. [CrossRef]
30. Ito, H.; Ohtsuka, T.; Tanaka, A. Conversion of chlorophyll b to chlorophyll a via 7-hydroxymethyl chlorophyll. *J. Biol. Chem.* **1996**, *271*, 1475–1479. [CrossRef]
31. Kobayashi, M.; Nakagawa, H.; Asaka, T.; Matoh, T. Borate $\pm$ rhamnogalacturonan II bonding reinforced by Ca^{2+} retains pectic polysaccharides in higher-plant cell walls. *Plant Physiol.* **1999**, *119*, 199–204. [CrossRef]
32. Park, S.; Fischer, A.L.; Steen, C.J.; Iwai, M.; Morris, J.M.; Walla, P.J.; Niyogi, K.K.; Fleming, G.R. Chlorophyll-carotenoid excitation energy transfer in high-light-exposed thylakoid membranes investigated by snapshot transient absorption spectroscopy. *J. Am. Chem. Soc.* **2018**, *140*, 11965–11973. [CrossRef]
33. Bolaños, L.; Lukaszewski, K.; Bonilla, I.; Blevins, D. Why boron? *Plant Physiol. Biochem.* **2004**, *42*, 907–912. [CrossRef]
34. Brown, P.H.; Shelp, B.J. Boron mobility in plants. *Plant Soil* **1997**, *193*, 85–101. [CrossRef]
35. Stangoulis, J.; Tate, M.; Graham, R.; Bucknall, M.; Palmer, L.; Boughton, B.; Reid, R. The mechanism of boron mobility in wheat and canola phloem. *Plant Physiol.* **2010**, *153*, 876–881. [CrossRef] [PubMed]
36. Cervilla, L.M.; Blasco, B.; Ríos, J.J.; Romero, L.; Ruiz, J.M. Oxidative stress and antioxidants in tomato (*Solanum lycopersicum*) plants subjected to boron toxicity. *Ann. Bot.* **2007**, *100*, 747–756. [CrossRef] [PubMed]
37. Hamurcu, M.; Demiral, T.; Hakki, E.E.; Turkmen, Ö.; Gezgin, S.; Bell, R.W. Oxidative stress responses in watermelon (*Citrullus lanatus*) as influenced by boron toxicity and drought. *Zemdirbyste/Agriculture* **2015**, *102*, 209–216. [CrossRef]
38. Samet, H.; Çıkılı, Y. Response of Purslane (*Portulaca oleracea* L.) to Excess Boron and Salinity: Physiological Approach. *Russ. J. Plant Physiol.* **2019**, *66*, 316–325. [CrossRef]
39. Paull, J.G.; Cartwright, B.; Rathjen, A.J. Responses of wheat and barley genotypes to toxic concentrations of soil boron. *Euphytica* **1988**, *39*, 137–144. [CrossRef]
40. Nable, R.O. Resistance to boron toxicity amongst several barley and wheat cultivars: A preliminary examination of the resistance mechanism. *Plant Soil* **1988**, *112*, 45–52. [CrossRef]
41. Subedi, K.D.; Gregory, P.J.; Gooding, M.J. Boron accumulation and partitioning in wheat cultivars with contrasting tolerance to boron deficiency. *Plant Soil* **1999**, *214*, 141–152. [CrossRef]
42. Francois, L.E. Effect of excess boron on broccoli, cauliflower, and radish. *J. Am. Soc. Hortic. Sci.* **1986**, *111*, 494–498. [CrossRef]
43. Huang, S.S.; Liao, Q.L.; Hua, M.; Wu, X.M.; Bi, K.S.; Yan, C.Y.; Chen, B.; Zhang, X.Y. Survey of heavy metal pollution and assessment of agricultural soil in Yangzhong district, Jiangsu Province, China. *Chemosphere* **2007**, *67*, 2148–2155. [CrossRef]
44. Wang, X.; Liu, Y.; Zeng, G.; Chai, L.; Song, X.; Min, Z.; Xiao, X. Subcellular distribution and chemical forms of cadmium in *Bechmeria nivea* (L.) Gaud. *Environ. Exp. Bot.* **2008**, *62*, 389–395. [CrossRef]
45. Kabata-Pendias, A. *Trace Elements in Soils and Plants*, 3rd ed.; CRC Press: Boca Raton, FL, USA, 2000; p. 432.
46. Kumar, A.; Singh, U.M.; Manohar, M.; Gaur, V.S. Calcium transport from source to sink: Understanding the mechanism(s) of acquisition, translocation, and accumulation for crop biofortification. *Acta Physiol. Plant.* **2015**, *37*, 1722. [CrossRef]
47. González-Fontes, A.; Navarro-Gochicoa, M.T.; Camacho-Cristóbal, J.J.; Herrera-Rodríguez, M.B.; Quiles-Pando, C.; Rexach, J. Is Ca^{2+} involved in the signal transduction pathway of boron deficiency? New hypotheses for sensing boron deprivation. *Plant Sci.* **2014**, *217*, 135–139. [CrossRef] [PubMed]

48. Moradi, L.; Ehsanzadeh, P. Effects of Cd on photosynthesis and growth of safflower (*Carthamus tinctorius* L.) genotypes. *Photosynthetica* **2015**, *53*, 506–518. [CrossRef]
49. García-Sánchez, F.; Simón-Grao, S.; Martínez-Nicolás, J.J.; Alfosea-Simón, M.; Liu, C.; Chatzissavvidis, C.; Pérez-Pérez, J.G.; Cámara-Zapata, J.M. Multiple stresses occurring with boron toxicity and deficiency in plants. *J. Hazard. Mater.* **2020**, *397*, 122713. [CrossRef]

horticulturae

MDPI

Article

Tomato Lines Tolerant to Sodium Chloride at Early Growth Stages

Alma Aurora Deanda-Tovar [1], Juan Enrique Rodríguez-Pérez [1,*], Jaime Sahagún-Castellanos [1], María Teresa Beryl Colinas-y-León [1], Paulino Pérez-Rodríguez [2] and Ana Elizabeth Paredes-Cervantes [1]

[1] Departamento de Fitotecnia, Instituto de Horticultura, Universidad Autónoma Chapingo, Km 38.5 Carretera México-Texcoco, Chapingo 56230, Estado de México, Mexico; almadeanda2a@gmail.com (A.A.D.-T.); jsahagunc@yahoo.com.mx (J.S.-C.); lozcol@gmail.com (M.T.B.C.-y.-L.); paredescerv29@gmail.com (A.E.P.-C.)
[2] Colegio de Postgraduados, Km 36.5 Carretera México-Texcoco, Montecillo 56230, Estado de México, Mexico; perpdgo@gmail.com
* Correspondence: erodriguezx@yahoo.com.mx

Abstract: High concentrations of sodium chloride (NaCl) in soil and water are increasingly common conditions in tomato (*Solanum lycopersicum* L.) production that impair the development and yield of this crop, generating the need for tolerant varieties. This research aimed to identify tomato lines tolerant to salinity during germination and early seedling development. A standard germination test was carried out in which 93 lines were evaluated under conditions of 0 and 80 mM NaCl for 12 days in a germination chamber with a temperature of 28 ± 1 °C and relative humidity of 80 ± 5%. At the seedling stage, 88 lines were evaluated under conditions of 0 and 150 mM NaCl in a floating raft system. During germination, saline conditions decreased germination percentage (37%), plumule (43%) and radicle (47%) length, dry matter (44%) and germination rate index (70%). At the seedling stage, NaCl decreased ($p \leq 0.05$) plant height (44%) and leaf area (50%), without modifying root, aerial and total dry matter or root length. Twenty-eight tolerant lines were identified at germination and twenty-three at the seedling stage, seven of which were tolerant at both stages. This implies that salinity tolerance mechanisms differ in the developmental stages studied and makes it possible to combine these mechanisms to prolong tolerance during plant development.

Keywords: salinity; germination; seedling; tolerance; *Solanum lycopersicum* L.

1. Introduction

Salinity is one of the major abiotic factors affecting agriculture worldwide and threatening food security [1], as it is estimated that 20% of cultivated land and 33% of irrigated agricultural area are affected by this condition [2,3]; this causes reductions in agricultural crop yields between 50 and 80% [4,5], with losses of up to USD 27.3 billion annually [6]. In addition, it is estimated that by 2050, half of all crops will be affected by salinity [2,7]. Mexico also faces this problem due to the fact that of the country's 9.8 million hectares of irrigated agricultural land, 34.9% are slightly affected by excess sodium and 25.1% by salinity [8]; this percentage is constantly increasing due to inadequate agricultural practices and use of poor-quality water.

Tomato (*Solanum lycopersicum* L.) is one of the most consumed vegetables worldwide, with a harvested area of 4,917,735 hectares in 2022 [9]. Mexico is the world's eighth largest producer and leading exporter of this vegetable [10]. The widespread cultivation of this crop implies that its establishment can occur under salinity stress conditions. Although

the crop is considered moderately tolerant to salts, up to 6 $dS \cdot m^{-1}$ [11], it shows disorders when grown in highly saline soils, with greater damage during germination and, to a lesser extent, during the seedling stage [12]. Saline conditions delay and reduce the germination of tomato seeds by altering their physiological and biochemical activity and by decreasing the water potential gradient and its surrounding environment [13,14]; saline conditions also reduce the germination rate due to the deterioration of enzymatic activity caused by osmotic stress or ionic toxicity caused by NaCl [15,16].

At the seedling stage, salinity reduces the height, growth and development of the stem, root and leaf area and, consequently, biomass accumulation [17,18]. High Na^+ and Cl^- concentrations in the soil solution generate osmotic stress, ionic imbalance, water deficit and oxidative stress in the plant [19]. Thus, as the concentration of salts and the stress period increase, the accumulation of Na^+ and Cl^- ions increases, which generates toxicity and inhibits the primary metabolism by damaging the photosynthetic machinery and accumulating excess reactive oxygen species (ROS) [20]. The high accumulation of ROS increases the permeability of the cell membrane due to the degradation of its functional and structural proteins [21]. In the root zone, osmotic stress reduces the ability to absorb water and nutrients, which decreases leaf and shoot growth [22].

Plants also have the ability to activate gene families involved in different metabolic, physiological and biochemical processes to tolerate salinity stress [23]. Among them, there are those that regulate stomatal closure, which prevents water loss and increase and maintains ionic homeostasis [24]; those that prevent Na^+ accumulation in roots [25]; and those that increase antioxidant activity, biomass accumulation and secondary metabolite accumulation [26]. These metabolites have the functions of preserving enzymatic activity, stabilizing structural proteins and scavenging reactive oxygen species to mitigate oxidative damage and enhance the tolerance response [22,27].

All of them together maintain root development in the face of salinity stress for the supply of nutrients. Since there is a genetic control of these processes involved in salt tolerance, some tomato breeding programs focus on the selection of these genes to obtain new tolerant varieties [28], particularly during the initial growth stages (germination, emergence and seedling), since the greatest vulnerability of tomato plants to saline conditions occurs during these stages in which the ability to adapt to salt stress is crucial to maintain crop productivity [29].

This research aimed to identify and select experimental tomato lines that are salinity tolerant at the germination and seedling stages and to design a strategy to evaluate a large number of genotypes using short-term tests and identify their degree of tolerance to salt stress in the early stages of development.

2. Materials and Methods

The genotypes evaluated were 93 homozygous lines (F_{17}–F_{19}) at germination and 88 lines at the seedling stage. The difference in the number of genotypes evaluated in the tests was due to seed availability. The lines were generated by the greenhouse tomato breeding program of the Universidad Autónoma Chapingo (UACh) and were obtained from balanced composites of segregating populations derived from crosses between commercial hybrids. Some characteristics of these lines are presented in Table S1 (fruit type, color and growth habit).

Two salt tolerance tests were carried out, one during germination (in 2022) and one at the seedling stage (in 2020). The NaCl concentrations studied were chosen based on Seth et al. [30] for germination, 80 mM NaCl, and Ahmed et al. [23] for seedling, 150 mM NaCl. These concentrations allowed to differentiate between tolerant and susceptible lines, without being lethal doses.

2.1. NaCl Tolerance at Germination Stage

The experiment was carried out in June and July 2022 in the seed laboratory of the Plant Science Department of the Universidad Autónoma Chapingo (UACh). Two standard germination tests were performed using saline treatment (80 mM NaCl) and a control. The saline solution was prepared with distilled and deionized water and 99.3% pure NaCl (High Purity®, Mexico city, Mexico).

The experimental unit (EU) was a 56 mm diameter Petri dish with 25 seeds. Filter paper was used as a substrate saturated with 2 mL of solution, either with distilled and deionized water or 80 mM NaCl, according to the corresponding treatment. The experimental design randomized complete blocks with two replicates in the case of the control and four replicates in the case of 80 mM NaCl. Under laboratory or greenhouse conditions, environmental variation tends to be considerably smaller, allowing for a more precise estimation of experimental error with a smaller number of replicates. In contrast, under stress conditions, this variation increases. Thus, the smaller number of replicates in the control setting does not compromise the statistical validity of the results.

The tests were carried out for twelve days in a germination chamber (Lab-Tech Inc.®, model D-7140, Hopkinton, MA, USA) with three days of darkness and nine days of artificial light. The temperature was maintained at 28 ± 1 °C and relative humidity at 80 ± 5%. Three 1 mL irrigations were made with the corresponding solutions, according to the water needs of the seedlings.

Germinated seeds were counted daily. A seed was considered germinated when the radicle protruded. At the end of the test, the following were evaluated:

Germination percentage (GP, in %) with respect to the total number of seeds sown.

Germination rate index (GRI) with the formula proposed by Maguire [31]:

$$GRI = \sum_{i=1}^{n} \frac{x_i}{d_i},$$

where n is the number of counts made during the trial, x_{i} is the number of seeds germinated in count i minus the number of seeds germinated in count $i-1$, and d_{i} is the number of days after sowing until count i.

Five seedlings were randomly selected from the EU, and the average plumule length (PL, in cm) and average radicle length (RL, in cm) were determined.

Seedlings from all the EU were dried to constant weight at 45 °C in an oven (Riossa®, model H-48, series 301007, Mexico city, Mexico). Subsequently, total dry matter (TDM, in mg) was determined on an analytical balance (Sartorius, practiucum224-1S, 0029604782, Goettingen, Germany).

2.2. NaCl Tolerance at the Seedling Stage

The evaluation was carried out from July to September 2020 under greenhouse conditions at the Colegio de Postgraduados, Montecillo campus (19°27′53″ N, 98°54′19″ W); temperatures inside the greenhouse ranged between 13.5 and 35 °C.

Eighty-eight experimental lines exposed during the seedling stage to 0 and 150 mM NaCl concentrations were evaluated. The lines were sown in 200-cavity polystyrene trays with peat foam (Oasis®, Columbus, OH, USA) as substrate. Transplanting was carried out 23 days after sowing in a floating raft system (Figure 1) under greenhouse conditions. Wooden containers measuring 2.4 × 1.2 × 0.2 m and covered with geomembrane and with a capacity of 500 L of nutrient solution were used. The nutrient solution used was that of Cadahia [32] at 50%. The experimental unit consisted of 5 seedlings, with a planting density of 166.6 plants·m^2. One container constituted a replicate. Four days after transplanting (DAT), 150 mM NaCl was added to the nutrient solution of three containers. Two other

containers corresponded to the control without NaCl. A randomized complete block experimental design was used with three replicates at 150 mM concentration and two replicates at the control.

Figure 1. Tomato lines evaluated in a floating raft system.

Seedling height (SH, in cm) was measured on three EU seedlings.

The test ended at 14 DAT. The average root length (RL, in cm) was then evaluated in three EU seedlings, and from the five EU seedlings, aerial dry matter (ADM, in g) and root dry matter (RDM, in g) were determined, both dried for 96 h at 46 °C. Leaf area (LA, in cm^2), for which digital photographs were captured, was subsequently determined using ImageJ software (v1.4.3.67; National Institutes of Health, Bethesda, MD, USA).

2.3. Statistical Analysis

The statistical analysis was similar in both tests. Initially, indices were obtained by the quotient of the response obtained in the saline condition divided by the average of the response obtained in the control. With the generated indices, a cluster analysis was carried out with Gower's [33] distance and Ward's [34] minimum variance algorithm. The cut-off height was determined by Hotelling's [35] T2 statistics and the pseudo-F statistic [36].

To corroborate the sets obtained by the cluster analysis, a discriminant analysis was performed, and resubstitution and cross-validation tests were applied [36]. Finally, with the original data, analysis of variance and comparison of means were performed with Tukey's test, considering the generated groups as a source of variation and the genotypes nested in this factor.

The analysis was performed with SAS statistical package (version 9.4., Cary, NC, USA) with the procedures UNIVARIATE, MEANS, DISTANCE, CLUSTER, DISCRIM and GLM.

3. Results and Discussion

3.1. Salinity Tolerance at Germination Stage

The dendrogram generated by the cluster analysis obtained from Gower's distance and Ward's minimum variance algorithm is presented in Figure 2. Hotelling's T^2 statistic and the pseudo-F statistic indicated the formation of three groups with a cut-off height of 0.05 of semipartial r^2. The groups were made up of 25, 28 and 40 genotypes.

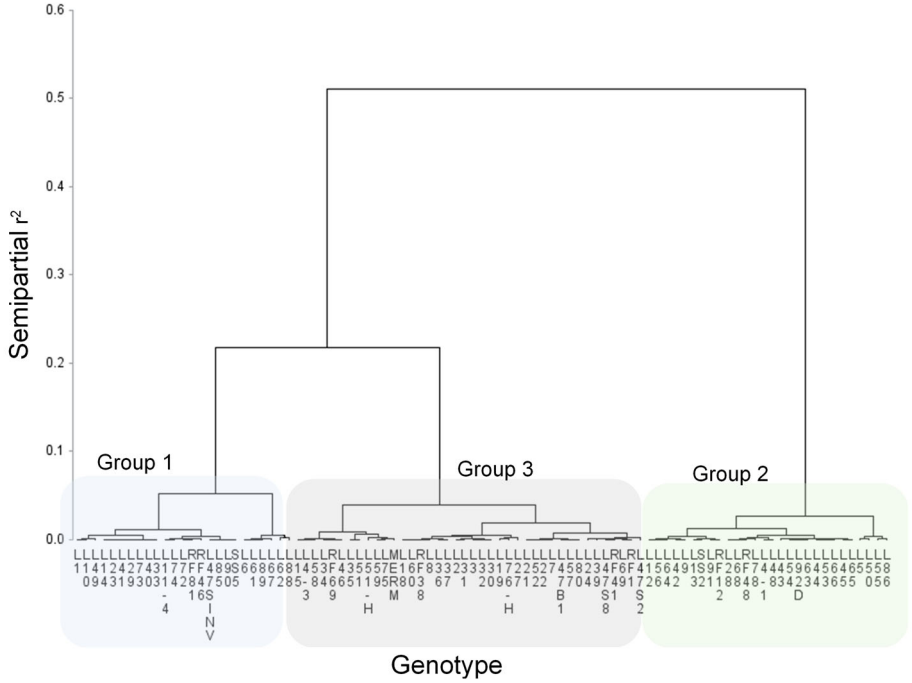

Figure 2. Hierarchical dendrogram generated from Gower's distance and Ward's minimum variance algorithm of NaCl tolerance indices of 93 experimental tomato lines evaluated under salt stress during germination.

The appropriateness of the achieved grouping was corroborated with a linear discriminant analysis, which indicated that the first discriminant variable (DV1), with an eigenvalue of 6.8, explained 97.4% of the variation in the data ($p \leq 0.0001$). The DV1 eigenvector indicated a greater relationship with germination percentage, germination rate index and total dry matter (Table 1); that is, lines with a high DV1 value identify lines with greater vigor during germination and vice versa. The second discriminant variable (DV2) described only 2.6% of the variation, which was not significant. Resubstitution and cross-validation tests showed adequate assignments in 90 of the 93 genotypes evaluated.

Table 1. Eigenvectors of the discriminant variables DV1 and DV2 generated from indices of 93 experimental tomato (*Solanum lycopersicum* L.) lines during the germination stage.

Variable	Eigenvectors		Discriminant Functions	
	DV1	DV2	DV1	DV2
Total dry matter (TDM)	0.98	−0.12	1.56	−2.39
Germination percentage (GP)	0.96	0.25	0.37	2.24
Plumule length (PL)	0.77	0.21	−0.08	0.93
Radicle length (RL)	0.49	−0.22	−0.20	−0.24
Germination rate index (GRI)	0.96	0.05	1.09	−0.42

The graphical representation of the genotypes based on the two discriminant variables is presented in Figure 3. Group 2 had the highest tolerance to salt stress, showing the greatest seed vigor with the highest DV1 values, associated with the greatest development of GP, TDM, PL, RL and GRI. In contrast, Group 1 was the most susceptible to NaCl, with the lowest seed vigor, while Group 3 showed intermediate tolerance.

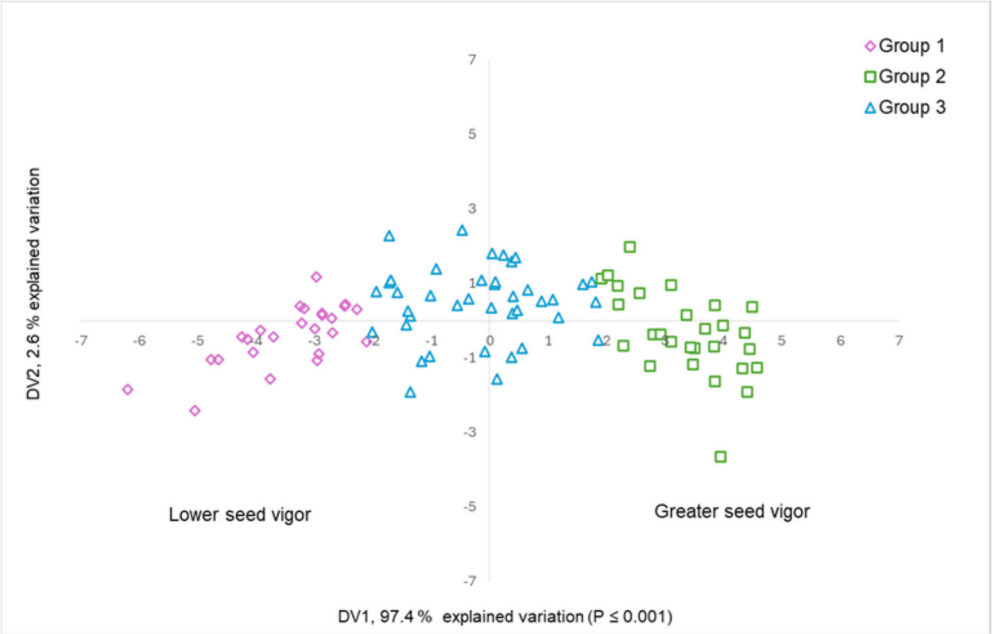

Figure 3. Graphical representation of discriminant variables of 93 tomato lines germinated under salinity conditions. DV1: discriminant variable 1; positive values are associated with a higher germination percentage, germination rate index and dry matter content and vice versa. DV2: discriminant variable 2 (not significant).

Analyses of variance were performed for original traits where NaCl concentrations, the generated groups and the genotypes nested within groups were considered, along with the corresponding interactions. These analyses showed significance for all sources of variation in the evaluated traits, except for GP and TDM in the concentration × genotype (group) interaction. Coefficients of variation ranged between 20 and 25%, except for radicle length, which was 40% (Table S2).

The evaluated traits were diminished by more than 37% by salinity stress (Table 2). Similar results were reported by Fadhil et al. [37] in commercial cultivars under salinity conditions between 70 and 170 mM NaCl, where a negative association was detected between the increase in saline condition with the germination percentage and biomass accumulation. At 100 mM, the reductions in these two traits corresponded to 95 and 100%, whereas, in the present study, at 80 mM NaCl, they were 37 and 44%, respectively.

Table 2. Comparisons of NaCl concentration means for the traits evaluated in 93 tomato (*Solanum lycopersicum* L.) lines germinated under salinity and control conditions.

NaCl (mM)	GP (%)		GRI		PL (cm)		RL (cm)		TDM (mg)	
0	80.62	a	6.84	a	3.40	a	1.08	a	0.028	a
80	50.87	b	2.04	b	1.94	b	0.58	b	0.015	b
% Reduction	37		70		43		47		44	
HSD	6.24		0.59		0.46		0.17		0.0029	

GP: germination percentage, GRI: germination rate index, PL: plumule length, RL: radicle length, TDM: total dry matter, % Reduction: percentage reduction from 0 to 80 mM NaCl concentration. HSD: honestly significant difference. Means with the same letter within columns do not differ statistically (Tukey, $p \leq 0.05$).

The evaluated lines showed reductions of less than 47% in seedling development (RL, PL and TDM) (Table 2); this contrasts with the reductions observed by Shanika and Seran [38] in the same variables and at the same NaCl concentration, which were greater than 50%. GRI was the most affected trait, being reduced by 70% over a 12-day period at

80 mM NaCl. This percentage was lower than that obtained in tomatoes native to Mexico (88%) germinated in 150 mM NaCl, although over a 20-day period [39]. At concentrations of 80 mM NaCl, the GRI reduction percentages are consistent with those observed in commercial varieties, in which they have been higher than 80% starting at 75 mM [40].

Comparisons of means of the group × NaCl concentration interaction (Table 3) indicated that in all groups the traits decreased ($p \leq 0.05$) under salt stress. However, Group 2 had greater tolerance, since it decreased the evaluated traits to a lesser extent, with appreciably smaller reductions than the other two groups; in the case of GP, PL, RL and TDM, they were less than 40%. Group 1, with the greatest susceptibility, had reduction percentages in the evaluated traits of between 57 and 84%. This is consistent with Figure 3, derived from the discriminant analysis previously performed.

Table 3. Comparisons of means of the group × NaCl concentration interaction of 93 experimental tomato (*Solanum lycopersicum* L.) lines germinated under saline conditions. Comparisons are made within each group between control (0 mM NaCl) versus saline condition (80 mM NaCl).

NaCl (mM)	GRO	GP (%)		GRI		PL (cm)		RL (cm)		TDM (mg)	
0	1	80.37	b	6.44	b	3.32	a	1.00	a	0.03	a
80	1	30.26	d	1.06	e	1.33	d	0.44	d	0.01	d
% Reduction		62		84		60		57		69	
0	2	86.37	a	7.85	a	3.40	a	1.06	a	0.03	a
80	2	75.07	b	3.38	c	2.52	b	0.73	b	0.02	b
% Reduction		13		57		26		31		14	
0	3	76.82	b	6.41	b	3.46	a	1.14	a	0.03	a
80	3	48.38	c	1.78	d	1.96	c	0.57	c	0.01	c
% Reduction		37		72		44		50		48	
HSD		3.05		0.17		0.13		0.07		0.0012	

GRO: group, % reduction: percentage reduction at 80 mM NaCl with respect to the control, GP: germination percentage, GRI: germination rate index, PL: plumule length, RL: radicle length, TDM: total dry matter, HSD: honestly significant difference. Means with the same letter within columns and group do not differ statistically (Tukey, $p \leq 0.05$).

The tolerant lines belonging to Group 2 (L4-1, L5, L9, L45 and L92D) showed no differences in GP, RL, PL and TDM ($p \leq 0.05$) between the saline condition (80 mM NaCl) and the control (Table 4). Previous research indicates that in various crops, including tomato, genotypes with salinity tolerance show minor reductions in these same traits [29,38,41,42].

Table 4. Comparisons of means of the concentration-by-genotype interaction nested in a group of experimental tomato (*Solanum lycopersicum* L.) lines selected from a set of 93 lines, germinated under salinity conditions. Comparisons are made within each genotype between control (0 mM NaCl) versus saline condition (80 mM NaCl).

NaCl (mM)	GEN	GRO	GP (%)		GRI		RL (cm)		PL (cm)		TDM (mg)	
0	L4-1	2	96	a	10.2	a	1.34	a	3.71	a	0.0258	a
80	L4-1	2	84	a	5.1	b	1.11	a	3.10	a	0.0252	a
% Reduction			13		50		17		17		2	
0	L45	2	94	a	8.0	a	0.90	a	3.37	a	0.0306	a
80	L45	2	80	a	3.5	b	0.66	a	2.63	a	0.0312	a
% Reduction			15		56		27		22		102	
0	L5	2	100	a	9.7	a	0.84	a	2.70	a	0.0299	a
80	L5	2	94	a	4.6	b	0.68	a	2.19	a	0.0300	a

Table 4. *Cont.*

NaCl (mM)	GEN	GRO	GP (%)		GRI		RL (cm)		PL (cm)		TDM (mg)	
% Reduction			6		53		19		19		103	
0	L9	2	92	a	7.6	a	1.20	a	3.50	a	0.0328	a
80	L9	2	78	a	3.3	b	0.77	a	2.57	a	0.0240	a
% Reduction			15		57		36		27		27	
0	L92D	2	98	a	9.9	a	0.94	a	3.15	a	0.0214	a
80	L92D	2	91	a	4.1	b	0.54	a	2.16	a	0.0193	a
% Reduction			7		59		43		32		10	
0	L29	1	94	a	8.7	a	1.41	a	3.35	a	0.0403	a
80	L29	1	36	b	1.3	b	0.43	b	1.59	b	0.0126	b
% Reduction			62		84		70		53		69	
0	L33	1	88	a	6.5	a	1.16	a	3.24	a	0.0402	a
80	L33	1	38	b	1.4	b	0.42	a	1.56	b	0.0131	b
% Reduction			57		79		64		52		67	
0	L40	1	80	a	7.0	a	0.94	a	4.13	a	0.0256	a
80	L40	1	27	b	1.0	b	0.33	a	1.64	b	0.0086	b
% Reduction			66		86		65		60		66	
0	L41	1	98	a	7.1	a	1.22	a	3.44	a	0.0354	a
80	L41	1	38	b	1.2	b	0.55	a	1.28	b	0.0102	b
% Reduction			61		83		55		63		71	
0	L73	1	94	a	8.4	a	1.52	a	3.81	a	0.0416	a
80	L73	1	36	b	1.1	b	0.45	b	1.755	b	0.0124	b
% Reduction			62		87		70		54		70	
HSD			34		1.8		0.78		1.47		0.0133	

GEN: genotype, GRO: group, % reduction: percentage reduction when going from 0 to 80 mM NaCl concentration, GP: germination percentage, GRI: germination rate index, PL: plumule length, RL: radicle length, TDM: total dry matter, HSD: honestly significant difference. Means with the same letter within columns and genotype do not differ statistically (Tukey, $p \leq 0.05$).

At a concentration of 70 mM, two commercial varieties showed germination percentages of 65% [43], while the tolerant lines in the present study (80 mM NaCl) had germination percentages above 78%.

According to previous information, it was possible to identify 28 genotypes with better performance under salt stress (Table S3) than those reported in other studies [37,38,41,44,45]. In contrast, susceptible genotypes were found with diminished development under this condition (Figure 4) and were clearly outperformed by both the tolerant genotypes in this work and those from other studies [14,15,39,40,43]. This shows the usefulness of the methodology employed for the selection of NaCl tolerance during germination with a high number of genotypes.

The tolerance expressed by the genotypes during a 12-day period to the salt stress that occurred in this research must be associated with both osmotic stress tolerance and ionic tolerance. The former occurs in the initial periods of exposure to NaCl, which causes a decrease in the osmotic potential that prevents water uptake during seed germination [5,15,46,47]. In contrast, ionic stress occurs during prolonged periods of NaCl exposure, caused by the toxicity of Na^+ and Cl^- upon entering embryonic tissues, resulting in the alteration of cellular metabolism, protein synthesis and ATP synthesis [23,48–50], reasons why the germination process is considered to be the most sensitive in plant development [29,44,51].

Under this reasoning, the genotypes of Group 2, with greater tolerance during germination, must possess mechanisms of tolerance to both types of stress due to the prolonged period of the test. Group 3, with partial tolerance to NaCl, could possess one of these two mechanisms, suggesting that the tolerance gene complexes are different.

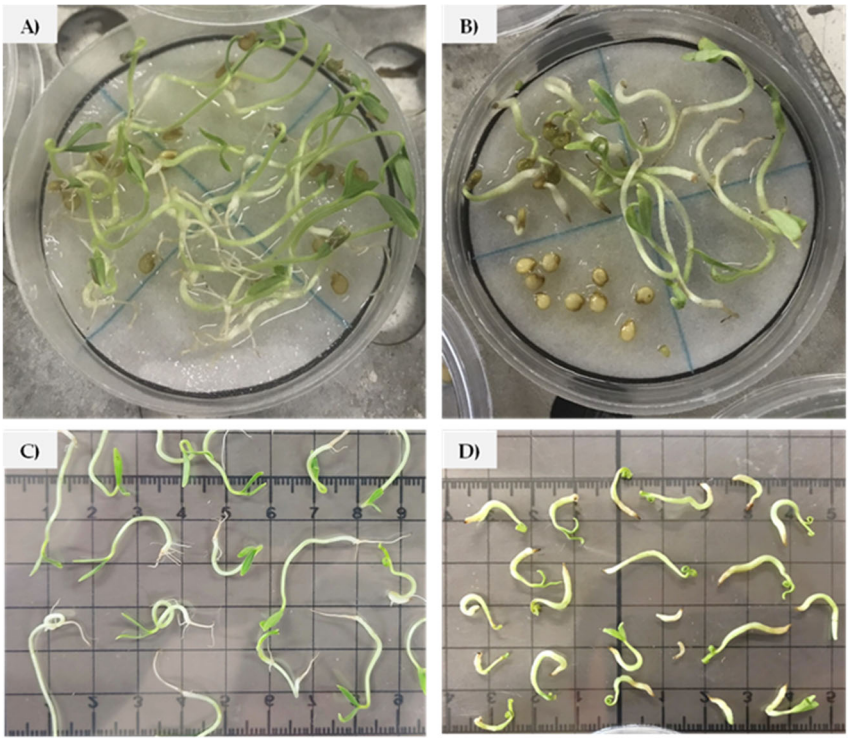

Figure 4. Tomato seeds at the end of germination test. (**A**) Control without NaCl; (**B**) 80 mM NaCl; (**C**) control treatment; (**D**) 80 mM NaCl. Saline conditions induce seed death and root necrosis in tomato seedlings and reduce seedling length.

3.2. Salinity Tolerance at Seedling Stage

An index was calculated for each trait, which consisted of dividing the result of the saline condition by the average of the result in the absence of salt, with which multivariate analyses were performed. The dendrogram, generated with Gower's distance and Ward's minimum variance algorithm, is presented in Figure 5. Hotelling's T^2 statistic and the pseudo-F statistic indicated the formation of three groups with a cut-off height of 0.05 of semipartial r^2.

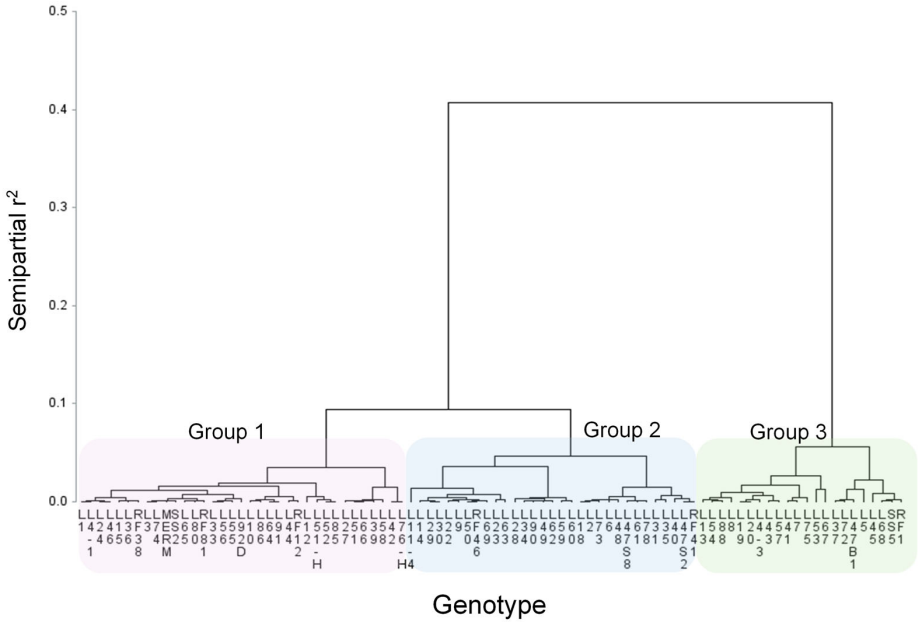

Figure 5. Hierarchical dendrogram generated from Gower's distance and Ward's minimum variance algorithm of NaCl tolerance indices of 88 experimental tomato lines evaluated under salt stress during initial seedling development.

A linear discriminant analysis was performed to corroborate the appropriateness of the grouping, which indicated that one discriminant variable (DV1), with an eigenvalue of 5.3, explained 97% of the variation in the data ($p \leq 0.0001$). The DV1 eigenvector showed a greater positive association with aerial dry matter accumulation, total dry matter and leaf area (Table 5); that is, lines with a high DV1 value indicate greater stem and leaf development. The cross-validation test showed adequate assignments in 80 of the 88 genotypes evaluated. Once the eight genotypes were reassigned, the three groups were made up of 36, 29 and 23 lines.

Table 5. Eigenvector of the variables generated from indices of 88 experimental tomato (*Solanum lycopersicum* L.) lines at seedling stage.

Variable	Eigenvectors		Discriminant Functions	
	VD1	VD2	VD1	VD2
Seedling height (SH)	0.28	0.62	0.36	0.74
Root length (RL)	0.07	0.23	−0.29	0.09
Root dry matter (RDM)	0.25	0.62	−0.07	0.93
Aerial dry matter (ADM)	0.97	−0.11	−1.76	1.83
Total dry matter (TDM)	0.98	−0.08	4.18	−2.30
Leaf area (LA)	0.62	0.31	0.02	0.05

The graphical representation of the genotype distribution based on discriminant variables DV1 and DV2 is presented in Figure 6. The Group 3 genotypes were the most tolerant to salt stress, showing higher DV1 values; that is, they had greater development of the aerial part and leaf area. In contrast, the Group 1 genotypes were susceptible, since they showed less development of the traits mentioned.

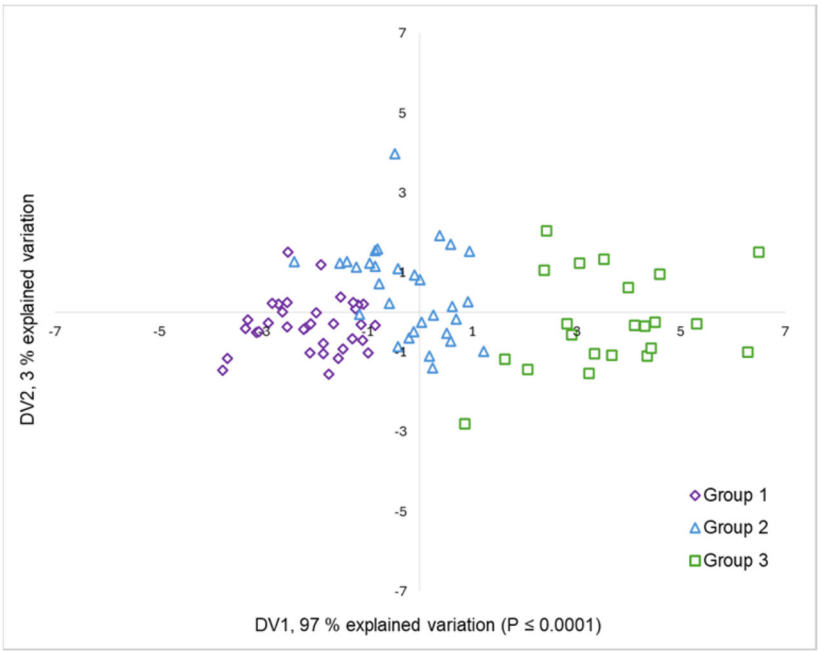

Figure 6. Graphical representation of discriminant variables of 88 tomato (*Solanum lycopersicum* L.) seedlings under saline conditions. DV1: discriminant variable 1; positive values are associated with higher aerial and total dry matter content, as well as greater leaf area and vice versa. DV2: discriminant variable 2; positive values are associated with greater root length and seedling height and vice versa.

The analyses of variance considered the sources of variation: NaCl concentration, groups, genotypes nested within groups and the corresponding interactions. In the sources of variation groups and concentration, significance was detected in the evaluated traits, except for RL in groups and TDM for concentrations. The genotypes within groups had differences ($p \leq 0.01$) in all evaluated traits. Regarding the concentrations × genotype interaction, statistical differences were only detected in SH and LA. Coefficients of variation were acceptable, between 12 and 21% in SH, RL and LA. For RDM, ADM and TDM, the coefficients of variation ranged between 34 and 37.5% (Table S4).

According to the comparisons of means for NaCl concentration, the saline condition drastically decreased SH and LA, without modifying RL, RDM, ADM or TDM (Table 6). In a previous study, tomato seedlings exposed to 105 mM NaCl had plant height reductions of 70% [43]. In commercial varieties, decreases of 30% in plant height were observed at a 100 mM NaCl concentration [41], which was 10% lower than the percentage obtained in the present study. In addition, the lines showed reductions of 50% in leaf area, results like those obtained in tomato lines native to Mexico at 205 mM NaCl, where the genotypes decreased their leaf area by 38% [52]. Similarly, at the same concentration, three commercial varieties decreased their leaf area by 50% [45].

Table 6. Comparisons of concentration means for the traits evaluated in 88 seedlings of experimental tomato (*Solanum lycopersicum* L.) lines under salinity conditions.

NaCl (mM)	SH (cm)		RL (cm)		RDM (g)		ADM (g)		TDM (g)		LA (cm^2)	
0	18.3	a	44.0	a	0.2	a	2.1	a	2.3	a	702.2	a
150	10.2	b	38.0	a	0.5	a	1.8	a	2.3	a	348.5	b
% Reduction	44		14		−187		13		0		50	
HSD	7.5		6.7		0.4		1.2		1.6		248.9	
CV	12.3		12.5		34.1		37.5		35.3		21.0	

% reduction: percentage reduction when going from 0 to 150 mM NaCl concentration (negative values indicate evaluated trait's increases in the saline condition), SH: seedling height, RL: root length, RDM: root dry matter, ADM: aerial dry matter, TDM: total dry matter, LA: leaf area, HSD: honestly significant difference. Means with the same letter within columns did not differ statistically (Tukey, $p \leq 0.05$).

The comparisons of means for the concentration × group interaction (Table 7) identify the genotypes of Group 3 as tolerant to NaCl, since they had fewer effects on SH, LA and RL; the percentages of reduction in the saline condition corresponded to 42, 14 and 43%, respectively, and RDM, ADM and TDM showed increases greater than 40% with respect to the control. In contrast, Group 1 genotypes were the most susceptible, showing reductions of more than 15% in the evaluated traits.

Table 7. Comparisons of group-by-concentration interaction means of 88 seedlings of tomato (*Solanum lycopersicum* L.) lines under salinity conditions. Comparisons are made within each group between control (0 mM NaCl) versus saline condition (150 mM NaCl).

NaCl (mM)	GRO	SH (cm)		RL (cm)		RDM (g)		ADM (g)		TDM (g)		LA (cm^2)	
0	1	19.5	a	44.9	a	0.19	c	2.65	a	2.85	a	771.5	a
150	1	10.3	d	38.1	b	0.51	a	1.84	bc	2.35	b	351.7	de
% reduction		47		15		−163		31		17		54	
0	2	18.4	b	43.7	a	0.16	c	2.07	b	2.24	b	718.8	b
150	2	10.5	d	38.3	b	0.50	a	1.89	bc	2.39	b	366.3	d
% reduction		43		13		−201		9		−7		49	

Table 7. *Cont.*

NaCl (mM)	GRO	SH (cm)		RL (cm)		RDM (g)		ADM (g)		TDM (g)		LA (cm^2)	
0	3	16.0	c	42.9	a	0.13	c	1.15	d	1.29	c	559.1	c
150	3	9.4	e	37.1	b	0.42	b	1.64	c	2.07	b	317.0	e
% reduction		42		14		−219		−42		−61		43	
HSD		6.42		1.97		0.062		0.28		0.31		40.16	

GRO: group, % reduction: percentage reduction when going from 0 to 150 mM NaCl concentration (negative values indicate evaluated trait's increases in the saline condition), SH: seedling height, RL: root length, RDM: root dry matter, ADM: aerial dry matter, TDM: total dry matter, LA: leaf area, HSD: honestly significant difference. Means with the same letter within columns and group do not differ statistically (Tukey, $p \leq 0.05$).

Under salinity conditions, the RDM of the tolerant genotypes of Group 3 increased by more than 100% ($p \leq 0.05$) with respect to the control (Table 7). Similar results were observed in tomato seedlings exposed to 150 mM NaCl, which increased root dry matter by 72% [53].

Table 8 shows the 10 best-performing genotypes from Group 3, which expressed the highest tolerance (Table 7); these, except in the case of SH, did not show statistical differences in the evaluated traits ($p \leq 0.05$) when going from the stress-free condition to the saline condition (150 mM NaCl). A tendency is observed in most of them to increase, although not significantly, RL, RDM and TDM; in addition, all, except one, did not reduce LA. Similar results were observed by López-Méndez et al. [39], where tolerant lines of wild tomatoes showed no statistical difference in biomass accumulation under 0 and 175 mM NaCl conditions. Previous research has indicated that as the NaCl concentration in the medium increases, stem and root length decreases, as well as dry matter accumulation [41,44,45,52]; however, in our research, aerial and root dry matter was not affected ($p \leq 0.05$) by the saline condition, and even tendencies to be increased in tolerant genotypes are observed (Figure 7). In contrast, the susceptible genotypes of Group 1 tended to increase only the RDM.

Table 8. Comparisons of means of tomato genotypes of Group 3 under two NaCl concentrations at seedling stage. Comparisons are made within each genotype between control (0 mM NaCl) versus saline condition (150 mM NaCl).

NaCl	GEN	SH (cm)		RL (cm)		RDM (g)		ADM (g)		TDM (g)		LA (cm^2)	
0	L13	18.3	a	50.5	a	0.109	a	0.99	a	1.10	a	518.7	a
150	L13	9.4	b	41.0	a	0.449	a	1.42	a	1.87	a	316.2	a
% reduction		49		19		−313		−44		−70		39	
0	L20	14.7	a	36.8	a	0.129	a	1.01	a	1.14	a	683.0	a
150	L20	8.8	a	36.2	a	0.357	a	1.41	a	1.77	a	340.3	a
% reduction		40		2		−176		−39		−55		50	
0	L43	14.5	a	40.8	a	0.090	a	0.68	a	0.77	a	455.7	a
150	L43	8.9	a	34.3	a	0.269	a	1.18	a	1.45	a	244.2	a
% reduction		39		16		−198		−72		−87		46	
0	L5	10.2	a	46.3	a	0.111	a	0.76	a	0.87	a	344.4	a
150	L5	8.4	a	33.7	a	0.204	a	1.06	a	1.27	a	205.0	a
% reduction		18		27		−84		−40		−45		40	
0	L75	15.1	a	37.8	a	0.085	a	0.84	a	0.93	a	409.1	a
150	L75	10.1	b	34.8	a	0.369	a	1.46	a	1.83	a	277.8	a
% reduction		33		8		−334		−74		−97		32	
0	L41	15.2	a	37.8	a	0.091	a	0.95	a	1.04	a	420.6	a
150	L41	8.8	b	39.5	a	0.369	a	1.43	a	1.80	a	279.0	a

Table 8. *Cont.*

NaCl	GEN	SH (cm)		RL (cm)		RDM (g)		ADM (g)		TDM (g)		LA (cm^2)	
% reduction		42		−5		−305		−51		−73		34	
0	L8	14.1	a	46.5	a	0.1	a	0.8	a	0.9	a	387.6	a
150	L8	7.6	b	44.0	a	0.4	a	1.2	a	1.5	a	280.1	a
% Reduction		46		5		−186		−49		−68		28	
0	L67	8.0	a	26.3	a	0.0	a	0.2	a	0.3	a	130.5	a
150	L67	4.4	b	27.8	a	0.1	a	0.4	a	0.5	a	114.6	a
% Reduction		44		−6		−150		−79		−89		12	
0	L4-3	18.6	a	33.0	a	0.1	a	1.0	a	1.1	a	487.4	a
150	L4-3	8.6	b	32.3	a	0.3	a	1.4	a	1.8	a	252.9	b
% reduction		53		2		−196		−40		−55		48	
0	L53	13.7	a	44.3	a	0.2	a	0.9	a	1.0	a	343.1	a
150	L53	8.3	b	31.2	a	0.3	a	1.8	a	2.2	a	230.3	a
% reduction		39		30		−103		−107		−107		33	

GEN: genotype, GRO: group, % reduction: percentage reduction when going from 0 to 150 mM NaCl concentration (negative values indicate evaluated trait's increases in the saline condition), SH: seedling height, RL: root length, RDM: root dry matter, ADM: aerial dry matter, TDM: total dry matter, LA: leaf area. Means with the same letter within columns and genotype do not differ statistically (Tukey, $p \leq 0.05$).

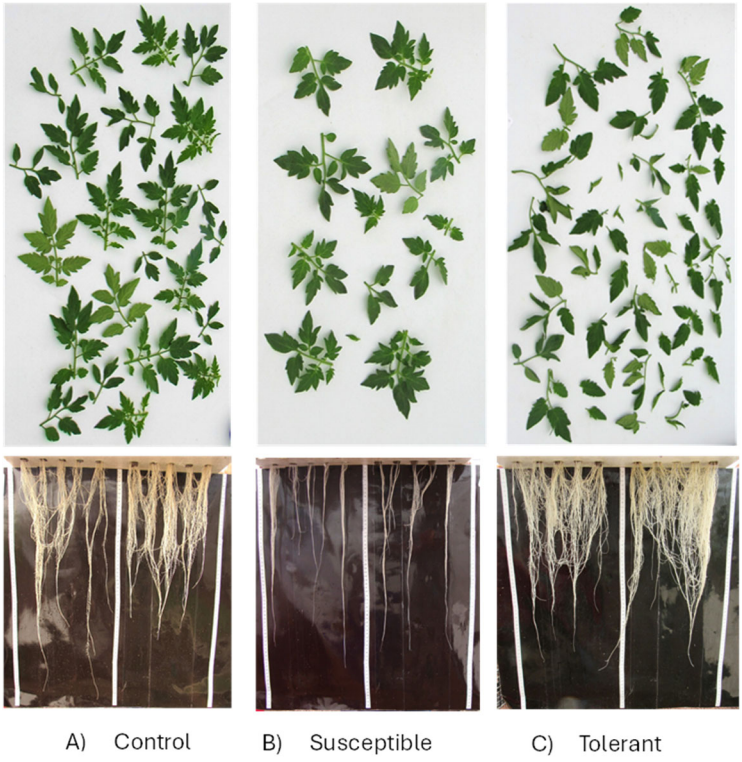

Figure 7. Root length and leaf area of seedlings tomato. (**A**) Control without NaCl; (**B**) susceptible line to 150 mM NaCl; (**C**) tolerant line to 150 mM NaCl. Saline conditions significantly reduce leaf area and root length in susceptible lines, whereas in tolerant lines, leaf area is affected, but root volume tends to increase.

Of the 88 lines evaluated in the seedling test, 23 were identified as tolerant (Table S5), showing better performance under saline conditions than other genotypes from previous research [39,44,45,52]. This resulted from increased development of SH, RL and LA, as well as the greater accumulation of dry matter by structures. This increase in dry matter as a mechanism of salt stress tolerance has also been reported in corn [54], sweet potato [55], barley [42] and tomato [41]; these responses are associated with increases in

the synthesis of organic solutes such as reducing sugars, total sugars, proline and amino acids, which help counteract osmotic effects and maintain plant water status [56–58]. In contrast, 36 susceptible genotypes were identified with impaired development in saline conditions, outperformed by the tolerant genotypes in this research, as well as those in other studies [16,40,51].

Under this reasoning, tolerant lines (Group 3) must have mechanisms that allow maintaining an adequate root system for the supply and distribution of water and nutrients to ensure the development and growth of seedlings, which must include tolerance to both osmotic stress and ionic toxicity by having the ability to accumulate Na^+ in the vacuole and restrict the entry and translocation of Na^+ [21,51,59]. Additionally, they participate in hormonal regulation that affects source–demand relationships and regulates the production and use of photoassimilates [60] that prevent ionic toxicity in photosynthetic tissues, which translates into greater biomass accumulation [61,62].

Upon consideration of the results of both tests, seven lines (L5, L13, L28, L43, L53, L54 and L68) were identified as salinity tolerant at the germination and seedling stages (Table 9). This set was characterized by having the lowest decreases in GP, PL and TDM during germination and RL, RDM, ADM and TDM in the seedling test when going from a normal condition to saline stress.

Table 9. Clustering groups for tomato (*Solanum lycopersicum* L.) lines in salinity tolerance tests at germination and seedling stages.

Seedling \ Germination	Tolerant Group 2	Intermediate Tolerance Group 3	Susceptible Group 1
Tolerant Group 3	L5, L13, L28, L43, L53, L54, L68	L4-3, L8, L19, L35, L37, L47B1, L57, L75, RF1	L7, L41, L67, L72, L88, SS5
Intermediate tolerance Group 2	L9, L45, L48, L63, L78	L2, L18, L22, L30, L31, L34, L47S2, L58, L59, L60, L69	L10, 11-4, L14, L23, L29, L40, L47S8, L49, L61, L62, L73, L90, RF46
Susceptible Group 1	L4-1, L12, L42, L44, L50, L55, L56, L64, L65, L66, L86, L91, L92D, RF12, SS2	L3, L15, L24, L27, L36, L39, L46, L51, L51H, L52, L76H, L80, MERM, RF38, RF41	L1, L6, L33, L74, L85, RF81

Growth assessment using rapid tests during germination and seedling development exposed to NaCl is an effective strategy for the preliminary identification of tolerant genotypes [37,44]. Several studies have shown that root growth and seedling length are correlated with salinity tolerance; therefore, these variables have been used as selection criteria for tolerant genotypes [38,39,41]. These conditions are observed in our results.

Leaf area, dry matter, seedling length and root length are required variables for the identification of genotypes tolerant to salt stress [43,45,52,53]. In this context, the floating raft system allows the evaluation of root development and growth through direct and non-destructive monitoring, which represents a great advantage over the use of solid substrates, in which the quantification of these characteristics is less precise [63].

The presence of tolerant lines in a single test implies that the tolerance mechanisms activated at each stage are different. For example, line L92D was tolerant in the germination test, while in the seedling test, it showed high susceptibility. Two lines derived from native populations were included in the study; SS2 exhibited the same behavior as L92D, while SS5 was tolerant in seedlings and susceptible during germination. Thus, salinity tolerance is a complex trait regulated by the expression of various metabolic and structural genes influenced by the presence of salt [64–67], such as those involved in the exclusion and

compartmentalization of toxic ions and transcription factors that participate in signaling pathways in the presence of stress [68,69] and by the adaptive responsiveness of the genotype to salt stress [51,70]. Although genotypes with different levels of tolerance were found, no associations between this behavior and their phenotypic characteristics (fruit color and shape, growth habit) were identified (Table S1).

Similar to the present results, previous research has detected as tolerant genotypes those with smaller reductions in seedling and root length, as well as in biomass accumulation. In addition, these studies have been able to associate this response with the accumulation of secondary metabolites such as carotenoids, flavonoids, amino acids and anthocyanins, which are indicators to salinity stress adaptation [15,45,53]. Therefore, it is highly likely that the tolerant lines identified in this research possess these mechanisms that allow them to counteract the negative effects of salt stress.

Having rapid initial tests that are easy to replicate in a large number of genotypes in order to identify those that are tolerant to salt stress in periods of less than 20 days, enough time to show tolerance to both osmotic stress and ionic stress during the germination and seedling stages, facilitates the breeding of this crop. However, a detailed study of selected materials in longer periods of exposure to stress is necessary in order to quantify the concentration of secondary metabolites and nutrients, which would allow confirming tolerance to salt stress, even at advanced phenological stages. Quantification of these metabolites can provide further evidence of NaCl tolerance, complementing information from growth assessments. Under prolonged salt stress, secondary metabolites play a crucial role in maintaining enzyme function, stabilizing membrane proteins and scavenging reactive oxygen species [58,71].

4. Conclusions

Salinity caused by NaCl produces negative effects on the early developmental stages, germination and seedling of tomato lines. Furthermore, the results of this research suggest that the response to salinity stress depends on the adaptability of the genotype and the developmental stage. This is attributed to the fact that the twenty-eight tolerant genotypes in germination were different from the twenty-three tolerant ones in the seedling stage, with only seven tolerant genotypes coinciding in both phenological stages, which implies that salt stress tolerance is regulated by the expression of different genetic complexes.

The differential behavior of the lines allowed us to identify genotypes that are tolerant and susceptible to salt stress by evaluating growth and development at the germination and seedling stages using the methodologies employed in this research.

The variation in salt stress tolerance observed in a large number of tomato lines during the germination and seedling stages allowed the initial selection of genotypes for use in breeding. Thus, the tolerant lines at both stages evaluated (L5, L13, L28, L43, L53, L54 and L68) can be considered as parents for obtaining future tolerant varieties, because these genotypes showed the best response in terms of salt tolerance at germination and seedling stages.

In the germination test, salt stress-tolerant genotypes did not decrease dry matter accumulation, germination percentage or plumule and radicle length with respect to the control; in contrast, during the seedling stage, the tolerant genotypes increased root length and dry matter as an adaptive response to salt stress. This suggests the usefulness of these traits for the early selection of salt-tolerant genotypes.

Supplementary Materials: The following supporting information can be downloaded at https://www.mdpi.com/article/10.3390/horticulturae11050532/s1: Table S1. Phenotypic characteristics of the greenhouse tomato breeding program lines of the Universidad Autónoma Chapingo; Table S2. Analysis of variance for the traits evaluated in 93 tomato lines (*Solanum lycopersicum* L.) germinated

under salinity conditions; Table S3. Comparisons of means of the concentration-by-genotype interaction in 93 experimental tomato (*Solanum lycopersicum* L.) lines, germinated under salinity conditions. Comparisons are made within each genotype between control (0 mM NaCl) versus saline condition (80 mM NaCl) (Tukey, $p \leq 0.05$); Table S4. Analysis of variance for the traits evaluated in 88 seedlings tomato lines (*Solanum lycopersicum* L.) under salinity conditions; Table S5. Comparisons of means of the concentration-by-genotype interaction in 88 seedlings of experimental tomato (*Solanum lycopersicum* L.) lines under salinity conditions. Comparisons are made within each genotype between control (0 mM NaCl) versus saline condition (150 mM NaCl) (Tukey, $p \leq 0.05$).

Author Contributions: Conceptualization, A.A.D.-T., J.E.R.-P., J.S.-C. and M.T.B.C.-y.-L.; methodology, A.A.D.-T., J.E.R.-P., J.S.-C., M.T.B.C.-y.-L. and A.E.P.-C.; validation, A.A.D.-T., J.E.R.-P., P.P.-R. and A.E.P.-C.; formal analysis, A.A.D.-T., J.E.R.-P., P.P.-R. and A.E.P.-C.; investigation, A.A.D.-T., J.E.R.-P. and A.E.P.-C.; resources, J.E.R.-P. and J.S.-C.; writing—original draft preparation, A.A.D.-T. and J.E.R.-P.; writing—review and editing, J.S.-C. and M.T.B.C.-y.-L.; visualization, A.A.D.-T. and J.E.R.-P.; supervision, J.E.R.-P., M.T.B.C.-y.-L., J.S.-C. and P.P.-R.; project administration, J.E.R.-P. and J.S.-C.; funding acquisition, J.E.R.-P. and J.S.-C. All authors have read and agreed to the published version of the manuscript.

Funding: This research received funding from Universidad Autónoma Chapingo through project D.G.I.P. 24002-EI2.

Data Availability Statement: Data are contained within the article. Additional information is available on request from the corresponding author.

Acknowledgments: For their assistance in the conduction of the experiments, thanks to Jorge Luis Sánchez Galicia and Ricardo Gaspar Hernández.

Conflicts of Interest: The authors declare no conflicts of interest.

References

1. Mukhopadhyay, R.; Sarkar, B.; Jat, H.S.; Sharma, P.C.; Bolan, N.S. Soil salinity under climate change: Challenges for sustainable agriculture and food security. *J. Environ. Manag.* **2021**, *280*, 111736. [CrossRef]
2. Shrivastava, P.; Kumar, R. Soil salinity: A serious environmental issue and plant growth promoting bacteria as one of the tools for its alleviation. *Saudi J. Biol. Sci.* **2015**, *22*, 123–131. [CrossRef] [PubMed]
3. Hopmans, J.W.; Qureshi, A.S.; Kisekka, I.; Munns, R.; Grattan, S.R.; Rengasamy, P.; Ben-Gal, A.; Assouline, S.; Javaux, M.; Minhas, P.S.; et al. Chapter One—Critical knowledge gaps and research priorities in global soil salinity. *Adv. Agron.* **2021**, *169*, 1–191. [CrossRef]
4. Vargas, R.; Pankova, E.I.; Balyuk, S.A.; Krasilnikov, P.V.; Khasankhanova, G.M. *Handbook for Saline Soil Management*; Food and Agriculture Organization of the United Nations: Rome, Italy; Lomonosov Moscow State University: Moscow, Russia, 2018.
5. Uçarlı, C. Effects of Salinity on Seed Germination and Early Seedling Stage. In *Abiotic Stress in Plants*; Fahad, S., Saud, S., Chen, Y., Wu, C., Wang, D., Eds.; IntechOpen: London, UK, 2021. [CrossRef]
6. Qadir, M.; Quillérou, E.; Nangia, V.; Murtaza, G.; Singh, M.; Thomas, R.J.; Drechsel, P.; Noble, A.D. Economics of salt-induced land degradation and restoration. *Nat. Resour. Forum.* **2014**, *38*, 282–295. [CrossRef]
7. Zhao, S.; Zhang, Q.; Liu, M.; Zhou, H.; Ma, C.; Wang, P. Regulation of Plant Responses to Salt Stress. *Int. J. Mol. Sci.* **2021**, *22*, 4609. [CrossRef] [PubMed]
8. Secretaría de Agricultura y Desarrollo Rural. Mapa Agrícola de Afectación por Salinidad en México. 2021. Available online: https://www.gob.mx/agricultura/acciones-y-programas/mapa-agricola-de-afectacion-por-salinidad-en-mexico (accessed on 20 July 2024).
9. Food and Agriculture Organization of the United (FAOSTAT). Data About Food and Agriculture. 2024. Available online: https://www.fao.org/faostat/en/#data (accessed on 5 July 2024).
10. Servicio de Información Agroalimentaria y Pesquera (SIAP). Panorama Agroalimentario 2024. Available online: https://www.gob.mx/agricultura/dgsiap/acciones-y-programas/panorama-agroalimentario-258035 (accessed on 6 April 2024).
11. Singh, A. Soil salinity: A global threat to sustainable development. *Soil Use and Manag.* **2022**, *38*, 39–67. [CrossRef]
12. Shams, M.; Khadivi, A. Mechanisms of salinity tolerance and their possible application in the breeding of vegetables. *BMC Plant Biol.* **2023**, *23*, 139. [CrossRef]
13. Zhao, C.; Zhang, H.; Song, C.; Zhu, J.-K.; Shabala, S. Mechanisms of Plant Responses and Adaptation to Soil Salinity. *Innovation* **2020**, *1*, 100017. [CrossRef]

14. Adilu, G.S.; Gebre, Y.G. Effect of salinity on seed germination of some tomato (*Lycopersicon esculentum* Mill.) varieties. *J. Aridland Agri.* **2021**, *7*, 76–82. [CrossRef]
15. Abdel-Farid, I.B.; Marghany, M.R.; Rowezek, M.M.; Sheded, M.G. Effect of Salinity Stress on Growth and Metabolomic Profiling of *Cucumis sativus* and *Solanum lycopersicum*. *Plants* **2020**, *9*, 1626. [CrossRef]
16. González-Grande, P.; Suárez, N.; Marín, O. Effect of salinity and seed salt priming on the physiology of adult plants of *Solanum lycopersicum* cv. 'Río Grande'. *Braz. J. Bot.* **2020**, *43*, 775–787. [CrossRef]
17. Osakabe, Y.; Osakabe, K.; Shinozaki, K.; Tran, L.-S.P. Response of plants to water stress. *Front. Plant Sci.* **2014**, *5*, 86. [CrossRef]
18. Zörb, C.; Geilfus, C.M.; Dietz, K.J. Salinity and crop yield. *Plant Biol.* **2019**, *21*, 31–38. [CrossRef]
19. Yang, Y.; Guo, Y. Elucidating the molecular mechanisms mediating plant salt-stress responses. *New Phytol.* **2018**, *217*, 523–539. [CrossRef]
20. Machado, R.; Serralheiro, R. Soil Salinity: Effect on Vegetable Crop Growth. Management Practices to Prevent and Mitigate Soil Salinization. *Horticulturae* **2017**, *3*, 30. [CrossRef]
21. Isayenkov, S.V.; Maathuis, F.J.M. Plant Salinity Stress: Many Unanswered Questions Remain. *Front. Plant Sci.* **2019**, *10*, 80. [CrossRef] [PubMed]
22. Jameel, J.; Anwar, T.; Majeed, S.; Qureshi, H.; Siddiqi, E.H.; Sana, S.; Zaman, W.; Ali, H.M. Effect of salinity on growth and biochemical responses of brinjal varieties: Implications for salt tolerance and antioxidant mechanisms. *BMC Plant Biol.* **2024**, *24*, 128. [CrossRef]
23. Ahmed, A.M.; Wais, A.H.; Ditta, A.; Islam, M.R.; Chowdhury, M.K.; Pramanik, M.H.; Ismaan, H.N.; Soufan, W.; El Sabah, A.; Islam, M.S. Seed Germination and Early Seedling Growth of Sorghum (*Sorghum bicolor* L. Moench) Genotypes Under Salinity Stress. *Pol. Environ. Stud.* **2024**, *33*, 3019–3032. [CrossRef]
24. Ludwiczak, A.; Osiak, M.; Cárdenas-Pérez, S.; Lubińska-Mielińska, S.; Piernik, A. Osmotic Stress or Ionic Composition: Which Affects the Early Growth of Crop Species More? *Agronomy* **2021**, *11*, 435. [CrossRef]
25. Abbas, A.; Mansha, S.; Waheed, H.; Siddiq, Z.; Hayyat, M.U.; Zhang, Y.-J.; Alwutayd, K. NaCl stress, tissue specific Na+ and K+ up-take and their effect on growth and physiology of *Helianthus annuus* L. and *Solanum lycopersicum* L. *Sci. Hortic.* **2024**, *326*, 112454. [CrossRef]
26. Meza, S.L.R.; Egea, I.; Massaretto, I.L.; Morales, B.; Purgatto, E.; Egea-Fernández, J.M.; Bolarin, M.C.; Flores, F.B. Traditional Tomato Varieties Improve Fruit Quality Without Affecting Fruit Yield Under Moderate Salt Stress. *Front. Plant Sci.* **2020**, *11*, 587754. [CrossRef] [PubMed]
27. Li, K.; Zhao, M.; Zhou, S.; Niu, L.; Zhao, L.; Xu, D. Effects of antibiotics on secundary metabolism and oxidative stress in oilseed rape seeds. *Env. Sci. Poll. Res.* **2024**, *31*, 27689–27698. [CrossRef] [PubMed]
28. Sytar, O.; Mbarki, S.; Zivcak, M.; Brestic, M. The Involvement of Different Secondary Metabolites in Salinity Tolerance of Crops. In *Salinity Responses and Tolerance in Plants*; Kumar, V., Wani, S., Suprasanna, P., Tra, L.S., Eds.; Springer: Cham, Switzerland, 2018; Volume 2, pp. 21–48. [CrossRef]
29. Ellouzi, H.; Ben Slimene Debez, I.; Amraoui, S.; Rabhi, M.; Hanana, M.; Alyami, N.M.; Debez, A.; Abdelly, C.; Zorrig, W. Effect of seed priming with auxin on ROS detoxification and carbohydrate metabolism and their relationship with germination and early seedling establishment in salt stressed maize. *BMC Plant Biol.* **2024**, *24*, 704. [CrossRef]
30. Seth, R.; Kendurkar, S. In vitro screening: An effective method for evaluation of commercial cultivars of tomato towards salinity stress. *Inter. J. Curr. Microbiol. Appl. Sci.* **2015**, *4*, 725–730.
31. Maguire, J.D. Speed of germination-aid in selection and evaluation for seedling emergence and vigor. *Crop Sci.* **1962**, *2*, 176–177. [CrossRef]
32. Cadahia López, C. *Fertirrigación: Cultivos Hortícolas y Ornamentales*, 2nd ed.; Mundiprensa: Barcelona, Spain, 2000.
33. Gower, J.C. A Comparison of Some Methods of Cluster Analysis. *Biometrics.* **1967**, *23*, 623. [CrossRef]
34. Ward, J.H. Hierarchical Grouping to Optimize an Objective Function. *J. Am. Stat. Assoc.* **1963**, *58*, 236–244. [CrossRef]
35. Hotelling, H. A Generalized T Test and Measure of Multivariate Dispersion. In Proceedings of the Second Berkeley Symposium on Mathematical Statistics and Probability; Neyman, J., Ed.; University of California Press: Berkeley, CA, USA, 1951; pp. 23–42. [CrossRef]
36. Johnson, D.E. *Applied Multivariate Methods for Data Analysts*; Brooks Cole Publishing Company: Pacific Grove, MA, USA, 1998.
37. Fadhil, A.A.; Swaid, S.Y.; Mohammed, S.J.; Al-Abboodi, A. Impact of Salinity on Tomato Seedling Development: A Comparative Study of Germination and Growth Dynamics in Different Cultivars. *J. Chem. Health Risks* **2024**, *14*, 183–190. [CrossRef]
38. Shanika, M.M.A.N.; Seran, T.H. Impact of salinity on seed germination and seedling performance of tomato (*Solanum lycopersicum* L.) cv KC-1. *J. Sci.* **2020**, *11*, 1–11. [CrossRef]
39. López-Méndez, A.G.; Rodríguez-Pérez, J.E.; Mascorro-Gallardo, J.O.; Sahagún-Castellanos, J.; Lobato-Ortiz, R. Sodium Chloride Tolerance during Germination and Seedling Stages of Tomato (*Solanum lycopersicum* L.) Lines Native to Mexico. *Horticulturae* **2024**, *10*, 466. [CrossRef]

40. de Oliveira, L.B.; de Oliveira, L.B. Effects of water salinization on tomato seedlings (*Solanum lycopersicum*). *Int. J. Adv. Eng. Res. Sci.* **2023**, *10*, 015–021. [CrossRef]
41. Ruiz Espinoza, H.F.; Villalpando Gutiérrez, R.L.; Murillo Amador, B.; Beltrán Morales, F.A.; Hernández Montiel, L.G. Respuesta diferencial a la salinidad de genotipos de tomate (*Lycopersicon esculentum* Mill.) en primeras etapas fenológicas. *Terra Latinoam.* **2014**, *32*, 311–323.
42. Mwando, E.; Angessa, T.T.; Han, Y.; Zhou, G.; Li, C. Quantitative Trait Loci Mapping for Vigour and Survival Traits of Barley Seedlings after Germinating under Salinity Stress. *Agronomy* **2021**, *11*, 103. [CrossRef]
43. Sané, A.K.; Diallo, B.; Kane, A.; Sagna, M.; Sané, D.; Sy, M.O. In Vitro Germination and Early Vegetative Growth of Five Tomato (*Solanum lycopersicum* L.) Varieties under Salt Stress Conditions. *Am. J. Plant Sci.* **2021**, *12*, 796–817. [CrossRef]
44. Chakma, P.; Hossain, M.M.; Rabbani, M.G. Effects of salinity stress on seed germination and seedling growth of tomato. *J. Bangladesh Agri. Univ.* **2019**, *17*, 490–499. [CrossRef]
45. Mustafa, A.A.; Abass, M.H.; Awad, K.M. Responses of three tomato (*Lycopersicon esculentum* L.) varieties to different salinity levels. *Plant Cell Biotechnol. Mol. Biol.* **2021**, *22*, 277–291.
46. Rajendran, K.; Tester, M.; Roy, S.J. Quantifying the three main components of salinity tolerance in cereals. *Plant Cell Environ.* **2009**, *32*, 237–249. [CrossRef]
47. Long, Y.; Chen, J.; Zeng, F.; Wu, S. An activatable NIR-II fluorescent probe for tracking heavy-metal ion and high-level salt-induced oxidative stress in plant sprouts. *Aggregate* **2023**, *4*, e288. [CrossRef]
48. Kaneko, M.; Itoh, H.; Ueguchi-Tanaka, M.; Ashikari, M.; Matsuoka, M. The α-Amylase Induction in Endosperm during Rice Seed Germination Is Caused by Gibberellin Synthesized in Epithelium. *Plant Physiol.* **2002**, *128*, 1264–1270. [CrossRef]
49. Zhang, P.; Senge, M.; Dai, Y. Effects of salinity stress on growth, yield, fruit quality and water use efficiency of tomato under hydroponics system. *Rev. Agric. Sci.* **2016**, *4*, 46–55. [CrossRef]
50. Li, J.; Wu, Y.; Feng, X.; Hussain, T.; Guo, K.; Liu, X. Nonuniform salinity regulates leaf characteristics and improve photosynthesis of cherry tomatoes under high salinity. *Environ. Exp. Bot.* **2024**, *217*, 105565. [CrossRef]
51. Nawaz, A.; Amjad, M.; Afzal, I.; Aslam Pervez, M. Effect of halopriming on germination and seedling vigor of tomato. *Afr. J. Agric. Res.* **2011**, *6*, 3551–3559.
52. Sanjuan-Lara, F.; Ramírez-Vallejo, P.; Sánchez-García, P.; Sandoval-Villa, M.; Livera-Muñoz, M.; Carrillo-Rodríguez, J.C.; Perales-Segovia, C. Tolerancia de líneas nativas de tomate (*Solanum lycopersicum* L.) a la salinidad con NaCl. *Interciencia* **2015**, *40*, 704–709.
53. Bogoutdinova, L.R.; Khaliluev, M.R.; Chaban, I.A.; Gulevich, A.A.; Shelepova, O.V.; Baranova, E.N. Salt Tolerance Assessment of Different Tomato Varieties at the Seedling Stage. *Horticulturae* **2024**, *10*, 598. [CrossRef]
54. Akram, M.; Yasin Ashraf, M.; Ahmad, R.; Waraich, E.A.; Iqbal, J.; Mohsan, M. Screening for salt tolerance in maize (*Zea mays* L.) hybrids at an early seedling stage. *Pak. J. Bot.* **2010**, *42*, 141–154.
55. Rodríguez-Delfín, A.; Posadas, A.; Quiroz, R. Rendimiento y absorción de algunos nutrimentos en plantas de camote cultivadas con estrés hídrico y salino. *Rev. Chapingo Ser. Hortic.* **2014**, *20*, 19–28. [CrossRef]
56. Babu, M.A.; Singh, D.; Gothandam, K.M. The effect of salinity on growth, hormones and mineral elements in leaf and fruit of tomato cultivar PKM1. *J. Anim. Plant Sci.* **2012**, *22*, 159–164.
57. Saha, J.; Brauer, E.K.; Sengupta, A.; Popescu, S.C.; Gupta, K.; Gupta, B. Polyamines as redox homeostasis regulators during salt stress in plants. *Front. Environ. Sci.* **2015**, *3*, 21. [CrossRef]
58. Sabzmeydani, E.; Sedaghathoor, S.; Hashemabadi, D. Salinity response of Kentucky bluegrass (*Poa pratensis* L.) as influenced by salicylic acid and progesterone. *Rev. Chapingo Ser. Hortic.* **2019**, *26*, 49–63. [CrossRef]
59. Parra-Terraza, S.; Angulo-Castro, A.; Sánchez-Peña, P.; Valdéz-Torres, J.B.; Rubio-Carrasco, W. Effect of Cl^- and Na^+ ratios in nutrient solutions on tomato (*Solanum lycopersicum* L.) yield in a hydroponic system. *Rev. Chapingo Ser. Hortic.* **2022**, *28*, 67–78. [CrossRef]
60. Pérez-Alfocea, F.; Albacete, A.; Ghanem, M.E.; Dodd, I.C. Hormonal regulation of source—Sink relations to maintain crop productivity under salinity: A case study of root-to-shoot signalling in tomato. *Funct. Plant Biol.* **2010**, *37*, 592. [CrossRef]
61. Roy, S.J.; Negrão, S.; Tester, M. Salt resistant crop plants. *Curr. Opin. Biotechnol.* **2014**, *26*, 115–124. [CrossRef] [PubMed]
62. Pailles, Y.; Awlia, M.; Julkowska, M.; Passone, L.; Zemmouri, K.; Negrão, S.; Schmöckel, S.M.; Tester, M. Diverse Traits Contribute to Salinity Tolerance of Wild Tomato Seedlings from the Galapagos Islands. *Plant Physiol.* **2020**, *182*, 534–546. [CrossRef] [PubMed]
63. Solanki, P.; Narayan, M.; Meena, S.S.; Srivastava, R.K. Floating raft wastewater treatment system: A review. *J. Pure App. Microbiol.* **2017**, *11*, 1113–1116. [CrossRef]
64. Yokoi, S.; Quintero, F.J.; Cubero, B.; Ruiz, M.T.; Bressan, R.A.; Hasegawa, P.M.; Pardo, J.M. Differential expression and function of *Arabidopsis thaliana* NHX Na+/H+ antiporters in the salt stress response. *Plant J.* **2002**, *30*, 529–539. [CrossRef]
65. Wu, X.; Shu, S.; Wang, Y.; Yuan, R.; Guo, S. Exogenous putrescine alleviates photoinhibition caused by salt stress through cooperation with cyclic electron flow in cucumber. *Photosynth. Res.* **2019**, *141*, 303–314. [CrossRef]
66. Yang, X.; Li, Y.; Chen, H.; Huang, J.; Zhang, Y.; Qi, M.; Liu, Y.; Li, T. Photosynthetic Response Mechanism of Soil Salinity-Induced Cross-Tolerance to Subsequent Drought Stress in Tomato Plants. *Plants* **2020**, *9*, 363. [CrossRef]

67. Akram, S.; Ghaffar, M.; Wadood, A.; Shokat, S.; Hameed, A.; Waheed, M.Q.; Arif, M.A.R. A GBS-based genome-wide association study reveals the genetic basis of salinity tolerance at the seedling stage in bread wheat (*Triticum aestivum* L.). *Front. Genet.* **2022**, *13*, 997901. [CrossRef]
68. Hichri, I.; Muhovski, Y.; Clippe, A.; Žižková, E.; Dobrev, P.I.; Motyka, V.; Lutts, S. SlDREB2, a tomato dehydration-responsive element-binding 2 transcription factor, mediates salt stress tolerance in tomato and Arabidopsis. *Plant Cell Ennviron.* **2015**, *39*, 62–79. [CrossRef]
69. Zhang, P.; Wang, R.; Yang, X.; Ju, Q.; Li, W.; Lü, S.; Tran, L.S.P.; Xu, J. The R2R3-MYB transcription factor AtMYB49 modulates salt tolerance in Arabidopsis by modulating the cuticle formation and antioxidant defence. *Plant Cell Ennviron.* **2020**, *43*, 1925–1943. [CrossRef]
70. Dogan, M.; Tipirdamaz, R.; Demir, Y. Salt resistance of tomato species grown in sand culture. *Plant Soil Environ.* **2010**, *56*, 499–507. [CrossRef]
71. Khalid, M.F.; Huda, S.; Yong, M.; Li, L.H.; Chen, Z.H.; Ahmed, T. Alleviation of drought and salt stress in vegetables: Crop responses and mitigation strategies. *Plant Growth Regul.* **2023**, *99*, 177–194. [CrossRef]

horticulturae

MDPI

Article

Response of Shoot Growth to Ecological Factors Highlights a Synergistic Relationship Between Yield and Catechin Accumulation in Tea Plant (*Camellia sinensis* L.)

Ping Xiang [1,2,3], Qiufang Zhu [4], Marat Tukhvatshin [4], Bosi Cheng [4], Meng Tan [4], Jianghong Liu [4], Jiaxin Huang [4], Yunfei Hu [4], Yutao Shi [4], Liangyu Wu [4] and Jinke Lin [4,*]

1 College of Life and Environmental Science, Hunan University of Arts and Science, Changde 415000, China; xiangping@huas.edu.cn
2 Agricultural Products Processing and Food Safety Key Laboratory of Hunan Higher Education, Changde 415000, China
3 College of Synthetic Biology Industry, Hunan University of Arts and Science, Changde 415000, China
4 College of Horticulture, Fujian Agriculture and Forestry University, Fuzhou 350002, China; zqf216@163.com (Q.Z.); 2191911001@fafu.edu.cn (M.T.); bobo311003@163.com (B.C.); tanmeng3236@163.com (M.T.); liu3125jianghong@163.com (J.L.); hjx94929@163.com (J.H.); huyunfei@fafu.edu.cn (Y.H.); ytshi@wuyiu.edu.cn (Y.S.); alex@fafu.edn.cn (L.W.)
* Correspondence: ljk213@163.com

Abstract: Ecological factors directly influence the growth and metabolism of tea plants (*Camellia sinensis* L.), and unfavorable environmental conditions cause abiotic stress to them. Abiotic stress causes damage to reliable, high-quality, and safe tea production, yet the optimal ecological conditions for enhancing both yield and quality remain unclear. To investigate the response patterns of shoot growth to ecological factors and its relationship with catechin accumulation, this study conducted the cultivation of tea plants with a precise modulation of both individual and combined ecological parameters. Under 30 °C and 90% air humidity, specific combinations of light intensity and substrate relative humidity ("250 μmol·m^{-2}·s^{-1} + 65%" or "350 μmol·m^{-2}·s^{-1} + 70%") significantly enhanced growth and yield. A significant correlation between shoot growth and catechin accumulation was observed, and mathematical models further revealed a synergistic response between shoot growth capacity and total catechin content to ecological factors. Furthermore, co-expression analysis indicated that catechin biosynthesis-related genes exhibited coordinated expression with key growth-related genes, including *CsTCP*, *CsErf*, and *CsXth*. In conclusion, these findings identify optimal ecological conditions to mitigate abiotic stress and reveal a synergistic relationship between catechin biosynthesis and shoot growth, providing an ecological basis for balancing yield and quality in tea production.

Keywords: tea; shoot growth; yield; catechins; EGCG; ecological factors; temperature; humidity; light intensity

1. Introduction

Tea is a popular non-alcoholic beverage worldwide, valued for its various health benefits [1]. Global tea leaf production reportedly exceeded 30 million metric tons in 2023 [2], with an import value reaching USD 6.57 billion. However, rising temperatures and inconsistent rainfall reduce tea yields in major producing countries, such as Sri Lanka [3,4], Kenya [5,6], India [7,8], and China [9,10]. Drought has reduced tea production by 30% in Kenya [11] and by 26% in Sri Lanka [4]. As global warming intensifies, future climate change is expected to cause further losses in tea production [11]. Projections indicate a

potential 5% decline in Kenya's tea yield between 2040 and 2070 due to heat and water stress [6]. Moreover, Sri Lanka's total tea production is estimated to decrease by 7.7%, 10.7%, and 22% over the next 10, 20, and 70 years, respectively [3].

Climate change negatively impacts both the yield and quality of tea, primarily through variations in temperature, light intensity, and humidity [12]. Previous studies show a direct negative correlation between minimum daily temperature and tea yield, as indicated by predictive models [13,14]. A decline in solar radiation during the growing season reduces yield, as both leaf number and weight increase with higher solar radiation [9,15]. An analysis of five studies concluded that excessive, insufficient, or unevenly distributed rainfall reduces tea yield [11]. Additionally, predictive models suggest that drought increases the risk of tea growth and yield reduction by over 40% [16]. The uncontrollable nature of the outdoor environment often necessitates pesticide and herbicide use, posing risks to the quality and safety of tea [17]. Therefore, ensuring a stable and optimized growing environment represents a significant challenge for sustainable tea cultivation and quality assurance.

Plant factories, which allow the precise monitoring and control of environmental factors such as temperature, humidity, light, and nutrients [18,19], offer a potential solution for stable and controlled cultivation. Plant factories can effectively mitigate natural disasters, reduce pesticide use, enhance crop yield and quality, and promote sustainable agriculture [20,21]. For instance, lettuce grown in plant factories can exhibit a shorter growth cycle with higher dry weight compared with greenhouses [22]. Moreover, optimizing cultivation conditions has significantly increased steviol glycoside content in stevia [23]. Research on artificial tea cultivation is emerging, led by groups like Fujian Sanan Sino-Science Photobiotech Co., Ltd. (SANANBIO, Quanzhou, China) in China and research teams in Japan. SANANBIO established a suitable method for indoor tea cultivation and subsequently applied for a related technical patent. Shunsuke Miyauchi et al. investigated artificial tea cultivation, focusing on light conditions to enhance green tea quality [24,25]. Furthermore, specific light conditions conductive to promoting tea plant growth in plant factories have been identified [17]. In summary, tea yield and quality face significant challenges from adverse ecological conditions, both currently and projected into the future. However, previous research has predominantly focused on the effects of light intensity or a specific light spectrum in isolation. A critical knowledge gap exists regarding the complex interplay between multiple key ecological factors and their combined influence on the growth, yield, and biochemical profile of tea plants grown indoors. Addressing this gap is crucial for developing optimized ecological conditions for high-quality indoor tea production.

Building on the team's previous findings in both field and controlled environments, we hypothesized that manipulating ecological factors could optimize tea shoot growth, likely showing diminishing returns or stress effects beyond certain thresholds. We further hypothesized that the response of catechin accumulation, a key quality indicator, to these environmental factors might have the same pattern as shoot growth, potentially creating opportunities to achieve a co-increase in yield and quality. To validate this hypothesis, experiments were conducted in artificial climate chambers with variations in light intensity (L150, L250, L350, L450, and L550 $\mu mol \cdot m^{-2} \cdot s^{-1}$), relative air humidity (AH40%, AH50%, AH70%, and AH90%), and substrate relative humidity (RH65%, RH70%, RH75%, RH80%, and RH85%), and the interactive effects of ecological factors across seventeen treatment combinations were assessed (T1–T17). This study provides novel insights into balancing yield and quality in tea production.

2. Materials and Methods

2.1. Plant Material

This study utilized the "Huangdan" tea cultivar (*Camellia sinensis* var. sinensis cv. Huangdan). One-year-old cuttings were purchased from the Qianhe Tea Cooperative (Anxi County, China). The cultivation protocol followed the optimized methods developed by Fujian Zhongke Biology Co., Ltd. (Quanzhou, China). Specifically, tea cuttings were pruned to 18–20 cm in height, with excess shoots removed to retain only 2–4 mature leaves on the stem, and fibrous roots were excised. The pruned cuttings were disinfected with a 1% potassium permanganate solution for 1 min before being planted in pots (16 cm in diameter, 18 cm in height). After the tea plants had successfully rooted and developed 2–3 new shoots, they were subjected to different ecological factor treatments. Each treatment consisted of 30 tea plants, which were randomly divided into three biological replicates. During the experiment, samples consisting of one bud and one leaf were collected. Half of the samples were dried and stored at −20 °C (drying conditions: 120 °C for 10 min, followed by 90 °C for 30 min) for HPLC analysis. The other half were frozen in liquid nitrogen and stored at −80 °C for qPCR analysis.

2.2. Environmental Conditions and Manipulation Methods

The artificial climate chamber, LED lamps, and nutrient solution were provided by Zhongke Biological Co., Ltd., Quanzhou, China. CO_2 concentration was maintained at 750 ± 50 μmol·mol^{-1}, automatically adjusted by the artificial climate chamber. The environmental parameters and manipulation methods are shown in Supplementary Table S1. In growth chambers, the ecological conditions experienced by individual plants fluctuate within a range rather than remain constant. However, the ranges of ecological factors were controlled to undergo minimal changes, and the ecological factors across different treatments fluctuated synchronously. The ecological conditions and duration for each treatment are provided in Supplementary Table S2.

2.3. Determination of Catechin Content

The method for catechin detection was consistent with that published by the research team in [26]. Tea samples (0.2 g, accurate to 0.0001 g) were weighed into a 10 mL centrifuge tube, and 5 mL of a pre-heated 70% methanol solution was added. After shaking on a mixer, the mixture was immediately transferred to a 70 °C water bath. It was incubated for 10 min, and shaken once at the 5 min mark. After 10 min, the centrifuge tube was centrifuged at 3500 r/min for 10 min, and the supernatant was transferred into a 10 mL brown volumetric flask. The residue was re-extracted with 5 mL of 70% methanol solution, and the procedure was repeated as above. The combined extract was adjusted to a volume of 10 mL and shaken well. Then, 1 mL of the solution was transferred into a 10 mL volumetric flask and diluted to 10 mL with the mobile phase. The mixture was then filtered through a 0.45 μM membrane before HPLC analysis.

The HPLC instrument was equipped with a Waters Acquity UPLC HSS T3 column (2.1 × 100 mm, RP18 1.7 μm) at a column temperature of 35 °C. Mobile phase A consisted of 97.98% pure water + 0.02% EDTA − 2Na + 2% glacial acetic acid, and mobile phase B comprised 98% acetonitrile + 2% glacial acetic acid. The photodiode array (PDA) detection conditions were as follows: a scanning range of 200–400 nm, a characteristic detection wavelength of 278 nm, a scanning time of 10 min, and an injection volume of 2 μL.

2.4. Measurement of Growth Indexes

Six tea plants were randomly selected from each treatment for measurements. The number of leaves, shoots, and buds per plant was counted. Leaf length, leaf width,

shoot length, and internode length were measured using a ruler, while leaf thickness and shoot diameter were measured using a vernier caliper. Leaf area was estimated using the following formula: LA = Leaf Length × Leaf Width × 0.7. A "shoot strength index" was determined by dividing the length measured from the first true leaf to the uppermost mature leaf by the number of internodes. The "shoot ratio" was calculated as the number of shoots divided by the total number of buds.

2.5. RNA Extraction and qRT-PCR

The methods for detecting and calculating gene expression levels were the same as those described in published paper [27]. Total RNA was extracted using the RNAprep Pure Plant Kit (Tiangen, Beijing, China), according to the manufacturer's instructions. First-strand cDNA was synthesized using the Script RT Kit (Tiangen, Beijing, China), and qRT-PCR was performed on an ABI 7500 Real-Time PCR System using the SuperReal PreMix Plus (SYBR Green) Kit (Tiangen, Beijing, China), following the manufacturer's protocol. The 20 μL reaction mixture included 0.6 μL of forward and reverse primers, 1 μL of cDNA, 10 μL of SuperReal PreMix Plus, and 7.8 μL of ddH_2O. The PCR program consisted of an initial denaturation at 95 °C for 15 min, followed by 40 cycles at 95 °C for 10 s and 61 °C for 32 s, and a melting curve analysis (95 °C for 15 s, 60 °C for 1 min, 95 °C for 30 s, and 60 °C for 15 s). GAPDH was used as the reference gene, and the relative expression levels of genes were calculated using the $2^{-\Delta\Delta Ct}$ method. The primer sequences are listed in Supplementary Table S3.

2.6. Data Analysis

Significance analysis, correlation analysis, partial least squares analysis (PLS), logistic regression, receiver operating characteristic (ROC) curve analysis, and multiple regression analysis were conducted using SPSS 21.0. Surface fitting was performed using Origin 2021. The co-expression was analyzed by https://www.bioinformatics.com.cn (accessed on 1 February 2025), and visualization was performed using Adobe Illustrator 2024.

3. Results

3.1. Growth Patterns of Tea Shoots in Response to Individual Changes in Ecological Factors

The changes in each ecological factor, including light intensity, relative air humidity, and relative substrate humidity, significantly influenced tea plant shoot growth. Extremely low light (L150) inhibited shoot elongation and germination, while moderately high light (L250–L550) promoted increases in shoot length, diameter, and internode length (Figure 1). Low relative air humidity (AH40%) caused comprehensive reductions in five shoot-growth-related indices, resulting in shorter plants. Compared to AH40%, the AH90% treatment increased shoot length and leaf number by 58.33% and 35.79%, respectively (Supplementary Figure S1A, Supplementary Table S4). Substrate drought (RH65%) significantly suppressed shoot elongation but enhanced bud density and leaf thickness. In contrast, high substrate humidity (RH85%) increased shoot ratio, internode length, and other indices by 32.74–247.69% (Supplementary Figure S1B, Supplementary Table S4). Collectively, moderate light enhancement, higher air humidity, and adequate substrate moisture promoted vigorous shoot growth, while drought stress inhibited bud development into shoots and leaf expansion.

To comprehensively elucidate the response patterns of shoot growth to individual variations in ecological factors, we employed principal component analysis (PCA) on ten indicators. The principal component analysis explained 74.87%, 72.37%, and 85.61% of the original data with regard to individual variations in light intensity, relative air humidity, and relative substrate humidity, respectively. The model score (F), an indicator of shoot

growth capacity, was significantly higher under moderate-light-intensity (L250–L450), AH70%, and RH80–85% treatments (Supplementary Figure S2).

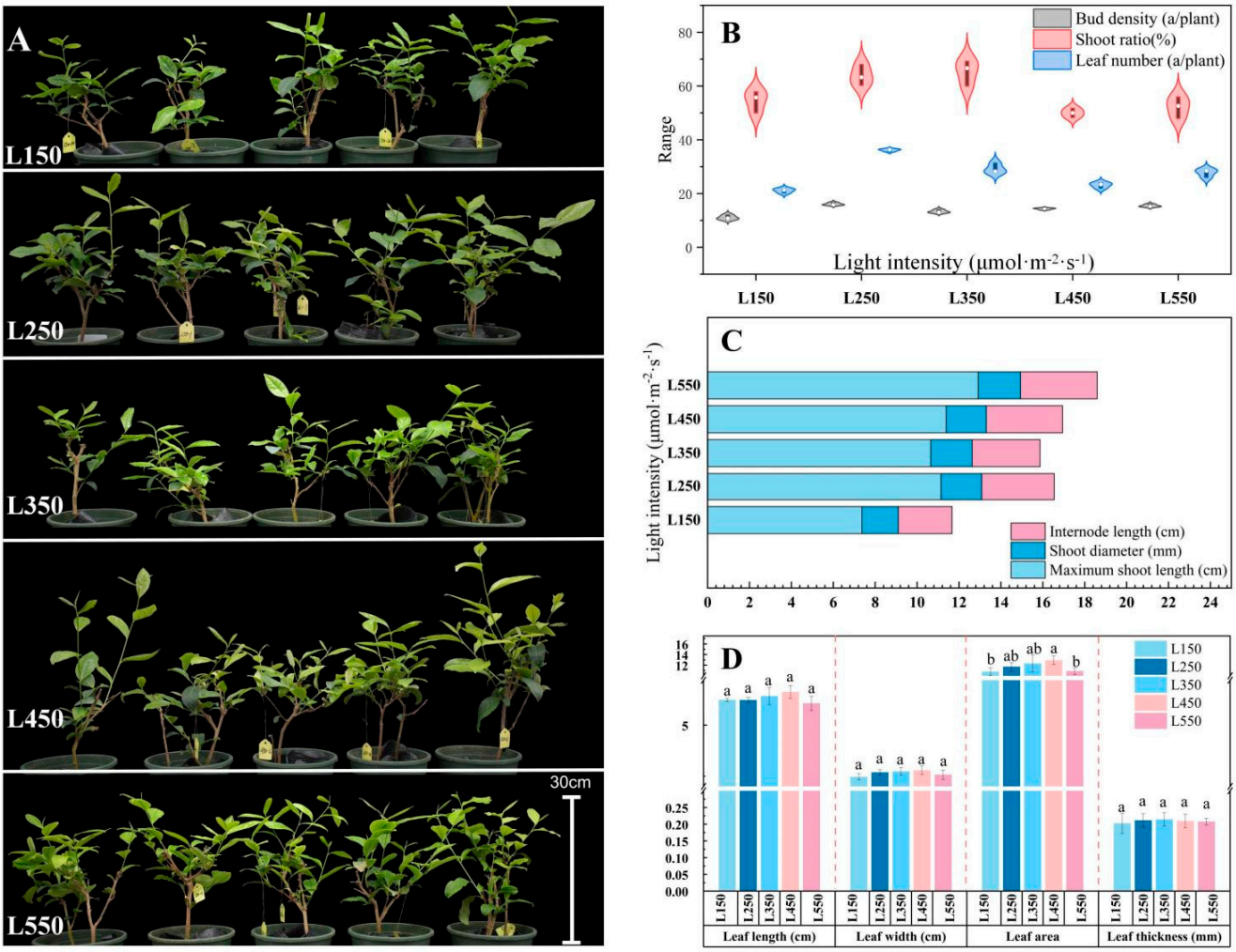

Figure 1. Effects of light intensity treatment on the growth of tea plant shoots. (**A**) Growth status of tea plants. (**B**) Buds number, shoot rate (number of shoots/number of buds), and leaf number. (**C**) Internode length, shoot diameter, and maximum length of shoot. (**D**) Leaf length, leaf width, leaf area, and leaf thickness. Different lowercase letters indicate significant differences at the 0.05 level.

3.2. Response of Tea Shoot Growth to the Interactive Changes in Ecological Factors

To elucidate the response patterns of tea shoot growth to the interactive variations in ecological factors, we employed the response surface methodology to design 17 treatments (T1–T17, Figure 2A). In treatments where both temperature and light intensity were increased (T11, T13, T12, T8, T9, and T15), there was an increase in shoot strength, shoot length, and internode length (Supplementary Table S5). This finding suggests that moderately elevated temperature and light intensity facilitate the elongation of tea shoots. Leaf area increased notably under treatments at 30 °C (T10–T13), was significantly lower at 25 °C (T1–T9), and reached its minimum at 20 °C (T14–T17). These results indicate that, within interacting ecological factors, tea leaves enlarge with rising temperature. In the principal component model, four principal components accounted for 88.50% of the original information, and the total score F represents the growth potential of tea shoots. Under moderately increased temperature, light intensity had a positive impact on growth capacity (T8 and T9 > T6 and T7; T11, T12 and T13 > T10). Conversely, under low-temperature

conditions, both extremely high and low light intensities inhibited shoot growth (T15 and T16 > T14 and T17, Figure 2B).

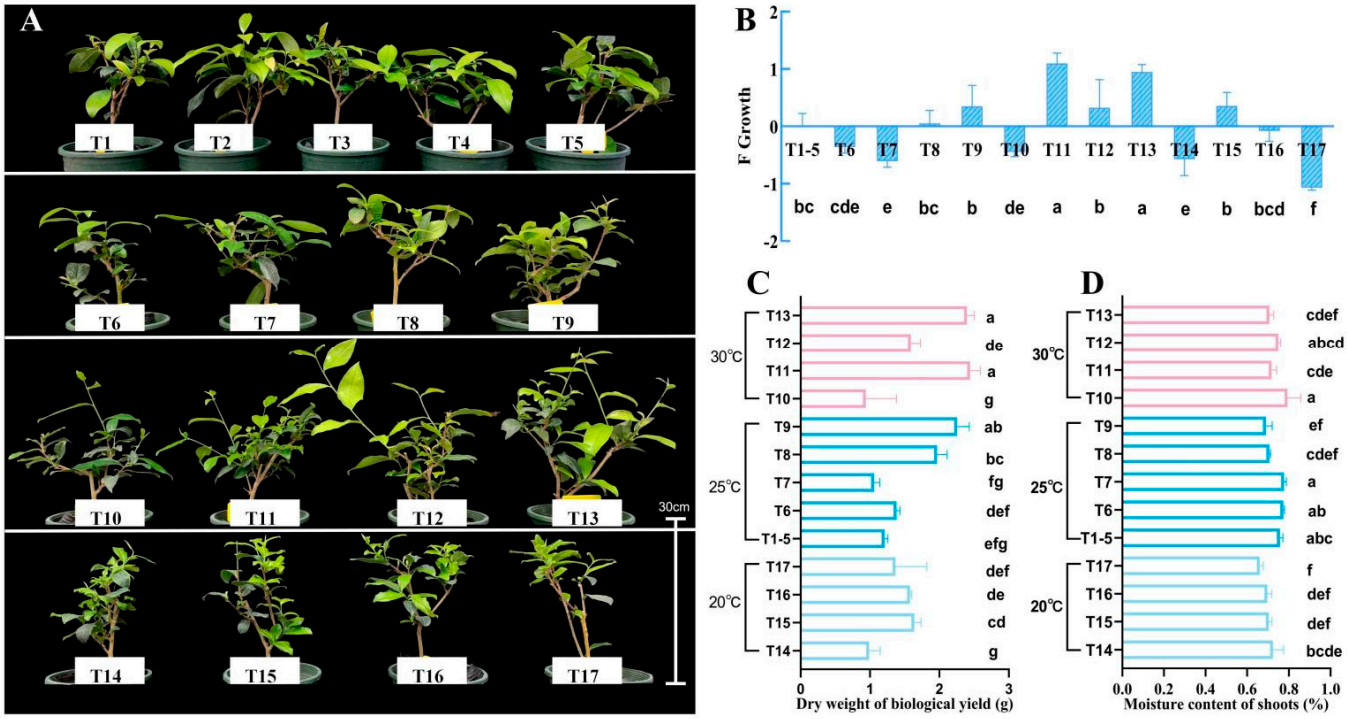

Figure 2. Effects of ecological factor interactions on the growth and yield of tea plant shoots. Different lowercase letters indicate significant differences at the 0.05 level. (**A**) Growth status of tea plants. (**B**) Total score (F) of the PCA model for growth indicators. F represents the shoot growth capacity. (**C**) Dry weight of biomass yield. (**D**) Water content of shoots.

The interactive changes in ecological factors significantly affected the biomass yield and water content of tea shoots (Figure 2C,D). The biomass yield was significantly higher under treatments with high light intensity (T13, T11, T9, and T8). Moreover, at 25 °C, the dry weight under treatments T8 and T9 (350 μmol·m^{-2}·s^{-1}) was significantly higher than that under treatments T6 and T7 (150 μmol·m^{-2}·s^{-1}). At 20 °C, treatment T14 (150 μmol·m^{-2}·s^{-1}) led to a decrease in dry weight but an increase in water content, and this response pattern was similar to that under 30 °C. Therefore, when the temperature is constant, higher light intensity promotes the biomass yield of tea shoots. Intriguingly, the response pattern of shoot water content was opposite to that of biomass yield, implying that increased light intensity promotes the lignification of tea shoots. In summary, both growth capacity and biomass yield were significantly enhanced under the ecological conditions of "90% AH + 30 °C + L250 + 65% RH" or "90% AH + 30 °C + L350 + 70% RH". This indicates that, under conditions of higher temperature and air humidity, both high light intensity and moderate substrate water deficit can independently promote shoot growth.

3.3. Gene Responses in Shoot Growth to Ecological Factor Changes

The *CsTCP* gene family plays a crucial role in shoot growth and exhibits a remarkable response to individual variations in ecological factors (Figure 3). When the light intensity was altered, treatment L150 maximized the expression of *CsTCP3*, *CsTCP4*, and *CsTCP6*, and treatment L450 up-regulated the expression of *CsTCP8b* (Figure 3A). Regarding changes in relative air humidity, the AH90% treatment enhanced the expression of *CsTCP3* and *CsTCP22* (Figure 3B). Similarly, regarding variations in relative substrate humidity, the expression levels of *CsTCP1*, *CsTCP4*, *CsTCP15*, and *CsTCP22* under RH80% treatment were

more than double those under RH65% treatment (Figure 3C). Evidently, the expression of *CsTCP22* is promoted by higher air and substrate humidity. When ecological factors changed interactively, the transcriptional level of *CsTCP12*, *CsTCP14*, and *CsTCP20* changed by less than 1.5-fold. The expression level of *CsPCF3* reached its peak under treatment T1 and its lowest point under treatment T14. Notably, the response pattern of the expression level of *CsTCP9* to the interactive changes in ecological factors was completely opposite to that of *CsPCF3* (Figure 3D). In conclusion, the *CsTCP* gene family exhibits significant responses to individual and interactive changes in ecological factors such as light, air humidity, and substrate humidity. Different *CsTCP* genes display diverse expression patterns. For example, the expression of *CsTCP22* is promoted by high humidity, and the response patterns of *CsPCF3* and *CsTCP9* are opposite.

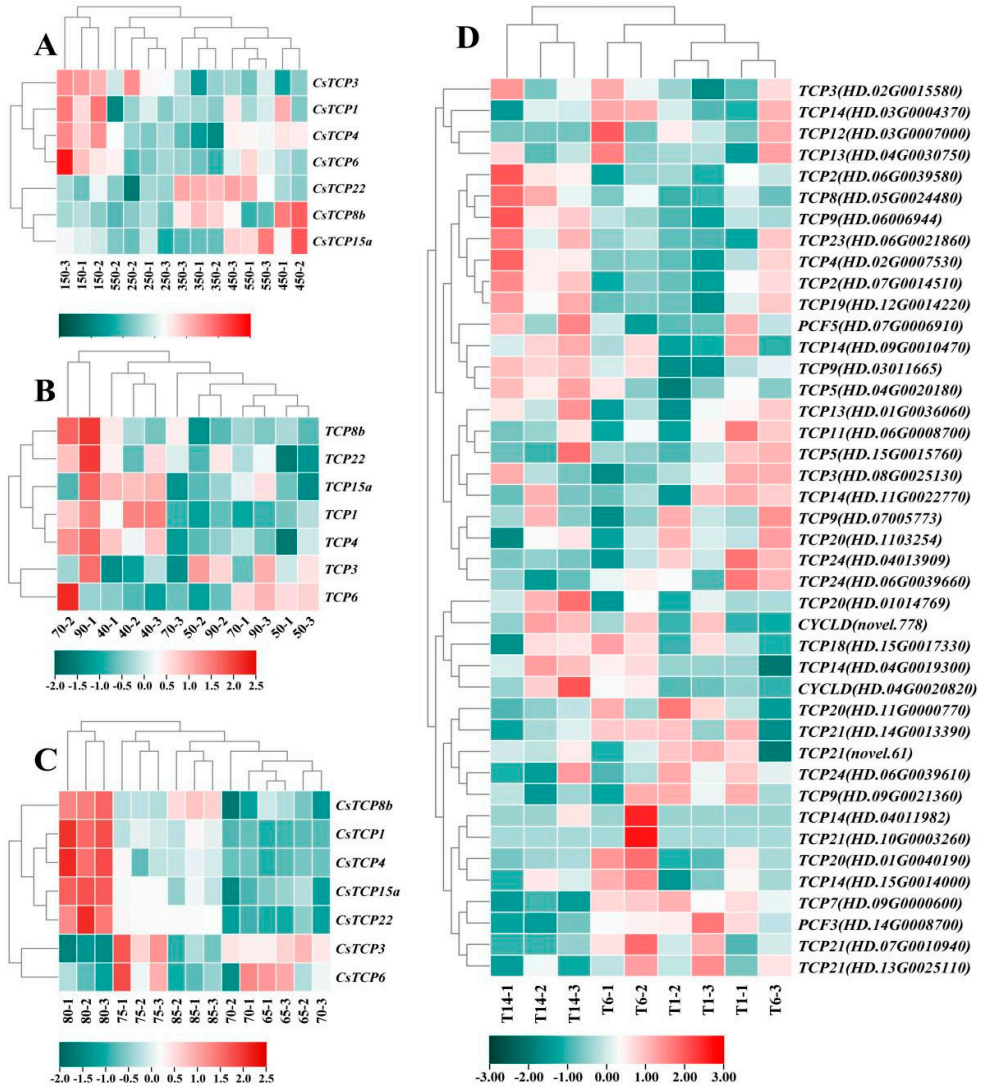

Figure 3. Response patterns of transcription factors related to growth with changes in ecological factors. (**A**) Response patterns to different light intensity treatments. (**B**) Response patterns to air humidity treatments. (**C**) Response patterns to substrate relative humidity treatments. (**D**) Response patterns to interactions of ecological factors.

3.4. Relationship Between Shoot Growth and Catechin Content in Response to Environmental Conditions

3.4.1. Correlation Analysis and Partial Least Squares Analysis

Shoot ratio, leaf length, leaf width, and leaf area were positively correlated with the content of ECG, EGCG, TEC, and TC, implying a synergistic response between shoot num-

ber, leaf size, and ester catechins (Figure 4A). Leaf number, maximum shoot length, shoot diameter, and internode length were negatively correlated with EGC and CG but positively correlated with EC. Interestingly, the diameter and maximum length of shoots showed a negative correlation with five catechin indicators. In contrast, there was a relatively weak correlation between leaf thickness, bud density, and catechin content, indicating that bud sprouting and leaf thickening in tea plants have no significant relationship with catechin accumulation. These results indicate that the relationship between the morphology and biochemical components of tea plants depends on their growth phases.

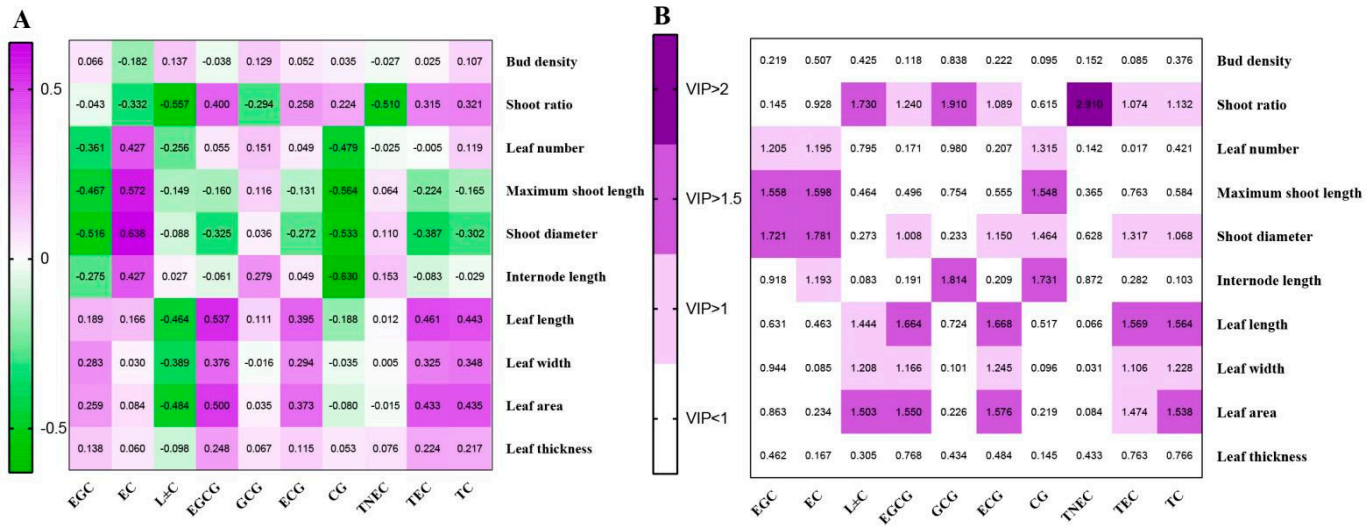

Figure 4. Relationship between growth indicators and catechin content in response to changes in ecological factors. (**A**) Pearson correlation coefficients between shoot growth indicators and catechin content. (**B**) Variable importance in projection of shoot growth indicators for catechin content in the partial least squares model.

Variable importance in projection (VIP) from the partial least squares (PLS) model revealed that bud density and leaf thickness showed values below 1 across all catechin indicators (Figure 4B). In contrast, leaf number and maximum shoot length had VIP values surpassing 1 for EGC, EC, and CG. Leaf size (leaf length, width, and area) VIP values were above 1 for C, EGCG, ECG, TEC, and TC. Remarkably, shoot ratio and shoot diameter exhibited VIP values greater than 1 for seven catechin indicators, with the shoot ratio being particularly prominent, as its VIP value for TNEC exceeded 2. To explore the relationship between shoot growth parameters and overall catechin accumulation in tea plants, the contents of seven catechin monomers were used as Y variables in the PLS analysis. The results showed that leaf number, maximum shoot length, shoot diameter, and internode length had a significant relationship with catechin accumulation (Supplementary Figure S3). In summary, leaf number, shoot length, shoot ratio, and shoot diameter synergistically respond to changes in ecological factors alongside catechin accumulation. Specifically, shoot ratio and leaf size have a synergistic relationship with total non-esterified catechin (TNEC) and total esterified catechin (TEC) content, respectively.

3.4.2. Regression Analysis and Surface Fitting

The L150, AH40%, RH65%, and T14 treatments were used as controls to determine whether the change trends of the F value and TC content were consistent. A consistent trend was coded as 1 and an inconsistent one as 0, on which logistic regression analysis and ROC curve analysis were conducted (Supplementary Table S6). The results showed that the logistic model was highly significant ($p < 0.01$) and the ROC area was 90.4% (Figure 5A). Consequently, variations in shoot growth were closely linked to changes in TC content

across the ecological factors, suggesting these two aspects respond synergistically to environmental shifts. We removed the independent variables exhibiting multicollinearity and performed a multiple regression analysis using seven growth indicators and TC content. The results showed that Durbin–Watson values were <2, overall model significance was <0.01, and R^2 was >70% (Figure 5D). The standardized residuals followed a normal distribution (Supplementary Figure S4). Using the resulting multiple regression equation, the predicted TC content fitted well with the actual measured values, suggesting a synergistic relationship between shoot growth and total catechin content. The results of the surface fitting between the F values (score of the PCA model) and the TC content conform to the Poly2D, Poly2D, and Fourier2D models, respectively, under different light intensity, AH, and RH treatments, with R^2 > 75% (Figure 5B,C,E). The relationship between F values and TC content followed the polynomial surface model when environmental factors were varied interactively (Figure 5F, R^2 = 63%). These results suggest that tea shoot growth ability exhibits a synergistic relationship with catechin accumulation in response to variations in ecological factors.

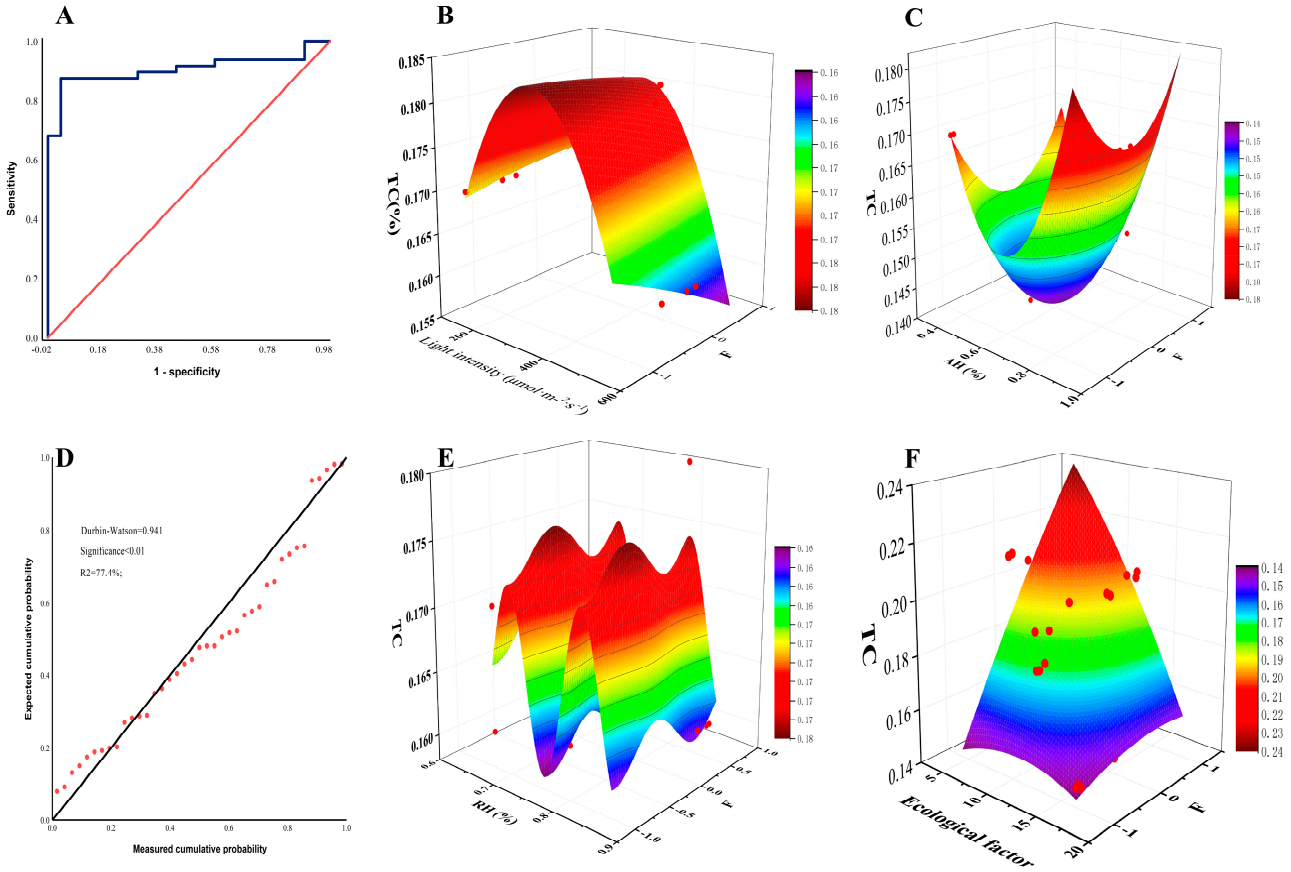

Figure 5. Surface fitting and regression analysis of growth indicators and catechin content in response to changes in ecological factors. (**A**) ROC curve analysis. F is the total score of the PCA model for growth indicators and represents the shoot growth capacity. (**B**,**C**,**E**,**F**) represent the surface fitting of TC content and F values under different light intensities, air humidities, substrate relative humidities, and interactions of ecological factor treatments, respectively. (**D**) Multiple regression analysis of seven growth indicators and TC content. The seven indicators are bud density, shoot percentage, leaf number, average shoot length, leaf area, leaf thickness, and shoot diameter.

3.5. Molecular Mechanisms of Shoot Growth Mediating Catechin Accumulation in Tea Plants

3.5.1. Co-Expression of Growth Transcription Factors and Catechin-Related Genes Under Individual Changes in Ecological Factors

When ecological factors changed individually, a significant correlation was observed between the expression levels of *CsTCP* and the genes associated with catechin biosynthesis (Figure 6A). Specifically, *CsTCP6* expression was significantly negatively correlated with the expression of ten catechin-related genes (e.g., *Cs4CL1*), while *CsTCP8b* and *CsTCP22* were positively correlated with them. Moreover, the expression of *CsCHS3* showed a significant positive correlation with four *CsTCPs*, indicating that *CsCHS3* cooperates with *CsTCP* in responding to individual changes in ecological factors. Similarly, there was a notable correlation between the expression levels of *CsTCP* and catechin accumulation (Figure 6B). The expression levels of two *CsTCP* transcription factors, *CsTCP15a* and *CsTCP22*, were significantly positively correlated with ECG content. However, *CsTCP3* expression was significantly negatively correlated with ECG and EGC content. Using a correlation coefficient greater than 0.6 or less than −0.6 as the standard, this study delineated the potential pathways through which shoot growth influences catechin accumulation (Figure 6C). *CsTCP6* inhibited the expression of genes such as *Cs4CL1*, leading to a reduction in the accumulation of esterified catechin monomers (EGCG, GCG, ECG) and TEC. Meanwhile, *CsTCP22* and *CsTCP1* promoted the expression of *CsCHS3*, thereby facilitating catechin accumulation. Additionally, *CsTCP1* might also enhance the accumulation of C and TNEC via the up-regulation of *CsF3H*, *CsF3′5′H*, and *CsCHS3*.

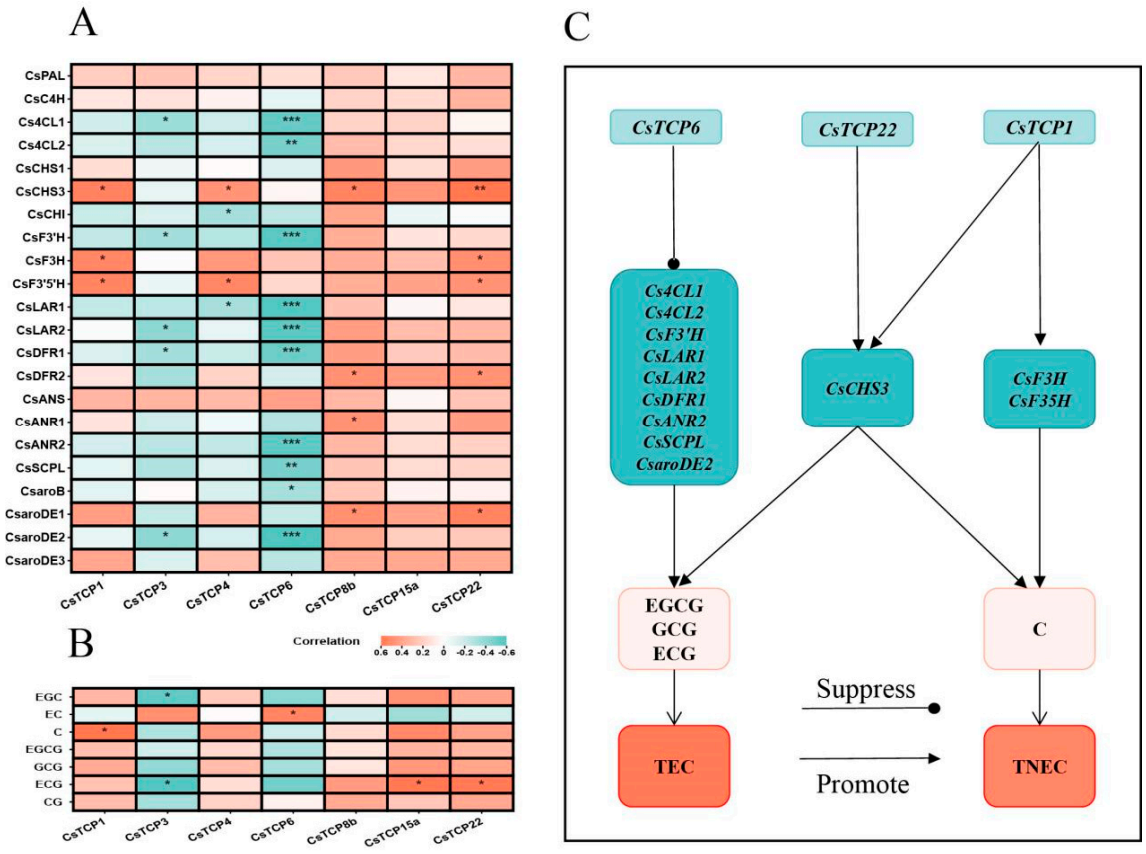

Figure 6. Synchronized responses of growth transcription factor and catechin biosynthesis genes to individual changes in ecological factors. (**A**) Pearson correlation between *CsTCP* expression levels and expression levels of catechin biosynthesis-related genes. (**B**) Pearson correlation between *CsTCP* expression and catechin content. (**C**) Potential pathways through which tea shoot growth affects catechin biosynthesis under individual changes in ecological factors. *, **, and *** represent significance levels of <0.05, <0.01, and <0.001, respectively.

3.5.2. Co-Expression of Growth Transcription Factors and Catechin-Related Genes Under Interactive Changes in Ecological Factors

Using a correlation coefficient threshold of >0.9 or <−0.9 as the screening criterion, we elucidated the potential pathways related to the coordinated response of tea shoot growth and catechin biosynthesis (Figure 7). Four *CsErf* transcription factors and *CsMYB93* cooperated with five catechin-related genes (*CsANS*, *Cs4CL*, *CsF3H*, *CsF3′5′H*, *CsaroDE*) to respond to interactive changes in ecological factors, thereby influencing catechin accumulation. Genes related to shoot growth also influenced catechin biosynthesis. *CsXth* positively affected the expression of *CsFLS*, *CsANR*, and *CsF3H*. Specifically, the expression of *CsF3′5′H* and *CsPAL* was enhanced by *CsLazy1*, which then exerted an impact on catechin accumulation. Furthermore, *CsDFR* and *CsANS* were, respectively, inhibited by *CsM3K20* and *CsGun25*. Notably, four *CsErf* genes and five *CsXth* genes significantly modulated the expression of genes associated with catechin biosynthesis. This finding strongly implies a pivotal role of *CsErf* and *CsXth* in regulating both tea shoot growth and catechin biosynthesis processes.

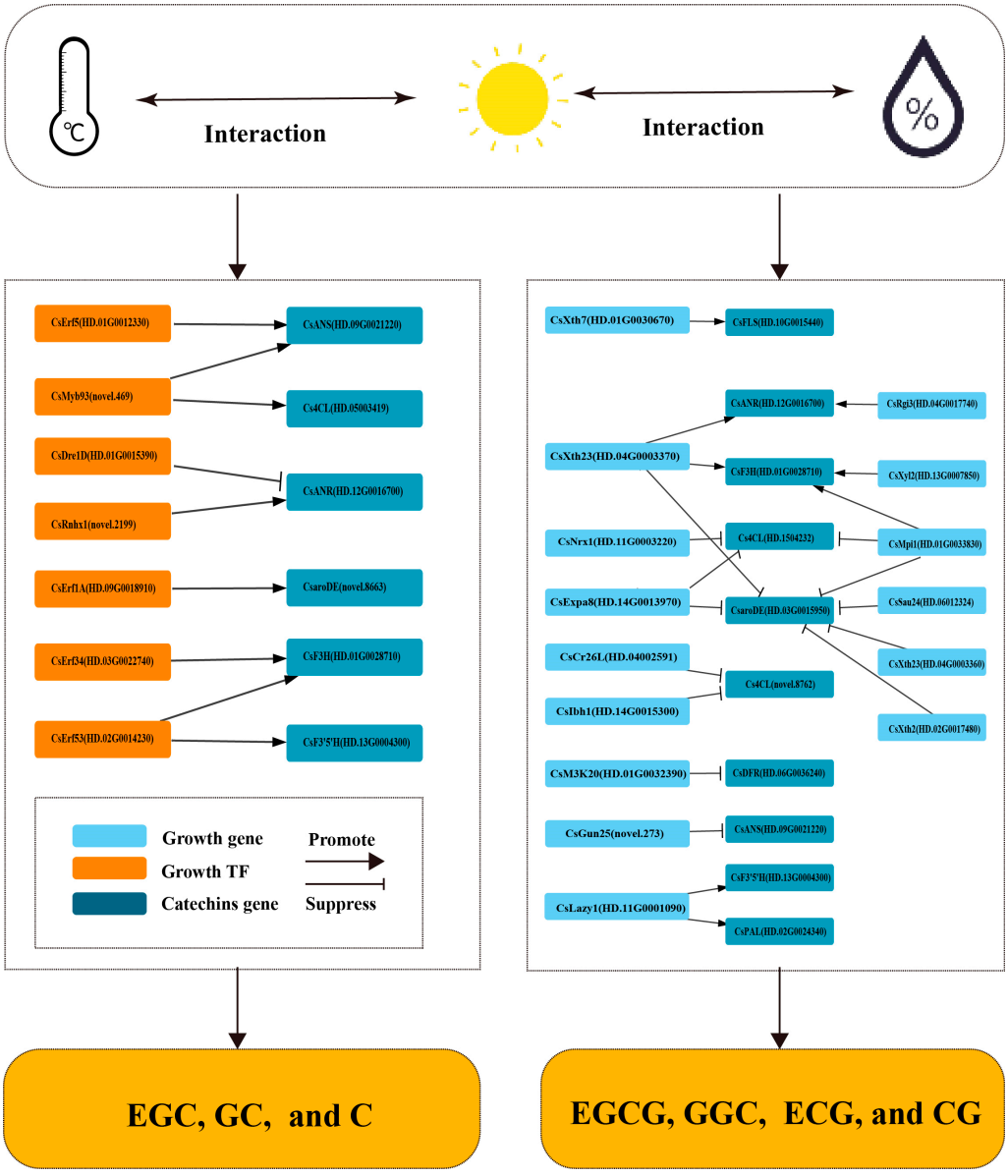

Figure 7. Potential working model of the coordinated response of tea shoot growth and catechin biosynthesis to interactions of ecological factors.

4. Discussion

4.1. Ecological Conditions for Enhancing Tea Growth and Yield

Under high temperature (30 °C) and air humidity (90%), the "L250 + 65% RH" and "L350 + 70% RH" treatments enhanced growth and yield. The current results differ from the optimal artificial settings established for dormancy release [28], likely due to differing ecological requirements for bud break and shoot elongation [29]. Field studies highlight strong temperature and water influences on tea growth [30,31]. Due to the variability in the ecological environment, field studies struggle to identify the specific effects of ecological factors on tea plant growth and development. However, plant factories can vary ecological factors independently and in combination to identify optimal tea growth conditions. Our findings indicate that under high temperature and air humidity, both high light intensity and moderate drought stress can independently promote biomass accumulation. When other ecological factors remained unchanged, the increased light intensity promoted vigorous growth and shoot elongation in tea plants. This finding is consistent with previous studies: under higher light intensity conditions, the thickness of tea leaves and dry matter accumulation significantly increase [32,33]. Fang et al. also reported that tea plants under non-shaded treatment exhibited the highest biomass [34], and the mechanism may be related to leaf isotope enrichment and enhanced starch synthesis driven by high light intensity [35,36].

Meanwhile, moderate deficit irrigation has been reported to maintain a similar tea yield to full irrigation [37]. Interestingly, experimental results show that drought stress increases bud density, aligning with previous studies indicating that drought stress raises the number of non-productive buds [38,39]. However, previous studies have reported that drought is unfavorable for tea plant growth and yield [40,41]. We speculate that this discrepancy arises from the combined influence of air relative humidity and substrate moisture on tea plant physiology. Even under moist soil conditions, vapor pressure deficit (VPD) can significantly affect tea yield [31]. In this study, higher air humidity reduced root water demand due to weakened transpiration, while moderate drought stress prevented root exposure to excessive moisture, thereby promoting tea plant growth. In addition, diurnal temperature variations are considered critical for shoot growth, and future research should investigate the optimal parameters for this variation.

4.2. Synchronous Relationship Between Catechin Biosynthesis and Shoot Growth

Metabolite accumulation in tea leaves depends on growth processes [42–44]. Previous studies have demonstrated that catechin content changes in alignment with shoot growth patterns. For example, shading reduces leaf number and simultaneously decreases EC and EGC content [32], and inter-cropping with soybeans increases non-esterified catechins and shoot growth [45]. A synchronous increase in catechin content and shoot biomass has been observed in response to elevated CO_2 [46], moderate–high temperatures [47], and increased Al concentrations [48]. Explorations have exhibited a significant synchronous pattern between catechin accumulation and shoot growth, likely due to the association between esterified catechin biosynthesis and vacuolization in stem meristematic tissue [49]. Interestingly, other studies found weak relationships between catechin content, the number of germinated buds, and leaf thickness, potentially attributed to metabolite differences across growth stages [50,51]. During the young phase, tea plants prioritize primary metabolic pathways to support growth, whereas maturation induces the biosynthesis of secondary metabolites, such as catechins, to enhance stress resistance [52]. To provide insights for high-quality tea cultivation and timely harvesting, future research could investigate the relationship between growth capacity and catechin accumulation at different growth stages.

Furthermore, linking this physiological response to potential regulatory mechanisms, a significant relationship was found between catechin accumulation and the expression of *CsTCP* and *CsErf*. Similarly, the transcription levels of *cin-type TCPs* have been significantly associated with catechin production [53], and *ERF014* may promote the decline in EGC during development [54]. Delving deeper into the regulatory basis for this observed coordination between growth and development with catechin content, the findings reveal that key shoot-development-related genes, namely *CsTCP*, *CsErf*, and *CsXth*, exhibited co-expression patterns with genes involved in catechin biosynthesis. This provides evidence supporting the role of these gene families and builds upon previous work showing the co-expression of *CsTCP1* and *CsTCP6* with *Cs4CL1* and *CsCHI* [55]. In other studies, the expression of *TCP3* activates genes involved in flavonoid biosynthesis [56], and *TCP15* induces the expression of catechin biosynthesis-related genes in Arabidopsis [57]. It has been found that *TCP* targets and regulates specific genes in catechin biosynthesis, such as *F3H* and *F3′5′H* [58]. *CsTCP3* regulates the activity of the *CsANS1* and *CsANR1* [53], and *TCP13* directly targets the *CHS* and *DFR* promoters [59]. Additionally, *AP2/ERF* exhibits strong co-regulatory effects on *C4H* [60]. Previous research has also demonstrated that *miR319* targets growth-related transcription factors [42,53,61], and flavonoid accumulation is associated with the *miR167d_1-ARF-GH3* and *miR319c_3-PIF-ARF* modules [62]. The synchronous response between catechin biosynthesis and shoot growth may also be regulated by miRNAs, though the precise mechanisms warrant further investigation.

This research comprehensively and precisely explored the response patterns of tea shoot growth to ecological factor variations and discovered a synergistic relationship between catechin accumulation and shoot growth. The optimal ecological conditions for tea cultivation offer practical guidance for tea production, providing a new ecological approach to balance tea yield and quality.

5. Conclusions

Under conditions of high temperature and air humidity (30 °C, 90%), moderately high light intensity or moderate substrate water deficit can promote tea plant growth. Specifically, the combinations of "250 $\mu mol \cdot m^{-2} \cdot s^{-1}$ + 65%" and "350 $\mu mol \cdot m^{-2} \cdot s^{-1}$ + 70%" were observed. This finding elucidated the precise response patterns of shoot growth to ecological factors and identified the optimal ecological conditions for promoting growth. Meanwhile, shoot growth ability and total catechin content exhibited high-fidelity modeling fits, suggesting a synergistic response between shoot growth and total catechin accumulation. Additionally, key growth-related genes (*CsTCP1*, *CsTCP6*, *CsTCP22*, *CsErf*, and *CsXth*) were co-expressed with catechin biosynthesis-related genes. Our results reveal the synergistic relationship between catechin accumulation and yield, providing an ecological perspective for improving both tea yield and quality.

Supplementary Materials: The following supporting information can be downloaded at: https://www.mdpi.com/article/10.3390/horticulturae11060624/s1, Figure S1: Growth state of tea plants under different humidity treatment; Figure S2: Response of tea shoot growth capacity (F) to individual changes in ecological factors; Figure S3: Variable Importance in Projection (VIP) of shoot growth influencing catechin accumulation in PLS analysis. The contents of seven catechin monomers as dependent variables, and the growth indicators of tea plants as the independent variables; Figure S4: Normal distribution of standardized residuals of the multiple regression; Table S1: Environmental indexs and manipulation methods; Table S2: Cultivation environment of tea plants; Table S3: The qPCR primers; Table S4: The response of shoot growth to air relative humidity and substrate relative humidity in tea plants; Table S5: Effects of ecological factors interaction on shoot growth and leaf size of tea plants; Table S6: Code about the trend between growth ability and total catechins content.

Author Contributions: P.X.: Investigation, Formal analysis, Writing—Original draft. Q.Z.: Investigation, Data curation. M.T. (Marat Tukhvatshin): Writing—review and editing. B.C., M.T. (Meng Tan): Investigation. J.L. (Jianghong Liu), J.H.: Methodology, Investigation. Y.H.: Investigation, Supervision. Y.S.: Visualization. L.W.: Conceptualization, Visualization. J.L. (Jinke Lin): Conceptualization, Writing—review and editing, Supervision, Project administration. All authors have read and agreed to the published version of the manuscript.

Funding: This work was supported by the Natural Science Foundation of Hunan Province (grant numbers 2023JJ50326); the National Natural Science Foundation of China (grant numbers 31870683); the Scientific Research Project of Hunan University of Arts and Sciences (grant numbers 22BSQD16); the Scientific research project of Hunan Provincial Department of Education (grant numbers 22A0487); and the Natural Science Foundation of Hunan Province (grant numbers 2023JJ30436).

Data Availability Statement: Requests to access the datasets should be sent via email to ljk213@163.com.

Acknowledgments: We express our gratitude to the Fujian Sanan Sino-Science Photobiotech Co., Ltd. for the site and nutrient solution for the study. This research was funded by the Provincial Applied Characteristic Discipline of Biology of Hunan University of Arts and Science.

Conflicts of Interest: The authors declare no conflicts of interest.

Abbreviations

The following abbreviations are used in this manuscript:

EGCG	Epigallocatechin gallate
CG	Catechin gallate
GCG	Gallocatechin gallate
ECG	Epicatechin gallate
TC	Total catechins
TNEC	Total non-esterified catechins
TEC	Total esterified catechins
PCA	Principal component analysis
PLS	Partial Least Squares
ARF	Auxin response factor
ERF	Ethylene response factor
RH	Relative humidity of substrate
AH	Relative humidity of air

References

1. Liao, Q.; Liang, P.-X.; Xing, Y.; Yao, Z.-F.; Chen, J.-P.; Pan, L.-P.; Deng, Y.-Q.; Liu, Y.-X.; Huang, D.-L. Optimizing Selenium Application for Enhanced Quality and Nutritional Value of Spring Tea (*Camellia sinensis*). *Horticulturae* **2025**, *11*, 423. [CrossRef]
2. FAOSTAT. Food and Agricultural Organization of the United Nations. Available online: http://www.fao.org/faostat (accessed on 23 March 2025).
3. Gunathilaka, R.P.D.; Smart, J.C.R.; Fleming, C.M. The impact of changing climate on perennial crops: The case of tea production in Sri Lanka. *Clim. Chang.* **2017**, *140*, 577–592. [CrossRef]
4. Wijeratne, M.A.; Anandacoomaraswamy, A.; Amarathunga, M.K.S.L.D.; Ratnasiri, J.; Kalra, N. Assessment of impact of climate change on productivity of tea (*Camellia sinensis* L.) plantations in Sri Lanka. *J. Natl. Sci. Found. Sri Lanka* **2007**, *35*, 119–126. [CrossRef]
5. Tim, B.; Michal, K.; Christoph, M.; Sibyll, S.; Yvonne, J. First process-based simulations of climate change impacts on global tea production indicate large effects in the World's major producer countries. *Environ. Res. Lett.* **2020**, *15*, e034023. [CrossRef]
6. Rigden, A.J.; Ongoma, V.; Huybers, P. Kenyan tea is made with heat and water: How will climate change influence its yield? *Environ. Res. Lett.* **2020**, *15*, e044003. [CrossRef]
7. Raj, E.E.; Ramesh, K.V.; Rajkumar, R. Modelling the impact of agrometeorological variables on regional tea yield variability in South Indian tea-growing regions: 1981–2015. *Cogent Food Agric.* **2019**, *5*, e1581457. [CrossRef]

8. Duncan, J.M.A.; Saikia, S.D.; Gupta, N.; Biggs, E.M. Observing climate impacts on tea yield in Assam, India. *Appl. Geogr.* **2016**, *77*, 64–71. [CrossRef]
9. Chen, H.; Liu, C.J.; Liu, C.F.; Hu, C.Y.; Hsiao, M.C.; Chiou, M.T.; Su, Y.S.; Tsai, H.T. A Growth Model to Estimate Shoot Weights and Leaf Numbers in Tea. *Agron. J.* **2019**, *111*, 2255–2262. [CrossRef]
10. Lou, W.; Sun, K.; Zhao, Y.; Deng, S.; Zhou, Z. Impact of climate change on inter-annual variation in tea plant output in Zhejiang, China. *Int. J. Climatol.* **2020**, *41*, 479–490. [CrossRef]
11. Jayasinghe, S.L.; Kumar, L. Potential Impact of the Current and Future Climate on the Yield, Quality, and Climate Suitability for Tea *Camellia sinensis* (L.) O. Kuntze: A Systematic Review. *Agronomy* **2021**, *11*, 619. [CrossRef]
12. Sun, L.; Li, X.; Shen, J.; Wang, S.; Xu, X.; Fan, K.; Wang, Y.; Bi, C.; Ding, Z. Optimizing tea plantation through rapeseed intercropping: Ecological and pest-resistant benefits. *Ind. Crop. Prod.* **2025**, *227*, e120821. [CrossRef]
13. Wang, C.; Zhao, B. Application of Apriori Algorithm in Meteorological Disaster Information Mining. In *Cooperative Design, Visualization, and Engineering, Proceedings of the 15th International Conference, CDVE 2018, Hangzhou, China, 21–24 October 2018*; Springer International Publishing: Cham, Switzerland, 2018; pp. 258–261. [CrossRef]
14. Edirisinghe, J.C.; Ranjan, H.; Herath, H.M.L.K.; Jayasinghe-Mudalige, U.K.; Wijeratne, M.; Kuruppu, V.; Jayathilake, C.; Wijesuriya, W.; Somarathna, K.; Karunaratne, S. Impact of climate on tea yield: An empirical investigation from Sri Lanka. *J. Natl. Sci. Found. Sri Lanka* **2024**, *52*, 183–190. [CrossRef]
15. Rebecca, B.; Sean, C.; Bruce, A.; Selena, A.; Timothy, G.; Albert, R.; John, S.; Wenyan, H.; Matt, H.; Colin, O. Association between Empirically Estimated Monsoon Dynamics and Other Weather Factors and Historical Tea Yields in China: Results from a Yield Response Model. *Climate* **2016**, *4*, 20. [CrossRef]
16. Wang, Y.-C.; Chen, C.-T.; Li, R.-Y.; Lu, Y.-H.; Chiang, L.-C. Climate risk analysis of low-altitude tea gardens in central Taiwan using a Bayesian network. *Environ. Monit. Assess.* **2024**, *196*, e809. [CrossRef]
17. Chang, C.-L.; Huang, C.-C.; Chen, H.-W. Design and Implementation of Artificial Intelligence of Things for Tea (*Camellia sinensis* L.) Grown in a Plant Factory. *Agronomy* **2022**, *12*, 2384. [CrossRef]
18. Zhiwei, T.; Wei, M.; Qichang, Y.; Famin, D. Application status and challenges of machine vision in plant factory—A review. *Inf. Process. Agric.* **2021**, *9*, 195–211. [CrossRef]
19. Kaya, C. Intelligent Environmental Control in Plant Factories: Integrating Sensors, Automation, and AI for Optimal Crop Production. *Food Energy Secur.* **2025**, *14*, e70026. [CrossRef]
20. Cai, W.; Bu, K.; Zha, L.; Zhang, J.; Lai, D.; Bao, H. Energy consumption of plant factory with artificial light: Challenges and opportunities. *Renew. Sustain. Energy Rev.* **2024**, *210*, e115235. [CrossRef]
21. Azad, M.O.K.; Gruda, N.S.; Naznin, M.T. Energy Efficiency of Glasshouses and Plant Factories for Sustainable Urban Farming in the Desert Southwest of the United States of America. *Horticulturae* **2024**, *10*, 1055. [CrossRef]
22. Graamans, L.; Baeza, E.; Andy, V.D.D.; Tsafaras, I.; Stanghellini, C. Plant factories versus greenhouses: Comparison of resource use efficiency. *Agric. Syst.* **2018**, *160*, 31–43. [CrossRef]
23. Yoneda, Y. Optimization Process of Plant Growth Environment for Improving Content Compounds Using Physiological and Genetic Information in a Closed-type Plant Factory. *Jpn. Agric. Res. Q.* **2021**, *55*, 201–208. [CrossRef]
24. Miyauchi, S.; Yuki, T.; Fuji, H.; Kojima, K.; Yonetani, T.; Tomio, A.; Bamba, T.; Fukusaki, E. High-quality green tea leaf production by artificial cultivation under growth chamber conditions considering amino acids profile. *J. Biosci. Bioeng.* **2014**, *118*, 710–715. [CrossRef] [PubMed]
25. Miyauchi, S.; Yonetani, T.; Yuki, T.; Tomio, A.; Bamba, T.; Fukusaki, E. Quality evaluation of green tea leaf cultured under artificial light condition using gas chromatography/mass spectrometry. *J. Biosci. Bioeng.* **2016**, *123*, 197–202. [CrossRef] [PubMed]
26. Tukhvatshin, M.; Peng, Q.; Zhao, X.; Liu, J.; Xiang, P.; Lin, J. Identifying meteorological factors influencing catechin biosynthesis and optimizing cultivation conditions of tea plant (*Camellia sinensis*). *Front. Plant Sci.* **2025**, *16*, e1532880. [CrossRef]
27. Xiang, P.; Zhu, Q.; Zhang, L.; Xu, P.; Liu, L.; Li, Y.; Cheng, B.; Wang, X.; Liu, J.; Shi, Y.; et al. Integrative analyses of transcriptome and metabolome reveal comprehensive mechanisms of Epigallocatechin-3-gallate (EGCG) biosynthesis in response to ecological factors in tea plant (*Camellia sinensis*). *Food Res. Int.* **2023**, *166*, e112591. [CrossRef]
28. Omae, H.; Takeda, Y. Modeling Winter Dormancy of Tea Buds and Simulation in Southern Japan. *Jpn. Agric. Res. Q.* **2003**, *37*, 189–194. [CrossRef]
29. Carr, M.K.V. The role of water in the growth of the tea (*Camellia sinensis*) crop: A synthesis of research in eastern africa. 1. water relations. *Exp. Agric.* **2010**, *46*, 327–349. [CrossRef]
30. Benti, T.; Debela, A.; Bekele, Y.; Suleman, S. Effect of seasonal variation on yield and leaf quality of tea clone (*Camellia sinensis* (L.) O. Kuntze) in South West Ethiopia. *Heliyon* **2023**, *9*, e14051. [CrossRef]
31. De Costa, W.A.J.M.; Mohotti, A.J.; Wijeratne, M.A. Ecophysiology of tea. *Braz. J. Plant Physiol.* **2007**, *19*, 299–332. [CrossRef]
32. Sano, T.; Horie, H.; Matsunaga, A.; Hirono, Y. Effect of shading intensity on morphological and color traits and on chemical components of new tea (*Camellia sinensis* L.) shoots under direct covering cultivation. *J. Sci. Food Agric.* **2018**, *98*, 5666–5676. [CrossRef]

33. Bahrami-Rad, S. Effect of light intensity on photosynthesis and antioxidant defense in boron deficient tea plants. *Acta Biol. Szeged.* **2011**, *55*, 265–272.
34. Fang, Z.-T.; Jin, J.; Ye, Y.; He, W.-Z.; Shu, Z.-F.; Shao, J.-N.; Fu, Z.-S.; Lu, J.-L.; Ye, J.-H. Effects of Different Shading Treatments on the Biomass and Transcriptome Profiles of Tea Leaves (*Camellia sinensis* L.) and the Regulatory Effect on Phytohormone Biosynthesis. *Front. Plant Sci.* **2022**, *13*, 909765. [CrossRef] [PubMed]
35. Xia, W.; Li, C.; Nie, J.; Shao, S.; Rogers, K.M.; Zhang, Y.; Li, Z.; Yuan, Y. Stable isotope and photosynthetic response of tea grown under different temperature and light conditions. *Food Chem.* **2022**, *368*, 130771. [CrossRef] [PubMed]
36. Zhang, X.; Liu, K.; Tang, Q.; Zeng, L.; Wu, Z. Light Intensity Regulates Low-Temperature Adaptability of Tea Plant through ROS Stress and Developmental Programs. *Int. J. Mol. Sci.* **2023**, *24*, 9852. [CrossRef]
37. Lin, S.K.; Lin, J.; Liu, Q.L.; Ai, Y.F.; Ke, Y.Q.; Chen, C.; Zhang, Z.Y.; He, H. Time-course of photosynthesis and non-structural carbon compounds in the leaves of tea plants (*Camellia sinensis* L.) in response to deficit irrigation. *Agric. Water Manag.* **2014**, *144*, 98–106. [CrossRef]
38. Cheruiyot, E.K.; Mumera, L.M.; Ng'Etich, W.K.; Hassanali, A.; Wachira, F. Polyphenols as Potential Indicators for Drought Tolerance in Tea (*Camellia sinensis* L.). *J. Agric. Chem. Soc. Jpn.* **2007**, *71*, 2190–2197. [CrossRef]
39. Ng'etich, W.K.; Stephens, W. Responses of tea to environment in kenya. 1. genotype × environment interactions for total dry matter production and yield. *Exp. Agric.* **2001**, *37*, 333–342. [CrossRef]
40. Zhang, Y.; Xiao, Y.; Zhang, Y.; Dong, Y.; Liu, Y.; Liu, L.; Wan, S.; He, J.; Yu, Y. Accumulation of Galactinol and ABA Is Involved in Exogenous EBR-Induced Drought Tolerance in Tea Plants. *J. Agric. Food Chem.* **2022**, *70*, 13391–13403. [CrossRef]
41. Dai, F.; Rong, Z.; Wu, Q.; Fathi Abd_Allah, E.; Liu, C.; Liu, S. Mycorrhiza improves plant growth and photosynthetic characteristics of tea plants in response to drought stress. *Biocell* **2022**, *46*, 1339–1346. [CrossRef]
42. Wu, Z.-J.; Wang, W.-L.; Zhuang, J. TCP family genes control leaf development and its responses to hormonal stimuli in tea plant *Camellia sinensis* (L.) O. Kuntze. *Plant Growth Regul.* **2017**, *83*, 43–53. [CrossRef]
43. Ashihara, H.; Deng, W.-W.; Mullen, W.; Crozier, A. Distribution and biosynthesis of flavan-3-ols in *Camellia sinensis* seedlings and expression of genes encoding biosynthetic enzymes. *Phytochemistry* **2010**, *71*, 559–566. [CrossRef] [PubMed]
44. Jiang, X.; Liu, Y.; Li, W.; Zhao, L.; Meng, F.; Wang, Y.; Tan, H.; Yang, H.; Wei, C.; Wan, X.; et al. Tissue-Specific, Development-Dependent Phenolic Compounds Accumulation Profile and Gene Expression Pattern in Tea Plant *Camellia sinensis*. *PLoS ONE* **2013**, *8*, e62315. [CrossRef] [PubMed]
45. Sun, L.; Dong, X.; Wang, Y.; Maker, G.; Agarwal, M.; Ding, Z. Tea-Soybean Intercropping Improves Tea Quality and Nutrition Uptake by Inducing Changes of Rhizosphere Bacterial Communities. *Microorganisms* **2022**, *10*, 2149. [CrossRef] [PubMed]
46. Ahammed, G.J.; Li, X.; Liu, A.; Chen, S. Physiological and Defense Responses of Tea Plants to Elevated CO_2: A Review. *Front. Plant Sci.* **2020**, *11*, e305. [CrossRef]
47. Li, X.; Li, M.-H.; Deng, W.-W.; Ahammed, G.J.; Wei, J.-P.; Yan, P.; Zhang, L.-P.; Fu, J.-Y.; Han, W.-Y. Exogenous melatonin improves tea quality under moderate high temperatures by increasing epigallocatechin-3-gallate and theanine biosynthesis in *Camellia sinensis* L. *J. Plant Physiol.* **2020**, *253*, e153273. [CrossRef]
48. Chen, Y.M.; Tsao, T.M.; Liu, C.C.; Lin, K.C.; Wang, M.K. Aluminium and nutrients induce changes in the profiles of phenolic substances in tea plants (*Camellia sinensis*). *J. Sci. Food Agric.* **2011**, *91*, 1111–1117. [CrossRef]
49. Cheruiyot, E.K.; Mumera, L.M.; Ngetich, W.K.; Hassanali, A.; Wachira, F.; Wanyoko, J.K. Shoot epicatechin and epigallocatechin contents respond to water stress in tea *Camellia sinensis* (L.) O. Kuntze. *Biosci. Biotechnol. Biochem.* **2008**, *72*, 1219–1226. [CrossRef]
50. Ryu, H.W.; Yuk, H.J.; An, J.H.; Kim, D.-Y.; Song, H.-H.; Oh, S.-R. Comparison of secondary metabolite changes in *Camellia sinensis* leaves depending on the growth stage. *Food Control* **2017**, *73*, 916–921. [CrossRef]
51. Jeon, D.B.; Hong, Y.S.; Lee, G.H.; Park, Y.M.; Lee, C.M.; Nho, E.Y.; Choi, J.Y.; Jamila, N.; Khan, N.; Kim, K.S. Determination of volatile organic compounds, catechins, caffeine and theanine in Jukro tea at three growth stages by chromatographic and spectrometric methods. *Food Chem.* **2017**, *219*, 443–452. [CrossRef]
52. Zeng, L.; Zhou, X.; Liao, Y.; Yang, Z. Roles of specialized metabolites in biological function and environmental adaptability of tea plant (*Camellia sinensis*) as a metabolite studying model. *J. Adv. Res.* **2021**, *34*, 159–171. [CrossRef]
53. Yu, S.; Li, P.; Zhao, X.; Tan, M.; Ahmad, M.Z.; Xu, Y.; Tadege, M.; Zhao, J. CsTCPs regulate shoot tip development and catechin biosynthesis in tea plant (*Camellia sinensis*). *Hortic. Res.* **2021**, *8*, e104. [CrossRef] [PubMed]
54. Chen, L.; Yan, J.; Miu, Y.; Huang, R.; Wei, H.; Wang, L.; Zhang, C.; Yuan, L.; Tong, H. The spatiotemporal variations of L-glutamic acid and catechins during the development of etiolated tea leaves in 'Huangjinye'. *Sci. Hortic.* **2024**, *328*, e112888. [CrossRef]
55. Xiang, P.; Wilson, I.W.; Huang, J.; Zhu, Q.; Tan, M.; Lu, J.; Liu, J.; Gao, S.; Zheng, S.; Lin, D.; et al. Co-regulation of catechins biosynthesis responses to temperature changes by shoot growth and catechin related gene expression in tea plants (*Camellia sinensis* L.). *J. Hortic. Sci. Biotechnol.* **2021**, *96*, 228–238. [CrossRef]
56. Li, S.; Zachgo, S. TCP3 interacts with R2R3-MYB proteins, promotes flavonoid biosynthesis and negatively regulates the auxin response in Arabidopsis thaliana. *Plant J.* **2013**, *76*, 901–913. [CrossRef]

57. Viola, I.L.; Camoirano, A.; Gonzalez, D.H. Redox-Dependent Modulation of Anthocyanin Biosynthesis by the TCP Transcription Factor TCP15 during Exposure to High Light Intensity Conditions in Arabidopsis. *Plant Physiol.* **2016**, *170*, 74–85. [CrossRef]
58. Mei, X.; Wan, S.; Lin, C.; Zhou, C.; Hu, L.; Deng, C.; Zhang, L. Integration of Metabolome and Transcriptome Reveals the Relationship of Benzenoid-Phenylpropanoid Pigment and Aroma in Purple Tea Flowers. *Front. Plant Sci.* **2021**, *12*, e762330. [CrossRef]
59. Hur, Y.-S.; Oh, J.; Kim, N.; Kim, S.; Son, O.; Kim, J.; Um, J.-H.; Ji, Z.; Kim, M.-h.; Ko, J.-H.; et al. Arabidopsis transcription factor TCP13 promotes shade avoidance syndrome-like responses by directly targeting a subset of shade-responsive gene promoters. *J. Exp. Bot.* **2024**, *75*, 241–257. [CrossRef]
60. Li, N.-N.; Lu, J.-L.; Li, Q.-S.; Zheng, X.-Q.; Wang, X.-C.; Wang, L.; Wang, Y.-C.; Ding, C.-Q.; Liang, Y.-R.; Yang, Y.-J. Dissection of Chemical Composition and Associated Gene Expression in the Pigment-Deficient Tea Cultivar '*Xiaoxueya*' Reveals an Albino Phenotype and Metabolite Formation. *Front. Plant Sci.* **2019**, *10*, e1543. [CrossRef]
61. Li, D.; Tang, X.; Dong, Y.; Wang, Y.; Shi, S.; Li, S.; Liu, Y.; Ge, H.; Chen, H. Comparative genomic investigation of TCP gene family in eggplant (*Solanum melongena* L.) and expression analysis under divergent treatments. *Plant Cell Rep.* **2022**, *41*, 2213–2228. [CrossRef]
62. Zhu, C.; Zhang, S.; Zhou, C.; Chen, L.; Zaripov, T.; Zhan, D.; Weng, J.; Lin, Y.; Lai, Z.; Guo, Y. Integrated Transcriptome, microRNA, and Phytochemical Analyses Reveal Roles of Phytohormone Signal Transduction and ABC Transporters in Flavor Formation of Oolong Tea (*Camellia sinensis*) during Solar Withering. *J.-Agric. Food Chem.* **2020**, *68*, 12749–12767. [CrossRef]

horticulturae

MDPI

Article

Phosphoric Acid and Magnesium Chloride Composite-Modified Biochar Improved Pakchoi Growth by Reducing Pb and Cd Accumulation and Altering Soil Properties and Microbial Communities

Xuejie Dong, Haojie Xu, Yanfang Ren *, Dongming Lin, Ke Li and Junyu He *

School of Environmental Science and Engineering, Changzhou University, Changzhou 213164, China; xuejiedong0415@163.com (X.D.); haojiexu1997@126.com (H.X.); lindongming2025@163.com (D.L.); xiaolike92@163.com (K.L.)

* Correspondence: yanfangren@126.com (Y.R.); junyuhe0303@126.com (J.H.)

Abstract: Soil heavy-metal pollution is one of the most serious environmental issues in the world. There is an urgent need to develop feasible strategies for the remediation of polluted soil. Biochar has great potential to reduce heavy metal phytotoxicity and promote plant growth, but its mechanisms are still unclear. In this study, phosphoric acid and magnesium composite-modified tea branch biochar (PMB) was prepared and characterized. The effects of PMB at 5% addition on pakchoi growth, Cd/Pb accumulation and subcellular distribution in pakchoi, soil physicochemical characteristics and enzyme activities, Cd/Pb bioavailability, bacterial community structure, and diversity in Cd/Pb co-contaminated soils was investigated by a pot experiment. The results showed that PMB significantly alleviated the phytotoxicity of Cd and Pb. The application of PMB effectively increased the plant height and biomass and Cd and Pb proportion in the cell wall, while reducing Cd and Pb accumulation and their distribution in cytoplasm and organelles in pakchoi plants. PMB significantly improved the activities of urease, invertase, and catalase and reduced the available Cd and Pb contents in soil. Moreover, PMB changed the structure and diversity of the soil bacterial community. The relative abundance of several beneficial microbial phyla, including *Acidobacteriota*, *Bacteroidota, Actinobacteriota*, and *Gemmatimonadota,* increased by 13.81%, 19.02%, 68.09%, and 34.79%, respectively. The Shannon and Chao1 index also increased significantly. This study provides an effective strategy for simultaneous Cd and Pb immobilization in soil, promoting plant growth and inhibiting heavy metal accumulation in vegetables, which highlights the application of PMB in sustainable agro-ecosystems.

Keywords: heavy metal contamination; soil amendment; passivation; bacterial diversity

1. Introduction

With the rapid development of industry and agriculture, heavy metals have entered the environment, causing serious pollution in soils due to metal smelting and processing, chemical wastewater discharge, mining, etc. [1]. Among them, cadmium (Cd) and lead (Pb) are the most common and widespread contaminants [2]. According to the *Bulletin of the National Soil Pollution Survey*, heavy metals accounted for 82.8% of the total amount of inorganic pollutants, while soil Cd and Pb contents exceeded the standard by 7.0% and 1.5%, respectively. Notably, Cd and Pb combined pollution occurred frequently. Both Cd and Pb have negative impact on plant growth, cell division, and metabolic processes,

resulting in declines in crop yield and quality. Long-term exposure to Cd and Pb can cause a variety of health problems in humans, such as cancer, anemia, kidney disorders, neurasthenia, etc. [3,4]. Therefore, it is imperative to explore promising strategies for high-efficiency remediation of soil simultaneously polluted with Pb and Cd.

Cd and Pb in soil are impossible to biodegrade. It is important to change their forms to reduce their ability to harm living organisms and their movement in the environment. Immobilization and stabilization are effective and easy-to-operate methods for remediating soil contaminated with heavy metals and reducing their toxic effects on living organisms [5]. Currently, various substances such as natural minerals, aggregates, and organic fertilizer are used for soil restoration. Due to its alkalinity, rich carbon content, functional groups, porosity, and high cation-exchange capacity, biochar is used in soil remediation, stabilizing heavy metals and improving soil fertility [6]. The alkaline ions of biochar can alter the forms of metals by changing soil pH, thereby decreasing the risk of Cd toxicity in the environment [7]. Biochar can also significantly reduce the mobility of Cd in the soil due to its good physical structure and rich surface functional groups [8]. Xu et al. [9] discovered that the addition of rice straw biochar significantly increased the pH value and cation exchange capacity of paddy soil and reduced the availability of Cd in rhizosphere soil. Coconut shell biochar could elevate soil pH and enzyme activity, reduce Cd bioavailability, and promote the germination of spinach [10]. Dewi et al. [11] reported that the addition of biochar increased the profit of the integrated agricultural system of soybeans and rice in field experiments by 10.1%. The application of biochar and its aging in the field both remarkably increased the immobilization of heavy metals in a field after 3 years of remediation [12]. However, the immobilization effect of pristine biochar on heavy-metal-polluted soil, especially for combined pollution, is far from satisfactory. In order to improve the repair effect, biochar modification has received increasing attention to modify the properties of biochar, which may contribute to its excellent immobilization behavior for heavy metals [13]. Recently, phosphorus (P)-modified biochar was considered as an efficient and low-cost way in soil remediation [14,15]. Phosphoric acid (H_3PO_4) with low corrosivity and environmental harmfulness is often used to modify biochar with the formation of functional groups, stable phosphorus complexes, and more micropores [16,17], which are suitable for HM immobilization in soil via metal-P precipitation and complexation [18]. For instance, it was reported that H_3PO_4-functionalized biochar showed excellent immobilization capacity for Cu(II) and Cd(II) due to highly improved surface pore structures and oxygen-containing groups [19]. P-rich biochar has good performance in Cd immobilization by improving soil physicochemical and biological properties [18,20]. Moreover, P-modified biochar can also provide soil with additional P fertilizer necessary for plant growth and promote plant growth [13,21]. Ahmad et al. [22] showed that 3% P-loaded biochar significantly increased the availability of soil P and obviously enhanced plant growth. Biochar modified by magnesium (Mg) ions can also significantly enhance its properties, including functional groups, cation exchange capacity, and pore structures [23,24], and thus can provide more adsorption sites for heavy metals, thereby reducing the available heavy metal content in the soil and increasing crop biomass [25]. Many studies have shown that combined modified biochar has a greater ability to immobilize heavy metals and inhibit their absorption by crops. Wang et al. [26] prepared EDTA-functionalized Mg/Al hydroxide-modified corn stover biochar, which introduced more functional groups and increased the chelating sites and ion exchange with Pb(II) and Cd(II). To date, the effects and mechanisms of P/Mg modified biochar on the sorption and immobilization of heavy metals in soil are still lacking.

Soil microorganisms play a key role in the transformation and translocation of nutrients from soil to plants, and the microbial community structure is often used as an indicator of soil quality. The porous structure of biochar could create a conductive environment

for beneficial soil microorganisms, heightening microbial diversity and activity, thereby fortifying heavy metal passivation in soil [21]. It was reported that bone biochar increased microbial biomass by up to 66%, altered the soil microbial community and promoted the abundance of taxa that promote soil repair, including *Actinomycetes, Firmicutes,* and *Proteobacteria* [27]. The application of BC-Fe-S treatment also induced an enhancement with most bacterial abundance, including *Ellin6067*, *Blastococcus*, *Pseudolabrys*, and *Ramlibacter*, etc., and most of these bacterial strains were related to heavy metal resistance, biotransformation, and biosorption [28]. Particularly, *Ellin6067* was found to contain genes resistant to cadmium, whereas *Blastococcus* had stress resistance which could grow vigorously under cadmium stress [29]. Moreover, these beneficial bacteria could not only facilitate heavy metal immobilization but also alter nitrogen and iron biogeochemical transformation in contaminated soil [30].

Tea branches have a large output in China. About 1 million tons of pruned tea branches (TBs) are produced annually. Currently, most of the TB waste is burned or discarded, which not only pollutes the environment but also wastes a large amount of potential biomass resources, presenting both a waste management challenge and an opportunity for value-added remediation materials [31]. Therefore, it is very important to find a suitable method to recycle and reuse tea branch waste. The tea branch is a cost-effective and lignocellulosic-rich material that can be the precursor of biochar and further applied in environmental rehabilitation. Our previous research showed tea branch biochar was porous and had a high specific surface area structure, which could effectively absorb heavy metals [31,32]. However, to the best of our knowledge, there have been few reports about its role and mechanisms in soil properties and heavy metal bioavailability under composite polluted soil. Pakchoi, rich in minerals and vitamins, is the most consumed vegetable in China. However, it is at high risk of heavy metal exposure [33]. Due to the frequent consumption of pakchoi in China, combined Cd and Pb pollution in soil has caused a decline in its yield [1]. Further, the accumulated heavy metals are easily transferred to humans through the food chain. Therefore, it is important to reduce Cd and Pb concentrations in pakchoi. We hypothesized that heavy metal bioavailability and pakchoi growth would probably be dominated by phosphoric acid and magnesium chloride composite-modified tea branch biochar (PMB). Therefore, the current study aimed to (i) examine the impact of PMB on the growth, accumulation, and subcellular distribution of Cd and Pb in pakchoi in Cd- and Pb-contaminated soil; (ii) explore the effect of PMB on soil physicochemical characteristics and enzymatic activity; and (iii) elucidate the response of soil bacterial community structure to PMB application. The application of PMB to heavy-metal-contaminated soil could provide a new way to increase the yield of pakchoi and guarantee food safety.

2. Materials and Methods

2.1. Soil Collection and Biochar Preparation

The soil in this experiment was obtained from the 0–20 cm surface layer of a farm located in Wujin District, Changzhou City, Jiangsu Province, China. The soil was classified as Luvisols with 42.5% clay, 39.2% silt, and 18.3% sand according to the World Reference Base classification. The basic physicochemical properties of the soil are listed in Table 1. After removing plant residues, the collected soil was air-dried at ambient temperature (20–25 °C) for one week and thereafter sieved through a mesh (2 mm) for further utilization. In the preparation of Cd- and Pb-contaminated soil, Cd^{2+} ($CdCl_2 \cdot 2.5H_2O$) and Pb^{2+} ($Pb(NO_3)_2$) solutions were added to soil sample to prepare simulated contaminated soil (5 mg/kg Cd^{2+} and 250 mg/kg Pb^{2+}), which was determined based on China's *Soil Environmental Quality Risk Control Standard* (GB 15618-2018) [34] and the current pollution situation in farmland surrounding industrial areas in China [35]. Polluted soil was incubated for 35 days, and

deionized water was regularly added to the polluted soil during the aging process to ensure that the soil water holding capacity remained at 70% of the maximum field water holding capacity. Then, the soil was allowed to dry naturally and ground through a 2 mm nylon sieve for the pot experiment.

Table 1. Basic physicochemical properties of the soil.

Soil Type	pH	Cation Exchange Capacity (cmol/L)	Organic Matter (g/kg)	Total Nitrogen (g/kg)	Available Phosphorus (mg/kg)	Available Potassium (mg/kg)
Yellow-brown soil	6.2	1.25	20.32	1.71	27.84	157.14

The PMB was prepared according to Xu et al. [35]. Specifically, tea branch (TB) powder was mixed with a H_3PO_4 solution in the ratio of 1:2 (g:mL) for 12 h at room temperature. The mixture was pyrolyzed at 600 °C for 2 h in a tubular furnace (OTF-1200X, Kejing, Hefei, China) with a nitrogen gas flow rate of 60 mL/min. Then, it was washed with deionized water to neutral and dried at 80 °C. The H_3PO_4-modified TB biochar was further mixed with magnesium chloride solution (1:12, g:mL) for 24 h. After washing with deionized water, the material (named PMB) was dried, sieved through a 100-mesh sieve, and stored in a sealed container for further use. The characteristics of the PMB were analyzed using standard techniques (Figure S1).

2.2. Pot Experiment

According to the literature, the common amount of biochar added to soil is 1~5%. In the actual soil remediation process, only an amount of biochar less than 5% prevented heavy metals from negatively affecting soil [36]. Therefore, 5% of PMB was added in this study. Four treatments were included as follows: Control (CK), 5% PMB (PMB), 250 mg/kg Pb + 5 mg/kg Cd (Pb + Cd), and 250 mg/kg Pb + 5 mg/kg Cd + 5% PMB (Pb + Cd + PMB). The PMB prepared above was applied to the well-aged, contaminated soil, stirred, mixed with the soil evenly, and then incubated at room temperature for 20 days. During the soil incubation process, the soil maintained 70% of the field water holding capacity. Then, the selected seeds of pakchoi (*Brassica rapa* subsp. *chinensis*) were sown and the pots were irrigated with distilled water to maintain about 70% of the soil water holding capacity. The plant was cultured in a control environmental room with 14 h day at 25 °C and 10 h night at 18 °C and a light intensity of 450 μmol/m/s. Hoagland's nutrient solution replaced distilled water every seven days until harvest. Each treatment consisted of three replications, with each replication including six pots. After 42 days, the pakchoi samples were collected, cleaned, and dried for subsequent analysis. At the same time, the fresh rhizosphere soils were collected and kept in a −80 °C refrigerator, which was divided into two parts: one part was used for the analysis of physical and chemical properties, enzyme activity, and available Pb and Cd contents; while the other part was used to analyze bacterial community structure diversity.

2.3. Growth Parameters and Pb and Cd Contents in Pakchoi

After measuring plant height and root length, the dried weight of both shoots and roots were determined using a milligram balance (INESA, Shanghai, China). Then, the dry samples were ground and approximately 0.05 g of powder was digested using an HNO_3-H_2O_2 system at 150 °C [37]. Cd and Pb contents were determined via AAS (AA-300, PerkinElmer, Waltham, MA, USA). The translocation factor (TF) was determined as the ratio of the Cd/Pb concentration in shoots to that in roots.

2.4. Pb and Cd Subcellular Distribution in Pakchoi

The subcellular distribution of Cd and Pb in pakchoi was determined by differential centrifugation [38]. Fresh roots and leaves (0.5 g) were ground in an extraction buffer (5 mmol/L, pH 7.5) containing 250 mmol/L sucrose, 50 mmol/L trimethylol aminomethane-hydrochloride, 1.00 mmol/L dithithreitol, and 5 mmol/L ascorbic acid for 10 min, and centrifuged at 3000× *g* for 15 min. The sedimentation was the cell wall component (T1). The supernatant was centrifuged at 15000× *g* for 30 min. The precipitate was the organelle component (T2), and the supernatant was the cell solute component (T3). The contents of Cd and Pb in each part were determined using AAS (AA-300, PerkinElmer, Waltham, MA, USA).

2.5. Determination of Soil Properties, Enzyme Activities, and Available Content of Heavy Metal

Soil pH was measured with a pH meter at soil-to-deionized-water ratios of 1:2.5 following 30 min of agitation [15]. The content of soil organic matter (SOM) was estimated based on soil organic carbon (SOC) and a constant (1.724). The content of soil organic carbon (SOC) was measured using the potassium dichromate oxidation method, wherein soil samples were digested with a mixture of $K_2Cr_2O_7$ and concentrated H_2SO_4, followed by titration with $FeSO_4$ [15]. The available phosphorus (AP) content was determined using the molybdenum–antimony colorimetric method following sodium bicarbonate extraction [39]. The available potassium (AK) content was measured by flame photometry following NH_4OAC (pH 7.0) extraction [39]. The alkaline hydrolysis of nitrogen (AHN) content was determined using the alkali-diffusion technique [39]. Soil urease activity (URA) was measured by an indophenol colorimeter at 630 nm [19]. Catalase activity (CAT) was determined via potassium permanganate titration [14]. Invertase activity (INV) was determined by 3,5-dinitrosalicylic acid colorimetry at 540 nm [14]. The contents of available Cd and Pb were determined by the DTPA extraction method. The chemical speciation of Cd and Pb in the soil sample was conducted using the BCR method [40].

2.6. Microbial Community Analysis

Total genetic DNA from soil samples was extracted using the E.Z.N.A™ Mag-Bind Soil DNA Kit (Omega Bio-tek, M5635-02, Norcross, GA, USA). The V3–V4 region of the soil 16S rRNA gene was amplified using PCR and universal primers 341F (CCTACGGGNGGCWGCAG) and 805R (GACTACHVGGGTATCTAATCC). After amplification, Hieff NGS™DNA Selection Beads (Yeasen Biotechnology, 10105ES03, Shanghai, China) were used to purify the amplified products by removing free primers and primer dimers. Purified PCR products of all samples were sequenced in the Illumina MiSeq system (Illumina, San Diego, CA, USA) to analyze bacterial community diversity.

2.7. Data Analysis

Data were expressed as mean ± standard deviation (SD) (n = 3). The differences among treatments were analyzed using a one-way ANOVA and the LSD test ($p < 0.05$) via the SPSS 20.0 software. The graphs were generated with Origin 2018. Relative abundance (>1%) was used to compare bacterial community composition, and the top 10 phyla were examined using Origin 2018. Alpha diversity indicators, including the Shannon and Chao1 indices, were calculated to estimate the complexity of species variety in a sample using Mothur software (version 1.48.0). Beta diversity was analyzed to estimate the similarity and difference of the microbial community, and a principal coordinate analysis (PCA) was performed on both weighted and unweighted UniFrac distances using Origin 2018. The LEFse based of OTUs was performed using R software (version 4.3.1).

3. Results

3.1. PMB Characterization

The physicochemical properties of the PMB are presented in Table S1. The PMB was alkaline, with a pH of 9.17. The main elements in the PMB were C, O, P, and Mg. Its BET surface area was 442.23 m^2/g, and the pore volume was 0.45 cm^3/g. The FTIR spectrum of the PMB exhibited several functional groups (Figure S1a), including -OH (3337 cm^{-1}), C-H (2852 and 903 cm^{-1}), -COOH/C=H (1620 cm^{-1}), and C=O/O-C=O (1395 cm^{-1}), which would favor the stabilization of heavy metals [31]. Further, peaks at 1169 cm^{-1} (P=O/P-O-C/P=OOH), 1068 cm^{-1} (PO_4^{3-}), and 620 cm^{-1} (Mg-O) were observed, indicating that P and Mg compounds existed in the PMB. The XRD analysis showed a strong diffraction peak at 25.91° associated with the typical graphite-like structure of PMB [1]. Moreover, the characteristic peaks at 13.59°, 31.27°, 26.66°, 35.42°, and 43.93° corresponded well with magnesium phosphate, calcium carbonate, calcium phosphate, and calcium carbide (Figure S1b). The SEM image of PMB showed many pore structures on the surface (Figure S1c), which was responsible for the high specific surface area. The EDS analysis confirmed that the elemental composition of PMB was dominated by C, P, O, and Mg (Figure S1d).

3.2. Effect of PMB on the Growth, Contents, and Subcellular Distribution of Cd and Pb of Pakchoi

Compared to CK, the Pb + Cd stress inhibited plant growth, leading to a significant reduction in plant height, root length, leaf dry weight, and root dry weight by 26.31%, 30.61%, 61.57%, and 49.71%, respectively (Table 2). These decreases indicated the toxicity of Pb + Cd to pakchoi growth. However, the addition of PMB reduced the inhibition in pakchoi growth caused by the Pb + Cd stress, leading to a significant increase in those parameters by 28.92%, 33.58%, 81.93%, and 71.59%, respectively, as compared to the Pb + Cd treatment. Furthermore, those growth parameters increased by 8.11%, 11.56%, 13.43%, and 17.71% under the PMB treatment alone, respectively. This indicated that the application of PMB could promote pakchoi plant growth.

Table 2. Plant height, root length, and biomass of pakchoi under Pb and Cd stress.

Treatments	Plant Height (cm)	Root Length (cm)	Leaf Dry Weight (g/plant)	Root Dry Weight (g/plant)
CK	20.60 ± 0.49 c	5.88 ± 0.23 ab	2.16 ± 0.14 c	0.175 ± 0.014 b
PMB	22.27 ± 0.76 a	6.56 ± 0.51 a	2.45 ± 0.16 a	0.206 ± 0.021 a
Cd + Pb	15.18 ± 0.42 d	4.08 ± 0.45 c	0.83 ± 0.054 d	0.088 ± 0.007 c
Cd + Pb + PMB	19.57 ± 0.35 b	5.45 ± 0.42 b	1.51 ± 0.12 b	0.151 ± 0.013 b

Note: Different lowercase letters after data in the same column indicate a significant difference at the 0.05 level.

As shown in Figure 1, under the Cd + Pb treatment, Cd and Pb contents in leaves and roots were significantly increased ($p = 0.037$). After the application of PMB, Cd and Pb contents markedly decreased ($p = 0.025$), which were decreased by 83.84% and 74.29% in leaves and by 51.91% and 47.93% in roots, respectively, compared with the Pb + Cd stress alone. Furthermore, the TFs of Cd and Pb were less than one, indicating a higher accumulation of Cd and Pb in the roots compared to the shoots. The application of PMB reduced the TFs of Cd and Pb by 67.91% and 50.62%, respectively (Figure S2).

In Figure 2, it is evident that Cd and Pb in both the leaves and roots of pakchoi mainly accumulated in the cell wall, followed by the cytoplasm and organelles. Upon the application of PMB, the levels of Cd and Pb in each subcellular component significantly decreased ($p = 0.034$). For leaves, the use of PMB reduced the contents of Cd and Pb in cell wall, cytoplasm, and organelles by 85.34% and 77.77%, 90.64% and 85.56%, and 84.45%

and 92.32%, respectively. For roots, the levels of Cd and Pb were reduced by 55.48% and 44.16%, 72.82% and 63.32%, and 79.69% and 76.43%, respectively.

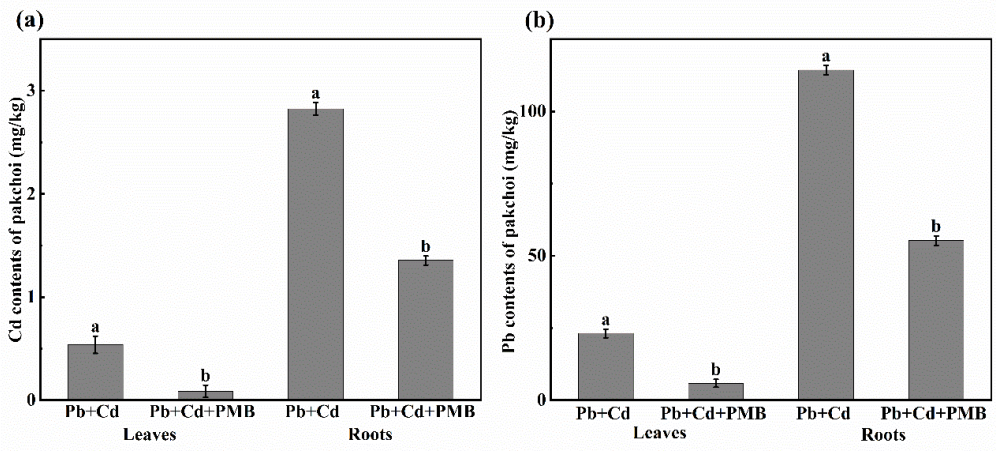

Figure 1. Effects of PMB on Cd (**a**) and Pb (**b**) contents in pakchoi. Different lowercase letters on the top of column indicate a significant difference at the 0.05 level.

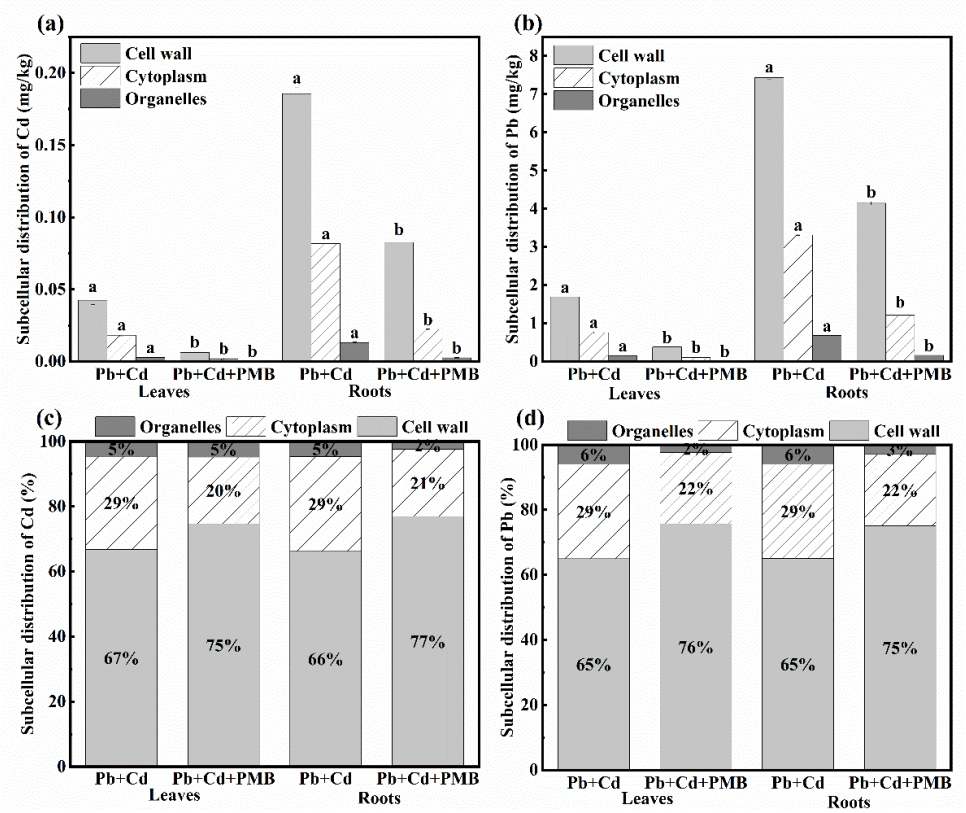

Figure 2. Effects of PMB on subcellular distribution of Cd (**a**,**c**) and Pb (**b**,**d**) in leaves and roots parts of pakchoi under Pb and Cd stress. Different lowercase letters on the top of column indicate a significant difference at the 0.05 level.

3.3. Effects of PMB on Soil Properties, Enzyme Activities, Cd and Pb Contents, and Their Chemical Speciation

As depicted in Figure S3, compared with CK, the soil pH, SOM, AP, AK, and AHN value of (Pb + Cd)-polluted soil decreased by 18.65%, 32.17%, 47.65%, 28.57%, and 30.96%, respectively. These values in PMB-added soil significantly increased by 17.92%, 33.14%, 47.82%, 30.33% and 34.36% under Pb + Cd stress, respectively, and they increased by 23.35%, 34.72%, 34.42%, 34.83% and 39.28%, respectively, when PMB was applied alone.

As shown in Figure S4, compared with CK, the urease, sucrase, and catalase activities under Pb + Cd stress decreased by 35.16%, 44.94%, and 48.64%, respectively. When PMB was applied to (Pb + Cd)-contaminated soil, the urease, invertase, and catalase activities increased by 66.30%, 51.71%, and 52.27%, respectively. Meanwhile, the urease, invertase, and catalase in soil treated by PMB alone increased by 35.16%, 25.35%, and 34.83%, respectively.

As depicted in Figure 3, the addition of PMB significantly decreased the contents of available Cd and Pb by 65.05% and 52.25%, respectively. Further, the addition of PMB significantly reduced the acid extractable state of Cd and Pb by 40.62% and 34.01%, respectively (Figure 3). However, the addition of PMB increased the reducible state, oxidizable state, and residual state of Cd and Pb by 5.59% and 0.36%, 10.19% and 5.73%, and 919.47% and 672.2%, respectively.

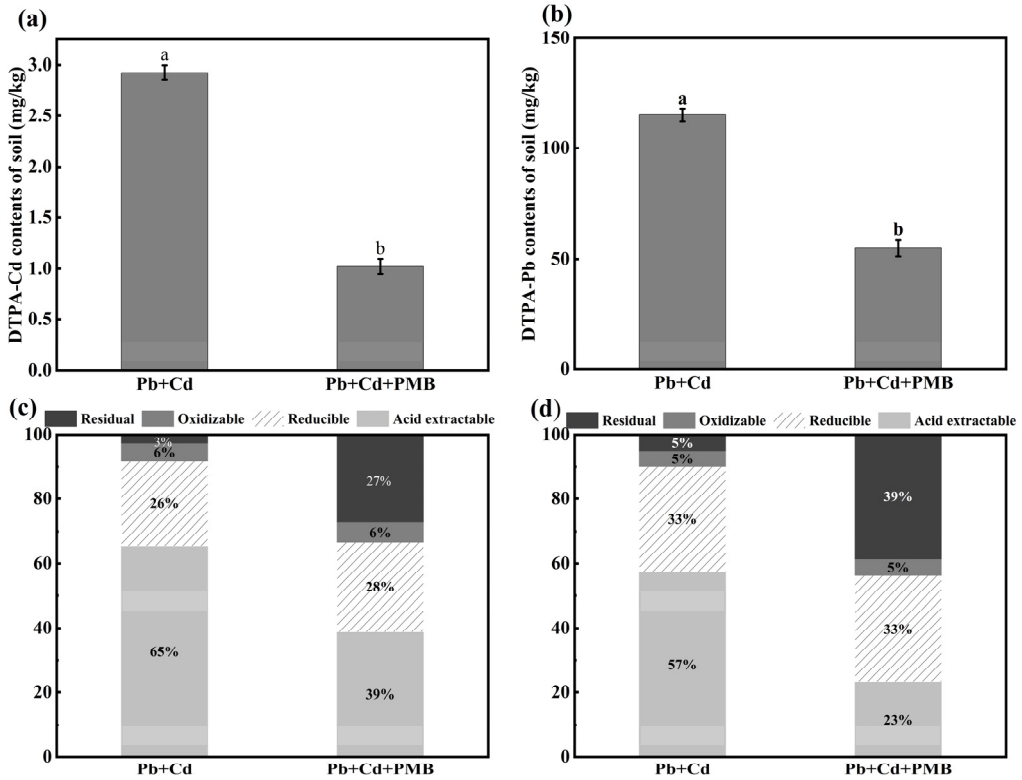

Figure 3. The available content and proportion of different forms of Cd (**a**,**c**) and Pb (**b**,**d**). Different lowercase letters on the top of column indicate a significant difference at the 0.05 level.

3.4. Effects of PMB on Soil Bacterial Communities

3.4.1. Soil Bacterial Community Composition

As shown in Figure 4a,c, there were notable differences in the relative abundance of bacteria at the phylum level. The ten dominant soil bacterial communities in all samples were *Proteobacteria*, *Bacteroidota*, *Acidobacteriota*, *Actinobacteriota*, *Gemmatimonadota*, *Patescibacteria*, *Verrucomicrobiota*, *Chloroflexi*, *Myxococcota,* and *Planctomycetota*, which accounted for 96.59%, 97.23%, 97.33%, and 96.20% of the total number of bacteria in CK, PMB, Pb + Cd, and Pb + Cd + PMB, respectively. Among them, *Proteobacteria* was the largest bacterial community. Compared with CK, the number of *Proteobacteria* under Pb + Cd stress increased by 6.01%. However, it decreased in the Pb + Cd + PMB treatment by 22.72% compared with the Pb + Cd treatment. When PMB was applied alone, the number of *Proteobacteria* decreased slightly by 5.32%.

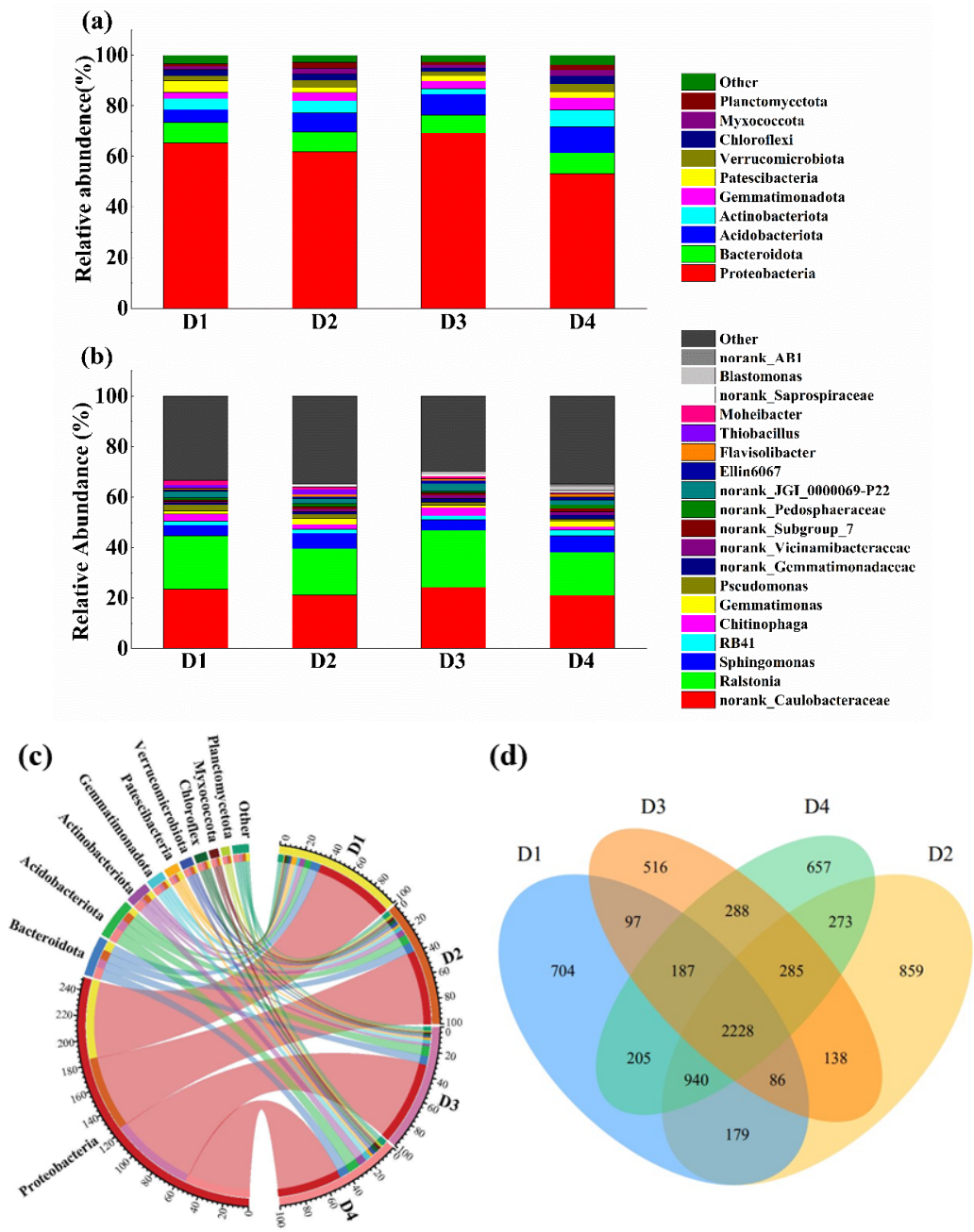

Figure 4. The changes in the rhizosphere soil microbial community under different treatments. (**a**) Relative abundance of bacteria, (**b**) relative abundance heat map, (**c**) collinearity diagram, (**d**) Venn diagram of OTU distribution of soil bacteria. D1 refers to CK, D2 refers to PMB, D3 refers to Pb + Cd, and D4 refers to Pb + Cd + PMB.

As depicted in Figure 4b, at the genus level, *norank_Caulobacteraceae*, *Sphingomonas*, *Gemmatimonas*, and *norank_Pedosphaeraceae* showed a marked decrease in the Pb + Cd treatment compared with CK. The addition of PMB increased these bacteria significantly under the Pb + Cd treatment and CK. Moreover, compared to CK, *RB41*, *norank_Gemmatimonadaceae*, and *norank_Vicinamibacteraceae* showed a significant increase in the Pb + Cd treatment. However, the addition of PMB decreased these bacteria significantly under the Pb + Cd treatment and CK.

In Figure 4d, the Venn diagram illustrated the differences in OTUs between different treatments. There were 2228 core OTUs present in all samples. Additionally, the PMB treatment had the highest number of unique OTUs (859), while the Pb + Cd group had

the lowest (516), and the CK and Pb + Cd + PMB groups had 704 and 657 unique OTUs, respectively. Compared to CK, the number of unique OTUs decreased by 26.70% under Pb + Cd stress. Under Pb + Cd stress, the addition of PMB increased the number of unique OTUs by 27.32%. PMB alone also increased it by 22.01% compared to CK.

3.4.2. Alpha and Beta Analyses of Soil Bacterial Community

Table 3 showed the alpha diversity index of soil bacteria based on the 16S rRNA gene. The Chao1 index and Shannon index were used to assess the richness and diversity of soil microbial communities. Compared to CK, the Chao1 and Shannon indices of bacteria in the Pb + Cd treatment group decreased by 14.51% and 7.75%, respectively. Under Pb + Cd stress, the addition of PMB increased the Chao1 and Shannon indices by 15.39% and 7.09%, respectively. The Chao1 and Shannon indices of bacteria treated with PMB alone increased by 10.93% and 11.14% compared to CK, respectively. The findings suggested that the addition of PMB markedly increased the diversity and abundance of soil bacteria.

Table 3. Richness and diversity indices of soil bacterial communities under different treatments.

Treatments	Chao1	Shannon
CK	2040.32 ± 73.48 b	4.13 ± 0.04 b
PMB	2263.10 ± 65.31 a	4.59 ± 0.04 a
Pb + Cd	1744.18 ± 81.64 c	3.81 ± 0.08 c
Pb + Cd + PMB	2012.62 ± 85.73 b	4.08 ± 0.11 b

Note: Different lowercase letters after data in the same column indicate a significant difference at the 0.05 level.

The principal coordinate analysis illustrated the soil bacterial communities in the four treatments (Figure 5). PC1 and PC2 axes explained 31.7% and 19.4% of the sample composition differentiation, respectively. There were noticeable differences among the four treatments according to their location in Figure 5, indicating that PMB had a significant separation effect on soil microorganisms.

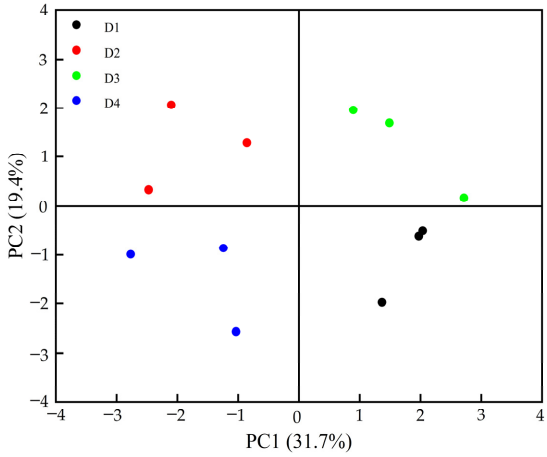

Figure 5. PCA principal coordinate analysis. D1 refers to CK, D2 refers to PMB, D3 refers to Pb + Cd, and D4 refers to Pb + Cd + PMB.

3.4.3. Correlation Analysis and LEFse Analysis

The correlation analysis (Figure 6) demonstrated that soil pH, SOM, AP, AK, AHN, CAT, URA, INV, plant height, root length, leaf dry weight, and root dry weight were significant and positive correlated with the phyla *Planctomycetota, Myxococcota,* and *Verrucomicrobiota* but negative correlated with *Proteobacteria* and *Patescibacteria.* Soil available Cd, available Pb, leaf Cd, leaf Pb, root Cd, and root Pb were positively correlated with *Proteobacteria* and *Acidobacteriota* but significantly and negatively correlated with *Bacteroidota*.

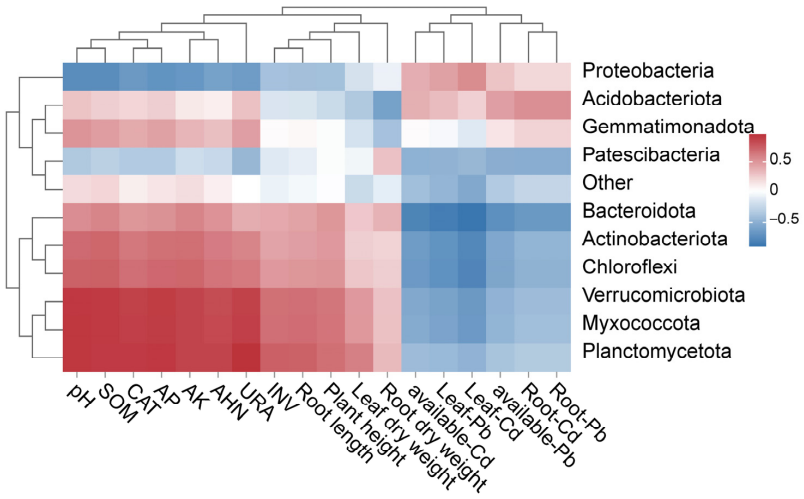

Figure 6. Correlation heatmap of bacterial community at the phylum level with soil and plant variables.

The taxonomic cladogram line discriminant analysis effect size (LEfSe) indicated the predominant discriminant taxa of the bacterial communities in the different treatments (Figure 7). In CK, *Bacteroidota* and *Chloroflexi* (phylum), *Chitinophagales* and *Cytophagales* (order), and *Chitinophaga* and *Gemmatimonas* (genus) were significantly enriched. For the Pb + Cd treatment, it merely enriched *Verrucomicrobiota* (Phylum), *Pedosphaerales* (order), and *norank_Pedosphaeraceae c6* (genus). After applying PMB under Pb + Cd, *RB41*, *norank_Subgroup_7*, *norank_Vicinamibacteraceae*, and *Cellulomonas* at the genus level were significantly enriched. After application of PMB alone, *Proteobacteria* (phylum), *Rickettsiales* (order), *norank_Bacteroidetes_VC2_1_Bac22* (family), and *Ellin6067* (genus) were significantly enriched.

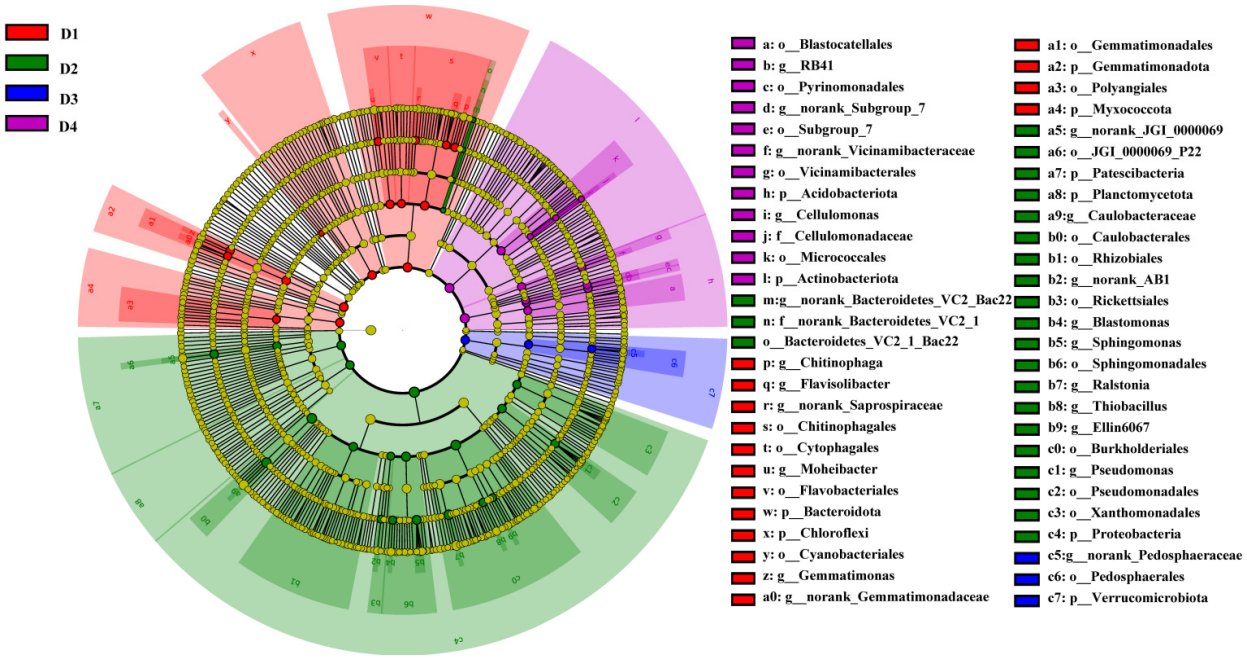

Figure 7. A taxonomic cladogram of line discriminant analysis effect size (LEfSe) based on OTUs. The cladogram shows the biomarker microbes of the microbial lineages from phylum to genus among four different treatments. Yellow dots represent microbes with no statistical differences among the five treatments. D1 refers to CK, D2 refers to PMB, D3 refers to Pb + Cd, and D4 refers to Pb + Cd + PMB.

4. Discussion

Many studies have found that biochar has a large specific surface area, rich functional groups, and a stable structure, which can adsorb and fix heavy metals in soil, improve soil physical and chemical properties, and promote plant growth [41]. In this study, the Pb + Cd treatment significantly decreased the plant height, root length, and the leaf and root weight of pakchoi; however, the application of PMB significantly increased these growth parameters of pakchoi under the Pb + Cd treatment. This suggested that PMB could promote pakchoi growth. This was consistent with the findings of Chen et al. [42]. This was because the addition of PMB to the soil reduced the Pb and Cd accumulation in roots and shoots and their translocation from the roots to the leaves. The transport of heavy metals from soil to plants was mainly influenced by the quantity of available metals in the soil [43]. Our findings indicated that the application of PMB in (Pb + Cd)-contaminated soil markedly reduced the content of bioavailable Cd and Pb in the soil. This was consistent with previous research [44], indicating that applying biochar could reduce the contents of Cd and Pb in bioavailable forms. This was because biochar exhibited a wide range of adsorption capabilities for heavy metals [41]. Generally, biochar rich in oxygen-containing functional groups, carbonate, or phosphate is conducive to the passivation of cationic heavy metals. Reduced bioavailability of heavy metals in soil inhibits plant absorption, thereby decreasing heavy metal bioaccumulation in plants. Our results also confirmed that PMB effectively reduced the Cd and Pb contents of pakchoi roots and leaves in (Pb + Cd)-polluted soil.

Compartmentalization is a key approach for detoxifying heavy metals in plant cells. The cell wall, as the primary physical barrier against heavy metals, can provide various negative functional groups, such as carboxyl and hydroxyl, to bind heavy metal ions and inhibit their translocation across the cytoplasmic membrane [3]. Simultaneously, heavy metal ions enter in the vacuole and are sequestered by organic ligands, therefore reducing the interference with cell organelles. In a previous study, Sun et al. [45] showed that most of the Cd^{2+} ions were immobilized by the hemicellulose 1 of the cell wall in pakchoi roots, and the content of hemicellulose was positively correlated with the Cd immobilization capacity. Pectin was identified as the main polysaccharide in the root cell wall of rice exhibiting significant Cd buildup. In this study, Cd and Pb in leaves and roots of pakchoi mainly accumulated in the cell wall, followed by the cytoplasm and organelles. After PMB was applied, the contents of Cd and Pb in each cell component were significantly decreased. However, the proportion of Cd and Pb content in the cell wall components increased significantly, indicating that more Cd and Pb were bound by these components in the cell wall, thus reducing the toxic effect of heavy metals on pakchoi.

The bioavailability of heavy metals in soils was related to the physical and chemical properties of the soil [28]. Biochar can significantly regulate the physical and chemical properties of the soil. In this study, the addition of PMB in both control and Pb + Cd composite-polluted soils increased the soil pH and SOM value. The increase was attributed to the presence of alkaline substances in biochar, including carbonates, phosphates, and silicates, which may consume protons in the soil solution, leading to an elevation in soil pH [46]. The increased pH value could deprotonate soil colloids, facilitating the electrostatic adsorption of Pb^{2+} and Cd^{2+} [9]. Hence, the addition of PMB was favorable for the stabilization of heavy metals in the soil. The increase in soil SOM caused by the addition of PMB was attributed to the carbon enrichment of biochar, as higher organic matter in the soil can facilitate the complexation of Cd and Pb in the soil [47]. Previous research also indicated that the improved capacity of biochar to mitigate heavy metal damage was primarily attributable to the alterations in soil physicochemical properties, which were beneficial for immobilizing heavy metals and reduced their mobility and effectiveness in

the soil [10,48]. In addition, applying PMB greatly reduced the acid extractable state of Cd and Pb, transforming them into a residual state with low bioavailability in this study. The residual state has the weakest migration ability in soil and is the form with the lowest bioavailability [18]. Both reduced bioavailability and reduced migration ability can be used as indicators to evaluate the effectiveness of the original passivation. Gondek et al. [49] applied biochar and zeolite to Cd, Pb, and Zn-contaminated soils to reduce the exchangeable states of Cd, Pb, and Zn and increase the parts with low bioavailability. The content of the residual state increased, and heavy metal stabilization was realized. The observed changes in soil properties in this investigation indicated that the application of PMB was a viable approach to decrease the bioavailability of Cd and Pb.

Biochar is primarily composed of carbon, nitrogen, phosphorus, and potassium, which can enhance the growth of microorganisms [41]. Soil enzymes are essential for soil physical and chemical reactions and highly sensitive to heavy metal contamination. Numerous research studies have indicated that the moderate amount of biochar could boost the activities of urease, sucrase, and catalase in the soil [10,49]. A similar role was confirmed in this study. This could be attributed to the layered porous structure of PMB, which created a better environment for microbial growth and enhanced enzyme activity in the soil. It may be attributed to heightened substrate utilization, which in turn stimulated the reaction of metals with organic substances, leading to the formation of metal–organic complexes and a reduction in the toxicity of Cd and Pb [50].

Soil microorganisms are highly sensitive indicators of changes in soil properties and play a crucial role in maintaining ecosystem health and nutrient cycling [51]. The use of PMB had a significant impact on the composition of the bacterial community at the phylum level and increased the number of operational taxonomic units (OTUs), bacterial diversity, and bacterial abundance under Pb + Cd stress, possibly due to the introduction of substantial quantities of phosphorus, oxygen-containing functional groups, and carbonate. Alpha diversity is an important indicator of bacterial richness and diversity. It was observed that the addition of PMB enhanced the abundance and diversity of bacteria and increased the Shannon and Chao1 indices. This could be attributed to the appropriate increase in soil pH, SOM, AP, AK, AHN, INV, URA, and CAT, due to the application of biochar, promoting the growth of certain bacteria [47], as evidenced by the increase in *Acidobacteriota* in the soil.

Previous research has demonstrated exposure to abiotic stresses such as heavy metals, wastewater, and pesticides can impact the beneficial microorganisms present in the soil, including *Proteobacteria*, *Acidobacteriota*, *Gemmatimonadota*, *Bacteroidota*, *Chloroflexi*, *Actinobacteriota,* and *Myxococcota* [52,53]. This research found that *Proteobacteria*, *Bacteroidota*, *Acidobacteriota*, and *Actinobacteriota* were the most predominant bacterial phyla in soil, similar to previous studies [54,55]. *Proteobacteria* is known for its high resistance to heavy metals due to its ability to adapt to extreme environments such as soil polluted with heavy metals [13]. *Actinobacteria* is predominant in carbon-rich environments and plays a crucial role in the carbon cycle. They are usually associated with the decomposition of organic materials such as chitin and cellulose and are thought to play a major role in converting soil organic matter in the ecosystem. In this study, the number of *Actinobacteriota* in PMB treatment increased significantly when compared with CK and the Cd + Pb treatment. This suggested that the PMB enhanced microbial activity involved in the carbon cycle. In addition, our study found that adding PMB in contaminated soil increased the abundance of beneficial microorganisms, including *Bacteroidota*, *Acidobacteriota*, *Gemmatimonadota*, and *Patescibacteria*. Previous research has showed that these beneficial microorganisms played a crucial role in immobilizing Cd and Pb in the soil [56], leading to the passivation of these metals and an increase in the proportion of fixed Cd and Pb in the soil. These bacteria could reduce the available Cd and Pb in soil via their complexation and absorption abilities [57].

In the present study, the correlation heatmap demonstrated that available Cd and Pb were positively correlated with *Proteobacteria* and *Acidobacteriota* but significantly and negatively correlation with *Bacteroidota*. *Bacteroidota* affects the cycling and persistence of soil carbon. This may relate to an alteration in soil pH, SOM, AP, AK, AHN, INV, URA, and CAT. Our research findings confirmed that PMB could potentially regulate the structure of soil microorganisms, altering the forms and availability of Cd and Pb, reduce absorption of these metals by plants, and enhance plant growth. Future research should focus on identifying its heavy metal passivation role in the different environmental factors, such as temperature and moisture. Additionally, field trials are essential to validate the broad applicability of our findings across environmental conditions and for long-term stability.

5. Conclusions

The present study demonstrated that PMB significantly promoted pakchoi growth in soil contaminated with Cd and Pb by reducing Cd and Pb accumulation in the plant and their migration from the roots to the shoots of pakchoi. PMB significantly reduced the available contents of Cd and Zn and converted bioavailable Cd and Pb into immobilized forms, while increasing soil pH, organic matter, and available nutrient content. PMB application also improved the activities of urease, invertase, and catalase. Additionally, PMB increased the relative abundance of beneficial bacteria in the soil, including *Bacteroidota*, *Acidobacteriota*, *Actinobacteriota*, and *Gemmatimonadota*. In summary, this study provided a new strategy for reducing heavy metal pollution in vegetables and fostering sustainable agro-ecosystem development. However, further research is essential to ascertain the effective application of PMB on a large scale under real-field conditions.

Supplementary Materials: The following supporting information can be downloaded at: https://www.mdpi.com/article/10.3390/horticulturae11060632/s1, Table S1: Physicochemical properties of PMB; Figure S1: FTIR (a), XRD (b), SEM (c) and EDS (d) of PMB; Figure S2: The translocation factor of Cd and Pb; Figure S3: Effects of PMB on soil pH (a), soil organic matter (b), available phosphorus (c), available potassium (d) and alkali hydrolyzed nitrogen (e); Figure S4: Effects of PMB on soil enzyme activity. (a) urease, (b) invertase, (c) catalase.

Author Contributions: X.D.: writing—original draft, visualization, methodology, investigation, formal analysis, data curation. H.X.: experimental operation, methodology, formal analysis, data curation. Y.R.: writing—review and editing, supervision. D.L.: formal analysis, data curation. K.L.: methodology, formal analysis. J.H.: writing—review and editing, supervision. All authors have read and agreed to the published version of the manuscript.

Funding: This work was funded by the National Natural Science Foundation of China [31460100].

Data Availability Statement: The original contributions presented in this study are included in the article. Further inquiries can be directed to the corresponding author.

Conflicts of Interest: The authors declare that the research was conducted in the absence of any commercial or financial relationships that could be construed as a potential conflict of interest.

References

1. Zhang, L.; Ren, Y.; Xue, Y.; Cui, Z.; Wei, Q.; Han, C.; He, J. Preparation of biochar by mango peel and its adsorption characteristics of Cd(II) in solution. *RSC Adv.* **2020**, *10*, 35878–35888. [CrossRef] [PubMed]
2. Gu, J.; Hu, C.; Jia, X.; Ren, Y.; Su, D.; He, J. Physiological and biochemical bases of spermidine-induced alleviation of cadmium and lead combined stress in rice. *Plant Physiol. Biochem.* **2022**, *189*, 104–114. [CrossRef] [PubMed]
3. Ji, Y.; Ren, Y.F.; Han, C.; Zhu, W.J.; Gu, J.Y.; He, J.Y. Application of exogenous glycinebetaine alleviates lead toxicity in pakchoi (*Brassica chinensis* L.) by promoting antioxidant enzymes and suppressing Pb accumulation. *Environ. Sci. Pollut. Res.* **2022**, *29*, 25568–25580. [CrossRef] [PubMed]

4. Li, K.; Ren, Y.; Lin, D.; Tong, M.; Yang, B.; Xiao, F.; Hou, Y.; Lu, Y.; He, J. Green preparation of bimetallic CuO/ZnO nanoparticles by using *Cinnamomum camphora* leaf and its potential for antifungal and cadmium removal applications. *Inorg. Chem. Commun.* **2025**, *178*, 114577. [CrossRef]
5. Lan, J.; Zhang, S.S.; Dong, Y.Q.; Li, J.H.; Li, S.Y.; Feng, L.; Hou, H.B. Stabilization and passivation of multiple heavy metals in soil facilitating by pinecone-based biochar: Mechanisms and microbial community evolution. *J. Hazard. Mater.* **2021**, *420*, 126588. [CrossRef]
6. Algethami, J.S.; Irshad, M.K.; Javed, W.; Alhamami, M.A.M.; Ibrahim, M. Iron-modified biochar improves plant physiology, soil nutritional status and mitigates Pb and Cd-hazard in wheat (*Triticum aestivum* L.). *Front. Plant Sci.* **2023**, *14*, 1221434. [CrossRef]
7. Bandara, T.; Franks, A.; Xu, J.; Bolan, N.; Wang, H.; Tang, C. Chemical and biological immobilization mechanisms of potentially toxic elements in biochar-amended soils. *Crit. Rev. Environ. Sci. Technol.* **2020**, *50*, 903–978. [CrossRef]
8. Haider, F.U.; Ain, N.; Khan, I.; Farooq, M.; Habiba Cai, L.; Li, Y. Co-application of biochar and plant growth regulators improves maize growth and decreases Cd accumulation in cadmium-contaminated soil. *J. Clean. Prod.* **2024**, *440*, 140515. [CrossRef]
9. Xu, M.L.; Dai, W.J.; Zhao, Z.L.; Zheng, J.T.; Huang, F.; Mei, C.; Huang, S.T.; Liu, C.F.; Wang, P.; Xiao, R.B. Effect of rice straw biochar on three different levels of Cd-contaminated soils: Cd availability, soil properties, and microbial communities. *Chemosphere* **2022**, *301*, 134551. [CrossRef]
10. Noronha, F.R.; Manikandan, S.K.; Nair, V. Role of coconut shell biochar and earthworm (*Eudrilus euginea*) in bioremediation and palak spinach (*Spinacia oleracea* L.) growth in cadmium-contaminated soil. *J. Environ. Manag.* **2022**, *302*, 114057. [CrossRef]
11. Dewi, R.K.; Huang, Q.; Hashimi, R.; Komatsuzaki, M. Enhancing agroecosystem sustainability: Integrative soil health strategies in regenerative organic soybean production on Andosol in Japan. *Geoderma Reg.* **2025**, *40*, e00910. [CrossRef]
12. Chen, X.; Jiang, S.; Wu, J.; Yi, X.; Dai, G.; Shu, Y. Three-year field experiments revealed the immobilization effect of natural aging biochar on typical heavy metals (Pb, Cu, Cd). *Sci. Total Environ.* **2024**, *912*, 169384. [CrossRef] [PubMed]
13. Mandal, S.; Pu, S.; He, L.; Ma, H.; Hou, D. Biochar induced modification of graphene oxide & nZVI and its impact on immobilization of toxic copper in soil. *Environ. Pollut.* **2020**, *259*, 113851. [CrossRef] [PubMed]
14. Huang, K.; Sun, X.; Sun, J.; Guo, Y.; Hu, X.; Hu, C.; Tan, Q. The role of phosphorus speciation of biochar in reducing available Cd and phytoavailability in mining area soil: Effect and mechanism. *Sci. Total Environ.* **2023**, *894*, 164868. [CrossRef]
15. Zhang, H.; Shao, J.; Zhang, S.; Zhang, X.; Chen, H. Effect of phosphorus-modified biochars on immobilization of Cu(II), Cd(II), and As(V) in paddy soil. *J. Hazard. Mater.* **2020**, *390*, 121349. [CrossRef]
16. Chu, G.; Zhao, J.; Huang, Y.; Zhou, D.D.; Liu, Y.; Wu, M.; Peng, H.B.; Zhao, Q.; Pan, B.; Steinberg, C.E.W. Phosphoric acid pretreatment enhances the specific surface areas of biochars by generation of micropores. *Environ. Pollut.* **2018**, *240*, 1–9. [CrossRef]
17. Dechapanya, W.; Khamwichit, A. Biosorption of aqueous Pb(II) by H_3PO_4-activated biochar prepared from palm kernel shells (PKS). *Heliyon* **2023**, *9*, e17250. [CrossRef]
18. Netherway, P.; Reichman, S.M.; Laidlaw, M.; Scheckel, K.; Pingitore, N.; Gasćo, G.; Méndez, A.; Surapaneni, A.; Paz-Ferreiro, J. Phosphorus-rich biochars can transform lead in an urban contaminated soil. *J. Environ. Qual.* **2019**, *48*, 1091–1099. [CrossRef]
19. Zhang, H.; Ke, S.; Xia, M.; Bi, X.; Shao, J.; Zhang, S.; Chen, H. Effects of phosphorous precursors and speciation on reducing bioavailability of heavy metal in paddy soil by engineered biochars. *Environ. Pollut.* **2021**, *285*, 117459. [CrossRef]
20. Ge, Q.; Tian, Q.; Wang, S.; Zhu, F. Synergistic effects of phosphoric acid modified hydrochar and coal gangue-based zeolite on bioavailability and accumulation of cadmium and lead in contaminated soil. *Chinese J. Chem. Eng.* **2022**, *46*, 150–160. [CrossRef]
21. Sahin, O.; Yagcioglu, K.D.; Kadioglu, Y.K.; Gunes, A. The importance of acidified biochar as a sustainable phosphorus source and its role in balanced nutrition for spinach (*Spinacia oleracea* L.). *J. Soil Sci. Plant Nutri.* **2024**, *24*, 8035–8045. [CrossRef]
22. Ahmad Munir Usman, A.R.A.; Al-Faraj, A.S.; Ahmad Mahtab Sallam, A.; Al-Wabel, M.I. Phosphorus-loaded biochar changes soil heavy metals availability and uptake potential of maize (*Zea mays* L.) plants. *Chemosphere* **2018**, *194*, 327–339. [CrossRef] [PubMed]
23. Behrooz, B.A.; Oustan, S.; Hosseini, H.M.; Etesami, H.; Padoan, E.; Magnacca, G.; Marsan, F.A. The importance of presoaking to improve the efficiency of $MgCl_2$-modified and non-modified biochar in the adsorption of cadmium. *Ecotoxicol. Environ. Saf.* **2023**, *257*, 114932. [CrossRef] [PubMed]
24. Deng, Y.; Li, X.; Ni, F.; Liu, Q.; Yang, Y.; Wang, M.; Ao, T.; Chen, W. Synthesis of magnesium modified biochar for removing copper, lead and cadmium in single and binary systems from aqueous solutions: Adsorption mechanism. *Water* **2021**, *13*, 599. [CrossRef]
25. Shan, R.; Li, W.; Chen, Y.; Sun, X. Effects of Mg-modified biochar on the bioavailability of cadmium in soil. *BioResources* **2020**, *15*, 8008–8025. [CrossRef]
26. Wang, Y.; Li, J.; Xu, L.; Wu, D.; Li, Q.; Ai, Y.; Liu, W.; Li, D.; Zhou, Y.; Zhang, B.; et al. EDTA functionalized Mg/Al hydroxides modified biochar for Pb(II) and Cd(II) removal: Adsorption performance and mechanism. *Sep. Purif. Technol.* **2024**, *335*, 126199. [CrossRef]

27. Azeem, M.; Ali, A.; Jeyasundar, P.G.S.A.; Li, Y.M.; Abdelrahman, H.; Latif, A.; Li, R.H.; Basta, N.; Li, G.; Shaheen, S.M.; et al. Bone-derived biochar improved soil quality and reduced Cd and Zn phytoavailability in a multi-metal contaminated mining soil. *Environ. Pollut.* **2021**, *277*, 116800. [CrossRef]
28. Qu, J.H.; Yuan, Y.H.; Zhang, X.M.; Wang, L.; Tao, Y.; Jiang, Z.; Yu, H.; Dong, M.; Zhang, Y. Stabilization of lead and cadmium in soil by sulfur-iron functionalized biochar: Performance, mechanisms and microbial community evolution. *J. Hazard. Mater.* **2022**, *425*, 127876. [CrossRef]
29. Wang, Y.; Ren, Q.; Li, T.; Zhan, W.; Zheng, K.; Li, Y.; Chen, R. Influences of modified biochar on metal bioavailability, metal uptake by wheat seedlings (*Triticum aestivum* L.) and the soil bacterial community. *Ecotox. Environ. Saf.* **2021**, *220*, 112370. [CrossRef]
30. Zhang, J.; Jiang, Y.; Ding, C.; Wnag, S.; Zhao, C.; Yin, W.; Wang, B.; Yang, R.; Wang, X. Remediation of lead and cadmium co-contaminated mining soil by phosphate-functionalized biochar: Performance, mechanism, and microbial response. *Chemosphere* **2023**, *334*, 138938. [CrossRef]
31. Han, C.; Wang, M.; Ren, Y.F.; Zhang, L.; Ji, Y.; Zhu, W.; Song, Y.; He, J.Y. Characterization of pruned tea branch biochar and the mechanisms underlying its adsorption for cadmium in aqueous solution. *RSC Adv.* **2021**, *11*, 26832–26843. [CrossRef] [PubMed]
32. Xu, H.J.; Zhou, Q.; Yan, T.Y.; Jia, X.W.; Lu, D.D.; Ren, Y.F.; He, J.Y. Enhanced removal efficiency of Cd^{2+} and Pb^{2+} from aqueous solution by H_3PO_4-modified tea branch biochar: Characterization, adsorption performance and mechanism. *J. Environ. Chem. Eng.* **2024**, *12*, 112183. [CrossRef]
33. Ren, Y.F.; Wang, W.; He, J.Y.; Zhang, L.; Wei, Y.; Yang, M. Nitric oxide alleviates salt stress in seed germination and early seedling growth of pakchoi (*Brassica chinensis* L.) by enhancing physiological and biochemical parameters. *Ecotox. Environ. Saf.* **2020**, *187*, 109785. [CrossRef] [PubMed]
34. *GB 15618-2018*; China: National Standard Soil Environmental Quality Risk Control Standard for Soil Contamination of Agricultural Land. USDA: Beijing, China, 2018.
35. Yang, Q.; Li, Z.; Lu, X.; Duan, Q.; Huang, L.; Bi, J. A review of soil heavy metal pollution from industrial and agricultural regions in China: Pollution and risk assessment. *Sci. Total Environ.* **2018**, *642*, 690–700. [CrossRef]
36. Bian, R.; Li, L.; Bao, D.; Zheng, J.; Zhang, X.; Zheng, J.; Liu, X.; Cheng, K.; Pan, G. Cd immobilization in a contaminated rice paddy by inorganic stabilizers of calcium hydroxide and silicon slag and by organic stabilizer of biochar. *Environ. Sci. Pollut. Res.* **2016**, *23*, 10028–10036. [CrossRef]
37. Su, D.M.; Wang, M.F.; Xu, H.J.; Zhang, Y.Z.; Hu, Q.F.; Ren, Y.F.; He, J.Y. Performance and mechanism of *Ficus carica* branch waste based biochar in removing Cd^{2+} from aqueous solution. *Biomass Convers. Bior.* **2024**, *14*, 24137–24150. [CrossRef]
38. Weigal, H.J. Jager HJ. Subcellular distribution and chemical form of cadmium in bean. *Plant Physiol.* **1980**, *65*, 480–482. [CrossRef]
39. Wang, W.; Ren, Y.F.; He, J.; Zhang, L.; Wang, X.; Cui, Z. Impact of copper oxide nanoparticles on the germination, seedling growth, and physiological responses in *Brassica pekinensis* L. *Environ. Sci. Pollut. Res.* **2020**, *27*, 31505–31515. [CrossRef]
40. Hamidpour, M.; Sadeghi, R.; Abbaszadeh-Dahaji, P.; Alaei, H.; Shafigh, M.; Omidvari, M.; Kariman, K. The effects of EDTA and Trichoderma species on growth and Cu uptake of maize (*Zea mays*) plants grown in a Cu-contaminated soil. *Environ. Geochem. Health* **2024**, *46*, 372. [CrossRef]
41. Lu, X.; Sun, J.; Pan, G.; Qi, W.; Zhang, Z.; Xing, J.; Gao, Y. Ball-milling-modified biochar with additives enhances soil Cd passivation, increases plant growth and restrains Cd uptake by chinese cabbage. *Horticulturae* **2025**, *11*, 168. [CrossRef]
42. Chen, X.L.; Ran, Z.F.; Li, R.; Duan, W.Y.; Song, Z.J.; Fang, L.; Guo, L.P.; Zhou, J. Biochar reduces the cadmium content of *Panax quinquefolium* L. by improving rhizosphere microecology. *Sci. Total Environ.* **2024**, *915*, 170005. [CrossRef] [PubMed]
43. Gu, T.Y.; Lu, Y.Q.; Li, F.; Zeng, W.M.; Shen, L.; Yu, R.L.; Li, J.K. Microbial extracellular polymeric substances alleviate cadmium toxicity in rice (*Oryza sativa* L.) by regulating cadmium uptake, subcellular distribution and triggering the expression of stress-related genes. *Ecotox. Environ. Saf.* **2023**, *257*, 114958. [CrossRef]
44. Awad, M.; El-Sayed, M.M.; Li, X.; Liu, Z.; Mustafa, S.K.; Ditta, A.; Hessini, K. Diminishing heavy metal hazards of contaminated soil via biochar supplementation. *Sustainability* **2021**, *13*, 12742. [CrossRef]
45. Sun, Q.H.; Zhang, Y.X.; Ming, C.S.; Wang, J.M.; Zhang, Y. Amended compost alleviated the stress of heavy metals to pakchoi plants and affected the distribution of heavy metals in soil-plant system. *J. Environ. Manag.* **2023**, *336*, 117674. [CrossRef] [PubMed]
46. Qi, X.; Gou, J.L.; Chen, X.M.; Xiao, S.Q.; Ali, I.; Shang, R.; Wang, D.; Wu, Y.W.; Han, M.W.; Luo, X.G. Application of mixed bacteria-loaded biochar to enhance uranium and cadmium immobilization in a co-contaminated soil. *J. Hazard. Mater.* **2021**, *401*, 123823. [CrossRef]
47. Liu, Q.Q.; Sheng, Y.Q.; Wang, W.J.; Liu, X.Z. Efficacy and microbial responses of biochar- nanoscale zero-valent during in-situ remediation of Cd-contaminated sediment. *J. Clean. Prod.* **2021**, *287*, 125076. [CrossRef]
48. Bashir, S.; Hussain, Q.; Zhu, J.; Fu, Q.L.; Houben, D.; Hu, H.Q. Efficiency of KOH- modified rice straw-derived biochar for reducing cadmium mobility, bioaccessibility and bioavailability risk index in red soil. *Pedosphere* **2020**, *30*, 874–882. [CrossRef]
49. Gondek, K.; Mierzwa-Hersztek, M.; Jarose, R. Effect of willow biochar and fly ash-derived zeolite in immobilizing heavy metals and promoting enzymatic activity in a contaminated sandy soil. *Catena* **2023**, *232*, 107429. [CrossRef]

50. Yang, X.; Wen, E.; Ge, C.; El-Naggar, A.; Yu, H.; Wang, S.S.; Kwon, E.E.; Song, H.; Shaheen, S.M.; Wang, H.L.; et al. Iron-modified phosphorus- and silicon-based biochars exhibited various influences on arsenic, cadmium, and lead accumulation in rice and enzyme activities in a paddy soil. *J. Hazard. Mater.* **2023**, *443*, 130203. [CrossRef]
51. Lentini, M.; Ciriello, M.; Rouphael, Y.; Campana, E.; Vaccari, F.P.; De Pascale, S. Harnessing biochar for sustainable horticulture: Strategies to cope with abiotic stress. *Horticulturae* **2025**, *11*, 73. [CrossRef]
52. Pradhan, S.K.; Singh, N.S.; Kumar, U.; Mishra, S.; Perumal, R.C.; Benny, J.; Thatoi, H. Illumina MiSeq based assessment of bacterial community structure and diversity along the heavy metal concentration gradient in Sukinda chromite mine area soils. *India Ecol. Genet. Genom.* **2020**, *15*, 100054. [CrossRef]
53. Narendrula-Kotha, R.; Nkongolo, K. Bacterial and fungal community structure and diversity in a mining region under long-term metal exposure revealed by metagenomics sequencing. *Ecol. Genet. Genom.* **2017**, *2*, 13–24. [CrossRef]
54. Ibrahim, M.M.; Tong, C.X.; Hu, K.; Zhou, B.Q.; Xing, S.H.; Mao, Y.L. Biochar-fertilizer interaction modifies N-sorption, enzyme activities and microbial functional abundance regulating nitrogen retention in rhizosphere soil. *Sci. Total Environ.* **2020**, *739*, 140065. [CrossRef] [PubMed]
55. Yang, W.H.; Li, C.J.; Wang, S.S.; Zhou, B.Q.; Mao, Y.L.; Rensing, C.; Xing, S.H. Influence of biochar and biochar-based fertilizer on yield, quality of tea and microbial community in an acid tea orchard soil. *Appl. Soil Ecol.* **2021**, *166*, 104005. [CrossRef]
56. Wu, S.J.; Zhou, Z.J.; Zhu, L.; Zhong, L.M.; Dong, Y.X.; Wang, G.J.; Shi, K.X. Cd immobilization mechanisms in a *Pseudomonas* strain and its application in soil cd remediation. *J. Hazard. Mater.* **2022**, *425*, 127919. [CrossRef]
57. Wang, P.; Cao, J.; Mao, L.; Zhu, L.; Zhang, Y.; Zhang, L.; Jiang, H.; Zheng, Y.; Liu, X. Effect of H_3PO_4-modified biochar on the fate of atrazine and remediation of bacterial community in atrazine-contaminated soil. *Sci. Total Environ.* **2022**, *851*, 158278. [CrossRef]

horticulturae

MDPI

Article

Genome-Wide Identification and Characterization of Trehalose-6-Phosphate Synthase/Phosphatases Gene Family in Petunia and Their Expression Profiling Under Abiotic Stresses

Renwei Huang [1], Daofeng Liu [2], Gonzalo H. Villarino [3] and Neil S. Mattson [3,*]

[1] Sichuan Provincial Key Laboratory for Development and Utilization of Characteristic Horticultural Biological Resources, College of Chemistry and Life Sciences, Chengdu Normal University, Chengdu 611130, China; swuhrw@126.com

[2] Key Laboratory of Agricultural Biosafety and Green Production of Upper Yangtze River (Ministry of Education), Chongqing Engineering Research Center for Floriculture, College of Horticulture and Landscape Architecture, Southwest University, Chongqing 400715, China; liu19830222@swu.edu.cn

[3] School of Integrative Plant Science, Cornell University, Ithaca, NY 14853, USA; ghv8@cornell.edu

* Correspondence: nsm47@cornell.edu

Abstract: Trehalose is a nonreducing disaccharide critical for cellular integrity and stress adaptation in plants, and its synthesis relies on trehalose-6-phosphate synthase (TPS) and trehalose-6-phosphate phosphatase (TPP). Despite their established roles in abiotic stress responses across model plants, these gene families remain underexplored in ornamental species like *Petunia hybrida*. Here, *TPS* and *TPP* genes in two wild petunia progenitors, *P. axillaris* and *P. inflata*, underwent a genome-wide analysis, with 10 *TPS* and 8–9 *TPP* genes being identified in each species. According to phylogenetic analysis, petunia TPS proteins cluster into two clades, while TPP proteins were classified into three clades, showing closer evolutionary ties to tomato homologs. *Cis*-acting elements profiling identified hormone- and stress-responsive regulatory elements (e.g., ABRE, TC-rich repeats). Expression analysis under drought, heat, and salt stress revealed dynamic temporal regulation. For instance, *PaTPS4*/*PaTPS9* were early responders (peak at 6 h) under drought and salt stress, while *PaTPS8* exhibited sustained upregulation during salt treatment. Heat stress uniquely suppressed *PaTPS1*,*2* and *PaTPP1*, contrasting with broad upregulation of other members. Notably, *PaTPP3* displayed delayed induction under heat. These findings underscore the functional diversity within *TPS*/*TPP* families, with specific members governing stress-specific responses. This study provides a foundational resource for leveraging these genes to enhance stress resilience and ornamental value in petunia.

Keywords: petunia; trehalose-6-phosphate synthase/phosphatases; gene family; expression profiling; abiotic stresses

1. Introduction

Trehalose is a nonreducing disaccharide encompassing two glucose units linked by α,α-1,1-glycosidic bonds [1], and exists in bacteria, yeast, fungi, insects, invertebrates, and both lower and higher plants [2]. Trehalose excels in maintaining cellular integrity in a variety of organisms, especially in plant growth and development [3]. Trehalose is linked to plant stress tolerance and helps protect cellular integrity under abiotic stresses (heat, cold, salinity, and drought) [2,4–7]. However, research shall be conducted in the future to examine the role of trehalose (or trehalose-6-phosphate (Tre6P), the precursor of trehalose) in stress regulation, especially in temperature stress.

Trehalose synthesis primarily relies on two essential enzymes: trehalose-6-phosphate synthase (TPS) and trehalose-6-phosphate phosphatase (TPP) [8], typically proceeding in two steps in plants: Firstly, Tre6P, an intermediate product, is formed by TPS. Subsequently, TPP induces Tre6P to be dephosphorylated, generating trehalose [9]. Large gene families take charge of encoding *TPS* and *TPP* in most sequenced higher plants. Specifically, Arabidopsis possesses 11 *TPS* genes (*AtTPS1–AtTPS11*) [10] and 10 *TPP* genes (*AtTPPA–AtTPPJ*) [11]; in comparison, rice possesses 11 *TPS* genes (*OsTPS1–OsTPS11*) and 11 *TPP* genes (*OsTPP1–OsTPP11*) [12,13]. The *TPS* family genes fall into two clades with different structures and biochemical activities. Class I and Class II members contain both TPS and TPP domains; however, Class I *TPSs* encode catalytically active TPS enzymes, Class II *TPSs* have no TPS or TPP enzymatic activity, most of which harbor conserved phosphatase domains [10,13,14]. The *TPP* family genes harbor a specific TPP domain with conserved phosphatase domains, all exhibiting TPP activities [15].

According to previous research, specific groups of *TPS* and *TPP* genes undergo differential regulation under varying abiotic stresses [16]. In detail, their overexpression or mutation can remarkably affect the tolerance to abiotic stress, e.g., *OsTPS1* overexpression makes transgenic rice seedlings more tolerant to low temperature, high salinity, and drought [17], *OsTPP1* overexpression makes transgenic rice more tolerant to salt and low-temperature stresses, while also promoting multiple stress-responsive genes to be expressed [12], and *OsTPP3* overexpression makes plants more sensitive to abscisic acid with corresponding higher tolerance to drought stress [18]. In Arabidopsis, the *Attppi* mutant is sensitive to low-temperature stress, whereas overexpressing plants exhibit tolerance [19]. Moreover, *AtTPPF* and *AtTPPI* coordinate the response to drought, while the overexpression of *AtTPPD* enhances tolerance to salt [20]. Recently, research has elucidated that the Tre6P signaling pathway is of significant importance for regulating soluble sugar metabolism and coordinating plant stress responses. For example, *OsTPP1* enhances sugar accumulation in panicles by inhibiting trehalose-6-phosphate (Tre6P) accumulation and promoting the expression of sugar transporter genes. Under low-temperature stress, these accumulated sugars ensure proper pollen development, ultimately improving cold tolerance in rice during the booting stage [21].

Petunia hybrid, a widely used ornamental plant in the Solanaceae family, is prized for its vibrant flowers, diverse colors, shapes, and ease of cultivation, making it a popular choice in gardens and landscaping [22,23]. *P. hybrid* also serves as an important model organism in scientific research, particularly in plant genetics, flower development, and pigment biosynthesis [24]. Significant progress has been made in the areas of flower organ development and color regulation in petunia [25,26]. In contrast, research on stress resistance genes in petunia has been less advanced. Identifying key genes responsible for stress resistance in petunia can crucially enhance their stress tolerance and ornamental value in landscaping [24]. Despite the effect of *TPS* and *TPP* genes on plant species' growth, development, and stress responses as evidenced in existing studies, their function in petunia has not been comprehensively analyzed. Additionally, current studies have not well explored their participation in environmental stress responses. The commercial *P. hybrida* is derived from crossbreeding between *P. axillaris* and species within the *P. integrifolia* clade [24]. Researchers have sequenced the whole genome of *P. axillaris* and *P. inflata* [24], providing an opportunity to analyze the *TPS* and *TPP* gene families in petunia under stress conditions.

The *TPS* and *TPP* genes in two petunia genomes underwent a genome-wide investigation herein, with relevant phylogeny, gene structures, conserved motifs, and *cis*-acting elements being examined, and expression patterns in abiotic stress conditions being analyzed in detail. All these assist in deeply comprehending the critical roles of the two

gene families in petunia growth, development, and stress responses, defining directions for future research.

2. Materials and Methods

2.1. TPS and TPP Gene Identification in Petunia

We downloaded the Arabidopsis TPS and TPP protein sequences from the Arabidopsis Information Resource (TAIR) database (http://www.rosaceae.org/, accessed on 9 June 2021). The genomic data regarding *P. axillaris* and *P. inflata* were publicly accessible at the Sol Genomics Network (SGN) (https://solgenomics.net/organism/Solanum_lycopersicum/genome, accessed on 27 July 2022). The Genome Database for *P. axillaris* and *P. inflata* was subjected to a BLASTP search using Arabidopsis TPS or TPP proteins as query sequences. The NCBI Conserved Domains (CD) search tools (http://www.ncbi.nlm.nih.gov/Structure/cdd/wrpsb.cgi, accessed on 5 May 2022) and the SMART program (http://smart.embl-heidelberg.de/, accessed on 20 January 2022) served to confirm each candidate *TPS* and *TPS* equence as a member of the *TPS* and *TPP* family [27]. Analysis was conducted on the physicochemical properties of TPS and TPP proteins, such as their physical locations, molecular weights (MW), and theoretical isoelectric points (pI) by virtue of the online ProtParam tool (http://web.expasy.org/protparam/, accessed on 11 August 2022). Subcellular localization prediction proceeded via the Plant-mPloc server (http://www.csbio.sjtu.edu.cn/bioinf/plant-multi/, accessed on 10 May 2022).

2.2. Phylogenetic Analysis of TPS and TPP Genes

We downloaded rice and tomato TPS and TPP protein sequences from NCBI (http://www.ncbi.nlm.nih.gov/, accessed on 10 May 2022) and the SGN (https://solgenomics.net/organism/Solanum_lycopersicum/genome, accessed on 31 May 2012), respectively, with relevant full-length amino acid (AA) sequences being compared via Clustal W with default parameters [28]. The neighbor-joining method assisted in phylogenetic analysis by virtue of MEGA version 11.0 (http://www.megasoftware.net/, accessed on 12 February 2023), followed by the calculation of the bootstrap value after 1000 iterations. The last step was the visualization of the ML tree under the aid of iTOL version 6.9 (https://itol.embl.de/, accessed on 5 July 2024) [29].

2.3. Gene Structure and Conserved Motif Analysis of TPS and TPP Genes

Utilizing the GFF file, we analyzed *TPS* and *TPP* genes' exon-intron structure by virtue of the Gene Structure Display Server (GSDS) version 2.0 (https://gsds.cgrpoee.top/, accessed on 21 March 2022) [30]. Conserved motifs in TPS and TPP protein sequences were identified through MEME Suite version 5.5.0 (https://meme-suite.org/meme/index.html, accessed on 20 March 2022) [31], with a maximum of 10 motifs, motif widths of 6–200 AAs, and a screening threshold of $E < 1 \times 10^{-10}$. Visualization was conducted on their gene structure and conserved motifs using TBtools version 2.056 [32].

2.4. Cis-Element Analysis

The study extracted the 2000 bp region upstream of each *TPS* and *TPP* gene as the putative promoter sequence. PlantCARE (http://bioinformatics.psb.ugent.be/webtools/plantcare/html/, accessed on 2 April 2022) was adopted for the prediction of *Cis*-acting elements [33], which were visualized with TBtools.

2.5. Plant Materials, Growth Conditions, and Stress Treatment

Plants of petunia, 'Mitchell Diploid' (a doubled haploid from *P. axillaris* and *P. hybrid* cv. 'Rose of Heaven'), were grown in pots (10 cm (diameter) $\times$ 9 cm (height)) with Cornell mix

and sand mixed in a ratio of 3:1. The growing conditions included a day/night temperature of 25/15 °C, 14 h photoperiod, and the presence of supplemental lights (Cornell University in Ithaca, NY, USA). With plants growing to 15–20 cm tall, experimenters selected uniform plants to conduct various stress treatments. Plants in the heat stress treatment were exposed to 42 °C for 3 days. Plants in the drought stress treatment were deprived of water for 3 days. When conducting the salt stress treatment, experimenters watered each pot with 300 mM NaCl for 3 days. Each treatment was repeated five times (n = 5) in a completely randomized design. Experimenters collected leaf samples at 0, 3, 6, 12, 24, 48, and 72 h following stress treatment. All the samples, after being frozen in liquid nitrogen, were preserved at −80 °C for subsequent analysis.

2.6. Total RNA Extraction and qRT-PCR Analysis

Experimenters ground petunia leaves in liquid nitrogen to a fine powder and extracted total RNA with the RNeasy Plant Mini Kit (Qiagen, Hilden, Germany). After RQ1 DNase treatment (Promega, Madison, WI, USA), total RNA was measured in terms of the quality and quantity by virtue of an Agilent 2100 Bioanalyzer (Agilent, Santa Clara, CA, USA), followed by agarose gel electrophoresis to ascertain the RNA integrity. Subsequently, the High-Capacity cDNA Reverse Transcription Kit (Applied Biosystems, Foster, CA, USA) was employed for reverse-transcribing equal amounts of total RNA for each sample into cDNA. Table S1 lists the gene-specific primers for expression analysis. 15 μL reactions underwent three rounds of real-time PCR using 7.5 μL of SYBR Green Supermix (Bio-Rad, Hercules, CA, USA), 0.75 μL of each primer (500 nM), 5.4 μL water, and 0.6 μL cDNA template, together with the negative controls without templates. PCR was carried out using an Icycler iQ5 (BioRad, Hercules, CA, USA) real-time system machine, as per the manufacturer's protocol. The ddCT method was used for data analysis by using the iQ5 2.0 software (Bio-Rad, Hercules, CA, USA) [34]. The *Actin* gene of petunia was used to calculate the relative transcript abundance. All quantitative PCRs specific to each gene adopted three biological replicates, and each experiment had three technical replicates.

2.7. Data Analysis

Data analysis relied on SPSS 20.0 (SPSS, Chicago, IL, USA), with data presented in the format of mean ± standard deviation (SD). Significant differences between treatments were assessed via one-way ANOVA coupled with Tukey's test ($p \leq 0.05$), which were illustrated by bar charts (Origin 2019, OriginLab Corporation, Northampton, MA, USA).

3. Results

3.1. Identification and Physicochemical Property Analysis of TPS and TPP Genes in Petunia

With the sequences of the Arabidopsis TPS and TPP proteins, we carried out local BLAST (version 2.12.0) analysis utilizing genome data of *P. axillaris* and *P. inflata*, and confirmed 10 *TPS* genes in both *P. axillaris* and *P. inflata*, designated as PaTPS1-10 and PiTPS1-10, respectively (Table 1). Among these TPS proteins, PiTPS1 and PiTPS9 were the shortest and longest proteins with 848 and 1028 AAs, respectively. The petunia TPS proteins had a pI of 5.58–7.19 and a MW of 96.23–116.45 kDa. According to the subcellular localization predictions, most TPS proteins were in the cytoplasm, while some were in the nucleus. Additionally, we identified 8 *TPP* genes in *P. axillaris*, named PaTPP1-8, and 9 *TPP* genes in *P. inflata*, named PiTPP1-9 (Table 2). Among these TPP proteins, PiTPP2 was the shortest with 276 AAs, while PiTPP5 was the longest with 414 AAs. The petunia TPP proteins had a pI of 6.04–9.65 and an MW of 31.47–46.45 kDa. According to subcellular localization predictions, most TPP proteins were found in the cytoplasm, while some were in the mitochondria, chloroplasts, or nucleus.

Table 1. Physicochemical properties of TPS proteins in the petunia genome.

Gene Name	Locus_ID	Position			Length (AA)	MW (Da)	pI	Subcellular Localization
		Scaffold Location	Start	End				
PaTPS1	*Peaxi162Scf00229g00096.1*	Peaxi162Scf00229	917,477	925,133	851	96.93	5.58	Cytoplasmic
PaTPS2	*Peaxi162Scf00469g00632.1*	Peaxi162Scf00469	667,063	671,245	871	98.92	5.72	Nuclear
PaTPS3	*Peaxi162Scf00202g00187.1*	Peaxi162Scf00202	1,815,219	1,819,743	855	96.39	5.70	Cytoplasmic
PaTPS4	*Peaxi162Scf00170g01223.1*	Peaxi162Scf00170	1,214,499	1,220,448	864	97.52	5.78	Cytoplasmic
PaTPS5	*Peaxi162Scf00275g00085.1*	Peaxi162Scf00275	813,026	816,592	856	97.16	5.66	Cytoplasmic
PaTPS6	*Peaxi162Scf00421g00116.1*	Peaxi162Scf00421	104,373	107,349	851	96.23	5.91	Cytoplasmic
PaTPS7	*Peaxi162Scf00297g00098.1*	Peaxi162Scf00297	982,826	985,666	863	97.97	6.01	Cytoplasmic
PaTPS8	*Peaxi162Scf00457g00215.1*	Peaxi162Scf00457	252,951	255,711	865	98.05	5.96	Cytoplasmic
PaTPS9	*Peaxi162Scf00022g02413.1*	Peaxi162Scf00022	2,390,346	2,421,693	975	110.65	6.03	Cytoplasmic
PaTPS10	*Peaxi162Scf00111g01324.1*	Peaxi162Scf00111	1,308,982	1,320,265	927	104.39	6.29	Cytoplasmic
PiTPS1	*Peinf101Scf00275g03007.1*	Peinf101Scf00275	406,279	412,631	848	96.55	5.67	Cytoplasmic
PiTPS2	*Peinf101Scf00442g03004.1*	Peinf101Scf00442	320,610	324,681	852	96.75	5.77	Nuclear
PiTPS3	*Peinf101Scf00994g03007.1*	Peinf101Scf00994	331,522	336,139	855	96.37	5.65	Cytoplasmic
PiTPS4	*Peinf101Scf01033g01017.1*	Peinf101Scf01033	150,487	155,519	864	97.51	5.78	Cytoplasmic
PiTPS5	*Peinf101Scf01456g02005.1*	Peinf101Scf01456g	225,034	228,660	856	97.16	5.66	Cytoplasmic
PiTPS6	*Peinf101Scf01436g11018.1*	Peinf101Scf01436	1,108,249	1,111,224	851	96.25	5.91	Cytoplasmic
PiTPS7	*Peinf101Scf00586g01015.1*	Peinf101Scf00586	115,175	118,018	868	98.67	6.01	Cytoplasmic
PiTPS8	*Peinf101Scf01850g03027.1*	Peinf101Scf01850	402,667	405,426	865	97.92	5.99	Cytoplasmic
PiTPS9	*Peinf101Scf00304g01004.1*	Peinf101Scf00304	68,073	93,541	1028	116.45	7.19	Cytoplasmic
PiTPS10	*Peinf101Scf00665g07025.1*	Peinf101Scf00665	722,849	733,623	927	104.39	6.29	Cytoplasmic

Table 2. Physicochemical properties of TPP proteins in the petunia genome.

Gene Name	Locus_ID	Position			Length (AA)	MW (Da)	pI	Subcellular Localization
		Scaffold Location	Start	End				
PaTPP1	*Peaxi162Scf00904g00003.1*	Peaxi162Scf00904	81,668	83,679	341	38.06	6.04	Cytoplasmic
PaTPP2	*Peaxi162Scf00711g00011.1*	Peaxi162Scf00711	115,934	118,338	276	31.56	6.62	Cytoplasmic
PaTPP3	*Peaxi162Scf00241g00319.1*	Peaxi162Scf00241	378,645	381,161	384	42.76	6.72	Chloroplast
PaTPP4	*Peaxi162Scf00002g00816.1*	Peaxi162Scf00002	860,185	862,872	391	44.18	7.66	Mitochondrial
PaTPP5	*Peaxi162Scf00041g00810.1*	Peaxi162Scf00041	797,885	799,770	357	40.06	9.13	Chloroplast
PaTPP6	*Peaxi162Scf00838g00003.1*	Peaxi162Scf00838	86,470	89,698	387	43.66	9.4	Chloroplast
PaTPP7	*Peaxi162Scf00295g00075.1*	Peaxi162Scf00295	757,573	761,478	316	35.94	9.65	Mitochondrial
PaTPP8	*Peaxi162Scf00295g00510.1*	Peaxi162Scf00295	578,702	582,229	376	42.29	9.22	Chloroplast
PiTPP1	*Peinf101Scf01632g02002.1*	Peinf101Scf01632	229,134	231,134	341	38.03	6.04	Cytoplasmic
PiTPP2	*Peinf101Scf03315g00014.1*	Peinf101Scf03315	71,337	73,493	276	31.47	6.41	Cytoplasmic
PiTPP3	*Peinf101Scf03555g01022.1*	Peinf101Scf03555	91,639	94,062	384	42.73	6.72	Chloroplast
PiTPP4	*Peinf101Scf00674g06014.1*	Peinf1011Scf00674	660,658	663,175	385	43.56	7.66	Mitochondrial
PiTPP5	*Peinf101Scf00173g02008.1*	Peinf1011Scf00173	222,878	225,001	414	46.45	9.15	Cytoplasmic
PiTPP6	*Peinf101Scf00966g00008.1*	Peinf101Scf00966	73,267	76,165	402	45.63	9.51	Mitochondrial
PiTPP7	*Peinf101Scf01178g05006.1*	Peinf101Scf01178	522,267	525,309	375	42.50	9.18	Nuclear
PiTPP8	*Peinf101Scf01178g06005.1*	Peinf101Scf01178	666,203	669,510	379	42.76	9.01	Nuclear
PiTPP9	*Peinf101Scf07373g00001.1*	Peinf101Scf07373	3	2454	362	40.58	6.12	Chloroplast

3.2. Phylogenetic Analysis of TPS and TPP Family Genes in Petunia

To reveal the evolutionary relationships between the petunia TPS and TPP families and those of other plant species, we built a phylogenetic tree by utilizing 64 TPS proteins and 56 TPP proteins from four model plants, including Arabidopsis, rice, tomato, and Populus (Figure 1).

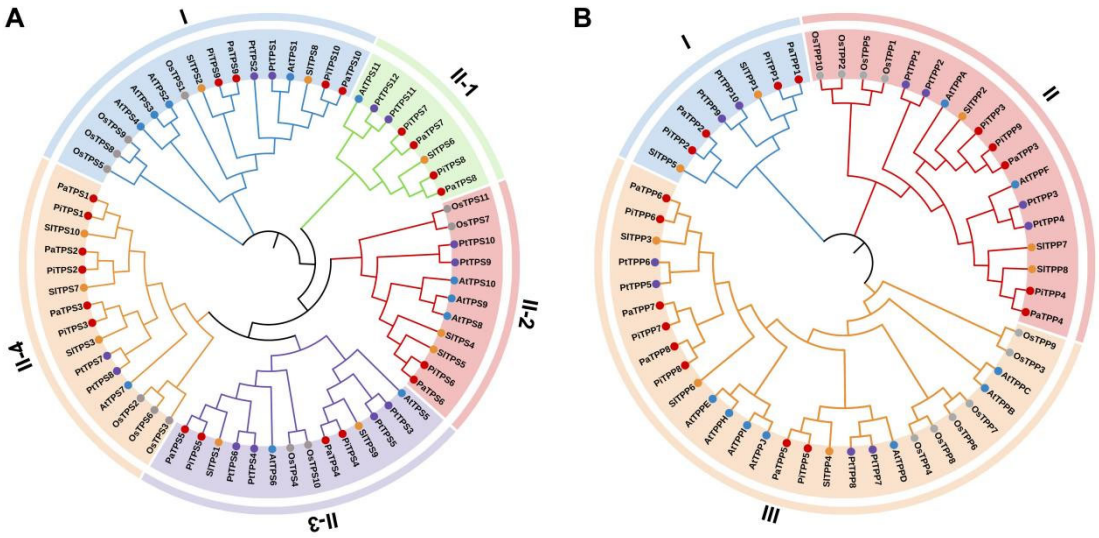

Figure 1. Phylogenetic analysis of *TPS* (**A**) and *TPP* (**B**) gene families in *P. inflata*, *P. axillaris*, *Arabidopsis thaliana*, *Oryza sativa*, *Populus trichocarpa*, and *Solanum lycopersicum*. Protein subfamilies are highlighted in distinct colors. The red, blue, orange, purple, and gray circles represent *P. inflata* (Pi) and *P. axillaris* (Pa), *A. thaliana* (At), *S. lycopersicum* (Sl), *P. trichocarpa* (Pt), and *O. sativa* (Os), respectively.

Considering the phylogenetic relationship in Arabidopsis, researchers classify the petunia TPS family into Clade I and Clade II (Figure 1A). Among these TPS proteins, PaTPS1-8 and PiTPS1-8 belong to Clade II, while PaTPS9-10 and PiTPS9-10 are placed in Clade I. Clade II is subsequently divided into four subgroups: Clade II-1 (PaTPS7-8 and PiTPS7-8), Clade II-2 (PaTPS6 and PiTPS6), Clade II-3 (PaTPS4-5 and PiTPS4-5), and Clade II-4 (PaTPS1-3 and PiTPS1-3). Comparative analysis reveals that most petunia TPS proteins are intensely associated with those of tomato, another member of the Solanaceae family, indicating a closer evolutionary relationship. The petunia TPP family is divided into three clades: Clade I, Clade II, and Clade III (Figure 1B). Among these TPP proteins, PaTPP1-2 and PiTPP1-2 are placed in Clade I, PaTPP3-4 and PiTPP3-4, 9 in Clade II, and PaTPP5-8 and PiTPP5-8 in Clade III. Similar to the TPS proteins, most petunia TPP proteins also show a closer genetic relationship to those of tomato.

3.3. Gene Structure and Conserved Motif Analysis of TPSs and TPPs

The TPS and TPP families were deeply investigated in terms of their inherent structures (Figure 2). According to gene structure analysis, the two subgroups exhibited remarkably different genetic structure of TPS members, with Class I genes having more exons and more complex gene structures than Class II genes (Figure 2A). Among the Class I *TPS* genes, *Pa/PiTPP9* has 19 exons, *Pa/PiTPP10* has 17 exons, while all Class II *TPS* genes contain 3 exons. Comparatively, the TPP subgroups have a slightly varied number of exons (Figure 2B). Class I *TPP* genes consistently have 8 exons, while in Class II, all *TPP* genes except *PiTPP9*, which contains 12 exons, have 11 exons. Among Class III *TPP* genes, *PaTPP5* and *PaTPP7* contain 8 exons, *PiTPP5* contains 9 exons, and the remaining genes consist of 8 exons.

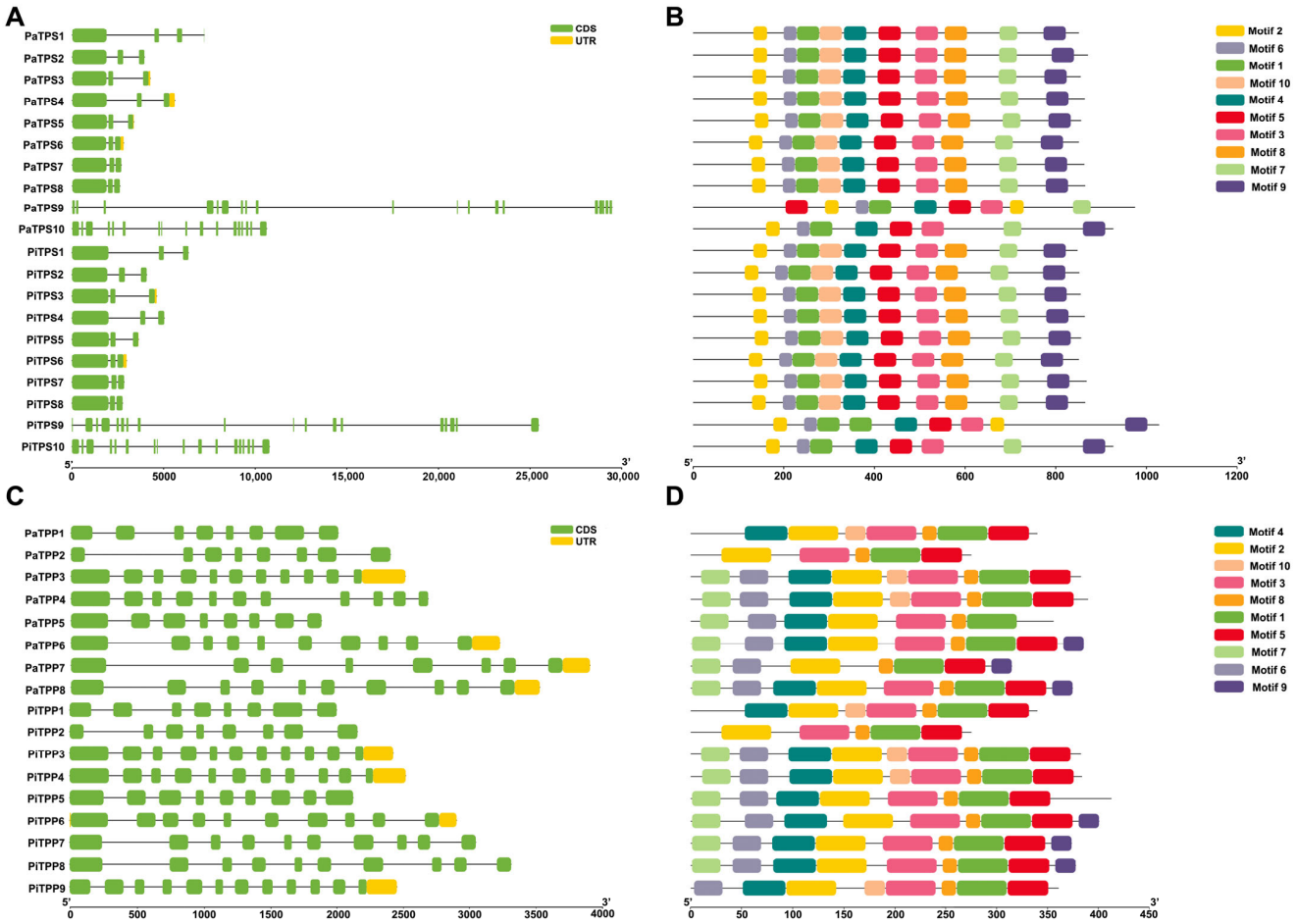

Figure 2. Gene structure and protein motif of the *TPS* and *TPP* genes in petunia. Gene structure of (**A**) *TPS* genes and (**C**) *TPP* genes. Conserved motif of (**B**) TPS proteins and (**D**) TPP proteins.

To investigate the evolutionary conservation and diversification patterns among TPS and TPP proteins, we conducted systematic motif identification across all family members using the MEME Suite version 5.5.0. Conservative motif analysis confirmed 10 conserved motifs, Motif 1 to Motif 10 (Figure 2B and Table S2). All TPS proteins contain motifs 1 through 10, except for PaTPS9,10 and PiTPS9,10 (Figure 2B). Among them, PaTPS9 lacks motifs 8, 9, and 10, PiTPS9 lacks motifs 7, 8, and 10, and Pa/PiTPS10 lack motifs 8 and 10. Motifs 1, 2, 3, 4, 5, 6, 8, and 10 constitute the TPS domain (Glyco_transf_20). Motifs 7 and 9 compose the TPP domain (HAD-like domain). Compared to TPS proteins, TPP proteins exhibit fewer motifs, with Pa/PiTPP2 having the least number of motifs (5) (Figure 2B). All TPP proteins contain motifs 1, 2, 3, 5, and 8. Motif 4 is absent only in Pa/PiTPP2, motif 6 is absent only in PaTPS1,2 and PiTPS1,2, motif 7 is present only in PaTPP3-8 and PiTPP3-8, motif 9 is present only in PaTPP6-8 and PiTPP6-8, and motif 10 is present only in PaTPP1,3,4,9 and PiTPP1,3,4,9. Motifs 1, 2, 3, 4, 5, and 6 together constitute the Trehalose_PPase domain.

3.4. Cis-Acting Elements Analysis of TPSs and TPPs

Cis-acting elements were analyzed for a better understanding of their regulatory mechanisms against the *TPS* and *TPP* gene expression in petunia (Figure 3, Table S3). In the *TPS* genes, most of the *cis*-acting elements regulate plants' hormone responses and stress responses, which include hormone-responsive elements of abscisic acid (ABRE), auxin (AuxRR-core and TGA-element), gibberellin (GARE-motif, P-box, and TATC-box), methyl jasmonate (CGTCA-motif and TGACG-motif), and salicylic acid (TCA-element), as well

as stress-associated elements like anaerobic induction (ARE), defense and stress responsiveness (TC-rich repeats), light response (C-box, G-box, GT1-motif, ect), low-temperature responsiveness (LTR). In the *TPP* genes, the *cis*-acting elements also affect plants' hormone responses and stress responses, with the most abundant category also related to light responses, similar to the *TPS* genes.

Figure 3. *Cis*-elements in the promoter regions of the *TPS* (**A**) and *TPP* (**B**) genes in petunia.

3.5. TPSs and TPPs Expression Pattern Analysis Under Different Stresses

The two genome sequences were compared with transcriptomics data from three unrelated *P. hybrida* lines—'Mitchell Diploid', 'R27', and 'R143', confirming the slim contribution of the *P. inflata* parent to the *P. hybrida* gene space [23]. With the objective of elucidating the expression patterns pertaining to petunia *TPS* and *TPP* family members during abiotic

stress, including heat, salt, and drought stress in petunia 'Mitchell Diploid', we designed the primers according to the *TPS* and *TPP* genes in *P. axillaris* for real-time PCR analysis (Figures 4–6). Given that primer design was exclusively based on *P. axillaris TPS*/*TPP* gene sequences, we retained the prefix 'Pa' for all expression analysis targets.

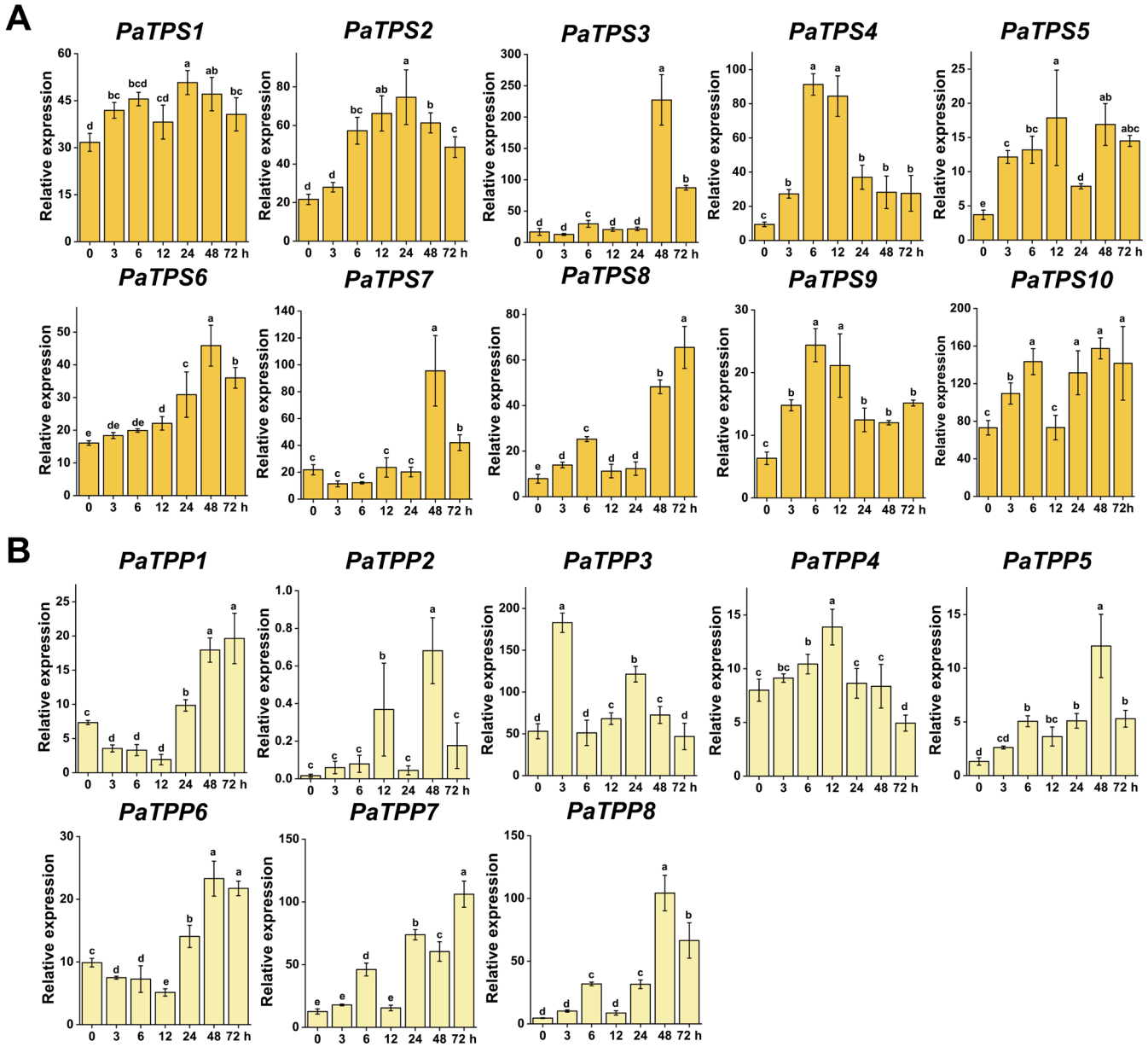

Figure 4. Expression patterns of *TPS* (**A**) and *TPP* (**B**) genes under drought stress in petunia. Letters above the bars represent significant differences ($p < 0.05$).

3.5.1. Drought Stress

In the *PaTPS* genes, all genes except *PaTPS1* showed upregulation in expression levels under drought treatment. Among them, *PaTPS4* and *PaTPS9* reached their peak expression at 6 h, *PaTPS5* at 12 h, *PaTPS2* at 24 h, and others at 48 or 72 h, indicative of their relatively similar expression pattern (Figure 4A). In the *PaTPP* genes, all genes showed upregulated expression. Among them, *PaTPP3* reached its peak expression at 3 h, *PaTPP4* at 12 h, and others at 48 or 72 h, displaying a similar expression pattern (Figure 4B).

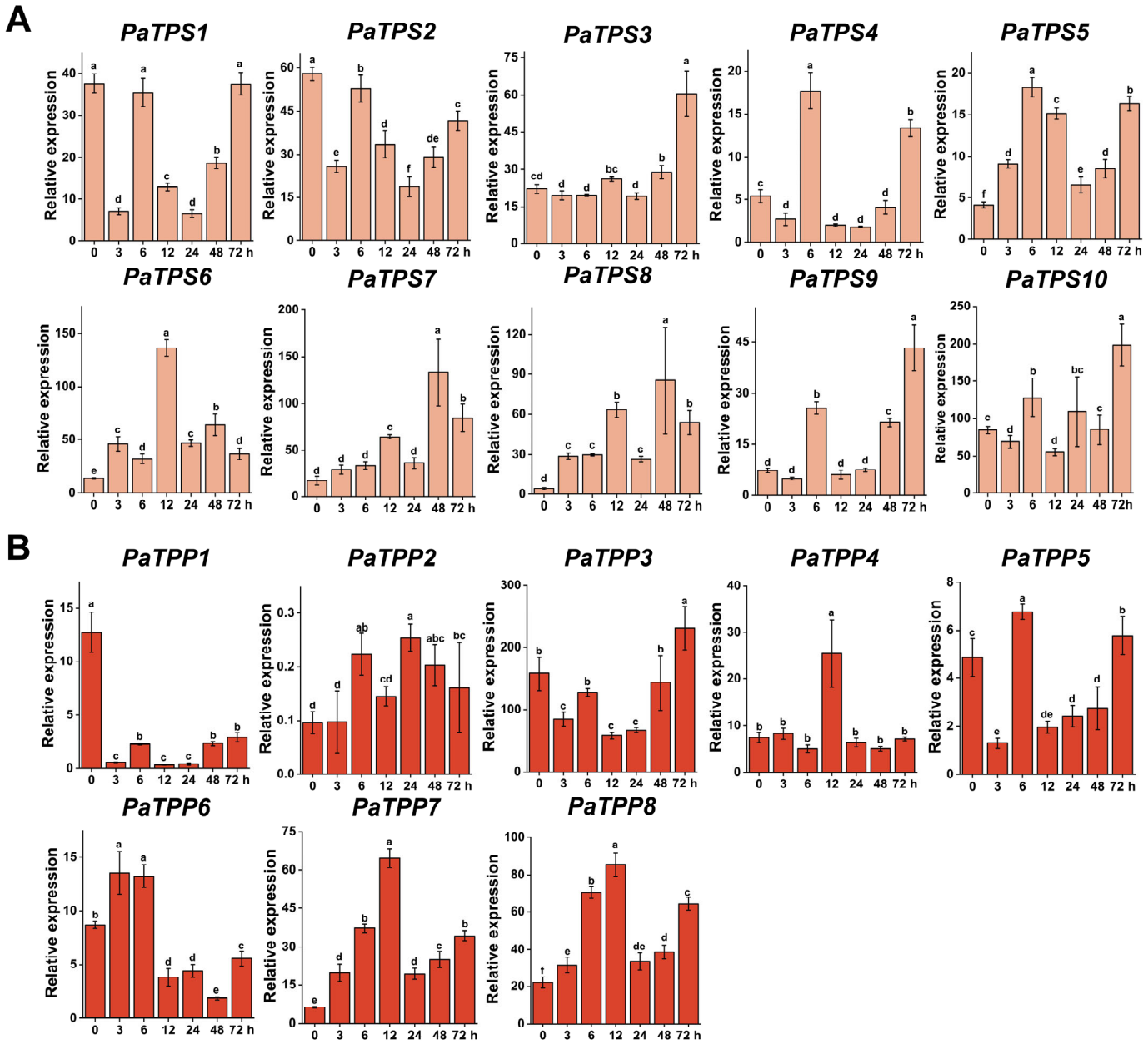

Figure 5. Expression patterns of *TPS* (**A**) and *TPP* (**B**) genes under heat stress in petunia. Letters above the bars represent significant differences ($p < 0.05$).

3.5.2. Heat Stress

In the *PaTPS* genes, *PaTPS1-2* showed downregulated expression under high-temperature treatment, while the other genes were also upregulated. Among the upregulated genes, *PaTPS4* and *PaTPS5* reached their peak expression at 6 h, *PaTPS6* at 12 h, and *PaTPS3*, *PaTPS7-10* at 48 or 72 h (Figure 5A). In the *PaTPP* genes, except for *PaTPP1*, which showed downregulation, all other *PaTPP* genes exhibited upregulation under high-temperature treatment. Among the upregulated genes, all except *PaTPP3* reached their peak expression within 24 h, with *PaTPP3* peaking at 72 h (Figure 5B).

3.5.3. Salt Stress

In the *PaTPS* genes, except for *PaTPS1*, all other *PaTPS* genes presented significantly upregulated expression under salt treatment. Among them, *PaTPS2*, *PaTPS4-5*, and *PaTPS9* reached their peak expression at 6 h, *PaTPS6* and *PaTPS10* at 12 h, and *PaTPS3* and *PaTPS7* at 24 h. Notably, *PaTPS8* reached its peak expression at 3 h and remained highly expressed

throughout the treatment (Figure 6A). In the *PaTPP* genes, the expression of *PaTPP1* and *PaTPP5* showed no significant change, while *PaTPP3* was significantly downregulated. The expression level of *PaTPP6* was significantly downregulated at 6h, and then displayed transient upregulation at 12h, followed by a return to initial levels at 24 h, 48 h, and 72 h. The remaining genes exhibited significant upregulation, with *PaTPP7-8* reaching their peak expression at 3 h, and *PaTPP2* and *PaTPP4* at 12 h (Figure 6B).

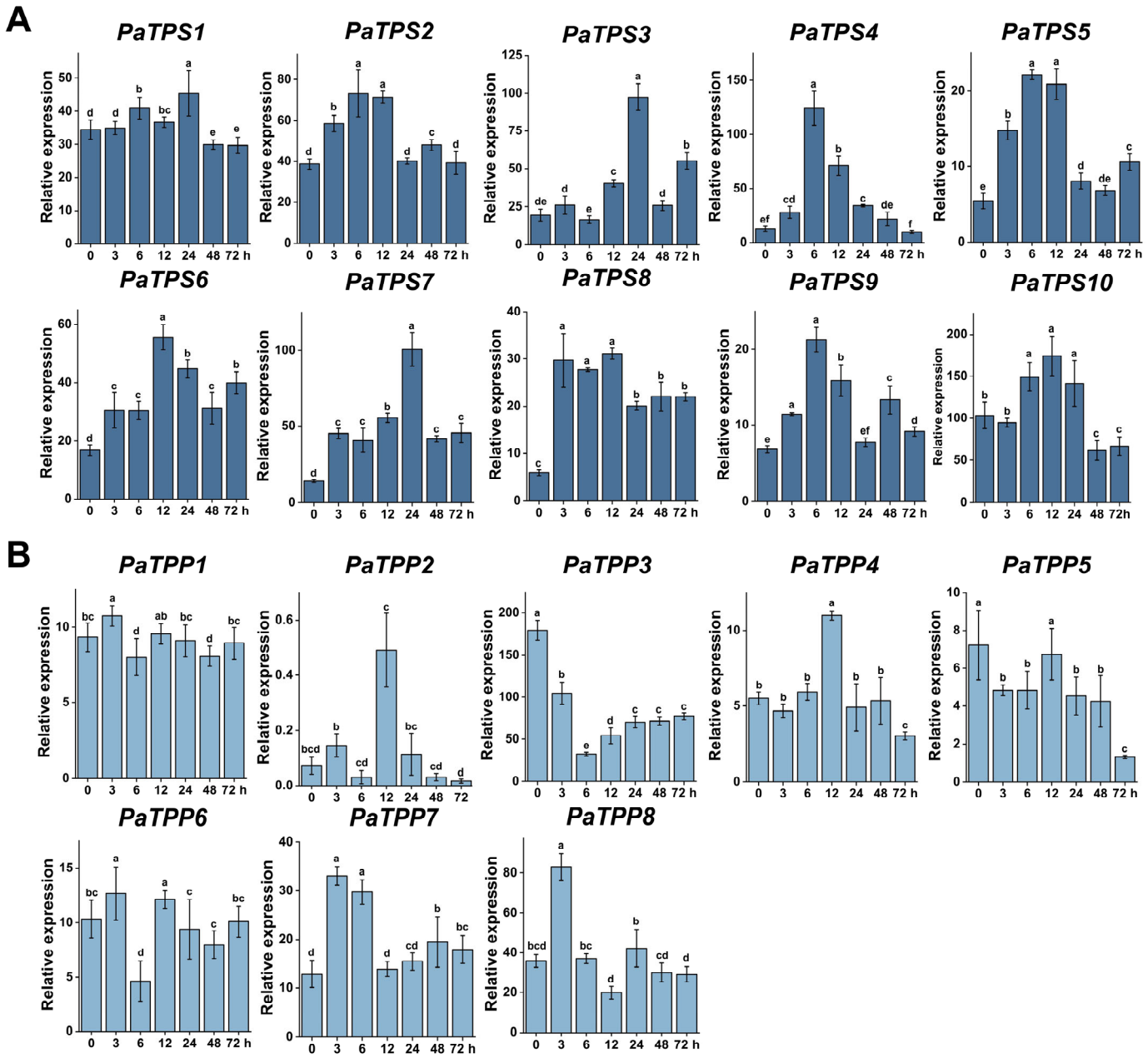

Figure 6. Expression patterns of *TPS* (**A**) and *TPP* (**B**) genes under salt stress in petunia. Letters above the bars represent significant differences ($p < 0.05$).

4. Discussion

Trehalose metabolism, mediated by TPS and TPP, pivotally affects plant growth, development, and stress responses [35,36]. *TPS* and *TPP* family genes can crucially regulate trehalose synthesis, and the relevant transcription and expression undergo differential regulation under varying abiotic stresses [16]. Extensive research has paid attention to the *TPS* and *TPP* gene family in Arabidopsis [10,11], rice [13,15], wheat [37,38], tomato [39],

and peanut [40], etc., after the whole genome sequencing. However, these gene families remain underexplored in ornamental species, such as petunia. Therefore, the *TPS* and *TPP* genes in two petunia genomes are subjected to comprehensive genome-wide analysis in the study, shedding light on their evolutionary relationships, structural features, and stress-responsive expression patterns.

The study identified 10 *PaTPS* genes and 8 *PaTPP* genes in the *P. axillaris* genome, and 10 *PiTPS* genes and 9 *PiTPP* genes in the *P. inflata* genome. Phylogenetic analysis classified petunia TPS proteins into two clades and TPP proteins into three clades, consistent with patterns observed in Arabidopsis and rice, etc. [10,11,13,15]. The close evolutionary relationship between petunia and tomato TPS/TPP proteins suggests conserved functional mechanisms within the Solanaceae family [41]. The diversity of exons and introns greatly affects the way gene families evolve [42]. Analyzing the structure of genes can help elucidate their functions [43]. Notably, Class I *TPS* genes (e.g., *Pa/PiTPS9-10*) exhibited more complex gene structures (17–19 exons) compared to Class II genes (3 exons), reflecting potential functional specialization. Similarly, *TPP* genes displayed clade-specific structural variations, with Class III genes (e.g., *Pa/PiTPP5*) showing fewer exons, possibly linked to functional divergence. Conserved motif analysis further underscored functional diversification. While most TPS proteins retained all 10 motifs, Pa/PiTPS9-10 lacked two key motifs, suggesting potential functional redundancy or neofunctionalization. In contrast, TPP proteins exhibited fewer motifs, with Pa/PiTPP2 having the least, indicating lineage-specific evolutionary pressures. These structural variations likely trigger the functional specialization of TPS and TPP proteins in stress responses.

We analyzed the promoter *cis*-acting elements and expression patterns with regard to the *TPS* and *TPP* gene families under varying stress conditions, confirming their crucial function in petunia growth and development, hormone regulation, and stress responses. *Cis*-acting element analysis elucidates the regulation of *TPS* and *TPP* genes by hormone-responsive (e.g., ABRE, AuxRR-core) and stress-related elements (e.g., TC-rich repeats, LTR), implicating their roles in abiotic stress signaling. The abundance of light-responsive elements suggests additional roles in photomorphogenesis, consistent with trehalose's involvement in carbon metabolism and energy homeostasis [44]. These regulatory features provide a molecular basis for the stress-responsive expression patterns observed in this study. Regulating *TPS* and *TPP* genes strengthens plants' tolerance to abiotic stress [12,17–20]. Our expression analysis under drought, heat, and salt stresses revealed dynamic and stress-specific regulation of these gene families. In drought stress conditions, most *TPS* and *TPP* genes were upregulated, with *PaTPS4/9* and *PaTPP3* emerging as early responders. This rapid induction likely facilitates osmotic adjustment and cellular protection, consistent with trehalose's role in stabilizing membranes and proteins under water deficit [45,46]. Heat stress uniquely suppressed *PaTPS1-2* and *PaTPP1*, while upregulating other members, such as *PaTPS4-5/9* and *PaTPP3*. The delayed induction of *PaTPP3* (peak at 72 h) suggests a specialized role in long-term thermotolerance, possibly through trehalose-mediated protein stabilization or reactive oxygen species (ROS) scavenging [47,48]. Salt stress triggered significant upregulation of *TPS* genes, with *PaTPS8* showing sustained high expression, indicating its potential role in ion homeostasis and Na^+ compartmentalization. In contrast, the downregulation of *PaTPP3/6* under salt stress may reflect a regulatory mechanism to maintain T6P levels for signaling while limiting trehalose accumulation, which could otherwise impose a metabolic burden [49,50]. While this study delineates the expression dynamics of *TPS/TPP* genes under controlled abiotic stresses, future studies are suggested to perform functional validation by virtue of CRISPR/Cas9-mediated gene editing or overexpression approaches, aiming at interpreting their exact mechanisms in stress adaptation.

Supplementary Materials: The following supporting information can be downloaded at: https://www.mdpi.com/article/10.3390/horticulturae11060695/s1, Table S1: Real-time PCR primers for *TPS* and *TPS* genes in petunia; Table S2: List of the conserved motifs of TPS and TPP proteins in petunia; Table S3: List of the *cis*-acting elements of *TPS* and *TPP* genes in petunia.

Author Contributions: Conceptualization, N.S.M. and D.L.; formal analysis, R.H. and D.L.; investigation, D.L.; writing-original draft preparation, D.L. and R.H.; writing-review and editing, R.H., G.H.V. and N.S.M.; visualization, R.H. and D.L.; supervision, project administration, and funding acquisition, N.S.M. All authors have read and agreed to the published version of the manuscript.

Funding: This work was supported under Accession Number 7005941 by the Cornell University Agricultural Experiment Station (Hatch/Multistate funds) received from the National Institute of Food and Agriculture (NIFA), U.S. Department of Agriculture (USDA). Any opinions, findings, conclusions, or suggestions in this publication are those of the authors and do not always represent the view of the USDA. The APC was funded by the High-Level Talent Introduction Program of Chengdu Normal University (YJRC2020-22) and the Sichuan Science and Technology Program (2023JDRC0114).

Data Availability Statement: All data that support this research result are available in the article and within its Supplementary Materials published online.

Conflicts of Interest: The authors declare no conflict of interest.

References

1. Paul, M.; Pellny, T.; Goddijn, O. Enhancing photosynthesis with sugar signals. *Trends Plant Sci.* **2001**, *6*, 197–200. [CrossRef] [PubMed]
2. Elbein, A.D.; Pan, Y.; Pastuszak, I.; Carroll, D. New insights on trehalose: A multifunctional molecule. *Glycobiology* **2003**, *13*, 17R–27R. [CrossRef] [PubMed]
3. O'Hara, L.E.; Paul, M.J.; Wingler, A. How do sugars regulate plant growth and development? New insight into the role of trehalose-6-phosphate. *Mol. Plant* **2013**, *6*, 261–274. [CrossRef]
4. Fernandez, O.; Bethencourt, L.; Quero, A.; Sangwan, R.S.; Clement, C. Trehalose and plant stress responses: Friend or foe? *Trends Plant Sci.* **2010**, *15*, 409–417. [CrossRef]
5. Kosar, F.; Akram, N.A.; Sadiq, M.; Al-Qurainy, F.; Ashraf, M. Trehalose: A key organic osmolyte effectively involved in plant abiotic stress tolerance. *J. Plant Growth Regul.* **2019**, *38*, 606–618. [CrossRef]
6. Villarino, G.H.; Bombarely, A.; Giovannoni, J.J.; Scanlon, M.J.; Mattson, N.S. Transcriptomic analysis of *Petunia hybrida* in response to salt stress using high throughput RNA sequencing. *PLoS ONE* **2014**, *9*, e94651. [CrossRef]
7. Villarino, G.; Hu, Q.W.; Scanlon, M.; Mueller, L.A.; Bombarely, A.; Mattson, N.S. Dissecting tissue-specific transcriptomic responses from leaf and roots under salt stress in *Petunia hybrida* Mitchell. *Genes* **2017**, *8*, 195. [CrossRef]
8. Smeekens, S. From leaf to kernel: Trehalose-6-phosphate signaling moves carbon in the field. *Plant Physiol.* **2015**, *169*, 912–913. [CrossRef]
9. Avonce, N.; Mendoza-Vargas, A.; Morett, E.; Iturriaga, G. Insights on the evolution of trehalose biosynthesis. *BMC Evol. Biol.* **2006**, *6*, 109. [CrossRef]
10. Vandesteene, L.; Ramon, M.; Roy, K.L.; Dijck, P.V.; Rolland, F. A single active trehalose-6-P synthase (TPS) and a family of putative regulatory TPS-like proteins in *Arabidopsis*. *Mol. Plant* **2010**, *3*, 406–419. [CrossRef]
11. Vandesteene, L.; Lopez-Galvis, L.; Vanneste, K.; Feil, R.; Maere, S.; Lammens, W. Expansive evolution of the trehalose-6-phosphate phosphatase gene family in Arabidopsis. *Plant Physiol.* **2012**, *160*, 884–896. [CrossRef] [PubMed]
12. Ge, L.F.; Chao, D.Y.; Shi, M.; Zhu, M.Z.; Gao, J.P.; Lin, H.X. Overexpression of the trehalose-6-phosphate phosphatase gene *OsTPP1* confers stress tolerance in rice and results in the activation of stress responsive genes. *Planta* **2008**, *228*, 191–201. [CrossRef] [PubMed]
13. Zang, B.; Li, H.; Li, W.; Deng, X.W.; Wang, X. Analysis of trehalose-6-phosphate synthase (TPS) gene family suggests the formation of TPS complexes in rice. *Plant Mol. Biol.* **2011**, *76*, 507–522. [CrossRef]
14. Dijck, P.V. The cytophaga hutchinsonii chtpsp: First characterized bifunctional TPS-TPP protein as putative ancestor of all eukaryotic trehalose biosynthesis proteins. *Mol. Biol. Evol.* **2010**, *27*, 359–369.
15. Shima, S.; Matsui, H.; Tahara, Y.; Imai, R. Biochemical characterization of rice trehalose-6-phosphate phosphatases supports distinctive functions of these plant enzymes. *FEBS J.* **2007**, *274*, 1192–1201. [CrossRef]
16. Iordachescu, M.; Imai, R. Trehalose biosynthesis in response to abiotic stresses. *J. Integr. Plant Biol.* **2008**, *50*, 1223–1229. [CrossRef]

17. Li, H.W.; Zang, B.S.; Deng, X.W.; Wang, X.P. Overexpression of the trehalose-6-phosphate synthase gene *OsTPS1* enhances abiotic stress tolerance in rice. *Planta* **2011**, *234*, 1007–1018. [CrossRef]
18. Jiang, D.; Chen, W.; Gao, J.; Yang, F.; Zhuang, C. Overexpression of the trehalose-6-phosphate phosphatase *OsTPP3* increases drought tolerance in rice. *Plant Biotechnol. Rep.* **2019**, *13*, 285–292. [CrossRef]
19. Lin, Q.; Wang, S.; Dao, Y.; Wang, J.; Wang, K. The Arabidopsis thaliana trehalose-6-phosphate phosphatase gene *AtTPP1* enhances drought tolerance by regulating stomatal apertures. *J. Exp. Bot.* **2020**, *71*, 1795–1807. [CrossRef]
20. Lin, Q.; Yang, J.; Wang, Q.; Zhu, H.; Chen, Z.; Dao, Y.; Wang, K. Overexpression of the trehalose-6-phosphate phosphatase family gene *AtTPPF* improves the drought tolerance of *Arabidopsis thaliana*. *BMC Plant Biol.* **2019**, *19*, 381. [CrossRef]
21. Li, J.; Guo, H.F.; Lou, Q.J.; Zeng, Y.W.; Guo, Z.H.; Xu, P.H.; Gu, Y.; Gao, S.; Xu, B.; Han, S.; et al. Natural variation of indels in the *CTB3* promoter confers cold tolerance in *japonica* rice. *Nat. Commun.* **2025**, *16*, 1613. [CrossRef] [PubMed]
22. Cao, Z.; Guo, Y.F.; Yang, Q.; He, Y.H.; Fetouh, M.I.; Warner, R.M.; Deng, Z. Genome-wide identification of quantitative trait loci for important plant and flower traits in petunia using a high-density linkage map and an interspecific recombinant inbred population derived from *Petunia integrifolia* and *P. axillaris*. *Hortic. Res.* **2019**, *6*, 27. [CrossRef] [PubMed]
23. Zentella, R.; Mascorro-Gallardo, J.O.; Van Dijck, P.; Folch-Mallol, J.; Bonini, B.; Van Vaeck, C.; Gaxiola, R.; Covarrubias, A.A.; Nieto-Sotelo, J.; Thevelein, J.M.; et al. A Selaginella lepidophylla trehalose-6-phosphate synthase complements growth and stress-tolerance defects in a yeast tps1 mutant. *Plant Physiol.* **1999**, *119*, 1473–1482. [CrossRef]
24. Bombarely, A.; Moser, M.; Amrad, A.; Bao, M.; Bapaume, L.; Barry, C.S.; Bliek, M.; Boersma, M.R.; Borghi, L.; Bruggmann, R.; et al. Insight into the evolution of the Solanaceae from the parental genomes of *Petunia hybrida*. *Nat. Plants* **2016**, *2*, 16074. [CrossRef]
25. Berardi, A.E.; Korinna, E.; Lea, J.; Therese, M.; Cannarozzi, G.M.; Cris, K. Complex evolution of novel red floral color in petunia. *Plant Cell* **2021**, *33*, 2273–2295. [CrossRef]
26. Patrick, R.M.; Xing-Qi, H.; Natalia, D.; Ying, L. Dynamic histone acetylation in floral volatile synthesis and emission in petunia flowers. *J. Exp. Bot.* **2021**, *72*, 3704–3718. [CrossRef]
27. Thompson, J.D.; Gibson, T.J.; Higgins, D.G. Multiple sequence alignment using ClustalW and ClustalX. *Curr. Protoc. Bioinform.* **2003**, *2*, 2–3. [CrossRef]
28. Lu, S.; Wang, J.; Chitsaz, F.; Derbyshire, M.K.; Geer, R.C.; Gonzales, N.R.; Gwadz, M.; Hurwitz, D.I.; Marchler, G.H.; Song, J.S.; et al. CDD/SPARCLE: The conserved domain database in 2020. *Nucleic Acids Res.* **2020**, *48*, 265–268. [CrossRef]
29. Ivica, L.; Peer, B. Interactive tree of life (iTOL) v6: Recent updates to the phylogenetic tree display and annotation tool. *Nucleic Acids Res.* **2024**, *52*, W78–W82.
30. Hu, B.; Jin, J.; Guo, A.-Y.; Zhang, H.; Luo, J.; Gao, G. GSDS 2.0: An upgraded gene feature visualization server. *Bioinformatics* **2015**, *31*, 1296–1297.
31. Bailey, T.L.; Boden, M.; Buske, F.A.; Frith, M.; Grant, C.E.; Clementi, L.; Ren, J.; Li, W.W.; Noble, W.S. MEME Suite: Tools for motif discovery and searching. *Nucleic Acids Res.* **2009**, *37*, W202–W208. [CrossRef] [PubMed]
32. Chen, C.; Chen, H.; Zhang, Y.; Thomas, H.R.; Frank, M.H.; He, Y.; Xia, R. TBtools: An integrative toolkit developed for interactive analyses of big biological data. *Mol. Plant* **2020**, *13*, 1194–1202. [CrossRef] [PubMed]
33. Lescot, M.; Déhais, P.; Thijs, G.; Marchal, K.; Moreau, Y.; Peer, Y.V.D.; Rouzé, P.; Rombauts, S. PlantCARE, a database of plant *cis*-acting regulatory elements and a portal to tools for in silico analysis of promoter sequences. *Nucleic Acids Res.* **2002**, *30*, 325–327. [CrossRef]
34. Livak, K.L.; Schmittgen, T.D. Analysis of relative gene expression data using real-time quantitative PCR and the 2(-Delta Delta C(T)) Method. *Methods* **2001**, *25*, 402–408. [CrossRef]
35. Sarkar, A.K.; Sadhukhan, S. Imperative role of trehalose metabolism and trehalose-6-phosphate signaling on salt stress responses in plants. *Physiol. Plant.* **2022**, *174*, e13647. [CrossRef]
36. Fichtner, F.; Lunn, J.E. The role of trehalose 6-phosphate (tre6p) in plant metabolism and development. *Annu. Rev. Plant Biol.* **2021**, *72*, 737–760. [CrossRef]
37. Zhao, L.; Zhao, X.; Francis, F.; Liu, Y. Genome-wide identification and characterization of the TPS gene family in wheat (*Triticum aestivum* L.) and expression analysis in response to aphid damage. *Acta Physiol. Plant.* **2021**, *43*, 64. [CrossRef]
38. Du, L.; Li, S.; Ding, L.; Cheng, X.; Kang, Z.; Mao, H. Genome-wide analysis of trehalose-6-phosphate phosphatases (TPP) gene family in wheat indicates their roles in plant development and stress response. *BMC Plant Biol.* **2022**, *22*, 120. [CrossRef]
39. Mollavali, M.; Börnke, F. Characterization of trehalose-6-phosphate synthase and trehalose-6-phosphate phosphatase genes of tomato (*Solanum lycopersicum* L.) and analysis of their differential expression in response to temperature. *Int. J. Mol. Sci.* **2022**, *23*, 11436. [CrossRef]
40. Zhong, C.; He, Z.; Liu, Y.; Li, Z.; Wang, X.; Jiang, C.; Kang, S.; Liu, X.; Zhao, S.; Wang, J.; et al. Genome-wide identification of *TPS* and *TPP* genes in cultivated peanut (*Arachis hypogaea*) and functional characterization of *AtTPS9* in response to cold stress. *Front. Plant Sci.* **2024**, *14*, 1343402. [CrossRef]
41. Doganlar, S.; Frary, A.; Daunay, M.C.; Lester, R.N.; Tanksley, S.D. Conservation of gene function in the solanaceae as revealed by comparative mapping of domestication traits in eggplant. *Genetics* **2002**, *161*, 1713–1726. [CrossRef] [PubMed]

42. Qi, L.; Chen, L.; Wang, C.; Zhang, S.; Yang, Y.; Liu, J.; Li, D.; Song, J.; Wang, R. Characterization of the auxin efflux transporter PIN proteins in pear. *Plants* **2020**, *9*, 349. [CrossRef] [PubMed]
43. Li, Y.; Chen, D.; Luo, S.; Zhu, Y.; Jia, X.; Duan, Y.; Zhou, M. Intron-mediated regulation of β-tubulin genes expression affects the sensitivity to carbendazim in *Fusarium graminearum*. *Curr. Genet.* **2019**, *65*, 1057–1069. [CrossRef]
44. Paul, M.J.; Primavesi, L.F.; Jhurreea, D.; Zhang, Y. Trehalose metabolism and signaling. *Annu. Rev. Plant Biol.* **2008**, *59*, 417–441. [CrossRef]
45. Jain, N.K.; Roy, I. Effect of trehalose on protein structure. *Protein Sci.* **2010**, *18*, 24–36. [CrossRef]
46. Sadak, M.S.; El-Bassiouny, H.M.S.; Dawood, M.G. Role of trehalose on antioxidant defense system and some osmolytes of quinoa plants under water deficit. *Bull. Natl. Res. Cent.* **2019**, *43*, 5. [CrossRef]
47. Yang, Y.; Yao, Y.; Li, J.; Zhang, J.; Zhang, X.; Hu, L.; Ding, D.; Bakpa, E.P.; Xie, J. Trehalose alleviated salt stress in tomato by regulating ros metabolism, photosynthesis, osmolyte synthesis, and trehalose metabolic pathways. *Front. Plant Sci.* **2022**, *13*, 772948. [CrossRef]
48. Nawaz, M.; Hassan, M.U.; Chattha, M.U.; Mahmood, A.; Shah, A.N.; Hashem, M.; Alamri, S.; Batool, M.; Rasheed, A.; Thabit, M.A.; et al. Trehalose: A promising osmo-protectant against salinity stress-physiological and molecular mechanisms and future prospective. *Mol. Biol. Rep.* **2022**, *49*, 11255–11271. [CrossRef]
49. Schluepmann, H.; Berke, L.; Sanchez-Perez, G.F. Metabolism control over growth: A case for trehalose-6-phosphate in plants. *J. Exp. Bot.* **2012**, *63*, 3379–3390. [CrossRef]
50. Paul, M. Trehalose 6-phosphate. *Curr. Opin. Plant Biol.* **2007**, *3*, 303–309. [CrossRef]

horticulturae

MDPI

Article

Expression Analysis of the ABF Gene Family in *Actinidia chinensis* Under Drought Stress and the Response Mechanism to Abscisic Acid

Haoyu Wang [1,†], Yinqiang Zi [1,†], Xu Rong [2,†], Qian Zhang [3], Lili Nie [3], Jie Wang [1], Hailin Ren [1], Hanyao Zhang [1,*] and Xiaozhen Liu [3,*]

[1] Key Laboratory for Forest Resources Conservation and Utilization in the Southwest Mountains of China, Ministry of Education, Southwest Forestry University, Kunming 650224, China; whyyx@swfu.edu.cn (H.W.); ziyinqiang@swfu.edu.cn (Y.Z.); wangjie1201@swfu.edu.cn (J.W.); 2113676876@swfu.edu.cn (H.R.)
[2] School of Chemical, Biological and Environmental, Yuxi Normal University, Yuxi 653100, China; xurong@yxnu.edu.cn
[3] Key Laboratory of Biodiversity Conservation in Southwest China, National Forest and Grassland Administration, Southwest Forestry University, Kunming 650224, China; 871970420@swfu.edu.cn (Q.Z.); nielily@swfu.edu.cn (L.N.)
* Correspondence: zhanghanyao@swfu.edu.cn (H.Z.); 15198729095@swfu.edu.cn (X.L.)
† These authors contributed equally to this work.

Abstract

Drought can limit plant growth. The ABRE binding factor (ABF) gene family is extensively involved in multifarious bioregulatory processes in plants. However, kiwifruit has not yet been systematically analyzed. This study analyzed the response of kiwifruit *AcABF* genes to drought stress. Eleven *AcABF* genes were distributed on nine chromosomes and clustered into three subfamilies with *Arabidopsis AtABF* genes, *AcABF2*, *AcABF3*, *AcABF8*, *AcABF9*, and *AcABF10*, which have drought resistance functions, and *AtABF1*, *AtABF2*, *AtABF3*, and *AtABF4* were clustered in Group I. The structural domains of the nine *ABF* genes in Group I were highly conserved, and the protein structures were highly similar. In the analysis of the five *AcABF* genes in Group I, all of their cis-acting elements were related to ABA, the content of ABA-like hormones was significantly increased after drought stress, and most of the GO (Gene Ontology) and KEGG (Kyoto Encyclopedia of Genes and Genomes) enrichment results were related to hormonal processes. A total of six *AcABF* genes were upregulated under drought stress. qRT-PCR was performed to validate the *AcABF* genes of Group I. The correlation coefficients of the results with the transcriptome data were all above 0.70, and the expression level of ABA increased under drought treatment. These results indicated that the five *AcABF* genes were positively correlated with ABA under drought stress and that, by synthesizing ABA and facilitating the expression of *ABF* gene family members, the tolerance of kiwifruit increased. These results provide a solid foundation for further research on improving drought tolerance in kiwifruit.

Keywords: drought; *Actinidia chinensis*; *ABF* gene; ABA; qRT-PCR

1. Introduction

Actinidia chinensis is an edible berry that originated in China [1]. Various vitamins, minerals, amino acids, and other metabolites are believed to be beneficial to human health [2]. More than 90% of the world's kiwifruit is exported from New Zealand and Chile, with Italy exporting approximately 75% [3]. Kiwifruit has become one of the most popular

fruits worldwide. 'Hongyang' kiwifruit, also known as red kiwifruit/red heart kiwifruit, is characterized by a medium to the skin color is darker color; short cylindrical fruits with greenish-brown, hairless skin; a very high sugar–acid ratio; and abundant anthocyanins. It has been widely cultivated for its high economic value [4,5].

Drought is a widespread environmental stress in the environment that severely hampers the growth and development of crops. Under drought stress, plant foliage will fall, curl, and wither, and stems will also bend, resulting in slow plant growth [6,7] and even a decrease in yield and quality, especially for major food crops such as wheat and corn, which are the main limiting factors for global food security and crop productivity [8,9]. Kiwifruit is relatively sensitive to arid environments, and many kiwifruit planting areas, including China, often experience drought stress [10]. Drought stress is one of the most important abiotic stresses affecting kiwifruit growth, development, and yield [11]. Plant drought stress includes moderate drought (40–45% of field water holding capacity) and severe drought (25–30% of field water holding capacity) [12]. The most obvious impact of drought stress on plants is through accelerating the transpiration rate, reducing photosynthesis, severely damaging the photosynthetic apparatus, reducing seed germination, and decreasing nutrient absorption [13,14]. To cope with survival and adversity pressures, plants must utilize a series of physiological and biochemical processes to adapt to environmental stresses. These processes are mediated through the activation or inhibition of gene-specific expression [15].

ABA (abscisic acid) is a plant hormone that accumulates under drought-induced osmotic stress conditions and plays a vital role in stress response and tolerance [16,17]. During plant growth, endogenous ABA content increase with unfavorable environmental conditions; for instance, salt stress bring about an increase in ABA concentration, prompting the activation of the ABA signaling pathway to alter downstream response of gene expression in salt-stressed environments [18,19]. It also promotes seed dormancy, inhibits seed germination, promotes stomatal closure, regulates root development, promotes tissue abscission, and defends against abiotic stressors such as drought, osmotic, and salt stress [20]. ABA signaling modulates the accumulation of other adaptive responses, such as osmoprotectants and antioxidants, in plants, further increasing their tolerance to drought [21].

The *b*ZIP (basic region/leucine zipper motif) gene family has a large variety, percentage, and number of members [22]. Plant *b*ZIP transcription factors are involved in the regulation of processes including but not limited to defense against pathogens, light and stress signaling, and seed and flower growth and development [23]. TFs (transcription factors) constitute one of the gene-specific expression pathways that not only interact with cis-acting elements but also activate or repress the specific expression of genes related to environmental stresses to maintain normal plant life activities [24]. The *ABF* gene family is a subfamily of ABA response element-binding factors and *b*ZIP transcription factors in plants. The *ABF* gene family plays crucial roles in ABA-dependent and ABA-independent signaling pathways and has a variety of downstream target genes that participate in the growth and development of plants and the response to adversity and stress [25,26]. *ABF* upregulates ABA-regulated genes through binding to ABRE cis-acting elements [27,28]. The *ABF* gene family has been identified in some species through previous studies, and all of these genes can act as crucial ABA signaling pathway transcription factors in response to abiotic stressors, such as salt, drought, and low temperature [29]. For example, BnaABF2 identified in *Arabidopsis* enhances its tolerance to salt and drought via the modulation of ABA-dependent stress signaling genes [30]. Most of the *TaABF* genes identified in wheat are highly expressed and upregulated in various tissues under abiotic stress conditions, such as low nitrogen, low temperature, and drought [31]. Many cis-acting elements have been postulated in the ABF genes identified in three orchids, and ABA (ABRE) and ET (ERE)

motifs were the most enriched among all the *ABF* genes [32]. All ten *SlABF* gene family members identified in tomatoes are responsive to ABA, and *SlABF3* demonstrated peak sensitivity to salt stress and low-temperature stress, with concurrent activation observed in *SlABF5* and *SlABF10* [25]. Eight *CoABF* genes have been detected and characterized in jute; *CoABFs* are widely involved in hormone response elements, and the expression levels of *CoABF3* and *CoABF7* show a positive correlation with ABA concentration under ABA treatment [28]. However, few studies have investigated the changes in the expression profile of the ABF gene family and ABA concentration occurring in kiwifruit under abiotic stress.

This study aimed to comprehensively investigate the members of the *ABF* gene family of *A. chinensis* by identifying them; analyzing their physicochemical properties; performing phylogenetic analysis; determining their gene structures and conserved motifs; performing cis-acting element analysis, chromosomal localization, and GO (Gene Ontology) and KEGG (Kyoto Encyclopedia of Genes and Genomes) enrichment; and analyzing their expression profiles and ABA contents under drought stress. This study lays the groundwork for further understanding ABF gene evolution and function in *A. chinensis*.

2. Materials and Methods

2.1. Plant Material

In this study, *A. chinensis* cv. 'Hongyang' histocultured seedlings in the histocultivation room of Southwest Forestry University were used as research materials. The best-growing tissue culture-generated seedlings were selected for refinement and transplanted into flower pots for cultivation. Finally, kiwifruit seedlings whose growth was similar to that of the subsequent experimental materials were selected [33,34].

2.2. Data Acquisition

The kiwifruit (Hongyang v3) genomic data were downloaded from the Kiwifruit Genome Database (KGB; https://kiwifruitgenome.org/, accessed on 1 May 2024) [35]. The conserved structural domain (PF00170) of the ABF transcription factor family was retrieved from the Pfam database (https://www.ebi.ac.uk/interpro/entry/pfam/?search=PF00170#table, accessed on 1 May 2024) [36]. The protein sequences and genomic data of nine *A. thaliana* ABF gene families were obtained from the *A. thaliana* genome website TAIR (https://www.Arabidopsis.org/, accessed on 1 May 2024) [28]. The genomic data of rice and apple were downloaded from the genome database of rice, JGI (https://riceome.hzau.edu.cn/, accessed on 1 May 2024), and the genome databases of Rosaceae, GDR (https://www.rosaceae.org/, accessed on 1 May 2024), respectively.

2.3. Identification and Physicochemical Properties of the ABF in A. chinensis

Initially, HMMER v3.4 software's hmmsearch tool was employed to identify sequences within the *A. chinensis* genome that harbor conserved structural domains characteristic of the *ABF* gene family (ID: to minimize the risk of false positives, we employed protein sequences with an E value below 1×10^{-20} as a filtering criterion, as detailed in reference [37]). Next, the BLASTP module within the TBtools v2.154 suite was employed to perform a sequence comparison of *A. chinensis* genome-derived protein sequences by aligning them against the reference set of *A. thaliana ABF* gene family proteins. A comprehensive analysis was conducted to compare the protein sequences of *A. chinensis*, which exhibited high similarity (E value < 1×10^{-5}) to those of the *A. thaliana ABF* gene family [38]. The hmmsearch program of the HMMER software was applied to search the protein sequences of the conserved structural domains (ID: PF00170) of the *A. chinensis* genomic protein data. A search for conserved structural domains within the *A. chinensis* protein sequences was conducted using the HMMER-based hmmsearch tool, which was applied to BLAST-identified data.

The proteins whose sequences exhibited an E-value threshold of less than 1×10^{-5} were selected for further analysis. In the final stage, the protein sequences derived from the two preceding processes were integrated to generate a comprehensive profile of the *ABF* gene family in *A. chinensis*. The structural domain of *ABF* was validated through the CDD tool available on NCBI's database (https://www.ncbi.nlm.nih.gov/Structure/cdd/wrpsb.cgi, accessed on 1 May 2024) as part of the NCBI sequence analysis. To isolate the *ABF* gene family members from *A. chinensis*, researchers utilized a method that involved eliminating non-existent or incomplete structural domains within the *ABF* gene. These genes were assigned the designation *AcABF1-AcABF11* based on their chromosomal locations and were subsequently subjected to molecular weight analysis. To analyze the properties of the protein, we will evaluate the number of amino acids present in the sequence, determine the isoelectric point, calculate the stability coefficient, and assess hydrophobicity using the online tool ProtParam (https://web.expasy.org/protparam/, accessed on 1 May 2024).

2.4. Multiple Sequence Alignment, Phylogenetic Analysis, and Three-Dimensional Structure Analysis of Proteins

Initially, 11 *A. chinensis AcABF* gene sequences, which were identified through prior research, were selected for pairwise sequence analysis and subsequent trimming using TBtools v2.154. This process was conducted in conjunction with MEGA11.0 software to refine the dataset [38]. Subsequently, phylogenetic trees were developed using the maximum likelihood (ML) approach with MEGA11.0 software and the IQtree algorithm. In conclusion, the evolutionary tree was constructed using the Chiplot tool (https://www.chiplot.online/, accessed on 1 May 2024), which allows for the visualization and analysis of phylogenetic relationships, and subsequently, the 11 *A. chinensis ABF* genes were classified in accordance with the known gene clustering patterns observed in the *A. thaliana* species.

2.5. Gene Structure and Conserved Motif Analysis

To further analyze the gene structure and composition of the conserved motifs in the *A. chinensis ABF* gene family, the gene structure of each gene was analyzed according to the kiwifruit genome annotation file (GFF3) using TBtools v2.154 software [35]. The conserved motifs contained in the *A. chinensis ABF* genes were also predicted via the online motif prediction tool MEME (https://meme-suite.org/meme/, accessed on 1 May 2024). Visualization was then performed using TBtools software.

2.6. Analysis of Promoter Cis-Acting Elements

Nucleotide sequences 2000 bp upstream of each *A. chinensis ABF* gene were extracted from the *A. chinensis* genome annotation file (GFF3) file using TBtools software and analyzed for promoter cis-acting elements via the online software PlantCARE (https://bioinformatics.psb.ugent.be/webtools/plantcare/html/, (accessed on 1 May 2024) for promoter cis-acting element analysis.

2.7. Chromosome Localization and Covariate Partitioning

The chromosomal positions of *AcABF* genes were mapped using TBtools based on the *A. chinensis* genome annotation (GFF3 file). Subsequently, TBtools was used to extract their genomic features (length, position, and density) and to analyze collinear relationships among *ABF* family members (using the MCSanX plugin v4.1.0). For interspecies collinearity analysis, GFF files and gene sequences of *A. thaliana*, rice (*Oryza sativa*), and apple (*Malus domestica*) were downloaded from TAIR, JGI, and GDR, respectively, and analyzed using TBtools v2.154.

2.8. Transcriptome Sequencing and ABA Content Determination

In this study, 18 kiwifruit seedlings of uniform size were selected as experimental materials. The eighteen kiwifruit seedlings were divided into two groups of nine plants each, of which nine plants were used as the control group, with the soil humidity maintained at 80–85%, and were then divided into three groups numbered CK1, CK2, and CK3; the other nine plants were subjected to drought treatment, where watering was discontinued until the soil humidity reached 40–45% [12], and were subjected to drought stress for 72 h. In addition to the drought treatment, the other nine plants were randomly divided into three groups numbered T1, T2, and T3. Indices such as the plant height and leaf relative water content were observed and recorded for each group. The leaves of each sample were removed, stored in liquid nitrogen, and then transferred to Wuhan Maiwei Metabolism Technology Co., Ltd. (Wuhan, China) for sequencing of the transcriptome and determination of the content of the phytohormone (ABA). After the transcriptome data were obtained, the expression data were standardized to ensure comparability of the expression levels, genes were clustered based on expression patterns, and heatmaps were drawn for visual adjustment. After obtaining the metabolic data, the data were standardized, and *p*-values were obtained using T-TST.

2.9. qRT-PCR Analysis

To further verify the expressions of the *AcABF2*, *AcABF3*, *AcABF5*, *AcABF8*, *AcABF9*, and *AcABF10* genes under drought stress, kiwifruit leaves grown at 80–85% soil moisture were used as the control groups (CK1, CK2, and CK3), and kiwifruit leaves grown under drought stress were used as the treatment groups (T1, T2, and T3). Total RNA from kiwifruit leaves was extracted with the Plant RNA Extraction Kit (DP432) (Tiangen Biochemical Technology (Beijing) Co., Ltd., Beijing, China) and reverse-transcribed into complementary DNA (cDNA) using the FastKing RT Kit (KR116) (Tiangen Biochemical Technology (Beijing) Co., Ltd., Beijing, China). Actin was used as an internal reference gene, and qRT-PCR primers (Table S1) were designed using Primer 6.0. Standard RT-PCR was then performed using a QIAGEN kit, with at least three replicates for each gene. All the data were processed and analyzed using SPASS v21 software. The reaction system was a 10 μL total reaction volume, and the mixture included 5 μL of 2× SYBR Green PCR Master Mix, 0.05 μL of QN ROX Reference Dye (Applied Biosystems instruments only), 0.7 μL of Primer A, 0.7 μL of Primer B, 2.55 μL of RNase-free water, and 1 μL of template gDNA or cDNA. The PCR procedure was as follows: predenaturation at 95 °C for 2 min; denaturation at 95 °C for 5 s; and annealing at 60 °C for 30 s, for a total of 40 cycles. Each gene was subjected to three repeated tests. The ACTIN gene was used as an internal standard, and the quantitative data were analyzed via the $2^{-\Delta\Delta CT}$ method. The primers used for qRT-PCR are listed in Supplementary Table S1.

3. Results

3.1. Identification and Physicochemical Properties of the ABF Gene Family in A. chinensis

On the basis of their positions on the chromosome, 11 *ABF* genes were ultimately identified and named *AcABF1–ACABF11* according to their locations. The aligned *A. thaliana ABF* gene protein sequences were further analyzed with *A. chinensis ABF* protein sequences, and the structures are shown (Figure 1, Table S2). The protein length of each *A. chinensis ABF* gene varied widely, ranging from 50 (*AcABF7*) to 717 (*AcABF6*) amino acids; the molecular weight varied from 10.63 (*AcABF4*) to 81.29 (*AcABF6*) kiloDalton (kDa); the isoelectric point (pI) ranged from 8.42 (*AcABF1*) to 10.96 (*AcABF4*); the instability index ranged from 37.51 (*AcABF7*) to 69.39 (*AcABF10*); and the lipolysis index ranged from 50.20 (*AcABF7*) to 84.81 (*AcABF6*). The physicochemical properties of the *AtABF1*, *AtABF2*,

AtABF3, and *AtABF4* genes in *A. thaliana* and the *AcABF2*, *AcABF3*, *AcABF8*, and *AcABF9* genes in kiwifruit are similar. It can be hypothesized that the *A. thaliana AtABF1*, *AtABF2*, *AtABF3*, and *AtABF4* genes have similar properties to the *A. chinensis AcABF2*, *AcABF3*, *AcABF8*, and *AcABF9* genes.

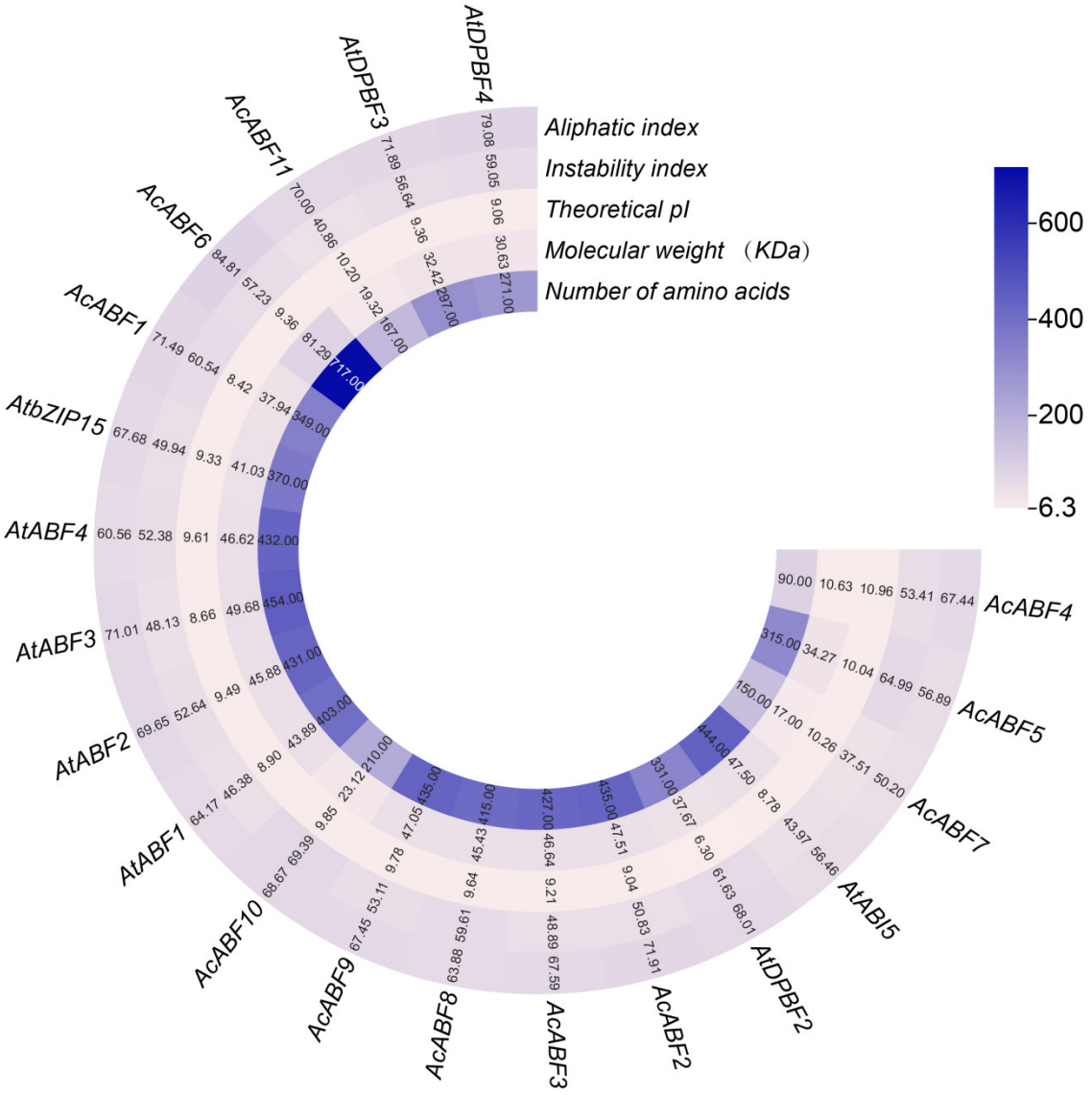

Figure 1. The physicochemical property analysis of the *A. thaliana ABF* genes and the *Actinidia chinensis ABF* genes. The numbers in the heatmap indicate numerical values, with larger values being darker; the outermost circle indicates the name of the gene, followed by the aliphatic index, instability index, theoretical pI, and molecular weight (kDa).

3.2. Phylogenetic Analysis of the ABF Gene Family of A. chinensis

To understand the correlations among the *ABF* genes of different species, the amino acid sequences encoded by 11 *A. chinensis ABF* genes and 9 *A. thaliana ABF* genes were compared to construct a phylogenetic tree. The clustering results (Figure 2a) revealed that according to the three *ABF* subfamilies of *A. thaliana*, the *A. chinensis ABF* genes were also categorized into three subfamilies, and each subfamily included *ABF* genes from both species. According to the gene data of each subfamily, the Group I subfamily had the greatest number of genes (10), in which the number of genes of *A. thaliana* was the same as that of *A. chinensis*, both with five genes; the number of genes in the Group II and Group III subfamilies was the same (both with ten genes), and the number of genes in each

subfamily was the same for both *A. thaliana* and kiwifruit. Kiwifruit also presented the same percentage of genes in each subfamily: three *A. thaliana* genes and two *A. chinensis* genes. Based on Figure 1, correlation analysis revealed that these genes may have similar properties; the *A. thaliana AtABF1*, *AtABF2*, *AtABF3*, and *AtABF4* genes and the *A. chinensis AcABF2*, *AcABF3*, *AcABF8*, *AcABF9*, and *AcABF10* genes clustered together in subfamily I, which increases the possibility that these genes have similar properties. The *A. thaliana AtABF1*, *AtABF2*, *AtABF3*, and *AtABF4* genes have all been shown to function in response to drought via ABA, as revealed in previous studies [39–41]. These findings suggest that *AcABF2*, *AcABF3*, *AcABF8*, *AcABF9*, and *AcABF10* may also have similar functions, such as drought resistance.

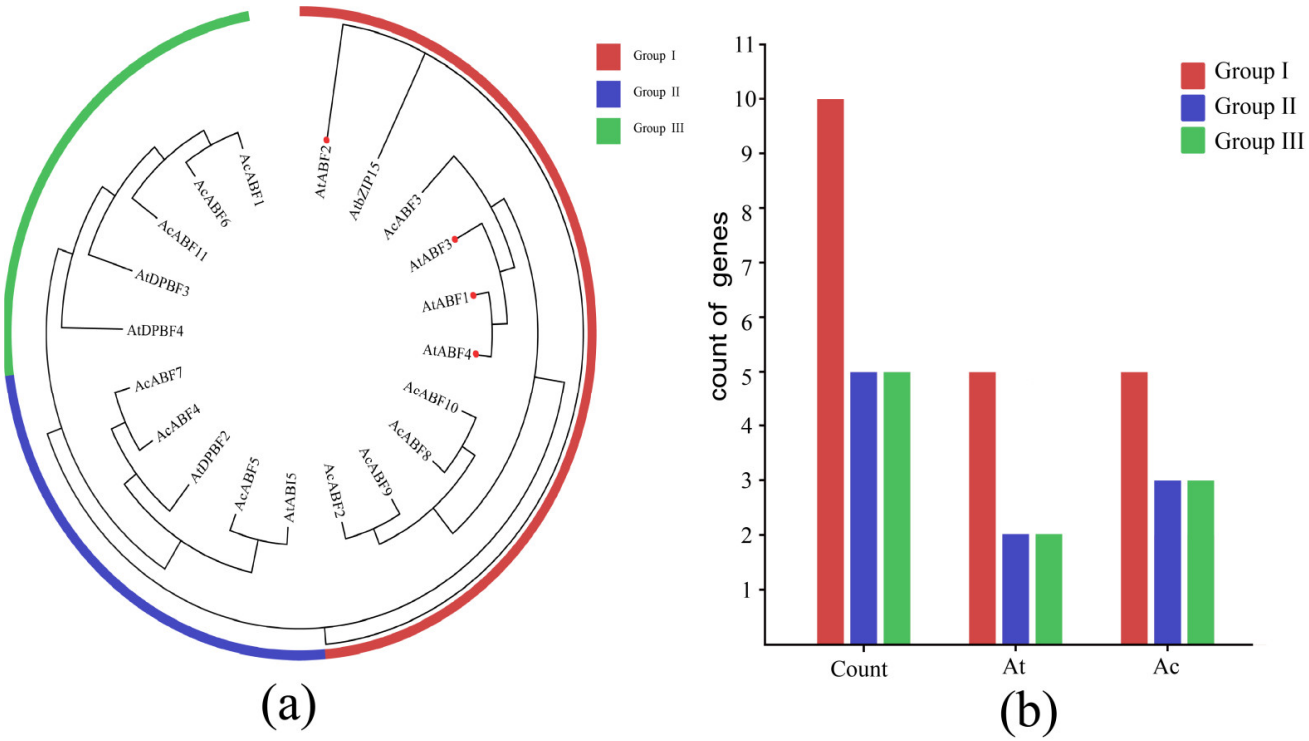

Figure 2. Phylogenetic tree of the *A. thaliana* and *A. chinensis ABF* gene families. (**a**) Phylogenetic tree plot constructed via the maximum likelihood (ML) method using 1000 replicated bootstrap values, with different subgroups denoted by different colors; in the figure, red denotes subfamily I, blue denotes subfamily II, green denotes subfamily III, red dots indicate *AtABF* genes that have been functionally validated. (**b**) Plot of the number of *A. thaliana* and *A. chinensis ABF* genes in each subclade, with light yellow-brown denoting subclade I, blue denoting subclade II, and red denoting subclade III.

Proteins with similar structural sequences have conserved three-dimensional structures, and conserved structural domains in different proteins have conserved functions. The protein tertiary structures of *AtABF1*, *AtABF2*, *AtABF4*, *AtABF3*, *AcABF2*, *AcABF3*, *AcABF8*, *AcABF9*, and *AcABF10* were constructed using SWISS-Model 2022 software. The results (Figure 3) revealed that the protein structures of the *ABF* genes of clade I were highly similar, having α-helix consistency over 70% with very close ratios of α-helices, β-folds, elongated strands, and free curls. These findings suggest that the structural domains of subclass I *ABF* proteins from *A. thaliana* and kiwifruit are similar and have conserved functions.

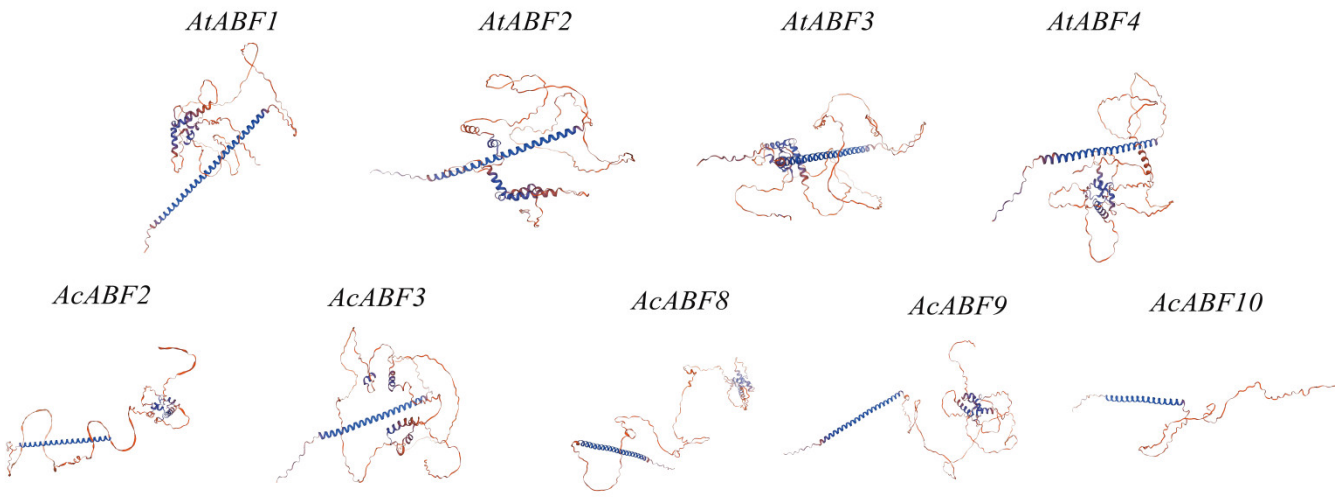

Figure 3. Protein tertiary structure diagrams of *AtABF1*, *AtABF2*, *AtABF3*, *AtABF4*, *AcABF2*, *AcABF3*, *AcABF8*, *AcABF9*, and *AcABF10*. The upper row represents the protein tertiary structure diagrams of *A. thaliana AtABF1*, *AtABF2*, *AtABF4*, and *AtABF3*; the lower row represents the protein tertiary structure diagrams of kiwifruit *AcABF2*, *AcABF3*, *AcABF8*, *AcABF9*, and *AcABF10*.

3.3. Analysis of the Gene Structure and Conserved Motifs of the A. chinensis ABF Gene Family

To characterize the amino acid sequence of the *AcABF* gene family, the gene composition of this protein sequence was analyzed via the MEME Suit 5.5.8 online tool. The results are shown in Figure 4b. Conserved motifs 1 and 8 are highly conserved. Additionally, all the *AREB/ABFs* from Group I are extremely similar except for *AcBF10*. However, the same motifs have different positions in different protein sequences, which are presumed to be related to the structure and function of this protein. Combined with the phylogenetic tree of *AcABF* (Figure 2a), the motif distribution of members of the same subfamily also showed some differences; for example, *AcABF4*, *AcABF5*, and *AcABF7* belong to subfamily II, but motif 3 appeared only in *AcABF5*, which might be caused by the differences between transcription factor families under specific conditions. Similarly, in subfamily III, *AcABF1* and *AcABF6* differ by only one motif, 4. In subfamily III, *AcABF1* and *AcABF6* contain five or more motifs, but *AcABF11* has only two motifs, which is hypothesized to be due to the unique evolutionary process related to this subfamily.

The distribution of conserved motifs in the *AcABF* gene family may also be influenced by gene structure. The key to studying evolution within gene families is the distribution of gene structure. Sequence comparison of the 11 *AcABF* genes and analysis based on gene structure revealed (Figure 4c) that 9 of the 11 *AcABF* gene family members (*AcABF2*, *AcABF3*, *AcABF4*, *AcABF5*, *AcABF7*, *AcABF8*, *AcABF9*, *AcABF10*, and *AcABF11*) were within 7.5 kb in length. The remaining two *AcABF* gene family members (*AcABF1* and *AcABF6*) were approximately 16 kb and 24 kb long, respectively. The difference in the number of introns and exons of *A. chinensis ABF* genes was not large, with the number of introns ranging from 1 to 8 and the number of exons ranging from 2 to 9. Among the *AcABF* gene family members, *AcABF6* not only had the longest gene length but also contained the greatest number of introns and exons. These results suggest that different *AcABF* gene family members may be functionally differentiated.

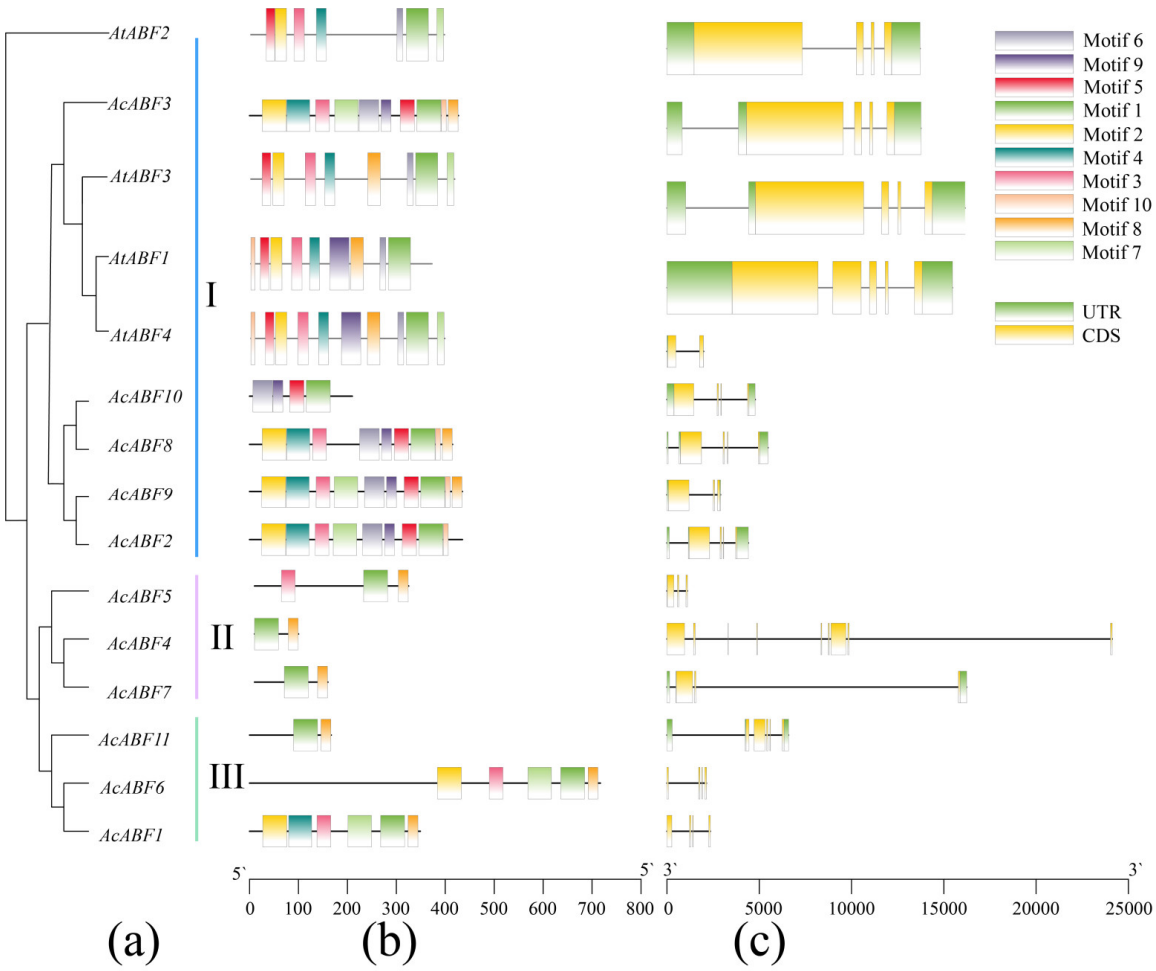

Figure 4. Conserved motifs and gene structure maps of the *A. thaliana AtABF1*, *AtABF2*, *AtABF3*, and *AtABF4* genes and the *A. chinensis ABF* gene family. (**a**) Members of the *A. thaliana AtABF1*, *AtABF2*, *AtABF3*, and *AtABF4* genes and the *A. chinensis ABF* gene family. (**b**) *A. thaliana AtABF1*, *AtABF2*, *AtABF3*, and *AtABF4* genes and *A. chinensis AcABF*. Distribution of conserved motifs; the motifs are indicated by colored boxes, and the black lines indicate the relative lengths of the proteins. The ruler represents the length of the motif. (**c**) Exon-intron structure diagrams of the *A. thaliana AtABF1*, *AtABF2*, *AtABF3*, and *AtABF4* genes and the *A. chinensis AcABF* genes, with green denoting the UTR, yellow showing the CDS, and the line segment in the center indicating the intron. The ruler represents the length of the genes.

3.4. Analysis of the Promoter Cis-Acting Elements of the A. chinensis ABF Gene Family

To investigate the response mechanism of *A. chinensis ABF* genes, 11 promoter cis-acting elements 2000 bp upstream of *A. chinensis* genes were predicted via the online software PlantCARE (https://bioinformatics.psb.ugent.be/webtools/plantcare/html/, accessed on 1 May 2024). The results (Figure 5) revealed 177 cis-acting elements, which could be divided into four categories: 80 light-responsive elements, 65 phytohormone-responsive elements, 26 environmental stress-responsive elements, and 6 plant-specific regulator-responsive elements. The proportion of these elements, from largest to smallest, was as follows: light-responsive elements (45%) > phytohormone-responsive elements (36%) > environmental stress-responsive elements (15%) > plant-specific regulatory elements (7%). Among the phytohormone elements, the main ones were ABA responsive elements, JA-responsive elements, and SA-responsive elements. Among them, the class I subclade *AcABF* genes (*AcABF2*, *AcABF3*, *AcABF8*, *AcABF9*, and *AcABF10*) all had ABA response elements, and the *A. thaliana AtABF1*, *AtABF2*, *AtABF3*, and *AtABF4* genes respond to drought stress through ABA, whereas the *A. chinensis AcABF2*, *AcABF3*, *AcABF8*, *AcABF9*, and *AcABF10* genes also have ABA responsive elements; thus, these

five genes may also have similar drought resistance functions. Among the 11 *AcABF* gene family members, the maximum number of individual cis-acting response elements was eight, and the minimum was zero. Two genes, *AcABF2* and *AcABF9*, had the maximum number of eight light response elements, and *AcABF5* also had the maximum number of eight MeJA (methyl jasmonate) response elements. In summary, in addition to light-responsive elements, 54.8% of promoter-acting elements can regulate gene expression and material metabolism in plants to increase their resistance and improve their maladaptability to adverse environments.

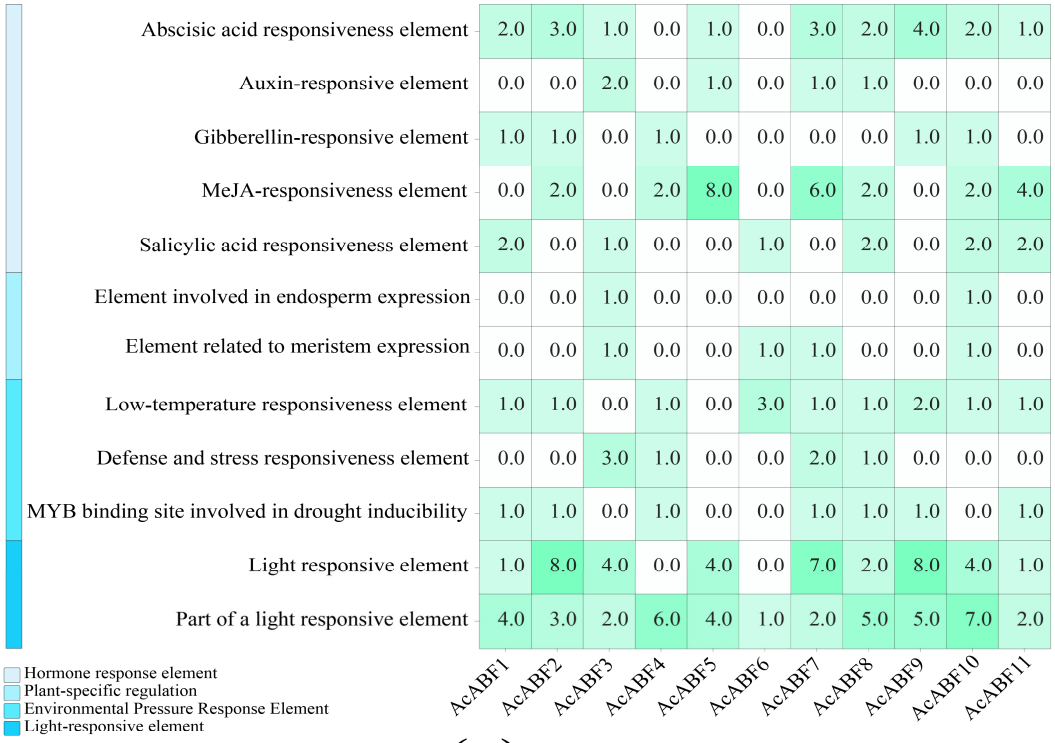

Figure 5. Cis-acting elements of *A. chinensis ABF* genes. (**a**) The number of cis-acting elements of each *ABF* gene and the numbers in the heatmap boxes indicate the number of different elements in these *AcABFs*; (**b**) the position of each cis-acting element.

3.5. Chromosomal Localization and Interspecific Covariance of the ABF Gene Family in A. chinensis

The results of chromosome localization revealed (Figure 6a) that the 11 *ABF* genes of *A. chinensis* were unevenly distributed on nine chromosomes. In addition, the ABF gene covariance among *A. chinensis*, rice, *A. thaliana*, and apple was also analyzed in this study, and the results (Figure 6b) revealed that *A. chinensis* and *A. thaliana* presented the greatest number of homologous gene pairs and that *A. chinensis* and rice presented the smallest number of homologous gene pairs. These findings indicate that the evolutionary relationship between the *A. chinensis ABF* and the *A. thaliana ABF* is relatively close and that the evolutionary relationship between the *A. chinensis ABF* and the rice *ABF* is strong.

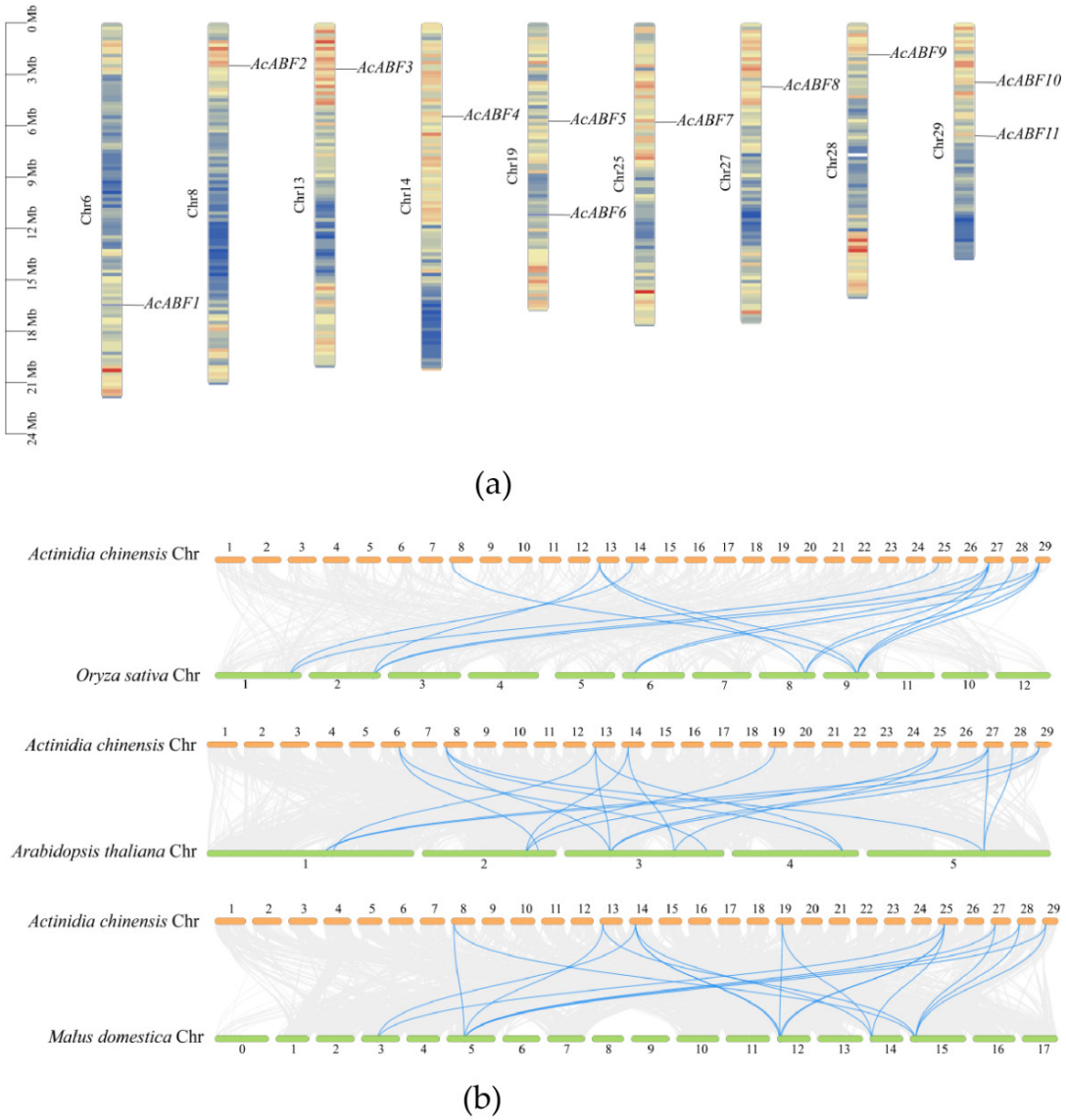

Figure 6. Chromosomal localization and covariance map of the *ABF* gene in *A. chinensis*. (**a**) Chromosomal localization map of the *ABF* gene in *A. chinensis*. (**b**) Covariance map between different species of kiwifruit, rice, *A. thaliana*, and apple. The gray lines denote the duplicated blocks, whereas the blue lines denote the covariant *ABF* gene pairs.

3.6. GO Function Enrichment Analysis

GO enrichment analysis helps to understand the various potential molecular functions of gene-encoded proteins to understand the functions of genes. The DEGs (differentially expressed genes) were analyzed via GO enrichment based on the transcriptome data to

understand the regulatory role of *A. chinensis* genes under stress. The results (Figure 7) present *A. chinensis* hormone processes under drought stress, such as GO:0009738 (abscisic acid-activated signaling pathway), GO:0009725 (response to hormone), GO:0009755 (hormone-mediated signaling pathway), and GO:0032870 (cellular response to hormone stimulus), among others. These results indicated that the biological processes associated with hormones were closely related to drought stress in *A. chinensis* and that the expression of all of these hormones was upregulated. The *AcABF* genes were annotated into three categories: biological process, cellular component, and molecular function. Among the biological process terms, most were related to hormone biological processes and osmoregulation; among the cellular component terms, most were related to biofilms. These findings suggest that *ABF* genes may adapt plants to adverse environments mainly by regulating ABA hormone levels and regulating the osmotic potential within the cell body.

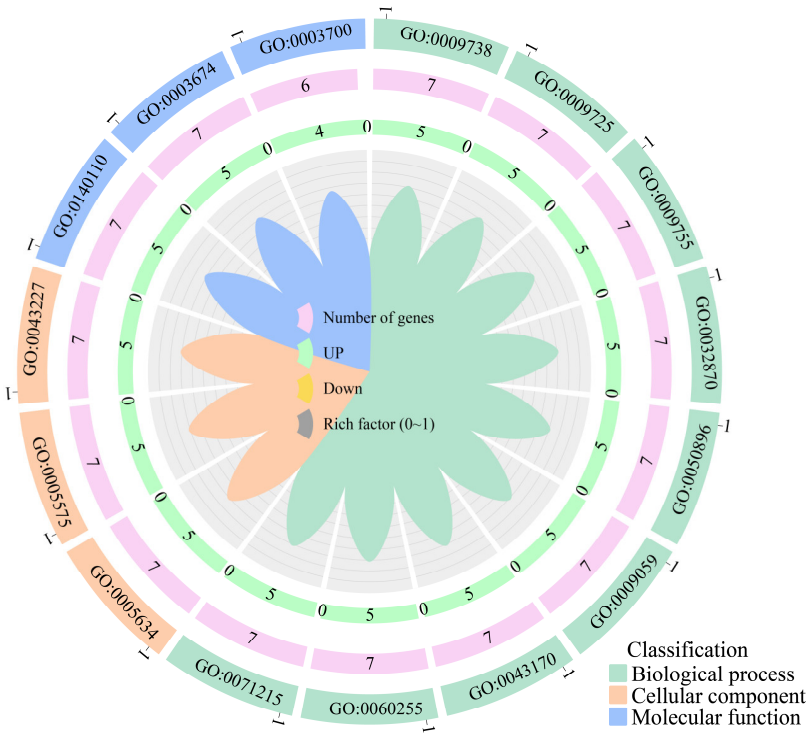

(a)

GO ID	Name
GO:0009738	abscisic acid-activated signaling pathway
GO:0009725	response to hormone
GO:0009755	hormone-mediated signaling pathway
GO:0032870	cellular response to hormone stimulus
GO:0050896	response to stimulus
GO:0009059	macromolecule biosynthetic process
GO:0043170	macromolecule metabolic process
GO:0060255	regulation of macromolecule metabolic process
GO:0071215	cellular response to abscisic acid stimulus
GO:0005634	nucleus
GO:0005575	cellular component
GO:0043227	membrane-bounded organelle
GO:0140110	transcription regulator activity
GO:0003674	molecular function
GO:0003700	DNA-binding transcription factor activity

(b)

Figure 7. GO enrichment analysis plot of the *AcABF* genes. (**a**) GO functional enrichment of the kiwifruit ABF gene; from the inside out, the 1st circle bar indicates the ratio of the number of genes with significant *AcABF* differences enriched with the same GO term to the total number of *AcABF* genes; the 2nd circle indicates the number of *AcABF* genes enriched with differences in upregulation and downregulation of the GO term, with green denoting upregulation and yellow denoting downregulation; the 3rd circle heatmap represents the total number of genes enriched with the corresponding GO term; and the 4th circle represents the GO number, and different classifications are indicated by different colors. (**b**) The name of the GO corresponding to the GO ID.

3.7. Changes in the ABA Content in Kiwifruit Leaves Under Drought Stress

Abscisic acid (ABA) regulates plant growth and development and adaptation to biotic and abiotic stresses. In this study, we determined the expression of abscisic acid phytohormones in the drought stress and control groups, and the results revealed that the expressions of ABA, ABA-GE (ABA-glucosyl ester), and ABA-ald (abscisic aldehyde) in kiwifruit were significantly greater than in the control group after drought stress (Figure 8, Table S3).

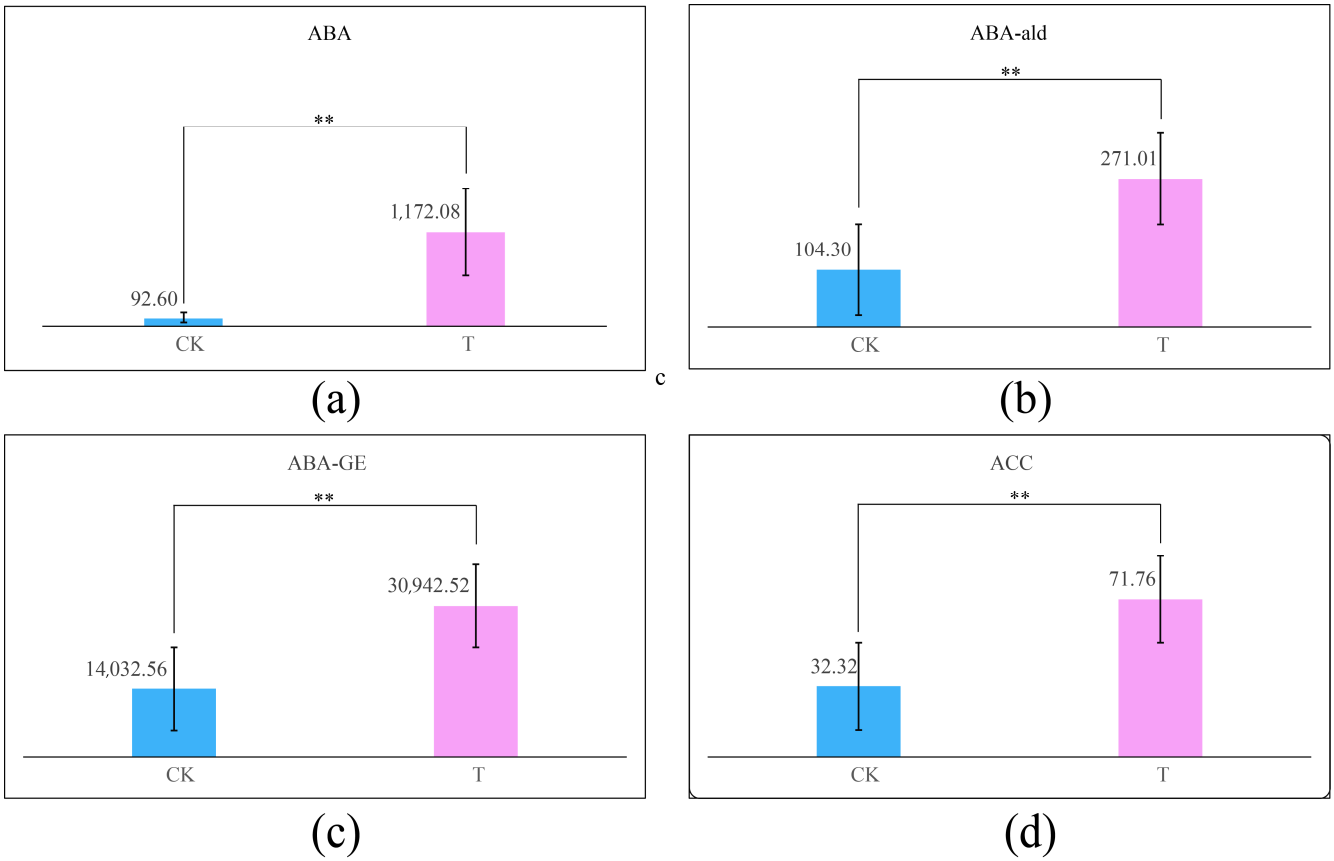

Figure 8. Comparative graphs of the physiological indices of *A. chinensis* histocultured seedlings in the control and drought stress-treated groups. (**a**) ABA; (**b**) ABA-ald (abscisic aldehyde); (**c**) ABA-GE (abscisic acid glucose ester); (**d**) ACC (desmotropic enzyme); CK: control group; T: treatment group; *p*-value obtained through hypothesis testing; ** denotes a *p*-value < 0.01.

3.8. KEGG Enrichment of the ABF Gene Family in A. chinensis Under Drought Stress

KEGG enrichment analysis was performed under drought stress to understand the biological function of AcABF genes under drought stress. KEGG enrichment analysis (Figure 9) revealed that the *AcABF2*, *AcBF3*, *AcABF8*, *AcABF9*, and *AcABF10* genes encode *ABF* genes in the ABA signaling pathway. ABA response elements were found in 2000 bp in all five *AcABF* genes. Under drought stress, carotenoid biosynthesis occurs through multiple conversions to form abscisic acid (ABA), which is transported to the ABA receptor PYR/PYL, which directly inhibits PP2C-type protein phosphatases in the presence of ABA, thereby inhibiting SnPK2 protease activity. The inhibition of SnPK2 protease activity promotes the expression of *ABF*-binding factors, which facilitate the closure of leaf stomata, thereby increasing plant tolerance to drought stress. These findings confirm that the *A. chinensis AcABF2*, *AcABF3*, *AcABF8*, *AcABF9*, and *AcABF10* genes activate relevant drought tolerance functions in response to ABA.

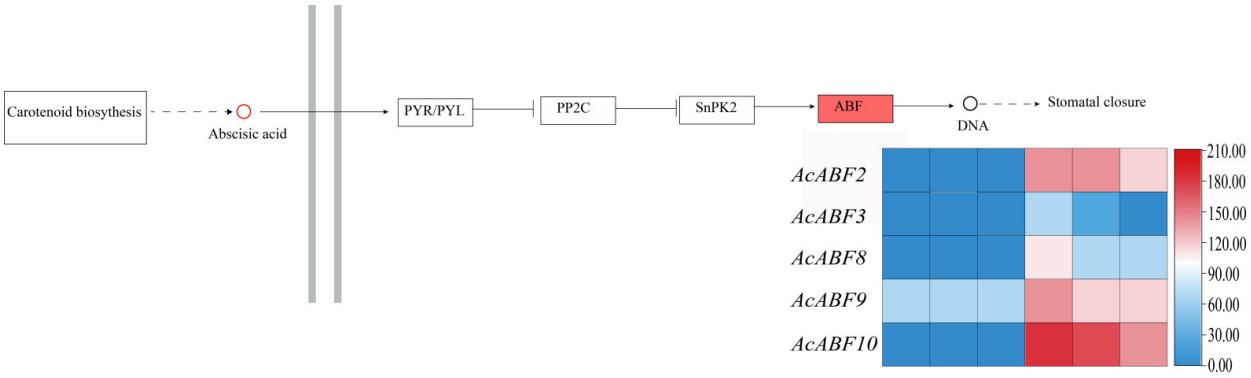

Figure 9. KEGG signaling pathway map of *ABF* (*AcABF2*, *AcABF3*, *AcABF8*, *AcABF9*, and *AcABF10*) genes. Carotenoid biosynthesis, abscisic acid (ABA); PYR/PYL: ABA receptor; PP2C: phosphatases of type 2C; SnPK2: related protein kinase 2. Two solid gray lines represent the cell membrane, solid arrows represent activation, dashed arrows represent indirect effects, dashed arrows represent state changes, straight lines represent binding, circles represent chemical compound, DNA and other molecule, and dashed lines represent inhibition. The four rectangles represent the complex.

3.9. Expression Pattern and qRT-PCR Analysis of ABF Family Members in A. chinensis Under Drought Stress

Transcriptome sequencing was performed on kiwifruit leaves to understand the expression patterns of *AcABF* genes under drought stress; kiwifruit seedlings grown at 80–85% soil moisture were used as controls, and kiwifruit seedlings grown at 40–45% soil moisture for 72 h composed the experimental group. The results (Figure 10a, Table S4) revealed that eight *AcABF* genes were expressed under drought stress compared with the control (CK), and six genes (*AcABF2*, *AcABF3*, *AcABF7*, *AcABF8*, *AcABF9*, and *AcABF10*) were upregulated, suggesting that the *AcABF* genes may be positively regulated through positively regulating the effects of drought stress on kiwifruit, thus maintaining its life activities.

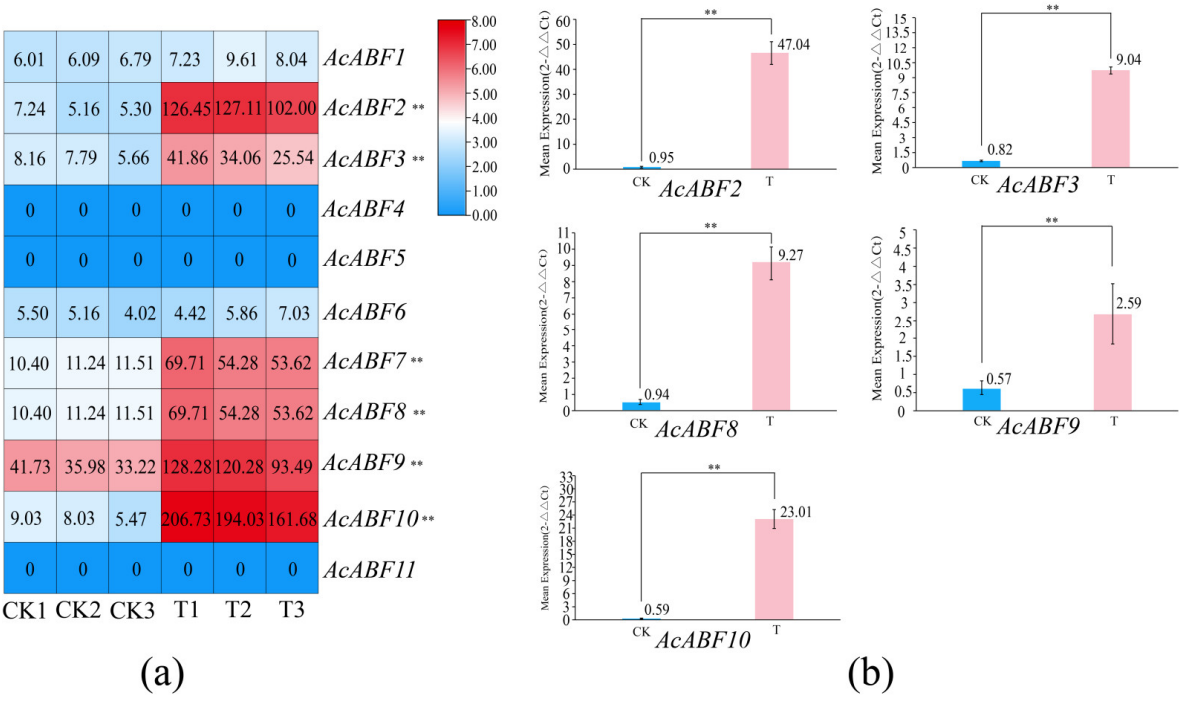

Figure 10. Heatmap of *AcABF* gene expression under drought stress and qRT-PCR results for five *AcABF* genes. (**a**) Heatmap of *AcABF* gene expression under drought stress; (**b**) qRT-PCR results of five *AcABF* genes; CK denotes the control; and T denotes drought stress for 72 h. **: $p < 0.01$.

To further confirm the accuracy of the transcriptome data, five *AcABF* genes whose transcriptome data were significantly different and designated in the ABA pathway were selected for qRT-PCR verification. The results (Figure 10b, Table S5) revealed that the expressions of *AcABF2*, *AcABF3*, *AcABF8*, *AcABF9*, and *AcABF10* were upregulated and that the differences were highly significant after drought stress compared with those of the control (CK). When we analyzed the correlation between the fragments per kilobase per million (FPKM) values and the qRT-PCR results from the transcriptome data (Table S6), the correlation coefficients were greater than 0.7, which indicated a strong correlation between the qRT-PCR results and the transcriptome data. These results confirmed the accuracy of the transcriptome data and verified the reliability of the differential genes in the transcriptome data. Moreover, these *AcABF* genes are crucial genes involved in the response of kiwifruit to drought stress.

4. Discussion

Kiwifruit is an important economic crop. Nonbiological stress can significantly reduce product quality and cause economic losses. Therefore, exploring the survival strategies and underlying coping mechanisms of kiwifruit is particularly important. Studies have shown that the *AREB/ABF* subfamily of the *bZIP* gene family can play an important role in plants under abiotic stress [29,42,43]. However, information about their properties and functions in kiwifruit, especially how they respond to drought stress, remains unclear.

In this study, we identified the *ABF* gene family in *A. chinensis*. The similarity of the *A. chinensis* gene family members *AcABF2*, *AcABF3*, *AcABF8*, *AcABF9*, and *AcABF10* with the *A. thaliana genes AtABF1*, *AtABF2*, *AtABF3*, and *AtABF4* with drought resistance functions was predicted via comparative analysis, and it was hypothesized that the *A. chinensis AcABF2*, *AcABF3*, *AcABF8*, *AcABF9* and *AcABF10* genes may have drought resistance functions. We also analyzed the expression patterns of the *ABF* gene, i.e., the *AcABF* gene, in *A. chinensis* under drought stress and the hormone (ABA) content of *A. chinensis* seedlings under drought stress, which can be used as a reference for the subsequent screening of drought resistance genes in kiwifruit and other related studies.

In this study, 11 *ABF* genes were identified in *A. chinensis*. However, nine *ABF* genes were identified in *A. thaliana* [44], ten in tomato [27], eight in jute [28], and nine in sweet potato [39], indicating that the number of *ABF* genes is independent of the genome size of different species. The Chinese kiwifruit *AcABF* gene family was categorized into three subfamilies based on the phylogenetic tree, and *Arabidopsis AtABF1*, *AtABF2*, *AtABF3*, and *AtABF4* belong to the same subfamily as Chinese kiwifruit *AcABF2*, *AcABF3*, *AcABF8*, *AcABF9*, and *AcABF10*, assuming that *AtABF1*, *AtABF2*, *AtABF3*, and *AtABF3* have functions similar to those of *AcABF2*. *AtABF1*, *AtABF2*, *AtABF3*, and *AtABF4* [39–41] in the annual herb *A. thaliana* and *GmABF3* in soybean [45]; *OsABF2* and *OsABF3* in the aquatic graminaceous plant rice increased the drought tolerance of the plants [46]; and the upregulation of *TaABF2* and *TaABF3* was induced by drought stress in cereal crop wheat, suggesting that the majority of species [44]. These findings indicate that the *ABF2* and *ABF3* genes of most species have the same function in response to drought stress. Notably, soybean *GmABF8* not only responds to drought stress but also increases its expression under osmotic stress together with *GmABF9* [47]; the relative expression levels of tomato *SlABF8*, *SlABF9*, and *SlABF10* are upregulated under osmotic stress as well as salt stress, presumably because of the slight differences in the function of the *ABF* genes in different species [25]. The upregulation of *SlABF8*, *SlABF9,* and *SlABF10* in tomatoes under salt stress was presumably due to slight differences in the functions of *ABF* genes in different species. The conserved motifs of *AcABF3* in kiwifruit were consistent with those of *AcABF9*, and there were only small differences between *AcABF2* and 8, so perhaps *AcABF8* and *AcABF*9 not only have similar functions but also have some special functions. In

contrast, *AcABF10* has a large gap with the other genes of the family I; however, *AcABF10* may still have specialized functions. Lu et al. reported that tea tree *CsABF2*, *CsABF8*, and *CsABF11* are key transcription factors for drought tolerance, whereas the conserved structural domains of *CsABF9* and *CsABF10* are significantly different from the conserved structural domains of the other transcription factors but still strongly expressed under drought stress conditions [48]. It may even function only as a drought suppressant in kiwifruit.

Gene structure analysis revealed that the difference in the number of introns in each of the *A. chinensis AcABF* genes was small, with the number of introns in each of the 11 *AcABF* genes ranging from 1 to 8. This gene is similar to the *ABF* gene in orchids [32], poplars [49], and carrots [50]. The gene structures of the *ABF* genes in clade I are highly similar to the conserved motifs, which further suggests that the more similar the genes are in evolution, the more similar they are in function, thus helping to screen for functionally similar *ABF* genes. For example, the 13 *TaABF* genes in wheat are regulated by 11 known miRNAs and play important roles in abiotic stress resistance, such as drought and salt stress [31]; the overexpression of *PtrABF* in tobacco enhances tolerance to dehydration shock and prolonged water stress (drought) [51]; the family of *CsABF* genes in tea trees regulates downstream genes by modulating them and generating a resistance response, such as the drought expression levels of *CsABF2*, *CsABF8*, *CsABF9*, and *CsABF13*, which are significantly upregulated under treatment; *CsABF6* and *CsABF7* are notably upregulated under cold stress treatment for part of the period; and *CsABF1*, *CsABF6*, and *CsABF9* are elevated under salt stress treatment, with *CsABF6* reaching the highest expression at the 48 h level [48]. It can be hypothesized that *AcABF* genes play important roles in regulating abiotic stresses, including drought stress.

Promoter cis-acting elements are crucial for transcription and gene expression regulation in plants. In this study, a variety of resistance-related cis-acting elements were identified in the 2000 bp sequence upstream of the *A. chinensis ABF* gene. Among them, the phytohormone response elements were the most abundant, mainly methyl jasmonate (MeJA), ABA, salicylic acid (SA), growth hormone and gibberellin-related response elements, which suggests that the expression of *AcABF* genes under drought stress may be related to these hormones; among them, all genes in group I have ABA response elements, indicating that *the AcABF* genes of group I may be involved in the ABA transduction process. This finding is consistent with the findings concerning *AREB/ABF* genes and ABA [28,43,52]. Studies have shown that the *b*ZIP (*ABF*) family is vital for the regulation of secondary metabolism, such as jasmonic acid (JA), carotenoids, and abscisic acid (ABA) [53–57]. Both MeJA and ABA can stimulate the expression of plant defense genes, inducing chemical defenses and some physiological and functional stress responses in plants [58–61]. *Arabidopsis AtABF* can be induced by light, ABA, and stress [43,62,63]. Potato *StABF1* can be induced by ABA, drought, cold, and salt stresses to act as a homeopathic element [64], and the expression of orchid *ABF* genes correlates with ABA, JA, and ET [32]. ABA, MEJA, and SA have been shown, by previous researchers, to initiate their own defense responses during mechanical damage and pathogen invasion, and eventually, plants achieve rebalancing of the intracellular environment under stress conditions through the expression of stress-related genes, secondary metabolic shifts, and the accumulation of antioxidants to achieve the ability to survive and, thus, improve the resistance of the plant [65,66]. The above analyses mutually confirmed that *ABF* genes contribute to drought tolerance in kiwifruit. GO enrichment analysis helped elucidate the biological processes in which the *AcABF* gene family is involved, and the results revealed that these genes are involved mainly in biological processes, which are closely related mainly to hormones and plant resistance, and the results of the analyses further corroborated the above results.

Studying the expression patterns of relevant genes based on transcriptomic data is a new approach. In this study, we analyzed the expression patterns of kiwifruit ABF genes under drought stress. All 11 *AcABF* genes presented differential changes in expression under drought stress, and 6 genes were significantly upregulated (Figure 10a). Among the significantly upregulated genes, five, which were clustered in the same subfamily as the *A. thaliana ABF* genes with clear drought resistance functions, were selected for qRT-PCR validation in conjunction with the above conjecture validation. The correlation between the results of qRT-PCR and the results of transcriptome sequencing was high, confirming the accuracy of the transcriptome data and verifying the reliability of the transcriptome data with the DEGs (Figure 10b). These DEGs were able to respond to kiwifruit drought stress.

ABA is key in the abiotic stress response [36]. ABA accumulates to varying degrees and can mediate abiotic stress through selective splicing when plants are subjected to environmental stressors such as drought, salinity, and extreme temperatures [36,67,68]. Therefore, when plants are subjected to drought stress for a long period of time, they can be maintained by increasing the level of ABA and inducing defoliation, for example. The presence of some genes under short-term environmental stress can contribute to the maintenance of carotenoid homeostasis and accumulation, protect plants from environmental stress, and improve their tolerance to environmental stress by controlling carotenoid biosynthesis [69]. In this study, the ABA content in kiwifruit leaves under drought stress was determined (Figure 8). The results revealed that the ABA content in kiwifruit leaves significantly increased under drought stress.

ABA synthesis occurs through the carotenoid pathway [70]. It is also one of the most crucial hormones in the plant's response to stress, and it plays a vital role in various physiological processes of the plant's life cycle and response to biotic and abiotic stresses [70–72]. These findings suggest that under abiotic stress, plants synthesize ABA in various organs and initiate defense mechanisms to regulate the stomatal aperture and the expression of defense-related genes, thereby conferring resistance to environmental stress [73]. Plants synthesize ABA through the carotenoid pathway, and when plants are subjected to drought stress, dehydrated roots increase their water absorption capacity by synthesizing ABA, thereby inhibiting lateral root growth and promoting deep root production [74]. ABA enhances plant drought tolerance by regulating stomata; reducing water loss, such as transpiration; increasing plant water use efficiency; and activating ABA-dependent gene regulatory networks [75]. ABA response element-binding factor (ABRE binding factor (*ABF*)) is a downstream target gene for ABA-dependent pathways [76]. The expression of the *ABF* binding factor promotes leaf stoma closure, increasing plant tolerance to drought stress.

Abscisic acid (ABA) regulates many crucial processes in plant development and adaptation to biotic and abiotic stresses. Under stress conditions, plants synthesize ABA in various organs and initiate defense mechanisms, such as the regulation of the stomatal aperture and the expression of defense-related genes [73]. The drought-induced increase in ABA in plant cells is synthesized mainly by defense cells through the carotenoid pathway, and the accumulated ABA is sensed by the receptor pyrabactin (PYR/PYL). The binding affinity of ABA-PYR/PYL is regulated by phosphatases (PP2Cs), which are considered ABA coreceptors, and PP2Cs play a negative role in ABA signaling through the inhibition of downstream targets [77]. ABA signaling plays a negative role in ABA signaling [78]. ABA-bound receptors form a complex with the plant protein phosphatase 2C phosphatase of type 2C (PP2C), which deregulates the inhibitory effect of PP2C on the related protein kinase 2 (SnRK2) protein kinase [78]. SnRK2 is then phosphorylated via autophosphorylation or other protein kinases (e.g., Raf-like MAPKKK). The phosphorylated state of SnRK2 activates the transcription factor ABA responsive element-binding factors (*AREB/ABFs*) through phosphorylation, thereby regulating various transcriptional and posttranslational levels

of physiological responses, such as seed maturation, leaf genesis, stem cell maintenance, stomatal movement, photosynthesis, carbon translocation, bud dormancy, flowering, fruit maturation, and senescence [79]. Kang et al. [80] and others have shown that overexpression of the *AtABF3* and *AtABF4* genes enhances tolerance to drought stress in *Arabidopsis*. Based on the phylogenetic tree, KEGG enrichment analysis, transcriptional data, and expression of ABA in the leaves of rhesus macaques after drought stress in this study, as well as [78] the coevolution of hormone metabolism and signaling networks, expanded plant adaptive plasticity, we can speculate a mechanistic model diagram of *AcABF* (*AcABF2*, *AcABF3*, *AcABF8*, *AcABF9*, and *AcABF10*) genes involved in ABA signaling to increase drought tolerance in kiwifruit (Figure 11). Under drought stress, kiwifruit may synthesize large amounts of ABA through the carotenoid pathway, and ABA binds to receptors (PYR/PYL); inhibits the activities of PP2C-type protein phosphatase and SnPK2 protease; promotes the expression of *ABF*, an ABA transcription factor; and then promotes the closure of stomata in kiwifruit leaves to increase drought stress tolerance. The above is only speculation, and further transgenic experiments and measurements of ABA content and stomatal closure in transgenic plants are needed to prove this speculation.

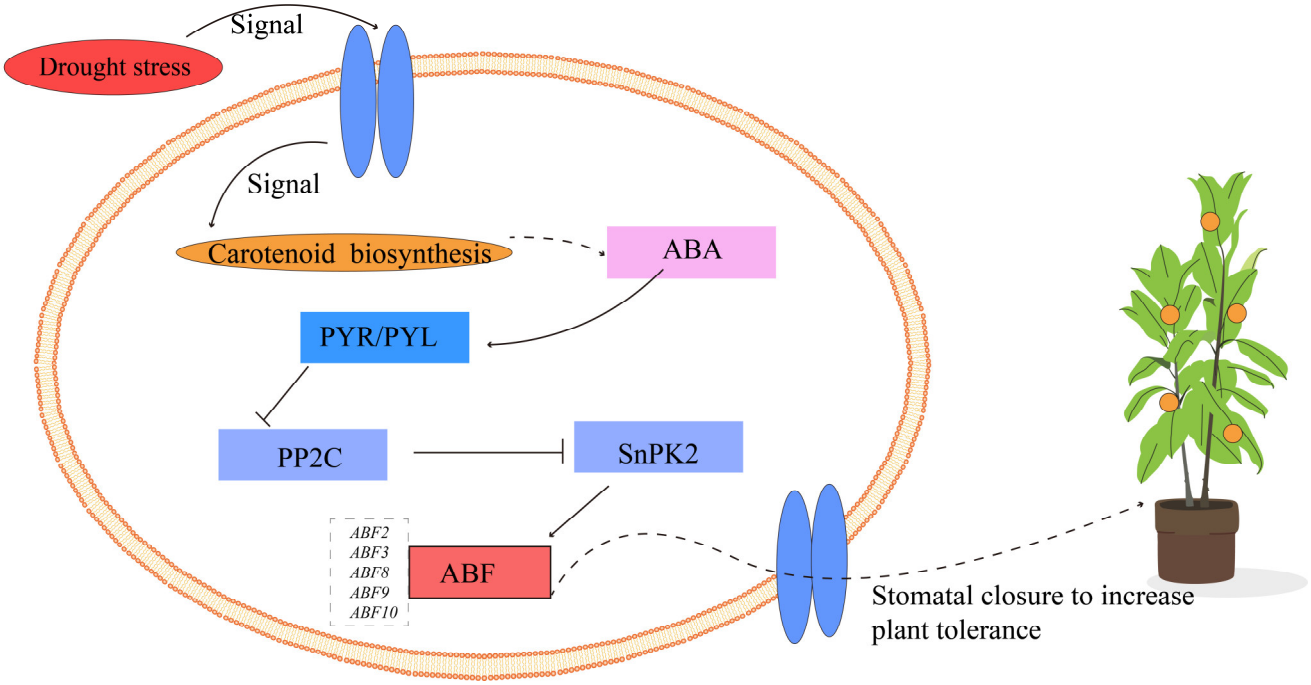

Figure 11. Putative map of the ABA signaling model involving *ABF* (*AcABF2*, *AcABF3*, *AcABF8*, *AcABF9*, and *AcABF10*) genes. ABA: abscisic acid; PYR/PYL: ABA receptor; PP2C: phosphatases of type 2C; SnPK2: sucrose nonfermenting 1-related protein kinase 2.

5. Conclusions

In this study, 11 *AcABF* genes were identified from the *A. chinensis* genome and phylogenetically categorized into three subfamilies, and members of these gene families were unevenly distributed on nine chromosomes. GO enrichment and cis-acting element analysis revealed that the *AcABF* genes were associated with ABA synthesis and metabolic pathways. Nine *AcABF* genes were expressed under drought stress, and six *AcABF* genes were DEGs. The qRT-PCR results strongly correlated with the transcriptome data, with correlation coefficients greater than 0.7. The contents of ABA phytohormones such as ABA, ABA-ald, ABA-GE, and ACC significantly increased, indicating that *A. chinensis* synthesizes a large amount of ABA to increase its tolerance to drought. Based on KEGG enrichment, *AcABF2*, *AcABF3*, *AcABF8*, *AcABF9*, and *AcABF10* were enriched in the ABA signaling

pathway and identified as binding factors of ABA response elements. The mechanism by which the kiwifruit *ABF* gene family responds to drought stress involves increasing the content of ABA in plants by promoting the expression of the ABA transcription factor *ABF* to increase the tolerance of these plants to drought stress.

Supplementary Materials: The following supporting information can be downloaded at: https://www.mdpi.com/article/10.3390/horticulturae11070715/s1, Table S1. Primer design for qRT-PCR. Table S2. Physicochemical properties of AcABF genes. Table S3. Expression of kiwifruit ABA analogs under drought and control conditions. Table S4. FPKM values of AcABF genes. Table S5. Raw CT values for the qRT-PCR data. Table S6. Correlations of the transcriptome data with the qRT-PCR results.

Author Contributions: Conceptualization, investigation, formal analysis, writing—original draft preparation, and software, H.W.; conceptualization, writing—original draft preparation, and software, Y.Z.; conceptualization and writing—original draft preparation, X.R.; software and data curation, Q.Z.; material provision and sampling, L.N.; validation, J.W.; validation, H.R.; review and editing, supervision, and funding acquisition, H.Z.; methodology, writing—review and editing, and funding acquisition, X.L. All authors have read and agreed to the published version of the manuscript.

Funding: This study is supported by the Agricultural Joint Key Projects in Yunnan Province (202301BD070001-003), the Rural Revitalization Science and Technology Project-Rural Revitalization Industry Key Technology Integration Demonstration Project (202304BP090005), the Yunnan Academician (Expert) Workstation Project (202305AF150020), the Yunnan First-class Construction Discipline of Forestry Science of Southwest Forestry University, and the Start-up Fund Project of Doctoral Research at Southwest Forestry University. The funders had no role in the design of the study; the collection, analysis, or interpretation of the data; or the writing of the manuscript.

Data Availability Statement: All data generated or analyzed during this study are included in this published article. Kiwifruit genome annotation files can be accessed at http://kiwifruitgenome.org/ (accessed on 1 May 2024). RNA-Seq (RNA sequencing) data under salt stress can be found at https://submit.ncbi.nlm.nih.gov/subs/sra/SUB14697397 (accessed on 1 May 2024). The RNA-Seq data are publicly available at the National Center for Biotechnology Information. The other data presented in this study are available in the Supplementary Materials.

Acknowledgments: The authors thank Deqiang Zhang, Beijing Forestry University, for his critical reading of the manuscript.

Conflicts of Interest: The authors declare that there are no conflicts of interest regarding any commercial or financial relationships pertaining to in this study.

References

1. Huang, S.; Ding, J.; Deng, D.; Tang, W.; Sun, H.; Liu, D.; Zhang, L.; Niu, X.; Zhang, X.; Meng, M.; et al. Draft genome of the kiwifruit *Actinidia chinensis*. *Nat. Commun.* **2013**, *4*, 2640. [CrossRef] [PubMed] [PubMed Central]
2. Latocha, P.; Debersaques, F.; Decorte, J. Varietal differences in the mineral composition of kiwiberry *Actinidia arguta* (Siebold et Zucc.) Planch, ex. Miq. *Acta Hortic.* **2015**, *1096*, 479–486. [CrossRef]
3. Ashraf, I.; Cipriani, G.; De Mori, G. Bridging the gap: Genetic insights into graft compatibility for enhanced kiwifruit production. *Int. J. Mol. Sci.* **2025**, *26*, 2925. [CrossRef] [PubMed]
4. Liu, Y.; Lv, G.; Yang, Y.; Ma, K.; Ren, X.; Li, M.; Liu, Z. Interaction of AcMADS68 with transcription factors regulates anthocyanin biosynthesis in red-fleshed kiwifruit. *Hortic. Res.* **2022**, *10*, uhac252. [CrossRef] [PubMed] [PubMed Central]
5. Bassi, I.; Mian, G.; Troiano, S.; Gori, E.; Iseppi, L. Assessing consumer preferences for new red-pulp kiwifruit: Application of a choice experiment between different countries. *Foods* **2023**, *12*, 2865. [CrossRef] [PubMed] [PubMed Central]
6. Zhang, Y.; Zhang, H.Z.; Fu, J.Y.; Du, Y.Y.; Qu, J.; Song, Y.; Wang, P.W. The GmXTH1 gene improves drought stress resistance of soybean seedlings. *Mol. Breed.* **2021**, *42*, 3. [CrossRef]
7. Razi, K.; Muneer, S. Drought stress-induced physiological mechanisms, signaling pathways and molecular response of chloroplasts in common vegetable crops. *Crit. Rev. Biotechnol.* **2021**, *41*, 669–691. [CrossRef]
8. Daryanto, S.; Wang, L.; Jacinthe, P. Global synthesis of drought effects on maize and wheat production. *PLoS ONE* **2017**, *11*, e0156362. [CrossRef]

9. Sallam, A.; Alqudah, M.A.; Dawood, A.F.M.; Baenziger, P.S.; Börner, A. Drought stress tolerance in wheat and barley: Advances in physiology, breeding and genetics Research. *Int. J. Mol. Sci.* **2019**, *20*, 3137. [CrossRef]
10. Judd, M.J.; McAneney, K.J.; Wilson, K.S. Influence of water stress on kiwifruit growth. *Irrig. Sci.* **1989**, *10*, 303–311. [CrossRef]
11. Chen, J.Y.; Fang, J.B.; Qi, X.J.; Gu, H.; Lin, M.M.; Zhang, W.Y.; Wei, C.G. Research progress on rootstocks of kiwifruit. *J. Fruit Sci.* **2015**, *32*, 959–968.
12. Bao, W.W.; Chen, X.; Li, R.N.; Li, M.; Xie, C.J.; Dou, M.R.; Zhang, K.Z.; Wang, J.; Gao, Z.X.; Liu, Z.D.; et al. Comprehensive assessment of drought resistance and recovery in kiwifruit genotypes using multivariate analysis. *Plant J.* **2024**, *119*, 100–114. [CrossRef] [PubMed]
13. Dubey, A.; Kumar, A.; Malla, M.A.; Chowdhary, K.; Singh, G.; Ravikanth, G.; Harish; Sharma, S.; Saati-Santamaria, Z.; Menéndez, E.; et al. Approaches for the amelioration of adverse effects of drought stress on crop plants. *Front. Biosci.* **2021**, *26*, 928–947. [CrossRef] [PubMed]
14. Mukarram, M.; Choudhary, S.; Kurjak, D.; Petek, A.; Khan, M.M.A. Drought: Sensing, signalling, effects and tolerance in higher plants. *Physiol. Plant.* **2021**, *172*, 1291–1300. [CrossRef] [PubMed]
15. Sun, X.; Wang, Y.; Sui, N. Transcriptional regulation of bHLH during plant response to stress. *Biochem. Biophys. Res. Commun.* **2018**, *503*, 397–401. [CrossRef] [PubMed]
16. Nakashima, K.; Yamaguchi-Shinozaki, K.; Shinozaki, K. The transcriptional regulatory network in the drought response and its crosstalk in abiotic stress responses including drought, cold, and heat. *Front. Plant Sci.* **2014**, *5*, 170. [CrossRef] [PubMed] [PubMed Central]
17. Nakashima, K.; Yamaguchi-Shinozaki, K. ABA signaling in stress-response and seed development. *Plant Cell Rep.* **2013**, *32*, 959–970. [CrossRef] [PubMed]
18. Du, F.; Wang, Y.; Wang, J.; Li, Y.; Zhang, Y.; Zhao, X.; Xu, J.; Li, Z.; Zhao, T.; Wang, W.; et al. The basic helix-loop-helix transcription factor gene, OsbHLH38, plays a key role in controlling rice salt tolerance. *J. Integr. Plant Biol.* **2023**, *65*, 1859–1873. [CrossRef] [PubMed]
19. Geilfus, C.M.; Mithöfer, A.; Ludwig-Müller, J.; Zörb, C.; Muehling, K.H. Chloride-inducible transient apoplastic alkalinizations induce stomatal closure by controlling abscisic acid distribution between leaf apoplast and guard cells in salt-stressed Vicia faba. *New Phytol.* **2015**, *208*, 803–816. [CrossRef] [PubMed]
20. Brookbank, B.P.; Patel, J.; Gazzarrini, S.; Nambara, E. Role of basal aba in plant growth and Development. *Genes* **2021**, *12*, 1936. [CrossRef] [PubMed] [PubMed Central]
21. Sato, H.; Mizoi, J.; Shinozaki, K.; Yamaguchi-Shinozaki, K. Complex plant responses to drought and heat stress under climate change. *Plant. J.* **2024**, *117*, 1873–1892. [CrossRef] [PubMed]
22. Zhao, J.; Guo, R.; Guo, C.; Hou, H.; Wang, X.; Gao, H. Evolutionary and expression analyses of the apple basic leucine zipper transcription factor Family. *Front. Plant Sci.* **2016**, *7*, 376. [CrossRef]
23. Jakoby, M.; Weisshaar, B.; Dröge-Laser, W.; Vicente-Carbajosa, J.; Tiedemann, J.; Kroj, T.; Parcy, F.; bZIP Research Group. bZIP transcription factors in Arabidopsis. *Trends Plant Sci.* **2002**, *7*, 106–111. [CrossRef] [PubMed]
24. Niu, X.; Fu, D. The Roles of BLH Transcription factors in plant development and environmental Response. *Int. J. Mol. Sci.* **2022**, *23*, 3731. [CrossRef]
25. Pan, X.; Wang, C.; Liu, Z.; Gao, R.; Feng, L.; Li, A.; Yao, K.; Liao, W. Identification of ABF/AREB gene family in tomato (*Solanum lycopersicum* L.) and functional analysis of ABF/AREB in response to ABA and abiotic stresses. *PeerJ* **2023**, *11*, e15310. [CrossRef] [PubMed] [PubMed Central]
26. Chang, H.C.; Tsai, M.C.; Wu, S.S.; Chang, I.F. Regulation of ABI5 expression by ABF3 during salt stress responses in *Arabidopsis thaliana*. *Bot. Stud.* **2019**, *60*, 16. [CrossRef]
27. Yoshida, T.; Fujita, Y.; Sayama, H.; Kidokoro, S.; Maruyama, K.; Mizoi, J. AREB1, AREB2, and ABF3 are master transcription factors that cooperatively regulate ABRE-dependent ABA signaling involved in drought stress tolerance and require ABA for full activation. *Plant J.* **2010**, *61*, 672–685. [CrossRef] [PubMed]
28. Fiallos-Salguero, M.S.; Li, J.; Li, Y.; Xu, J.; Fang, P.; Wang, Y.; Zhang, L.; Tao, A. Identification of AREB/ABF gene family involved in the response of aba under salt and drought stresses in jute (*Corchorus olitorius* L.). *Plants* **2023**, *12*, 1161. [CrossRef] [PubMed]
29. Fujita, Y.; Yoshida, T.; Yamaguchi-Shinozaki, K. Pivotal role of the AREB/ABF-SnRK2 pathway in ABRE-mediated transcription in response to osmotic stress in plants. *Physiol. Plant.* **2012**, *147*, 15–27. [CrossRef]
30. Zhao, B.Y.; Hu, Y.F.; Li, J.; Yao, X.; Liu, K. BnaABF2, a bZIP transcription factor from rapeseed (*Brassica napus* L.), enhances drought and salt tolerance in transgenic *Arabidopsis*. *Bot. Stud.* **2016**, *57*, 12. [CrossRef]
31. Yang, F.; Sun, X.; Wu, G.; He, X.; Liu, W.; Wang, Y.; Sun, Q.; Zhao, Y.; Xu, D.; Dai, X.; et al. Genome-wide identification and expression profiling of the abf transcription factor family in wheat (*Triticum aestivum* L.). *Int. J. Mol. Sci.* **2024**, *25*, 3783. [CrossRef] [PubMed] [PubMed Central]
32. Xie, X.; Lin, M.; Xiao, G.; Wang, Q.; Li, Z. Identification and characterization of the AREB/ABF gene family in three orchid species and functional analysis of DcaABI5 in Arabidopsis. *Plants* **2024**, *13*, 774. [CrossRef] [PubMed] [PubMed Central]

33. Sinkar, R.S.; Rai, M. *Plant Tissue Culture:Theory and Practical Approach*; CRC Press: Boca Raton, FL, USA, 2025.
34. Loyola-Vargas, V.M.; Ochoa-Alejo, N. An Introduction to plant cell, tissue, and organ culture: Current status and perspectives. *Methods Mol. Biol.* **2024**, *2827*, 1–13. [CrossRef] [PubMed]
35. Tao, J.; Jia, H.; Wu, M.; Zhong, W.; Jia, D.; Wang, Z. Genome-wide identification and characterization of the TIFY gene family in kiwifruit. *BMC Genom.* **2022**, *23*, 179. [CrossRef] [PubMed]
36. Yang, Y.; Chen, L.; Su, G.; Liu, F.; Zeng, Q.; Li, R. Identification and expression analysis of the lipid phosphate phosphatases gene family reveal their involvement in abiotic stress response in kiwifruit. *Front. Plant Sci.* **2022**, *13*, 942937. [CrossRef]
37. Potter, S.C.; Luciani, A.; Eddy, S.R.; Park, Y.; Lopez, R.; Finn, R.D. HMMER web server, 2018 update. *Nucleic Acids Res.* **2018**, *46*, W200–W204. [CrossRef]
38. Chen, C.; Chen, H.; Zhang, Y.; Thomas, H.R.; Frank, M.H.; He, Y. TBtools, an integrative toolkit developed for interactive analyses of big biological data. *Mol. Plant.* **2020**, *13*, 1194–1202. [CrossRef]
39. Muñiz García, M.N.; Cortelezzi, J.I.; Fumagalli, M.; Capiati, D.A. Expression of the Arabidopsis ABF4 gene in potato increases tuber yield, improves tuber quality and enhances salt and drought tolerance. *Plant Mol. Biol.* **2018**, *98*, 137–152. [CrossRef]
40. Liu, J.; Shu, D.; Tan, Z.; Ma, M.; Guo, N.; Gao, S.; Duan, G.; Kuai, B.; Hu, Y.; Li, S.; et al. The Arabidopsis IDD14 transcription factor interacts with bZIP-type ABFs/AREBs and cooperatively regulates ABA-mediated drought tolerance. *New Phytol.* **2022**, *236*, 929–942. [CrossRef]
41. Yoshida, T.; Fujita, Y.; Maruyama, K.; Mogami, J.; Todaka, D.; Shinozaki, K. Four *Arabidopsis* AREB/ABF transcription factors function predominantly in gene expression downstream of SnRK2 kinases in abscisic acid signalling in response to osmotic stress. *Plant Cell Environ.* **2014**, *38*, 35–49. [CrossRef]
42. Maszkowska, J.; Szymańska, K.P.; Kasztelan, A.; Krzywińska, E.; Sztatelman, O.; Dobrowolska, G. The Multifaceted Regulation of SnRK2 Kinases. *Cells* **2021**, *10*, 2180. [CrossRef] [PubMed]
43. Choi, H.; Hong, J.; Ha, J.; Kang, J.; Kim, S.Y. ABFs, a family of ABA-responsive element binding factors. *J. Biol. Chem.* **2000**, *275*, 1723–1730. [CrossRef] [PubMed]
44. Li, F.; Mei, F.; Zhang, Y.; Li, S.; Kang, Z.; Mao, H. Genome-wide analysis of the AREB/ABF gene lineage in land plants and functional analysis of TaABF3 in Arabidopsis. *BMC Plant Biol.* **2020**, *20*, 558. [CrossRef] [PubMed] [PubMed Central]
45. Li, C.; Chen, Y.; Hu, Q.; Yang, X.; Zhao, Y.; Lin, Y.; Yuan, J.; Gu, J.; Li, Y.; He, J.; et al. Pseudoresponse regulator 3b and transcription factor ABF3 modulate abscisic acid-dependent drought stress response in soybean. *Plant Physiol.* **2024**, *195*, 3053–3071. [CrossRef]
46. Hossain, M.A.; Cho, J.I.; Han, M.; Ahn, C.H.; Jeon, J.S.; An, G.; Park, P.B. The ABRE-binding bZIP transcription factor OsABF2 is a positive regulator of abiotic stress and ABA signaling in rice. *J. Plant Physiol.* **2010**, *167*, 1512–1520. [CrossRef] [PubMed]
47. Zhang, B.S.; Li, M.Y.; Song, Z.; Han, J.P.; Cheng, Z.Q.; Chen, X.J.; Han, D.Z.; Hu, Z.B.; Liu, C.Y.; Yang, M.L.; et al. Characterization of the soybean ABF gene family and the key regulatory function of GmABF1 in salt stress response. *Int. J. Biol. Macromol.* **2025**, *317*, 144763. [CrossRef] [PubMed]
48. Lu, J.; Du, J.; Tian, L.; Li, M.; Zhang, X.; Zhang, S.; Wan, X.; Chen, Q. Divergent response strategies of CsABF facing abiotic stress in tea plant: Perspectives from drought-tolerance studies. *Front. Plant Sci.* **2021**, *12*, 763843. [CrossRef] [PubMed] [PubMed Central]
49. Ji, L.; Wang, J.; Ye, M.; Li, Y.; Guo, B.; Chen, Z.; Li, H.; An, X. Identification and characterization of the *Populus* AREB/ABF Subfamily. *J. Integr. Plant Biol.* **2013**, *55*, 177–186. [CrossRef] [PubMed]
50. Wang, Y.H.; Que, F.; Li, T.; Zhang, R.R.; Khadr, A.; Xu, Z.S.; Tian, Y.S.; Xiong, A.S. DcABF3, an ABF transcription factor from carrot, alters stomatal density and reduces ABA sensitivity in transgenic *Arabidopsis*. *Plant Sci.* **2021**, *302*, 110699. [CrossRef] [PubMed]
51. Huang, X.S.; Liu, J.H.; Chen, X.J. Overexpression of *PtrABF* gene, a bZIP transcription factor isolated from *Poncirus trifoliata*, enhances dehydration and drought tolerance in tobacco via scavenging ROS and modulating expression of stress-responsive genes. *BMC Plant Biol.* **2010**, *10*, 230. [CrossRef] [PubMed] [PubMed Central]
52. Uno, Y.; Furihata, T.; Abe, H.; Yoshida, R.; Shinozaki, K.; Yamaguchi-Shinozaki, K. Arabidopsis basic leucine zipper transcription factors involved in an abscisic acid-dependent signal transduction pathway under drought and high-salinity conditions. *Proc. Natl. Acad. Sci. USA* **2000**, *97*, 11632–11637. [CrossRef] [PubMed] [PubMed Central]
53. Cao, S.; Cai, Y.; Yang, Z.; Joyce, D.C.; Zheng, Y. Effect of MeJA treatment on polyamine, energy status and anthracnose rot of loquat fruit. *Food Chem.* **2014**, *145*, 86–89. [CrossRef] [PubMed]
54. Berens, M.L.; Berry, H.M.; Mine, A.; Argueso, C.T.; Tsuda, K. Evolution of hormone signaling networks in plant defense. *Annu. Rev. Phytopathol.* **2017**, *55*, 401–425. [CrossRef]
55. Laura, B.; Silvia, P.; Francesca, F.; Benedetta, S.; Carla, C. Epigenetic control of defense genes following MeJA-induced priming in rice (*O. sativa*). *J. Plant Physiol.* **2018**, *228*, 166–177. [CrossRef]
56. Ma, Y.; Cao, J.; He, J.; Chen, Q.; Li, X.; Yang, Y. Molecular mechanism for the regulation of ABA homeostasis during plant development and stress Responses. *Int. J. Mol. Sci.* **2018**, *19*, 3643. [CrossRef]

57. Osakabe, Y.; Yamaguchi-Shinozaki, K.; Shinozaki, K.; Tran, L.P. ABA control of plant macroelement membrane transport systems in response to water deficit and high salinity. *New Phytol.* **2014**, *202*, 35–49. [CrossRef]
58. Chini, A.; Gimenez-Ibanez, S.; Goossens, A.; Solano, R. Redundancy and specificity in jasmonate signalling. *Curr. Opin. Plant Biol.* **2016**, *33*, 147–156. [CrossRef] [PubMed]
59. Zhou, M.; Memelink, J. Jasmonate-responsive transcription factors regulating plant secondary metabolism. *Biotechnol. Adv.* **2016**, *34*, 441–449. [CrossRef]
60. Aleman, F.; Yazaki, J.; Lee, M.; Takahashi, Y.; Kim, A.Y.; Li, Z. An ABA-increased interaction of the PYL6 ABA receptor with MYC2 transcription factor, A putative link of ABA and JA signaling. *Scientific Rep.* **2016**, *6*, 28941. [CrossRef]
61. Walter, M.H.; Strack, D. Carotenoids and their cleavage products, biosynthesis and functions. *Natural Product Rep.* **2011**, *28*, 663–692. [CrossRef]
62. Kim, S.; Kang, J.Y.; Cho, D.I.; Park, J.H.; Kim, S.Y. ABF2, an ABRE-binding bZIP factor, is an essential component of glucose signaling and its overexpression affects multiple stress tolerance. *Plant J.* **2004**, *40*, 75–87, Erratum in: *Plant J.* **2005**, *43*, 467. [CrossRef] [PubMed]
63. Xu, D.; Li, J.; Gangappa, S.N.; Hettiarachchi, C.; Lin, F.; Andersson, M.X.; Jiang, Y.; Deng, X.W.; Holm, M. Convergence of Light and ABA signaling on the ABI5 promoter. *PLoS Genet.* **2014**, *10*, e1004197. [CrossRef] [PubMed] [PubMed Central]
64. Muñiz García, M.N.; Giammaria, V.; Grandellis, C.; Téllez-Iñón, M.T.; Ulloa, R.M.; Capiati, D.A. Characterization of StABF1, a stress-responsive bZIP transcription factor from *Solanum tuberosum* L. that is phosphorylated by StCDPK2 vitro. *Planta* **2012**, *235*, 761–778. [CrossRef] [PubMed]
65. Schopfer, P. Biomechanics of plant growth. *Am. J. Bot.* **2006**, *93*, 1415–1425. [CrossRef]
66. Wang, D.; Pajerowska-Mukhtar, K.; Culler, A.H.; Dong, X. Salicylic acid inhibits pathogen growth in plants through repression of the auxin signaling Pathway. *Curr. Biol.* **2007**, *17*, 1784–1790. [CrossRef] [PubMed]
67. Zhang, A.; Yang, X.; Lu, J.; Song, F.; Sun, J.; Wang, C.; Lian, J.; Zhao, L.; Zhao, B. OsIAA20, an Aux/IAA protein, mediates abiotic stress tolerance in rice through an ABA pathway. *Plant Sci.* **2021**, *308*, 110903. [CrossRef] [PubMed]
68. Min, M.K.; Kim, R.; Hong, W.J.; Jung, K.H.; Le, J.Y.; Kim, B.G. OsPP2C09 is a bifunctional regulator in both ABA-dependent and independent abiotic stress signaling pathways. *Int. J. Mol. Sci.* **2021**, *22*, 393. [CrossRef] [PubMed]
69. Kim, H.S.; Ji, C.Y.; Lee, C.J.; Kim, S.E.; Park, S.C.; Kwak, S.S. Orange: A target gene for regulating carotenoid homeostasis and increasing plant tolerance to environmental stress in marginal lands. *J. Exp. Bot.* **2018**, *69*, 3393–3400. [CrossRef] [PubMed]
70. Guilfoyle, T.; Hagen, G.; Dong, T.; Park, Y.; Hwang, I. Abscisic acid: Biosynthesis, inactivation, homoeostasis and signalling. *Essays Biochem.* **2015**, *58*, 29–48. [CrossRef]
71. Chernys, J.T.; Zeevaart, J.A. Characterization of the 9-cis-epoxycarotenoid dioxygenase gene family and the regulation of abscisic acid biosynthesis in avocado. *Plant Physiol.* **2000**, *124*, 343–354. [CrossRef]
72. Zhu, J.K. Salt and drought stress signal transduction in plants. *Annu. Rev. Plant Biol.* **2002**, *53*, 247–273. [CrossRef]
73. Lim, C.W.; Baek, W.; Jung, J.; Kim, J.H.; Lee, S.C. Function of ABA in stomatal defense against biotic and drought stresses. *Int. J. Mol. Sci.* **2015**, *16*, 15251–15270. [CrossRef] [PubMed]
74. Lee, S.C.; Luan, S. ABA signal transduction at the crossroad of biotic and abiotic stress responses. *Plant Cell Environ.* **2011**, *35*, 53–60. [CrossRef] [PubMed]
75. Daszkowska-golec, A.; Szarejko, I. The molecular basis of ABA-mediated plant response to drought. *PLoS ONE* **2013**, *177*, 103–134.
76. Soma, F.; Takahashi, F.; Yamaguchi-Shinozaki, K.; Shinozaki, K. Cellular phosphorylation signaling and gene expression in drought stress responses, ABA-dependent and ABA-independent regulatory systems. *Plants* **2021**, *10*, 756. [CrossRef] [PubMed]
77. Gong, Z.; Xiong, L.; Shi, H.; Yang, S.; Herrera-Estrella, L.R.; Xu, G. Plant abiotic stress response and nutrient use efficiency. *Sci. China-Life Sci.* **2020**, *63*, 635–674. [CrossRef] [PubMed]
78. Weng, J.K.; Ye, M.; Li, B.; Noel, J.P. Co-evolution of hormone metabolism and signaling networks expands plant adaptive plasticity. *Cell* **2016**, *166*, 881–893. [CrossRef]
79. Umezawa, T.; Sugiyama, N.; Takahashi, F.; Anderson, J.C.; Ishihama, Y.; Peck, S.C.; Shinozaki, K. Genetics and Phosphoproteomics Reveal a Protein Phosphorylation Network in the Abscisic Acid Signaling Pathway in *Arabidopsis thaliana*. *Sci. Signal.* **2013**, *6*, rs8. [CrossRef]
80. Kang, J.Y.; Choi, H.I.; Im, M.Y.; Kim, S.Y. Arabidopsis basic leucine zipper proteins that mediate stress-responsive abscisic acid signaling. *Plant Cell* **2002**, *14*, 343–357. [CrossRef]

horticulturae

MDPI

Article

Transcriptome Analysis Reveals Key Pathways and Candidate Genes for Resistance to *Plasmodiophora brassicae* in Radish

Yinbo Ma [1,†], Xinyuan Li [1,†], Feng Cui [1], Qian Yu [1], Baoyang Liu [1], Xinyi Guo [1] and Liwang Liu [1,2,*]

[1] College of Horticulture and Landscape Architecture, Yangzhou University, Yangzhou 225009, China
[2] National Key Laboratory of Crop Genetics & Germplasm Enhancement and Utilization, Key Laboratory of Horticultural Crop Biology and Genetic Improvement (East China) of MOAR, College of Horticulture, Nanjing Agricultural University, Nanjing 210095, China
* Correspondence: nauliulw@njau.edu.cn
† These authors contributed equally to this work.

Abstract

Clubroot disease, caused by the soil-borne pathogen *Plasmodiophora brassicae*, poses a severe threat to the global production of Brassicaceae crops, including radish (*Raphanus sativus* L.). Although resistance breeding is an important method for sustainable disease management, the molecular mechanism underlying clubroot resistance remains elusive in radish compared to other Brassicaceae species. In this study, 52 radish inbred lines were screened for disease responses following *P. brassicae* inoculation, with the resistant line T6 and the susceptible line T14 selected for transcriptome analysis. RNA-Seq was performed at 10, 20, and 30 days post inoculation (DPI) to elucidate transcriptional responses. The susceptible line T14 exhibited a higher number of differentially expressed genes (DEGs) and persistent upregulation across all time points, indicating ineffective defense responses and metabolic hijacking by the pathogen. In contrast, the resistant line T6 displayed temporally coordinated defense activation marked by rapid induction of core immune mechanisms: enhanced plant–pathogen interaction recognition, MAPK cascade signaling, and phytohormone transduction pathways, consistent with effector-triggered immunity priming and multilayered defense orchestration. These findings indicate that resistance in T6 could be mediated by the rapid activation of multilayered defense mechanisms, including *R* gene-mediated recognition, MAPK-Ca^{2+}-ROS signaling, and jasmonic acid (JA) pathway modulation. The outcomes of this study would not only facilitate clarifying the molecular mechanism underlying clubroot resistance, but also provide valuable resources for genetic improvement of clubroot resistance in radish.

Keywords: radish; clubroot disease; transcriptome analysis; plant–pathogen interaction; resistance gene

1. Introduction

Radish (*Raphanus sativus* L.), a member of the Brassicaceae family, is an economically significant vegetable crop cultivated globally, particularly in Asian agroecosystems [1]. As a versatile crop, various radish types contribute substantially to global vegetable production and agricultural economies [2]. Nutritionally, radish is recognized as an essential component of human diets due to its high dietary fiber content, abundance of water-soluble vitamins (such as vitamin C), and valuable mineral profiles, including potassium and calcium [3,4]. Beyond basic nutrition, radish roots and leaves contain various bioactive compounds, notably glucosinolates and phenolic compounds, which are associated with

antioxidant and health-promoting properties [5–7]. Furthermore, *Semen Raphani*, recorded in the Chinese Pharmacopoeia (2015 edition), consists of the dried seeds of radish, with therapeutic applications for digestive ailments, including indigestion and gastric pains [8]. Otherwise, the radish is also used as a household remedy for gallstones, liver diseases, rectal prolapse, and other diseases in Unani, Greco-Arabic, and Indian medicine [9]. Therefore, radish holds an important position in human livelihoods due to its multifaceted roles in dietary nutrition, therapeutic applications, and agricultural systems.

Despite its agronomic and medicinal importance, radish production faces a critical threat from clubroot disease, caused by the obligate biotrophic plasmodiophorid protist *P. brassicae* [10,11]. This pathogen exhibits a complex life cycle involving the primary infection of root hairs and secondary infection of the root cortex, leading to the characteristic gall formation, and produces highly persistent resting spores that can remain viable in soil for over a decade, making eradication extremely difficult [12,13]. The historical origins of clubroot can be traced back to its initial identification on the west coast of the Mediterranean Sea in 1737 [14]. Subsequently, this pathogenic agent has disseminated globally, especially exhibiting a particular affinity for temperate regions and locations characterized by weakly acidic soils [15]. Moreover, the intensified and continuous cultivation practices applied to Brassicaceae crops have accelerated the widespread dissemination of clubroot, transforming it into a profoundly impactful soil-borne disease on a global scale [16]. Clubroot induces large root galls that impair plant growth and reduce both the yield and quality of economically important crops such as Chinese cabbage, cabbage, rapeseed, and radish. For instance, in Canada in 2005, canola yield losses reached as high as 50%, while annual yield losses of 20–30% have been reported for Brassicaceae crops in China [17,18]. Beyond yield implications, clubroot exerts a discernible influence on crop quality, with documented reductions in seed oil content by 2–6% in oil crops [19]. The persistent nature of *P. brassicae* resting spores in soil poses a long-term challenge for sustainable agriculture, demanding effective and durable management strategies.

Currently, managing clubroot disease remains a significant challenge in Brassicaceae crops. Traditional methods such as crop rotation have limited efficacy due to the longevity of resting spores [20]. Soil pH adjustment through liming can reduce disease severity, but it is not always practical or sufficient. Chemical control using fungicides has shown limited success and raises environmental concerns [21]. Consequently, developing and cultivating clubroot-resistant cultivars is considered the most effective strategy for preventing and controlling this devastating disease. In recent years, significant progress has been made in identifying and mapping clubroot resistance (CR) genes/loci in several Brassica species. Numerous quantitative trait loci (QTLs) and resistance genes, such as *CRa*, *CRb*, and *WeiTsing*, have been characterized in *Brassica rapa* (Chinese cabbage, turnip) and *Brassica oleracea* (cabbage, broccoli, cauliflower), providing valuable resources for resistance breeding in these crops [22–26]. However, compared to these species, the molecular basis of clubroot resistance in radish remains poorly understood. Although several QTLs (e.g., *Crs1*, *RsCr6*) [27–29] have been identified, the functional genes conferring resistance have yet to be characterized, which limits the application of marker-assisted selection and gene editing in resistance breeding.

RNA-Seq has emerged as a powerful tool to systematically investigate gene expression dynamics during plant–pathogen interactions. Transcriptomic analysis enables the identification of DEGs and regulatory networks activated upon pathogen infection, thereby providing insights into resistance mechanisms and candidate resistance genes. In the context of plant immunity, key defense responses are often associated with the activation of specific metabolic and signaling pathways. Notably, the plant–pathogen interaction pathway, MAPK cascades, and plant hormone signaling are critical in initiating and co-

ordinating immune responses [30,31]. Additionally, secondary metabolic pathways such as the phenylpropanoid biosynthesis pathway contribute to cell wall reinforcement and the synthesis of antimicrobial compounds [32,33], while calcium signaling and reactive oxygen species production further mediate rapid local defense responses [34,35]. In this study, we performed a comparative transcriptomic analysis of resistant (T6) and susceptible (T14) radish inbred lines at three time points following inoculation with *P. brassicae*. By characterizing global gene expression profiles and enriched pathways, this study aimed to uncover the molecular basis of clubroot resistance in radish and to identify key genes and regulatory mechanisms involved in defense responses. These findings provide valuable insights into the molecular basis of clubroot resistance in radish and lay the foundation for the genetic improvement in radish breeding programs.

2. Materials and Methods

2.1. Plant Materials and P. brassica Inoculation

Totally, 52 inbred lines collected from our laboratory germplasm repository were selected for clubroot resistance evaluation. Ten plants per line were grown in 50-well plastic trays filled with a sterilized growing medium consisting of vermiculite, peat moss, and soil in a 1:1:1 ratio. The plants were maintained in a controlled growth chamber at 25/20 °C (day/night) with a 16/8 h photoperiod. The investigation of clubroot disease was carried out 4 weeks post-inoculation. The pathogen isolation protocol, inoculation methodology, and disease index (DI) calculation for *P. brassicae* suspension preparation followed established procedures described in the previous study [28]. Briefly, the concentration of resting spores was determined using a hemocytometer and adjusted to 1×10^7 spores/mL for inoculation. Ten days after sowing, each seedling was inoculated by injecting 1 mL of the spore suspension into the soil near the root. The disease index (DI) was assessed four weeks post-inoculation based on a 0–4 scale as follows: 0, no galling; 1, a few small galls on lateral roots; 2, moderate galling on lateral roots or main root; 3, numerous galls on the main roots; and 4, clubroot rot or plant death.

To elucidate the molecular mechanisms underlying clubroot resistance following *P. brassicae* inoculation in radish, transcriptome analysis was performed. Based on the initial screening, lines exhibiting contrasting phenotypes (susceptible and resistant) were selected for further analysis. The experimental design included parallel treatments where both resistant and susceptible lines were inoculated with *P. brassicae* at 10 days post-sowing, with corresponding mock controls treated with distilled water. To systematically capture the molecular responses during disease progression and resistance activation, a total of 36 root samples were collected from susceptible and resistant lines at 10, 20, and 30 DPI following either pathogen inoculation or mock treatment. Each sample consisted of three roots pooled from three plants. Three independent biological replicates were included for each treatment (inoculated and mock-inoculated) and each time point. All samples were immediately immersed in liquid nitrogen and stored at −80 °C until further processing for RNA extraction and sequencing or RT-qPCR analysis.

2.2. RNA Extraction and Sequencing

Total RNAs for transcriptome sequencing were extracted using the Eastep® Super Total RNA Extraction Kit (Promega Co., Ltd., Shanghai, China) following the manufacturer's protocol. For transcriptome sequencing, mRNA was purified from total RNA using poly-T oligo-attached magnetic beads. The purified mRNA was then fragmented and used as a template for first-strand cDNA synthesis with random hexamer primers, followed by second-strand cDNA synthesis. The resulting cDNA fragments were subjected to end-repair, A-tailing, and adapter ligation. After PCR amplification, the final cDNA

libraries were constructed. The library construction and sequencing were performed by Annaroad Gene Technology Co., Ltd. (Beijing, China) on an Illumina NovaSeq 6000 platform, generating 150 bp paired-end reads.

2.3. Analysis of the RNA-Seq Data

Raw sequencing data underwent FastQC (v0.11.9) [36] quality evaluation, examining per-base scores, adapter content, and duplication rates. Filtering via fastp (v0.23.2; defaults) [37] included trimming low-quality bases (Q < 20), removing adapters, and discarding reads <36 bp, producing clean reads validated through post-filtering FastQC. Using HISAT2 (v2.2.1) [38], processed reads were aligned to the radish genome [39], generating BAM-formatted alignments. Gene quantification was performed using featureCounts (v2.0.1; Subread) [40] with GTF annotations. FPKM normalization was used to compensate for variations in transcript length and sequencing depth. DEGs were identified using DESeq2 (v1.34.0) [41] with a negative binomial model ($|\log_2 FC| \geq 1$, adjusted $q \leq 0.05$). KEGG pathway analysis was performed using clusterProfiler (v4.2.2) [42] with functional enrichment adjusted by the Benjamini–Hochberg correction.

2.4. Real-Time qPCR Analysis

To evaluate the accuracy of transcriptome data, quantitative RT-qPCR analyses were performed. The RT-qPCR primers were designed based on the available radish sequence information (Supplementary Table S1). The RT-qPCR analysis was performed using the CFV96™ Real-Time System (Bio-Rad, Berkeley, CA, USA) and the SYBR Green Supermix (Transgen, Beijing, China). The PCR program was as follows: 95 °C for 3 min, 39 cycles of 95 °C for 15 s, and 58 °C for 20 s. Data were acquired during the annealing/extension step and were analyzed using the CFX Manager software (version 2.1) (Bio-Rad). Three replicates of each sample were analyzed, and mean gene expression levels were normalized against 18S rRNA levels.

3. Results

3.1. The Investigation of the Resistance to P. brassicae in 52 Radish Lines

Based on the phenotypic evaluation of clubroot resistance (Table 1), six radish lines (T6, T11, T30, T35, YZ-8, and YZ-11) were identified as completely resistant, as they exhibited normal growth without any clubroot symptoms. In contrast, seven lines (T7, T8, T14, YZ-6, YZ-18, YZ-20, and YZ-21) displayed severe clubroot symptoms, including extensive galling on both taproots and lateral roots, stunted plant growth, and leaf yellowing, and were classified as completely susceptible. The remaining 39 lines showed intermediate levels of susceptibility, with varying degrees of root galling and reduced growth compared to the control. To investigate the molecular mechanisms underlying clubroot resistance, lines T6 and T14 (Figure 1), representing the resistant and susceptible phenotypes, respectively, were selected for further transcriptome analysis.

Table 1. Disease index of 52 radish lines after inoculation with *P. brassicae*.

Name	Plant NO. [a]	DI [b]	Phenotype [c]	Name	Plant NO.	DI	Phenotype
T1	10	3.40 ± 1.34	S	19_12	9	1.33 ± 0.82	S
T2	10	0.67 ± 1.63	S	19_16	10	3.83 ± 0.41	S
T3	10	2.00 ± 2.83	S	MYB01	9	1.80 ± 1.48	S
T5	10	3.17 ± 1.60	S	MYB02	10	3.60 ± 0.89	S
T6	9	0.00 ± 0.00	R	YZ-1	10	3.22 ± 1.39	S
T7	10	4.00 ± 0.00	S	YZ-2	10	2.27 ± 1.74	S

Table 1. *Cont.*

Name	Plant NO. [a]	DI [b]	Phenotype [c]	Name	Plant NO.	DI	Phenotype
T8	9	4.00 ± 0.00	S	YZ-3	8	3.40 ± 1.26	S
T9	10	2.67 ± 2.07	S	YZ-4	10	3.10 ± 1.66	S
T10	8	3.25 ± 1.50	S	YZ-5	10	2.88 ± 1.81	S
T11	10	0.00 ± 0.00	R	YZ-6	10	4.00 ± 0.00	S
T13	10	2.25 ± 1.71	S	YZ-7	10	3.83 ± 0.41	S
T14	10	4.00 ± 0.00	S	YZ-8	10	0.00 ± 0.00	R
T15	10	2.00 ± 1.90	S	YZ-9	10	1.23 ± 1.92	S
T16	10	2.83 ± 1.47	S	YZ-10	9	2.88 ± 1.81	S
T17	10	3.60 ± 0.55	S	YZ-11	10	0.00 ± 0.00	R
T20	8	3.50 ± 1.00	S	YZ-12	10	2.62 ± 1.76	S
T21	10	3.20 ± 1.79	S	YZ-13	9	2.14 ± 1.68	S
T22	9	3.40 ± 1.34	S	YZ-14	10	3.82 ± 0.60	S
T23	10	2.67 ± 2.07	S	YZ-15	10	3.86 ± 0.38	S
T24	10	0.20 ± 0.45	S	YZ-16	9	2.56 ± 1.51	S
T25	9	0.80 ± 1.79	S	YZ-17	10	3.40 ± 0.97	S
T26	10	0.20 ± 0.45	S	YZ-18	9	4.00 ± 0.00	S
T30	9	0.00 ± 0.00	R	YZ-19	10	3.43 ± 1.13	S
T31	10	0.83 ± 1.60	S	YZ-20	9	4.00 ± 0.00	S
T33	9	0.67 ± 1.63	S	YZ-21	10	4.00 ± 0.00	S
T35	10	0.00 ± 0.00	R	YZ-22	10	3.17 ± 1.33	S

Note: [a] The number of plants used in the experiments was consistent across each radish line; [b] DI: disease index; [c] R: resistance; S: susceptible.

Figure 1. The root phenotypes of T14 and T6 at 30 days after *P. brassica* inoculation.

3.2. Sequencing Data Analysis

To obtain a global view of the transcriptomic changes of the radish plants in response to *P. brassica* infection, the expression profiles of pathogen-infected radish samples were compared to those of the mock-inoculated control plants by high-throughput sequencing. The RNA-Seq generated between 43,088,690 and 49,731,344 raw reads for the *P. brassicae* infected group and between 42,013,050 and 49,757,114 raw reads for the control group. Following the removal of low-quality reads and adapter sequences, the number of clean reads ranged from 40,728,900 to 47,626,288 in the infected group and from 43,233,294 to 47,710,712 in the control group (Supplementary Table S2). Alignment of these clean reads to the radish reference genome yielded mapping percentages between 92.63% and 95.81% for the infected group and between 92.61% and 97.61% for the control group. The RNA-Seq data have been deposited in the Genome Sequence Archive (GSA) of the National Genomics Data Center (NGDC) under the project accession number PRJCA030868.

3.3. DEGs Between Resistant and Susceptible Radish Lines in Uninoculated or Inoculated Conditions

To investigate the gene expression patterns in susceptible and resistant plant lines, we analyzed DEGs in resistant (T6) and susceptible (T14) radish lines at 10, 20, and 30 DPI with *P. brassica*. Significant differences in gene expression patterns were observed between the two lines. The susceptible line T14 exhibited a persistent dominance of up-regulated over down-regulated genes across all time points (Figure 2). Specifically, T14 showed 2221 up-regulated vs. 1589 down-regulated genes at 10 DPI, 3586 vs. 2946 at 20 DPI, and 3354 vs. 2453 at 30 DPI. Conversely, the resistant line T6 demonstrated an inverse regulatory pattern, with down-regulated genes consistently outnumbering up-regulated counterparts: 1107 vs. 2004 at 10 DPI, 2280 vs. 2991 at 20 DPI, and 388 vs. 665 at 30 DPI (Figure 2B). Furthermore, the overall magnitude of the transcriptional response, indicated by the total number of DEGs, was markedly higher in the susceptible line T14 than in the resistant line T6 across all examined time points (Figure 2). To identify the core DEGs involved in pathogen response, a Venn analysis of temporally regulated genes was performed. In the comparative combinations of mock vs. treatment of T14, 53 DEGs were significantly regulated after *P. brassica* treatment at three time points. In the resistance plant line T6, six DEGs were significantly regulated after *P. brassica* treatment at three time points (Figure 3).

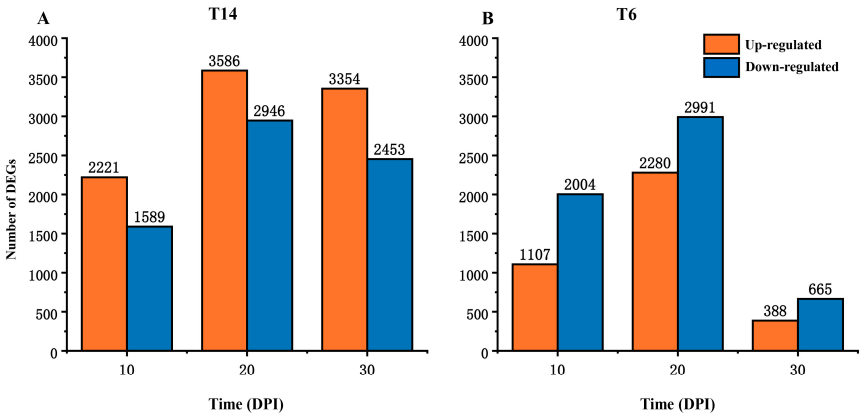

Figure 2. The number of DEGs of T14 (**A**) and T6 (**B**) at 10, 20, and 30 days post inoculation (DPI).

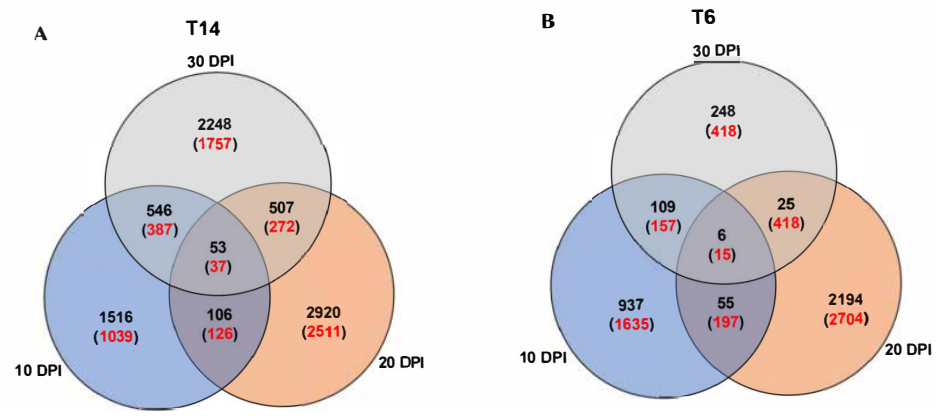

Figure 3. Venn diagrams represented common and specific up and down DEGs identified at 10, 20, and 30 DPI in T14 (**A**) and T6 (**B**). The black numbers represent the number of up-regulated genes, and the red numbers represent the number of down-regulated genes.

3.4. Differential Enrichment of Metabolic Pathways in Resistant and Susceptible Lines

KEGG pathway analysis was employed to elucidate the biological processes associated with the DEGs identified in the resistant (T6) and susceptible (T14) lines at 10, 20, and 30 DPI, relative to mock-inoculated controls (Figures 3 and 4). This analysis highlighted significant

enrichment of DEGs in several key pathways pertinent to plant–microbe interactions in both lines, notably including 'plant–pathogen interaction', 'MAPK signaling pathway', and 'Plant hormone signal transduction'.

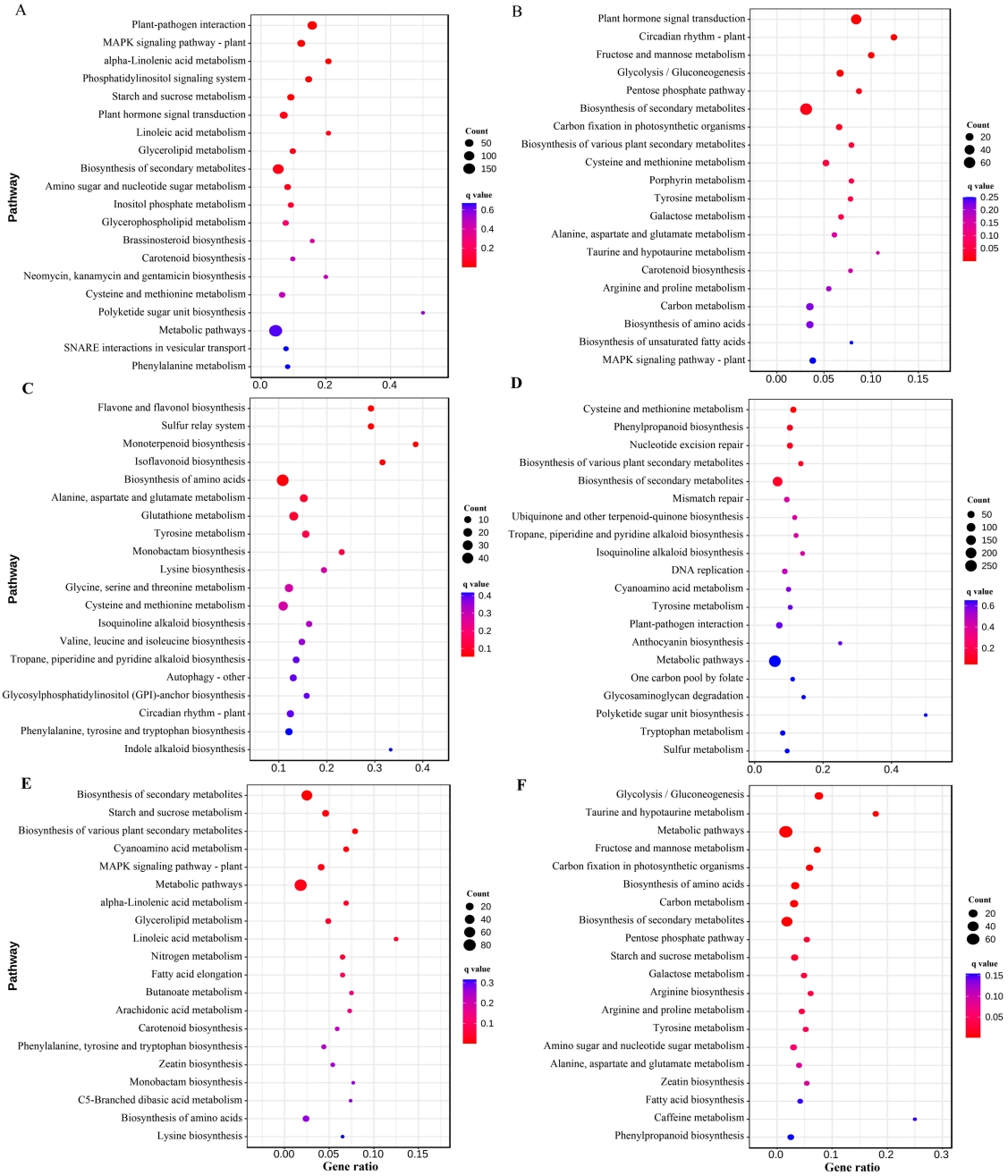

Figure 4. Top 20 KEGG pathways enriched in DEGs for T14. The size of each circle represents the number of DEGs, and the rich factor was calculated using the number of enriched genes divided by the total number of background genes in the corresponding pathway. (**A**,**C**,**E**), down-regulated DEGs of T14 at 10, 20, and 30 DPI. (**B**,**D**,**F**) up-regulated DEGs of T14 at 10, 20, and 30 DPI. The q value was calculated using the Benjamini–Hochberg correction.

The 'plant–pathogen interaction' pathway plays a pivotal regulatory role in plant immune responses. Transcriptomic analysis revealed distinct dynamics: at 10 days post inoculation, significant enrichment of DEGs occurred in this pathway in both lines (Figures 4 and 5). However, the susceptible line T14 was dominated by down-regulation (72 DEGs down vs. 5 up), whereas the resistant line T6 exhibited a clear activation profile (50 DEGs up vs. 25 down). By 20 DPI, T14 initiated a defense-related gene response

(33 DEGs up vs. 28 down), while T6 maintained a relatively balanced regulatory state (37 DEGs up vs. 36 down). At 30 DPI, T6 displayed robust pathway activation, characterized by a surge in up-regulated genes (82 DEGs up vs. 22 down). In contrast, the immune response in T14 was markedly attenuated (three DEGs up vs. eight down), indicating that the resistant line possesses the capacity for sustained and amplified defense signaling.

The MAPK signaling pathway demonstrates critical involvement in plant disease resistance mechanisms. This study analyzed gene expression in the susceptible line T14 and the resistant line T6 at three time points following pathogen infection. The results showed that in the susceptible line T14, the number of down-regulated genes associated with the MAPK signaling pathway exceeded that of up-regulated genes across the three examined time points (Figure 6). Conversely, the resistant line T6 exhibited a prevalence of up-regulated genes over down-regulated ones within this pathway. Furthermore, plant hormone signaling not only regulates plant growth and development but also plays a pivotal role in disease response. A comparison of DEGs between the two lines post-infection revealed significant enrichment of DEGs associated with ethylene (ET) and JA signaling pathways (Figure 7, Supplementary Tables S3 and S4), with 131 and 191 DEGs identified, respectively. Additionally, 16 DEGs related to ABA and 9 DEGs linked to SA were detected (Figure 6A). Further analysis indicated that following infection by *P. brassicae*, DEGs were also identified in the calcium ion (Ca^{2+}) signaling and reactive oxygen species (ROS) metabolic pathways (Figure 7B). Notably, the starch metabolism pathway was also impacted, particularly in the susceptible line T14, where a total of 52 DEGs associated with this pathway were identified.

3.5. Differential Gene Ontology Enrichment and Expression Patterns Between Resistant and Susceptible Lines

To characterize the functional implications of transcriptional changes following inoculation, gene ontology (GO) enrichment analysis was performed on the DEGs identified at three time points comparing inoculated versus control samples within both the resistant (T6) and susceptible (T14) lines. DEGs were categorized into the three main GO domains: biological process, cellular component, and molecular function. Across all time points and both lines, prominent terms within the cellular component category included 'cell part' and 'organelle'. Within the molecular function category, 'catalytic activity' and 'binding' were highly represented. A comparative analysis of DEG profiles between the resistant (T6) and susceptible (T14) lines post-inoculation revealed distinct overall patterns. Notably, the susceptible line T14 exhibited a preponderance of up-regulated DEGs compared to down-regulated DEGs (Supplementary Figure S1). Conversely, the resistant line T6 displayed a predominance of down-regulated DEGs relative to up-regulated DEGs (Supplementary Figure S2).

Based on GO annotations and resistance gene characteristics, 51 putative resistance (R) genes were identified (Figure 6A). Among these, 47 genes contained the nucleotide-binding site and leucine-rich repeat (NB-ARC) domain, 2 were classified as receptor-like kinases (RLKs), and 2 as receptor-like proteins (RLPs). At 10 DPI, the expression levels of *R* genes in the resistant line T6 were significantly up-regulated and generally higher compared to their counterparts in the susceptible line T14 at the same time point. Notably, however, two specific genes (*Rsa6g032250* and *Rsa6g032260*) exhibited significantly higher expression levels in the susceptible line T14 compared to the resistant line T6 across all three examined time points. The calcium signaling pathway, including calcium-dependent protein kinases (CPKs) and calmodulin-like proteins (CMLs), displayed distinct regulation: 14 CPK and 4 CML genes were up-regulated in T6 at 10 DPI (Figure 7B). A comparative analysis of peroxidase genes revealed 11 significantly differentially expressed members. At 10 DPI, T14 showed five down-regulated and six up-regulated peroxidase genes, whereas T6 exhibited two down-regulated and nine up-regulated genes. By 20 DPI, all peroxidase genes in

T14, except *Rsa5g023890*, were up-regulated. A total of 11 significantly differentially expressed peroxidase genes were detected between the two lines. At 10 DPI, T14 exhibited down-regulation of 5 and upregulation of 6 peroxidase genes, whereas T6 showed down-regulation of two and upregulation of nine such genes. By 20 DPI, nearly all identified peroxidase genes in T14 were up-regulated, except for *Rsa5g023890*. Callose synthase (CALS) contributes to plant defense via callose deposition at infection sites. The results showed that the CALS gene *Rsa2g028300* was up-regulated in the susceptible line T14 but down-regulated in the resistant line T6.

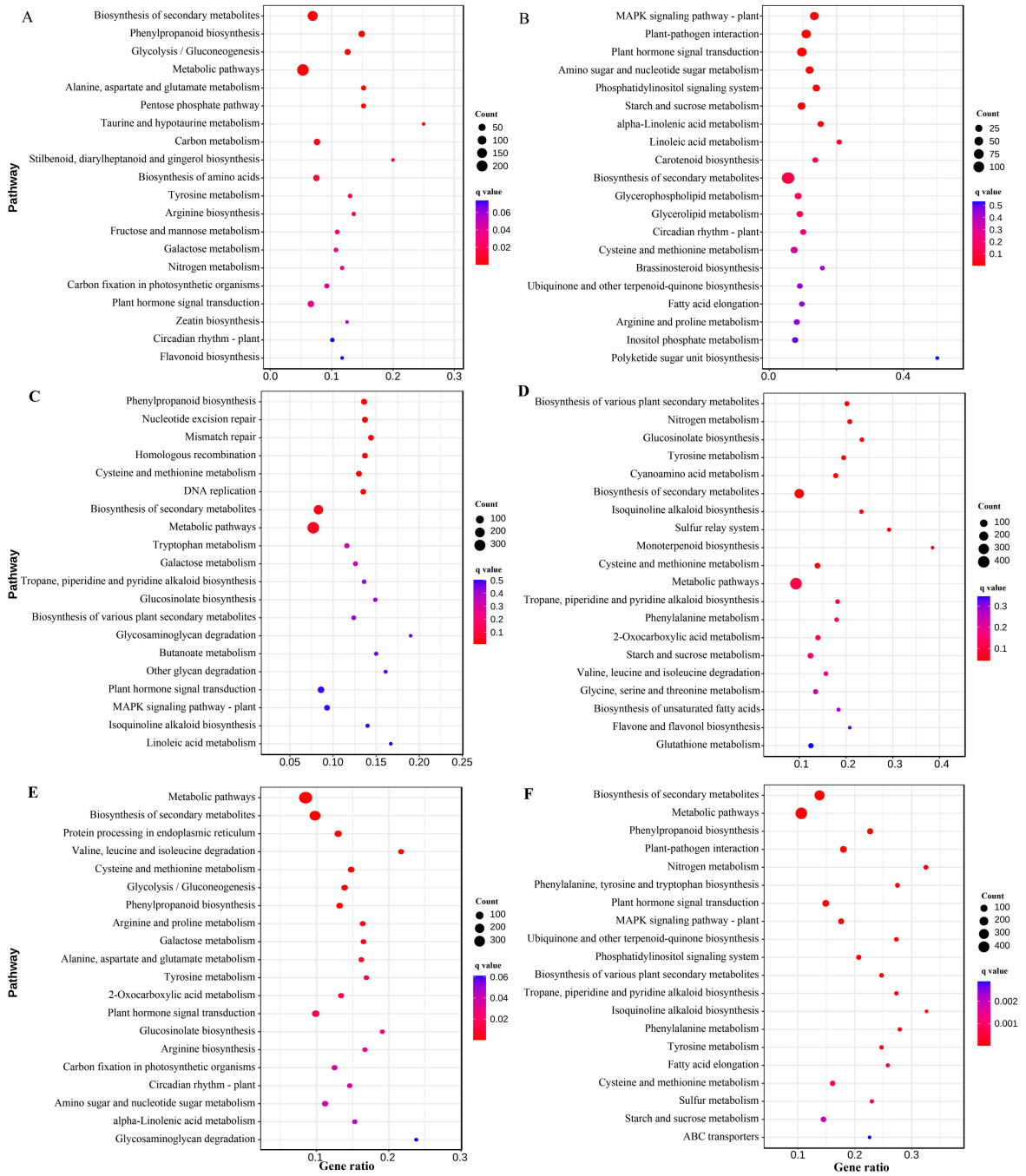

Figure 5. Top 20 KEGG pathways enriched in DEGs for T6. The size of each circle represents the number of DEGs, and the rich factor was calculated using the number of enriched genes divided by the total number of background genes in the corresponding pathway. (**A**,**C**,**E**), down-regulated DEGs of T6 at 10, 20, and 30 DPI. (**B**,**D**,**F**) up-regulated DEGs of T6 at 10, 20, and 30 DPI. The q value was calculated using the Benjamini–Hochberg correction.

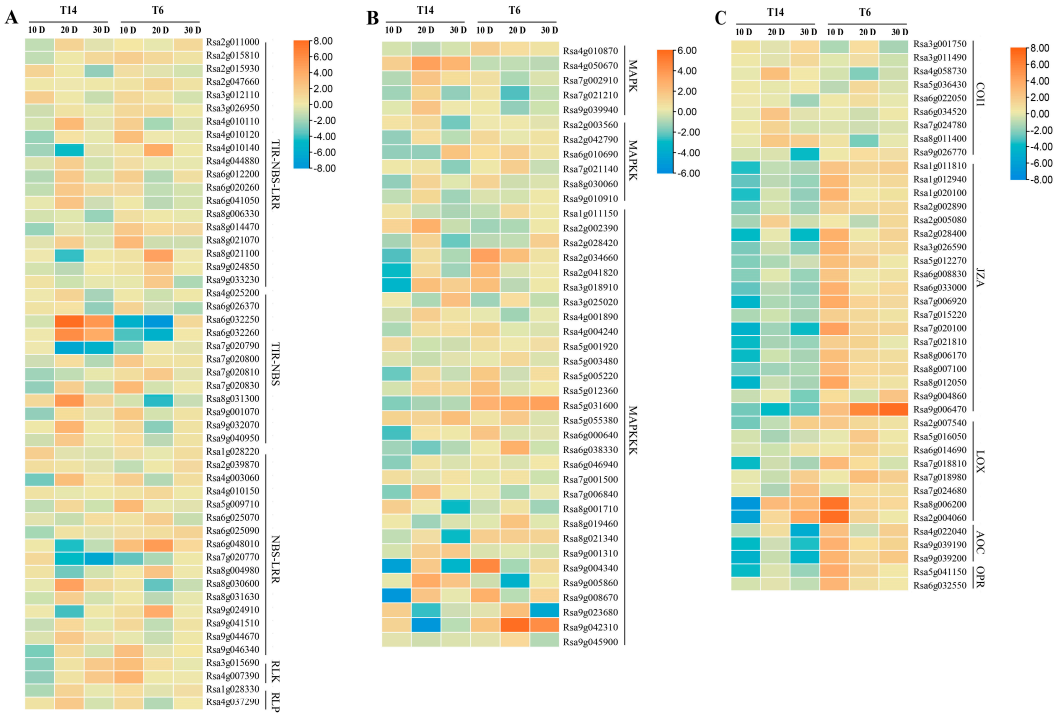

Figure 6. Heatmap of DEGs related to resistance genes (**A**), MAPK signaling (**B**), and jasmonic acid (**C**) of two varieties (T14 and T6) at 10, 20, and 30 DPI. The intensity of the color represents the level of expression.

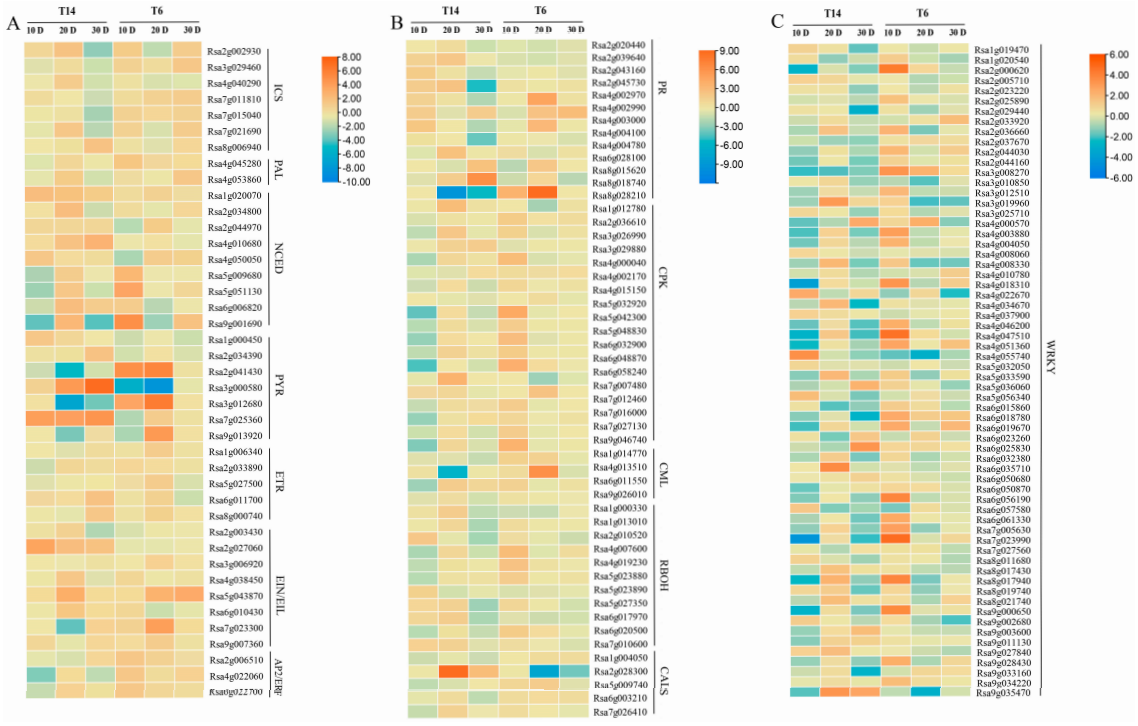

Figure 7. Heatmap of DEGs related to plant hormone signal transduction (**A**), Ca^{2+} (**B**), and transcription factors WRKYs (**C**) of two varieties (T14 and T6) at 10, 20, and 30 DPI. The intensity of the color represents the level of expression.

Jasmonic acid (JA) is a critical phytohormone, regulating defense responses, growth, and stress adaptation. Key genes in JA signaling (Figure 6C), *Coronatine Insensitive 1* (*COI1*), and *Jasmonate ZIM-domain* (*JAZ*), displayed contrasting regulation. Following infection, most *JAZ* genes in T14 were negatively regulated across the three time points, while they were generally

positively regulated in the resistant line T6. The gene *Rsa9g006470* showed a particularly pronounced expression difference between the lines. The genes involved in JA biosynthesis, including *Lipoxygenases* (*LOXs*), *Allene Oxide Cyclase* (*AOC*), and *OPDA Reductase* (*OPR*), also exhibited specific patterns. The expression trends of *AOC* and *OPR* genes paralleled those of *JAZ* genes (down-regulated in T14, up-regulated in T6). However, *LOX* genes differed in their expression patterns: they were consistently up-regulated in T6 across all time points, whereas in T14, they were down-regulated at 10 and 20 DPI, but five *LOX* genes were up-regulated at 30 DPI. Notably, *Rsa2g004060* and *Rsa8g006200* displayed highly significant expression differences between the lines at 10 DPI. A preliminary analysis of genes related to SA, ABA, and ethylene (ET) signaling pathways indicated divergent responses among PYR/PYL/RCAR receptor genes in the ABA pathway (Figure 7A). Specifically, *Rsa3g000580* and *Rsa7g025360* were highly expressed in the susceptible line T14 and lowly expressed in the resistant line T6, whereas *Rsa3g012680* and *Rsa2g041430* showed the inverse pattern.

Among the DEGs, 64 members belonging to the WRKY transcription factor (TFs) family were identified (Figure 7C). At 10 DPI, these WRKY genes were predominantly up-regulated in the resistant line T6 and down-regulated in the susceptible line T14. Finally, an analysis of genes associated with the starch regulatory pathway revealed that most of these genes were up-regulated in the susceptible line T14 at later time points (20 and 30 DPI).

3.6. Validation of RNA-Seq Data by RT-qPCR

To validate the RNA-Seq expression profiles, the RT–qPCR analysis was performed on eight selected DEGs. These included three putative disease-associated genes (*Rsa6g032250*, *Rsa2g028300*, *Rsa7g020770*), two MAPK pathway genes (*Rsa5g031600*, *Rsa9g042310*), two JA pathway genes, and one ABA pathway gene (*Rsa3g000580*). The relative expression levels measured by RT-qPCR in resistant and susceptible lines at three time points (inoculated vs. uninoculated controls) showed trends largely consistent with the RNA-Seq data, thereby corroborating the transcriptomic findings. However, the RNA-Seq analysis exhibited a broader dynamic range, detecting fold changes of greater magnitude compared to RT-qPCR (Figure 8).

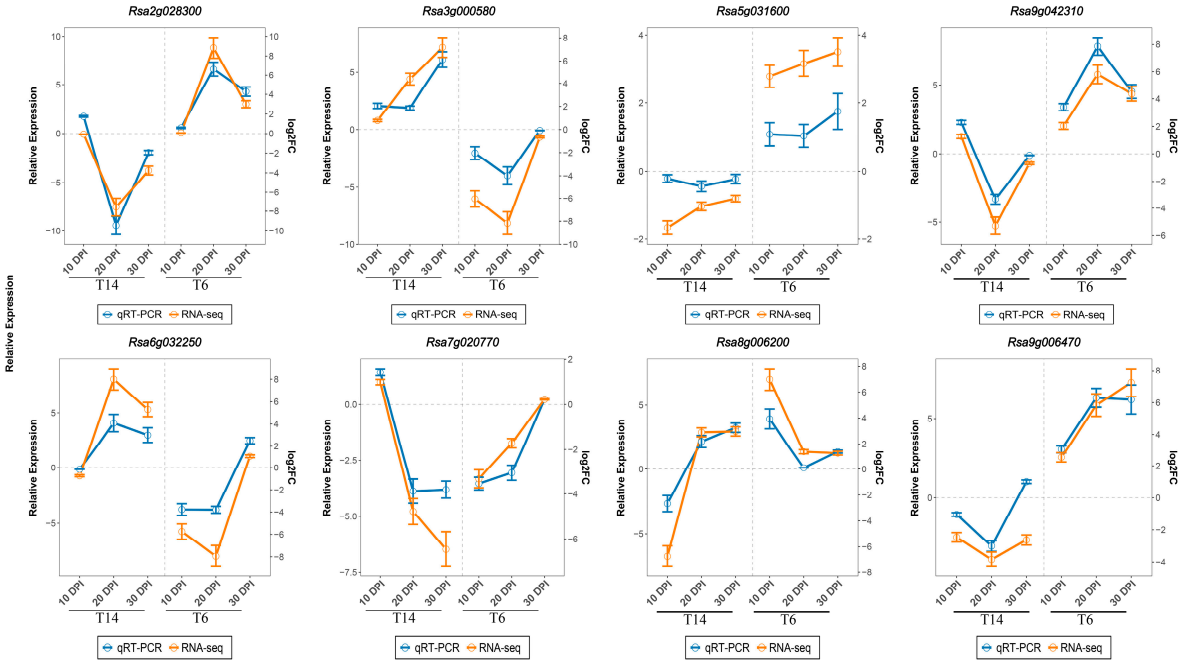

Figure 8. Validation of RNA–seq data by RT–qPCR. Blue lines represent the relative gene expression levels as measured by RT–qPCR (left y-axis), while orange lines indicate the $\log_2$ fold change ($\log_2$FC) derived from RNA-Seq read counts (right y-axis). Error bars denote the standard error of the mean (n = 3).

4. Discussion

Clubroot disease, caused by the obligate biotrophic plasmodiophorid protist *P. brassicae*, poses a significant threat to global cruciferous crop production. While resistance breeding remains the most effective control strategy, the molecular mechanisms underlying clubroot resistance in radishes are less understood compared to related *Brassica* species [25,26]. In this study, a total of 52 radish inbred lines were screened for their disease responses following inoculation with *P. brassicae*, resulting in the identification of six resistant and seven highly susceptible lines. Subsequently, transcriptomic reprogramming in susceptible (T14) and resistant (T6) radish lines following infection with *P. brassicae* revealed distinct defense strategies and susceptibility determinants. Notably, the resistant line T6 exhibited rapid activation of defense pathways, contrasting with delayed or dysregulated responses in T14, suggesting pathogen manipulation of host processes.

Transcriptomic analysis in susceptible and resistant lines during *P. brassicae* infection

The susceptible line (T14) displayed a global transcriptional upheaval, marked by a higher number of DEGs and predominant upregulation across all time points (Figure 2A). This pattern could suggest a potential reallocation of resources from growth toward defense, a strategy often associated with the 'growth-defense trade-off' hypothesis in plant immunity. The subsequent reduction in the number of DEGs at 30 DPI in the T6 line may indicate a successful containment of the pathogen, allowing the plant to restore metabolic homeostasis.

Multilayered defense activation in resistant and susceptible lines

We identified 51 putative *R* genes, predominantly encoding NB-ARC domain proteins, which were markedly up-regulated in T6 at 10 DPI. This aligns with effector-triggered immunity (ETI), where R proteins recognize pathogen effectors to initiate defense cascades. Intriguingly, two R-like genes (*Rsa6g032250* and *Rsa6g032260*) were constitutively up-regulated in T14, potentially functioning as susceptibility (S) genes or ineffective R alleles specific to race 4.

In the early activation of defense signaling pathways, plant–pathogen interaction was activated in T6 at 10 DPI (50 up vs. 25 down DEGs), while it was suppressed in T14 (5 up vs. 72 down) (Figures 4 and 5). MAPK cascades, critical for relaying pathogen-associated molecular pattern (PAMP) signals [43], likely coordinate downstream responses such as calcium signaling (14 CPKs and 4 CMLs up-regulated) and reactive oxygen species (ROS) production (nine peroxidase genes were up-regulated). This rapid signaling network activation may underpin T6's ability to limit pathogen spread through oxidative bursts and cellular reinforcement [44]. Among 64 WRKY transcription factors identified, most were up-regulated in T6 but down-regulated in T14. WRKY proteins, acting downstream of MAPK cascades, regulate defense gene expression by binding W-box elements in promoters [45]. Their early induction in T6 suggests a coordinated amplification of defense signals, contrasting with T14's failure to activate this regulatory network.

Hormonal crosstalk appears to be critical in modulating resistance outcomes. Our analysis revealed a striking divergence in the jasmonic acid (JA) pathway, where key components, including JAZ repressors and biosynthesis genes (AOC, OPR), were up-regulated in the resistant T6 line but suppressed in the susceptible T14 line. While JA typically mediates resistance to necrotrophic pathogens, its role in biotrophic interactions involves fine-tuning responses to balance defense and fitness costs [46,47]. The sustained upregulation of *LOX* genes in T6, contrasted with the transient suppression in T14, highlights the temporal regulation of JA biosynthesis. The highly differential *Rsa9g006470* (*JAZ*) warrants functional validation to elucidate its role in resistance. Our results also suggest the involvement of abscisic acid (ABA) and cross-pathway interactions. Specifically, ABA receptor genes

(*PYR/PYL/RCAR*) showed genotype-specific expression, with *Rsa3g000580* highly expressed in the susceptible T14 line and *Rsa2g041430* highly expressed in the resistant T6 line. This finding suggests a potential dual role for ABA as a defense modulator in this pathosystem. ABA may antagonize JA signaling in T14, exacerbating susceptibility, as observed in other pathosystems. Although SA-related DEGs were limited, SA-JA interplay likely influences defense prioritization against *P. brassicae*'s biotrophic lifestyle [48].

The susceptible phenotype in T14 correlated with delayed defense initiation and metabolic manipulation by *P. brassicae*. Suppression of JA signaling and late-stage upregulation of starch metabolism genes (20–30 DPI) suggest pathogen-driven resource reallocation to support gall formation [49]. The paradoxical upregulation of callose synthase (*Rsa2g028300*) in T14 might reflect futile defense attempts or pathogen subversion of callose deposition, a mechanism observed in other susceptible interactions.

5. Conclusions

This transcriptomic study reveals the molecular mechanisms underlying clubroot resistance and susceptibility in radish. The resistant line T6 employs a multilayered defense strategy characterized by rapid activation of 51 putative *R* genes, MAPK-Ca^{2+}-ROS signaling, and JA-mediated regulation, enabling effective pathogen restriction through effector-triggered immunity and sustained defense signaling. In contrast, T14's susceptibility stems from delayed and dysregulated defense responses, marked by suppressed JA and MAPK pathways, pathogen-driven starch metabolism upregulation, and potential susceptibility genes, facilitating gall formation and disease progression. Key pathways, including plant–pathogen interaction, MAPK signaling, and hormonal crosstalk, exhibit divergent regulation, with T6 prioritizing early, coordinated immunity, and T14 succumbing to metabolic hijacking. These findings not only elucidate the different strategies radish employs in response to clubroot but also provide important molecular resources and a theoretical basis for improving clubroot resistance in radish.

Supplementary Materials: The following supporting information can be downloaded at https://www.mdpi.com/article/10.3390/horticulturae11070777/s1. Figure S1: Classification of gene ontology (GO) analysis of DEGs for T14; Figure S2: Classification of gene ontology (GO) analysis of DEGs for T6; Table S1: The primer sequence for RT-qPCR; Table S2: Summary of the RNA-seq experimental design and read alignment; Table S3: Expression of DEG involved ethylene biosynthesis pathway between T14 and T6; Table S4: Relative expression of DEGs involved jasmonic acid biosynthesis pathway between T14 and T6.

Author Contributions: Study conception and revising the manuscript: L.L.; writing the draft manuscript: Y.M. and X.L.; reviewing and creating figures and tables: F.C., Q.Y., B.L. and X.G.; reviewing and improving the manuscript: L.L. All authors have read and agreed to the published version of the manuscript.

Funding: This work was supported by grants from the Natural Science Foundation of Jiangsu Province (BK20220573), the Jiangsu Seed Industry Revitalization Project [JBGS(2021)071], the Key Technology R&D Program of Jiangsu Province (BE2023366).

Data Availability Statement: All data generated in this study are available within the paper and its additional files. The raw sequence data reported in this paper have been deposited in the National Genomics Data Center (NGDC) under the project accession number PRJCA030868.

Conflicts of Interest: The authors declare that they have no conflicts of interest.

References

1. Swaamy, K. Origin, distribution, genetic diversity and breeding of radish (*Raphanus sativus* L.). *Int. J. Dev. Res.* **2023**, *13*, 61657–61673.
2. Nishio, T. Economic and academic importance of radish. In *The Radish Genome*; Springer: Berlin/Heidelberg, Germany, 2017; pp. 1–10.
3. Gaba, J.; Bhardwaj, G.; Sharma, A.; Nayik, G.; Gull, A. *Antioxidants in Vegetables and Nuts-Properties and Health Benefits*; Springer: Berlin/Heidelberg, Germany, 2020.
4. Goyeneche, R.; Roura, S.; Ponce, A.; Vega-Gálvez, A.; Quispe-Fuentes, I.; Uribe, E.; Di Scala, K. Chemical characterization and antioxidant capacity of red radish (*Raphanus sativus* L.) leaves and roots. *J. Funct. Foods* **2015**, *16*, 256–264. [CrossRef]
5. Baenas, N.; Piegholdt, S.; Schloesser, A.; Moreno, D.A.; García-Viguera, C.; Rimbach, G.; Wagner, A.E. Metabolic activity of radish sprouts derived isothiocyanates in *Drosophila melanogaster*. *Int. J. Mol. Sci.* **2016**, *17*, 251. [CrossRef] [PubMed]
6. Ishida, M.; Kakizaki, T.; Morimitsu, Y.; Ohara, T.; Hatakeyama, K.; Yoshiaki, H.; Kohori, J.; Nishio, T. Novel glucosinolate composition lacking 4-methylthio-3-butenyl glucosinolate in Japanese white radish (*Raphanus sativus* L.). *Theor. Appl. Genet.* **2015**, *128*, 2037–2046. [CrossRef] [PubMed]
7. Malik, M.S.; Riley, M.B.; Norsworthy, J.K.; Bridges, W., Jr. Variation of glucosinolates in wild radish (*Raphanus raphanistrum*) accessions. *J. Agric. Food Chem.* **2010**, *58*, 11626–11632. [CrossRef]
8. Chinese Pharmacopoeia Commission. *Pharmacopoeia of the People's Republic of China*; China Medical Science Press: Beijing, China, 2015; Volume 1, pp. 188–189.
9. Shukla, S.; Chatterji, S.; Mehta, S.; Rai, P.K.; Singh, R.K.; Yadav, D.K.; Watal, G. Antidiabetic effect of *Raphanus sativus* root juice. *Pharm. Biol.* **2011**, *49*, 32–37. [CrossRef] [PubMed]
10. Xu, X.; Wu, C.; Zhang, F.; Yao, J.; Fan, L.; Liu, Z.; Yao, Y. Comprehensive review of *Plasmodiophora brassicae*: Pathogenesis, pathotype diversity, and integrated control methods. *Front. Microbiol.* **2025**, *16*, 1531393. [CrossRef]
11. Saharan, G.S.; Mehta, N.K.; Meena, P.D. The pathogen: *Plasmodiophora brassicae*. In *Clubroot Disease of Crucifers: Biology, Ecology and Disease Management*; Springer: Berlin/Heidelberg, Germany, 2021; pp. 87–120.
12. Ma, Y.; Meng, Y.; Wang, Y.; Xu, L.; Chen, Y.; Yuan, Y.; Zhang, X.; Wang, L.; Wei, X.; Li, B.; et al. Research progress on clubroot disease in Brassicaceae crops–advances and perspectives. *Veg. Res.* **2024**, *4*, e022. [CrossRef]
13. Javed, M.A.; Schwelm, A.; Zamani-Noor, N.; Salih, R.; Vañó, M.S.; Wu, J.; García, M.G.; Heick, T.M.; Luo, C.; Prakash, P. The clubroot pathogen *Plasmodiophora brassicae*: A profile update. *Mol. Plant Pathol.* **2022**, *24*, 89. [CrossRef]
14. Ainsworth, G.C. *Introduction to the History of Plant Pathology*; Cambridge University Press: Cambridge, UK, 1981.
15. Karling, J.S. *The Plasmodiophorales*, 2nd ed.; Hafner Publishing Company: New York, NY, USA, 1968.
16. Dixon, G.R. The occurrence and economic impact of *Plasmodiophora brassicae* and clubroot disease. *J. Plant Growth Regul.* **2009**, *28*, 194–202. [CrossRef]
17. Tewari, J.; Strelkov, S.; Orchard, D.; Hartman, M.; Lange, R.; Turkington, T. Identification of clubroot of crucifers on canola (*Brassica napus*) in Alberta. *Can. J. Plant Pathol.* **2005**, *27*, 143–144. [CrossRef]
18. Chai, A.; Xie, X.; Shi, Y.; Li, B. Research status of clubroot (*Plasmodiophora brassicae*) on cruciferous crops in China. *Can. J. Plant Pathol.* **2014**, *36* (Suppl. S1), 142–153. [CrossRef]
19. Engqvist, L. Distribution of clubroot (*Plasmodiophora brassicae* Wor) in Sweden and the effect of infection on oil content of oilseed rape (*Brassica napus* L.). *Sver. Utsädesförenings Tidskr.* **1994**, *104*, 82–86.
20. Hwang, S.; Ahmed, H.; Zhou, Q.; Turnbull, G.; Strelkov, S.; Gossen, B.; Peng, G. Effect of host and non-host crops on *Plasmodiophora brassicae* resting spore concentrations and clubroot of canola. *Plant Pathol.* **2015**, *64*, 1198–1206. [CrossRef]
21. Botero-Ramirez, A.; Kirk, B.; Strelkov, S.E. Optimizing clubroot management and the role of canola cultivar mixtures. *Pathogens* **2024**, *13*, 640. [CrossRef] [PubMed]
22. Shah, N.; Li, Q.; Xu, Q.; Liu, J.; Huang, F.; Zhan, Z.; Qin, P.; Zhou, X.; Yu, W.; Zhu, L. *CRb* and *PbBa8. 1* synergically increases resistant genes expression upon infection of *Plasmodiophora brassicae* in *Brassica napus*. *Genes* **2020**, *11*, 202. [CrossRef]
23. Hatakeyama, K.; Suwabe, K.; Tomita, R.N.; Kato, T.; Nunome, T.; Fukuoka, H.; Matsumoto, S. Identification and characterization of *Crr1a*, a gene for resistance to clubroot disease (*Plasmodiophora brassicae* Woronin) in *Brassica rapa* L. *PLoS ONE* **2013**, *8*, e54745. [CrossRef] [PubMed]
24. Hatakeyama, K.; Yuzawa, S.; Tonosaki, K.; Takahata, Y.; Matsumoto, S. Allelic variation of a clubroot resistance gene (*Crr1a*) in Japanese cultivars of Chinese cabbage (*Brassica rapa* L.). *Breed. Sci.* **2022**, *72*, 115–123. [CrossRef]
25. Yang, Z.; Jiang, Y.; Gong, J.; Li, Q.; Dun, B.; Liu, D.; Yin, F.; Yuan, L.; Zhou, X.; Wang, H. *R* gene triplication confers European fodder turnip with improved clubroot resistance. *Plant Biotechnol. J.* **2022**, *20*, 1502–1517. [CrossRef]
26. Wang, W.; Qin, L.; Zhang, W.; Tang, L.; Zhang, C.; Dong, X.; Miao, P.; Shen, M.; Du, H.; Cheng, H. *WeiTsing*, a pericycle-expressed ion channel, safeguards the stele to confer clubroot resistance. *Cell* **2023**, *186*, 2656–2671.e18. [CrossRef]
27. Kamei, A.; Tsuro, M.; Kubo, N.; Hayashi, T.; Wang, N.; Fujimura, T.; Hirai, M. QTL mapping of clubroot resistance in radish (*Raphanus sativus* L.). *Theor. Appl. Genet.* **2010**, *120*, 1021–1027. [CrossRef] [PubMed]

28. Gan, C.; Deng, X.; Cui, L.; Yu, X.; Yuan, W.; Dai, Z.; Yao, M.; Pang, W.; Ma, Y.; Yu, X. Construction of a high-density genetic linkage map and identification of quantitative trait loci associated with clubroot resistance in radish (*Raphanus sativus* L.). *Mol. Breed.* **2019**, *39*, 116. [CrossRef]
29. Gan, C.; Yan, C.; Pang, W.; Cui, L.; Fu, P.; Yu, X.; Qiu, Z.; Zhu, M.; Piao, Z.; Deng, X. Identification of novel locus *RsCr6* related to clubroot resistance in radish (*Raphanus sativus* L.). *Front. Plant Sci.* **2022**, *13*, 866211. [CrossRef]
30. Sun, T.; Zhang, Y. MAP kinase cascades in plant development and immune signaling. *EMBO Rep.* **2022**, *23*, e53817. [CrossRef] [PubMed]
31. Zhang, M.; Zhang, S. Mitogen-activated protein kinase cascades in plant signaling. *J. Integr. Plant Biol.* **2022**, *64*, 301–341. [CrossRef]
32. Yadav, V.; Wang, Z.; Wei, C.; Amo, A.; Ahmed, B.; Yang, X.; Zhang, X. Phenylpropanoid pathway engineering: An emerging approach towards plant defense. *Pathogens* **2020**, *9*, 312. [CrossRef]
33. Li, Q.; Liu, Z.; Jiang, Z.; Jia, M.; Hou, Z.; Dou, D.; Yu, J. Phenylalanine metabolism-dependent lignification confers rhizobacterium-induced plant resistance. *Plant Physiol.* **2025**, *197*, kiaf016. [CrossRef]
34. Gogoi, K.; Gogoi, H.; Borgohain, M.; Saikia, R.; Chikkaputtaiah, C.; Hiremath, S.; Basu, U. The molecular dynamics between reactive oxygen species (ROS), reactive nitrogen species (RNS) and phytohormones in plant's response to biotic stress. *Plant Cell Rep.* **2024**, *43*, 263. [CrossRef]
35. Gao, M.; He, Y.; Yin, X.; Zhong, X.; Yan, B.; Wu, Y.; Chen, J.; Li, X.; Zhai, K.; Huang, Y. Ca^{2+} sensor-mediated ROS scavenging suppresses rice immunity and is exploited by a fungal effector. *Cell* **2021**, *184*, 5391–5404.e17. [CrossRef]
36. Anders, S.; Huber, W. Differential expression analysis for sequence count data. *Nat. Preced.* **2010**. [CrossRef]
37. Chen, S. Ultrafast one-pass FASTQ data preprocessing, quality control, and deduplication using fastp. *Imeta* **2023**, *2*, e107. [CrossRef] [PubMed]
38. Kim, D.; Paggi, J.M.; Park, C.; Bennett, C.; Salzberg, S.L. Graph-based genome alignment and genotyping with HISAT2 and HISAT-genotype. *Nat. Biotechnol.* **2019**, *37*, 907–915. [CrossRef] [PubMed]
39. Xu, L.; Wang, Y.; Dong, J.; Zhang, W.; Tang, M.; Zhang, W.; Wang, K.; Chen, Y.; Zhang, X.; He, Q. A chromosome-level genome assembly of radish (*Raphanus sativus* L.) reveals insights into genome adaptation and differential bolting regulation. *Plant Biotechnol. J.* **2023**, *21*, 990–1004. [CrossRef] [PubMed]
40. Liao, Y.; Smyth, G.K.; Shi, W. The Subread aligner: Fast, accurate and scalable read mapping by seed-and-vote. *Nucleic Acids Res.* **2013**, *41*, e108. [CrossRef]
41. Love, M.; Anders, S.; Huber, W. Differential analysis of count data–the DESeq2 package. *Genome Biol.* **2014**, *15*, 10–1186.
42. Yu, G. Thirteen years of clusterProfiler. *Innovation* **2024**, *5*, 100722. [CrossRef]
43. Taj, G.; Giri, P.; Tasleem, M.; Kumar, A. MAPK signaling cascades and transcriptional reprogramming in plant–pathogen interactions. In *Approaches to Plant Stress and Their Management*; Springer: Berlin/Heidelberg, Germany, 2014; pp. 297–316.
44. Torres, M.A.; Jones, J.D.; Dangl, J.L. Reactive oxygen species signaling in response to pathogens. *Plant Physiol.* **2006**, *141*, 373–378. [CrossRef]
45. Chi, Y.; Yang, Y.; Zhou, Y.; Zhou, J.; Fan, B.; Yu, J.-Q.; Chen, Z. Protein–protein interactions in the regulation of WRKY transcription factors. *Mol. Plant* **2013**, *6*, 287–300. [CrossRef]
46. Lorang, J. Necrotrophic exploitation and subversion of plant defense: A lifestyle or just a phase, and implications in breeding resistance. *Phytopathology* **2019**, *109*, 332–346. [CrossRef]
47. Huot, B.; Yao, J.; Montgomery, B.L.; He, S.Y. Growth–defense tradeoffs in plants: A balancing act to optimize fitness. *Mol. Plant* **2014**, *7*, 1267–1287. [CrossRef]
48. Van der Does, D.; Leon-Reyes, A.; Koornneef, A.; Van Verk, M.C.; Rodenburg, N.; Pauwels, L.; Goossens, A.; Körbes, A.P.; Memelink, J.; Ritsema, T. Salicylic acid suppresses jasmonic acid signaling downstream of SCFCOI1-JAZ by targeting GCC promoter motifs via transcription factor ORA59. *Plant Cell* **2013**, *25*, 744–761. [CrossRef] [PubMed]
49. Ma, Y.; Choi, S.R.; Wang, Y.; Chhapekar, S.S.; Zhang, X.; Wang, Y.; Zhang, X.; Zhu, M.; Liu, D.; Zuo, Z. Starch content changes and metabolism-related gene regulation of Chinese cabbage synergistically induced by *Plasmodiophora brassicae* infection. *Hortic. Res.* **2022**, *9*, uhab071. [CrossRef] [PubMed]

horticulturae

MDPI

Article

Integrated Transcriptomic and Functional Analyses Reveal the Role of the Plant–Pathogen Interaction Pathway in *Fusarium solani* Infection of *Zingiber officinale*

Lingling Zhang [1,2], Qie Jia [2], Lei Liu [1,*] and Yiqing Liu [2,3,*]

[1] College of Architecture and Design, Yangtze University College of Arts and Sciences, Jingzhou 434020, China; llzhchina@163.com
[2] Hubei Key Laboratory of Spices & Horticultural Plant Germplasm Innovation & Utilization, Yangtze University, Jingzhou 434025, China; jiaqie020@163.com
[3] College of Smart Agriculture, Chongqing University of Arts and Sciences, Chongqing 402160, China
* Correspondence: baryll@163.com (L.L.); liung906@163.com (Y.L.)

Abstract

Fusarium wilt, caused by *Fusarium solani*, is a devastating disease that leads to significant losses in ginger (*Zingiber officinale*) crops worldwide. To explore the molecular mechanisms underlying *F. solani* infection and disease progression, we performed a comparative transcriptome analysis of ginger rhizomes during storage, comparing inoculated and non-inoculated samples. A total of 647 and 6398 DEGs were identified in the 1.5- and 2-day infection groups, respectively. KEGG analysis revealed that most DEGs were enriched in the plant–pathogen interaction pathway, with both PTI and ETI being activated. Six DEGs in this pathway were validated by qRT-PCR at two time points, showing a strong correlation with FPKM values from the transcriptome data. Furthermore, transient expression analysis in *Nicotiana benthamiana* leaves demonstrated that overexpressing ZoCEBiP1 helped scavenge excess ROS, thereby reducing disease severity. Transcriptional profiling of DEGs in the plant–pathogen interaction pathway revealed significant changes in genes involved in ROS and NO metabolism. In *F. solani*-infected ginger rhizomes, levels of H_2O_2 and O_2^- were elevated, along with increased activities of antioxidant enzymes (POD, CAT, SOD, and APX) and higher NO content and NOS activity. These findings elucidated the early defense response of ginger rhizomes to *F. solani* infection and provided insights for developing effective strategies to manage fungal diseases.

Keywords: ginger rhizome; *Fusarium solani*; Fusarium wilt; CEBiP; postharvest storage

1. Introduction

Ginger (*Zingiber officinale*), a perennial plant in the Zingiberaceae family, is extensively grown for its fragrant rhizomes, which hold significant value in culinary, medicinal, and economic contexts [1,2]. Despite its economic significance, ginger faces considerable postharvest challenges, particularly fungal infections that result in severe spoilage and quality degradation during storage [3]. Factors such as mechanical damage, surface wounds caused by the division of rhizomes before germination, and the warm, humid conditions necessary for germination are primary contributors to pathogen infection [4]. Among these pathogens, *Fusarium solani* is one of the most prominent, causing Fusarium wilt of the rhizomes [5], thereby reducing both the marketability and shelf life of ginger. In addition to impacting ginger yield and seed quality, *F. solani* also poses a direct threat to human health,

causing diseases such as tinea and fungal keratitis [6]. Furthermore, during its metabolic processes, *F. solani* produces a variety of toxic secondary metabolites, including mycotoxins, which are harmful to humans and exhibit carcinogenic properties [6]. Therefore, enhancing control over *F. solani* during the postharvest storage of ginger is crucial to ensuring the quality and safety of this agricultural product.

Up to now, research on ginger rhizome loss due to postharvest diseases has mainly focused on chemical treatments [7] and biological control methods [4,5] to enhance disease resistance and elucidate their underlying mechanisms. However, there has been limited research on the resistance of ginger to *F. solani* infection caused by Fusarium wilt, and the molecular mechanisms underlying ginger's interaction with pathogenic fungi are not yet fully understood. Plant–pathogen interactions involve sophisticated and multi-layered biological processes that are dynamically regulated during infection [8]. Transcriptome sequencing offers enhanced insights into plant–pathogen interactions, aids in the discovery of novel disease resistance genes, and provides a more thorough understanding of plant immune responses [9]. At present, transcriptome technology has significantly advanced our understanding of disease resistance mechanisms in postharvest horticultural crops such as kiwifruit [9], mango fruit [10], Lanzhou lily [11], and button mushroom [12]. For example, Yang et al. [12] used RNA-Seq analysis to characterize ten differentially expressed genes (DEGs) that played crucial roles in the initial defense of *Agaricus bisporus* against *Pseudomonas tolaasii*. Furthermore, combining physiological and transcriptomic findings, they concluded that jasmonate acid (JA)-mediated defense mechanisms were fundamentally involved in the antifungal response. However, the transcriptomic characteristics of ginger rhizome in response to *F. solani* infection during postharvest storage remain unexplored.

Thus, transcriptomic and physiological analyses were employed to identify DEGs and characterize the associated physiological changes in ginger rhizomes during the early responses to *F. solani* inoculation, thereby providing a solid theoretical foundation and valuable insights for preserving ginger rhizome quality and developing targeted disease management strategies.

2. Materials and Methods

2.1. Plant Material and Fungal Pathogen

'Zhugen' ginger is a local cultivar widely cultivated in the Shandong and Sichuan provinces of China, known for its crisp and juicy texture, low fiber content, and rich ginger aroma. In our previous assessment of Fusarium wilt disease resistance, 'Zhugen' ginger was classified as having a light resistance level (data not published). Healthy ginger rhizomes were obtained from the experimental farm of Yangtze University and immediately transported to the laboratory. The selected rhizomes displayed uniform morphological features, with no visible signs of physical damage or disease.

The fungal pathogen *Fusarium solani* (strain D6), originally isolated from symptomatic ginger rhizomes in Enshi County, Hubei Province, was maintained on potato dextrose agar (PDA) slants at 4 °C in our microbial culture collection. For experimental purposes, the fungus was subcultured on PDA plates and incubated at 25 ± 1 °C in the dark for 7 d. Conidial suspensions were prepared by gently scraping the mycelial mat with sterile 0.05% Tween-80 solution, followed by filtration to remove the hyphae. The spore concentration was then adjusted to 1×10^8 sporangia mL^{-1}. All reagents were purchased from Beijing Solarbio Science & Technology Co., Ltd. (Beijing, China), unless otherwise specified.

2.2. Ginger Rhizome Treatment

The surface-sterilized ginger rhizomes were wounded at two opposite points using a sterile borer to create consistent inoculation sites (3 mm deep × 3 mm diameter). The

rhizomes were then randomly assigned to two groups: the *F. solani* treatment group, which received 10 μL of spore suspension, and the control group, which was injected with 10 μL of sterile water. Following complete absorption of the inoculum, the ginger rhizomes were incubated in sterile containers at 28 °C with 85% relative humidity [13]. Tissue samples from a 1 cm radius around the inoculation sites were harvested in 1.5 and 2 d post-inoculation, immediately frozen in liquid nitrogen, and stored at −80 °C for subsequent analysis. Each group was replicated three times.

2.3. Determination of Disease Spot Diameter, Decay Rate, Water Loss, Hardness, and F. solani Biomass

To evaluate disease progression and physiological changes in ginger rhizomes following *F. solani* infection, the disease spot diameter, decay rate, water loss, and hardness were measured at 1.5 and 2 d post-inoculation. Lesion diameters were measured using digital calipers. Decay was assessed by observing visible mycelial growth on the rhizome surface. The disease incidence rate (%) and water loss rate (%) were calculated as follows:

Disease incidence rate (%) = [(Number of decaying ginger rhizomes)/(Total number of ginger rhizomes)] × 100

Water loss rate (%) = [(Initial weight of ginger rhizomes − Weight of stored ginger rhizomes)/(Initial weight of ginger rhizomes)] × 100

Ginger rhizome's hardness was performed using a texture analyzer (TA.XT Plus, Stable Micro Systems, Godalming, UK) with a 5-mm cylindrical probe penetrating to 3 mm depth at 1 mm s^{-1}, recording maximum force (N) as an indicator of tissue firmness.

The biomass of *F. solani* in ginger rhizomes was analyzed using Quantitative real-time PCR (qRT-PCR). Total RNA was isolated from ginger rhizome with the MagicPure Total RNA Kit (TransGen, Beijing, China). For qRT-PCR, cDNA was synthesized from the RNA with the Fast Quant RT Kit (Tiangen, Beijing, China). Reactions were run on a QuantStudio 5 Real-Time PCR System (Bio-Rad, Hercules, CA, USA) with ChamQ Universal SYBR qPCR Master Mix (Vazyme, Nanjing, China). The *Fusarium solani EF-1α* (*FsEF-1α*) (KX940968.1) primers (Table S1) were used, and expression levels were normalized to the *Zingiber officinale RBP* gene [14] using the $2^{-\Delta\Delta Ct}$ method. Three technical replicates were performed per sample.

2.4. RNA-Seq Analysis

Total RNA was isolated from ginger rhizome with the MagicPure Total RNA Kit (TransGen, Beijing, China). For library preparation, polyadenylated mRNA was extracted from 1 μg of RNA with oligo (dT)-conjugated magnetic beads, then fragmentation and cDNA synthesis. The mRNA was purified, fragmented, and both the first- and second-strand cDNA were synthesized. The library fragments were purified with the AMPure XP system (Beckman Coulter, Brea, CA, USA) and assessed using the Agilent Bioanalyzer 2100 (Agilent Technologies, Santa Clara, CA, USA). The clean reads were then aligned to the *Zingiber officinale* reference genome [15] using HISAT2 (v2.2.1). RNA-seq data were generated using the Illumina NovaSeq 6000 platform to ensure reproducibility and have been deposited in the NCBI database (PRJNA1279401). Further analysis was performed using the BMKCloud bioinformatics platform (www.biocloud.net accessed on 15 March 2025). Gene expression levels were quantified by fragments per kilobase of transcript per million reads (FPKM), accounting for gene lengths and sequencing biases. DEGs were identified with a $\log2|\text{fold change}| \geq 1$ and false discovery rate (FDR) < 0.05. Three biological replicates were used in RNA-seq analysis.

2.5. qRT-PCR Validation

The cDNA samples used for qRT-PCR assays were prepared following in Section 2.4. The primer sequences are provided in Table S1, with the specific method referring to Section 2.3.

2.6. Transient Agroinfiltration Assays

Based on integrated analysis of RNA-Seq and qRT-PCR data, the critical DEG associated with ginger rhizome's defense response against *F. solani* infection was identified. To investigate the biological function of the critical DEG, we performed transient expression analysis in *Nicotiana benthamiana*, followed by *Phytophthora infestans* inoculation assays.

2.6.1. Transient Transformation and Inoculation Treatment of *N. benthamiana* Leaves

The coding sequence of the target DEG was amplified using 2 × Phanta Max Master Mix (Vazyme, Nanjing, China) according to the manufacturer's protocol. The purified PCR products were then directionally cloned into a linearized pBWA(V)BS-GFP vector (digested with BsaI/Eco31I) through homologous recombination using the ClonExpress II cloning system (Vazyme, Nanjing, China). The primer sequences are provided in Table S1. For transient expression assays, recombinant pBWA(V)BS-ZoCEBiP1-GFP and an empty vector control were introduced into *Agrobacterium* GV3101 competent cells. GV3101 carrying vectors were pressure-injected into the abaxial surface of *N. benthamiana* leaves. After 36 h of overexpression, detached *N. benthamiana* leaves were inoculated with *P. infestans* (strain 88,069) sporangial suspension (4×10^4 sporangia mL^{-1}), following the method described by Li et al. [16]. At 5 d of inoculation, lesion diameters were documented and visualized under a handheld long-wavelength UV light (Analytic Jena, Jena, Germany). The experiment was performed with three biological replicates, each containing 10 leaves.

2.6.2. DAB Histochemical Staining

To further assess the oxidative burst induced during the defense response, hydrogen peroxide (H_2O_2) accumulation was assessed using the 3,3-diaminobenzidine (DAB) staining method [5]. Detached *N. benthamiana* leaves, collected 2 d post-inoculation, were immersed in freshly prepared DAB solution and vacuum infiltrated for 15 min. The leaves were then incubated in the dark, shaking at 100 rpm for 4 h. Following staining, the leaves were boiled in 95% ethanol to decolorize, leaving the unstained areas nearly colorless. Afterward, the leaves were air-dried and photographed for documentation. DAB staining was performed with three biological replicates, each containing three leaves.

2.7. Determination of H_2O_2, O_2^- Content, Enzyme Activities, NO Content, and NOS Activity

The contents of hydrogen peroxide (H_2O_2) and superoxide anion (O_2^-) were quantified using commercial assay kits (Solarbio, Beijing, China) following the manufacturer's protocols; the absorbances were measured at 415 and 530 nm, respectively. Results were expressed as mmol g^{-1} for O_2^- and μmol g^{-1} FW for H_2O_2.

Frozen ginger tissues (3 g) were homogenized in 9 mL ice-cold 0.1 M sodium phosphate buffer (pH 7.0). The homogenate was centrifuged at 12,000× *g* for 10 min at 4 °C, and the resulting supernatant served as the crude enzyme extract for determining the activities of peroxidase (POD) [17], catalase (CAT) [18], superoxide dismutase (SOD) [19], and ascorbate peroxidase (APX) [20]. Results were expressed as U g^{-1} FW for those enzyme activities.

The endogenous nitric oxide (NO) content was determined by the Griess reagent method [21]. The nitric oxide synthase (NOS) activity was analyzed by nitric oxide synthase assay kit (Jiancheng, Nanjing, China) according to the manufacturer's instructions.

2.8. Statistical Analysis

All results were obtained from a minimum of three independent biological replicates to account for biological variability. The statistical evaluation was performed using SPSS Statistics v27.0. Student's *t*-test was employed to determine significant differences between mean values at the 0.05 level. Data visualization was created using GraphPad Prism v9.0.

3. Results

3.1. Symptoms of Ginger Rhizomes Inoculated with F. solani

As shown in Figure 1A, the initial invading hyphae began to form 1.5 d after infection. By 2 d post-inoculation, the hyphae had penetrated the ginger tissue and rapidly expanded on the wound surfaces, while the uninfected rhizome remained free of rot. Therefore, ginger rhizome samples were initially collected at 1.5 d after infection with *F. solani* to capture the early interaction between the ginger and the pathogen, during which no visible disease symptoms were present. A subsequent sampling at 2 d, when extensive infection had spread across the rhizome, was chosen to investigate disease progression during the rapid pathogenic expansion.

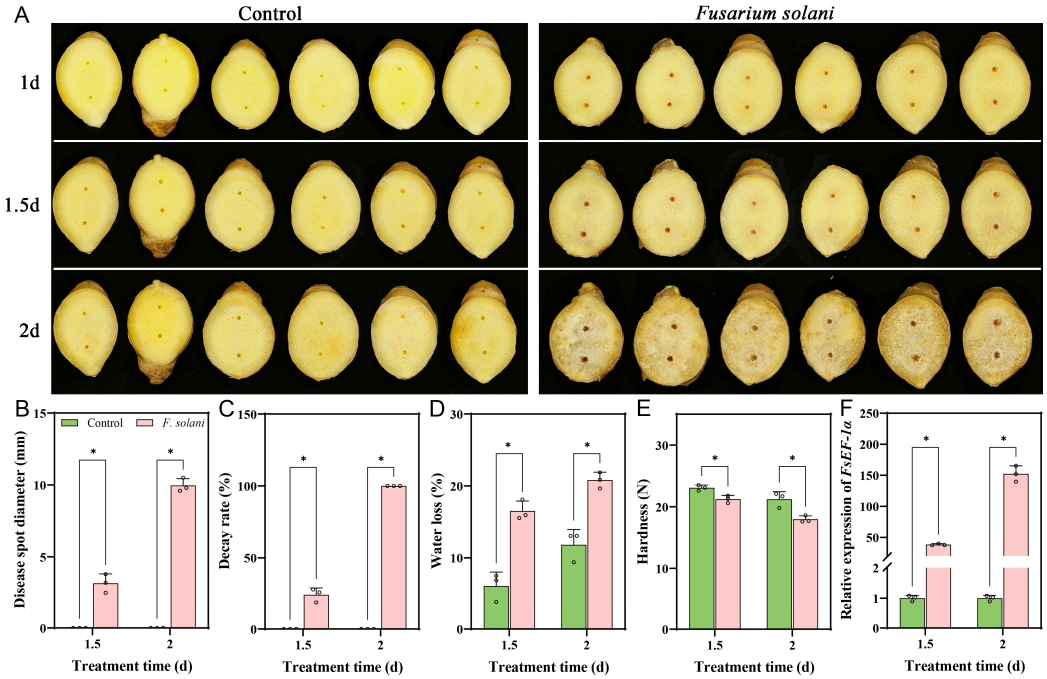

Figure 1. Effects of *F. solani* inoculation on the development of Fusarium wilt disease in ginger rhizomes. (**A**) Time series of *F. solani* infection on ginger rhizome at 1, 1.5, and 2 d. (**B**–**E**) Effects of *F. solani* inoculation on the disease spot diameter (**B**), decay rate (**C**), water loss (**D**), hardness (**E**), and *F. solani* biomass (**F**) of ginger rhizomes after 1.5 and 2 d. Results represent the mean ± standard deviation (SD). * indicated $p < 0.05$.

Moreover, the inoculation of *F. solani* caused Fusarium wilt disease, as evidenced by the disease spot diameter and decay rate. After 1.5 d of *F. solani* inoculation, the disease spot diameter and decay rate were 3.2 mm and 24.3%, respectively. After 2 d of inoculation, the disease spot diameter and decay rate reached up to 10.0 mm and 100%, respectively. The ginger rhizomes in the control group showed no Fusarium wilt symptoms (Figure 1B,C). Additionally, compared to the control, the water loss of ginger rhizomes in the *F. solani* treatment group increased by 171.7% after 1.5 d and 75.9% after 2 d (Figure 1D). The firmness of the *F. solani*-inoculated group decreased by 7.9% and 15.3%, respectively (Figure 1E). The biomass of *F. solani* was further analyzed to investigate Fusarium wilt

progression after inoculation. The results showed that, compared to the control, the biomass of *F. solani* in ginger rhizomes increased 38.3-fold at 1.5 d after inoculation and 152.4-fold at 2 d after inoculation (Figure 1F). These results indicated that the *F. solani* strain could cause the typical characteristic Fusarium wilt symptoms, significantly increase weight loss, reduce rhizome hardness, and increase *F. solani* biomass of ginger rhizome.

3.2. Sequencing Data Quality Evaluation

In order to determine the genes responsive to *F. solani* infection and compare the gene expression patterns of infected ginger rhizome at 1.5 and 2 d post-inoculation, 12 ginger rhizome libraries were constructed. The RNA-Seq sequencing of 12 libraries produced a total of 40,341,026~49,445,898 raw bases (Table S2). The Q30 was 94.23~94.95%, and the GC content of 47.49~49.83%, respectively (Table S3). Quality assessment of the RNA-seq data (error rate distribution along reads and GC content distribution) revealed excellent sequencing performance (Figures S1 and S2). Alignment to the *Zingiber officinale* reference genome using the HISAT2 demonstrated consistently high mapping efficiencies ranging from 90.16% to 92.34% (Table S4).

The volcano plot provides a clear visualization of the overall distribution of DEGs (Figure 2). In total, 647 DEGs were identified, with 374 up-regulated and 374 down-regulated in the 1.5 d infection group (CK1.5 vs. FS1.5), and 6398 DEGs were identified, with 3108 up-regulated and 3290 down-regulated in the 2 d infection group (CK2 vs. FS2). Notably, a higher number of differential genes were regulated in the 2 d infection group.

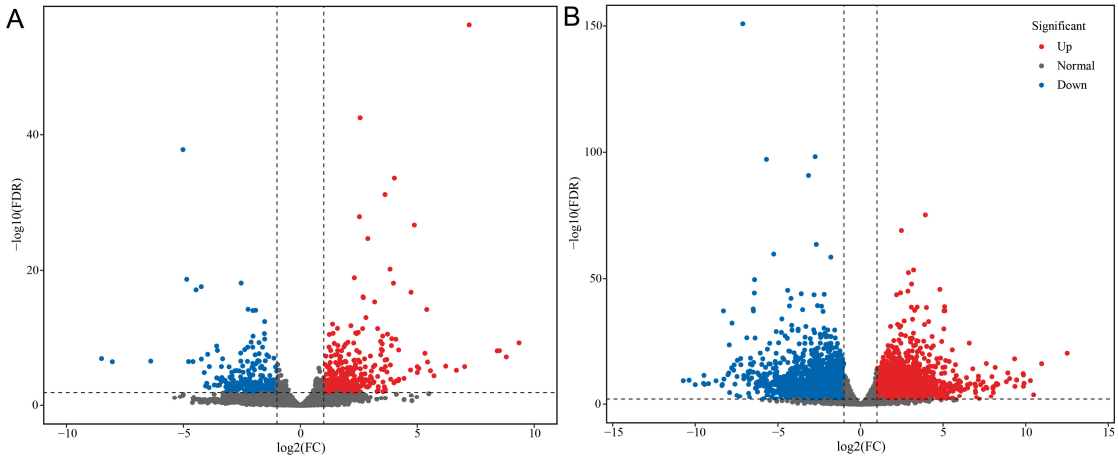

Figure 2. Differential gene volcano plot. Red means up-regulation genes, blue means down-regulation genes, and grey means no significant genes: (**A**) CK1.5 vs. FS1.5 and (**B**) CK2 vs. FS2.

3.3. GO Function Annotation

GO functional annotation was performed on DEGs to explore their functions across three categories: Biological Process (BP), Cellular Component (CC), and Molecular Function (MF). At 1.5 d, 17 GO terms, such as 'metabolic process' and 'single-organism process', were enriched at the BP level. At the CC level, 15 GO terms, including 'cell' and 'cell part', were predominantly enriched. The MF level was predominantly associated with 11 GO terms, such as 'binding' and 'catalytic activity' (Figure 3A). At 2 d, 20 GO terms, such as 'metabolic process' and 'cellular process', were enriched at the BP level. In the CC level, 18 GO terms such as 'cell' and 'cell part' were mainly enriched. At the MF level, 12 GO terms, such as 'binding' and 'catalytic activity', were mostly enriched (Figure 3B).

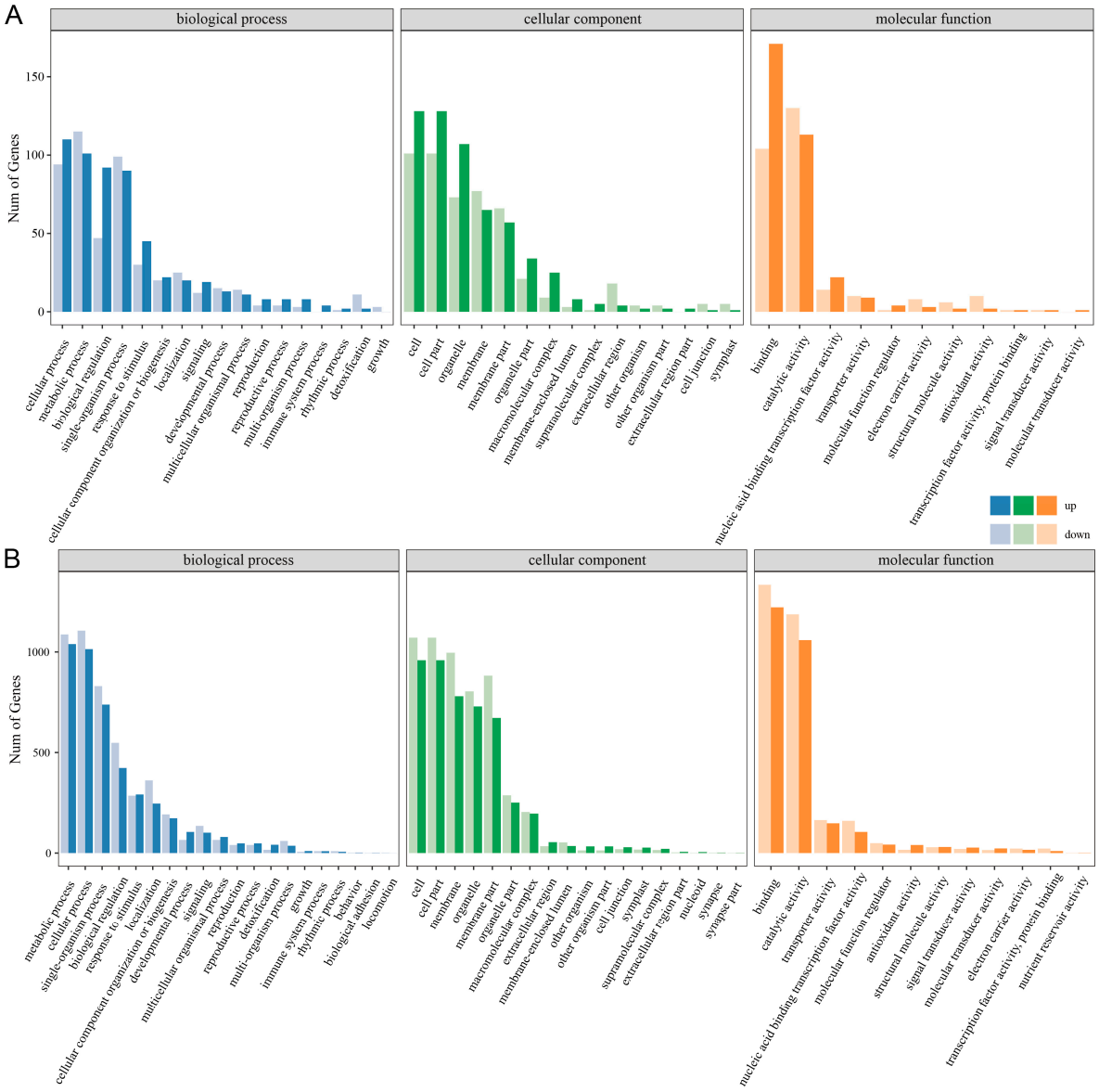

Figure 3. GO classification of DEGs: (**A**) CK1.5 vs. FS1.5 and (**B**) CK2 vs. FS2.

3.4. KEGG Metabolic Pathway

To elucidate the functional roles and molecular networks of DEGs in the ginger rhizome transcriptome, KEGG pathway analysis was conducted. KEGG pathway annotation revealed that the DEGs were primarily associated with five major functional categories: Cellular Processes, Environmental Information Processing, Genetic Information Processing, Metabolism, and Organismal Systems. At 1.5 d, the DEGs were significantly enriched in pathways such as 'Plant–pathogen interaction' and 'Plant hormone signal transduction' (Figure 4A). At 2 d, the DEGs showed significant enrichment in pathways such as 'Plant–pathogen interaction', 'Plant hormone signal transduction', and 'MAPK signaling pathway' (Figure 4B). KEGG pathway enrichment analysis identified 217 and 2109 significantly enriched pathways for CK1.5 vs. FS1.5 and CK2 vs. FS2, respectively (Tables S5 and S6). To sum up, the infection of ginger rhizome tissue induces physiological responses, which may contribute to enhancing resistance to *F. solani* infection through the coordinated regulation of metabolic processes, cellular compartmentalization, and molecular interactions.

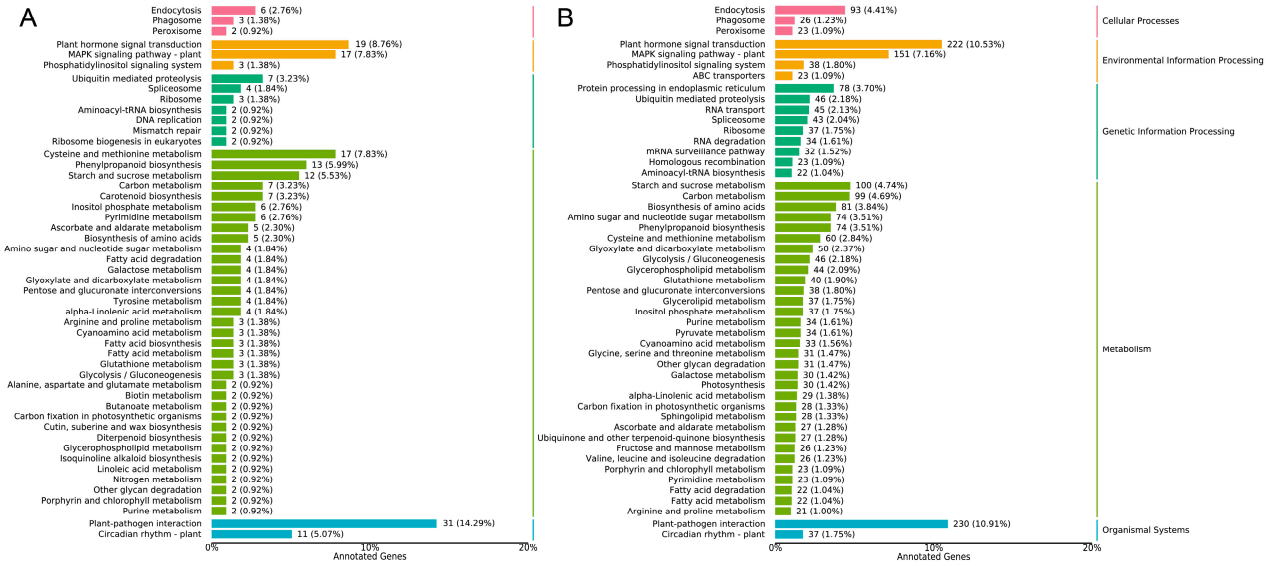

Figure 4. KEGG classification of DEGs: (**A**) CK1.5 vs. FS1.5 and (**B**) CK2 vs. FS2.

3.5. DEGs Related to Plant–Pathogen Interaction Pathway in Ginger Rhizome Against F. solani

KEGG enrichment analysis showed that the plant–pathogen interaction pathway (ko04626) was the most significantly enriched pathway in ginger rhizomes at both 1.5 and 2 d post-inoculation with *F. solani* (Tables S4 and S5). Based on this result, we conducted cluster analysis of the DEGs ($|\log2(\text{FoldChange})| > 1.5$ and FDR < 0.05) associated with this pathway and subsequently validated their expression patterns using qRT-PCR.

A total of 17 DEGs ($|\log2(\text{FoldChange})| > 1.5$ and FDR < 0.05) in the plant–pathogen interaction pathway were identified at 1.5 d post-inoculation with *F. solani*. Among these, fourteen genes showed significant up-regulation, including pattern recognition receptors (CEBiP and FLS2), resistance proteins (RPS2 and RRS1-R), signaling components (PBS1, CNGCs, and UPA20), transcription factors (WRKY22 and Pti5/1), and defense-related genes (FRK1 and EIX1/2). Conversely, three genes were down-regulated: one WKK4/5, one EIX1/2, and one Pti5/1 (Figure 5A). RNA-Seq analysis identified 106 significantly DEGs ($|\log2\text{FoldChange}| > 1.5$, FDR < 0.05) in the plant–pathogen interaction pathway at 2 d post-inoculation with *F. solani*. Of these, 68 genes were significantly up-regulated, including pattern recognition receptors (two CEBiP, two CERK1, two FLS2, two EFR), resistance proteins (four RPM1, four RPS2, one RRS1-R), signaling components (seven PBS1, seven UPA20, seven CDPK, two CaMCML), transcription factors (three Pti5/6/1, one WRKY22), defense-related genes (two EIX1/2, three Pto, two PR1, five FRK1), and other components (four MKK4/5, one MEKK1, two CNGCs, one NOS). Conversely, thirty-eight genes showed significant down-regulation, comprising pattern recognition receptors (one CERK1, three FLS2, two EFR), signaling components (two RIN4, one PBS1, two UPA20, two CDPK), transcription factors (six WRKY33, two WRKY22, four Pti5/6/1), defense-related genes (one EIX1/2, two FRK1), and other components (three RRS1-R, one RPS2, one MEKK1, five Rboh) (Figure 5B).

In agreement with RNA-Seq analysis, qRT-PCR experiments further confirmed that Pti1 (Maker00011524.gene), CEBiP (Maker00045267.gene), RPS2 (Maker00011463.gene), UPA20 (Maker00077866.gene), and FLS2 (Maker00028416.gene) were up-regulated, and MKK4/5 (Maker00034618.gene) was down-regulated upon *F. solani* treatment 1.5 d, compared to the control (Figure 5(C1)). Moreover, CEBiP (Maker00045267.gene), CERK1 (Maker00028603.gene), UPA20 (Maker00004882.gene), and PR1 (Maker00071011.gene) were up-regulated, and EIX1/2 (Maker00069746.gene) and WRK33 (Maker00007282.gene) were down-regulated upon *F. solani* treatment 2 d, compared to the control (Figure 5(C2)). This

consistency suggested the reliability of the RNA-Seq data. This comprehensive expression profiling reveals a complex regulatory network in ginger rhizomes during *F. solani* infection.

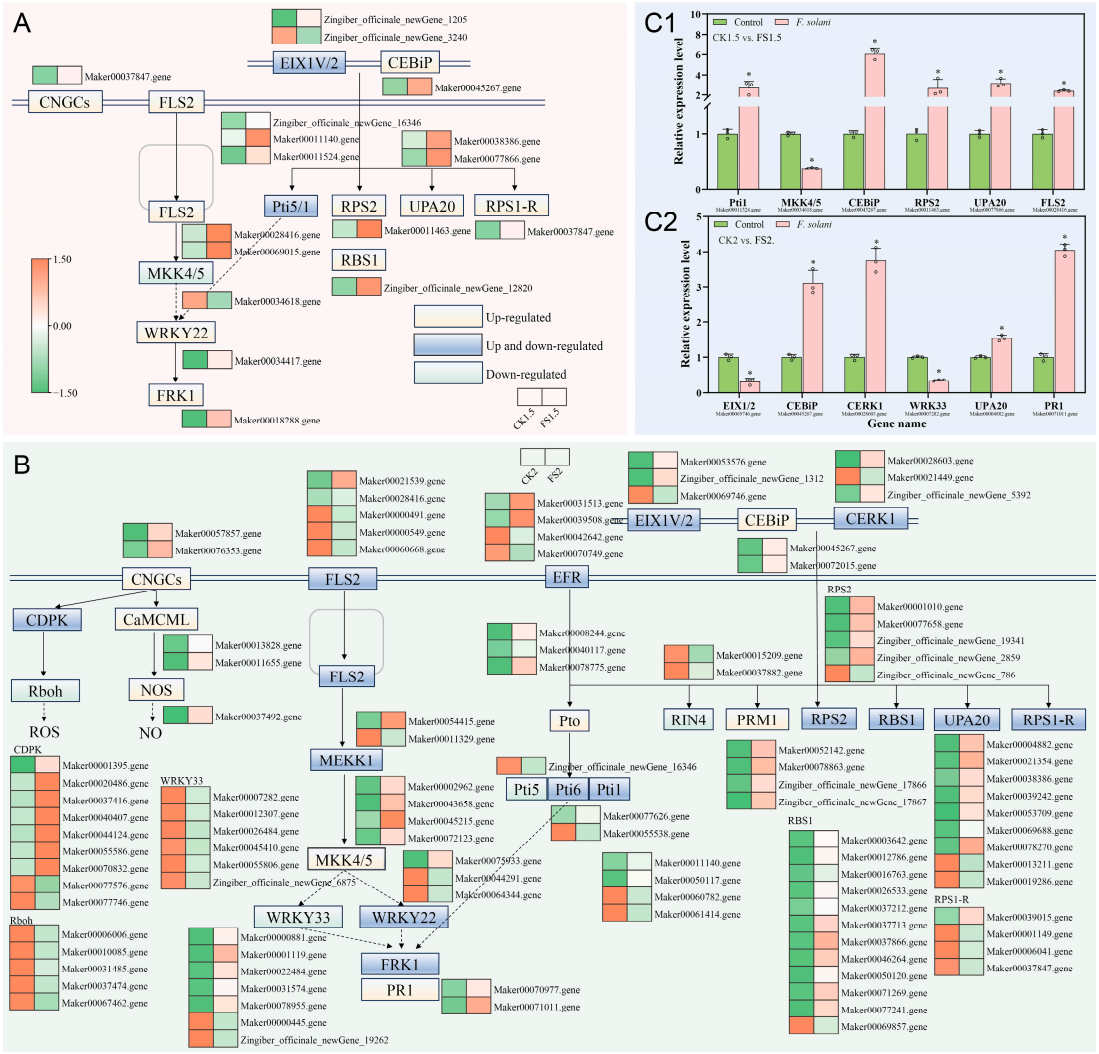

Figure 5. Transcriptional changes in DEGs involved in the plant–pathogen interaction pathway response to *F. solani* in ginger rhizomes. (**A**) KEGG mapping and heatmap of DEGs involved in the plant–pathogen interaction pathway at 1.5 d post-inoculation with *F. solani*. (**B**) KEGG mapping and heatmap of DEGs involved in the plant–pathogen interaction pathway at 2 d post-inoculation with *F. solani*. (**C1**,**C2**) qRT-PCR confirmation. EIX1/2, ethylene-inducing xylanase receptor 1/2; CEBiP, chitin elicitor binding protein; CERK1, chitin elicitor receptor kinase 1; RIN4, RPM1-interacting protein 4; PRM1, resistance to *Pseudomonas maculicola* 1; RPS2, resistance to *Pseudomonas syringae* 2; PBS1, AvrPphB susceptible 1; UPA20, ubiquitin-associated protein 20; RRS1-R, resistance to *Ralstonia solanacearum* 1-required; EFR, EF-Tu receptor, Pto, *Pseudomonas syringae* pv. tomato resistance protein; Pti5/6/1, Pto-interacting protein 5/6/1; FLS2, flagellin-sensitive 2; MEKK1, mitogen-activated protein kinase kinase kinase 1; MKK4/5, mitogen-activated protein kinase kinase 4/5; WRKY33, WRKY transcription factor 33; WRKY22, WRKY transcription factor 22; FRK1, flagellin-induced receptor kinase 1; PR1, pathogenesis-related protein 1; CNGCs, cyclic nucleotide-gated ion channels; CDPK, calcium-dependent protein kinase; Rboh, respiratory burst oxidase homolog; CaMCML, calmodulin-like protein; NOS, nitric oxide synthase. * indicated $p < 0.05$.

Moreover, among the DEGs, five genes encoding CEBiP (Maker00045267.gene), FLS2 (Maker00028416.gene), Pti5 (Zingiber_officinale_newGene_16346), Pti1 (Maker00011140.gene), and RPS1-R (Maker00037847.gene) were involved in defense response to *F. solani* against Fusarium wilt (Figure 5A,B). Especially, CEBiP (Maker00045267.gene), which was renamed

as ZoCEBiP1, exhibited the most significant regulation, with expression levels more than 6.1 and 3.7 times higher than those of the control at 1.5 and 2 d post-inoculation, respectively (Figure 5(C1,C2)).

3.6. Functional Analysis of ZoCEBiP1

To investigate the biological function of ZoCEBiP1 in plant defense, we performed molecular cloning and transient expression analysis in *N. benthamiana*, followed by *P. infestans* inoculation assays.

The full-length coding sequence of ZoCEBiP1 (1248 bp) was successfully amplified, purified, and verified by sequencing (Figure 6A). Sequence alignment using DNAMAN demonstrated 100% identity with the predicted sequence in the ginger genome, confirming accurate gene annotation. Domain architecture analysis through SMART revealed that ZoCEBiP1 contains two characteristic LysM domains, showing conserved structural features with the known chitin receptor *Oryza sativa* LYP4 (OsLYP4) (Figure 6B).

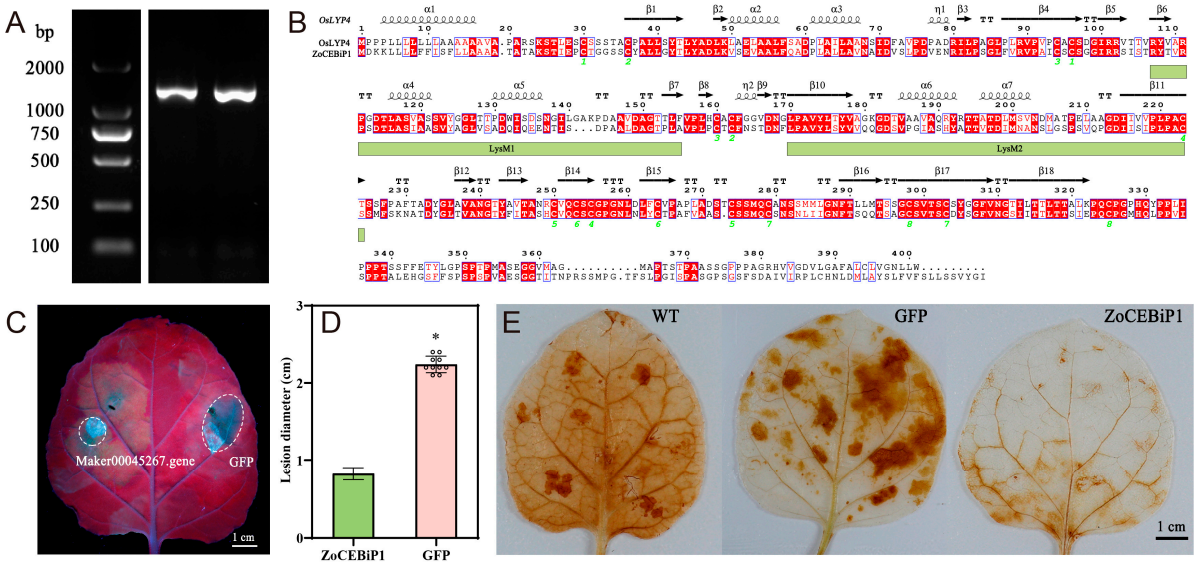

Figure 6. Gene cloning, sequence characteristics, and function analysis of ZoCEBiP1. (**A**) PCR amplification result. (**B**) Protein sequence alignment of ZoCEBiP1 and OsLYP4, similarities are highlighted in red, while the green box indicated the position of the LysM (Lysin-motif) domain. (**C**) Effects of transient overexpression of ZoCEBiP1 and GFP in transient overexpression *N. benthamiana* leaves on disease progression, (**D**) disease spot diameter, and (**E**) H_2O_2 accumulation. * indicated $p < 0.05$.

For functional characterization, ZoCEBiP1 was transiently overexpressed in *N. benthamiana* leaves via Agrobacterium-mediated transformation. Subsequent inoculation with *P. infestans* showed that ZoCEBiP1 overexpression significantly enhanced disease resistance (Figure 6C), with lesion diameters reduced by 63.4% compared to GFP-expressing control leaves (Figure 6D). The DAB staining results showed that 72 h after *P. infestans* inoculation, the tobacco leaves of the WT and GFP control exhibited darker brown staining. In contrast, the leaves with transient overexpression of ZoCEBiP1 showed only a few light brown spots at the inoculation sites (Figure 6E). These results demonstrated that ZoCEBiP1 functions as a pathogen resistance gene.

3.7. Effects of ROS Accumulation, Antioxidant Enzyme Activities, NOS Activity, and NO Content of Ginger Rhizome After Infection with F. solani

Transcriptional profiling of DEGs in the plant–pathogen interaction pathway revealed that *F. solani* infection in ginger rhizomes caused significant changes in the expression of multiple genes related to ROS and NO metabolism. In the context of ROS metabolism,

antioxidant enzymes like POD, CAT, SOD, and APX help modulate the levels of ROS such as H_2O_2 and O_2^- [22]. Meanwhile, NO, a crucial signaling molecule, is synthesized through the activity of NOS, with NOS activity directly regulating the production of NO [23,24]. To functionally validate these transcriptional changes, we subsequently quantified ROS accumulation, antioxidant enzyme activities (POD, CAT, SOD, and APX), NOS activity, and NO content in *F. solani*-infected ginger rhizomes to validate the functional consequences of these transcriptional changes.

As shown in Figure 7A,B, ginger rhizomes treated with the control showed an increase in ROS accumulation, while treatment with *F. solani* resulted in a decrease at 2 d. However, the H_2O_2 and O_2^- contents in the *F. solani* treatment group were significantly higher compared to the control group; the H_2O_2 content increased by 49.6% and 51.4%, while O_2^- levels increased by 20.7% and 33.0% at both time points, respectively. The antioxidant enzyme activities of ginger rhizomes were increased after 2 d of the control and *F. solani* treatments. Compared with the control, *F. solani* treatment enhanced the POD activity by 30.8% and 27.2% at 1.5 and 2 d, respectively (Figure 7C); increased CAT activity by 49.3% and 53.7%, respectively (Figure 7D); increased the SOD activity by 19.7% and 27.4%, respectively (Figure 7E); elevated the APX activity by 33.6% and 29.2%, respectively (Figure 7F). As shown in Figure 7G, *F. solani* treatment increased the NO content by 30.3% and 33.8% compared to the control at 1.5 and 2 d, respectively. Similarly, inoculation with *F. solani* treatment significantly increased the activity of NOS at 1.5 and 2 d, which were 41.4% and 49.3% higher than those of the control (Figure 7H). These data suggested that *F. solani* infection triggered an oxidative burst in ginger rhizomes, activating both ROS-scavenging systems and NO-mediated defense signaling. The temporal coordination of these responses indicated a dynamic interplay between oxidative stress and nitric oxide signaling during fungal infection.

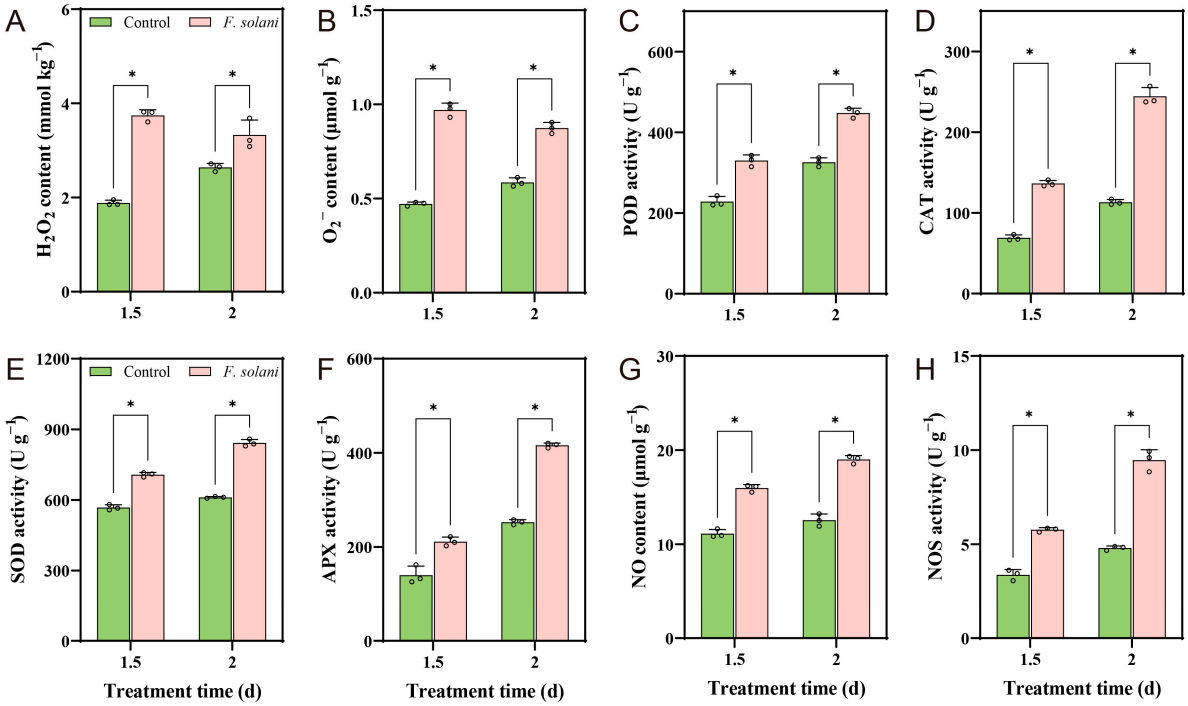

Figure 7. Effects of *F. solani* treatment on the contents of (**A**) H_2O_2 (**B**) O_2^-, the activities of (**C**) POD, (**D**) CAT, (**E**) SOD, (**F**) APX, (**G**) NO content, and (**H**) NOS activity in ginger rhizomes. Results represent the mean ± standard deviation (SD). * indicated $p < 0.05$.

4. Discussion

Fusarium wilt, caused by *F. solani*, is one of the most prevalent and damaging fungal diseases of ginger during postharvest storage, which is responsible for high economic loss globally [4]. In our previous research on biological control approaches for postharvest ginger diseases, we identified several promising alternatives, including eugenol [2], chitosan [5], silica nanoparticles [25], and hydrogen sulfide [7], for suppressing Fusarium wilt progression. However, despite these advances, conventional disease management strategies remain inadequate for controlling *F. solani* under commercial storage conditions. This highlights the urgent need for a deeper understanding of ginger–pathogen interactions at the molecular level to develop more effective, targeted control measures.

Recently, RNA-seq analysis has been widely utilized to investigate pathogen–plant interactions. For example, in the study by Jiang et al. [10], the analysis of DEGs in mango fruit treated with *Bacillus siamensis* demonstrated that the fruit's response to the treatment was most prominent during the early days of storage. Xu et al. [26] identified several key mechanisms involved in the pear's response to *Penicillium expansum*, as revealed by transcriptome analysis. In our study, compared with the control, 647 genes were significantly affected by *F. solani* at 1.5 d post-infection, and the expressions of 5751 DEGs were increased by treatment at 2 d post-infection, indicating that the early response of the ginger rhizome to *F. solani* infection was activated in 2 d. In addition, by 2 d post-infection, the number of enriched GO terms had increased, indicating a more complex and intensified defense response.

KEGG pathway enrichment analysis revealed that the plant–pathogen interaction was the most enriched at both 1.5 and 2 d post-treatment, indicating that this process played a central role in the ginger rhizome's response to *F. solani*. In plants, the plant–pathogen interaction pathway is considered as a key defense mechanism during fungal pathogen invasion, involving both pathogen-associated molecular pattern (PAMP)-triggered immunity (PTI) and effector-triggered immunity (ETI) pathways [27]. PTI is the first layer of plant immune response, triggered by the recognition of PAMPs by pattern recognition receptors (PRRs) on the plant cell surface [28]. In this study, several PRRs, including CEBiP and FLS2, were significantly upregulated at both 1.5 and 2 d post-inoculation with *F. solani*. The upregulation of these PRRs suggested that ginger rhizomes were actively engaging PTI mechanisms to counteract the pathogen. ETI is a more specific and robust immune response activated by the recognition of pathogen effectors by intracellular nucleotide-binding leucine-rich repeat (NLR) proteins [29]. In our study, multiple NLR genes, such as RPS2 and RRS1-R, were significantly upregulated at both time points, indicating that the ginger rhizome was also mounting a specific ETI response to *F. solani*. Those results were consistent with the findings of Xiong et al. [30], who reported that several PRR genes, kinase genes, and genes involved in PTI and ETI signaling pathways were significantly induced in the *Botrytis cinerea*–strawberry interaction. Therefore, these results underscore the specific roles of these genes in plant defense, further supporting the idea that both PTI and ETI pathways were essential for successful pathogen defense in ginger.

It is worth noting that ZoCEBiP1 played an important role in the early defense response of *F. solani* against Fusarium wilt disease. *Oryza sativa* CEBiP (OsCEBiP) was the first identified polysaccharide receptor that binds fungal chitin elicitors, playing a crucial role in detecting chitin signals and initiating signal transduction [31,32]. It contains two LysM domains and one transmembrane domain. Knockout of the CEBiP gene severely impaired chitin-induced ROS bursts and the expression of chitin-responsive genes, leading to reduced disease resistance in rice plants [32]. Similarly, in this study, ZoCEBiP1 also contained two LysM domains, indicating that CEBiP was highly conserved across species, and transient overexpression experiments in tobacco demonstrated that ZoCEBiP1 could

enhance the disease resistance of tobacco seedlings by scavenging ROS. These results demonstrated that ZoCEBiP1 functioned as a pathogen resistance gene, likely serving as a pattern recognition receptor in the plant immune system. However, its precise molecular function requires further investigation. The upregulation of signaling components (PBS1, CNGCs) and transcription factors (WRKY22, Pti5/1) in ginger rhizomes highlighted a sophisticated, multi-layered defense strategy against *F. solani* infection. These molecular players activate canonical immune pathways: PBS1 initiates MAPK cascades [33], while CNGCs mediate calcium signaling [34], representing conserved convergence points for both PTI and ETI responses. In the transcriptional response of Wolfberry to the infection by the endophytic fungus *Fusarium nematophilum*, the activation of FRK1 and EIX1/2 played a crucial role [35]. In our study, the strong induction of defense executors like FRK1 and EIX1/2 also demonstrated the activation of downstream antimicrobial mechanisms. Conversely, the downregulation of certain genes, such as WKK4/5 and specific isoforms of EIX1/2 and Pti5/1, may reflect a fine-tuning of the immune response. Studies have shown that certain transcription factors and signaling components could act as negative regulators to balance immune responses. For example, *Arabidopsis thaliana* WRKY50/51 (AtWRKY50/51) mediated low oleic acid- and SA-dependent repression of JA signaling, leading to increased susceptibility to *Botrytis cinerea* [36]. In addition, *Gossypium hirsutum* WRKY25 (GhWRKY25) negatively regulated *B. cinerea* infection [37]. This could involve negative regulatory mechanisms to prevent excessive immune activation, which can be detrimental to the plant.

The plant–pathogen interaction pathway involves a complex network of signaling cascades and defense responses that plants utilize. Activation of this pathway triggers downstream signaling events, including the production of ROS and NO, which are crucial components of the plant's defense arsenal. In this study, the significant upregulation of genes associated with ROS and NO metabolism suggested that ROS and NO could be essential in the defense response of ginger rhizomes to *F. solani* infection. ROS are essential players in plant defense against pathogens; they serve both as signaling molecules and as direct antimicrobial agents. Rapid accumulation of ROS has been considered as one of the earliest events strongly associated with plant resistance to pathogens and involved in the development of disease resistance in ginger rhizomes [38], grapes [39], and kiwifruit [40] during postharvest storage. In the present study, H_2O_2 contents and H_2O_2 and O_2^- levels significantly increased in *F. solani*-infected ginger rhizomes, indicating a robust oxidative burst. However, ROS can also be detrimental to plant cells if not properly managed. The observed increase in antioxidant enzyme activities (POD, CAT, SOD, and APX) suggested that ginger rhizomes were actively balancing ROS production and scavenging to prevent oxidative damage. Similarly, H_2S induced resistance in ginger rhizomes via increasing the capacity for antioxidant defense [7]. Therefore, the enhanced activities of these antioxidant enzymes indicated that the plant was effectively managing oxidative stress during infection. NO is another important signaling molecule involved in plant defense against pathogens. Studies have shown that NO treatment could enhance disease resistance in horticultural crops, such as kiwifruit [41] and tomato [23]. NOS was a key enzyme for the NO production [24]. For instance, melatonin has been reported to trigger NO accumulation by activating NOS, improving cold tolerance in postharvest litchi fruit [42]. Additionally, NO interacts with ROS signaling pathways, strengthening the overall defense response. For instance, NO application to *Arabidopsis* roots could rapidly activate protein kinases with MAPK properties [43]. In this study, the significant increase in NO content and NOS activity in *F. solani*-infected ginger rhizomes indicated the role of NO in mediating defense responses. Notably, a dynamic interplay between ROS and NO occurs during pathogenic fungal infection [39]. Future research can focus on

unraveling the specific signaling pathways and molecular interactions between ROS and NO in ginger rhizomes.

In addition, our findings demonstrate that ginger rhizomes exhibit distinct phased immune responses during *F. solani* infection. In the early infection stage (1.5 d), although there were not many significantly upregulated defense-related genes in the plant–pathogen interaction pathway (Figure 5A), the recognition of PAMPs such as chitin through significantly upregulated pattern recognition receptors like ZoCEBiP1 (Figure 5(C1)) successfully activated early immune responses characterized by ROS burst [32]. This rapid accumulation of H_2O_2 and O_2^- (Figure 7A,B), consistent with typical pathogen recognition responses reported in postharvest ginger [5,7,13,25] and other crops [40,41], likely effectively restricted fungal spread before effector secretion [44], indicating that ginger rhizomes preferentially initiate PTI rather than comprehensive defense responses at this stage. As infection progressed to 2 d, we observed reduced activation of ZoCEBiP1, suggesting diminished pathogen recognition capacity. However, defense responses were significantly enhanced, manifested by increased enrichment of differentially expressed genes associated with the plant–pathogen interaction pathway, along with elevated antioxidant enzyme activities, NO content, and NOS activity. When the disease developed to the necrotic stage, *F. solani* likely secreted effectors to suppress PTI, thereby ensuring successful infection [44–47]. This dynamic pattern reveals the temporal characteristics of ginger's defense strategy: early emphasis on pathogen recognition and rapid response, followed by transition to more comprehensive defense execution, which ultimately could be overcome by the pathogen's virulence strategies.

While previous disease resistance evaluations confirmed that the 'Zhugen' ginger cultivar exhibits resistance to Fusarium wilt, this study further demonstrates its ability to activate defense responses upon *F. solani* inoculation. However, a comparison with susceptible varieties was not conducted. In subsequent experiments, we will systematically compare resistant and susceptible ginger varieties under pathogen challenge to identify and validate key regulators that positively correlate with resistance or negatively correlate with susceptibility [48].

5. Conclusions

This research provided comprehensive insights into the molecular defense mechanisms of ginger rhizomes against *F. solani* infection through transcriptomic and functional analyses. The results revealed a strong activation of the plant–pathogen interaction pathway, with significant upregulation of genes associated with both PTI and ETI, including PRRs like CEBiP and FLS2, and NLR proteins such as RPS2 and RRS1-R. The upregulation of signaling components (PBS1, CNGCs) and transcription factors (WRKY22, Pti5/1) highlighted a multi-layered defense strategy. Furthermore, the critical role of ZoCEBiP1 was identified in early defense through transient transformation of *N. benthamiana* leaves. The marked significance in ROS and NO metabolism genes, along with effective ROS management, coupled with elevated NO content and NOS activity, suggested that ROS and NO were essential players in the defense response (Figure 8). These findings not only advance our understanding of ginger immunity but also identify specific molecular targets for developing innovative control strategies against Fusarium wilt.

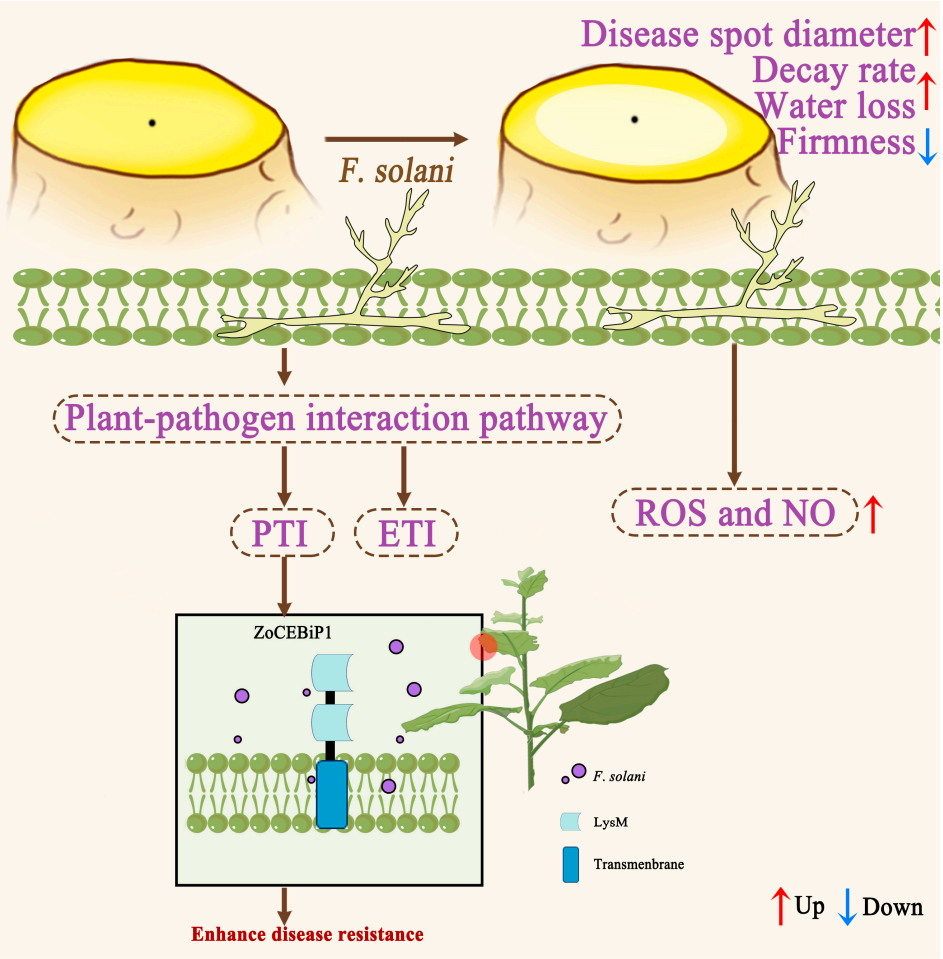

Figure 8. Molecular network of interaction between saffron and *F. solani*.

Supplementary Materials: The following supporting information can be downloaded at https://www.mdpi.com/article/10.3390/horticulturae11070791/s1, Figure S1. Error rate distribution along reads. Horizontal is position along reads, ordinate is error rate (%); Figure S2. GC content distribution. Horizontal is position along reads, ordinate is the proportion of single base (%), different colors represent different base types; Table S1: Primers' sequence information used in this study; Table S2: List of quality of RNA-Seq data; Table S3: Quality control of the control/*F. solani*-treated; Table S4: The mapping efficiency percentage of reads mapped to the *Zingiber officinale* reference genome; Table S5: The KEGG pathways enrichment analysis of the control/*F. solani*-treated at 1.5 d; Table S6: The KEGG pathways enrichment analysis of the control/*F. solani*-treated at 2 d.

Author Contributions: L.Z.: writing—original draft and data curation. Q.J.: methodology, writing—review and editing, and funding acquisition. L.L.: project administration and funding acquisition. Y.L.: conceptualization, funding acquisition, and resources. All authors have read and agreed to the published version of the manuscript.

Funding: This work was funded by the Natural Science Foundation of Hubei Province (2023AFB1001).

Data Availability Statement: The RNA-seq data were deposited in the NCBI database (PRJNA1090657).

Conflicts of Interest: The authors declare no conflicts of interest.

References

1. Srinivasan, K. Ginger rhizomes (*Zingiber officinale*): A spice with multiple health beneficial potentials. *PharmaNutrition* **2017**, *5*, 18–28. [CrossRef]
2. Zhou, X.; Ma, H.H.; Xiong, S.J.; Zhang, L.L.; Zhu, X.D.; Zhu, Y.X.; Zhou, L.R. Evaluation of the inhibitory efficacy of eugenol against the pathogen of Fusarium wilt in ginger seedlings. *Horticulturae* **2023**, *9*, 1024. [CrossRef]
3. Choi, J.H.; Nah, J.Y.; Lee, M.J.; Yim, S.B.; Jang, J.Y.; Lee, T.; Kim, J. Fungal diversity in ginger and effect of storage conditions on occurrence of *Fusarium* and its mycotoxins. *Food Control* **2024**, *165*, 110631. [CrossRef]
4. Meng, X.L.; Wu, W.J.; Niu, B.; Liu, R.L.; Chen, H.Z.; Gao, H.Y.; Chen, H.J. Inhibitory effect and action mechanism of perillaldehyde on the *Fusarium graminearum* in postharvest fresh ginger. *Postharvest Biol. Technol.* **2024**, *209*, 112674. [CrossRef]
5. Zhang, L.L.; Fang, S.Y.; Sun, C.; Liang, H.R.; Ma, J.W.; Jia, Q.; Yin, J.L.; Zhu, Y.X.; Liu, Y.Q. Chitosan boosts ginger disease resistance: Insights from transcriptomic and metabolomic analyses. *LWT* **2024**, *205*, 116478. [CrossRef]
6. Ferreira da Cunha Neto, J.; da Silva Rocha, W.P.; Makris, G.; Sandoval-Denis, M.; Hagen, F.; Crous, P.W.; Chaves, G.M. Fusarioid keratitis and other superficial infections: A 10-years prospective study from Northeastern Brazil. *PLOS Neglected Trop. Dis.* **2024**, *18*, e0012247. [CrossRef]
7. Zhang, L.L.; Wu, X.Q.; Zhong, Y.; Yang, Y.; Wei, S.W.; Sun, C.; Wei, L.J.; Liu, Y.Q. Hydrogen sulfide enhances the disease resistance of ginger to rhizome rot during postharvest storage through modulation of antioxidant response and nitric oxide-mediated *S*-nitrosylaion. *Postharvest Biol. Technol.* **2025**, *220*, 113321. [CrossRef]
8. Abdullah, A.S.; Moffat, C.S.; Lopez-Ruiz, F.J.; Gibberd, M.R.; Hamblin, J.; Zerihun, A. Host-multi-pathogen warfare: Pathogen interactions in co-infected plants. *Front. Plant Sci.* **2017**, *8*, 1806. [CrossRef]
9. Zhao, L.N.; Zhou, Y.L.; Quan, S.H.; Qiu, J.E.; Dhanasekaran, S.; Li, B.; Gu, X.Y.; Zhang, H.Y. Transcriptome analysis reveals mechanisms of the disease resistance in postharvest kiwifruit induced by *Meyerozyma caribbica*. *Sci. Hortic.* **2023**, *322*, 112452. [CrossRef]
10. Jiang, Z.C.; Li, R.; Tang, Y.; Cheng, Z.Y.; Qian, M.J.; Li, W.; Shao, Y.Z. Transcriptome analysis reveals the inducing effect of *Bacillus siamensis* on disease resistance in postharvest mango fruit. *Foods* **2022**, *11*, 107. [CrossRef]
11. Li, X.; Zhang, C.; Wang, X.Y.; Liu, X.Q.; Zhu, X.L.; Zhang, J. Integration of metabolome and transcriptome profiling reveals the effect of modified atmosphere packaging (MAP) on the browning of fresh-cut Lanzhou lily (*Lilium davidii* var. unicolor) bulbs during storage. *Foods* **2023**, *12*, 1335. [CrossRef]
12. Yang, X.M.; Yang, K.X.; Wang, X.H.; Wang, Y.T.; Zhao, Z.Y.; Meng, D.M. Transcriptomic analysis reveals the mechanism of bacterial disease resistance of postharvest button mushroom (*Agaricus bisporus*). *Physiol. Mol. Plant Pathol.* **2022**, *122*, 101903. [CrossRef]
13. Zhang, L.L.; Yang, Y.; Zhu, Y.X.; Hu, H.J.; Jia, Q.; Sun, C.; Zhu, X.D.; Liu, Y. Antifungal activity and mechanism of chitosan against *Fusarium solani* caused ginger soft rot during postharvest storage. *Postharvest Biol. Technol.* **2024**, *208*, 112680. [CrossRef]
14. Li, H.L.; Wu, L.; Dong, Z.M.; Jiang, Y.S.; Jiang, S.J.; Xing, H.T.; Li, Q.; Liu, G.C.; Tian, S.M.; Wu, Z.Y.; et al. Haplotype-resolved genome of diploid ginger (*Zingiber officinale*) and its unique gingerol biosynthetic pathway. *Hortic. Res.* **2021**, *8*, 189. [CrossRef]
15. Li, G.; Ma, J.W.; Yin, J.L.; Guo, F.L.; Xi, K.Y.; Yang, P.H.; Cai, X.D.; Jia, Q.; Li, L.; Liu, Y.Q.; et al. Identification of reference genes for reverse transcription-quantitative PCR analysis of ginger under abiotic stress and for postharvest biology studies. *Front. Plant Sci.* **2022**, *13*, 893495. [CrossRef] [PubMed]
16. Li, Y.T.; Liu, X.; Xiao, Y.; Wen, Y.; Li, K.K.; Ma, Z.L.; Yin, J.L.; Yang, L.J.; Zhu, Y.X. Genome-wide characterization and function analysis uncovered roles of wheat LIMs in responding to adverse stresses and TaLIM8-4D function as a susceptible gene. *Plant Genome* **2022**, *15*, e20246. [CrossRef] [PubMed]
17. Trinder, P. Determination of blood glucose using an oxidase-peroxidase system with a non-carcinogenic chromogen. *J. Clin. Pathol.* **1969**, *22*, 158–161. [CrossRef]
18. Bergmeyer, H.U. *Methods of Enzymatic Analysis*; Academic Press: New York, NY, USA, 2012.
19. Sun, Y.I.; Oberley, L.W.; Li, Y. A simple method for clinical assay of superoxide dismutase. *Clin. Chem.* **1988**, *34*, 497–500. [CrossRef]
20. Kırgeç, Y.; Batı-Ay, E.; Açıkgöz, M.A. The effects of foliar salicylic acid and zinc treatments on proline, carotenoid, and chlorophyll content and anti-oxidant enzyme activity in *Galanthus elwesii* Hook. *Horticulturae* **2023**, *9*, 1041. [CrossRef]
21. Wei, L.J.; Zhang, J.; Wei, S.H.; Hu, D.L.; Liu, Y.Y.; Feng, L.; Li, C.X.; Wang, C.L.; Liao, W.B. Nitric oxide enhanced salt stress tolerance in tomato seedlings, involving phytohormone equilibrium and photosynthesis. *Int. J. Mol. Sci.* **2022**, *23*, 4539. [CrossRef]
22. Lei, S.; Rossi, S.; Huang, B. Metabolic and physiological regulation of aspartic acid-mediated enhancement of heat stress tolerance in Perennial Ryegrass. *Plants* **2022**, *11*, 199. [CrossRef] [PubMed]

23. Shu, P.; Li, Y.J.; Wang, X.Y.; Yao, L.; Sheng, J.P.; Shen, L. Exogenous ferulic acid treatment increases resistance against *Botrytis cinerea* in tomato fruit by regulating nitric oxide signaling pathway. *Postharvest Bio. Technol.* **2021**, *182*, 111678. [CrossRef]
24. Sharma, A.; Soares, C.; Sousa, B.; Martins, M.; Kumar, V.; Shahzad, B.; Sidhu, G.P.; Bali, A.S.; Asgher, M.; Bhardwaj, R.; et al. Nitric oxide-mediated regulation of oxidative stress in plants under metal stress: A review on molecular and biochemical aspects. *Physiol. Plant.* **2020**, *168*, 318–344. [CrossRef]
25. Zhou, J.; Liu, X.L.; Sun, C.; Li, G.; Yang, P.M.; Jia, Q.; Cai, X.D.; Zhu, Y.X.; Yin, J.L.; Liu, Y.Q. Silica nanoparticles enhance the disease resistance of ginger to rhizome rot during postharvest storage. *Nanomaterials* **2022**, *12*, 1418. [CrossRef]
26. Xu, M.Q.; Zhang, X.Y.; Dhanasekaran, S.; Godana, E.A.; Yang, Q.Y.; Zhao, L.N.; Zhang, H.Y. Transcriptome analysis of postharvest pear (*Pyrus pyrifolia* Nakai) in response to *Penicillium expansum* infection. *Sci. Hortic.* **2021**, *288*, 110361. [CrossRef]
27. Ortiz-Morea, F.A.; Liu, J.; Shan, L.B.; He, P. Malectin-like receptor kinases as protector deities in plant immunity. *Nat. Plants* **2022**, *8*, 27–37. [CrossRef] [PubMed]
28. Zipfel, C. Early molecular events in PAMP-triggered immunity. *Curr. Opin. Plant Biol.* **2009**, *12*, 414–420. [CrossRef]
29. Yuan, M.H.; Jiang, Z.Y.; Bi, G.Z.; Nomura, K.; Liu, M.H.; Wang, Y.P.; Cai, B.Y.; Zhou, J.M.; He, S.Y.; Xin, X.F. Pattern-recognition receptors are required for NLR-mediated plant immunity. *Nature* **2021**, *592*, 105–109. [CrossRef]
30. Xiong, J.S.; Zhu, H.Y.; Bai, Y.B.; Liu, H.; Cheng, Z.M. RNA sequencing-based transcriptome analysis of mature strawberry fruit infected by necrotrophic fungal pathogen *Botrytis cinerea*. *Physiol. Mol. Plant Pathol.* **2018**, *104*, 77–85. [CrossRef]
31. Akamatsu, A.; Wong, H.L.; Fujiwara, M.; Okuda, J.; Nishide, K.; Uno, K.; Imai, K.; Umemura, K.; Kawasaki, T.; Kawano, Y.; et al. An OsCEBiP/OsCERK1-OsRacGEF1-OsRac1 module is an essential early component of chitin-induced rice immunity. *Cell Host Microbe* **2013**, *13*, 465–476. [CrossRef]
32. Kaku, H.; Nishizawa, Y.; Ishii-Minami, N.; Akimoto-Tomiyama, C.; Dohmae, N.; Takio, K.; Minami, E.; Shibuya, N. Plant cells recognize chitin fragments for defense signaling through a plasma membrane receptor. *Proc. Natl. Acad. Sci. USA* **2006**, *103*, 11086–11091. [CrossRef] [PubMed]
33. Haider, M.S.; Kurjogi, M.M.; Khalil-Ur-Rehman, M.; Fiaz, M.; Pervaiz, T.; Jiu, S.T.; Jia, H.F.; Chen, W.; Fang, J.G. Grapevine immune signaling network in response to drought stress as revealed by transcriptomic analysis. *Plant Physiol. Biochem.* **2017**, *121*, 187–195. [CrossRef]
34. DeFalco, T.A.; Moeder, W.; Yoshioka, K. Opening the gates: Insights into cyclic nucleotide-gated channel-mediated signaling. *Trends Plant Sci.* **2016**, *21*, 903–906. [CrossRef] [PubMed]
35. Yan, S.Y.; Li, J.; Zhang, Q.C.; Jia, S.X.; Zhang, Q.Q.; Wang, R.T.; Ju, M.X.; Gu, P.W. Transcriptional response of wolfberry to infestation with the endophytic *Fusarium nematophilum* strain NQ8GII4. *Plant Dis.* **2024**, *108*, 1514–1525. [CrossRef]
36. Gao, Q.M.; Venugopal, S.; Navarre, D.; Kachroo, A. Low oleic acid-derived repression of jasmonic acid-inducible defense responses requires the WRKY50 and WRKY51 proteins. *Plant Physiol.* **2011**, *155*, 464–476. [CrossRef]
37. Liu, X.F.; Song, Y.Z.; Xing, F.Y.; Wang, N.; Wen, F.J.; Zhu, C.X. GhWRKY25, a group I WRKY gene from cotton, confers differential tolerance to abiotic and biotic stresses in transgenic *Nicotiana benthamiana*. *Protoplasma* **2016**, *253*, 1265–1281. [CrossRef]
38. Peng, H.M.; Hu, H.J.; Xi, K.Y.; Zhu, X.M.; Zhou, J.; Yin, J.L.; Guo, F.L.; Liu, Y.Q.; Zhu, Y.X. Silicon nanoparticles enhance ginger rhizomes tolerance to postharvest deterioration and resistance to *Fusarium solani*. *Front. Plant Sci.* **2022**, *13*, 816143. [CrossRef]
39. Ding, L.N.; Li, Y.T.; Wu, Y.Z.; Li, T.; Geng, R.; Cao, J.; Zhang, W.; Tan, X.L. Plant disease resistance-related signaling pathways: Recent progress and future prospects. *Int. J. Mol. Sci.* **2022**, *23*, 16200. [CrossRef]
40. Pan, L.Y.; Zhao, X.Y.; Chen, M.; Fu, Y.Q.; Xiang, M.L.; Chen, J.Y. Effect of exogenous methyl jasmonate treatment on disease resistance of postharvest kiwifruit. *Food Chem.* **2020**, *305*, 125483. [CrossRef]
41. Yang, R.; Wang, J.; Cai, Z.P.; Shen, Y.G.; Gan, Z.Y.; Duan, B.; Yuan, J.; Huang, T.H.; Zhang, W.; Du, H.Y.; et al. Transcriptome profiling to elucidate mechanisms of the enhancement of the resistance to *Botryosphaeria dothidea* by nitric oxide in postharvest kiwifruit during storage. *LWT* **2022**, *159*, 113187. [CrossRef]
42. Liu, J.L.; Zhang, W.L.; Hu, M.J.; Pan, Y.G.; Jiang, Y.M.; Zhang, Z.K.; Jiang, G.X. Nitric oxide is involved in melatonin-induced cold tolerance in postharvest litchi fruit. *Postharvest Bio. Technol.* **2023**, *196*, 112157. [CrossRef]
43. Capone, R.; Tiwari, B.S.; Levine, A. Rapid transmission of oxidative and nitrosative stress signals from roots to shoots in *Arabidopsis*. *Plant. Physiol. Biochem.* **2004**, *42*, 425–428. [CrossRef] [PubMed]
44. Weralupitiya, C.; Eccersall, S.; Meisrimler, C.N. Shared signals, different fates: Calcium and ROS in plant PRR and NLR immunity. *Cell Rep.* **2024**, *43*, 114910. [CrossRef]
45. He, Q.; McLellan, H.; Hughes, R.K.; Boevink, P.C.; Armstrong, M.; Lu, Y.; Banfield, M.J.; Tian, Z.; Birch, P.R.J. *Phytophthora infestans* effector *SFI3* targets potato *UBK* to suppress early immune transcriptional responses. *New Phytol.* **2019**, *222*, 438–454. [CrossRef] [PubMed]
46. Kong, L.; Ma, X.Y.; Zhang, C.; Kim, S.I.; Li, B.; Xie, Y.P.; Yeo, I.C.; Thapa, H.; Chen, S.; Devarenne, T.P.; et al. Dual phosphorylation of DGK5-mediated PA burst regulates ROS in plant immunity. *Cell* **2024**, *187*, 609–623. [CrossRef]

47. Zhu, Y.T.; Zhao, M.; Li, T.T.; Wang, L.Z.; Liao, C.L.; Liu, D.X.; Zhang, H.M.; Zhao, Y.P.; Liu, L.S.; Ge, X.Y.; et al. Interactions between *Verticillium dahliae* and cotton: Pathogenic mechanism and cotton resistance mechanism to Verticillium wilt. *Front Plant Sci.* **2023**, *14*, 1174281. [CrossRef]
48. Chakraborty, N.; Basak, J. Comparative transcriptome profiling of a resistant vs. susceptible *Vigna mungo* cultivar in response to Mungbean yellow mosaic India virus infection reveals new insight into MYMIV resistance. *Curr. Plant Biol.* **2018**, *15*, 8–24. [CrossRef]

horticulturae

MDPI

Article

Exogenous 24-Epibrassinolide Alleviated Selenium Stress in Peach Seedling

Zhiyu Hang [1], Qizhe Cao [1], Yunyao Du [1], Jinrong Zhang [2], Lijin Lin [1], Mingfei Zhang [1,*] and Xun Wang [1,*]

[1] College of Horticulture, Sichuan Agricultural University, Chengdu 611130, China; 18976798029@163.com (Z.H.); yushengASLN@163.com (Q.C.); 17323200084@163.com (Y.D.); 14208@sicau.edu.cn (L.L.)

[2] School of Agriculture and Horticulture, Chengdu Agriculturall College, Chengdu 611130, China; 13980460749@163.com

* Correspondence: zhang_mingfei@sicau.edu.cn (M.Z.); wx0104@sicau.edu.cn (X.W.)

Abstract

Selenium stress can adversely affect plants by inhibiting growth, impairing oxidative stress resistance, and inducing toxicity. In this experiment, we investigated the effect of exogenous 24-epibrassinolide (24-EBL; 2.0 mg/L), a brassinosteroid (BR), on alleviating selenium stress in peach trees by analyzing its impact on biomass, selenium accumulation, and the expression of selenium metabolism-related genes in peach seedlings. The results demonstrated that 24-EBL could effectively mitigate biomass loss in peach seedlings exposed to selenium stress. Compared to the Se treatment alone, the 24-EBL+Se treatment resulted in a significant 16.55% increase in root selenium content and a more pronounced 30.39% increase in selenium content in the aboveground parts. Regarding the subcellular distribution, the cell wall was the primary site of Se deposition, accounting for 42.3% and 49.8% in the root and aboveground parts, respectively, in the Se treatment. 24-EBL further enhanced Se distribution at this site, reaching 42.9% and 63.2% in root and aboveground parts, respectively, in the 24-EBL+Se treatment. The 24-EBL+Se treatment significantly increased the contents of different chemical forms of Se, including ethanol-soluble, water-soluble, and salt-soluble Se. The quantitative real-time PCR (qRT-PCR) results indicated that the Se treatment promoted the expression of organic Se assimilation genes (*SATs*, *OAS-TL B*, and *OAS-TL C*), and 24-EBL application further increased their expression. Meanwhile, the Se-only treatment up-regulated the organic Se metabolism gene *CGS1*. Consequently, we propose that 24-EBL alleviates Se stress in peach seedlings by enhancing Se uptake and assimilation, and by adjusting subcellular distribution and chemical forms.

Keywords: brassinosteroids; selenium determination; gene expression

1. Introduction

Selenium is an essential trace element for human health, but the human body cannot synthesize it and must obtain it from external sources [1,2]. However, naturally occurring selenium cannot be directly absorbed or utilized by humans. Plants serve as a critical intermediary in selenium metabolism by absorbing inorganic selenium from the soil and converting it into bioavailable organic forms [3]. As a result, crops, fruits, and vegetables are ideal dietary sources of selenium, constituting the primary route of human selenium intake [4]. This has led to the widespread use of selenium-enriched fertilizers in agriculture to enhance the selenium content of food products [5].

However, excessive application of selenium fertilizers in agriculture can lead to environmental selenium pollution, posing risks to human health, disrupting ecosystems, and harming agricultural productivity [5]. For example, an intake of >400 μg/day is generally considered the threshold for toxic levels for humans [6,7]. The widespread use of selenium-enriched fertilizers may result in the gradual accumulation of selenium in soil and groundwater [8]. Elevated selenium levels can adversely affect plants by inhibiting growth, impairing oxidative stress resistance, and inducing toxicity [9]. Specifically, it disrupts root physiology, damages antioxidants, suppresses antioxidant enzyme activity, and destabilizes the plant's antioxidant defense system [9,10].

Selenium induces stress in plants through multiple mechanisms. The bioavailable forms of selenium for plant uptake in soil are primarily inorganic selenate (SeO_4^{2-}) and selenite (SeO_3^{2-}) [11]. These inorganic selenium species induce oxidative stress by generating excessive reactive oxygen species (ROS), disrupting intracellular antioxidant defenses, and causing phytotoxicity [12]. Furthermore, selenite is readily assimilated into organic forms. Excessive accumulation of organic selenium compounds, particularly selenocysteine (SeCys) and selenomethionine (SeMet), can lead to nonspecific incorporation into proteins, where they displace their sulfur (S) analogues. This substitution alters protein structure, impairs functionality, and disrupts enzymatic processes critical for plant metabolism [13].

Brassinosteroids (BRs) are a class of ubiquitous plant sterol hormones. They can enhance plant stress resistance by boosting antioxidant enzyme activity, optimizing antioxidant systems, and maintaining intracellular homeostasis [14,15]. These properties of BRs enable plants to tolerate various abiotic stresses such as extreme temperatures, salinity, drought, heavy metals, and pesticides [16]. Specifically, BRs have been shown to strengthen antioxidant defense systems in rice (*Oryza sativa*) under heavy metal (cadmium; Cd) stress [17] and reduce Cd and also phenanthrene (PAH) accumulation in tomato (*Solanum lycopersicum*) leaves and roots [18]. Recent studies demonstrated that synthesized BR (24-epibrassinolide; 24-EBL) alleviated zinc (Zn) stress in mung bean (*Vigna radiata*) seedlings, significantly improving germination rate, germination velocity, and seedling vigor index [19]. Our previous work also demonstrated the alleviating effect of 24-epibrassinolide on Se toxicity [20,21]. However, the metabolic mechanisms by which 24-EBL alleviates Se-induced stress in plants remain unclear.

Peach fruit has gained global popularity due to its delightful taste and nutritional benefits. As the foundation for nutrient absorption in peach trees, rootstock selection is crucial for cultivation. Fluffy peach ("MaoTao"), a native Chinese germplasm, serves as one of the most widely used rootstocks in peach production regions of China. This study investigated the potential of BRs to mitigate selenium stress in peach plants using fluffy peach seedlings as experimental material. We examined the effects of exogenous 24-EBL application on plant biomass and total selenium accumulation, subcellular selenium distribution patterns, chemical forms of selenium, and expression profiles of selenium metabolism-related genes. Our findings provide valuable insights into using 24-EBL as a potential treatment for enhancing plant tolerance to selenium stress, offering practical references for peach cultivation under selenium-rich conditions.

2. Materials and Methods

2.1. Plant Material and Growth Condition

Fluffy peach (*Prunus persica* (L.) Batsch) seeds were obtained from Chengdu, Sichuan Province, China. The experiment was conducted from March to May 2024 in the greenhouse of Sichuan Agricultural University, Chengdu Campus (30°43′ N, 103°52′ E), with day/night temperatures maintained at 25/20 °C, relative humidity at 70%/90%, and a 14/10 h photoperiod at 10,000 lx intensity. Seeds were germinated in perlite-filled trays under

controlled conditions. After emergence, seedlings were irrigated with Hoagland nutrient solution (Betensh, Hubei, China) every 3 days. When seedlings reached 10 cm height, uniform plants were transplanted into 32-cell plug trays (4 × 8 arrangement), containing perlite substrate, continuing with triweekly Hoagland solution irrigation. The Hoagland nutrient solution was pH 6.0. The main nutrient elements in the Hoagland solution were as follows: Ca^{2+} 23.625 mEq/L, K^{+} 15.425 mEq/L, $NH_4{}^{+}$ 2.375 mEq/L, Mg^{2+} 20.54 mEq/L, NO^{3-} 34.8 mEq/L, and $PO_4{}^{3-}$ 1.15 mEq/L. Each treatment was replicated in three trays.

2.2. Experimental Treatments

Ten days post-transplantation, three treatments were initiated: (1) Control (CK) receiving standard Hoagland solution; (2) Selenium treatment (Se) with 0.1 mg/L sodium selenite in Hoagland solution applied every 3 days [22]; and (3) Combined treatment (24-EBL+Se) receiving both the selenium solution and foliar sprays of 2.0 mg/L 24-EBL weekly for 4 weeks [21]. Each treatment included three biological replicates (trays). After one month of treatment, when seedlings reached 32–38 cm height with 21–25 leaves, complete plants (aboveground part and root) were harvested from all treatments for subsequent analysis of growth parameters, selenium content, subcellular distribution, chemical form, and gene expression related to selenium metabolism.

2.3. Plant Biomass Determination

The aboveground parts and roots were washed with tap water, followed by repeated rinsing with deionized water. Plant materials were then deactivated at 105 °C in a drying oven for 15 min and dried to constant weight at 70 °C. The biomass of roots and aboveground parts was measured separately using an electronic balance.

2.4. Total Selenium Content Determination

Dried plant materials were ground and sieved through a 100-mesh sieve. Exactly 0.500 g samples were weighed into Erlenmeyer flasks containing 9 mL concentrated nitric acid (analytical grade) and 1 mL perchloric acid (analytical grade). After 12 h of predigestion, samples were digested on an electric hot plate until the solution became transparent. After complete cooling, the solution was diluted to 25 mL with potassium ferricyanide solution (100 g/L). Selenium concentration was determined using an atomic fluorescence spectrometer (AFS-9700, Beijing Haiguang Instrument Co., Ltd., Beijing, China).

2.5. Inorganic Se and Organic Se Contents Determination

Dry plant materials (0.20–0.50 g) were digested with 20 mL 6 mol/L HCl at 70 °C for 2 h in a water bath shaker. After cooling and volume adjustment, the mixture was filtered through degreased cotton. The filtrate was heated in a boiling water bath for 20 min, cooled, and 1 mL was transferred to a 25 mL stoppered colorimetric tube. Following dilution to 10 mL with deionized water, 2 mL concentrated HCl and 1 mL potassium ferricyanide solution (100 g/L) were added to obtain the inorganic Se (Inorg-Se) content. Organic Se (Org-Se) content was calculated as the difference between total Se and inorganic Se. Selenium concentration was determined using an atomic fluorescence spectrometer (AFS-9700, Beijing Haiguang Instrument Co., Ltd., Beijing, China).

2.6. Selenium Content Determination in Plant Subcellular Distribution

Subcellular fractions from peach aboveground parts were extracted by differential centrifugation. Exactly 1.0 g of fresh root tissue was weighed and homogenized in a precooled mortar with extraction buffer (250 mmol/L sucrose, 50 mmol/L Tris-HCl [pH 7.5], and 1.0 mmol/L dithioerythritol) at a 1:10 (w/v) ratio. The homogenate was filtered through cheesecloth, with the residue washed into a beaker to obtain the cell wall fraction (CW-Se).

The filtrate was centrifuged at 20,000× *g* for 45 min at 4 °C to separate organelle fraction (O-Se, excluding vacuoles) in the pellet from the free fraction (F-Se) in the supernatant. All fractions were analyzed for selenium content by atomic fluorescence spectrometer (AFS-9700, Beijing Haiguang Instrument Co., Ltd., Beijing, China).

2.7. Determination of Selenium Chemical Forms

The analysis of selenium chemical forms was performed using a sequential extraction method. Dried aboveground part and root samples were defatted by stirring with acetone (1:10 *w*/*v*) for 4 h, repeated three times. After each defatting step, centrifugation was performed at 5000 rpm for 40 min. The combined supernatants yielded the water-soluble Se form (Fw). The residue was then extracted with 0.5 mol/L NaCl solution (2 h stirring) followed by centrifugation (5000 rpm, 4 °C, 20 min), repeated three times to obtain the salt-soluble Se form (Fs). Subsequent extractions with 0.6 mol/L acetic acid (HAC) solution and 80% ethanol under identical conditions yielded the weak acid-soluble (F_A) and ethanol-soluble (F_E) forms, respectively. The final residue represented the residual Se form (F_R). All speciations were analyzed for selenium content by atomic fluorescence spectrometer (AFS-9700, Beijing Haiguang Instrument Co., Ltd., Beijing, China).

2.8. Gene Expression Analysis Using Quantitative Real-Time PCR (qRT-PCR)

The expression levels of 14 selenium metabolism-related genes (*SULTR2;1*, *SULTR3;1*, *SULTR3;4*, *SULTR4;1*, *APS1*, *APR1*, *SAT3;1*, *SAT2;2*, *SAT1;1*, *OAS-TL B*, *OAS-TL C*, *NFS1*, *CGS1*, and *MS1*) in peach seedlings were analyzed using the primers listed in Table S1. Total RNA was extracted from leaves using the RNAprep Pure Plant Total RNA Extraction Kit (Tiangen Biotech, Beijing), followed by first-strand cDNA synthesis with the EasyScript One-Step gDNA Removal and cDNA Synthesis Kit (TransGen Biotech, Beijing, China). qRT-PCR was performed using TransStart Top Green qPCR SuperMix (TransGen Biotech, Beijing, China). The reaction system consisted of 1 μL cDNA, 0.4 μL forward primer, 0.4 μL reverse primer, 5 μL Green qPCR SuperMix, and 3.2 μL water. The thermal cycling program was as follows: 95.0 °C for 1 min, followed by 95.0 °C for 5 s and 55.0 °C for 30 s, repeated for 39 cycles, and finally, 95.0 °C for 10 s and 65.0 °C for 5 s. The *actin* gene was used as the internal reference gene. Relative gene expression levels were calculated using the $2^{-\Delta\Delta Ct}$ method with three technical replicates.

2.9. Statistical Analysis

Statistical analyses were performed using SPSS software SPSS 19.0 (IBM Corporation, Armonk, NY, USA). Significant differences among treatments were assessed using one-way analysis of variance (ANOVA) followed by *F*-tests, with a significance threshold of $p < 0.05$. Post hoc multiple comparisons were conducted using the Least Significant Difference (LSD) method.

3. Result

3.1. Biomass of Peach Seedlings

Under selenium stress conditions, both root and aboveground biomass of peach seedlings showed significant reductions ($p < 0.05$) compared to the control, decreasing by 15.24% and 6.24%, respectively (Figure 1). However, when selenium-stressed plants were treated with 24-EBL (24-EBL+Se treatment), both root and aboveground part biomass increased significantly by 7.84% and 3.69% relative to the selenium-only treatment, respectively ($p < 0.05$). These results demonstrated that foliar application of 24-EBL can effectively mitigate biomass loss in peach seedlings exposed to selenium stress.

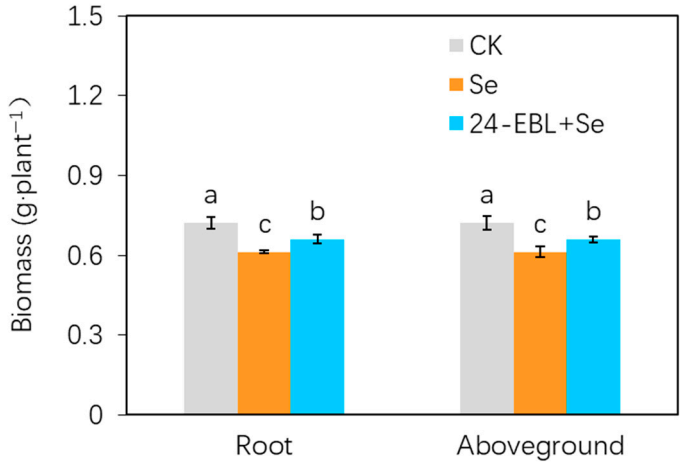

Figure 1. The biomass of root and aboveground parts. The lowercase letters a, b, and c denote statistically significant differences ($p < 0.05$).

3.2. Selenium Content in Peach Seedling

In both Se and 24-EBL+Se treatments, the majority of absorbed selenium accumulated in the root system (2.682 mg/kg and 3.126 mg/kg, respectively), with significantly lower concentrations detected in aboveground parts (0.362 mg/kg and 0.472 mg/kg, respectively) (Figure 2). Compared to the Se treatment alone, the 24-EBL+Se treatment resulted in a significant 16.55% increase in root selenium content (from 2.682 to 3.126 mg/kg) and a more pronounced 30.39% increase in selenium content in the aboveground part (from 0.362 to 0.472 mg/kg). In both the root and aboveground parts, the organic selenium content was significantly higher than the inorganic selenium content (Figure 2).

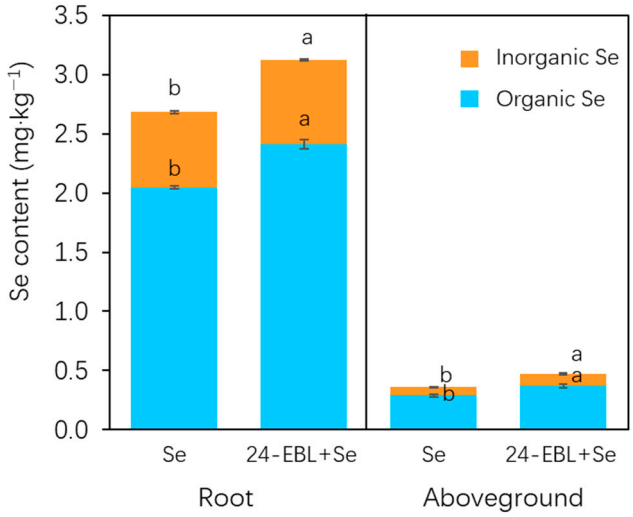

Figure 2. The selenium contents in root and aboveground parts. The lowercase letters a and b denote statistically significant differences ($p < 0.05$).

3.3. Subcellular Distribution of Selenium in Peach Seedlings

Both CW-Se and F-Se selenium fractions in 24-EBL+Se treatment showed significantly higher concentrations compared to the Se-only treatment, while the O-Se remained unchanged (Figure 3). In the aboveground part, 24-EBL+Se treatment also significantly increased CW-Se fractions (Figure 3). Consequently, in roots, the proportional Se distribution under Se treatment was CW-Se (42.3%), O-Se (23.1%), and F-Se (34.6%), which was similar to that in the 24-EBL+Se treatment: CW-Se (42.9%), O-Se (21.6%), and F-Se (35.5%) (Figure 4). By comparison, the distribution pattern shifted from CW-Se (49.8%),

O-Se (20.9%), and F-Se (29.3%) in the Se treatment to CW-Se (63.2%), O-Se (16.4%), and F-Se (20.4%) in the 24-EBL+Se treatment, with the cell wall-bound Se fraction increasing sharply while the organelle-bound and free Se fractions decreased proportionally (Figure 4). This suggested that the cell wall is the primary site of Se deposition, and 24-EBL further enhanced Se accumulation in this site.

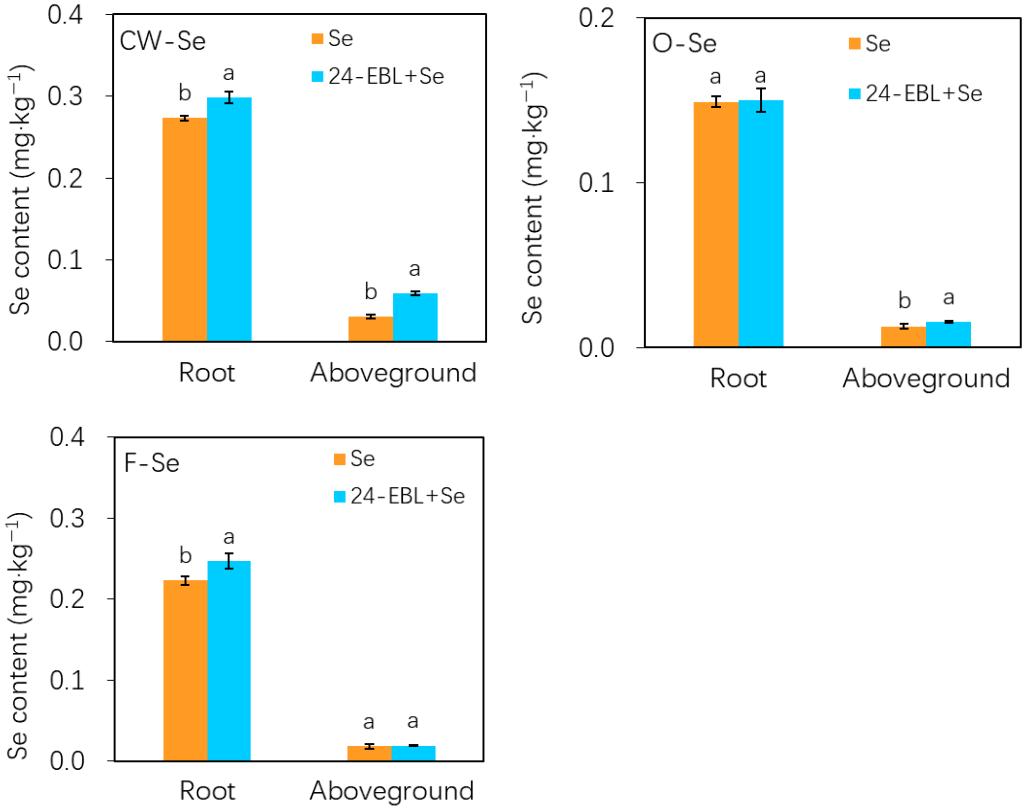

Figure 3. The selenium contents in subcellular fractions in root and aboveground parts. CW-Se, cell wall fraction Se; O-Se, organelle fraction Se; F-Se, free fraction Se. The lowercase letters a and b denote statistically significant differences ($p < 0.05$).

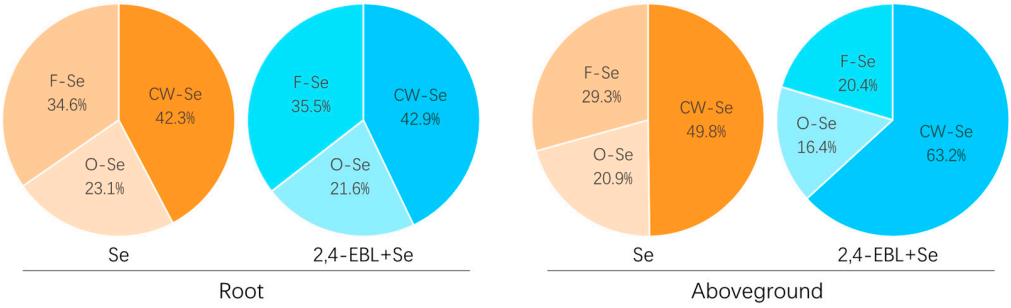

Figure 4. The proportional Se subcellular distribution in root and aboveground parts. CW-Se, cell wall fraction Se; O-Se, organelle fraction Se; F-Se, free fraction Se.

3.4. Chemical Forms of Selenium in Peach Seedlings

The 24-EBL+Se treatment significantly increased the contents of F_E (0.714 vs. 0.567 mg/kg), F_W (0.575 vs. 0.448 mg/kg), and F_S (0.440 vs. 0.380 mg/kg) in roots compared to the Se treatment alone (Figure 5). Similarly, in the aboveground part, the contents of F_E (0.151 vs. 0.104 mg/kg), F_W (0.065 vs. 0.051 mg/kg), and F_S (0.056 vs. 0.048 mg/kg) were significantly higher in the 24-EBL+Se treatment than in the Se-only treatment (Figure 5). However, the F_A content in both roots and aboveground parts significantly decreased

under 24-EBL+Se treatment, while no significant differences in F_R content were observed between the two treatments.

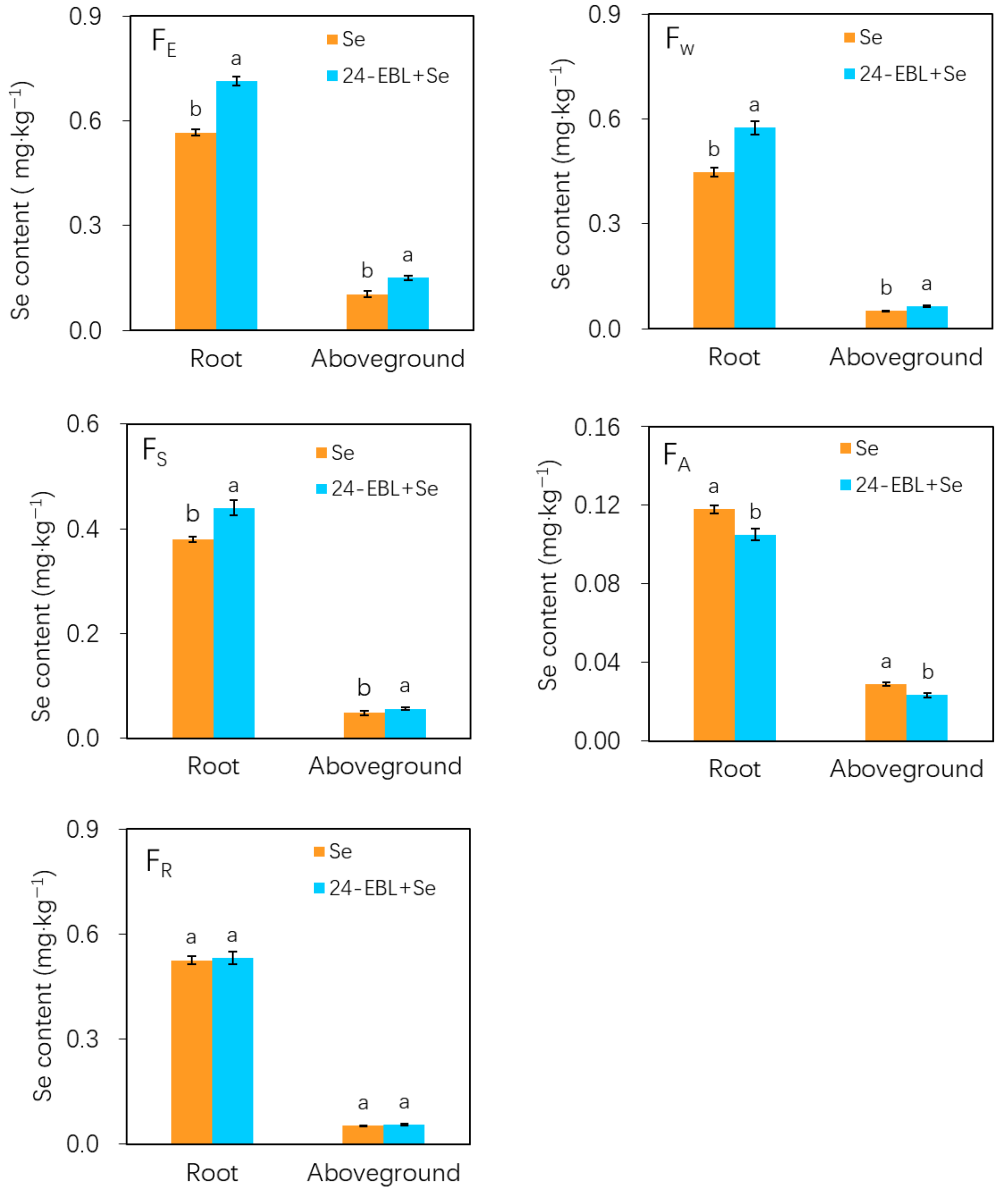

Figure 5. The selenium contents in different chemical forms in the root and aboveground parts. F_E, ethanol-soluble Se; F_W, water-soluble Se; F_S, salt-soluble Se; F_A, weak acid-soluble Se; F_R, residual Se. The lowercase letters a and b denote statistically significant differences ($p < 0.05$).

3.5. Expression Analysis of Selenium Metabolism-Related Genes in Peach Seedlings

Among the 14 genes tested, Se stress induced down-regulation of *SULTR2;1*, *SULTR3;4*, *APS1*, and *APR1* genes, while up-regulating *SAT3;1*, *SAT2;2*, *SAT1;1*, *OAS-TL C*, and *CGS1* (Figures 6 and 7) compared to the control. In the 24-EBL+Se treatment, similar expression patterns for the aforementioned genes were observed. Additionally, it significantly up-regulated *SULTR3;1* and *OAS-TL B* but did not alter the expression levels of *APS1* and *CGS1* significantly. Compared to the Se treatment, 24-EBL+Se significantly up-regulated the expression of *SULTR2;1*, *APS1*, *SAT3;1*, *OAS-TL B*, and *OAS-TL C*, while significantly down-regulating *SULTR3;1*, *APR1*, *NFS1*, and *CGS1* (Figures 6 and 7).

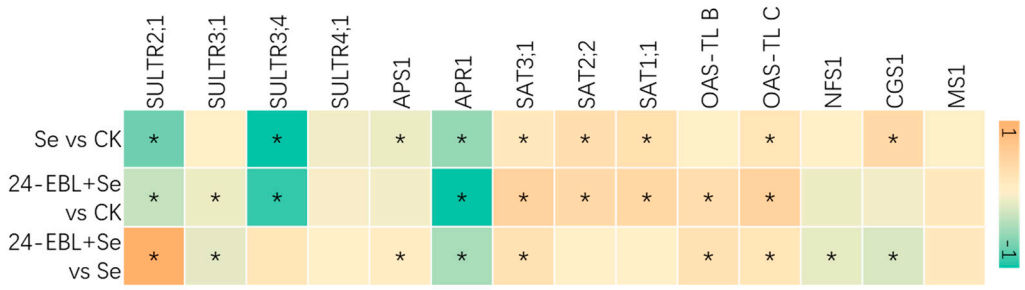

Figure 6. The qRT-PCR analysis of selenium metabolism-related genes. The colors show the $\log_{10}$ of different treatment ratios. "*" denotes the differentially expressed genes with a significance threshold of $p < 0.05$.

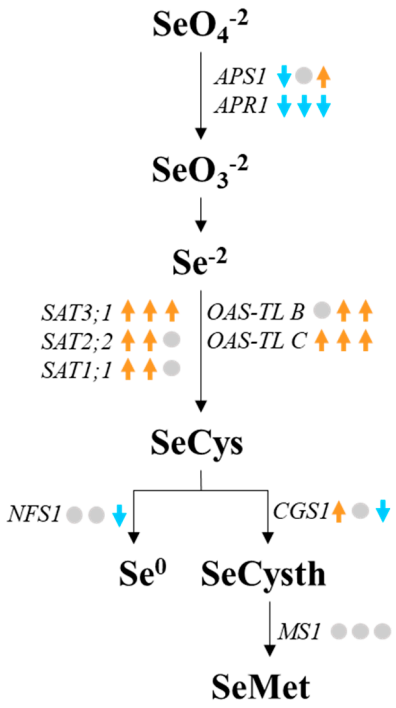

Figure 7. Schematic model of Se metabolism in peach seedling. The three arrows/circles next to gene names are Se vs. CK, 24-EBL+Se vs. CK, and 24-EBL+Se vs. Se. The orange up arrows indicate significantly up-expression, blue down arrows indicate significantly down-expression, and grey circles indicate no significant change.

4. Discussion

In this study, we used exogenous BR (24-EBL) to alleviate the effects of Se stress on the growth of peach seedlings, as indicated by the increased biomass in the 24-EBL+Se treatment compared to the Se-only treatment (Figure 1). By measuring the Se content in the plants, we found that the 24-EBL+Se treatment promoted the uptake of Se by the plants rather than inhibiting it (Figure 2). Therefore, 24-EBL might have activated certain metabolic mechanisms in the peach seedlings to prevent excessive damage caused by the absorbed Se. Similar functions of BRs have also been reported in alleviating the stress caused by cadmium, phenanthrene, and zinc [17–19]. Moreover, it indicated that the 24-EBL+Se treatment induced a more pronounced increase in organic Se content compared to inorganic Se (Figure 2). Since the organic Se in plants is derived from the assimilation of inorganic Se [23,24], these findings in the present study demonstrated that 24-EBL enhanced the assimilation process of inorganic Se in peach seedlings.

Plants employ subcellular distribution as a strategy to remove heavy metal toxicity [25,26]. Se can be bound to the cell wall, thereby limiting its effect on other intracellular

physiological and metabolic processes [27]. Our findings demonstrated that 24-EBL treatment significantly enhanced selenium sequestration in cell walls (CW-Se), particularly in the aboveground parts (Figures 3 and 4). This indicated that 24-EBL might mitigate selenium toxicity through preferential distribution to the cell wall, thereby protecting vital organelles from selenium-induced damage.

The results of selenium chemical speciation in the present study revealed that the 24-EBL+Se treatment significantly enhanced the levels of water-soluble, ethanol-soluble, and salt-soluble Se forms (Figure 5). The water-soluble form contains predominantly inorganic Se species along with small selenoamino acids, including selenolanthionine, glutamyl-methylselenocysteine (γGMSC), se-methylselenocysteine (MeSeCys), SeCys, and SeMet [28,29]. The ethanol-soluble form comprises monosaccharides, disaccharides, and low-molecular-weight organic Se compounds, while the salt-soluble form includes protein-bound Se and exchangeable Se species [29]. The findings in the present study demonstrated that the organic Se that 24-EBL+Se treatment promoted in peach seedlings was particularly stored as small-molecule organic Se, which contained several low-toxicity compounds, such as MeSeCys [30], selenocystathionine (SeCysth) [31], selenolanthionine [32], and γGMSC [33]. This shift in Se speciation likely contributed to the improvement in Se tolerance in peach seedlings under 24-EBL treatment. Concurrently, the increased incorporation of Se into proteins, as evidenced by elevated ethanol- and salt-soluble Se forms, might explain the relatively minor impact on biomass accumulation in the 24-EBL+Se treatment compared to the control (Figure 1).

The sulfate transporter gene *SULTR1;2*, known to mediate selenium/sulfate uptake from soil and their subsequent distribution to leaf tissues [34], exhibited low transcriptional expression in peach seedlings under both control (CK) and selenium stress conditions in the present research. Notably, 24-EBL application significantly upregulated *SULTR1;2* expression relative to both CK and selenium-treated plants (Figure 6), demonstrating that BRs enhance selenium acquisition through sulfate transport systems while facilitating root-to-shoot selenium translocation.

The SAT-OASTL enzyme complex (serine acetyltransferase (SAT) and O-acetylserine (thiol) lyase (OASTL)) is responsible for the assimilation of inorganic Se into organic Se [35,36]. The present study revealed that under Se stress, the expression of *SATs*, *OAS-TL C*, and *OAS-TL B* was upregulated (Figures 6 and 7). Following 24-EBL application, the expression of these genes was further enhanced. This upregulation might ultimately lead to a significant increase in organic Se content in the 24-EBL+Se treatment (Figure 2).

One of the mechanisms of selenium toxicity in plants is the misincorporation of organic selenium species (e.g., SeCys and SeMet) into cysteine and methionine residues, then disrupting normal metabolic processes [37–39]. In contrast, the accumulation of water-soluble, non-protein-bound selenium forms is less toxic [6]. Other detoxification strategies in plants involve reducing selenate to elemental Se (Se^0) and selenide (Se^{2-}), which can then be volatilized as dimethylselenide (DMSe) or dimethyldiselenide (DMDSe) [40]. We investigated three key genes in organic selenium metabolism, cysteine desulfurase (*NFS1*), cystathionine γ-synthase (*CGS1*), and methionine synthase (*MS1*) (Figures 6 and 7). NFS1 catalyzes the reduction of SeCys to Se^0, while CGS1 and MS1 mediate the conversion of SeCys to SeMet [27]. Notably, Se treatment alone significantly upregulated *CGS1* expression, suggesting enhanced SeMet biosynthesis. However, in the 24-EBL+Se treatment, *CGS1* expression levels showed no significant difference from the control and were even significantly lower than in Se-treated plants, indicating that attenuated SeMet production likely contributed to the reduction in selenium toxicity. Furthermore, our selenium chemical speciation analysis (Figure 5) suggested that 24-EBL promotes the accumulation of less

toxic water-soluble small selenoamino acids, providing the enhanced selenium tolerance observed in 24-EBL-treated peach seedlings.

5. Conclusions

This study demonstrated that 24-EBL application effectively mitigated selenium stress while promoting selenium accumulation in peach seedlings. Foliar application of 24-EBL enhanced plant biomass and total selenium content under selenium stress, facilitated organic selenium translocation from roots to aboveground, reduced selenium toxicity through cell wall sequestration of inorganic selenium, and upregulated key selenium metabolism genes (*Sultr1;2*, *SATs*, *OAS-TLs*, and *CGS1*). These molecular and physiological modifications collectively regulated organic selenium assimilation and conversion, minimized damage from excessive selenocysteine accumulation, and enhanced plant selenium enrichment capacity. Our findings provide a scientific foundation for employing 24-EBL, offering practical applications for selenium-enriched agricultural production systems. Future studies should employ more precise metabolite profiling (e.g., high-performance liquid chromatography (HPLC)) and comprehensive transcriptome analysis to better understand the mechanisms of 24-EBL in alleviating Se stress.

Supplementary Materials: The following are available online at https://www.mdpi.com/article/10.3390/horticulturae11080909/s1, Table S1: Primers for qRT-PCR.

Author Contributions: Z.H.: Formal analysis, Investigation, Resources, Writing—original draft. Q.C.: Investigation, Resources, Writing—original draft. Y.D.: Investigation, Resources, Writing—original draft. J.Z.: Resources, Supervision, Writing—review and editing. L.L.: Resources, Supervision. M.Z.: Conceptualization, Writing—review and editing. X.W.: Formal analysis, Conceptualization, Writing—review and editing. All authors have read and agreed to the published version of the manuscript.

Funding: Sichuan "Double High-Level" Crop Production and Management Professional Cluster Program (0200590060202).

Institutional Review Board Statement: Not applicable.

Informed Consent Statement: Not applicable.

Data Availability Statement: Data are contained within the article and Supplementary Materials.

Conflicts of Interest: The authors declare that they have no known competing financial interests or personal relationships that could have appeared to influence the work reported in this paper.

References

1. Hartikainen, H. Biogeochemistry of selenium and its impact on food chain quality and human health. *J. Trace Elem. Med. Biol.* **2005**, *18*, 309–318. [CrossRef]
2. Lv, Q.; Liang, X.; Nong, K.; Gong, Z.; Qin, T.; Qin, X.; Wang, D.; Zhu, Y. Advances in research on the toxicological effects of selenium. *Bull. Environ. Contam. Toxicol.* **2021**, *106*, 715–726. [CrossRef]
3. Rayman, M.P.; Infante, H.G.; Sargent, M. Food-chain selenium and human health: Spotlight on speciation. *Br. J. Nutr.* **2008**, *100*, 238–253. [CrossRef]
4. Yu, Y.; Liu, Z.; Luo, L.Y.; Fu, P.N.; Wang, Q.; Li, H.F. Selenium uptake and biotransformation in brassica rapa supplied with selenite and selenate: A hydroponic work with HPLC speciation and RNA-sequencing. *J. Agric. Food Chem.* **2019**, *67*, 12408–12418. [CrossRef]
5. Song, J.; Yu, S.; Yang, R.; Xiao, J.; Liu, J. Opportunities for the use of selenium nanoparticles in agriculture. *NanoImpact* **2023**, *31*, 100478. [CrossRef]
6. Fordyce, F.M. Selenium deficiency and toxicity in the environment. In *Essentials of Medical Geology*, 1st ed.; Selinus, O., Ed.; Springer: Dordrecht, The Netherlands, 2013; pp. 375–416.
7. Thiry, C.; Ruttens, A.; Temmerman, L.D.; Schneider, Y.J.; Pussemier, L. Current knowledge in species-related bioavailability of selenium in food. *Food Chem.* **2012**, *130*, 767–784. [CrossRef]

8. Winkel, L.H.; Johnson, C.A.; Lenz, M.; Grundl, T.; Leupin, O.X.; Amini, M.; Charlet, L. Environmental selenium research: From microscopic processes to global understanding. *Environ. Sci. Technol.* **2012**, *46*, 571–579. [CrossRef]
9. Liu, Y.; Ma, J.; Li, F.; Zeng, X.; Wu, Z.; Huang, Y.; Xue, Y.; Wang, Y. High concentrations of Se inhibited the growth of rice seedlings. *Plants* **2024**, *13*, 1580. [CrossRef]
10. Xue, T.; Hartikainen, H.; Piironen, V. Antioxidative and growth-promoting effect of selenium on senescing lettuce. *Plant Soil* **2001**, *237*, 55–61. [CrossRef]
11. Li, J.; Liang, D.; Qin, S.; Feng, P.; Wu, X. Effects of selenite and selenate application on growth and shoot selenium accumulation of pak choi (*Brassica chinensis* L.) during successive planting conditions. *Sci. Pollut. Res.* **2015**, *22*, 11076–11086. [CrossRef]
12. Reynolds, R.J.B.; Pilon-Smits, E.A.H. Plant selenium hyperaccumulation-Ecological effects and potential implications for selenium cycling and community structure. *Biochim. Biophys. Acta (BBA) Gen. Subj.* **2018**, *1862*, 2372–2382. [CrossRef]
13. Feng, R.; Wei, C.; Tu, S. The roles of selenium in protecting plants against abiotic stresses. *Environ. Exp. Bot.* **2013**, *87*, 58–68. [CrossRef]
14. Wani, A.S.; Ahmad, A.; Hayat, S.; Tahir, I. Epibrassinolide and proline alleviate the photosynthetic and yield inhibition under salt stress by acting on antioxidant system in mustard. *Plant Physiol. Biochem.* **2019**, *135*, 385–394. [CrossRef]
15. Ali, M.M.; Anwar, R.; Malik, A.U.; Khan, A.S.; Ahmad, S.; Hussain, Z.; Hasan, M.U.; Nasir, M.; Chen, F. Plant Growth and Fruit Quality Response of Strawberry is Improved After Exogenous Application of 24-Epibrassinolide. *J. Plant Growth Regul.* **2021**, *41*, 1786–1799. [CrossRef]
16. Krishna, P.; Prasad, B.D.; Rahman, T. Brassinosteroid action in plant abiotic stress tolerance. *Methods Mol. Biol.* **2017**, *1564*, 193–202. [CrossRef]
17. Sharma, P.; Kumar, A.; Bhardwaj, R. Plant steroidal hormone epibrassinolide regulate-heavy metal stress tolerance in *Oryza sativa* L. by modulating antioxidant defense expression. *Environ. Exp. Bot.* **2016**, *122*, 1–9. [CrossRef]
18. Ahammed, G.J.; Choudhary, S.P.; Chen, S.; Xia, X.J.; Shi, K.; Zhou, Y.; Yu, J. Role of brassinosteroids in alleviation of phenanthrene–cadmium co-contamination-induced photosynthetic inhibition and oxidative stress in tomato. *J. Exp. Bot.* **2013**, *64*, 199–213. [CrossRef]
19. Kumar, N.; Sharma, V.; Kaur, G.; Lata, C.; Dasila, H.; Perveen, K.; Khan, F.; Gupta, V.K.; Khanam, M.N. Brassinosteroids as promoters of seedling growth and antioxidant activity under heavy metal zinc stress in mung bean (*Vigna radiata* L.). *Front. Microbiol.* **2023**, *14*, 1259103. [CrossRef]
20. Dai, Z.; Zhang, D.; Li, Z.; Liu, X.; Liu, H.; Yan, K.; Liu, B.; Zhang, J.; Lin, L. Melatonin and 24-epibrassinolide promote the growth and selenium uptake of wild peach seedlings under selenium stress. *Environ. Prog. Sustain. Energy* **2025**, *44*, e14615. [CrossRef]
21. Lin, L.J.; Li, Z.Y.; Wang, J.; Liang, D.; Xia, H.; Lv, X.L.; Tang, Y.; Wang, X.; Deng, Q.X.; Liao, M. 24-epibrassinolide promotes selenium uptake in grapevine under selenium stress. *Sci. Hortic.* **2023**, *308*, 111564. [CrossRef]
22. Xu, Y.; Zhang, L.; Wang, J.; Liang, D.; Xia, H.; Lv, X.; Deng, Q.; Wang, X.; Luo, X.; Liao, M.; et al. Gibberellic acid promotes selenium accumulation in *Cyphomandra betacea* under selenium stress. *Front. Plant Sci.* **2022**, *13*, 968768. [CrossRef]
23. Wirtz, M.; Hell, R. Functional analysis of the cysteine synthase protein complex from plants: Structural, biochemical and regulatory properties. *J. Plant Physiol.* **2006**, *163*, 273–286. [CrossRef]
24. Wirtz, M.; Beard, K.F.M.; Lee, C.P.; Boltz, A.; Schwarzländer, M.; Fuchs, C.; Meyer, A.J.; Heeg, C.; Sweetlove, L.J.; Ratcliffe, R.G.; et al. Mitochondrial cysteine synthase complex regulates *O*-acetylserine biosynthesis in plants. *J. Biol. Chem.* **2012**, *287*, 27941–27947. [CrossRef]
25. Li, H.; Luo, N.; Zhang, L.J.; Zhao, H.M.; Li, Y.W.; Cai, Q.Y.; Wong, M.H.; Mo, C.H. Do arbuscular mycorrhizal fungi affect cadmium uptake kinetics, subcellular distribution and chemical forms in rice? *Sci. Total Environ.* **2016**, *571*, 1183–1190. [CrossRef]
26. Hall, J.L. Cellular mechanisms for heavy metal detoxification and tolerance. *J. Exp. Bot.* **2002**, *53*, 1–11. [CrossRef]
27. Wang, K.; Wang, Y.; Li, K.; Wan, Y.; Wang, Q.; Zhuang, Z.; Guo, Y.; Li, H. Uptake, translocation and biotransformation of selenium nanoparticles in rice seedlings (*Oryza sativa* L.). *J. Nanobiotechnol.* **2020**, *18*, 103. [CrossRef]
28. Tangjaidee, P.; Swedlund, P.; Xiang, J.; Yin, H.; Quek, S.Y. Selenium-enriched plant foods: Selenium accumulation, speciation, and health functionality. *Front. Nutr.* **2023**, *9*, 962312. [CrossRef]
29. Liu, H.; Shi, Z.; Li, J.; Zhao, P.; Qin, S.; Nie, Z. The impact of phosphorus supply on selenium uptake during hydroponics experiment of winter wheat (*Triticum aestivum*) in China. *Front. Plant Sci.* **2018**, *9*, 373. [CrossRef]
30. Pilon-Smits, E.A.H.; Quinn, C.F.; Hell, R.; Mendel, R.R. Selenium metabolism in plants. In *Cell Biology of Metals and Nutrients*, 1st ed.; Hell, R., Mendel, R.R., Eds.; Springer: Berlin/Heidelberg, Germany, 2010; pp. 225–241. [CrossRef]
31. Freeman, J.L.; Zhang, L.H.; Marcus, M.A.; Fakra, S.; McGrath, S.P.; Pilon-Smits, E.A. Spatial imaging, speciation, and quantification of selenium in the hyperaccumulator plants Astragalus bisulcatus and Stanleya pinnata. *Plant Physiol.* **2006**, *142*, 124–134. [CrossRef]
32. Both, E.B.; Shao, S.; Xiang, J.; Jókai, Z.; Yin, H.; Liu, Y.; Magyar, A.; Dernovics, M. Selenolanthionine is the major water-soluble selenium compound in the selenium tolerant plant Cardamine violifolia. *Biochim. Biophys. Acta (BBA) Gen. Subj.* **2018**, *1862*, 2354–2362. [CrossRef]

33. Freeman, J.L.; Tamaoki, M.; Stushnoff, C.; Quinn, C.F.; Cappa, J.J.; Devonshire, J.; Fakra, S.C.; Marcus, M.A.; McGrath, S.P.; Van Hoewyk, D.; et al. Molecular mechanisms of selenium tolerance and hyperaccumulation in *Stanleya pinnata*. *Plant Physiol.* **2010**, *153*, 1630–1652. [CrossRef] [PubMed]
34. Shibagaki, N.; Rose, A.; McDermott, J.P.; Fujiwara, T.; Hayashi, H.; Yoneyama, T.; Davies, J.P. Selenate-resistant mutants of Arabidopsis thaliana identify *Sultr1;2*, a sulfate transporter required for efficient transport of sulfate into roots. *Plant J.* **2002**, *29*, 475–486. [CrossRef] [PubMed]
35. Trippe, R.C.; Elizabeth, A.H.; Smits, P. Selenium transport and metabolism in plants: Phytoremediation and biofortification implications. *J. Hazard. Mater.* **2021**, *404*, 124178. [CrossRef] [PubMed]
36. Revilleza, M.J.; Galvez, A.F.; Krenz, D.C.; Lumen, B.O.D. An 8 kDa methionine-rich protein from soybean (*Glycine max*) cotyledon: Identification, purification, and n-terminal sequence. *J. Agric. Food Chem.* **1996**, *44*, 2930–2935. [CrossRef]
37. White, P.J.; Bowen, H.C.; Marshall, B.; Broadley, M.R. Extraordinarily high leaf selenium to sulfur ratios define 'Se-accumulator' plants. *Ann. Bot.-Lond.* **2007**, *100*, 111–118. [CrossRef]
38. Finley, J.W.; Sigrid-Keck, A.; Robbins, R.J.; Hintze, K.J. Selenium enrichment of broccoli: Interactions between selenium and secondary plant compounds. *J. Nutr.* **2005**, *135*, 1236–1238. [CrossRef]
39. Kaur, M.; Sharma, S. Selenium affects protein accumulation and its distribution in different protein fractions in developing wheat grains. *Cereal Res. Commun.* **2021**, *49*, 109–117. [CrossRef]
40. Dumont, E.; Vanhaecke, F.; Cornelis, R. Selenium speciation from food source to metabolites: A critical review. *Anal. Bioanal. Chem.* **2006**, *385*, 1304–1323. [CrossRef]

horticulturae

MDPI

Article

The Transcriptome and Metabolome Reveal the Mechanism by Which Melatonin Enhances Drought Tolerance in *Platycrater argutae*

Xule Zhang [1,†], Yaping Hu [1,†], Zhengjian Jiang [2], Xiaohua Ma [1], Qingdi Hu [1], Lei Feng [1] and Jian Zheng [1,*]

[1] Key Laboratory of Plant Innovation and Utilization, Institute of Subtropical Crops of Zhejiang Province, Wenzhou 325005, China; zhangxl@zaas.ac.cn (X.Z.); huyp@zaas.ac.cn (Y.H.); maxiaohua1120@126.com (X.M.); qingdihu@163.com (Q.H.); fengl@zaas.ac.cn (L.F.)

[2] Zhejiang Juyoupin Biotechnology Co., Ltd., Wenzhou 325615, China; zhengjianjiang@163.com

* Correspondence: zjyzs@126.com

† These authors contributed equally to this work.

Abstract

Drought stress severely impacts the survival of *Platycrater arguta*, an endangered tertiary relict plant. This study investigated the mechanism by which exogenous melatonin enhances drought tolerance in *P. arguta* seedlings through integrated physiological, transcriptomic, and metabolomic analyses. Under 30% PEG-6000-induced drought, seedlings exhibited leaf wilting, reduced relative water content (RWC: 78.6% vs. 84.8% in controls), and elevated oxidative damage (malondialdehyde increased by 62.94%, H_2O_2 by 83.78%). Exogenous melatonin application, particularly at 100 μM (T3), significantly alleviated drought symptoms, restoring RWC to 83.7%, reducing membrane permeability (relative electrical conductivity 1.38-fold vs. CK vs. 2.55-fold in PEG), and lowering oxidative markers (MDA and H_2O_2 accumulation by 28.33% and 27.84%, respectively). T3 treatment also enhanced osmolyte synthesis, increasing proline content by 90.14% and soluble sugars by 47.25% compared to the controls. Transcriptome sequencing revealed 31,870 differentially expressed genes in T3, predominantly enriched in carbohydrate metabolism, oxidative phosphorylation, and tryptophan metabolism pathways. Metabolomic profiling demonstrated that 100 μM melatonin elevated endogenous melatonin levels 19.62-fold and modulated tryptophan-derived metabolites, including indole derivatives and benzoic acid compounds. These findings indicate that melatonin mitigates drought stress by enhancing antioxidant capacity, osmotic adjustment, and metabolic reprogramming, with 100 μM as the optimal concentration. This study provides critical insights into melatonin-mediated drought resistance mechanisms, offering a theoretical foundation for conserving and restoring *P. arguta* populations in arid habitats.

Keywords: *Platycrater argutae*; drought relief; melatonin; tryptophan

1. Introduction

As a critically endangered tertiary relic, the deciduous shrub *Platycrater arguta* (Hydrangeaceae) faces survival challenges due to combined pressures from biotic and abiotic stress factors. This species is the sole extant member of its genus [1,2], representing a unique lineage with significant evolutionary and conservation value. Studying such relic species offers insights into historical biogeography, adaptation mechanisms, and the impacts of contemporary climate change on vulnerable biodiversity. Among these, drought stress

stands as one of the most prevalent abiotic stressors in natural ecosystems and serves as a critical environmental factor influencing plant growth and development [3–5]. For *P. arguta*, whose current fragmented distribution is closely linked to specific microclimates, particularly water availability, understanding drought tolerance mechanisms is paramount for its survival and effective conservation.

Drought stress directly impacts plant physiological processes by disrupting photosynthetic characteristics, reactive oxygen species (ROS) metabolism, and osmotic regulation [4,6,7]. These disruptions lead to cellular dehydration, plasmolysis, and damage to cell membranes and enzyme systems, ultimately resulting in metabolic imbalance, growth inhibition, and reduced productivity. Studies have demonstrated that water availability is a pivotal determinant of *P. arguta*'s geographical distribution [1]. Plants deploy complex physiological and molecular responses to counter drought, including osmotic adjustment, enhanced antioxidant defense, and stress signaling pathways.

Melatonin (MT), an indoleamine compound ubiquitously present in animals and plants, functions both as an endogenous phytohormone synthesized by plants and as an exogenous regulator absorbed and accumulated from the environment [8–10]. Melatonin, a highly effective scavenger of free radicals and secondary antioxidant, is essential for mediating stress responses in plants [11,12]. It modulates multiple metabolic pathways to alleviate damage caused by diverse abiotic stresses, including heavy metal toxicity, drought, and extreme temperatures [13–15].

Focusing on the threatened relict species *P. arguta*, this study specifically investigates the efficacy of exogenous melatonin in mitigating drought stress in this vulnerable plant. Given its unique phylogenetic position and high conservation urgency, understanding its stress response mechanisms is ecologically significant. The findings could inform conservation strategies not only for *P. arguta* but potentially for other endangered species facing similar climatic pressures. This study elucidates the protective mechanisms of melatonin supplementation (100~200 μM) against water deficit-induced alterations in biomass allocation, photosynthetic efficiency, and redox homeostasis in *P. arguta* juveniles. The findings will provide critical insights into whether exogenous melatonin mitigates drought-induced stress damage in *P. arguta*, while establishing a theoretical foundation for enhancing the conservation and field population expansion of this endangered species.

2. Materials and Methods

2.1. Experimental Materials and Treatments

Two-year-old *P. arguta* seedlings with uniform growth and no signs of pests or diseases were selected for this study. The experiment was conducted in a controlled environment at the Wenzhou Jingshan Plant Resource Nursery, with temperatures maintained between 16 °C and 29 °C. Drought stress was induced by irrigating each pot daily with 100 mL of 30% polyethylene glycol 6000 (PEG-6000, Sinopharm Chemical Reagent Co., Ltd., Shanghai, China) solution. To prevent leakage, the pots were placed in blue plastic trays. Prior to the experiment, the seedlings were thoroughly watered for three days and subjected to no further irrigation during the trial. Six treatments were established, each with five pots and three biological replicates:

(1) CK: normal watering;
(2) T1: drought stress (PEG);
(3) T2: drought stress + 50 μM melatonin (PEG + MT50)
(4) T3: drought stress + 100 μM melatonin (PEG + MT100)
(5) T4: drought stress + 200 μM melatonin (PEG + MT200)

Melatonin solutions (Merck KGaA, Darmstadt, Germany) were uniformly sprayed onto both leaf surfaces using a fine mist sprayer at 17:00–18:00 for five consecutive days before drought induction. The control groups received equivalent volumes of distilled water.

On the 10th day of treatment, fully expanded functional leaves (3rd–4th from the apex of current-year branches) were collected at 7:30 AM, sealed with parafilm, and immediately transported to the laboratory. Fresh leaves were used to measure cell membrane permeability, chlorophyll content, relative water content, and leaf mass per area. The remaining samples were stored at −80 °C for metabolomic, transcriptomic.

2.2. Determination of Physiological Indicators

The measurements of MDA, H_2O_2, SS, and Pro all require the use of crude enzyme extract. The preparation method for crude enzyme extract is as follows: The veins of *P. arguta* leaves were removed, and the leaves were cut into small pieces. One gram of the leaf pieces was placed in a pre-cooled mortar and ground into a homogenate under liquid nitrogen. The homogenate was then poured into a test tube, and nine milliliters of phosphate buffer solution with a concentration of 0.1 mol·L^{-1} and a pH of 7 was added. The centrifuge was set to a temperature of 4 °C and a speed of 10,000 r/min, and the mixture was centrifuged for 10 min. After the mixture was stratified, the supernatant, which served as the crude enzyme extract, was collected and stored in a refrigerator at 4 °C for future use.

The MDA content was measured using the thiobarbituric acid (TBA) colorimetric method [16]. The SS content was determined using the anthrone colorimetric method [17]. The Pro content was assayed using the acidic ninhydrin colorimetric method [18].

2.3. Transcriptomic Sequencing and Analysis

Total RNA was extracted from frozen leaf tissues using MJzol Reagent (Magen, Shanghai, China) and purified using magnetic bead-based methods. RNA quality was assessed using a Nanodrop2000 (NanoDrop Technologies LLC, Waltham, MA, USA), agarose gel electrophoresis, and an Agilent 2100 Bioanalyzer (RIN $\geq$ 7.0) (Agilent, Santa Clara, CA, USA). Following poly(A) mRNA selection using oligodeoxythymidine-coated magnetic beads, RNA fragments of ~300 nucleotides were generated through chemical fragmentation for subsequent cDNA synthesis. Library preparation was performed with the NEBNext Ultra II RNA Library Prep Kit (New England Biolabs (Beijing) Ltd., Beijing, China), followed by paired-end sequencing (2 × 150 bp) on an Illumina NovaSeq 6000 sequencing system (BGI, Shenzhen, China).

Raw sequencing data underwent quality control filtering prior to genome alignment via HISAT2 (v2.2.1) against the GRCh38 reference assembly. Differentially expressed genes (DEGs) were identified using DESeq2 (v1.30.1) based on read counts mapped to genes. Genes were defined as DEGs using the default significance thresholds: a false discovery rate (FDR) < 0.05 and an absolute $\log_2$ fold change > 1.0 (equivalent to a fold change > 2.0 or < 0.5).

GO term enrichment analysis for gene sets was performed using Goatools (v1.2.3). Fisher's exact test was employed, and GO terms with an adjusted *p*-value < 0.05 were considered significantly enriched. KEGG pathway enrichment analysis was conducted using KOBAS (v3.0) with similar statistical principles to the GO analysis. Fisher's exact test was applied, followed by multiple testing corrections using the Benjamini–Hochberg (BH) procedure (FDR) to control the false positive rate. KEGG pathways with a corrected *p*-value (FDR) < 0.05 were defined as significantly enriched within the DEGs.

2.4. Metabolomic Profiling

Cryopreserved *P. arguta* leaf samples were pulverized into fine powder using a grinding mill (30 Hz, 1 min). Aliquots (50 mg) of homogenized tissue were mixed with 10 μL of internal standard mixture solution (100 ng/mL) and 1 mL of extraction solvent (methanol/water/formic acid, 15:4:1, $v/v/v$). After vortexing for 10 min, the mixtures were centrifuged at 12,000 rpm for 5 min (4 °C). The supernatants were transferred to new tubes, concentrated under reduced pressure, and reconstituted in 100 μL of 80% methanol/water. Finally, the samples were filtered through 0.22 μm membranes into HPLC vials for LC-MS/MS analysis.

Chromatographic separation was performed on a Waters ACQUITY UPLC HSS T3 (Jitai Biotechnology Co., Ltd., Shanghai, China) C18 column (1.8 μm, 100 × 2.1 mm i.d.) maintained at 40 °C. The mobile phase consisted of (A) ultrapure water with 0.04% acetic acid and (B) acetonitrile with 0.04% acetic acid. A gradient elution program was applied at 0.35 mL/min as follows: 0–1.0 min, 95% A; 1.0–8.0 min, 95%→5% A; 8.0–9.0 min, 5% A; 9.0–9.1 min, 5%→95% A; 9.1–12.0 min, 95% A. The injection volume was 2 μL.

Analysis was conducted on a Q-Trap 6500+ system equipped with an electrospray ionization (ESI) source. Key parameters included the following: ESI temperature 550 °C; ion spray voltage 5500 V (positive mode) or −4500 V (negative mode); curtain gas (CUR) 35 psi. Compound-specific detection was achieved through multiple reaction monitoring (MRM) using optimized declustering potentials (DP) and collision energies (CE) for each ion transition.

Qualitative identification was performed against the MetWare Database (MWDB) established using authentic standards. Quantitative analysis was conducted in MRM mode with triple quadrupole detection. Chromatographic peaks of all target compounds were integrated, and concentrations were determined using standard calibration curves.

2.5. Data Analysis and Statistical Methods

Data were processed using Microsoft Excel 2010. One-way analysis of variance (ANOVA) was conducted to assess the significance of differences across various indices. Figures were generated using Origin 2020. A comprehensive approach involving Duncan's method, Tukey's HSD test, and the aov function from the R package agricolae (v1.3-7) was employed for multiple comparisons and ANOVA.

3. Results

3.1. Effects of Exogenous Melatonin on the Phenotype of P. arguta

Under normal watering conditions (CK), plants exhibited healthy growth with normal leaf color and no signs of wilting. In contrast, all seedlings subjected to 30% PEG-6000 treatment displayed varying degrees of leaf wilting. Exogenous melatonin application at different concentrations differentially alleviated drought-induced wilting, resulting in distinct phenotypic responses. Among the treatments, 100 nM melatonin (PEG+MT100) showed the most significant mitigation effect, followed by 200 nM (PEG+MT200), while 50 nM (PEG+MT50) provided minimal relief. Specifically, leaves treated with 100 nM melatonin displayed slight wilting and curling at the margins, with limited affected areas. At 200 nM, the leaves exhibited curling but no wilting or drooping. In contrast, seedlings treated with 50 nM melatonin experienced severe leaf wilting, desiccation, and even abscission, accompanied by pronounced water loss (Figure 1).

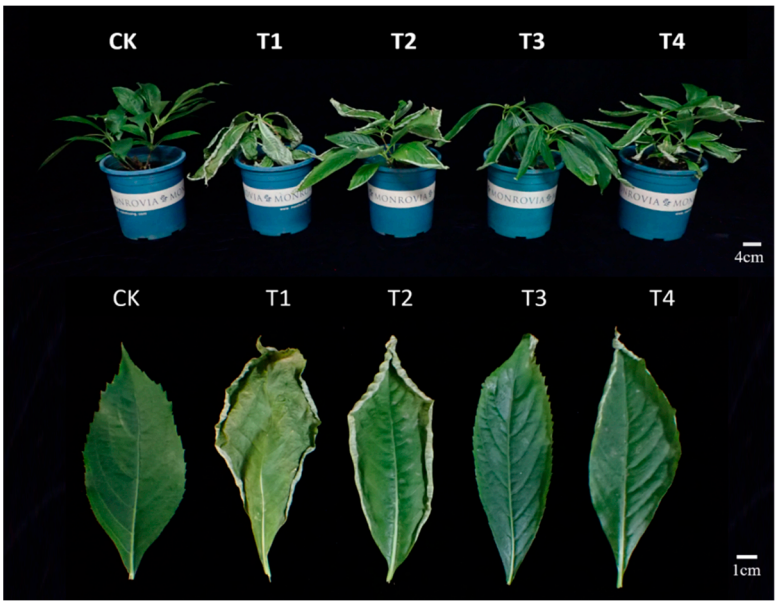

Figure 1. The hydrotoponic response of *P. arguta* to PEG-6000-induced osmotic perturbation was characterized through comprehensive morphometric analysis under whole-basin growth conditions.

After 10-day drought exposure, leaf RWC—a key parameter reflecting cellular hydration status—showed a progressive decline across experimental groups. The most severe dehydration occurred in PEG-treated specimens (78.6% RWC), representing a 7.3% reduction compared to well-watered controls (CK: 84.8%). Exogenous melatonin application significantly attenuated this dehydration effect, with 100 μM demonstrating superior efficacy (83.7% RWC) over both lower (50 μM: 81.4%) and higher (200 μM: 80.4%) concentrations in maintaining membrane-bound water (Figure 2a). Relative electrical conductivity (REC), reflecting cell membrane damage, increased substantially in drought-stressed plants. The untreated PEG group reached 76.6% REC, 2.55-fold higher than the CK group. In contrast, REC values for 50, 100, and 200 μM melatonin treatments were 2.10-, 1.38-, and 2.07-fold higher than CK, respectively. These results demonstrate that exogenous melatonin application significantly reduced membrane damage, with 100 μM showing the most pronounced protective effect (Figure 2b).

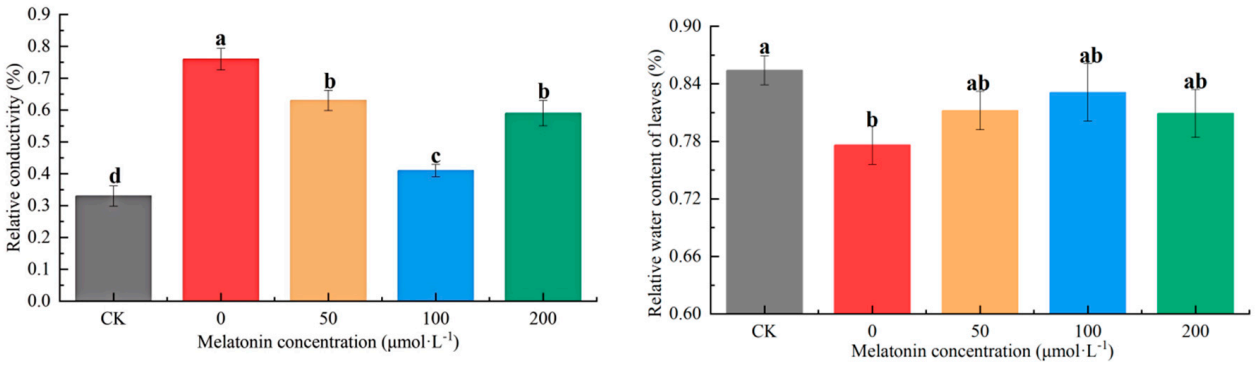

(**a**) (**b**)

Figure 2. Dose-dependent effects of exogenous melatonin on leaf physiological parameters: (**a**) relative electrolyte leakage (REC) and (**b**) relative water content (RWC) across MT concentration gradients. Alphabetic superscripts (a–d) denote statistically distinct clusters identified through Tukey's HSD test ($\alpha = 0.05$), where non-overlapping letters reflect membrane integrity–water retention coordination under osmotic stress.

3.2. Effects of Exogenous Melatonin on Peroxide Accumulation in P. arguta

As the final byproduct generated through polyunsaturated fatty acid peroxidation in cellular membranes, malondialdehyde (MDA) concentration directly reflects the degree of oxidative damage in biological systems. In this experiment, the CK group exhibited a significantly lower MDA content compared to all other treatments. The untreated drought-stressed group (0 μM melatonin) showed a 62.94% increase in MDA relative to CK, while 50, 100, and 200 μM melatonin treatments resulted in 33.78%, 28.33%, and 28.47% increases, respectively. Notably, MDA levels in melatonin-treated groups showed no significant differences among concentrations, with values intermediate between CK and untreated drought-stressed plants (Figure 3a).

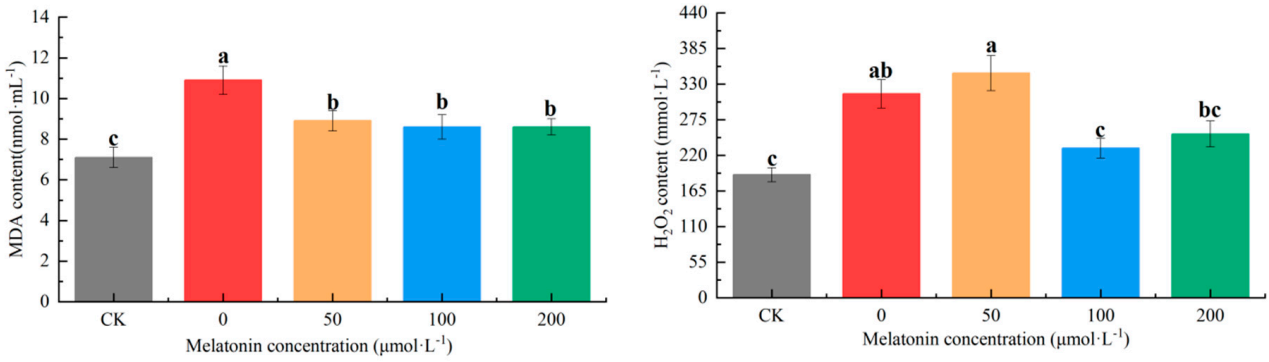

(**a**) (**b**)

Figure 3. (**a**) MDA content (reflecting membrane oxidative damage); (**b**) H_2O_2 accumulation across all experimental groups. Alphabetic superscripts (a–c) denote statistically distinct clusters identified through Tukey's HSD test ($\alpha = 0.05$), where non-overlapping letters reflect membrane integrity–water retention coordination under osmotic stress.

Hydrogen peroxide (H_2O_2) content, which rises under drought stress and induces cytotoxicity at elevated levels, was significantly lower in the CK- and 100 μM melatonin-treated groups compared to other treatments. The 200 μM melatonin group showed moderate H_2O_2 accumulation, while the untreated (0 μM) and 50 μM melatonin groups exhibited the highest levels, exceeding CK by 83.78% and 97.21%, respectively. The 50 μM melatonin treatment group exhibited a 2-fold increase in hydrogen peroxide accumulation compared to the control (CK), demonstrating significant drought-induced oxidative injury at the cellular level. In contrast, the 100 and 200 μM melatonin treatments limited H_2O_2 increases to 27.84% and 41.35% above CK, respectively, demonstrating a concentration-dependent mitigation effect (Figure 3b).

3.3. Effects of Exogenous Melatonin on Osmolyte Accumulation in P. arguta

Soluble sugars and proline, key osmoregulatory substances, are critical for maintaining cellular osmotic balance under drought stress. In this study, the observed differential in soluble carbohydrates—with consistently elevated levels across drought treatments relative to CK—reflects active osmotic adjustment as a key physiological adaptation strategy. The untreated drought-stressed group (0 μM melatonin) exhibited a 77.12% increase in soluble sugar content compared to CK, while 50, 100, and 200 μM melatonin treatments resulted in increases of 40.92%, 47.25%, and 60.18%, respectively. Notably, the 50 μM melatonin group showed the lowest soluble sugar accumulation among melatonin-treated plants, with values closer to CK (Figure 4a). Proline content varied markedly across treatments, peaking in the 100 μM melatonin group. The untreated drought-stressed group (0 μM) and 200 μM melatonin group displayed moderate proline levels, whereas the CK and 50 μM

melatonin treatments showed the lowest accumulation. Specifically, proline content in the 0, 50, 100, and 200 μM melatonin groups exceeded CK by 30.38%, 9.86%, 90.14%, and 29.61%, respectively. This highlights the superior efficacy of 100 μM melatonin in enhancing proline synthesis to counteract osmotic stress (Figure 4b).

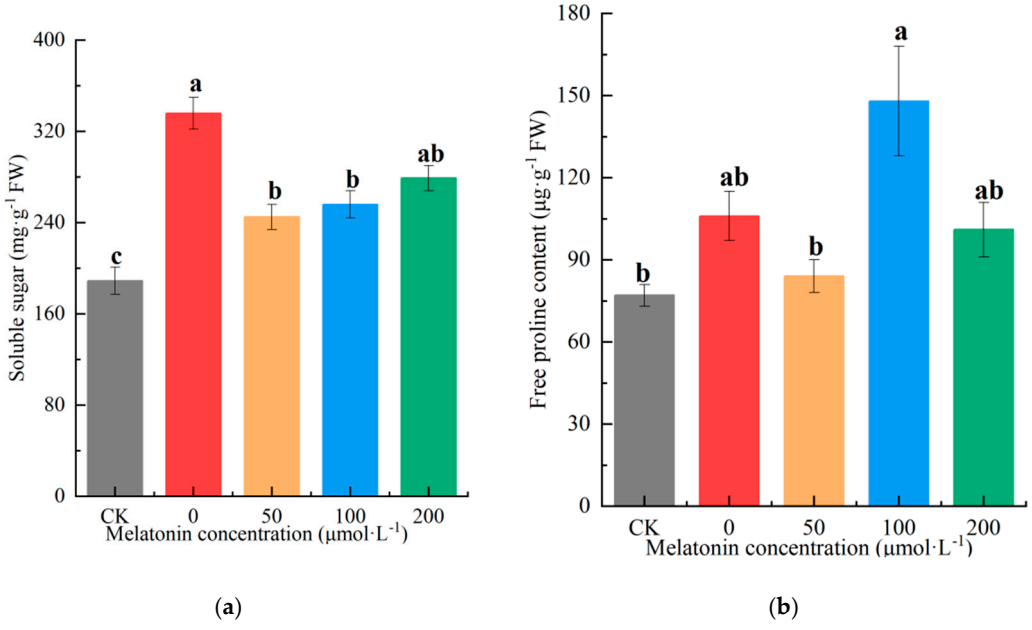

(**a**) (**b**)

Figure 4. (**a**) Soluble sugar content; (**b**) free proline content. Alphabetic superscripts (a–c) denote statistically distinct clusters identified through Tukey's HSD test (α = 0.05), where non-overlapping letters reflect membrane integrity–water retention coordination under osmotic stress.

3.4. Transcriptome Sequencing Alignment, Annotation, and Differential Gene Analysis

The de novo transcriptome reconstruction using the Trinity assembler yielded 316,538 RNA isoforms (301.34 Mbp total length), exhibiting broad size distribution from 952 bp average to 17.2 kb maximum contigs. These spliced variants underwent systematic functional characterization through six-tiered bioinformatic pipelines (Non-Redundant Protein, Swiss-Prot/UniProtKB, Pfam domain architecture, Clusters of Orthologous Groups, GO, and KEGG), with cross-database annotation landscapes quantitatively profiled in Figure 5.

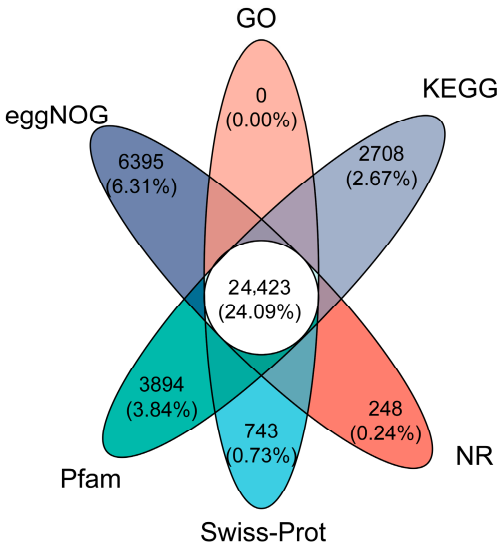

Figure 5. Gene annotation of each database.

Differential expression analysis identified distinct gene sets across comparisons. Specifically, 720 (2.49%), 206 (0.71%), 9728 (33.58%), and 149 (0.51%) genes were uniquely expressed in T1 vs. CK, T2 vs. CK, T3 vs. CK, and T4 vs. CK, respectively. Comparisons between melatonin-treated and drought-stressed groups revealed 30 (0.10%), 46 (0.16%), and 517 (1.78%) unique genes in T2 vs. PEG, T3 vs. PEG, and T4 vs. PEG, respectively. Cross-treatment comparisons yielded 114 (0.39%), 80 (0.28%), and 1,019 (3.52%) unique genes in T2 vs. T3, T2 vs. T4, and T3 vs. T4, respectively.

When T3 was compared to CK, a total of 31,870 differentially expressed genes (DEGs) were detected, with 22,324 being upregulated and 9546 downregulated. In the T3 versus T1 comparison, 27,068 DEGs were identified, consisting of 229 upregulated and 26,839 downregulated genes. Similarly, the contrast between T3 and T2 yielded 11,832 DEGs, including 4462 upregulated and 7370 downregulated transcripts. Finally, the T3 vs. T4 comparison displayed 22,598 DEGs, of which 5618 were upregulated and 16,980 downregulated. These results underscore the pronounced transcriptional reprogramming induced by 100 μM melatonin, aligning with its superior efficacy in enhancing drought tolerance.

3.5. Functional Enrichment Analysis of Differentially Expressed Genes

In the T3 vs. CK comparison, GO enrichment analysis revealed distinct functional categories. For biological processes (BP), DEGs were predominantly enriched in macromolecule modification (836 genes), phosphorus metabolic processes (761), cellular protein modification (757), protein modification (757), and phosphorus compound metabolism (728). Cellular component (CC) terms included cell part (7334 genes), cellular anatomical entity (6880), membrane-bounded organelle (2810), intracellular membrane-bounded organelle (2798), intrinsic membrane component (2552), membrane part (2534), and membrane (1496). Molecular functions (MF) were enriched in catalytic activity (1340 genes), kinase activity (701), phosphotransferase activity (630), and DNA binding (621).

KEGG pathway analysis highlighted distinct metabolic reprogramming across comparisons. Pathway enrichment analysis revealed distinct metabolic and regulatory patterns across the comparisons (Figure 6). In T3, relative to CK, the predominant pathways were associated with "Biosynthesis of cofactors," "Oxidative phosphorylation," and "Glycolysis/Gluconeogenesis." When contrasting T3 with T1, the most significantly enriched pathways included "Starch and sucrose metabolism," "Peroxisome," and "Pentose and glucuronate interconversions." For T3 versus T2, DEGs were primarily linked to "Plant hormone signal transduction," "Protein processing in endoplasmic reticulum," and "Plant-pathogen interaction." Meanwhile, the comparison between T3 and T4 highlighted pathways such as "Ribosome," "Oxidative phosphorylation," and "Carbon fixation in photosynthetic organisms."

Integrated analysis demonstrated that T3-specific DEGs were primarily associated with carbohydrate metabolism (e.g., glycolysis, starch/sucrose metabolism, pentose/glucuronate interconversions) and oxidative phosphorylation. Cross-group comparisons further revealed enrichment in pathways such as "Plant hormone signal transduction," antioxidant metabolism ("Oxidative phosphorylation," "Peroxisome"), and carbon metabolism ("Carbon fixation"). These findings align with melatonin's role in enhancing drought resilience through the coordinated regulation of energy metabolism, stress signaling, and redox homeostasis.

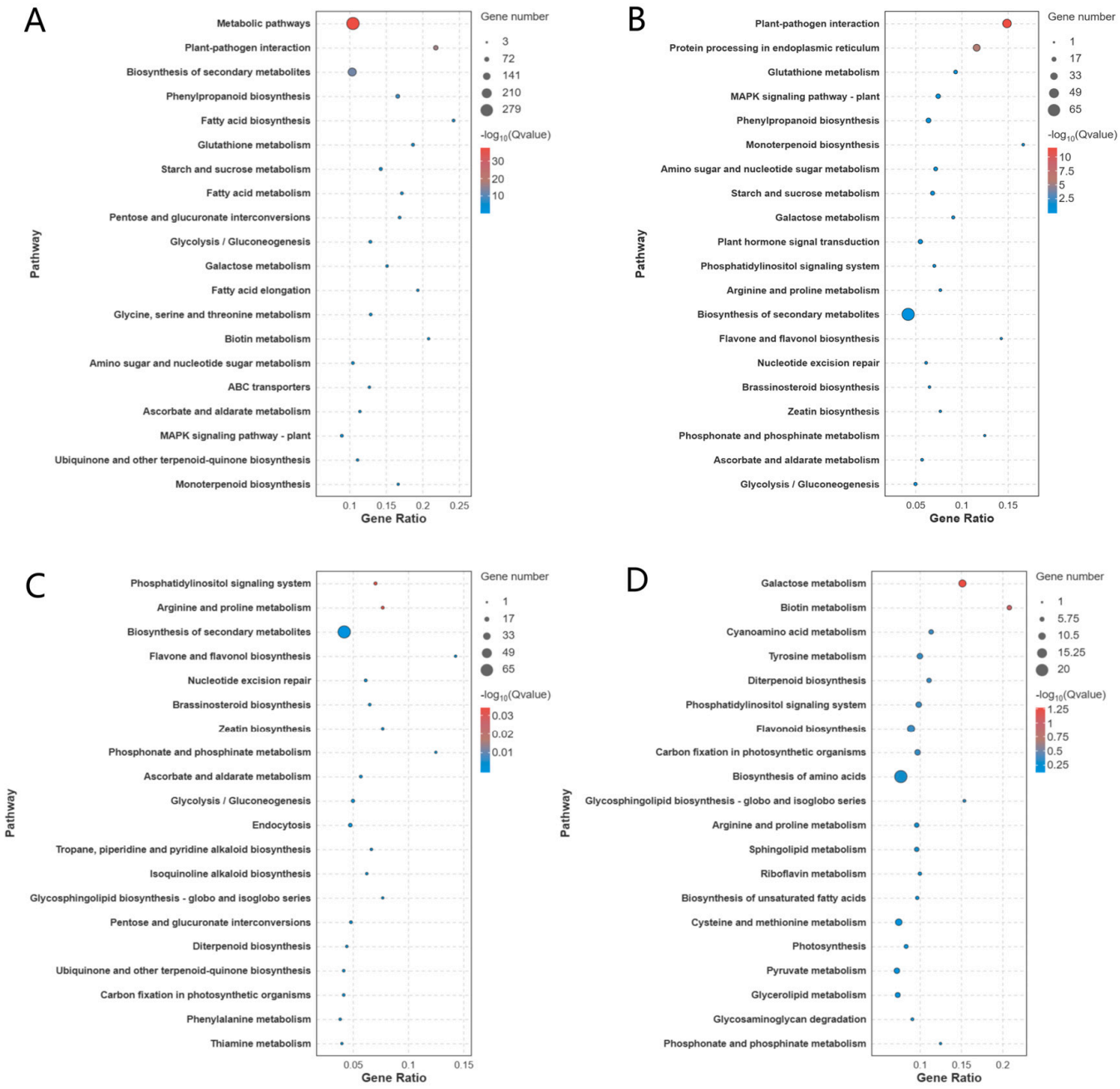

Figure 6. Enrichment analysis of KEGG differential genes in different treatment groups of *P. arguta*. (**A**) CK VS PEG; (**B**) CK VS PEG + MT50; (**C**) CK VS PEG+MT100; (**D**) CK VS PEG+MT200.

3.6. Tryptophan Metabolite Analysis

In this experiment, 31 tryptophan metabolic pathway-related metabolites were quantitatively analyzed. A total of 16 metabolites across 7 classes were detected with differential expression between treatments: aniline compounds (1 species: 2-aminophenol, 2-AF), benzoic acid derivatives (1 species: 2-aminobenzoic acid, 2-AA), indole derivatives (8 species: 6-hydroxymelatonin, 6-HMLT; tryptamine, TRM; N-acetylserotonin, NAS; melatonin, MLT; L-tryptophan, L-TRP; DL-indole-3-lactic acid, ILA; 5-hydroxytryptophol, 5_HTOL), medium-chain keto acids (1 species: 2-ketoadipic acid, 2-KA), carbonyl compounds (1 species: L-kynurenine, L-KYN), pyridine derivatives (2 species: picolinic acid, PA; nicotinic acid, N-Acid), and quinoline carboxylic acids (2 species: xanthurenic acid, XA; quinolinic acid, QA).

Among the indole derivatives, two melatonin-related compounds, MLT and 6-HMLT, exhibited a relatively high abundance. The MLT contents in the CK~T4 treatment groups were 1.3518 ng/g, 2.0171 ng/g, 11.0537 ng/g, 29.5711 ng/g, and 67.6499 ng/g, respectively. Significant differences were observed between the CK/T1 groups and the T2/T3/T4 groups. The CK group had the lowest MLT content, accounting for only 2.00%, 2.98%, 16.34%, and 43.71% of the other treatment groups. The treatment groups sprayed with exogenous melatonin showed significantly higher MLT content than the CK and PEG groups, with levels 5.84-, 9.76-, and 19.62-fold higher than those of the CK group. These results indicate that higher exogenous melatonin concentrations lead to greater endogenous melatonin accumulation. Additionally, the indole derivative IGA displayed substantial variation among treatments, with contents of 20.8052 ng/g, 51.7191 ng/g, 18.0867 ng/g, 24.2732 ng/g, and 19.1119 ng/g across the groups. The T2 group had the lowest IGA content, while the other groups showed 1.15-, 2.86-, 1.34-, and 1.06-fold higher levels compared to T2.

Among the benzoic acid derivatives, 2-AA exhibited significant variations across the treatment groups. The 2-AA content was notably lower in melatonin-sprayed groups (14.37 ng/g, 12.30 ng/g, and 20.98 ng/g), with the lowest observed in the T3 group, representing only 17.64%, 15.97%, 85.60%, and 58.64% of the levels in the other treatment groups. In contrast, the PEG-stressed group showed the highest 2-AA accumulation.

Overall, exogenous melatonin application modulated the content of tryptophan-related compounds in *P. arguta* leaf tissues, with melatonin-treated groups displaying intermediate levels between the CK control and PEG-stressed groups. Notably, the T2 and T3 treatments outperformed T4 in balancing tryptophan metabolism under drought stress.

3.7. KEGG Enrichment Analysis of Tryptophan-Related Differential Metabolites

Experimental evaluation of exogenous melatonin dosage variations on drought-stressed *P. arguta* demonstrated that the 100 μM/L concentration (T3) optimally enhanced both phenotypic resilience and physiological homeostasis among all treatments. Combined with the analysis of tryptophan-related compound contents, this further confirmed that 100 μM/L melatonin is the optimal concentration for enhancing drought resistance in *P. arguta*. Therefore, the KEGG functional annotation and enrichment analysis of tryptophan-related differential metabolites focused on comparing the enrichment differences between the T3 and other treatment groups.

In the comparison between T3 and CK, the pathways with the most enriched differentially expressed genes were 'biosynthesis of secondary metabolites' and 'tryptophan metabolism'. Between T3 and T1, the most enriched pathways were 'tryptophan metabolism', 'nicotinate and nicotinamide metabolism', and 'metabolic pathways'. For T3 versus T2, the predominant enriched pathways were 'metabolic pathways' and 'tryptophan metabolism'. Similarly, in T3 versus T4, the top enriched pathways were 'metabolic pathways' and 'tryptophan metabolism'.

Collectively, the differentially expressed genes between the T3 and other treatment groups were primarily enriched in 'metabolic pathways' and 'tryptophan metabolism'. Pairwise comparisons among other treatment groups revealed additional enriched pathways, including 'nicotinate and nicotinamide metabolism', 'biosynthesis of secondary metabolites', and 'biosynthesis of amino acids'. These results underscore the central role of tryptophan metabolism and broader metabolic reprogramming in the drought resistance mechanisms regulated by melatonin in *P. arguta*.

4. Discussion

Melatonin is synthesized and transported in plants, with a mechanism similar to that in animals, both using tryptophan as the precursor. The biosynthesis of melatonin in plants follows a four-step enzymatic cascade starting from tryptophan, with the involvement of six key enzymes: tryptophan decarboxylase initiates the pathway, followed by tryptophan hydroxylase, and tryptophan 5-hydroxylase for hydroxylation. Subsequently, serotonin N-acetyltransferase catalyzes acetylation, while N-acetylserotonin methyltransferase and caffeic acid O-methyltransferase mediate the final methylation steps to yield melatonin. Therefore, studying the tryptophan metabolic pathway is crucial for understanding the role of melatonin in drought resistance mechanisms of *P. arguta.*

P. arguta exhibited distinct morphological, peroxidative, and osmoregulatory responses under drought stress with exogenous melatonin treatments. Observations in *Rosa sertata* × *R. rugosa* showed that PEG-induced drought stress significantly inhibited plant growth, causing leaf curling and wilting, and a decrease in relative water content [19]. Exogenous melatonin application alleviated these symptoms, improving RWC in a dose-dependent manner. Similar studies on *Zanthoxylum bungeanum* demonstrated that melatonin (200 μM) effectively restored leaf turgor and chlorophyll content under drought, highlighting its species-specific optimal concentration for stress mitigation [20].

Drought-induced cellular damage, marked by elevated malondialdehyde (MDA), hydrogen peroxide (H_2O_2), and relative electrical conductivity (REC), was mitigated by melatonin in *P. arguta*. This aligns with findings in *Z. bungeanum*, where melatonin reduced MDA and H_2O_2 levels by 33% and 30%, respectively, under drought [21]. The reduction in membrane permeability and oxidative markers underscores melatonin's role in scavenging reactive oxygen species (ROS) and stabilizing membrane integrity, a conserved mechanism across plant species [22–24].

Carbohydrate metabolism, which is critical for osmotic adjustment and energy homeostasis, was significantly enriched in drought-stressed *P. arguta*, as revealed by transcriptomic analysis. Similar patterns were reported in *Agropyron mongolicum*, where drought-responsive genes were enriched in starch/sucrose metabolism pathways [25,26]. These findings suggest a universal adaptive strategy where plants prioritize carbon allocation to sustain cellular functions under water deficit [27]. Furthermore, melatonin's interaction with phytohormones, such as auxin and abscisic acid (ABA), may coordinate stress signaling. For instance, in *Arabidopsis*, tryptophan metabolism modulates auxin-ABA crosstalk, balancing growth and stress responses [28]. Drought-induced H_2O_2 accumulation suppresses tryptophan synthase activity, reducing auxin synthesis while promoting ABA accumulation—a dynamic interplay potentially regulated by melatonin [29–31].

Transcriptomic enrichment in metabolic pathways, particularly tryptophan metabolism, in the T3 group (100 μM melatonin) highlights melatonin's dual role as a metabolic regulator and antioxidant. Studies on *Arabidopsis* TSB1 (tryptophan synthase β-subunit 1) revealed its involvement in abiotic stress adaptation by fine-tuning auxin and ABA homeostasis [32]. In *P. arguta*, melatonin likely mitigates drought-induced oxidative stress by modulating tryptophan-derived metabolites, thereby influencing H_2O_2 levels and hormone signaling. This mechanistic overlap suggests that melatonin enhances drought resilience through conserved pathways involving redox balance and hormone coordination [33].

Growing evidence emphasizes phytohormones as pivotal mediators of drought adaptation. Melatonin, acting synergistically or antagonistically with hormones like ABA, ethylene, and jasmonic acid, orchestrates complex signaling networks to optimize stress responses. Our findings corroborate this paradigm, positioning melatonin as a master regulator bridging metabolic reprogramming and hormonal crosstalk under drought.

This study highlights the potential application of exogenous melatonin in enhancing drought tolerance in *P. arguta.* Melatonin is commercially available through chemical synthesis or microbial fermentation, with relatively high costs for plant applications. However, considering its significant benefits in improving drought resistance, the cost is acceptable, especially for endangered species or regions prone to drought. Additionally, foliar spraying of melatonin has shown promising results, but its effectiveness may vary under different environmental conditions. Future studies should focus on optimizing spray frequency, concentration, and timing to maximize its benefits in diverse conditions, particularly in arid areas. Thus, melatonin holds great potential for agricultural and ecological applications, especially for plants in drought-prone regions.

5. Conclusions

This study demonstrated the pivotal role of exogenous melatonin in enhancing drought stress tolerance in *P. arguta* through physiological and transcriptomic analyses. Under drought stress, *P. arguta* plants exhibited growth inhibition, elevated peroxide content, and reduced antioxidant enzyme activity. However, exogenous melatonin treatment mitigated leaf dehydration, elevated relative water content in leaves, and improved drought tolerance through the upregulation of antioxidant enzymes to eliminate reactive oxygen species (ROS), alongside the accumulation of osmoprotectants to reduce osmotic potential. Transcriptomic profiling revealed that differentially expressed genes in melatonin-treated leaves were predominantly enriched in pathways related to carbohydrate metabolism (including ribosome, glycolysis/gluconeogenesis, starch and sucrose metabolism, fructose and mannose metabolism, pentose and glucuronate interconversions), antioxidant metabolism, and carbon metabolism.

It is noteworthy that this research focused primarily on melatonin-mediated metabolic and transcriptional responses in leaves, while root development and regulatory mechanisms under drought stress remain unexplored. Future studies should integrate phenotypic and physiological assessments with genomic-level analyses to establish a comprehensive evaluation system for accurately quantifying drought resistance in *P. arguta*, thereby advancing the development of standardized resistance indicators.

Author Contributions: Data curation, X.Z., Z.J. and Y.H.; formal analysis, L.F. and Y.H.; funding acquisition, X.Z. and J.Z.; investigation, X.M., Z.J. and Y.H.; project administration, J.Z.; software, Q.H.; supervision, X.Z.; validation, Q.H.; writing—review and editing, X.Z. and Y.H. All authors have read and agreed to the published version of the manuscript.

Funding: This research was funded by Wenzhou Forestry and Flower Breeding Cooperation Group Project, grant number ZX2024004-3, and The APC was funded by Wenzhou Forestry and Flower Breeding Cooperation Group Project.

Data Availability Statement: The raw data supporting the conclusions of this article will be made available by the authors on request.

Conflicts of Interest: Author Zhengjian Jiang was employed by the company Zhejiang Juyoupin Biotechnology Co., Ltd. The remaining authors declare that the research was conducted in the absence of any commercial or financial relationships that could be construed as a potential conflict of interest.

References

1. Qi, X.-S.; Yuan, N.; Comes, H.P.; Sakaguchi, S.; Qiu, Y.-X. A strong 'filter' effect of the East China Sea land bridge for East Asia's temperate plant species: Inferences from molecular phylogeography and ecological niche modelling of *Platycrater arguta* (Hydrangeaceae). *BMC Evol. Biol.* **2014**, *14*, 41. [CrossRef]
2. Wingfield, J.C. Ecological processes and the ecology of stress: The impacts of abiotic environmental factors. *Funct. Ecol.* **2013**, *27*, 37–44. [CrossRef]

3. Farooq, M.; Wahid, A.; Kobayashi, N.; Fujita, D.; Basra, S.M.A. Plant drought stress: Effects, mechanisms and management. *Agron. Sustain. Dev.* **2009**, *29*, 185–212. [CrossRef]
4. Seleiman, M.F.; Al-Suhaibani, N.; Ali, N.; Akmal, M.; Alotaibi, M.; Refay, Y.; Dindaroglu, T.; Abdul-Wajid, H.H.; Battaglia, M.L. Drought Stress Impacts on Plants and Different Approaches to Alleviate Its Adverse Effects. *Plants* **2021**, *10*, 259. [CrossRef]
5. Bashir, S.S.; Hussain, A.; Hussain, S.J.; Wani, O.A.; Nabi, S.Z.; Dar, N.A.; Baloch, F.S.; Mansoor, S. Plant drought stress tolerance: Understanding its physiological, biochemical and molecular mechanisms. *Biotechnol. Biotechnol. Equip.* **2021**, *35*, 1912–1925. [CrossRef]
6. Impa, S.M.; Nadaradjan, S.; Jagadish, S.V.K. Drought Stress Induced Reactive Oxygen Species and Anti-oxidants in Plants. In *Abiotic Stress Responses in Plants*; Springer: New York, NY, USA, 2012.
7. Qi, J.; Song, C.P.; Wang, B.; Zhou, J.; Kangasjärvi, J.; Zhu, J.K.; Gong, Z. Reactive oxygen species signaling and stomatal movement in plant responses to drought stress and pathogen attack. *J. Integr. Plant Biol.* **2018**, *60*, 805–826. [CrossRef] [PubMed]
8. Mannino, G.; Pernici, C.; Serio, G.; Gentile, C.; Bertea, C.M. Melatonin and phytomelatonin: Chemistry, biosynthesis, metabolism, distribution and bioactivity in plants and animals—An overview. *Int. J. Mol. Sci.* **2021**, *22*, 9996. [CrossRef] [PubMed]
9. Ross, I.A. Melatonin in Plants and Animals. In *Plant-Based Therapeutics, Volume 2: The Brassicaceae Family*; Springer: Berlin/Heidelberg, Germany, 2024; pp. 735–812.
10. Ahmad, I.; Song, X.; Hussein Ibrahim, M.E.; Jamal, Y.; Younas, M.U.; Zhu, G.; Zhou, G.; Adam Ali, A.Y. The role of melatonin in plant growth and metabolism, and its interplay with nitric oxide and auxin in plants under different types of abiotic stress. *Front. Plant Sci.* **2023**, *14*, 1108507. [CrossRef]
11. Khan, A.; Numan, M.; Khan, A.L.; Lee, I.-J.; Imran, M.; Asaf, S.; Al-Harrasi, A. Melatonin: Awakening the defense mechanisms during plant oxidative stress. *Plants* **2020**, *9*, 407. [CrossRef]
12. Li, J.; Liu, J.; Zhu, T.; Zhao, C.; Li, L.; Chen, M. The Role of Melatonin in Salt Stress Responses. *Int. J. Mol. Sci.* **2019**, *20*, 1735. [CrossRef] [PubMed]
13. Zeng, W.; Mostafa, S.; Lu, Z.; Jin, B. Melatonin-Mediated Abiotic Stress Tolerance in Plants. *Front. Plant Sci.* **2022**, *13*, 847175. [CrossRef]
14. Hoque, M.N.; Tahjib-Ul-Arif, M.; Hannan, A.; Sultana, N.; Akhter, S.; Hasanuzzaman, M.; Akter, F.; Hossain, M.S.; Sayed, M.A.; Hasan, M.T.; et al. Melatonin modulates plant tolerance to heavy metal stress: Morphological responses to molecular mechanisms. *Int. J. Mol. Sci.* **2021**, *22*, 11445. [CrossRef]
15. Debnath, B.; Islam, W.; Li, M.; Sun, Y.; Lu, X.; Mitra, S.; Hussain, M.; Liu, S.; Qiu, D. Melatonin Mediates Enhancement of Stress Tolerance in Plants. *Int. J. Mol. Sci.* **2019**, *20*, 1040. [CrossRef]
16. Schmedes, A.; Hølmer, G. A new thiobarbituric acid (TBA) method for determining free malondialdehyde (MDA) and hydroperoxides selectively as a measure of lipid peroxidation. *J. Am. Oil Chem. Soc.* **1989**, *66*, 813–817. [CrossRef]
17. Leng, F.; Sun, S.; Jing, Y.; Wang, F.; Wei, Q.; Wang, X.; Zhu, X. A rapid and sensitive method for determination of trace amounts of glucose by anthrone-sulfuric acid method. *Bulg. Chem. Commun.* **2016**, *48*, 109–113.
18. Doi, E.; Shibata, D.; Matoba, T. Modified colorimetric ninhydrin methods for peptidase assay. *Anal. Biochem.* **1981**, *118*, 173–184. [CrossRef] [PubMed]
19. Li, L.; Zhu, H.; Ju, Y.; Lv, Z.; Qian, C.; Zhang, C.; Lu, Y.; Wang, J.; Li, W. Comparison of microstructure and physiological response of the leaves of six *Rosa rugosa* genotypes under drought stress. *Ornam. Plant Res.* **2024**, *4*, e016. [CrossRef]
20. Su, C.; Wang, P.; Wu, J.; Wang, H.; Fan, J.; Gong, W.; Hui, W.; Wang, J. Effects of melatonin on the photosynthetic characteristics of *Zanthoxylum armatum* under waterlogging stress. *Russ. J. Plant Physiol.* **2023**, *70*, 82. [CrossRef]
21. Hu, H.; Fei, X.; He, B.; Chen, X.; Ma, L.; Han, P.; Luo, Y.; Liu, Y.; Wei, A. UPLC-MS/MS profile combined with RNA-Seq reveals the amino acid metabolism in *Zanthoxylum bungeanum* leaves under drought stress. *Front. Nutr.* **2022**, *9*, 921742. [CrossRef]
22. García, J.J.; López-Pingarrón, L.; Almeida-Souza, P.; Tres, A.; Escudero, P.; García-Gil, F.A.; Tan, D.X.; Reiter, R.J.; Ramírez, J.M.; Bernal-Pérez, M. Protective effects of melatonin in reducing oxidative stress and in preserving the fluidity of biological membranes: A review. *J. Pineal Res.* **2014**, *56*, 225–237. [CrossRef]
23. Afzal, A. Melatonin as a multifunctional modulator: Emerging insights into its role in health, reproductive efficiency, and productive performance in livestock. *Front. Physiol.* **2024**, *15*, 1501334. [CrossRef] [PubMed]
24. Ganie, S.A.; Dar, T.A.; Bhat, A.H.; Dar, K.B.; Anees, S.; Zargar, M.A.; Masood, A. Melatonin: A potential anti-oxidant therapeutic agent for mitochondrial dysfunctions and related disorders. *Rejuvenation Res.* **2016**, *19*, 21–40. [CrossRef]
25. Zhao, Y.; Gao, C.; Shi, F.; Yun, L.; Jia, Y.; Wen, J. Transcriptomic and proteomic analyses of drought responsive genes and proteins in *Agropyron mongolicum* Keng. *Curr. Plant Biol.* **2018**, *14*, 19–29. [CrossRef]
26. Ma, Y.; Yu, X.; Yu, Z.; Sun, F.; Li, X.; Li, X. RNA-Seq of *Agropyron mongolicum* Keng in response to drought stress. *Grassl. Sci.* **2018**, *64*, 3–15. [CrossRef]
27. Hartmann, H.; Bahn, M.; Carbone, M.; Richardson, A.D. Plant carbon allocation in a changing world–challenges and progress. *New Phytol.* **2020**, *227*, 981–988. [CrossRef]

28. Parwez, R.; Aftab, T.; Gill, S.S.; Naeem, M.J.E.; Botany, E. Abscisic acid signaling and crosstalk with phytohormones in regulation of environmental stress responses. *Environ. Exp. Bot.* **2022**, *199*, 104885. [CrossRef]
29. Li, J.; Li, Y.; Du, M.; Zang, D.; Men, Q.; Su, P.; Guo, S. Exogenous melatonin improves drought stress tolerance via regulating tryptophan metabolism and flavonoid biosynthesis pathways in wheat. *Physiol. Plant.* **2024**, *176*, e70006. [CrossRef]
30. Shao, C.; Chen, J.; Lv, Z.; Gao, X.; Guo, S.; Xu, R.; Deng, Z.; Yao, S.; Chen, Z.; Kang, Y.; et al. Staged and repeated drought-induced regulation of phenylpropanoid synthesis confers tolerance to a water deficit environment in *Camellia sinensis*. *Ind. Crop. Prod.* **2023**, *201*, 116843. [CrossRef]
31. Qiu, C.-W.; Ma, Y.; Wang, Q.-Q.; Fu, M.-M.; Li, C.; Wang, Y.; Wu, F. Barley HOMOCYSTEINE METHYLTRANSFERASE 2 confers drought tolerance by improving polyamine metabolism. *Plant Physiol.* **2023**, *193*, 389–409. [CrossRef]
32. Liu, W.-C.; Song, R.-F.; Zheng, S.-Q.; Li, T.-T.; Zhang, B.-L.; Gao, X.; Lu, Y.-T. Coordination of plant growth and abiotic stress responses by tryptophan synthase β subunit 1 through modulation of tryptophan and ABA homeostasis in Arabidopsis. *Mol. Plant* **2022**, *15*, 973–990. [CrossRef]
33. El-Yazied, A.A.; Ibrahim, M.F.; Ibrahim, M.A.; Nasef, I.N.; Al-Qahtani, S.M.; Al-Harbi, N.A.; Alzuaibr, F.M.; Alaklabi, A.; Dessoky, E.S.; Alabdallah, N.M.; et al. Melatonin mitigates drought induced oxidative stress in potato plants through modulation of osmolytes, sugar metabolism, ABA homeostasis and antioxidant enzymes. *Plants* **2022**, *11*, 1151. [CrossRef] [PubMed]

MDPI AG
Grosspeteranlage 5
4052 Basel
Switzerland
Tel.: +41 61 683 77 34

Horticulturae Editorial Office
E-mail: horticulturae@mdpi.com
www.mdpi.com/journal/horticulturae

Academic Open
Access Publishing

mdpi.com

ISBN 978-3-7258-6327-3